Identifying Genetic Dependencies and Potential Novel Therapeutic Targets for Osteosarcoma

Harriet Katie Holme

University College London

Submitted for degree of Doctor of Philosophy

Statement of Contribution

I, Harriet Katie Holme confirm that the work presented in this thesis is my own. Where information has been derived from other sources, I confirm that this has been indicated in the thesis.

Helen Pemberton and Rachel Brough taught me how to prepare the siRNA screening plates for the siRNA libraries. Statistical analysis was performed with assistance from James Campbell Institute of Cancer Research, UK (ICR) and Aditi Gulati (ICR). The non-osteosarcoma tumour cell line data set (siRNA and drug sensitivities) used for data comparison was compiled by multiple members of the Lord / Ashworth Gene Function laboratory group at the ICR (Rachel Brough, Helen Pemberton, Jessica Frankum, Ilirjana Bajrami, Irene Chong, Rowan Miller, Ruman Rafiq, Sophie Postel-Vinjay, Chris Williamson, and Sara Costa-Cabral).

Rumana Rafiq (ICR) performed the preparation of the drug plates for the drug inhibitor screens for drug library, and performed the drug sensitivity profiling of the OS tumour cell line panel using this library presented in Chapter 7. Malini Menon (ICR) performed the preparation of the additional drug library.

Jenni Nikkilä (ICR) provided guidance with FACS cell cycle staining and gating presented in Chapter 6.

Rachel Brough (ICR) assisted me on the Echo to perform combination screens presented in Chapter 7. Rachel also categorised the breast cancer cell line panel used for comparison of *RB1* deficient dependencies.

Jessica Frankum (ICR) assisted with the staining and interpretation of the Rad 51 assays presented in Chapter 7.

Ilirjana Bajrami determined the BRCA1/2 mutations in the non-osteosarcoma tumour cell line panel.

Amy Dréan engineered the tumour cell lines CAPAN1.B2*.S and SUM149.B1*.S and performed the dose response sensitivity experiment illustrated in Figure 124.

Colm Ryan (Systems Biology Ireland, University College Dublin, Ireland) performed quantification and analysis of protein abundance by mass spectroscopy.

James Campbell (ICR) analysed the exome sequencing and Aditi Gulati RNA sequencing data generated by the Tumour Profiling Unit at the ICR.

Inger Brandsma (ICR) engineered a SUM149 *REV7* mutant clone with a truncating mutation in *REV7* (*MADL2L2*) and a SUM149 *53BP1* mutant clone with a truncating mutation in *53BP1* by CRISPR-Cas9 mutagenesis, used in Chapter 7 as controls. The SUM149 *PARP1* mutant clone with a missense mutation in *PARP1* was created by Stephen Pettitt (ICR), and used as a control in Chapter 7.

Ultan McDermott directed the exome sequencing and analysis of some of the osteosarcoma tumour cell lines at the Wellcome Trust Sanger Institute.

Fernanda Amary categorised a subset of the OS tumour cell lines according to *FGFR1* amplification and polysomy using fluorescent in situ hybridisation, presented in Chapter 7.

Acknowledgements

I would like to thank my supervisors Dr Sandra Strauss, Professor Chris Lord, Professor Alan Ashworth and Professor Adrienne Flanagan for giving me the opportunity to undertake this project and their guidance throughout.

I would like to sincerely thank Sandra Strauss for her critical appraisal and support. It has been an absolute privilege to work at the ICR and I am indebted to Chris Lord and Alan Ashworth for adopting me into their groups. I am very grateful for the patience, support, financial commitment and clarity of thought from Chris Lord. All the members of the Lord laboratory group have provided me with unwavering kindness, guidance and friendship, with particular thanks to my mentor Rachel Brough, Ilirjana Bajrami, Jessica Frankum and Rumana Rufiq. Rachel and Ilirjana educated me in laboratory techniques and I am eternally grateful for their mentorship.

Finally I would like to thank my family for the support and patience exhibited by my husband, Gurhan Erturan, and my parents.

Abstract

With little recent improvement in osteosarcoma (OS) outcomes, identification of therapeutic targets is critical. RNA interference (RNAi) and drug screens using OS tumour cell lines (TCL) were used to identify novel genetic dependencies and validate tractable therapeutic targets.

Cell viability data from RNAi screens in 18 OS TCL was integrated with whole-exome sequencing and protein expression data. Comparison with non-osteosarcoma TCL, demonstrated OS to be more reliant on skeletal morphogenesis pathways and *FGFR1/2*, with increased sensitivity to FGFR1 inhibitors. OS TCL positive for *FGFR1* amplification and polysomy were significantly more sensitive to FGFR1 inhibitors than unknown or non-amplified OS TCL, providing further evidence for a clinical trial in an enriched population.

Correlation of RNAi results with the presence of recurrent driver gene alterations revealed that sensitivity to selective silencing of *DYRK1A* was associated with deficiency of *RB1*. This finding was validated using RNAi in the OS TCL, an additional 34 breast TCL, and a *DYRK1A* kinase inactive model. Harmine, a DYRK1A inhibitor, resulted in greater apoptosis in an *RB1* deficient OS TCL than in a *RB1* wildtype model. DYRK1A has been identified as a protein interaction partner of RB1 and is pharmacologically tractable. Further work is necessary to mechanistically understand this synthetic lethality.

The model system was also used as a tool to validate the potential role of BRCAness in OS, recently identified as a potential target in genomic studies. This determined the majority of OS TCL not to be profoundly sensitive to PARP inhibition. However, LM7 (an OS TCL) created by repeated pulmonary murine passage of SAOS2, demonstrated this acquired phenotype. Absence of RAD51 foci in LM7 in contrast to SAOS2, identifies this as a suitable, mechanistically relevant, tool for studying ‘BRCAness’ in OS.

Integrated screens provided a framework for pre-clinical identification and validation of tractable therapeutic targets to facilitate translation into development of clinical trials.

Table of contents

List of Figures

List of Tables

List of Appendix Tables

Abbreviations

53BP1	p53-binding protein 1
ABCA12	ATP Binding Cassette Subfamily A Member 12
ABL	Proto-Oncogene 1, Non-Receptor Tyrosine Kinase
ACSL	Acyl-CoA Synthetase Long-Chain Family Member
ACVR2B	Actin A Receptor Type 2B
AGPAT3	1-Acylglycerol-3-Phosphate O-Acyltransferase 3
AKT	phosphoinositide 3-kinase
ALK	Anaplastic Lymphoma Receptor Tyrosine Kinase
AMPK	Protein Kinase AMP-Activated Catalytic Subunit Alpha 1
ANKRD50	Ankyrin Repeat Domain 50
ANOVA	analysis of variance
APC	Adenomatous Polyposis Coli
APE1	Apurinic/Apyrimidinic Endodeoxyribonuclease 1
ARHGAP26	Rho GTPase Activating Protein 26
ARID	AT-Rich Interaction Domain
ATCC	American Type Culture Collection
ATG4A	Autophagy Related 4A Cysteine Peptidase
ATM	Ataxia-Telangiectasia Mutated
ATR	ATM-Rad3-related protein kinase
ATRX	Alpha Thalassemia/Mental Retardation Syndrome X-Linked
AUC	Area Under the Curve
AURKA	Aurora Kinase A
AXL	AXL Receptor Tyrosine Kinase
BAP1	BRCA1 Associated Protein 1
BARD1	BRCA1 Associated RING Domain 1
BCKDK	Branched Chain Ketoacid Dehydrogenase Kinase
Bcl-2	BCL2, Apoptosis Regulator
BDH1	3-Hydroxybutyrate Dehydrogenase 1
BIRC3	Baculoviral IAP Repeat Containing 3
BRAF	B-Raf Proto-Oncogene Serine/Threonine Kinase
BRCA1	Breast cancer 1
BRCA2	Breast cancer 2
BSA	Bovine serum albumin
BTK	Bruton Tyrosine Kinase

C	Celsius
C17orf75	Chromosome 17 Open Reading Frame 75
C7	Complement C7
C8orf34	Chromosome 8 Open Reading Frame 34
CAMK4	Calcium/Calmodulin Dependent Protein Kinase IV
CAMTA1	Calmodulin Binding Transcription Activator 1
CASP10	Caspase 10
CB1	cannabinoid receptor
CCL25	C-C Motif Chemokine Ligand 25
CCLE	Cancer Cell Line Encyclopaedia
CCND3	Cyclin D3
CCNE1	Cyclin E1
CCR	C-C Motif Chemokine Receptor
CDC	Cell Division Cycle
CDK	cyclin-dependent kinases
CDKL	cyclin-dependent like kinases
CDKN1A	Cyclin Dependent Kinase Inhibitor 1A
CDKN1C	Cyclin Dependent Kinase Inhibitor 1C
CDKN2A	Cyclin Dependent Kinase Inhibitor 2A
cDNA	complementary deoxyribonucleic acid
CENPE	Centromere Protein E
CETP	Cholesteryl Ester Transfer Protein
CFHR2	Complement Factor H Related 2
CHK	Checkpoint Kinase
CHURC1	Churchill Domain Containing 1
CK1ε	Casein Kinase 1 Epsilon
cKIT	c-KIT Proto-Oncogene Receptor Tyrosine Kinase
cMET	c-MET Proto-Oncogene, Receptor Tyrosine Kinase
CNTNAP2	Contactin Associated Protein-Like 2
CNV	Copy Number Variants
COPB2	Coatomer Protein Complex Subunit Beta 2
COPS3	COP9 Signalosome Subunit 3
COSMIC	Catalogue of somatic mutations in cancer
COX2	Prostaglandin-Endoperoxide Synthase 2
COX6C	Cytochrome C Oxidase Subunit 6C

CRCP	CGRP Receptor Component
crDNA	CRISPR RNA
CRISPR	clustered regularly interspaced short palindromic repeats
CTG	CellTiter Glo
CTLs	Cytotoxic T lymphocytes
CUL4B	Cullin 4B
CXCR1	C-X-C Motif Chemokine Receptor 1
CYBRD1	Cytochrome B Reductase 1
CYP17A1	Cytochrome P450 Family 17 Subfamily A Member 1
D	dimensional
DAPI	4',6-diamidino-2-phenylindole
DDR	DNA damage response
DE	drug effect
DF4	Dharmafect 4
DHFR	Dihydrofolate Reductase
DLG1	Discs Large MAGUK Scaffold Protein 1
DMGDH	Dimethylglycine Dehydrogenase
DMSO	Dimethylsylfoxide
DNA	Deoxyribonucleic acid
DNA-PK	DNA-dependent protein kinase
DNM2	Dynamin 2
DP1	dimerization protein 1
DSB	double strand breaks
DYRK	dual-specificity tyrosine-regulate kinase
DYRK1A	dual-specificity tyrosine-regulate kinase 1A
E2F	E2F Transcription Factor
ECSCR	Endothelial Cell Surface Expressed Chemotaxis And Apoptosis Regulator
EDTA	ethylenediaminetetraacetate
EDU	5-ethynyl-2′-deoxyuridine
EFCAB13	EF-Hand Calcium Binding Domain 13
EFS	Event free survival
EGFR	Epidermal Growth Factor Receptor
EHD1	EH Domain Containing 1
EIF4A2	Eukaryotic Translation Initiation Factor 4A2

EME2	Essential Meiotic Structure-Specific Endonuclease Subunit 2
EPS15	Epidermal Growth Factor Receptor Pathway Substrate 15
ERBB	Erb-B2 Receptor Tyrosine Kinase
ERCC3	ERCC Excision Repair 3, TFIIH Core Complex Helicase Subunit
ERCC5	ERCC Excision Repair 5, Endonuclease
ERK2	Mitogen-Activated Protein Kinase 1
EURAMOS	European and American Osteosarcoma Study Group
EXT1	Exostosin Glycosyltransferase 1
EYA4	EYA Transcriptional Coactivator And Phosphatase 4
FAAH	Fatty Acid Amide Hydrolase
FACS	Fluorescence-activated cell sorting
FAK	Protein Tyrosine Kinase 2
FAM98A	Family With Sequence Similarity 98 Member A
FANC	Fanconi Anaemia Complementation Group
FAS	Fas Cell Surface Death Receptor
FBXW7	F-Box And WD Repeat Domain Containing 7
FDA	Food and Drug Administration
FDR	False Discovery Rate
FGFR	Fibroblast Growth Factor Receptor
FIP1L1	Factor Interacting With PAPOLA And CPSF1
FISH	Fluorescence in situ hybridisation
FLT 1/3/4	Fms Related Tyrosine Kinase 1/3/4
FOXM1	Forkhead box protein M1
FUK	Fucokinase
FXR	Nuclear Receptor Subfamily 1 Group H Member 4
g	gram
GALK1	Galactokinase 1
GATA3	GATA Binding Protein 3
GD2Bi-aATC	chimeric T cells with GD2 antibody
gDNA	genomic DNA
GDP	guanosine diphosphate
GLI2	GLI Family Zinc Finger 2
GLT6D1	Glycosyltransferase 6 Domain Containing 1
GMFG	Glia Maturation Factor Gamma

GNE	Glucosamine (UDP-N-Acetyl)-2-Epimerase/N-Acetylmannosamine Kinase
GPC3	Glypican 3
GPR40	Free Fatty Acid Receptor 1
GRM4	Glutamate Metabotropic Receptor 4
GSK	Glycogen Synthase Kinase
GTP	guanosine triphosphate
GUCY2D	Guanylate Cyclase 2D
Gy	Gray
H2BFWT	H2B Histone Family Member W, Testis Specific
HDAC	Histone Deacetylase
HDM2	MDM2 Proto-Oncogene
HER2	Erb-B2 Receptor Tyrosine Kinase 2
HIF	Hypoxia Inducible Factor
Hip-1	huntingtin-interacting protein 1
HIST2H2AB	Histone Cluster 2 H2B Family Member A
HMGCoA	3-Hydroxy-3-Methylglutaryl-CoA reductase (NADPH)
HMTase	histone methyltransferase
HNRNPA2B1	Heterogeneous Nuclear Ribonucleoprotein A2/B1
HOXA13	Homeobox A13
HOXD13	Homeobox D13
HR	homologous recombination
HRAS	HRas Proto-Oncogene, GTPase
HSP90	Heat shock protein 90
HSP90AA1	Heat Shock Protein 90 Alpha Family Class A Member 1
HUS1	HUS1 Checkpoint Clamp Component
IAP	Baculoviral IAP Repeat Containing 3
IC50	half maximal inhibitory concentration
ICL	interstrand cross-links
ICR	The Institute of Cancer Research, London, UK.
IDS	Iduronate 2-Sulfatase
IGF	Insulin Like Growth Factor
IGF1R	Insulin Like Growth Factor 1 Receptor
IkB	Inhibitor Of Nuclear Factor Kappa B Kinase Subunit Beta (IKK)
IKZF1	IKAROS Family Zinc Finger 1

IL1	Interleukin 1
indel	short insertion/deletion
INIP	INTS3 And NABP Interacting Protein
IR	Ionising radiation
IR	Insulin receptor
IRS4	Insulin Receptor Substrate 4
JAK2	Janus Kinase 2
JNK	c-Jun N-terminal kinase
K-RAS	KRAS Proto-Oncogene, GTPase
kDa	kilo Dalton
KLHL29	Kelch Like Family Member 29
KLK12	Kallikrein Related Peptidase 12
KR	kinase inactive DYRK1A-K188R
KRT8	Keratin 8
KSP	Kinesin spindle protein
L	Litre
LAK	Alpha Kinase 1
LF2000	Lipofectamine 2000
LFS	Li-Fraumeni syndrome
LIN37	Lin-37 DREAM MuvB Core Complex Component
LIN52	Lin-52 DREAM MuvB Core Complex Component
LIN54	Lin-54 DREAM MuvB Core Complex Component
LIN9	Lin-9 DREAM MuvB Core Complex Component
LOH	loss of homozygosity
LOH18CR1	TNF Receptor Superfamily Member 11a
M	Molar
m	millie
MAD	median absolute deviation
MAD2	mitotic checkpoint protein
MAO	monoamine oxidase
MAP	methotrexate, doxorubicin and cisplatin
MAPK	Mitogen-activated protein kinase
MAPK8	Mitogen-Activated Protein Kinase 8
Max	RNAmax
MAX	MYC Associated Factor X

MDM2	MDM2 Proto-Oncogene
MDM4	MDM4, P53 Regulator (MDMX)
MEI1	Meiotic Double-Stranded Break Formation Protein 1
MEK1	Mitogen-Activated Protein Kinase Kinase 1
MGC4796	Serine/Threonine Kinase 40 (STK40)
MGMT	O-6-Methylguanine-DNA Methyltransferase
miR-182	MicroRNA 182
miRNA	micro-ribonucleic acid
MLPA	muliplex ligation-dependent probe amplification
MMP	Matrix Metallopeptidase
MNX1	Motor Neuron And Pancreas Homeobox 1
MOPS	3-(N-morpholino)propanesulfonic acid
MORF4L2	Mortality Factor 4 Like 2
MPP3	Membrane Palmitoylated Protein 3
MPT	median permutation test
mRNA	messenger RNA
MRPL45	Mitochondrial Ribosomal Protein L45
MSC	mesenchymal stem cells
MSP1	Merozoite surface protein 1
MTAP	Methylthioadenosine Phosphorylase
MTD	maximum tolerated dose
mTOR	Mechanistic Target Of Rapamycin
MTP-PE	muramyl tripeptide phosphatidylethanolamine
MUTYH	MutY DNA Glycosylase
MuvB	multi-vulval class B
MYC	V-Myc Avian Myelocytomatosis Viral Oncogene Homolog
MYLK	Myosin Light Chain Kinase
n	nano
NAD	Nicotinamide adenine dinucleotide
NAGK	N-Acetylglucosamine Kinase
NAMPT	Nicotinamide Phosphoribosyltransferase
NBN	Nibrin
NCOA	Nuclear Receptor Coactivator
NEK	NIMA Related Kinase
NER	nucleotide excision repair

NF-kB	nuclear factor kappa-light-chain-enhancer of activated B cells
NF1	Neurofibromin 1
Nfkb	nuclear factor-κB
NHEJ	nonhomologous end-joining
NICE	National Institute of Clinical Excellence
NK	Natural Killer
NOS2	Nitric Oxide Synthase 2
NPI	Normalised percentage inhibition
NR	non-replicating
NS	non-silencing
NUDT1	Nudix Hydrolase 1
NUMA1	Nuclear Mitotic Apparatus Protein 1
OGG1	8-Oxoguanine DNA Glycosylase
OR	odds ratio
ORR	overall response rate
OS	osteosarcoma
p130	RB Transcriptional Corepressor Like 2 (RBL2)
P16INKa	Cyclin Dependent Kinase Inhibitor 2A (CDKN2A)
p21	Cyclin Dependent Kinase Inhibitor 1A (CDKN1A)
p27 ^{Kipl}	Cyclin Dependent Kinase Inhibitor 1B (CDKN1B)
PAK4	p-21 activated kinase 4
PAL	phenylalanine ammonia lyase
PALB2	Partner And Localizer Of BRCA2
PALM2	Paralemmin 2
PAM	protospacer adjacent motif
PARP	Poly ADP-ribose polymerase
PARPBP	PARP1 Binding Protein
PBRM1	Polybromo 1
PBS	phosphate buffered saline
PCDHA1	Protocadherin Alpha 1
PCDHB5	Protocadherin Beta 5
PCR	Polymerase Chain Reaction
PCTK3	Cyclin Dependent Kinase 18
PD	pharmacodynamics
PDCD1LG2	Programmed Cell Death 1 Ligand 2

PDGFR	Platelet derived growth factor receptor
PDL1	Programmed cell death ligand 1
PDPK1	3-Phosphoinositide Dependent Protein Kinase 1
PDX	patient derived xenograft
PFS	progression free survival
PHACTR1	Phosphatase And Actin Regulator 1
PI3 kinase	Peptidase Inhibitor 3
PIK3CA	Phosphatidylinositol-4,5-Bisphosphate 3-Kinase Catalytic Subunit Alpha
PIM	Pim Proto-Oncogene, Serine/Threonine Kinase
PK	pharmacokinetics
PKC	Protein Kinase C
PKM	Pyruvate Kinase, Muscle
PLK1	Polo Like Kinase 1
PMS2	PMS1 Homolog 2, Mismatch Repair System Component
POLG	DNA Polymerase Gamma, Catalytic Subunit
PPAR	Peroxisome Proliferator Activated Receptor
PRKCD	Protein Kinase C Delta
PRKCL1	Protein Kinase N1
PRKCN	Protein Kinase D3
PTEN	Phosphatase And Tensin Homolog
PTPRC	Protein Tyrosine Phosphatase, Receptor Type C
PYCS	Pyrroline-5-Carboxylate Synthetase
PYROXD1	Pyridine Nucleotide-Disulphide Oxidoreductase Domain 1
QN	Quantile normalisation
r^2	Spearman's rank correlation coefficient
RAC	Ras-Related C3 Botulinum Toxin Substrate
RAD50	RAD50 Double Strand Break Repair Protein
RAD51	RAD51 Recombinase
RAF1	Raf-1 Proto-Oncogene, Serine/Threonine Kinase
RAGE	Advanced Glycosylation End-Product Specific Receptor
RANK	Receptor Activator of Nuclear Factor κ B
RANK	TNF Receptor Superfamily Member 11a
RAR	Retinoic Acid Receptor
RB1	Retinoblastoma 1

RBBP4	RB Binding Protein 4, Chromatin Remodeling Factor
RECQL2/3/4	RecQ Like Helicase 2/3/4
RECQL5	RecQ Like Helicase 5
RET	Ret Proto-Oncogene
REV7	MAD2 Mitotic Arrest Deficient-Like 2 (MADL2L2)
RHOH	Ras Homolog Family Member H
RICTOR	RPTOR Independent Companion Of MTOR Complex 2
RIPK1	Receptor Interacting Serine/Threonine Kinase 1
RISC	RNA-induced silencing complex
RNA	ribonucleic acid
RNA seq	RNA sequencing
RNAi	ribonucleic acid inhibition
RNF168	Ring Finger Protein 168
RNF20	Ring Finger Protein 20
ROCK	Rho Associated Coiled-Coil Containing Protein Kinase
RP11-420A23.1	Uncharacterized LOC100507487
RP2D	recommended phase II dose
RP4-724E16.2	Uncharacterized LOC101927770
RPA	Replication Protein A
RTK	receptor tyrosine kinases
rtPCR	Real-time PCR
RTS	Rothmund-Thomson Syndrome
RUNX1	Runt Related Transcription Factor 1
S1P	Sphingosine-1-Phosphate
SCNA	somatic copy-number alterations
SD	standard deviation
SEM	standard error of the mean
SERPINB10	Serpin Family B Member 10
SF	survival fraction
SF-1	Nuclear Receptor Subfamily 5 Group A Member 1
SF50	Survival Fraction 50
SGK	Serum/Glucocorticoid Regulated Kinase 1
SGLT	Solute Carrier Family 5 Member
SHFM1	Split Hand/Foot Malformation (Ectrodactyly) Type 1
shRNA	small hairpin ribonucleic acid

siCON	small interfering ribonucleic acid control (non-targeting)
siRNA	small interfering ribonucleic acid
SIRT1	Sirtuin 1
SKP2	S Phase Kinase-associated protein
SLC19A1	Solute Carrier Family 19 Member 1
SLC45A3	Solute Carrier Family 45 Member 3
SLX1A	SLX1 Homolog A, Structure-Specific Endonuclease Subunit
SMARC	SWI/SNF Related Matrix Associated Actin Dependent Regulator Of Chromatin Subfamily
SNP	single nucleotide polymorphism
SNV	single nucleotide variants
SOSS	sensor of single strand DNA
SPARC	Secreted Protein Acidic And Cysteine Rich
SPPI	Secreted Phosphoprotein 1
SQSTM1	Sequestosome 1
SRB	sulforhodamine-B
SRC	SRC Proto-Oncogene, Non-Receptor Tyrosine Kinase
SSTR1	Somatostatin Receptor 1
ST6GAL1	ST6 Beta-Galactoside Alpha-2,6-Sialyltransferase 1
STAT	Signal Transducer And Activator Of Transcription
STK22C	Serine/Threonine-Protein Kinase 22C
STK33	Serine/Threonine Kinase 33
STR	short tandem repeat
SYK	Spleen Associated Tyrosine Kinase
TALEN	Transcription-Activator Like Effector Nuclease
TBC1D9B	TBC1 Domain Family Member 9B
TBK1	TANK Binding Kinase 1
TCA	trichloroacetic acid
TCF7L2	Transcription Factor 7 Like 2
TCTN3	Tectonic Family Member 3
TERT	Telomerase Reverse Transcriptase
Tet-on	Tetracycline-controlled transcriptional activation
TET2	Tet Methylcytosine Dioxygenase 2
TGF	transforming growth factor
THBS3	Thrombospondin 3

TIE2	TEK Receptor Tyrosine Kinase
TJP2	Tight Junction Protein 2
TNF	Tumour Necrosis Factor
TNKS	Tankyrase
TORC1	raptor-mTOR protein complex
TORC2	rictor-mTOR protein complex
TP53	Tumour Protein P53
TREX2	Three Prime Repair Exonuclease 2
TrkA	Neurotrophic Receptor Tyrosine Kinase 1
TSC2	Tuberous Sclerosis 2
TTC6	Tetratricopeptide Repeat Domain 6
UAP1L1	UDP-N-Acetylglucosamine Pyrophosphorylase 1 Like 1
UBC	Ubiquitin C
UBE2A	Ubiquitin Conjugating Enzyme E2 A
USA	United States of America
USP1	Ubiquitin Specific Peptidase 1
USP53	Ubiquitin Specific Peptidase 53
VEGF	Vascular Endothelial Growth Factor
VRK2	Vaccinia Related Kinase 2
WBSCR	GTF2I Repeat Domain Containing 1
WDR60	WD Repeat Domain 60
WEE1	WEE1 G2 Checkpoint Kinase
WHO	World Health Organisation
WIPF2	WAS/WASL Interacting Protein Family Member 2
WRN	Werner syndrome helicase
WT	wildtype
WTSI	Wellcome Trust Sanger Institute
WWTR1	WW Domain Containing Transcription Regulator 1
XRCC	X-ray repair cross-complementing
YBX1	Y-Box Binding Protein 1
ZNF	Zinc-Finger Nuclease
γH2AX	Histone H2A, Serine 139 phosphorylated
μ	micro

Publications and presentations from this thesis

Original publications

Campbell J, Ryan CJ, Brough R, Bajrami I, Pemberton HN, Chong IY, Costa-Cabrai S, Frankum J, Gulati A, Holme H, Miller R, Postel-Vinay S, Rafiq R, Wei W, Williamson CT, Quigley DA, Tym J, Al-Lazikani B, Fenton T, Natrajan R, Strauss S, Ashworth A, Lord CJ. Large-Scale Profiling of Kinase Dependencies in Cancer Cell Lines. Cell Reports. 2016 Mar15;14(10):2490-501.

Presentations

Connective Tissue Oncology Society (CTOS). Lisbon, Portugal November 2016.

Poster Presentation: Identification Of Pharmacologically Tractable Targets In Osteosarcoma. **Holme H,** Brough R, Pemberton H, Campbell J, Ryan CJ, Flanagan A, Ashworth A, Lord CJ, Strauss SJ.

British Sarcoma Group (BSG). Bristol February 2017.

Oral podium presentation: Identification Of Potential Novel Therapeutic Targets In Osteosarcoma. **Holme H,** Brough R, Pemberton H, Campbell J, Ryan CJ, Flanagan A, Ashworth A, Lord CJ, Strauss SJ.

UCL Cancer Institute student presentation

Poster Presentation: Identification Of Genetic Dependencies and Pharmacologically Tractable Targets In Osteosarcoma. **Holme H,** Brough R, Pemberton H, Campbell J, Ryan CJ, Ilirjana Bajrami, Aditi Gulati, Flanagan A, Ashworth A, Lord CJ, Strauss SJ. Identifying Genetic Dependencies and Potential Novel Therapeutic Targets for Osteosarcoma

1 Introduction

1.1 OSTEOSARCOMA

1.1.1 Incidence and mortality of Osteosarcoma

Osteosarcoma (OS) is the most common primary tumour of bone, occurring more frequently in males than females (ratio 1.3:1) (Whelan, McTiernan, Cooper, *et al.*, 2012). The incidence of osteosarcoma has a bimodal distribution, with the first peak occurring in adolescence (10-24 years), and a second occurring in those aged 70 years and over (Whelan, McTiernan, Cooper, *et al.*, 2012). Patients 40 years and older have been shown to have a worse outcome than those under 40 years of age, and have an overall survival at five years of just 22% compared to 53% (Whelan, McTiernan, Cooper, *et al.*, 2012). The overall five year survival across all age groups is under 45%, and no significant improvement in outcome has been achieved since 1987 (Whelan, McTiernan, Cooper, *et al.*, 2012). The site of disease also influences survival, with non-extremity (cranial, thoracic, spinal and pelvic) osteosarcoma having an inferior outcome (16%) compared to extremity (48%) and craniofacial tumours (52%) (p<0.0001) (Gorlick, Anderson, Andrulis, *et al.*, 2003).

1.1.2 Treatment of Osteosarcoma

Historical treatment of osteosarcoma focused on amputation, with dismal survival rates of 15-20% (Eilber, Giuliano, Eckardt, *et al.*, 1987), and patients succumbing to pulmonary metastases. In the 1970s, the M.D. Anderson Hospital, Houston, studied a combination of cytoxan, vincristine, melphalan, and adriamycin which delivered an overall two year survival rate of over 50% (Sutow, Sullivan, Fernbach, *et al.*, 1975; Sutow, Sullivan, Wilbur, *et al.*, 1975). Further studies from several institutions at this time showed a definite disease-free and overall survival advantage for patients receiving chemotherapy (Eilber, Giuliano, Eckardt, *et al.*, 1987). Methotrexate was first used in osteosarcoma in 1974, in combination with vincristine, after local control by surgery or irradiation with a significant reduction in reported pulmonary metastases (Jaffe, Frei, Traggis, *et al.*, 1974). Subsequent trials confirmed the benefit of multi-agent therapy comprising of neo-adjuvant and adjuvant chemotherapy (high-dose methotrexate, doxorubicin, and cisplatin), and surgical resection (Eilber, Giuliano, Eckardt, *et al.*, 1987) and shaped modern multi-

modality treatment (Bacci, Briccoli, Longhi, *et al.*, 2005; Kempf-Bielack, Bielack, Jürgens, *et al.*, 2005; Bacci, Picci, Ruggieri, *et al.*, 1990).

At present, in patients with localised, operable disease, histological response to neo-adjuvant chemotherapy is the most robust clinical marker of outcome, with 'good' response generally classified as a tumour showing 90% or more necrosis, and 'poor' if less than 90% tumour necrosis (Bacci, Mercuri, Longhi, *et al.*, 2005; Bacci, Picci, Ruggieri, *et al.*, 1990; Pakos, Nearchou, Grimer, *et al.*, 2009; Bielack, Kempf-Bielack, Delling, *et al.*, 2002). For patients with a good response, event free survival is in the order of 70% whilst those with a 'poor' response this lies below 50% (Bielack, 2002).

Collaboration between European and American clinicians led to the largest randomised Phase III trial to date, European and American Osteosarcoma Study Group 1 (EURAMOS 1), which investigated optimising treatment strategies based on the histological response to two cycles of neo-adjuvant chemotherapy (Marina, Bielack, Whelan, *et al.*, 2009). The study investigated the benefit of the addition of interferon maintenance therapy to methotrexate, doxorubicin and cisplatin (MAP) chemotherapy for 'good' responders (Bielack, Smeland, Whelan, *et al.*, 2015), and the addition of ifosfamide and etoposide for patients with a 'poor response' (Marina, Smeland, Bielack, *et al.*, 2016). Neither of the experimental arms was found to confer any benefit, thus, the standard of care remains MAP (Marina, Smeland, Bielack, *et al.*, 2016) and unfortunately despite international collaboration, there has been little improvement in survival over the past two decades since the introduction of this therapy (Kempf-Bielack, Bielack, Jürgens, *et al.*, 2005; Janeway, Barkauskas, Krailo, *et al.*, 2012; Mirabello, Troisi & Savage, 2009) with 5 year survival remaining in the order of 70% for young patients with localised disease. For those with metastatic disease at diagnosis, outcome is poor with only 20-30% surviving for 5 years and remains even more dismal for those with recurrence (Luetke, Meyers, Lewis, *et al.*, 2014). There is a paucity of early phase clinical trials available for these patients and unfortunately results from these have generally been disappointing. The Children's Oncology Group recently performed an analysis of outcome of patients with recurrent osteosarcoma treated on seven phase II clinical trials, demonstrating a very poor event free survival of 12 % at 4 months (Lagmay, Krailo, Dang, *et al.*, 2016).

Recently, liposomal muramyl tripeptide phosphatidylethanolamine (MTP-PE) has been approved by the National Institute of Clinical Excellence (NICE) as an adjunct to standard first line therapy in patients up to 30 years presenting with non-metastatic osteosarcoma. MTP-PE is now part of established therapy in the United Kingdom, in combination with post-operative MAP, in patients with resectable disease, after macroscopically complete surgical resection. MTP-PE is reported to be a nonspecific immune modulator; it is a synthetic analogue of a component of bacterial cell walls, which once incorporated into macrophages and monocytes residing in the lungs, activates these cells to become tumouricidal (Chou, Kleinerman, Krailo, *et al.*, 2009). However, the role of MTP-PE in the treatment of osteosarcoma remains unclear. Meyers *et al.* performed a Phase III study to answer two independent questions: first, if the addition of ifosfamide to standard MAP chemotherapy improved event free survival (EFS); and second, if the addition of MTP-PE improved EFS (Meyers, Schwartz, Krailo, *et al.*, 2016a). Patients under thirty years with OS were randomised at diagnosis to either regimen A^- (MAP), A^+ (MAP plus MTP-PE) or regimen B^- (MAP plus ifosfamide (MAPI)) or B^+ (MAPI plus MTP-PE). Clinically detectable metastases were not absolute exclusion criteria, but patients with metastatic disease were only enrolled at certain institutions and then analysed separately. They used a factorial 2x2 design that assumed that there were no interactions between the interventions tested, so that the four study arms could be collapsed, and aggregated together to analyse the results for each question (Meyers, Schwartz, Krailo, *et al.*, 2016a). Describing the patients with clinically undetectable disease, the percentage of necrosis at resection was only available for 264 of 559 (47.1%) patients, but although the difference between the four arms was not considered statistically significant, a greater number of patients in A^+ had less than 95% necrosis than the other arms. The five year EFS for each arm was as follows: A^-: 64%; A^+ 63%; B^- 56%; and B^+ 72%. From this analysis, the authors concluded there was an interaction between ifosfamide and MTP-PE which had not previously been recognised and so were unable to analyse the data as first anticipated, making the study under powered to analyse each of the four arms separately. From these limited results, it therefore appeared that in patients under the age of thirty years with clinically undetectable metastases, MTP-PE in combination with MAP and ifosfamide might provide some benefit (Meyers, Schwartz, Krailo, *et al.*, 2016a). Further analysis of this data by the authors lead to a second publication, which ascertained that no interaction had been observed between MTP-PE and ifosfamide, enabling the authors to analyse the study as first anticipated (Meyers, Schwartz, Krailo, *et al.*, 2016b). The six year EFS for the four individual arms at six years was reported as: A^-:

64%; A^+ 63%; B^- 58%; and B^+ 71%. Once the data was aggregated the authors reported that there was no significantly different (p = 0.91) EFS at four or six years between A^- (MAP) or B^- (MAPI) with overall EFS post chemotherapy of 61% at six years (Meyers, Schwartz, Krailo, *et al.*, 2016b). The overall reported EFS for patients treated with chemotherapy and MTP-PE was 67% at six years, which was not significantly different from chemotherapy alone 61% (p = 0.08), while overall survival at six years was 78 % with chemotherapy and MTP-PE, and 70% with chemotherapy alone (p = 0.03) (Meyers, Schwartz, Krailo, *et al.*, 2016b). The authors concluded from this study that the addition of ifosfamide to MAP did not improve outcome, but the addition of MTP-PE in patients with clinically undetectable metastases did improve overall survival (Meyers, Schwartz, Krailo, *et al.*, 2016b). The outcome for the 91 patients with clinically detectable metastases at diagnosis were reported in a further paper (Chou, Kleinerman, Krailo, *et al.*, 2009). The five year EFS for each of the regimens was as follows: A^-: 29%; A^+ 41%; B^- 23%; and B^+ 44%. No statistically significant differences between the five-year EFS between these groups were recorded. Once the data was aggregated the authors reported that there was no significantly different (p = 0.91) EFS at five years between A^- (MAP) or B^- (MAPI) with overall EFS post chemotherapy of 26% at six years. The overall reported EFS for patients treated with chemotherapy and MTP-PE was 42% at six years, which was not significantly different from chemotherapy alone (p = 0.23). A similar trend was observed, with five-year overall survival for patients who received chemotherapy of 40% and addition of MTP-PE of 53%, which was not significantly different (p=0.27). The authors concluded from this study that the addition of MTP-PE to chemotherapy did not improve outcome in patients with clinically detectable metastases (Chou, Kleinerman, Krailo, *et al.*, 2009). There are a number of limitations to this trial. Firstly, at present histological response to neo-adjuvant chemotherapy is the most robust clinical marker of outcome but concerns were raised that a greater proportion of patients in regimen A^+ had a poorer histological response. Second, the test for statistical interaction between MTP-PE and ifosfamide for disease-free survival was very close to the pre-specified threshold for interaction of 0.01 (p = 0.102), which would have invalidated the method of aggregation and analysis.

A number of unanswered questions remain but would require a further costly Phase III study sufficiently powered to answer the questions: (i) does the addition of MTP-PE to standard MAP significantly improve survival in patients randomised on the basis of histological response at resection with or without metastases; (ii) what are the effects on

survival in patients greater than 30 years; (iii) are there robust biomarkers of sensitivity to MTP-PE. A clinical trial to determine if ABCB1/P-glycoprotein over-expression can be used as a biological stratification factor for outcome of patients with localised disease undergoing treatment with either standard MAP or the addition of ifosfamide and MTP-PE is currently recruiting (NCT01459484). Another trial aiming to understand why some patients respond differently to MTP-PE alone and in combination with ifosfamide has just completed and the results are awaited (NCT02441309).

Neo-adjuvant and adjuvant chemotherapy along with resection is the conventional treatment for all histological variants of high-grade osteosarcoma. Complete surgical resection of both primary and relapsed disease (Wong, Lee, Shing, *et al.*, 2013; Kempf-Bielack, Bielack, Jürgens, *et al.*, 2005; Ferrari, Briccoli, Mercuri, *et al.*, 2003), comprising limb salvage surgery where possible (85% of children) (Grimer, 2005), is vital for cure (Bacci, Briccoli, Longhi, *et al.*, 2005). The use of radiotherapy in osteosarcoma is limited to local treatment of un-resectable disease, intra-lesional resection (DeLaney, Park, Goldberg, *et al.*, 2005) or as palliation of symptomatic metastases (Schwarz, Bruland, Cassoni, *et al.*, 2009).

1.1.3 Overview of clinical trials in OS

The objectives of Phase I clinical trials are to determine the maximum tolerated dose of the agent, toxicity profile, adverse events, pharmacokinetics and pharmacodynamics. Phase II trial objectives are to determine the efficacy of the agent by measuring response of the tumour, or a measure of survival (overall or event/progression free). Phase III trials are used to compare treatment with the novel agent with the recognised standard of care for a specific tumour type. These trials are usually randomised. Phase IV studies are used to gather further information about agents that have already been approved for use, such as quality of life metrics, longer-term safety and cost-effectiveness.

A literature search and summary of clinical trials between 1990 and 2010 enrolling patients with Ewing's sarcoma and OS was performed (van Maldegem, Bhosale, Gelderblom, *et al.*, 2012a). Of the 42 trials identified, 20 were specific for patients with OS (two phase I, 16 phase II, two phase I/II), with a total of 1114 patients enrolled, which represented only 0.2% of the world-wide potential patient recruitment (van Maldegem, Bhosale, Gelderblom, *et al.*, 2012a). From the twenty OS specific trials, 780 patients were

enrolled, 762 were evaluable with only 58 patients (8%) achieving a complete response, 21 (2.8%) a partial response, and 30 (4%) had stable disease (van Maldegem, Bhosale, Gelderblom, *et al.*, 2012a). At the time of this review, the majority of phase III trials were still chemotherapy, despite a shift towards more biologically based treatments in phases I/II (van Maldegem, Bhosale, Gelderblom, *et al.*, 2012a).

At present, 44 registered clinical trials (phase I: 15; phase Ib: two; phase I/II: seven; phase II: seventeen; phase II/II: two; phase IV: one) testing chemotherapy or biological treatments are currently actively recruiting patients with OS (Table 1). The majority of these studies are open for patients with either sarcoma in general, or solid tumours, only 12/44 (27%) are for the investigation of patients with OS alone. At present there is one phase IV trial actively recruiting patients with OS to determine if the addition of lithium carbonate to standard chemotherapy improves outcome (NCT01669369). The phase II/III studies are to first determine if MAPI chemotherapy plus MTP-PE in patients who over express ABCB1/P-glycoprotein improves outcome compared to MAP chemotherapy in patients who do not over express ABCB1/P-glycoprotein (NCT01459484), and second to answer if apatinib improves progression free survival in patients (>14 years) with relapsed and unresectable OS. Of the 44 studies, 27 are for chemotherapeutic agents, while 17 are for biological agents, which include anti-PDL1 anti-bodies (pembrolizumab, nivolumab, duralumab and avelumab), anti-GD2 antibodies (Hu14.18K322A), anti-receptor activator of nuclear factor kappa-B ligand (RANKL) antibodies (denosumab), T cells with a GD2 antibody in combination with interleukin 2, dendritic cells vaccine, activated Natural Killer cells, anti-B7-H3 antibodies (enoblituzumab), an oncolytic virus (HSV1716), anti-CTLA-4 antibodies (iIpilimumab, tremelimumab), and anti-cyclin dependent kinases 4/6 (CDK4/6) antibodies (abemaciclib).

Table 1 Actively recruiting clinical trials in patients with osteosarcoma

Trial	Phase	Treatment	Primary Aims
NCT01459484	II/III	MAP/MAPI + MTP-PE	Overall survival
NCT03063983	II	Cyclophosphamide MTX	EFS
NCT03013127	II	Pembrolizumab	PFS
NCT02718482	II	Gemcitabine and docetaxel or ifosfamide	PFS
NCT03006848	II	Avelumab	PFS
NCT01669369	IV	Lithium carbonate	PFS
NCT01987102	I/II	Leucovorin rescue	Toxicity
NCT02502786	II	Humanised anti-GD2 antibody	EFS
NCT03163381	II	Apatinib	PFS
NCT02711007	II/III	Apatinib	PFS
NCT02470091	II	Denosumab	Disease control rate
NCT02517918	Ib	Sirolimus, MTX, zoledronic acid and cyclophosphamide	Maximum tolerated dose
NCT02273583	II	Cyclophosphamide and MTX	EFS
NCT02432274	I/II	Lenvatinib, ifosfamide and etoposide	RP2D PFS
NCT02389244	II	Regorafenib	PFS
NCT02173093	I/II	IL2, GD2Bi-aATC	MTD
NCT02357810	II	Pazopanib hydrochloride and topotecan	PFS
NCT02301039	II	pembrolizumab	ORR
NCT01803152	I	Dendritic cells vaccine, imiquimod and gemcitabine	Toxicity
NCT02409576	I/II	Activated Natural Killer cells and radiotherapy	Toxicity Disease response
NCT02159443	I	Hu14.18K322A (anti GD2 monoclonal antibody)	Efficacy of antibody epitope binding
NCT02811523	I	In vivo lung perfusion of doxorubicin	Toxicity MTD
NCT02945800	II	Nab-paclitaxel and gemcitabine	PFS
NCT02013336	I	Irinotecan and cyclophosphamide	MTD
NCT02100891	II	Natural Killer cells post	DCR

[IL2: interleukin 2; GD2Bi-aATC: chimeric T cells with GD2 antibody; MTD: maximum tolerated dose; RP2D: recommended phase II dose; ORR: objective response rate; PK: pharmacokinetics; PD: pharmacodynamics; TAEST16001: TCR Affinity Enhancing Specific T cell Therapy; PFS: progression free survival; MAP: methotrexate, cisplatin, doxorubicin; MTX: methotrexate].

In addition to patient recruitment, due to the rarity of the disease, there are other challenges for clinical trials in OS. The need to acrue patients must be balanced by recruitment of a heterogeneous group of patients with OS, which imposes limitations on what conclusions can be drawn (Janeway & Gorlick, 2016). EURAMOS1 demonstrated that international collaboration is feasible, enrolling 2260 patients with OS over six years (Whelan, Bielack, Marina, et al., 2015; Bielack, Smeland, Whelan, et al., 2015). Most clinical trials use the WHO radiographic response criteria, or Response Evaluation Criteria in Solid Tumours (Eisenhauer, Therasse, Bogaerts, et al., 2009) for response to treatment, or radiological assessment of disease response. However, in localised OS, optimal assessment of tumour response is limited by calcified tumour matrix, and in metastatic OS, surgical excision where possible of pulmonary metastases is standard, resulting in minimal residual disease and possible exclusion from trials that require measurable disease for enrolment (Lagmay, Krailo, Dang, et al., 2016; van Maldegem, Bhosale, Gelderblom, et al., 2012b). Even with complete histological necrosis, radiological response to neo-adjuvant therapy is rare (Lagmay, Krailo, Dang, et al., 2016). Instead of radiological response, survival has been employed as an alternative end point. Therefore, for clinical trials to be successful in OS they must take into consideration these challenges.

1.1.4 Molecular and genomic biology of osteosarcoma

Osteosarcoma derives from primitive bone-forming mesenchymal cells and is typically composed of spindle cell lineages that produce osteoid (Gorlick, 2009). The current World Health Organisation (WHO) classification (Whelan, McTiernan, Cooper, *et al.*, 2012; Raymond, Ayala & Knuutila) describes three major subtypes of high-grade osteosarcoma: osteoblastic which comprise the majority (~60%), and approximately equal representation of fibroblastic and chondroblastic subtypes (Kempf-Bielack, Bielack, Jürgens, *et al.*, 2005; Bacci, Longhi, Fagioli, *et al.*, 2005; Janeway, Barkauskas, Krailo, *et al.*, 2012; Mirabello, Troisi & Savage, 2009). A fourth rare subtype telangectatic osteosarcoma occurs in less than 12% of patients (Angelini, Mavrogenis, Trovarelli, *et al.*, 2016). Although differences exist in response to chemotherapy between the subtypes, no overall survival differences have been demonstrated between these groups and thus, currently no stratification of therapy exists on the basis of subtype.

Limited understanding of the molecular and cellular mechanisms that influence the behaviour of osteosarcoma has potentially hindered the development of novel therapeutics. Early genetic events are thought to relate to the deletion or mutation of tumour suppressors such as Tumour Protein P53 (*TP53)* and other genetic abnormalities including deletion of Cyclin Dependent Kinase Inhibitor 2A (*CDKN2A*) and MDM2 Proto-Oncogene (*MDM2*) amplification. However, currently no molecular sub-classification of osteosarcoma exists on which stratification of therapy is based (Kansara & Thomas, 2007; Gorlick, 2009; Kuijjer, Hogendoorn & Cleton-Jansen, 2013) apart from the detection of *MDM2* amplification in low grade central and parosteal osteosarcomas, which helps classify these tumours as not requiring adjuvant therapy (Mejia-Guerrero, Quejada, Gokgoz, *et al.*, 2010). At present there are a small number of reports which correlate gene expression with clinical outcome, (PosthumaDeBoer, Witlox, Kaspers, *et al.*, 2011; Angstadt, Motsinger-Reif, Thomas, *et al.*, 2011; Man, Lu, Jaeweon, *et al.*, 2004; Sadikovic, Park, Selvarajah, *et al.*, 2013). For example expression of Thrombospondin 3 (THBS3), and Secreted Protein Acidic And Cysteine Rich (SPARC) are associated with poor outcome, whereas Secreted Phosphoprotein 1 (SPPI) expression is associated with good outcome (Dalla-Torre, Yoshimoto, Lee, *et al.*, 2006). However, these only serve to increase the limited understanding of the biology of the disease, and have not yet translated into clinical practice. Fibroblastic growth factor receptor 1 (*FGFR1*) gene amplification assessed by interphase fluorescence in situ hybridization of the tumour samples from 288 patients was reported in 18.5% of patients whose tumours responded poorly to chemotherapy, but not seen in patients whose tumours responded well (Fernanda Amary, Ye, Berisha, *et al.*, 2014). In addition, amongst the rare histological variants of osteosarcoma, *FGFR1* amplification was more frequent (Fernanda Amary, Ye, Berisha, *et al.*, 2014). A greater understanding about the role of FGFR in OS and investigation of inhibition is worthy of exploration.

Osteosarcomas are typically aneuploid (Schlabach, Luo, Solimini, *et al.*, 2008; Kansara & Thomas, 2007), with frequent extensive genomic aberrations (Kresse, Rydbeck, Skårn, *et al.*, 2012; Tarkkanen, Karhu, Kallioniemi, *et al.*, 1995). Unlike other types of sarcoma such as Ewings sarcoma, which are characterised by gene fusions of *EWS* to different members of the *ETS* transcription factor gene family (Toomey, Schiffman & Lessnick, 2010), there do not appear to be unifying genetic aberrations amongst high grade osteosarcomas. Contrary to other malignancies such as colorectal adenocarcinoma, no precursor lesions have been identified in OS (Mohseny, Hogendoorn & Cleton-Jansen,

2012). It is likely that there is extensive genetic heterogeneity both between and within high-grade osteosarcomas (Kansara & Thomas, 2007; Burrell, McGranahan, Bartek, *et al.*, 2013; Gorlick, 2009; Kuijjer, Hogendoorn & Cleton-Jansen, 2013; Behjati, Tarpey, Haase, *et al.*, 2017). This genetic heterogeneity has helped to obscure the identification of potential driver alterations involved in OS genesis.

Mutations in Retinoblastoma 1 (*RB1*), *CDKN2A* and *TP53* are the most common known recurrent mutational events in sporadic osteosarcoma (Gorlick, Anderson, Andrulis, *et al.*, 2003). The frequency of these events varies widely between reported cohorts, with some reporting that 20-70% of osteosarcomas harbour mutations of *TP53* (Gokgoz, Wunder, Mousses, *et al.*, 2001), and more recently when structural variants in the first intron were included, as many as 80% harbour a mutation (Chen, Bahrami, Pappo, *et al.*, 2014). Structural alterations of *RB1* have been reported in up to 35% of sporadic cases of osteosarcoma (Araki, Uchida, Kimura, *et al.*, 1991).

Very recently, eight out of 112 (7%) tumour OS samples that were either whole genome or exome sequenced were found to have mutations of the IGF signalling pathway (Behjati, Tarpey, Haase, *et al.*, 2017). Dependency on IGF-1R signalling and activation of IGF-1R by IGF-1 leading to stimulation of the growth of OS tumour cells both *in vitro* (Kappel, Velez-Yanguas, Hirschfeld, *et al.*, 1994) and *in vivo* (Kolb, Gorlick, Houghton, *et al.*, 2008) has already been described. Blockade of this pathway was thought to be therapeutically attractive (Kuijjer, Peterse, van den Akker, *et al.*, 2013; Fleuren, Versleijen-Jonkers, Boerman, *et al.*, 2014) with a number of IGF-1R inhibitors which entered early phase trial. However, all clinical trials in sarcoma have been closed or halted due to perceived lack of activity and no biomarker to stratify patients for therapy.

Molecular characterisation by whole exome sequencing (n = 59), whole genome sequencing (n = 13) and RNA-sequencing (n = 35) of OS tumour samples, identified alterations in the Phosphoinositide-3-Kinase, Catalytic, Alpha Polypeptide / Mechanistic Target Of Rapamycin (PI3K/mTOR) pathway in 24% of patients with OS (Perry, Kiezun, Tonzi, *et al.*, 2014). Perry *et al*. therefore hypothesised that the PI3K/mTOR pathway was a unifying vulnerability required for OS tumour proliferation, which could be exploited therapeutically; using the dual PIK3CA/mTOR inhibitors GSK2126458 and BEZ235, they demonstrated sensitivity in four OS tumour cell lines to the dual PIK3CA/mTOR inhibitors GSK2126458 and BEZ235 that was comparable with the breast cancer cell line MCF7,

known to harbour a PIK3CA p.E545K mutation, and previously established to undergo apoptosis in response to treatment with these inhibitors (Perry, Kiezun, Tonzi, *et al.*, 2014). Inhibitors of mTOR in early clinical trials have demonstrated clinical activity in OS, but not thought sufficient to be incorporated into treatment protocols (Chawla, Staddon, Baker, *et al.*, 2012; Demetri, Chawla, Ray-Coquard, *et al.*, 2013; Broto, Redondo, Valverde, *et al.*, 2015).

Chromothripsis, which describes the fragmentation of a single chromosome, which is then reassembled, was proposed as a mechanism for genetic instability in 2-3% of a diverse panel of 746 cancer cell lines (Bignell, Greenman, Davies, *et al.*, 2010), but is observed in up to 29% of OS samples affecting several chromosomes, creating hundreds of genetic rearrangements (Behjati, Tarpey, Haase, *et al.*, 2017; Stephens, Greenman, Fu, *et al.*, 2011). Kuijjer *et al*. have postulated that this process many explain the considerable complexity and heterogeneity seen within the disease and sudden onset (Kuijjer, Hogendoorn & Cleton-Jansen, 2013). Many of these genomic aberrations might not provide a growth advantage, representing instead collateral damage caused by chromothripsis (Kresse, Rydbeck, Skårn, *et al.*, 2012). A recent analysis of 37 whole genome sequences from OS tumour samples demonstrated three cytogenetic configurations of the OS genome; 11% (4/37) exhibited few or no rearrangements likely to represent an artifact due to inadequate tumour content; 30% (11/37) harboured chromothripsis on one or more chromosomes while 59% (22/37) exhibited combined chromothripsis and amplification (Behjati, Tarpey, Haase, *et al.*, 2017). Of these 22 genomes, chromothripsis amplification recurrently affected discrete genomic regions including chromosomes five, 12 and 17 postulated by the authors to represent chromosomal fragility or be the result of selection for driver events such as amplification of RPTOR Independent Companion Of MTOR Complex 2 (*RICTOR*) (4/37), Telomerase Reverse Transcriptase (*TERT*) (2/37) and disruption of *TP53* (5/37) and Neurofibromin 1 (*NF1*) (3/37) (Behjati, Tarpey, Haase, *et al.*, 2017).

Recent whole genome sequencing of 20 osteosarcoma tumour samples has also reported the presence of areas of kataegis, (hypermutation localized to small genomic regions (Alexandrov, Nik-Zainal, Wedge, *et al.*, 2013)), in approximately half of the samples, although these were not of recurrent regions of the genome, or associated with recurrently mutated genes (Chen, Bahrami, Pappo, *et al.*, 2014). This study of whole-genome sequencing of 20 osteosarcoma tumour samples and matched normal tissue,

observed that the most frequent method of mutation was by structural variation and copy number alteration, not single-nucleotide variations (SNVs), occurring in *TP53, RB1* and Alpha Thalassemia/Mental Retardation Syndrome X-Linked (*ATRX*) (Chen, Bahrami, Pappo, *et al.*, 2014). Whole genome sequencing of 37 and exome sequencing of 75 OS tumour samples confirmed recurrent genetic alterations in *TP53, RB1, CDKN2A, ATRX* and the insulin like growth factor (IGF) signalling pathway despite considerable inter-tumour heterogeneity (Behjati, Tarpey, Haase, *et al.*, 2017). Structural variations of *TP53* have only previously been reported in osteosarcoma and prostate cancers (Chen, Bahrami, Pappo, *et al.*, 2014; Berger, Lawrence, Demichelis, *et al.*, 2011). Since most *TP53* mutations are structural variants in intron 1, suggesting either a high frequency or susceptibility, Chen *et al.* postulate that the "genomic instability characterised by high rates of copy number variants and structural variants may precede *TP53* inactivation, and may be the underlying mechanism that initiates and promotes osteosarcoma" (Chen, Bahrami, Pappo, *et al.*, 2014). Others previously postulated the reverse, that mutations of the mitotic check points led to this genomic instability or at least permit cell viability in the face of genomic instability (Cahill, Lengauer, Yu, *et al.*, 1998).

Comparison of genome-wide expression profiles from tumour samples of osteoblastomas with high-grade osteosarcomas identified cell cycle regulation as the most prominently changed pathway (Cleton-Jansen, Anninga, Briaire-de Bruijn, *et al.*, 2009; Lovejoy, Li, Reisenweber, *et al.*, 2012). A recent genome-wide association study using germ-line DNA from patients with OS, and matched cancer-free controls, highlighted loci for further investigation (Savage, Mirabello, Wang, *et al.*, 2013); a locus in the Glutamate Metabotropic Receptor 4 (*GRM4*) gene at 6p21.3 which encodes the glutamate receptor metabotropic 4 which has been implicated in intracellular signalling (Savage, Mirabello, Wang, *et al.*, 2013). The GRM4 receptor is expressed in osteoblasts and osteoclasts and a possible role in involvement in cell differentiation and regulation during bone formation and resorption (Savage, Mirabello, Wang, *et al.*, 2013). The second locus is within a gene desert at 2p25.2, with some evidence that this region might affect gene expression (Savage, Mirabello, Wang, *et al.*, 2013). Kuijjer *et al*. integrated DNA copy number profiles from tumour samples with expression profiles of high-grade OS as compared to mesenchymal stem cells or osteoblasts and suggested 31 new OS driver genes by this method (Kuijjer, Rydbeck, Kresse, *et al.*, 2012); these warrant further investigation.

1.1.4.1 BRCAness phenotype and osteosarcoma

A recent publication revealed a significant proportion of OS tumours to potentially have a 'BRCAness' phenotype (Kovac, Blattmann, Ribi, *et al.*, 2015), which describes tumour cells that possess histopathological and molecular characteristics similar to tumour cells with Breast cancer 1 (*BRCA1*) or Breast cancer 2 (*BRCA2*) gene defects (Lord & Ashworth, 2016; Turner, Tutt & Ashworth, 2004). BRCA1 has a number of cellular roles, such as chromatin remodelling, transcriptional regulation, and DNA repair (Turner, Tutt & Ashworth, 2004). In contrast, BRCA2 is primarily involved in DNA recombination and repair, including interaction with RAD51, a protein with a critical role in the catalysis reaction required for homologous recombination (HR) (Turner, Tutt & Ashworth, 2004; Tarsounas, Davies & West, 2004). In the presence of DNA double strand breaks (DBSs), cells which are deficient for *BRCA1* or *BRCA2* are unable to perform DNA repair by the conservative HR, but are forced to rely on potentially mutagenic mechanisms such as NHEJ and single strand annealing (Turner, Tutt & Ashworth, 2004). BRCAness therefore describes a phenotype with an underling distinctive DNA-repair defect arising from loss of HR, due to deficiency of the BRCA pathways (Turner, Tutt & Ashworth, 2004); tumour cells with this phenotype are therefore more dependent on base excision repair, conferring sensitivity to inhibition of PARP, as the tumour cells are unable to repair the cumulative DNA damage and undergo cell death (Lord, Tutt & Ashworth, 2015; Lord & Ashworth, 2013).

The mutational spectra of whole genome sequencing from tumour samples have recently been classified according to the six base substitutions and information of the bases immediately 3' and 5' to the mutated base, resulting in 21 different 'mutational signatures' (Alexandrov, Nik-Zainal, Wedge, *et al.*, 2013). Different mutational processes have been shown to generate different combinations of mutation signatures, for example, mutation signature three, is strongly associated with tumours that harbour *BRCA1* and *BRCA2* mutations and exhibit approximately equal representation of all possible 96 mutations (Alexandrov, Nik-Zainal, Wedge, *et al.*, 2013).

Kovac *et al.* performed whole-exome sequencing on 31 treatment naive OS tumour samples (Kovac, Blattmann, Ribi, *et al.*, 2015). The single nucleotide variant (SNV) spectrum showed the majority of tumours (29/31) had C:G>T:A changes, followed by C:G>A:T and T:A>C:G changes (Kovac, Blattmann, Ribi, *et al.*, 2015). Some tumours had a mutation spectra (Signature three) associated with kataegis strongly associated

with mutations of *BRCA1* and *BRCA2* mutations within breast and pancreatic cancer types (Kovac, Blattmann, Ribi, *et al.*, 2015; Alexandrov, Nik-Zainal, Wedge, *et al.*, 2013). In addition to the previously reported driver mutations (*TP53* and *RB1*), Kovac *et al.* reported driver mutations not previously reported in OS (Ret Proto-Oncogene (*RET*), MutY DNA Glycosylase (*MUTYH*), Nuclear Mitotic Apparatus Protein 1 (*NUMA1*), Fanconi Anaemia Complementation Group (*FANCA*), Breast cancer 2 (*BRCA2*) and Ataxia-Telangiectasia Mutated (*ATM*)) that were either truncating / spice mutations or protein coding mutations present in two or more tumours (Kovac, Blattmann, Ribi, *et al.*, 2015). Somatic copy-number alterations (SCNA) of single-nucleotide polymorphism arrays identified large-scale genomic instability and LOH signatures similar to that of breast and ovarian cancers with BRCA1 inactivation using this methodology in 91% and BRCA2 inactivation in 78% of the OS tumour samples (Kovac, Blattmann, Ribi, *et al.*, 2015). SCNA mutations were also reported in *BRCA1* (26%) and other members of the HR pathway such as BRCA1 Associated Protein 1 (*BAP1*) (38%), Phosphatase And Tensin Homolog (*PTEN*) (50%) and Partner And Localizer Of BRCA2 (*PALB2*) (43%), in the absence of identification of mutations by exome sequencing (Kovac, Blattmann, Ribi, *et al.*, 2015). Kovac *et al.* reported that of the 31 tumours samples profiled, a typical OS sample carried 17 SCNA mutations in *BRCA* genes and their core binding partners (Kovac, Blattmann, Ribi, *et al.*, 2015). To further validate the observed copy number changes, whole genome copy number profiles of 123 independent OS tumour samples were used; 85% had copy number changes with hallmarks of *BRCA1/2* mutated breast cancer (Nik-Zainal, Alexandrov, Wedge, *et al.*, 2012; Alexandrov, Nik-Zainal, Wedge, *et al.*, 2013; Kovac, Blattmann, Ribi, *et al.*, 2015).

Mutations of genes known to be involved in HR such as *PALB2,* Checkpoint Kinase 2 (*CHEK2*), *PTEN* and *ATM* can have functionally equivalent results to *BRCA* deficiency, resulting in chromosomal instability (Kovac, Blattmann, Ribi, *et al.*, 2015). The notion of 'BRCAness' in OS has been offered as an explanation of how the vulnerability to chromosomal breakage may be sustained in the absence of *TP53* mutations or in parallel, not as a replacement of the existing view of OS as a monoclonal expansion of one initial *TP53* mutant cell (Kovac, Blattmann, Ribi, *et al.*, 2015).

Kovac *et al.* postulated that a BRCA-like phenotype is a unifying trait of OS, independent of driver mutation, with varying degrees of BRCAness acquired throughout polyclonal OS evolution (Kovac, Blattmann, Ribi, *et al.*, 2015). They therefore postulated that a BRCA-

like phenotype could therefore represent a potential therapeutic opportunity in OS (Kovac, Blattmann, Ribi, *et al.*, 2015; Engert, Kovac, Baumhoer, *et al.*, 2016). Four (MG63, ZK58, SAOS2, and HOSMMNG) OS tumour cell lines known to have disruptive gains in *PTEN* and *FANCD2* and / or losses of *ATM, BAP1,* BRCA1 Associated RING Domain 1 (*BARD1*)*, FANCA* or *CHK2* and therefore functionally analogous to *BRCA* mutations, were observed to be susceptible to PARP inhibition by talazoparib (BMN-673 (Engert, Kovac, Baumhoer, *et al.*, 2016).

Whole genome sequencing was recently performed on thirty-seven OS tumour samples and suggests only one, a radiation-induced OS, harboured evidence of HR deficiency using HRdetect methodology (mutational signature three) (Behjati, Tarpey, Haase, *et al.*, 2017; Davies, Glodzik, Morganella, *et al.*, 2017). From this series, nine different mutational signatures were represented, the most prevalent were signatures five (age-related mutational process), and eight (unknown origin) (Behjati, Tarpey, Haase, *et al.*, 2017). It was determined from that analysis that detection of the BRCAness molecular phenotype should only be performed on whole genome sequencing, not the whole-exome sequencing performed by Kovac *et al.* (Kovac, Blattmann, Ribi, *et al.*, 2015). In addition, the doses of talazoparib utilised in the above analysis by Engert *et al.* were noted to be higher than those used in similar studies in other malignancies.

1.1.4.2 Familial pre-disposition syndromes in osteosarcoma

While the majority of OS are sporadic, a minority are radiation-induced (Hawkins, Wilson, Burton, *et al.*, 1996), and there is a cluster of familial syndromes that predispose to the development of OS: Li-Fraumeni is an autosomal dominant disorder associated with a germ-line mutation of *TP53*; Familial Retinoblastoma is associated with germ-line mutation of *RB1*, a gate-keeper tumour suppressor, involved in the cell cycle checkpoint; the DNA helicase disorders include Werner Syndrome, Bloom Syndrome and Rothmund-Thomson Syndrome (RTS) and are associated with germ-line mutations of RecQ Like Helicases 2, 3 and 4 (*RECQL2*, *RECQL3* and *RECQL4*) respectively (Vogelstein, Papadopoulos, Velculescu, *et al.*, 2013; Kansara & Thomas, 2007); Pagetic bone diseases may occur as an inherited disorder, and are associated with mutations of Sequestosome 1 (*SQSTM1*) and Mitogen-Activated Protein Kinase 8 (*MAPK8*) in the (Receptor Activator of Nuclear Factor κ B) RANK signalling pathway, and TNF Receptor Superfamily Member 11a (*LOH18CR1*) in Interleukin1/Tumour necrosis factor (IL-1/TNF)

signalling (Kansara & Thomas, 2007). *RECQL4* mutations have not been observed in sporadic OS. Recently in 1120 oncology patients of less than 20 years of age, the whole genomes (n = 595), whole exomes (n = 456) or both (n = 69) were sequenced (Zhang, Walsh, Wu, *et al.*, 2015). The DNA sequences of 565 genes were analysed for the presence of germline mutations. Probably pathogenic or pathogenic mutations were identified in 8.5 % of cancer patients compared to 1.1% in the 1000 Genomes project (Ishida, Kitagawa, Hatakeyama, *et al.*, 2000). The most commonly mutated genes in the affected patients were *TP53* (n = 50), Adenomatous Polyposis Coli (*APC*) (in 6), *BRCA2* (n = 6), Neurofibromin 1 (*NF1*) (n = 4), PMS1 Homolog 2 Mismatch Repair System Component (*PMS2*) (n = 4), *RB1* (n = 3), and Runt Related Transcription Factor 1 (*RUNX1*) (n = 3) (Zhang, Walsh, Wu, *et al.*, 2015). Fifty-eight patients with a predisposing mutation had available information on family history, and of these 40% had a family history of cancer (Zhang, Walsh, Wu, *et al.*, 2015). The study concluded that family history did not predict the presence of an underlying predisposition syndrome in most patients (Zhang, Walsh, Wu, *et al.*, 2015).

Combinations of mutations in the p53 and RB pathways have been demonstrated in the majority of sporadic OS (Wang, Luo & Kelley, 2004; Wang, Levy, Lewis, *et al.*, 2001; Miller, Aslo, Tsay, *et al.*, 1990; Toguchida, Yamaguchi, Ritchie, *et al.*, 1992; Duan, Zhang, Choy, *et al.*, 2012; Marina, Gebhardt, Teot, *et al.*, 2004), however, they are rare (~3%) in germline DNA of these patients (Yamaguchi, Honda, Satow, *et al.*, 2009; Marina, Gebhardt, Teot, *et al.*, 2004). In contrast, germ-line *TP53* mutations, particularly of the core DNA binding domain are found in the majority (>50%) (Birch, Blair, Kelsey, *et al.*, 1998) of cases with Li-Fraumeni cancer predisposition syndrome (Duan, Jia, Koshkina, *et al.*, 2006; Li & Fraumeni, 1969). Despite being the second most frequent malignancy in Li-Fraumeni Syndrome, OS only has a 12% incidence in these patients (Siddiqui, Onel, Facio, *et al.*, 2005), suggesting a role for other driver mutations or epigenetic drivers in addition to *TP53*. Structural rearrangements of *RB1* have been observed in 30% of primary OS tumours, with point mutations in a further 10%, and loss of heterozygosity in 60% (Kansara & Thomas, 2007).

1.1.4.3 The role of RB1 in osteosarcoma

As discussed above, RB1 is recurrently altered in sporadic OS (Kansara & Thomas, 2007) and long-term survivors of retinoblastoma with germline mutations of *RB1* have a

twenty-fold increased risk of developing a secondary malignancy (including OS) and death (Kleinerman, Schonfeld & Tucker, 2012). RB1 plays a central role as a negative regulator of cell proliferation, and is frequently mutated in a number of different tumour types (Knudsen & Wang, 2010). Active RB1 binds the E2F transcription factors, thereby repressing expression of cell cycle genes, and preventing cell cyling beyond the G1 restriction point (Mittnacht, 2005; Knudsen & Wang, 2010; Dyson, 2016). Phosphorylation of RB1 leads to inactivation, dissociation of the E2F transcription factors with resultant expression of cell cycle genes needed for proliferation and progression past the G1 restriction point. Phosphorylation of RB1 is controlled by Cyclin D1 and E, which are regulated by the cyclin dependent kinases (Mittnacht, 2005; Dyson, 2016; Knudsen & Wang, 2010).

OS are characterised by a high degree of genomic instability but also frequent activation of the alternative lengthening of telomeres pathway of telomere maintenance, associated with karyotypic instability (Gonzalez-Vasconcellos, Anastasov, Sanli-Bonazzi, *et al.*, 2013). In addition to cell proliferation via control of the G1 restriction point, there is some evidence that heterozygous loss of Rb1 in mouse models is associated with spontaneous genomic instability and sustained telomeric attrition and in cells of the osteoblastic lineage (Gonzalez-Vasconcellos, Anastasov, Sanli-Bonazzi, *et al.*, 2013).

Osteosarcomas are characterized by the frequent activation of the alternative lengthening of telomeres pathway of telo- mere maintenance (10) and a high degree of genomic insta- bility. As the loss of telomeric DNA may lead to karyotypic instability (11), and as RB1 haploinsufficiency has been asso- ciated with increased genomic instability in premalignant retinoma cells (12), we postulate that the Rb1 gene may be the common denominator-linking susceptibility, genomic instability, and telomeric integrity. We report here that the loss of a single copy of the Rb1 gene is sufficient to cause sustained telomeric attrition and spontaneous genomic insta- bility in cells of the osteoblastic lineage. The extent of the genomic instability is increased after exposure to radiation.

A recent meta-analysis found that loss of *RB1* function results in a 1.62 fold increase in the mortality rate for patients with OS, a significant increase in metastasis (OR 3.95), and a significant reduction in the histological response to chemotherapy (OR 0.35) (Ren & Gu, 2015), with suggestions that RB1 status could be used as an additional prognostic

marker. However, at present it is unknown if *RB1* status predicts response to chemotherapy or outcome in OS.

1.1.4.3.1 DYRK1A

One of the most profound candidate genetic dependencies associated with *RB1* deficiency was DYRK1A. The DYRK (dual-specificity tyrosine-regulated kinase) family represents a highly conserved subfamily of seven protein kinases (DYRK1A, DYRK1B, DYRK1C, DYRK2, DYRK3, DYRK4A, and DYRK4B), that auto-phosphorylate a conserved tyrosine residue in their own activation loop during translation, but phosphorylate their substrates at serine or threonine residues (Fernández-Martínez, Zahonero & Sánchez-Gómez, 2015; Himpel, Panzer, Eirmbter, *et al.*, 2001). Members of this family have been identified as cell cycle regulators in a range of organisms (Becker, 2012). The *DYRK1A* gene is the only member of the DYRK family to be located on chromosome 21 in the Down Syndrome critical region and is ubiquitously expressed in mammalian tissues (Guimera, Casas, Estivill, *et al.*, 1999). Absence of *DRYK1A* in mice has been shown to be lethal at the embryonic stage, while heterozygous animals are viable but have a persistently reduced size (Fernández-Martínez, Zahonero & Sánchez-Gómez, 2015). Over expression and reduced expression of DYRK1A lead to deregulation of neurogenesis and resultant neuro-developmental alterations in transgenic models in mice, chicken and *Drosophila* (Tejedor & Hämmerle, 2011). Furthermore, truncation of the protein leads to microcephaly in humans (Møller, Kübart, Hoeltzenbein, *et al.*, 2008), while 1.5 fold overexpression in Trisomy 21, is thought to play a role in the altered brain development associated with the syndrome (Dowjat, Adayev, Kuchna, *et al.*, 2007; Tejedor & Hämmerle, 2011).

DYRK1A and *DYRK1B* have been described as paralogous genes (Aranda, Laguna & la Luna, 2011), however, differing functions have been reported. Litovchick *et al.* demonstrated *in vitro* phosphorylation of LIN52 DREAM MuvB Core Complex Component (LIN52) by DYRK1B, but could not replicate this observation *in vivo* (Litovchick, Florens, Swanson, *et al.*, 2011). Phosphorylation of LIN52, appears to be one of the key roles of DYRK1A, controlling formation of the DREAM complex (Litovchick, Florens, Swanson, *et al.*, 2011; Sadasivam & Decaprio, 2013).

1.1.5 Murine models of osteosarcoma

Preclinical models of disease are valuable to investigate biology. Tumour cell lines have pragmatic utility, but are limited by lack of three-dimensional structure, presence of tumour-associated osteoid, vascularisation and interaction with the immune response. To mitigate some of these challenges, mouse models can be employed. Previous murine models of osteosarcoma created by radiation or carcinogens have been limited by low disease penetrance of an unpredictable nature. Furthermore, the majority of osteosarcoma formation in humans is sporadic, meaning that comparison with these models is potentially less valuable. Germ-line homozygous deletion of *RB1* is fatal (Jones, 2011), while mice germ-line heterozygous for *RB1* develop neither OS nor retinoblastoma (Walkley, Qudsi, Sankaran, *et al.*, 2008), despite being associated with a 500-fold increased risk of formation of OS in humans (Clarke, Maandag, van Roon, *et al.*, 1992). Recent studies have demonstrated inactivation of the p53 pathway as the driving genetic alteration required to generate experimental OS, and that concurrent deletion of *RB1* potentiates OS formation, although deletion of *RB1* is insufficient to initiate tumour formation alone (Mutsaers, Ng, Baker, *et al.*, 2013; Kansara & Thomas, 2007). Cre-lox homozygous silencing of germ-line *RB1* created a mouse model with radiation susceptibility to osteosarcoma which is also seen in patients with germ-line *RB1* mutations (Gonzalez-Vasconcellos, Anastasov, Sanli-Bonazzi, *et al.*, 2013).

Mouse models of Li-Fraumeni syndrome (LFS) have been established by engineering structural or contact point mutations of *TP53* common to patients with LFS, into endogenous *TP53*, which demonstrated dominant negative effects over the wildtype allele (Olive, Tuveson, Ruhe, *et al.*, 2004). One of these models was shown to induce the formation of twice as many osteosarcomas, compared to a $p53^{+/-}$ model (Olive, Tuveson, Ruhe, *et al.*, 2004). Tractable genetically defined murine models of OS based on the genetics of human disease have only recently been established, and are thought to be more representative of sporadic disease (Mutsaers, Ng, Baker, *et al.*, 2013). Cre-Lox conditional silencing technology has been used to tissue restrict inactivation of *RB1* and *Tp53* in osteoblastic lineage in mice following Cre expression, which have a high penetrance of development of predominantly poorly differentiated/fibroblastic OS (Walkley, Qudsi, Sankaran, *et al.*, 2008; Berman, Calo, Landman, *et al.*, 2008). These models reproduce some of the key features of human osteosarcoma including comparable gene expression signatures, cytogenetic complexity, histology and metastiatic behaviour providing valueable insights into the disease (Walkley, Qudsi,

Sankaran, *et al.*, 2008). For example, these models have added further evidence that mutation of Rb alone is insufficient to act as an initiating event of OS formation, but instead likely acts as a potentiator (Walkley, Qudsi, Sankaran, *et al.*, 2008).

Mutsears *et al.* created a murine model that is highly representative of osteoblastic OS, by *in vivo* lineage restricted shRNA technology to deliver osteoblast specific silencing of *Tp53* and concomitant *Rb1* (Mutsaers, Ng, Baker, *et al.*, 2013). These tumours frequently develop in the long bones, demonstrating a homogenous osteoblastic OS phenotype, and are highly metastatic to the lungs (Mutsaers, Ng, Baker, *et al.*, 2013). Using comparative genomic techniques, these offer a new avenue for understanding the driving molecular events of OS.

Orthotopic mouse models created by human xenograft transplantation into nude mice are limited to cells that grow in culture, with potential transformation from original tumour biology and thus potential loss of microenvironment (Mills, Matos, Charytonowicz, *et al.*, 2009). Murine models of colonising and non-colonising OS have been created by orthotopic intra-tibial injection of the human OS cell line HOS and its derivatives 143b (virally transformed using a *K-Ras* oncogene (Rhim, Park, Arnstein, *et al.*, 1975)) and HOSMNNG (chemically transformed by N-methyl-N-nitro-N-nitrosoguanidine (Rhim, Park, Arnstein, *et al.*, 1975)), which demonstrated that HOS was tumorigenic, but non-colonising to secondary sites, while 143b and HOSMNNG were both tumorigenic and colonised the lungs (Luu, Kang, Park, *et al.*, 2005; Mohseny, Machado, Cai, *et al.*, 2011). Furthermore, LM7-J99 was developed by multiple *in vitro* selection of SAOS2 cells in nude mice with pulmonary metastases (Jia, Worth & Kleinerman, 1999). Since these parental lines and their derivates are genetically similar, for example HOS, 143b and HOSMNNG all possess an identical *TP53* mutation, additional events must be needed for metastatic potential (Mohseny, Machado, Cai, *et al.*, 2011). Of interest, no association with patient outcome or metastasis formation has been found with *TP53* status (Wunder, Gokgoz, Parkes, *et al.*, 2005) which suggests additional genetic events are required for metastatic spread other than loss/gain of function of *TP53*. These models provide feasible models for investigation of both progression and metastases in osteosarcoma.

Patient derived xenograft (PDX) mouse models may help to conserve more of the molecular characteristics of the tumour sample, but still lack the interactions with tumour microenvironment (Goodspeed, Heiser, Gray, *et al.*, 2016). As yet, this methodology is

nascent in OS, and requires further investigation by comparison of molecular differences between OS PDX models and the parental tumour samples.

1.2 RATIONALE FOR PhD / OVERALL RESEARCH APPROACH

1.2.1 Synthetic lethality and oncogenic addiction

The reliance of a tumour cell on an oncogene is termed oncogenic addiction (Weinstein & Joe, 2008). This concept is seen in chronic myeloid leukaemia, where the translocation of chromosome 9:22 causes constitutive activation of the *BCR-ABL* fusion gene (Konopka, Watanabe & Witte, 1984), which can be exploited by the use of inhibitors of Proto-Oncogene 1 Non-Receptor Tyrosine Kinase (ABL), such as imatinib (Druker, Talpaz, Resta, *et al.*, 2001).

The concept of synthetic lethality, where loss of function of gene A or B does not alter the fitness of the cell, but the combination of loss of function of both A and B is lethal, is well established (Ashworth, Lord & Reis-Filho, 2011; Lord, Tutt & Ashworth, 2015). Furthermore, synthetic lethalities that are relatively unaffected by changes in additional genes are termed 'hard', whereas those that can be readily rescued by alterations in other genes are termed 'soft' (Ashworth, Lord & Reis-Filho, 2011). This concept of synthetic lethality has been exploited by the use of (Poly ADP-ribose) polymerase (PARP) inhibitors in tumour cells harbouring *BRCA1* or *BRCA2* mutations derived from a number of tumour types and is an example of a 'hard' synthetic lethality (Bryant, Schultz, Thomas, *et al.*, 2005; Farmer, McCabe, Lord, *et al.*, 2005). Subsequent clinical trials using PARP inhibitors have validated the concept in patients with durable antitumor activity being demonstrated in some *BRCA* mutation carriers (Fong, Boss, Yap, *et al.*, 2009; Tutt, Robson, Garber, *et al.*, 2010). Genetic interactions involving *RAS* such as Tank Binding Kinase 1 (*TBK1*) and Serine/Threonine Kinase 33 (*STK33*)(Ashworth, Lord & Reis-Filho, 2011; Barbie, Tamayo, Boehm, *et al.*, 2009), have been shown to be more susceptible to changes in genetic background, cell type and context, and are therefore examples of 'soft' synthetic lethalities.

One approach to systematically identifying oncogene addiction and synthetic lethality effects has been to use high-throughput small interfering ribonucleic acid (siRNA) viability profiling. For example Brough *et al.* defined in detail the genetic dependencies for a set of

pharmacologically tractable genes in a panel of 20 breast tumour cell line models, using a library of siRNA targeting the kinome (Brough, Frankum, Sims, *et al.*, 2011). Each cell line was characterised by RNA interference (RNAi) targeting 720 genes. Cell viability was estimated five days later and this data was used to calculate a cell inhibitory Z score for each gene in each cell line. Each model was then classified according to mutations in well-established driver genes, for example the identification of two cohorts Phosphatidylinositol-4,5-Bisphosphate 3-Kinase Catalytic Subunit Alpha (*PIK3CA*) mutant and *PIK3CA* wildtype. Using the RNAi data they were able to identify siRNA that selectively targeted cell lines with *PIK3CA* mutations but not wildtype, by the use of statistical methods such as the median difference permutation test and Student's t test. By combining the RNAi analysis with gene expression, gene mutation and genomic analysis, they were able to reaffirm the impact of Peptidase Inhibitor 3 (PI3) kinase and Erb-B2 Receptor Tyrosine Kinase 2 (ERBB2) signalling in breast cancer, but also to identify essential determinants of specific breast cancer subtypes, which are potential novel therapeutic targets (Brough, Frankum, Sims, *et al.*, 2011). This approach has been used to comprehensively detail genetic dependencies for a number of other tissue types in the Lord / Ashworth laboratory, including cancer cell lines derived from the pancreas, ovary, brain and gastrointestinal tract. This methodology was utilised as a framework for identifying genetic dependencies in osteosarcoma (Figure 2).

The Lord / Ashworth group have now screened a total of 99 cell lines derived from 10 tissue types, which provides a valuable resource for comparison with data generated from screening the osteosarcoma cell lines. A number of candidate targets generated from these screens have been published (Brough, Frankum, Sims, *et al.*, 2011; Campbell, Ryan, Brough, *et al.*, 2016). Optimisation and screening methods are well established. One of the most challenging aspects of such screens is validation of results due to the expected high level of false positive results seen with any high-throughput screening methodology. Methods used by the group to improve validation include deconvolution using siRNA, targeted chemical inhibition where possible, and genome editing by use of clustered regularly interspaced short palindromic repeats (CRISPR) methodology (Mali, Yang, Esvelt, *et al.*, 2013).

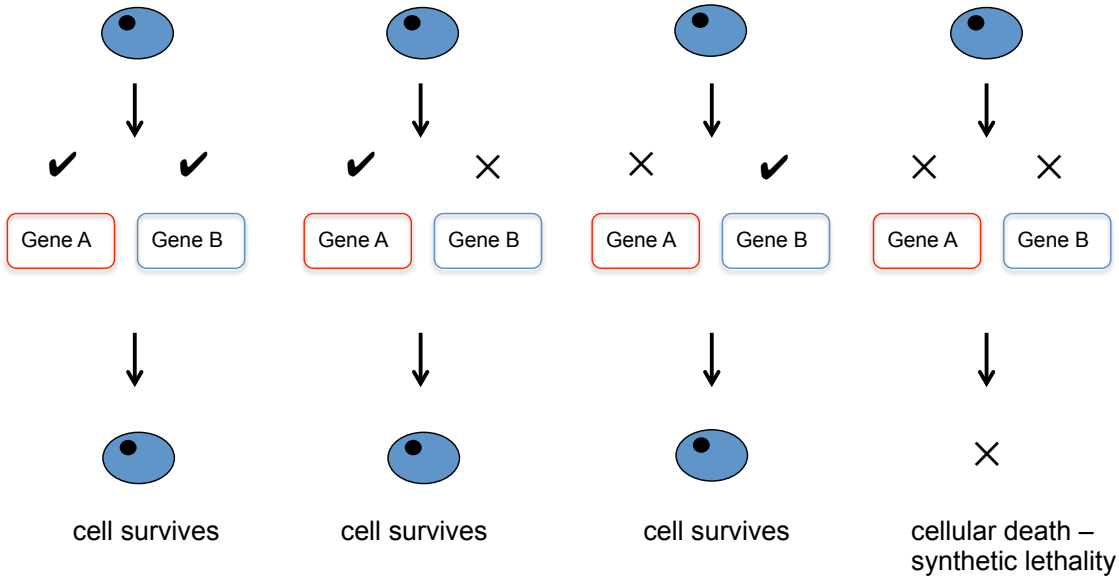

Figure 1 Schematic of synthetic lethality.

The cellular inhibition or dysfunction of either gene A or gene B is compensated by the action of the remaining gene. However, cellular inhibition or dysfunction of both genes A and B results in synthetic lethality and cellular death.

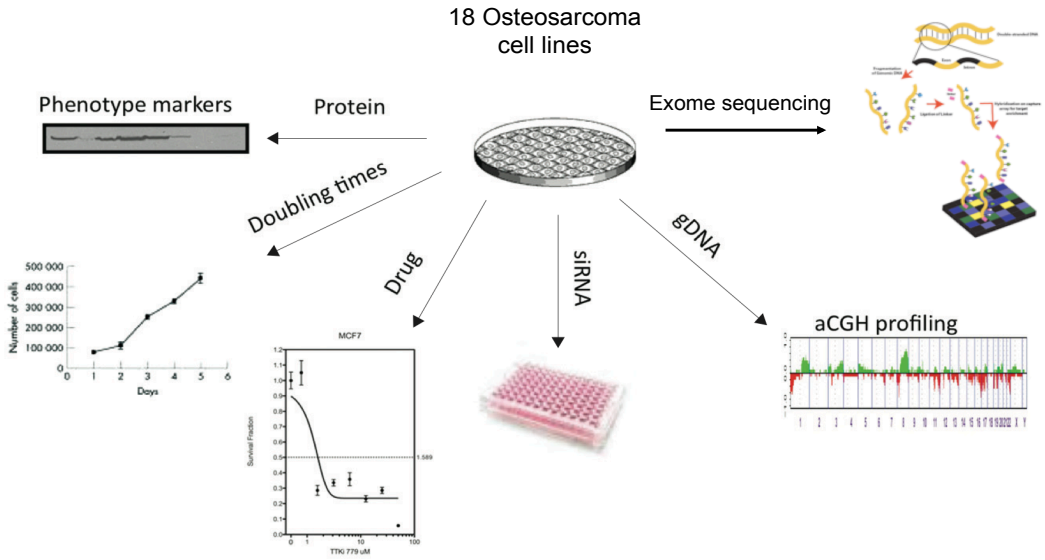

Figure 2: Summary of methodology.

A panel of 18 osteosarcoma tumour cell lines was used to investigate genetic vulnerabilities and drug dependencies for a set of pharmacologically tractable genes. Molecular characterisation of the tumour cell lines was performed by exome sequencing, transcriptome profiling, protein expression by western blotting, and protein abundance by mass spectrometry to enable identification of genetic vulnerabilities and drug dependencies associated with recurrent driver alterations. This data set was integrated with RNAi and drug screens. The Wellcome Trust Sanger Institute and the Tumour Profiling Unit at the ICR performed exome sequencing of the tumour cell lines, while copy number profiling and transcriptome data was obtained from the publically available Catalogue of somatic mutations in cancer (COSMIC http://cancer.sanger.ac.uk/cancergenome/projects/cosmic/) and Cancer Cell Line Encyclopaedia (CCLE www.broadinstitute.org/ccle) data bases. Adapted from Brough *et al.* (Brough, Frankum, Sims, *et al.*, 2011).

1.2.2 RNA interference

Tumour cells commonly exhibit between 10^3 and 10^5 genetic changes when compared to germline DNA, but theoretical estimates have suggested that it is likely fewer than 10 are critical 'drivers' of tumour formation and its survival (Schlabach, Luo, Solimini, *et al.*, 2008), with the remaining 'passenger' mutations conferring no selective growth advantage (Vogelstein, Papadopoulos, Velculescu, *et al.*, 2013). RNAi enables post-transcriptional gene silencing and has been performed using either small interfering RNA (siRNA) or small hairpin RNA (shRNA) (Willingham, Deveraux, Hampton, *et al.*, 2004; Lord, Martin & Ashworth, 2009; Brough, Frankum, Sims, *et al.*, 2011; Iorns, Lord, Turner, *et al.*, 2007) to identify novel genes involved in biological processes. The ability to modulate expression artificially of a single target gene enables dissection of the biological processes of the cell and identification of synthetic lethal relationships (Iorns, Lord, Turner, *et al.*, 2007). Identification of genetic dependencies, also termed 'addiction', by this method, distinguishes these critical driver mutations from passenger mutations. RNAi screening has already enabled the identification of genetic dependencies in cancer cells derived from a range of tissue types (Brough, Frankum, Sims, *et al.*, 2011; Schlabach, Luo, Solimini, *et al.*, 2008; Iorns, Lord, Grigoriadis, *et al.*, 2009; Arora, Gonzales, Hagelstrom, *et al.*, 2010). Both methodologies have advantages and disadvantages which are summarised by Lord *et al.* (Lord, Martin & Ashworth, 2009). One of the major limitations of using siRNA, is off-target effects caused by degradation of siRNAs that have only partial complementarity by acting as microRNAs (miRNAs) (Doench, Petersen & Sharp, 2003), reinforcing the need for robust validation.

At present, RNAi has only been applied to a limited number of models of osteosarcoma. Apurinic/Apyrimidinic Endodeoxyribonuclease 1 (*APE1*) silencing by siRNA was shown to enhance the sensitivity of osteosarcoma to DNA damaging agents in a single cell line (HOS) (Wang, Luo & Kelley, 2004). Polo Like Kinase 1 (*PLK1*) was initially identified as a potential therapeutic target in a function genomic screen (Yamaguchi, Honda, Satow, *et al.*, 2009; Duan, Ji, Weinstein, *et al.*, 2010), but has since been shown to be ubiquitously fatal amongst many tumour types and is now commonly used as a positive control for RNAi silencing (Brough, Frankum, Sims, *et al.*, 2011). An siRNA screen of the kinome in a single cell line (KHOS) demonstrated Cyclin Dependent Kinase 11 (*CDK11*) has a role in cell survival, validated by immunohistochemistry of 57 tumour samples and xenograft mouse model (Duan, Zhang, Choy, *et al.*, 2012). In two cell lines (KHOS and U2OS), Rho

Associated Coiled-Coil Containing Protein Kinase 1 (*ROCK1*) (Liu, Choy, Hornicek, *et al.*, 2011) and GLI Family Zinc Finger 2 (*GLI-2*) were demonstrated as having a role in cell survival by shRNA silencing. This was validated again by immunohistochemistry (approximately 50 tumour samples). siRNA silencing in MG63, HOSMNNG and SAOS2 demonstrated that Y-Box Binding Protein 1 (*YBX-1*) has a role in proliferation, which was validated by immunohistochemistry of 40 tumour samples (Fujiwara-Okada, Matsumoto, Fukushi, *et al.*, 2013). In the mouse (cell line K7M2), *Erbb3* has been shown to play a role in survival and migration by shRNA screening (Jullien, Dieudonné, Habel, *et al.*, 2013). These RNAi screens have been limited by inclusion of only a small number of cell lines and mouse models, with limited clinical correlation and small number of genes.

RNA interference (RNAi) screening technology enables dissection of biological processes and disease-related phenotypes by silencing specific genes, resulting in the selective death of cells that are 'addicted' to these genes (Iorns, Lord, Turner, *et al.*, 2007). Deregulation of genes that result in this 'addiction' are tractable drug targets; kinases appear particularly important in cancer survival, demonstrated by successful development of therapeutics against deregulated epidermal growth factor receptor, B-Raf Proto-Oncogene Serine/Threonine Kinase (*BRAF*) and others (Zhang, Yang & Gray, 2009). To date, there are no published studies that have undertaken a comprehensive genetic screening approach to generate a framework of genetic dependency profiles of this disease (Duan, Ji, Weinstein, *et al.*, 2010; Yamaguchi, Honda, Satow, *et al.*, 2009; Zhang, Yang & Gray, 2009).

1.3 SUMMARY

Osteosarcoma represents a malignancy with significant unmet clinical need. Despite increased understanding of the molecular landscape of OS, this has not yet translated into any specific therapies. Although tumour cell models of OS exist, to date a systematic analysis of genetic dependencies in these models has not been performed. Identification of such dependencies may in turn identify novel targets in OS.

Recent analyses of clinical samples have determined the mutation spectrum of osteosarcoma to exhibit a significant amount of inter-tumoural heterogeneity (Alexandrov, Nik-Zainal, Wedge, *et al.*, 2013; Chen, Bahrami, Pappo, *et al.*, 2014; Behjati, Tarpey, Haase, *et al.*, 2017), however, mutation of *TP53*, *RB1* and *CDKN2A* are recurrent. This

raises the possibility that targeting *RB1* deficiency might be one approach to developing novel therapies for OS, forming the basis of this thesis.

1.4 AIMS

The aim of this project was to identify potential novel therapeutic targets in OS that could be translated into clinical use, by the following objectives: (i) identification of genetic dependencies specific to OS via genetic perturbation screens in OS tumour cell lines, (ii) identification of genetic dependencies specific to recurrent known mutations in OS such as *RB1*, (iii) identification of potential novel therapeutic drug targets in OS, (iv) validation of potential genetic dependencies and drug targets.

To systematically identify genetic dependencies in OS, a disease that is known to be genetically heterogeneous, as large a panel as possible of well-characterised OS cell lines was compiled, totalling 18 different lines to reflect the genetic and histopathological diversity (five osteoblastic; five fibroblastic; two chondroblastic; one osteoblastic/telangectatic; three epithelial; one mixed and two unknown). These cell lines exhibit the recurrent tumour suppressor gene mutations seen in OS, described in Chapter 3, and have been demonstrated to be representative of the clinical disease, thus providing useful clinically relevant models for investigation of genetic dependency analysis.

With the aim of identification of genetic and drug dependencies specific to *RB1* dependency, in the absence of an available isogenic model of *RB1* deficiency in OS, two stable isogenic models were generated using CRISPR-Cas9 methodology. The generation and characterisation of these models is described in Chapter 4, together with discussion of the advantages and disadvantages of use of both an isogenic model and a diverse panel of tumour cell lines.

To characterise the genetic and drug dependencies of osteosarcoma, a relatively unbiased approach was undertaken using parallel high-throughput RNAi and chemical screening. Comparison of data generated from screening the OS tumour cell lines was possible with a diverse panel of 99 non-osteosarcoma tumour cell lines, which provided context for both scale of effects observed and OS specific dependencies. Chapter 5 describes the use of siRNA screens using a library that targeted the kinome, tumour

suppressor genes and the Cancer Gene Census thought to be the most tractable targets within the genome. Identification of genes which cause significant loss of viability in some tumour cell lines, but not all were identified as thought more likely to identify genes representing tumour-specific dependencies and potential candidate therapeutic targets.

Identification of genetic dependencies associated with specific driver mutations, in particular associated with deficiency of *RB1*, known to be recurrent in up to 30% of OS tumours (Araki, Uchida, Kimura, *et al.*, 1991) were deemed worthy of investigation. Identification of genetic dependencies associated with *RB1* deficiency in OS using both the panel of 18 OS tumour cell lines and isogenic models are described in Chapter 6. An association between *RB1* deficiency and a genetic dependency with DYRK1A was identified, and experiments are described with the aim of investigation of the mechanism of this dependency.

In the absence of stratification of drugs for the treatment of OS at present, a focused high-throughput cell based drug screen using both the OS tumour cell line panel and *RB1* deficient isogenic models with the aim of identification of potential novel therapeutic targets was performed and observations described in Chapter 7. Given the recent interest in the potential BRCAness of OS, investigation of the relative sensitivity of the OS tumour cell line panel in comparison to *BRCA1/2* deficient models, known to exhibit sensitivity to PARP inhibitors in the clinic was performed to determine any potential therapeutic potential in OS.

This thesis describes (i) characterisation of osteosarcoma cell line models, (ii) screening with high-throughput cell based RNAi libraries to characterise the candidate genetic dependencies of OS, (iii) more specifically *RB1* synthetic lethalities, (iv) high-throughput cell based drug screens to identify potential therapeutics for OS, and (v) PARP inhibitor sensitivity in OS and identification of an isogenic model for ‘BRCAness’ of osteosarcoma. A flow chart describes the data presented in each Chapter (Figure 3).

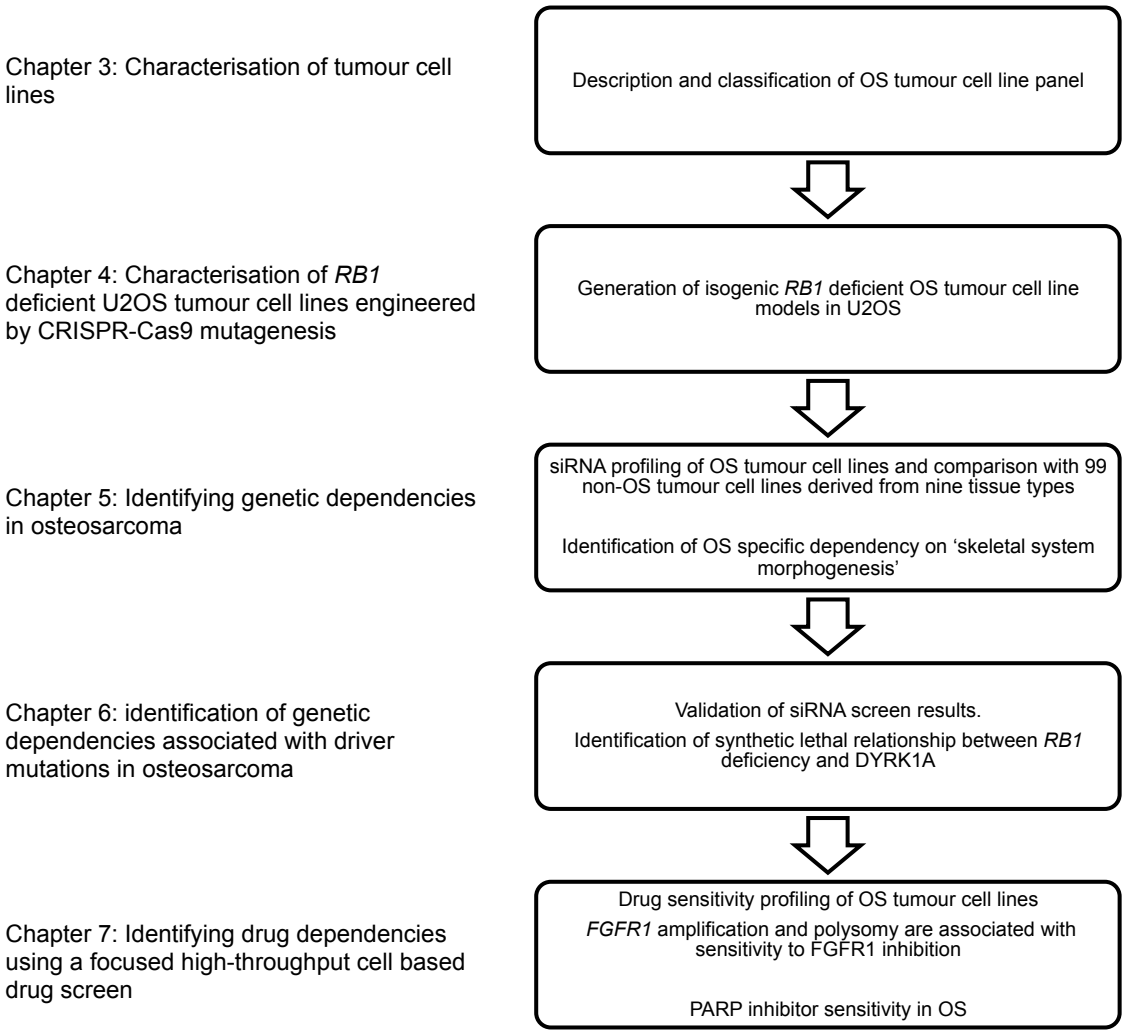

Figure 3 Summary of data presented in this thesis.

Schematic illustration of the work presented in each chapter of this thesis, including approach and findings.

[OS: osteosarcoma]

2 Materials and Methods

2.1 REAGENTS

2.1.1 General chemicals and solutions

All chemicals were purchased from Sigma unless otherwise stated.

PBS: 137nM NaCl, 2mM KCL, 8mM Na_2HPO, 1.5mM KH_2PO_4 in H_2O. pH adjusted to 7.4 with HCL.

NP250 lysis buffer: 10ml Tris pH 7.6 (1M), 1000µl EDTA (0.5M), 2500µl NP450 (5M), 500mls H_2O, 25mls NaCl (5M)

Lysis buffer for proteomic abundance via mass spectroscopy: 1% SDS, Tris 7.5 (20mM) and NaCl (150mM) with protease inhibitors.

EDTA 0.5M: di-sodium salt of ethylenediaminetetraacetate in H_2O. pH adjusted to 8.0 with NaOH.

MOPS: 3-(N-morpholino)propanesulfonic acid (Invitrogen)

Transfer buffer: 14.4g glycine, 3.03g Tris, 200ml methanol made up to 1 litre with H_2O.

10x TBS-T: 200ml 1M Tris pH 7.5, 300ml 5M NaCl, 10ml Tween in 1L of H_2O.

Tris: tris(hydroxymethyl)aminomethane (Invitrogen)

TCA: 10% trichloroacetic acid in H_2O.

IFF (Immunofluorescence buffer): PBS, 1% bovine serum albumin (Sigma, UK) and 2% foetal calf serum (Life Technologies, UK), filtered through a 0.2µM filter)

PFAL 4% (w/v) paraformaldehyde in PBS

10x TAE: 48.4g Trizma base, 20ml of EDTA pH 8.0 (0.5M), and 11.44ml glacial acetic acid, to a final volume of 1000ml with deionised H_2O.

2.1.2 Drugs

All cell lines were profiled using a customised in-house drug library containing 80 drugs, which have either been licenced for clinical use in cancer or are in early phase clinical trials and are listed by their primary target (Table 2). All drugs were purchased from Sigma, except those listed below, dissolved in 100% DMSO and stored at -20˚C unless otherwise stated.

AZ20 (Selleckchem)

AZD6738 (Selleckchem)

Cisplatin (Selleckchem)

Doxorubicin (Selleckchem)
Hydroxyurea (Selleckchem)
VE821 (Selleckchem)
VX970 (Selleckchem)
DMX_1783 (Domainex)
DMX_2320 (Domainex)
DMX_051_1783 (Domainex)
DMX_051_2384 (Domainex)
Blasticidin: dissolved in deionised H2O (Invitrogen)

Each drug was dissolved to give 5mM and 2.5mM stock solutions and then diluted to 500, 250, 50, 25, 5, 2.5, 0.5, 0.25uM stocks in 96-well 2D-matrix plates. 384-well daughter plates were then aliquoted from the master plates using the Hamilton Microlab Star robotic liquid handler platform. Drugs were stored under a nitrogen atmosphere using a StoragePod (Roylan Developments). Final plate concentrations were 0.5, 1, 5, 10, 50, 100, 500 and 1000nM and final concentration of DMSO in all wells was 0.2% (v/v). Controls for viability included 0.2% (v/v) DMSO and controls for cell death included 100 % DMSO.

An additional library consisting of 395 drugs, which have either been licenced for clinical use in cancer or are in early phase clinical trials prepared in the same manner, was also used to screen only the isogenic RB1 deficient U2OS models created by CRSIPR-Cas9 mutagenesis (**Table 3**). Final plate concentrations were 0.5, 5, 50, and 500nM with controls as above.

2.1.3 Antibodies

Primary antibodies are listed in Table 4, and all were incubated overnight at 4°C. HRP-conjugated secondary antibodies were purchased from Sigma and diluted 1:10,000. For images obtained using the Odyssey Infrared Imaging System from LI-COR, LI-COR fluorescent dye labelled secondary antibodies at 800CW or 650CW were purchased from Odyssey and diluted 1:10,000.

Table 2 Drug library

Compound	Mechanism of action	Compound	Mechanism of action
MK-2206	AKT inhibitor	17-AAG	HSP 90 inhibitor
Carboplatin	Alkylating agent	PF-04929113	HSP 90 inhibitor
Doxorubicin	Anthracyline	Decitabine	Hypomethylating agent
5-fluorouracil	Anti-metabolite	Linsitinib (OSI-906)	IGF1R, IR inhibitor
Gemcitabine	Anti-metabolite	GSK1904529A	IGF1R, IR inhibitor
methotrexate	Anti-metabolite	BMS-911543	JAK2 inhibitor
Vinorelbine	Anti-mitotic	Lestaurtinib	JAK2, FLT3 and TrkA receptor tyrosine kinase inhibitor
Bleomycinsulfate	Anti-tumour antibiotic	Nutlin-3	MDM2 inhibitor
KU60019	ATM inhibitor	PD-184352	MEK inhibitor
PF-03814735	Aurora kinase inhibitor	PF-02341066	MET/ALK inhibitor
Temozolomide	Alkylating agent	Paclitaxel	microtubule poison
ABT-737	Bcl-2 inhibitor	Everolimus	mTOR inhibitor
Dasatinib	Bcr-Abl, Src inhibitor	BEZ-235	mTOR/PI3K inhibitor
Nilotinib	Bcr-Abl, c-Kit, PDGR inhibitor	MLN-4924	NEDDylation inhibitor
Crizotonib	c_MET, ALK inhibitor	Sapacitabine	Nucleoside analogue
Foretinib	c-MET inhibitor	PF-03758309	PAK inhibitor
Flavopiridol	CDK inhibitor	Canertinib	pan-ErbB inhibitor
RO-3306	CDK1 inhibitor	PF-00299804	pan-ErbB inhibitor
Palbociclib	CDK4/6 inhibitor	AG-14699	PARP inhibitor
PF-332991	CDK4/6 inhibitor	BMN-673	PARP inhibitor
PF-00477736	CHEK1 inhibitor	Olaparib	PARP inhibitor
SAR-20106	CHEK1 inhibitor	Imatinib	PDGFR inhibitor
Cabozantinib	VEGF2, c-MET, RET, KIT, FLT1/3/4, TEK, AXL inhibitor	Sunitinib	PDGFR inhibitor
Celecoxib	COX2 inhibitor	PF-04691502	PI3K inhibitor
MDV-3100	CRCP inhibitor	Sotrastaurin/AEB071	PKC inhibitor
Abiraterone	CYP17A1 inhibitor	BI2536	PLK1 inhibitor
KU0057788	DNA-PK inhibitor	PLX-4720	RAF inhibitor
MSC2358705A	DNA-PK inhibitor	Sorafenib	Raf inhibitor
Tamoxifen	EF inhibitor	Resveratrol	SIRT1 activator
Erlotinib	EGFR inhibitor	YM155	Survivin- suppressant
Gefitinib	EGFR inhibitor	6-thioguanine	Thiopurine
BIBW2992	EGFR/HER2 inhibitor	DMX_1783	TNKS inhibitor
GSK2194069A	FAS inhibitor	DMX_2320	TNKS inhibitor
AZ4547	FGFR inhibitor	XAV-939	TNKS/Wnt signalling inhibitor
PD173074	FGFR inhibitor	Camptothecin	Topoisomerase inhibitor
MK-0752	Gamma secretase inhibitor	Etoposide	Topoisomerase inhibitor
voronostat	HDAC inhibitor	Salinomycin	Unknown
GDC-0449	hedgehog/smoothened signalling inhibitor	Lenvatinib	VEGFR1/2/3 inhibitor
lapatinib	HER2 inhibitor	MK-1175	Wee1 inhibitor
2-Methoxyestradiol	HIF inhibitor		

Table 3 Additional drug library

Drug	Mechanism of action	Drug	Mechanism of action
Zileuton	5-lipooxygenase	AT-406	IAP inhibitor
Pentostatin	Adenosine Deaminase Inhibitor	GSK1904529A	IGR1, IR inhibitor
GDC-0068	AKT inhibitor	Linsitinib (OSI-906)	IGFR1, IR inhibitor
GSK690693	AKT inhibitor	BAY11-7082	IKK inhibitor
MK-2206	AKT inhibitor	Dexamethasone	IL receptor inhibitor / steroid
Perifosine	AKT inhibitor	Mycophenolic	inhibitor of inosine monphosphate dehydrogenase
Triciribine	AKT inhibitor	TPCA-1	IκB/IKK inhibitor
EBPC	aldose reductase	CEP33779	JAK inhibitor
LDN193189	ALK inhibitor	Cyt387	JAK inhibitor
TAE684	ALK inhibitor	NVP-BSK805	JAK inhibitor
Bendamustine	Alkylating agent	Ruxolitinib	JAK inhibitor
Carboplatin	Alkylating agent	S-Ruxolitinib	JAK inhibitor
Cisplatin	Alkylating agent	Tofacitinib	JAK inhibitor
Dacarbazine	Alkylating agent	TG101348	JAK2 inhibitor
Doxercalciferol	Alkylating agent	BI78D3	JNK inhibitor
Ifosfamide	Alkylating agent	S7333KRAS	K-RAS G12C inhibitor
Oxaliplatin	Alkylating agent	Ispinesib	kinesin spindle inhibitor
Procarbazine	Alkylating agent	SB 743921	kinesin spindle inhibitor
Clafen	Alkylating agent	GW3965	liver x receptor inhibitor
Altretamine	Alkylating agent	Nutlin-3	MDM2 inhibitor
Cyclophosphamide	Alkylating agent	SJ172550	MDMX inhibitor
Lomustine	Alkylating agent	AZD6244	MEK inhibitor
Tosedostat	aminopeptidase	CI-1040	MEK inhibitor
A-769662	AMPK inhibitor	GSK1120212	MEK inhibitor
Andarine	androgen receptor inhibitor	PD0325901	MEK inhibitor
Bicalutamide	androgen receptor inhibitor	TAK-733	MEK inhibitor
Flutamide	androgen receptor inhibitor	BMS794833	MET/VEGFR2 inhibitor
Ostarine	androgen receptor inhibitor	Lomeguatrib	MGMT inhibitor
Doxorubicin	Anthracyline	EpothiloneA	microtubule inhibitor
Epirubicin	Anthracyline	EpothiloneB	microtubule inhibitor
MDV3100	anti-androgen	NPI-2358	microtubule inhibitor
Pomalidomide	anti-angiogenesis	Vinblastine	microtubule inhibitor
Itraconazole	anti-angiogenic and Hh signalling inhibitor	Nocodazole	microtubule poison
Phloretin	anti-inflammatory and immuno-suppressive	Paclitaxel	microtubule poison
Capecitabine	Anti-metabolite	Lonidamine	mitochondrial hexokinase inhibitor
Cladribine	Anti-metabolite	Vincristine	mitotic inhibitor
Clofarabine	Anti-metabolite	Marimastat	MMP inhibitor

Floxuridine	Anti-metabolite	AZ3146	MSP1 inhibitor
Ftorafur	Anti-metabolite	Rapamycin	mTOR inhibitor
Gemcitabine	Anti-metabolite	AZD8055	mTOR inhibitor
Pemetrexed	Anti-metabolite	Deforolimus	mTOR inhibitor
Azathioprine	Anti-metabolite	Everolimus	mTOR inhibitor
ABT-751	anti-mitotic	INK 128	mTOR inhibitor
Docetaxel	anti-mitotic	KU-0063794	mTOR inhibitor
Bleomycin	Anti-tumour antibiotic	Temsirolimus	mTOR inhibitor
(-)-Epigallocatechin	Antioxidant	Torin2	mTOR inhibitor
TAME	APC inhibitor	WYE-354	mTOR inhibitor
Aminoglutethimide	Aromatase	BEZ235	mTOR/PI3K inhibitor
Anastrozole	Aromatase	APO866	NAMPT inhibitor
Exemestane	Aromatase	FK866	NAMPT inhibitor
Formestane	Aromatase	Bay117085	NF-κB inhibitor
Letrozole	Aromatase	QNZ	NF-κB inhibitor
CP-466722	ATM inhibitor	L-NNA	NOS inhibitor
KU-55933	ATM inhibitor	Isotretinoin	nucelar RAR activator
KU-60019	ATM/ATR inhibitor	Toremifene	oestrogen inhibitor
NU6027	ATR inhibitor	Evista	oestrogen inhibitor
VE-821	ATR inhibitor	DFMO	ornithine decarboxylase inhibitor
Vx-970	ATR inhibitor	PH-797804	p38 MAPK inhibitor
AMG 900	Aurora kinase inhibitor	SB 203580	p38 MAPK inhibitor
AT9283	Aurora kinase inhibitor	BIRB796	p38 MAPK inhibitor
Barasertib	Aurora kinase inhibitor	LY2228820	p38 MAPK inhibitor
CYC116	Aurora kinase inhibitor	PF03758309PAKi	PAK inhibitor
Danusertib	Aurora kinase inhibitor	BMS-599626	pan HER inhibitor
JNJ-7706621	Aurora kinase inhibitor	ABT-888	PARP inhibitor
MLN8237	Aurora kinase inhibitor	AG14361	PARP inhibitor
PF-03814735	Aurora kinase inhibitor	BMN673	PARP inhibitor
SNS-314Mesylate	Aurora kinase inhibitor	Iniparib	PARP inhibitor
VX-680	Aurora kinase inhibitor	Olaparib	PARP inhibitor
Temozolomide	Alkylating agent	Rucaparib	PARP inhibitor
Vemurafenib	B-Raf inhibitor	UPF1035	PARP inhibitor
ABT-263	Bcl-2 inhibitor	AnagrelideHCl	PDE inhibitor
ABT-737	Bcl-2 inhibitor	Imatinib	ABL, KIT, PDGFR inhibitor
Obatoclax	Bcl-2 inhibitor	Sunitinib	PDGFR, VEGFR, KIT, RET, CSF-1R, Flt3 inhibitor
TW-37	Bcl-2 inhibitor	3-Methyladenine	PI3K inhibitor
Bafetinib	Bcr-Abl inhibitor	AS-605240	PI3K inhibitor
Dasatinib	Bcr-Abl, Src inhibitor	BKM120	PI3K inhibitor
DCC-2036	Bcr-Abl inhibitor	CAL-101	PI3K inhibitor

Nilotinib	Bcr-Abl, c-Kit, PDGR inhibitor	CH5132799	PI3K inhibitor
Ponatinib	Bcr-Abl, VEGF, FGFR, TIE2, Flt3 inhibitor	GDC-0941	PI3K inhibitor
WP1130	Bcr-Abl, Deubiquitinase inhibitor	GSK2126458	PI3K inhibitor
Ibrutinib	Btk inhibitor	IC-87114	PI3K inhibitor
Amuvatinib	c_KIT inhibitor	LY294002	PI3K inhibitor
Masitinib	c_KIT inhibitor	PF-04691502	PI3K inhibitor
OSI-930	c_KIT inhibitor	PI-103	PI3K inhibitor
SU11274	c_MET inhibitor	PIK-75	PI3K inhibitor
BMS 777607	c_MET inhibitor	PIK-90	PI3K inhibitor
Crizotinib	c_MET, ALK inhibitor	XL147	PI3K inhibitor
JNJ-26481585	c_MET inhibitor	YM201636	PI3K inhibitor
JNJ-38877605	c_MET inhibitor	ZSTK474	PI3K inhibitor
PF-04217903	c_MET inhibitor	PIK-93	PI4K inhibitor
PHA-665752	c_MET inhibitor	SGI-1776	PIM inhibitor
SGX-523	c_MET inhibitor	TCSPIM	PIM-1/-2 Kinase inhibitor
TTP22	caesin kinase 2 inhibitor	PIM-1Inhibitor	PIM1 inhibitor
CX-4945	caesin kinase 2 inhibitor	Chelerythrine	PKC inhibitor
CyclosporinA	Calcineurin Inhibitor	Enzastaurin	PKC inhibitor
Calpeptin	calpain inhibitor	Sotrastaurin	PKC inhibitor
PAC-1	caspase inhibitor	BI2536	PLK1 inhibitor
LY320135	CB1 receptor inhibitor	GSK461364	PLK1 inhibitor
Maraviroc	CCR inhibitor	BI6727	PLK1 inhibitor
NSC663284	Cdc25 inhibitor	Rigosertib	PLK1 inhibitor
ML-141	Cdc42 inhibitor	Rosiglitazone	PPAR inhibitor
AT7519	CDK inhibitor	GSK3787	PPARδ inhibitor
Flavopiridol	CDK inhibitor	Mifepristone	progesterone inhibitor
PHA-793887	CDK inhibitor	Bortezomib	proteasome inhibitor
Roscovitine	CDK inhibitor	MLN2238	proteasome inhibitor
SNS-032	CDK2,7,9 inhibitor	MLN9708	proteasome inhibitor
Palbociclib	CDK4/6 inhibitor	Disulfiram	PTEN inhibitor
Dalcetrapib	CETP inhibitor	Mercaptopurine	purine nucleoside analogue
AZD7762	CHK1 inhibitor	Nelarabine	purine nucleoside analogue
PF477736	CHK1 inhibitor	Carmofur	pyrimidine analogue
LY2603618	CHK2 inhibitor	NSC23766	Rac1 inhibitor
BML-277	CHK2 inhibitor	AZ628	Raf inhibitor
Ezetimibe	cholesterol absorption inhibitor	GDC-0879	Raf inhibitor
PF670462	CK1ε inhibitor	SB590885	Raf inhibitor
Celecoxib	COX-2 inhibitor	Sorafenib	Raf inhibitor
SB265610	CXCR2 inhibitor	CD437	retinoid
Abiraterone	CYP17A1 inhibitor	Fenretinide	retinoid

Mycophenolate	dehydrogenase inhibitor	Hydroxyurea	ribonucleotide reductase inhibitor
Abitrexate	DHFR inhibitor	Necrostatin-1	RIPK1 inhibitor
Azacitidine	DNA methyl transferase inhibitor	Triptolide	RNA poly II inhibitor
RG108	DNA methyltransferase inhibitor	Y-27632	ROCK inhibitor
NU7441	DNA-PK inhibitor	Pazopanib	RTK inhibitor
Vx-984	DNA-pk inhibitor	Fingolimod	S1P receptor inhibitor
Adrucil	DNA/RNA Synthesis inhibitor	PF-4708671	S6 kinase inhibitor
DMXAA	DT-diaphorase inhibitor	Ranolazine	selective inhibition of late sodium currents
Harmine	DYRK1A inhibitor	SID7969543	SF-1 inhibitor
SMER3	E3 Ubiquitin Ligase (SCF) Inhibitor inhibitor	GSK650394	SGK inhibitor
Tamoxifen	EF inhibitor	Canagliflozin	SGLT inhibitor
Afatinib	EGFR inhibitor	Dapagliflozin	SGLT inhibitor
Chrysophanicacid	EGFR inhibitor	PB28	Sigma 2 receptor inhibitor
CUDC-101	EGFR inhibitor	SRT1720	SIRT1 activator
Dacomitinib	EGFR inhibitor	EX527	SIRT1 inhibitor
Erlotinib	EGFR inhibitor	Quercetin	Sirtuin inhibitor
Gefitinib	EGFR inhibitor	Sirtinol	Sirtuin inhibitor
OSI-420	EGFR inhibitor	SANT1	smoothened inhibitor
PD153035	EGFR inhibitor	SK1	Sphingosine Kinase-1 Inhibitor
Pelitinib	EGFR inhibitor	SKI_II	Sphingosine Kinase-1 Inhibitor
WZ4002	EGFR inhibitor	Bosutinib	Src inhibitor
GSK264220A	endothelial lipase inhibitor	KX2-391	src inhibitor
Zibotentan	endothelin receptor inhibitor	Saracatinib	Src inhibitor
FR180204	ERK1/2 inhibitor	SrcI1	Src inhibitor
Fulvestrant	Estrogen receptor inhibitor	Fludarabine	STAT inhibitor
PF-3845	FAAH inhibitor	Fludarabine	STAT inhibitor
PF 573228	FAK inhibitor	STAT5Inhibitor	STAT5 inhibitor
PF-562271	FAK inhibitor	Hydrocortisone	steroid
GSK837149A	FAS inhibitor	YM155	Survivin inhibitor
PD173074	FGFR inhibitor	R406	Syk inhibitor
Quizartinib	FLT3 inhibitor	R935788	Syk inhibitor
Crenolanib	FLT3 inhibitor	Estrone	synthetic oestrogen
Dovitinib	FLT3 inhibitor	Estradiol	Synthetic oestrogen
ENMD-2076	FLT3 inhibitor	Medroxyprogesterone	synthetic progesterone
Tandutinib	FLT3 inhibitor	Megestrol	synthetic progesterone
GW4064	FXR inhibitor	BX795	TBK1/IKKepsilon inhibitor
WAY-362450	FXR inhibitor	BIBR1532	Telomerase inhibitor

DAPT	Gamma secretase inhibitor	LY2109761	TGF beta receptor inhibitor
YO-01027	Gamma secretase inhibitor	SB42	TGF beta/ smad inhibitor
MK-0752	Gamma secretase inhibitor	LY2157299	TGF beta/Smad inhibitor
SecinH3	GDP/GTP Exchange Factor inhibitor	SB525334	TGF beta/Smad inhibitor
Pioglitazone	glitazones	Raltitrexed	thymidylate synthase inhibitor
Gossypol	glycolytic inhibitor	Tie2	Tie-2 inhibitor
GW9508	GPR40 inhibitor	MG149	TIP60 Histone Acetyltransferase inhibitor
AR-A014418	GSK-3 inhibitor	Lenalidomide	TNF- alpha inhibitor
CHIR-99021	GSK-3 inhibitor	2131TNKSi	TNKS inhibitor
SB 216763	GSK-3 inhibitor	877TNKSi	TNKS inhibitor
4-Phenylbutyrate	HDAC inhibitor	C43TNKSi	TNKS inhibitor
AR-42	HDAC inhibitor	DMX_051_1783	TNKS inhibitor
Belinostat	HDAC inhibitor	DMX_051_2384	TNKS inhibitor
Entinostat	HDAC inhibitor	JW55	TNKS inhibitor
Mocetinostat	HDAC inhibitor	camptothecin	Topoisomerase I inhibitor
Panobinostat	HDAC inhibitor	Irinotecan	Topoisomerase I inhibitor
PCI-24781	HDAC inhibitor	Topotecan	Topoisomerase I inhibitor
Pyroxamide	HDAC inhibitor	Daunorubicin	Topoisomerase inhibitor
SB939	HDAC inhibitor	Etoposide	Topoisomerase inhibitor
Trichostatin	HDAC inhibitor	Idarubicin	Topoisomerase inhibitor
Valproic	HDAC inhibitor	Irinotecan	Topoisomerase inhibitor
Vorinostat	HDAC inhibitor	MitoxantroneHCl	Topoisomerase inhibitor
JNJ 26854165	HDM2 inhibitor	Palomid529	TORC1/2 inhibitor
Cyclopamine	Hedgehog signalling inhibitor	Tipifarnib	transferase inhibitor
JK184	Hedgehog signalling inhibitor	ITX3	TrioN RhoGEF inhibitor
LDE225	hedgehog/smoothened signalling inhibitor	CombretastatinA4	Tubulin polymerisation inhibitor
Vismodegib	hedgehog/smoothened signalling inhibitor	Axitinib	VEGFR inhibitor
AEE788	HER1/2, VEGFR1/2 inhibitor	BIBF1120	VEGFR1/2/3, FGFR1/2/3, PDGFR inhibitor
Lapatinib	HER2 inhibitor	Cediranib	VEGFR inhibitor
2-Methoxyestradiol	HIF inhibitor	E7080	VEGFR inhibitor
SKF91488	histamine N-methyltransferase inhibitor	Linifanib	VEGFR inhibitor
Fluvastatin	HMGCoA reductase inhibitor	Motesanib	VEGFR inhibitor
BIX01294	HMTase inhibitor	Tivozanib	VEGFR inhibitor
Elesclomol	HSP 90 inhibitor	Vandetanib	VEGFR inhibitor
17-AAG	HSP 90 inhibitor	Vatalanib	VEGFR inhibitor
17-DMAG	HSP 90 inhibitor	Brivanib	VEGFR,FGFR inhibitor
AUY922	HSP 90 inhibitor	Regorafenib	VEGFR2-TIE2 inhibitor

BIIB021	HSP 90 inhibitor	Telatinib	VEGGFR2/3,C-KIT,PDGFR inhibitor
CCT18159	HSP 90 inhibitor	MK-1775	Wee1 inhibitor
Ganetespib	HSP 90 inhibitor	MK1775	Wee1 inhibitor
Geldanamycin	HSP 90 inhibitor	PD407824	Wee1/Chk1 inhibitor
Decitabine	Hypomethylating agent	Febuxostat	Xanthine oxidase inhibitor

2.1.4 SiRNA library targeting the human genome

A SMARTpool® kinase siRNA custom library comprised of 720 kinases (Appendix Table 1), 80 tumour suppressor genes (Appendix Table 2) and 480 genes included in the Cancer Gene Census (Appendix Table 3), was obtained from GE life sciences. The library was supplied in 96 well plate format with each well representing one gene, with 80 genes per plate. Each well contained four individual siRNA species that targeted the same gene, with different target sequences, termed a SMARTpool®. Target sequence information was not supplied. Additional positive (siPLK) and non-targeting controls (siAllstar, siControl1, and siControl2) were added to the plate, prior to being aliquoted by the Hamilton Robot into 384 well daughter plates for use for the screens. All siRNA oligonucleotides were supplied by GE healthcare, except siAllstar from Qiagen.

2.1.5 SiRNA oligonucleotides

Individual siRNA oligonucleotides were purchased from GE Life Sciences and were supplied lyophilised and 2'ACE protected. DEPC (0.1% diethylpyrocarbonate) treated water (Ambion) was used to reconstitute the siRNA to 20μM, and aliquots were stored at -20˚Celcius.

2.1.6 CRISPR constructs

Edit-R crRNA and tracer RNA targeting two individual sequences of *RB1* were purchased from GE Life Sciences and were supplied lyophilised. Both were reconstituted with DEPC treated water (Ambion) and stored at -80˚Celcius.

2.2 PROTOCOLS

2.2.1 Tissue culture

2.2.1.1 Cell line identification confirmation

Short Tandem Repeat (STR) typing performed using GenePrint 10 (Promega UK Ltd) was used to confirm identification of the cell lines at the ICR. The Leibniz-Institute DSMZ-Deutsche Sammlung von Mikroorganismen und Zellkulturen GmbH online STR analysis website (http://www.dsmz.de/fp/cgi-bin/str.html), was used as reference for the STR cell

line profiles. Genome wide array single nucleotide polymorphisms (SNP) 6.0 (Affymetrix) were performed at the Wellcome Trust Sanger Institute (WTSI) instead of STR typing.

2.2.1.2 Cell lines

A total of 18 cell lines comprising a range of histological subtypes of osteosarcoma as classified by tumour of origin (Table 5), were used: 143b and HOSMMNG were purchased from the American Type Culture Collection (ATCC); G292 clone A141B1, MG63, CAL72, HU03N1, OSA/SJSA-1, NOS1, SAOS2, U2OS, HU09, NY and HOS were gifts from Ultan McDermott at the Wellcome Trust Sanger Institute (WTSI); LM7, OHSN, OSH25HAL (HAL) MHM, and KPD were kind gifts from Ola Myklebost, Norway. Included in this panel two isogenic models of murine metastasis formation derived from HOS (HOSMNNG and 143b), and SAOS2 (daughter LM7).

In addition, isogenic models of *RB1* deficiency were also used. Two isogenic *RB1* deficient and wildtype breast models were kind gifts from Eric Knudsen, Thomas Jefferson University, Philadelphia, USA; metastatic breast adencarcinoma tumour cell line (MDAMB231) and a non-tumourigenic epithelial breast cell line (MCF10A) both created by shRNA mediated silencing of *RB1*. Two *RB1* isogenic models (U2OS clone 4.2 and 4.5) generated in the OS cell line U2OS by CRISPR-Cas9 mutagenesis, described in Chapter 4.

Table 4 Compilation of primary antibodies used

Antibody	Supplier	Product Number	Secondary	Dilution
RB1 (C-terminus)	Cell signalling	9309	Mouse	1:1000
P16INKa	Abcam	Ab108349	Rabbit	1:1000
PARP	Santa cruise	D513	Mouse	1:1000
Actin	Santa cruise	G1814	Goat	1:1000
RB1 (N-terminus)	Antibodies online	ABIN 78590	Rabbit	1:2000
pTP53 (Serine15)	Cell signalling	9284	Rabbit	1:2000
P21 waf/lip1	Cell signalling	2946s	Mouse	1:1000
CHK1	Cell signalling	Sc-8408	Mouse	1:500
pCHK1 (S345)	Cell signalling	2348s	Rabbit	1:1000
CHK2	Abcam	Ab109413	Rabbit	1:1000
pCHK2 (Thr68)	Cell signalling	CS2661	Rabbit	1:1000
$P27^{Kipl1}$	Cell signalling	2552	Rabbit	1:1000
SKP2	Cell signalling	4358	Rabbit	1:1000
Cyclin E1	Cell signalling	HE12	Mouse	1:1000
Cyclin A2	Cell signalling	BF683	Mouse	1:1000
DYRK1A	Abcam	Ab69811	Rabbit	1:1000
DYRK1A	Cell signalling	2771	Rabbit	1:1000
ATM	Cell signalling	2873	Rabbit	1:1000
pATM (Ser1981)	Cell signalling	4526S	Mouse	1:1000
BRCA2	Genetex	GTX70121	Mouse	1:500
ATR	Cell signalling	SCC0514	Goat	1:1000
pATR (Thr1989)	GENETEX	GTX128145	Rabbit	1:1000
Cyclin B1	Cell signalling	12231S	Rabbit	1:1000

RB1 (C-terminus epitope)	Cell signalling	9309	Mouse	1:1000
RB1 (N-terminus epitope)	Antibodies-online.com	ABIN785970	Rabbit	1:1000

A number of mutant clones of SUM149 and CAPAN1 were created by CRISPR-Cas9 mutagenesis within the Lord laboratory. Two isogenic *BRCA* deficient and proficient models were created by Amy Dréan using CRISPR-Cas9 mutagenesis of the pancreatic ductal adenocarcinoma cell line CAPAN1 (*BRCA2* defective: c.6174delT, p.S1982fs*22) (Edwards, Brough, Lord, *et al.*, 2008) to create an intragenic mutation in *BRCA2* that restored the native open reading frame termed CAPAN1.B2.S* (Dréan, Williamson, Brough, *et al.*, 2017). This secondary mutation restored BRCA2 function. Amy Dréan used the same method to restore BRCA1 function to the *BRCA1* deficient breast tumour cell line SUM149 (*BRCA1* mutant c.2288delT, p.N723fsX13) (Elstrodt, Hollestelle, Nagel, *et al.*, 2006), creating a *BRCA1* 'revertant' clone termed SUM149.B1.S* (Dréan, Williamson, Brough, *et al.*, 2017). A SUM149 *REV7* mutant clone with a truncating mutation in *REV7* (*MADL2L2*) and a SUM149 *53BP1* mutant clone with a truncating mutation in *53BP1* were created by Inger Brandsma, ICR. A SUM149 *PARP1* mutant clone with a missense mutation in *PARP1* was created by Stephen Pettitt, ICR.

2.2.1.3 U2OS tetracycline inducible cell lines

Tetracycline-controlled transcriptional activation (Tet-on) U2OS cells generated using pRev Tet-On system (Clontech Takara Bio) were a generous gift from James DeCaprio, Dana-Farber Cancer Institute, Boston (Litovchick, Florens, Swanson, *et al.*, 2011). Litovchick *et al.* sublconed human DYRK1A complementary DNA (cDNA) (gift of W. Hahn) into tet-inducible pRevTre vector and generated a kinase-inactive DYRK1A-K188R by site-directed mutagenesis (QuikChange; Agilent)(Litovchick, Florens, Swanson, *et al.*, 2011).

2.2.1.4 Media

DMEM, RPMI, MEM, F12, IMDM and McCoys's were all supplied by Gibco and supplemented with 5mL L-Glutamine (Gibco) and five or ten percent Fetal Bovine Serum (FBS) (Gibco) depending on the cell line (Table 5). Penicillin-streptomycin 5ml (Invitrogen) was added to media for routine culture only.

Table 5 Origins and growth conditions for cell lines used.

[OS: osteosarcoma; ATCC: American Type Culture Collection; Wellcome Trust Sanger Institute: WTSI; FBS: Foetal bovine serum; EGF: epidermal growth factor]

Cell Lines	Tissue Type	Histology	Source	Media	FBS	Additives
CAL72	OS	Osteoblastic	Ultan McDermott, WTSI	DMEM	10%	2mM L-Glutamine
NOS-1	OS	Osteoblastic	Ultan McDermott, WTSI	DMEM	10%	2mM L-Glutamine
OS25-HAL	OS	Osteoblastic	Ola Myklebost, Norway	RPMI	10%	2mM L-Glutamine
HU09	OS	Osteoblastic	Ultan McDermott, WTSI	RPMI	10%	2mM L-Glutamine
OHSN	OS	Osteoblastic	Ola Myklebost, Norway	RPMI	10%	2mM L-Glutamine
KPD	OS	Chondroblastic	Ola Myklebost, Norway	RPMI	10%	2mM L-Glutamine
MHM	OS	Chondroblastic	Ola Myklebost, Norway	RPMI	10%	2mM L-Glutamine
G292 clone A141B1	OS	Osteoblastic / telangectatic	ATCC	McCoys	10%	2mM L-Glutamine
OSA/ SJSA-1	OS	Fibroblastic	Ultan McDermott, WTSI	RPMI	10%	2mM L-Glutamine
MG63	OS	Fibroblastic	Ultan McDermott, WTSI	RPMI	10%	2mM L-Glutamine
LM7	OS	Fibroblastic	Ola Myklebost, Norway	DMEM	10%	2mM L-Glutamine
HOS	OS	Fibroblastic	Ultan McDermott, WTSI	MEM	10%	2mM L-Glutamine
143B	OS	Epithelial	ATCC	DMEM	10%	2mM L-Glutamine
HOSMNNG	OS	Epithelial	ATCC	DMEM	10%	2mM L-Glutamine
SAOS2	OS	Epithelial	Ultan McDermott, WTSI	DMEM	10%	2mM L-Glutamine
U2OS	OS	Mixed histology	Ultan McDermott, WTSI	DMEM	10%	2mM L-Glutamine
HUO3N1	OS	Unknown histology	Ultan McDermott, WTSI	RPMI	10%	2mM L-Glutamine
NY	OS	Unknown histology	Ultan McDermott, WTSI	RPMI	10%	2mM L-Glutamine
MDAMB231	Breast	Adenocarcinoma	Eric Knudsen, USA	DMEM	10%	2mM L-Glutamine
MCF10A	Breast	Epithelial breast tissue (non-tumourigenic)	Eric Knudsen, USA	DMEM/ F12		20ng/ml EGF 0.5mg/ml hydrocortisone 100ng/ml chloera toxin 10µg/ml insulin 5% horse serum
CAPAN1	Pancreas	Adenocarcinoma	ATCC	IMDM	20%	2nm L-Glutamine
SUM149	Breast	Triple negative breast cancinoma	ATCC	DMEM/F 12	5%	2nM L-Glutamine 5µm/ml insulin 1µg/ml hydrocortisone

2.2.1.5 General culture conditions

Cells were maintained at 37 °C in a humidified atmosphere at 5% CO_2. Antibiotic-free media specific to each cell line (Table 5) was used for all drug and siRNA screening. To passage cells, growth media was removed, the cells washed with PBS and the cells incubated at 37˚C in a covering volume of trypsin/EDTA (Sigma). Once the cells detached, media was added to the cells to neutralise the trypsin and the cells seeded into new flasks or plates. To count the cell density, a single cell suspension was ensured by running the cells through a pipette multiple times, a 10µL alliquote of the cells was then stained with an equal volume of trypan blue and counted using the Countess automated cell counter (Invitrogen), which also provided an estimate of viability. Cells were frozen in a solution of 90% FBS and 10% DMSO, and maintained in liquid nitrogen. As per laboratory protocol, cell lines were tested monthly for mycoplasma infection.

2.2.1.6 Reverse transfection of siRNA

A transfection mix of serum free media (Opti-MEM, Gibco) and transfection reagent lipofectamine 2000 (Life Technologies), lipofectamine 3000 (Life Technologies), RNAimax (Life Technologies), or Dharmafect 4 (GE Lifesciences) was incubated at room temperature for 10 minutes according to the manufacturer's instructions. The siRNA was added to the transfection mix, and incubated for 10 minutes before being mixed with the cell suspension and plated at the required density. The final concentration of siRNA was 20nM.

For reverse transfection using siRNA oligonucleotides targeting two different genes, the same volume of siRNA was used as above, so the final concentration of each species of siRNA remained 20nM, but overall was 40nM.

2.2.1.7 Clonogenic / colony formation cell survival assays

Cells were plated in triplicate at a density of 500 cells per well of a 6 well plate for each condition, and repeated in triplicate. The media (tetracycline free and doxycycline positive) was replaced every four days. After 14 days, the cells were fixed in 10% trichloroacetic acid (TCA) and incubated overnight at 4^{o}C. The cells were then stained with sulforhodamine-B (SRB) for 30 minutes after which excess dye was removed by repeated washing with 1% (vol/vol) acetic acid, and the colonies counted. For cell lines

that failed to form discrete colonies, after 14 days the media was discarded, and cells were incubated in CTG (Promega), shaken for 10 minutes, transferred to a 96 well plate, and then luminescence measured using the Victor X5 Multilabel plate reader (Perkin Elmer) as a measure of viability. The survival fraction (cell viability) was then calculated as a fraction of the luminescence in vehicle treated wells, and GraphPad Prism was used to plot dose response curves.

2.2.1.8 High-throughput drug library screens

Cell lines were profiled using a customised in-house drug library containing 80 drugs (Table 2) and an additional library consisting of 395 drugs was also used to screen the isogenic *RB1* deficient U2OS models created by CRSIPR-Cas9 mutagenesis (Table 3). Cell lines were seeded at a density of 500 cells well using antibiotic free media, into white 384-well plates (Greiner Bio-one) using a MultiDrop Combi Dispenser (Thermo Fisher Scientific) and incubated overnight. Replicate cell plates were then loaded onto the Microlab Star screening platform and drug plates were serially diluted (final 1:500 fold dilution) in media before being added to the cell plates. After five days of continuous exposure to drug, cell viability was quantified via a highly sensitive luminescent assay measuring cellular ATP levels (CellTiter Glo; Promega) and using a Victor X5 Multilabel plate reader luminescence protocol (Perkin Elmer Las UK Ltd). Each screen was performed in triplicate on the same day.

2.2.1.9 Smaller scale drug screens

For smaller-scale drug screens and revalidation, the Echo Acoustic (Labcyte) was used because of ease of performing combination screens. Cells were first plated at a density of 500 cells per well into a 384 well plate (Greiner Bio-one) using a MultiDrop Combi Dispenser (Thermo Fisher Scientific) and incubated overnight. Drugs were prepared in a 384 well plate at doses of 10μM and 0.1μM. The Echo Acoustic was used to eject small droplets of liquid from wells of the mother plate using ultrasonic acoustic energy at the meniscus of the fluid sample, and position them precisely onto a surface (daughter plate) suspended above the ejection point. From this method seven final drug concentrations can be achieved (0.01, 0.05, 0.1, 0.5, 1, 5, 10μM). After five days of continuous exposure to drug, cell viability was quantified via a highly sensitive luminescent assay measuring cellular ATP levels (Cell Titer-Glo; Promega) and using a Victor X5 Multilabel plate reader

luminescence protocol (Perkin Elmer Las UK Ltd). Each screen was performed in triplicate on the same day.

2.2.1.10 High-throughput siRNA screen

A siRNA library targeting 720 known and putative human protein kinases (Appendix Table 1), 80 tumour suppressor genes (Appendix Table 2), and 480 genes included in the Cancer Gene Census (Appendix Table 3), was obtained in 384 well plates from GE Life Sciences. Each well contained 5μL (200nM) of a SMART pool of four distinct siRNA species targeting different sequences of the single target transcript. Additional positive (siRNA targeting PLK1 (GE Life Sciences)) and negative (nontargeting siRNA: siCON1, siCON2 (GE Life Sciences), and siAllstar (Qiagen)) controls were added to the edges of each plate (8 wells of each control), with an internal well of siPLK within the first plate (each screen consisted of three 384 well plates).

Cell lines were transfected with SMART pool siRNA using RNAiMAX (Invitrogen), Lipofectamine 2000 (Invitrogen) or Dharmafect4 (GE Life Sciences) according to results of prior optimisation. After the addition of 35μL cell suspension to each well, the final concentration of siRNA was 20nM. Each cell line was screened in triplicate on the same day. At 90% confluency (approximately five population doublings (Brough, Frankum, Sims, *et al.*, 2011)), established via prior microscopy, cell viability was measured as before (CellTiter-Glo; Promega).

For the olaparib resistance screen, 24 hours post reverse transfection, olaparib at a final concentration of 500nM or DMSO was added to the wells. After five days of continuous drug exposure, cell viability was then estimated using CellTiter Glo (Promega).

2.2.1.11 siRNA validation of target inhibition

To validate siRNA silencing of a target gene, protein expression level by western blotting and cell viability were determined using individual oligonucleotides targeting different regions of the same gene. Cells were reverse transfected in 6-well plates in duplicate with four individual oligonucleotide siRNAs (GE Life Sciences). Forty-eight hours post reverse transfection half the cells were collected for preparation of protein lysates and viability was assessed for the remainder using CellTiter Glo.

2.2.2 Analysis of cell cycle distribution by Fluorescence-activated cell sorting

Cells were plated at a density of $1x10^6$ cells per 10cm plate. After 24 hours of incubation the drugs and vehicles were added. At 24 and 48 hours post commencement of drug exposure, the cells were stained with 5-ethynyl-2′-deoxyuridine (EDU) (1:1000 incubated for 90 minutes) and both the adherent and non-adherent cells were collected for fixing. Prior to fixing, the cells were washed with 500µl of 1% Bovine serum albumin (BSA), centrifuged at 300g for five minutes, re-suspended in 100µl 1% BSA, mixed with 100µl Click-It Fixative (from the Click-iT® EdU Alexa Fluor® 488 Imaging Kit, Thermo Fisher) as per the manufacture's instructions, incubated for 15 minutes in the dark, centrigued at 300g for five minutes, re-suspended in 300µl PBS, and then 700µl ice-cold 100% ethanol added drop wise while gently vortexed. Fixed cells were then stored at -20˚C until ready for staining.

Cells were washed with 100µl of saponin-based permeabilisation and wash reagent (from the Click-iT® EdU Alexa Fluor® 488 Imaging Kit, Thermo Fisher), incubated for 30 minutes in the dark, centrifuged for five minutes at 300g, and then resuspended in 500µl 5% goat serum (made in 1% BSA). Cells were then incubated for an hour in the dark. After which they were further centrifuged at 300g for five minutes, and then 120µl of 1:200 diluted (using the saponin-based permeabilisation and wash reagent) anti-H3-Ser10 mouse antibody (Millipore 05-806) was added. The cells were then incubated at 4˚Celcius overnight in the dark. Next 500µl of saponin-based-permeabilisation and wash reagent was added, cells centrifuged for five minutes at 300g, 120µl of 1:500 diluted (using the saponin-based permeabilisation and wash reagent) secondary mouse-633 antibody was added and incubated for one hour in the dark. Cells were then washed with 500µl of saponin-based permeabilisation and wash reagent, centrifuged for 5 minutes at 300g, washed with 500µl 1% BSA, and centrifuged for five minutes at 300g. The Click-It cocktail (from the Click-iT® EdU Alexa Fluor® 488 Imaging Kit, Thermo Fisher), was prepared according to the manufacture's instructions and 500µl was added to each tube. The cells were then incubated again for 30 minutes in the dark, and centrifuged for five minutes at 300g. The cells were suspended in 500µl saponin-based permeabilisation and wash reagent with 1:10000 4',6-diamidino-2-phenylindole (DAPI) and incubated for a further 30 minutes in the dark. Each sample was then filtered into a FACS-cuvette and placed on ice in the dark until analysed on the BD LSR II Flow Cytometer (BD Biosciences) using BD FACSDiva software (BD Biosciences).

2.2.2.1 Apoptosis assay

OS tumour cells were plated at high density (10,000 cells per well) in a 96 well plate. After 24 hours of incubation the drugs and vehicle (DMSO) were added. At 24 and 48 hours post addition of drug, the Apo-Tox-Glo Triplex Assay (Promega) was performed as per the manufacture's instructions. The Victor X5 (Perkin Elmer) was used to measure luminescence. CellTiter-Glo was used in parallel to estimate cell viability.

2.2.2.2 Tetracycline inducible cell line U2OS

The three tumour cell lines U2OS preRev (empty vector), KR (kinase inactive *DYRK1A-K188R*), and WT (wildtype *DYRK1A*) were grown for one week in tetracycline free media, before division and the addition of doxycycline at 5µg/ml to half of the cells. After four days, cells were reverse transfected with a siRNA smart-pools targeting *RB1, PLK* and a non-targeting control (Allstar). At 24 hours, cells were then seeded in triplicate at low density (500 cells per well of six well plate), and after two weeks, the cells were fixed and stained (Figure 4 and Figure 58).

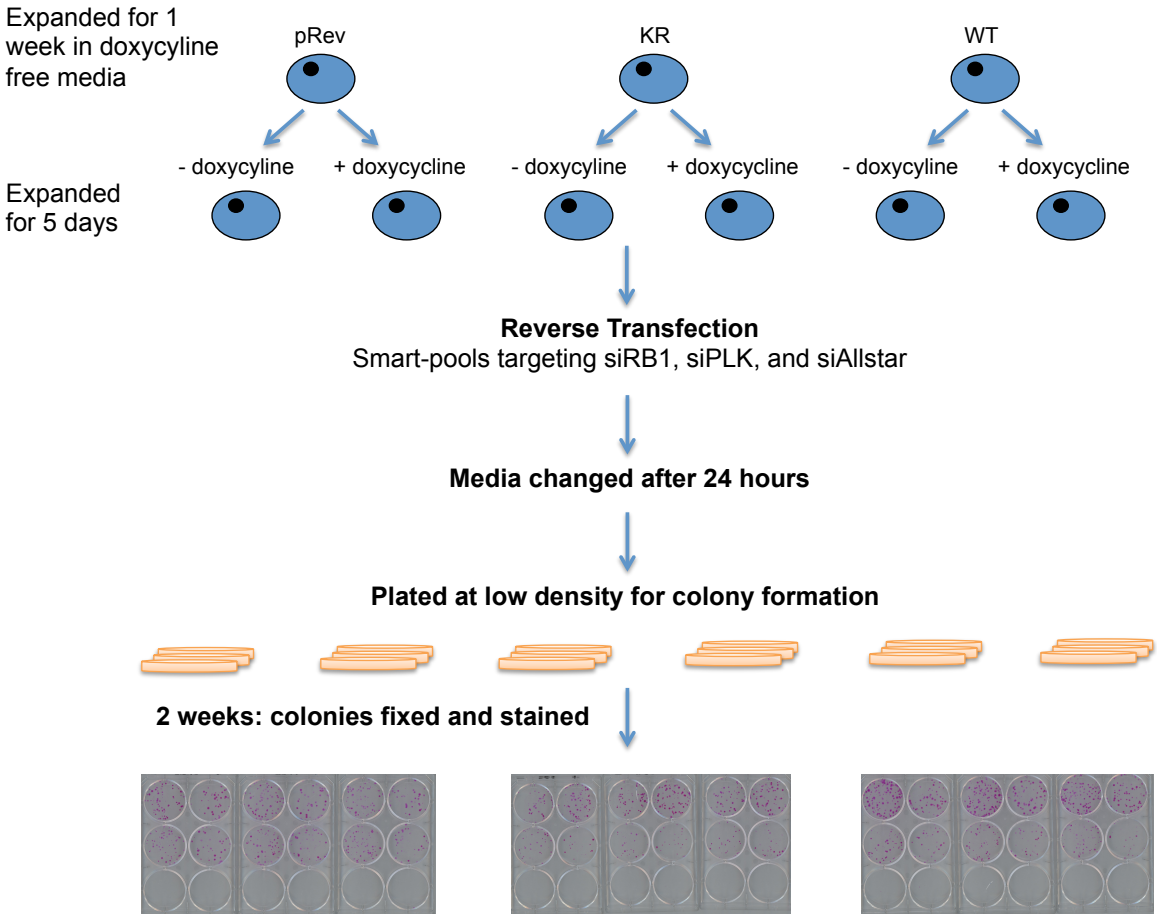

Figure 4 Schematic of methodology of colony formation assay post reverse transfection with siRNA.

Three U2OS tumour cell lines were used with either a tetracycline inducible empty vector (pRev), kinase inactive *DYRK1A-K188R* (KR), or wildtype *DYRK1A* (WT). Each U2OS tumour cell line was expanded for a week in tetracycline free media, split and half were treated with doxycycline (5µg/ml) for five days. Cells were then reverse transfected with siRNA targeting *RB1*, Allstar (negative control), and *PLK* (positive control), and after 24 hours plated at low density (500 cells per well) for colony formation. After two weeks the colonies were fixed and stained (Figure 58).

2.2.3 Protein manipulation

2.2.3.1 Western blots

Cells were washed twice with cold PBS and lysed at 4°C for 30 minutes in buffer (100 mmol/L NaCl, 1 mmol/L phenylmethylsulfonyl fluoride, 1% Triton X-100, 0.1% SDS, 0.5% sodium deoxycholate, 20 µg/mL aprotinin, 20 µg/mL leupeptin). Insoluble material was removed by centrifugation at 4°C for 30 minutes at 16,000g, and protein concentrations were determined by Bradford Assay using a BCA protein assay kit (Pierce, United States of America). For each lysate, 1ml of BioRad Protein assay [5x] diluted in 1:5 with ultra-filtered water was used and loaded into a cuvette. Absorbance values for each lysate were then interpolated on GraphPadPrism using a standard curve of absorbance value for known concentrations of BSA. For each lysate, fifty was then divided by the interpolated concentration, and the resultant value combined with 10µl of NuPAGE sample buffer (Life Technologies), which was heated to 96˚C for 10 minutes and snap frozen on dry ice.

Cell lysates were separated using either 4-12% SDS-PAGE Bis-Tris gels or 3-8% Tris-Acetate Gel, transferred to nitrocellulose membrane, blocked in 5% milk and blotted with antibodies as per the manufacturers instructions. Blots were washed using Tris-buffered saline tween (TBST) (500mls ultra-filtered water, 50mls Tris-buffered saline (TBS) [10x], 500µL Tween 20). All secondary antibodies were IRDye 700CW and 800CW (LI-COR Ltd), diluted 1:10000 in 5% milk, and incubated for one to two hours at room temperature in the dark. Blots were imaged for two minutes using the LI-COR Odyssey FC imager according to the manufacturer's instructions. Image-studio lite (LI-COR) was used for graphic display of blots. All primary anti-bodies and conditions used for western blot are listed in Table 4.

2.2.3.2 Proteomic Abundance

Proteomic abundance for the panel of OS tumour cell lines and isogenic *RB1* deficient U2OS models generated by CRISPR-Cas9 mutagenesis was performed in collaboration with Colm Ryan (Systems Biology Ireland, University College Dublin, Ireland). Cells were washed twice with cold PBS to remove all traces of serum proteins, and then air-dried by tilting plate on ice for 30 seconds to remove the PBS. Cell lysis was performed using a

lysis buffer (2.1.1), and transferred into eppendorfs. Following lysis, protein purification, and tryptic digest, peptides were separated by liquid chromatography and measured by mass spectrometer as described in Ryan *et al.* (Ryan, Kennedy, Bajrami, *et al.*, 2017). Label-free proteome quantification was performed using the MaxQuant software environment (Coscia, Watters, Curtis, *et al.*, 2016; Cox, Hein, Luber, *et al.*, 2014) to determine the quantitative abundance of 6696 peptides with a false discovery rate of less than one percent.

2.2.4 DNA analysis

2.2.4.1 Extraction of genomic DNA from cell lines

Extraction of the DNA from cell lines was performed using the DNeasy Kit (Qiagen Ltd), according to the manufacturer's recommendations and stored at -20˚Celcius.

2.2.4.2 Spectrophotometric quantification of DNA

The concentration of DNA was determined by measuring the UV absorbance at 260nm of diluted samples on a spectrophotometer.

2.2.4.3 Sanger sequencing

The DNeasy Kit (Qiagen Ltd.) was used to extract DNA from cell lines according to the manufacturer's recommendations. Sanger sequencing was performed by Eurofins Genomics, Germany, using standard methods and RB1 primers.

2.2.4.4 Polymerase Chain Reaction (PCR)

Sequencing primers were synthesised by Integrated DNA technologies and purchased as lyophilised powder, which was resuspended in DEPC-treated H_2) (Ambion) to a concentration of 100μM and stocks stored at -20˚C. Prior to use in PCR reactions, the stock primers were further diluted to 10μM. PCR products were approximately 330 base pairs in length. PCR reactions were performed in 50 or 100μl volumes using Q5® High-Fidelity DNA Polymerase (New England Biolabs) and purified using the QUIquick PCR purification kit (Qiagen Ltd.). The following RB1 primers were used:

RB1 1D forwards: 5' – CCGCGGAAAGGCGTCAT – 3'
RB1 1D reverse: 3' – GAACCCAGAATCCTGTCACCA – 5'

The following PCR conditions were used on a thermocycler:

1. 94˚C three minutes
2. 94˚C one minute (melting)
3. 57.5˚C two minutes (annealing)
4. 72˚C one minute (elongation)
5. go to step two for 29 cycles
6. 72˚C three minutes
7. 4˚C for ever

Agarose gel electrophoresis was used to separate the PCR products. Agarose gels were made as follows: 1.5% ultra-pure agarose (Life Technologies) dissolved in 1xTAE butter + 1/10,000 GelRed nucleic acid stain (Biotum). Hyperladder 1 (Bioline) was used to estimate the length of PCR products. DNA was visualised using an ultraviolet trans-illuminator (Syngene).

2.2.4.5 Generation of CRISPR-Cas9 induced mutant clones

RB1 encodes for a phosphoprotein 928 amino acids in length comprised of 27 exons. Two CRISPR guides (CrAA4 and CrAA5), were designed by Professor Alan Ashworth, both of which targeted a different 21 base pair region in Exon 1 of *RB1* (Table 6). To amplify Exon 1 of RB1 by PCR, a pair of oligonucleotides flanking Exon 1 of *RB1*, was designed (Table 7).

U2OS cells were reverse transfected with the Cas9 plasmid, tracer RNA, and guide RNA and controls were transfected with the Cas9 plasmid alone. Transfection efficiency was confirmed at 24-48 hours, by presence of green luminescence in a cohort of cells treated with GFP. At 72 hours cells were selected in blastocydin (10µg/µl) and plated at a low density (5000 cells per 15cm dish in 25mls of media). Once colonies were established, 100 clones were picked and expanded. Sixteen of the fastest growing clones were picked, and pelleted for genomic DNA (gDNA). The Gentra Puregene cell kit (Qiagen Ltd.) was used to prepare DNA according the manufacturer's instructions.

To efficiently screen for mutations generated by CRISPR-Ca9 mutagenesis in the selected clones, the Surveyor assay (Integrated DNA technologies) was used. Firstly PCR amplification of Exon 1 of *RB1* was performed for each of the selected clones, and PCR product confirmed on a TAE 1.5% agarose gel (Figure 5).

The remaining PCR product for each clone was quantified, and then mixed in equal quantities with the Cas9 control (U2OS cells reverse transfected with Cas9 alone). The Surveyor assay kit (Integrated DNA technologies), an enzyme mismatch cleavage assay, was followed according to manufacture's instructions and a known mutant was used as a positive control. The Surveyor nuclease recognised and cleaved mismatches due to the presence of single nucleotide polymorphisms (SNPs), or small indels. The subsequent product was then confirmed on a further TAE 1.5% agarose gel and the presence of multiple bands used to confirm the existence of mutants (Figure 6). The 1kb Hyperladder I (BioLine) which contained 14 bands from 200bp to 10,037bp, was used as a size marker.

2.2.4.6 Topo Cloning

To amplify as many alleles of Exon one of *RB1* as possibe, each CRISRP-Cas9 generated mutant clone was subcloned. Competent *Escherichia coli* cells were used to subclone cleaned PCR product from each clone. Vector sample was prepared using the Topo TA cloning kit (Invitrogen) according to the manufacturer's instructions. Topovector (1µl), sodium chloride (1µl), DEPC treated water (2.3µl) and cleaned PCR product (2µl) from each clone were mixed and incubated at room temperature for 20 minutes. 1µl of vector sample was added to 40µl of competent *E.coli* and incubated on ice for 30 minutes. This was then heat shocked at 42˚Celcius for one minute, and incubated on ice for a further two minutes. Next 900µl of warmed L-broth was added and incubated at 37˚Celcius for an hour. Ampicillin selection marker agar plates were pre-warmed at 37˚Celcius and stained with 30µl of B3928 blue-white select screening reagent (Sigma Ltd.) for selection of recombinant bacterial colonies and left to dry for 20 minutes. The *E.coli* cells were centrifuged and re-suspended in 40µl of warmed L-broth and plated out onto the ampicillin selection agar plates and incubated overnight, inverted at 37˚Celcius. Twenty-five white colonies were picked per mutant clone and amplified by miniprep using Quiaprep spin miniprep kit (Quiagen) and cleaned using QUIAquick PCR purification kit (Quiagen) according to the manufacturer's instructions. The amplified *RB1* PCR product

from each clone was then Sanger sequenced by Eurofins Genomics, (Ebersberg, Germany) using Sanger sequencing methodology.

2.2.4.7 Exome sequencing

The OS tumour cell lines LM7, SAOS2, U2OS 4.2, U2OS 4.5, U2OS 9.1 were exome-sequenced by the Tumour Profiling Unit (TPU), ICR. Targeted exome capture was performed using SureSelect Human All Exome v5 reagents (Agilent). Paired-end libraries were prepared from the captured target regions and sequenced on a HiSeq2500 (Illumina) using v4 chemistry acquiring two x 100 bp reads. Bcl2fastq software (v1.8.4, Illumina) was used for converting the raw basecalls to fastqs and to further demultiplex the sequencing data. The paired-end fastq files were used for further analysis.

The OS tumour cell lines SAOS2, 143b, HOS, HOSMNNG, MG63, CAL72, U2OS, KPD, MHM, OHS25, OHSN, SJSA-1/OSA, NY, NOS1, HU09, HU03N1 and G292 Clone A141B1 were whole exome sequenced by the Wellcome Trust Sanger Institute (WTSI) as described by Garnett *et al.* (Garnett, Edelman, Heidorn, *et al.*, 2012). Mutations were considered driver events if they represented canonical changes.

2.2.4.8 Fluorescence in situ hybridisation (FISH)

FISH was performed by Fernanda Amary as described by Amary *et al.* and FGFR1 amplification was classified as positive if ≥10% of the cells showed (a) FGFR1/CEN8 ratio >2, (b) clusters of FGFR1 signals, or (c) >15 copies of FGFR1 per cell (Fernanda Amary, Ye, Berisha, *et al.*, 2014).

2.2.5 RNA manipulation

2.2.5.1 RNA extraction

The RNAeasy kit (Qiagen Ltd.) was used to extract RNA from cell lines according to the manufacturer's instructions, eluted in 50µl water and stored at – 80˚Celcius. Concentration and quality of the RNA was measured using a 2100 Bioanalyzed® platform (Agilent® technologies) and a spectrophotometer.

Table 6 CRISPR guides targeting Exon 1 of *RB1*

CRISPR guide	Guide Sequence 5' – 3'	Region of *RB1* targeted 5' – 3'
CrAA4	GCTCTGGGTCCTCCTCAGGAG TTTTAGAGCTATGCTGTTTTG	GCTCTGGGTCCTCCTCAGGA
CrAA5	GAGGACCCAGAGCAGGACAGG TTTTAGAGCTATGCTGTTTTG	GAGGACCCAGAGCAGGACAG

Table 7 Oligonucleotide primers for a 336 base pair region including Exon 1 of *RB1*

	RB1 1D forwards 5' – 3'	RB1 1D reverse 5' – 3'
Sequence	CCGCGGAAAGGCGTCAT	GAACCCAGAATCCTGTCACCA
Length (base pairs)	17	21
Melting temperature (°C)	58.8	56.8
Optimum temperature (°C)	57.5	57.5

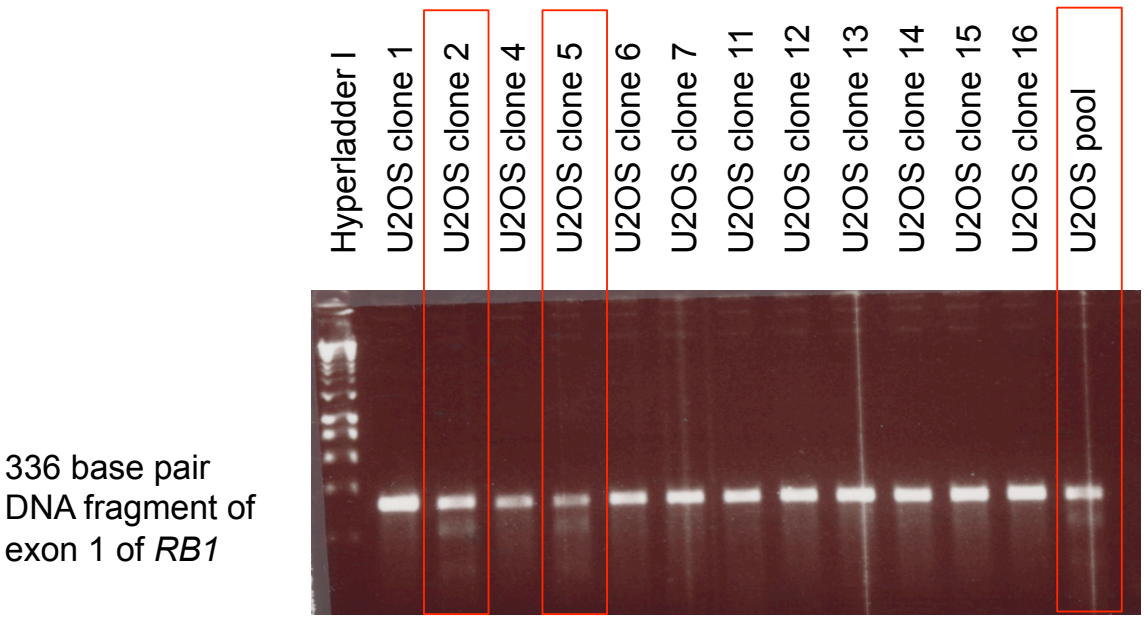

Figure 5 PCR amplification of Exon 1 of *RB1* in 12 U2OS CRISPR-Cas9 transfected clones. The CRISPR crDNA crAA4 was used to generate these clones using the OS tumour cell line U2OS. Individual numbered clones and all clones pooled together were visualised using a 1.5% TAE agarose gel. The RB1 oligonucleotide primers RB1 1D forwards and reverse were used to amplify a 336 base pair fragment shown here. Red boxes highlight clones with multiple band sizes suggesting possible mutations of this amplified region.

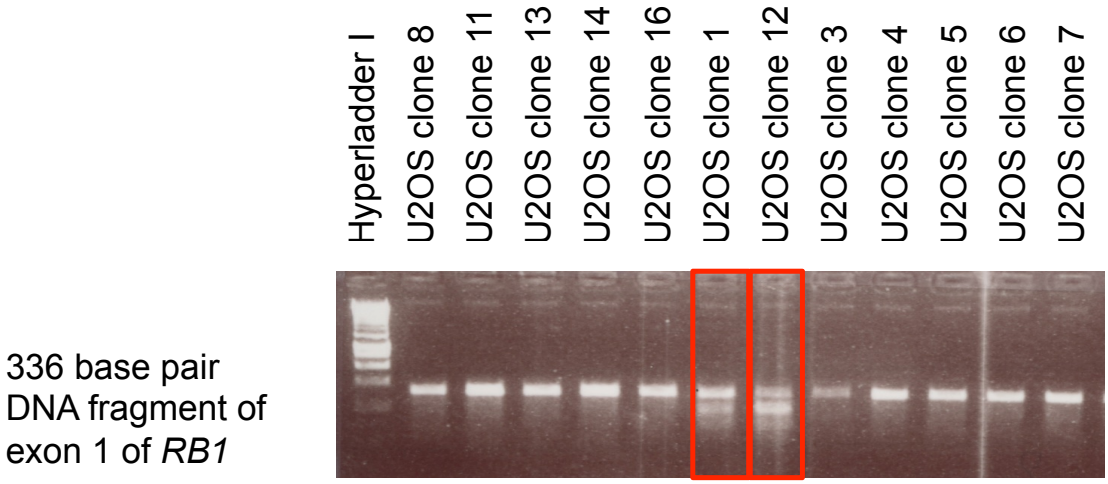

Figure 6 The surveyor assay was used to screen for generation of mutants generated by CRISPR-Cas9 mutagenesis.

A 336 base pair fragment of Exon 1 of *RB1* was amplified by PCR from each U2OS CRISPR-Cas9 transfected clone, and mixed in equal quantities with that from control (U2OS reverse transfected with Cas9 only). The surveyor assay (Integrated DNA technologies), an enzyme mismatch cleavage assay, was used to screen for generation of mutants generated by CRISPR-Cas9 mutagenesis. The surveyor nuclease recognised and cleaved mismatches, which were seen on agarose gel as multiple bands, highlighted here by red boxes. The CRISPR crDNA crAA5 was used to generate the clones using the OS tumour cell line U2OS.

2.2.5.2 Whole transcriptome Sequencing / RNA-seq

Whole transcriptome sequencing was performed by the Tumour Profiling Unit, Institute of Cancer Research. Samples were sequenced and checked for quality. The Ribo-zero kit (Illumina) was used to select the RNA according to the manufacturer's instructions. Strand specific libraries were generated from the RNA using the NEBnext ultra directional RNA library preparation kit (Illumina) as specified by the manufacturer. Paired-end libraries were sequenced on a HiSeq2500 (Illumina) using v4 chemistry acquiring 2X75bp paired-end (PE) reads. Bcl2fastq software (v1.8.4, Illumina) was used for converting the raw basecalls to fastqs and to further demultiplex the sequencing data. The paired-end fastq files were used for further analysis.

2.2.5.3 Real-time PCR (rtPCR)

The Superscript III First Strand Synthesis System for rt-PCR (Invitrogen) using oligo-hexamers according to the manufacturer's instructions was used to prepare cDNA. Quantatitive rtPCR was performed using Taqman Universal mastermix II with UNG (Thermo Fisher) according to the manufacturer's instructions in 96-well optical plates (Applied Biosystems). The following primer/probe sets were purchased from Thermo Fisher: DYRK1A (Hs00176369_m1) and endogenous control GAPDH (Hs03929097_g1). Real-time PCR was performed on the 7900HT HT Fast Real-Time PCR System (Applied Biosystems) according to the manufacturer's instructions. Target gene expression was calculated as expression relative to the expression of control cDNA after adjusting for expression of GAPDH as the endogenous control.

2.2.5.4 RAD51 foci assay

Cells were plated in triplicate at 500,000 cells per well of 6 well plates on sterile coverslips. After 24 hours the tumour cells were irradiated at 10Gray. Four hours post irradiation the cells were fixed using a covering volume of 4% Paraformaldehyde (PFA) in PBS for one hour at room temp and then washed with PBS before staining. Cells were permeabilised using a covering volume of 0.2% Triton X-100 in PBS for 10 minutes at room temp. Next, the coverslips were washed three times with PBS. The coverslips were inverted onto a 50µL drop of DNAse I (Thermo Fisher)(10,000 units/mL stock diluted 1:10 in PBS) for two hours at 37˚C in a humidified container, prior to three washes in PBS. The

coverslips were incubated for 30 minutes at room temperature in a covering volume of IFF (1% BSA, 2% FCS in PBS). The coverslips were inverted onto a 50µl drop of RAD51 primary antibody (Abcam) and phospho-γH2AX Millipore primary antibody diluted 1:1000 in IFF, prior to incubation for one hour at room temperature in an air tight container. The coverslips were washed three times in PBS, prior to inversion onto a 50µl drop of secondary Rabbit 488 and Mouse 555 antibody diluted 1:1000 in IFF, and incubated in the dark for 40 minutes at room temperature. The coverslips were then washed twice with PBS and then once with DAPI (1:10,000 dilution in PBS). Each coverslip was then rinsed in distilled water and blotted dry. To mount, each coverslip was inverted onto a 4ml drop of vector shield (Vector Laboratories) and sealed with nail varnish. The Leica or Ziess confocal microscopes with a 63x objective were used to visualise and score the phospho-γH2AX and RAD51 foci. Cells were scored as positive for foci if they contained at least five or more foci, and at least 100 cells were counted per condition.

2.3 STATISTICAL ANALYSIS

2.3.1 General statistical analysis

Microsoft Excel or GraphPad Prism were used to perform statistical tests except for the median permutation test (MPT) which was performed in R using a custom script. All tests were two-sided unless otherwise stated. The MPT is a random sampling test that calculates the p (probability) value whether or not there is an observed difference between the median Z scores of two groups. One million random samples for the two groups were performed. A False Discovery Rate (FDR), a method for conceptualising the number of False Positive errors was set at 0.1, meaning 10% of significant tests will be false positives. This test accounts for multiple test corrections. The MPT was used to compare non-parametric datasets, while the Student's t-tests used for parametric datasets. Significance was set at $p<0.05$.

2.3.1.1 Drug dose response curves

Survival fractions for each well of a 96 or 384-well plate were calculated as follows: luminescence in drug treated well / luminescence in vehicle (DMSO) treated well. Survival fractions were expressed as a percentage and plotted in GraphPad Prism where a five-parameter logistic equation with preliminary Log-transformation of the data, was

used to draw dose response curves. Comparison of dose-response curves was performed using the two-way ANOVA function in GraphPad Prism for the median effect of each drug compared to a control curve as indicated in the figures. For comparison of repeated measures, the ANOVA and the Bonferroni post hoc test was calculated using GraphPad Prism. The Survival Fraction 50 (SF_{50}), the drug concentration required to elicit a 50% inhibition of the cell population, and the SF_{80} (concentration required to elicit an 80% inhibition of the cell population) were calculated from the dose response curves using GraphPad Prism. The Area Under the Curve (AUC) for each dose response curve was also calculated using GraphPad Prism. Comparison of SF_{50} and AUC was by a two-sided Student's t-test.

2.3.1.2 Viability assessment post-siRNA transfection

Survival fractions for siRNA of interest were generated by dividing the luminescence readings from each well by the median of the negative non-targeting controls (siCON1, siCON2, siAllstar) for each plate:

Surviving fraction = (luminescence in siRNA of interest treated well) / (luminescence in non-targeting siRNA treated wells)

2.3.1.3 Analysis of high-throughput siRNA screen data

Raw luminescence values were first analysed using the CellHTS2 software (BioConductor) (Boutros, Brás & Huber, 2006). The dynamic range of each screen was determined by calculating Z prime values (Zhang, Chung & Oldenburg, 1999), based on positive (siPLK) and negative (siCON1, siCON2 and allstar) control wells in each plate, which were used as a marker of quality. A minimum of two negative controls and one positive control was used for each analysis. Z prime values greater than >0.3 have been shown to be representative of reproducible data (Zhang, Chung & Oldenburg, 1999), and were considered acceptable, with a Z prime 0.5 – 1 demonstrating a robust and powerful screen (Brough, Frankum, Sims, *et al.*, 2011). The Z prime for each screen was calculated using a modified version of the script HTS on the statistical program R:

$$Z\ prime = 1 - 3(\sigma_p + \sigma_n) / (\mu_p - \mu_n)$$

Where σ_p and σ_n refer to the mean of the positive and negative controls respectively, and μ_p and μ_n refer to the standard deviations of the positive and negative controls respectively.

Spearman Rank Correlation determined the reproducibility between the replicates and was calculated as follows using Microsoft Excel:

$$\text{Spearman's Rank Correlation} = 1 - 6\,\Sigma D^2 / n(n^2-1)$$

Where n refers to the number of wells, and D is the difference between rank order of size of the two replicates. A cut off of Spearman's Rank Correlation co-efficient was set at >0.7.

To account for the plate-to-plate variation common in high-throughput screens, raw luminescence readings from each well were log transformed, centred by the plate median and standardised using a Z score, calculated as follows:

$$Z = (x\text{-median screen}) / \text{median absolute deviation}$$

Where x represents the plate centred $\log_2$ luminescence value, median screen represents the median luminescence value for all the siRNAs in the screen, and the median absolute deviation (MAD) the standard deviation of all the siRNAs (Brough, Frankum, Sims, *et al.*, 2011; Boutros, Brás & Huber, 2006). The distribution of each screen was assumed to approximate to normal, allowing comparison of the individual siRNA effects across cell lines. A Z score of zero represented no change in viability, while a negative Z score represented loss of viability (Brough, Frankum, Sims, *et al.*, 2011).

Quantile normalisation of the Z scores was performed by James Campbell using the preProcessCore package (Bioconductor). This method (originally described by Bolstad *et al.* (Bolstad, Irizarry, Astrand, *et al.*, 2003)) adjusts the distribution of z-scores for each cell line so as to make each of them identical whilst maintaining the approximate magnitude of the original z-scores. The principle of quantile normalisation is to first rank order (sort) z-scores for each cell line, average the values across each rank and then return the averaged values to the original order.

As a graphical measure of similarity between two groups of cell lines, heatmaps were generated by comparison of QN Z scores of each group by the median difference permutation test, using an in-house R script at the ICR. To identify genetic dependencies associated with a particular subtype of cell line, the cell lines were divided into two conditions, for example loss of function of *RB1,* and wildtype *RB1*. Both the median difference permutation test using an in-house R script at the ICR and the student's T test were used to calculate the probability of the difference between the QN Z scores of each group.

2.3.1.4 High-throughput siRNA screen with olaparib and calculation of Drug Effect

The effect of each siRNA on olaparib sensitivity was determined by calculation of a drug effect (DE) score for each siRNA. DE scores were calculated by the difference between the median of replicate wells with drug and median of replicate corresponding wells with no drug for each siRNA. The median absolute deviation (MAD) was used to account for variance of the DE data. The DE was calculated as follows:

DE of siRNA = (drug effect of each siRNA – median drug effect of all siRNA) / standard deviation of DE values for all siRNA in the screen

Negative DE scores suggested the siRNA increased sensitivity to olaparib, while positive DE suggested increased resistance. DE scores of -2 < or > 2 were considered significant for sensitising and resistance causing effects. The Delta Drug Effect was calculated as the difference between the DE for each tumour cell line.

2.3.1.5 Drug Screen Analysis

The quality of the data was examined using Z prime (Zhang, Chung & Oldenburg, 1999), based on positive (puromycin-treated) and negative (DMSO-treated) control wells in each plate to determine the dynamic range of the screen. Spearman's Rank Correlation was performed to determine the reproducibility between the plates and was calculated on Excel for the 3 combinations of pairs of replicates for each of the drug plates.

Spearman's Rank Correlation = $1 - 6 \Sigma D^2 / n(n^2-1)$

Where n refers to the number of wells, and D is the difference between rank order of size of the 2 replicates. Stringent quality control with Spearman's Rank correlation approaching 1 and Z prime >0.7 were set (Iorns, Lord, Grigoriadis, *et al.*, 2009).

2.3.1.6 Exome sequencing

Exome sequencing analysis for the cell lines LM7, SAOS2, U2OS 4.2, U2OS 4.5, and U2OS 9.1 sequenced by the TPU was performed by James Campbell, ICR, according to the following steps: Burrow Wheeler Aligner (BWA)-mem (v0.7.5a) (University of Birmingham), was used to align reads to the human reference genome (GRCh37). PCR duplicates were removed prior to further processing and variant detection. Variant calling was done using GATK Broad Best Practice pipeline V3 (Broad Institute), with standard settings. Variants called in regions not covered by the capture probes were excluded, as were those with genotype qualities below 20 and those covered by fewer than 10 reads in either sample.

Somatic single nucleotide variants (SNV) were identified using MuTect (v1.1.4) (Broad Institute). Short insertion/deletion (indel) mutations were selected from the complete set of variants called using the GATK HaplotypeCaller (Broad Institute) based on differences in the variant allele fractions observed in the tumour and normal exome sequence data. Indel variants were considered to be candidate somatic mutations where the variant was detected at less than 5% in the normal sample and greater than 15% in the tumour sample. Additionally, indel variants detected when the depth of coverage in either sample was less than 10 reads were rejected. All mutations were annotated using the SnpEff (v3.3h) (Source Forge), (Cingolani, Platts, Wang, *et al.*, 2012) which provided information on genes affected by mutations and the likely consequences for the encoded gene products. Analysis was performed using CNVkit software tool (v0.7.8) (Talevich, Shain, Botton, *et al.*, 2016). For this, the exome-sequencing data on blood samples from nine patients sequenced by Irene Chong, ICR, was used as normal samples. The copy number scores were represented as log2 ratio of the read depths of each tumour and nine pooled normal samples. The differences in Copy Number Variants (CNVs) between the two tumour cell line models (LM7 and SAOS2) were Z-normalized to determine the distribution of CNVs. Further analyses for detection of LOH regions and data visualization were performed using R programming.

2.3.1.7 Analysis of RNA-seq data

The Tophat2 spliced alignment software (v2.0.7) was used to align reads to the reference genome (GRCH37) in combination with Bowtie2 (v2.1.0). Once the reads were aligned, HTSeq-count (HTSeq v0.6.1) was used to count the number of reads mapping unambiguously to genomic features in each sample. Differential expression analysis of the count data was performed by James Campbell and Aditi Gulati, from the ICR, in R using the Bioconductor package, DESeq2 (v1.14.1). The package used negative binomial generalized linear models to test for differential expression. The results were reported as log2 fold changes in expression along with associated p-values and adjusted p-values. The results were visualized as MA plots using the inbuilt plotting function of the package.

3 Characterisation of tumour cell lines

3.1 INTRODUCTION

My primary aim was to identify therapeutic vulnerabilities in osteosarcoma via a series of parallel high-throughput genetic and chemical screens. To do this I first collated and characterised a panel of osteosarcoma tumour cell lines that were representative of the histological subtypes of OS. Completion of exome sequencing and characterisation of the remaining tumour cell line models was performed to assess whether these reflected the mutational spectrum of the disease, and confirm a clinically relevant model for investigation of recurrent driver mutations in OS.

To identify the presence or absence of cancer driver gene defects in osteosarcoma, a large panel of 18 OS tumour cell lines was assembled. These were molecularly profiled to detect pathogenic mutations and then classified into groups; those with a pathogenic mutation in an oncogene or tumour suppressor (deficient) and those without (wildtype). This enabled a 'class analysis' by comparison of deficient and wildtype phenotypes for specific driver genes. The phenotype of the 'wildtype' cohort was used as a surrogate to estimate the effect of target inhibition in a non-tumour cell, in an attempt to minimise the risk of identification of targets that would also impair essential processes in normal cells. This 'class analysis' approach is limited by potential cancer-specific alterations in the 'wildtype' group that phenocopy the cancer driver gene defect seen in the 'deficient' group. For example while defects in *TP53* are proposed to be tumourigenic, disruption of apoptosis downstream of TP53, phenocopies TP53 loss with respect to its impact on tumour onset and dissemination (Schmitt, Fridman, Yang, *et al.*, 2002). The presence of these phenocopy effects, whether they are well described at the molecular level or not ('cryptic phenocopies'), most likely impair the power of any class analysis that makes the assumption that the "wild type" cohort of tumour cells lines has a relatively minor proportion of phenocopies.

Therefore characterisation of the panel of tumour cell lines by exome sequencing, mRNA expression, copy number profiling, protein expression by western blotting, and proteomic profiling was performed in order to classify the panel according to *RB1* status. This enabled classification of the panel into 'deficient' and 'wildtype' *RB1* groups, enabling class analyses to be performed to identify candidate genetic dependencies in the presence of deficient *RB1*. To identify the genetic and therapeutic dependencies of the

panel of osteosarcoma tumour cell lines thought to be representative of the disease, parallel high-throughput siRNA screens and drug screens were performed. Integration of the screen data and molecular characterisation was performed to identify the genetic vulnerabilities and drug dependencies associated with driver alterations in osteosarcoma, and any possible tractable targets (Figure 7).

This panel of OS tumour cell lines was further comprised of both non-isogenic and isogenic models (HOS and SAOS2), which have inherent advantages and disadvantages. Isogenic models all derive from a single progenitor cell line, whereby a specific genetic deficiency is engineered in daughter cells by genetic manipulation. This results in a minimal number of genetic differences between the daughter and parental cell lines, so that any observed differences are likely to be due to the gene of interest (Rehman, Lord & Ashworth, 2010). However, the limitation of an isogenic system is that any candidate genetic dependency identified has the potential to be context specific to the cell line, preventing extrapolation to a wider panel of tumour cell lines or clinical samples, and can be readily rescued by alterations in other genes (Ashworth, Lord & Reis-Filho, 2011). While non-isogenic models may more closely represent the tumour heterogeneity observed in the clinical setting, the observations seen may be due to mutations in genes other than the gene of interest, and thus make interpretation more challenging (Rehman, Lord & Ashworth, 2010). Therefore, both isogenic and non-isogenic OS tumour cell line models were used to investigate for candidate genetic dependencies. Any synthetic lethalities identified in a panel of tumour cell lines, are more likely a 'hard' synthetic lethality, relatively unaffected by changes in additional genes (Rehman, Lord & Ashworth, 2010). Therefore an ideal approach would be to use the isogenic model for discovery of candidate genetic dependencies, which could then be validated to confirm clinical relevance using a panel of tumour cell lines.

At the beginning of this thesis, a number of OS tumour cell lines were in the process of characterisation by the Wellcome Trust Sanger Institute. However, no human isogenic models of loss of *RB1*, or *CDKN2A* in osteosarcoma had been described. Therefore, the panel of tumour cell lines was used to perform genetic perturbation and drug screens in osteosarcoma, while isogenic models (*RB1* deficient and wildtype U2OS tumour cell lines created by CRISPR-Cas9 mutagenesis described in the next chapter) were used to assess candidate synthetic lethalities from the screen.

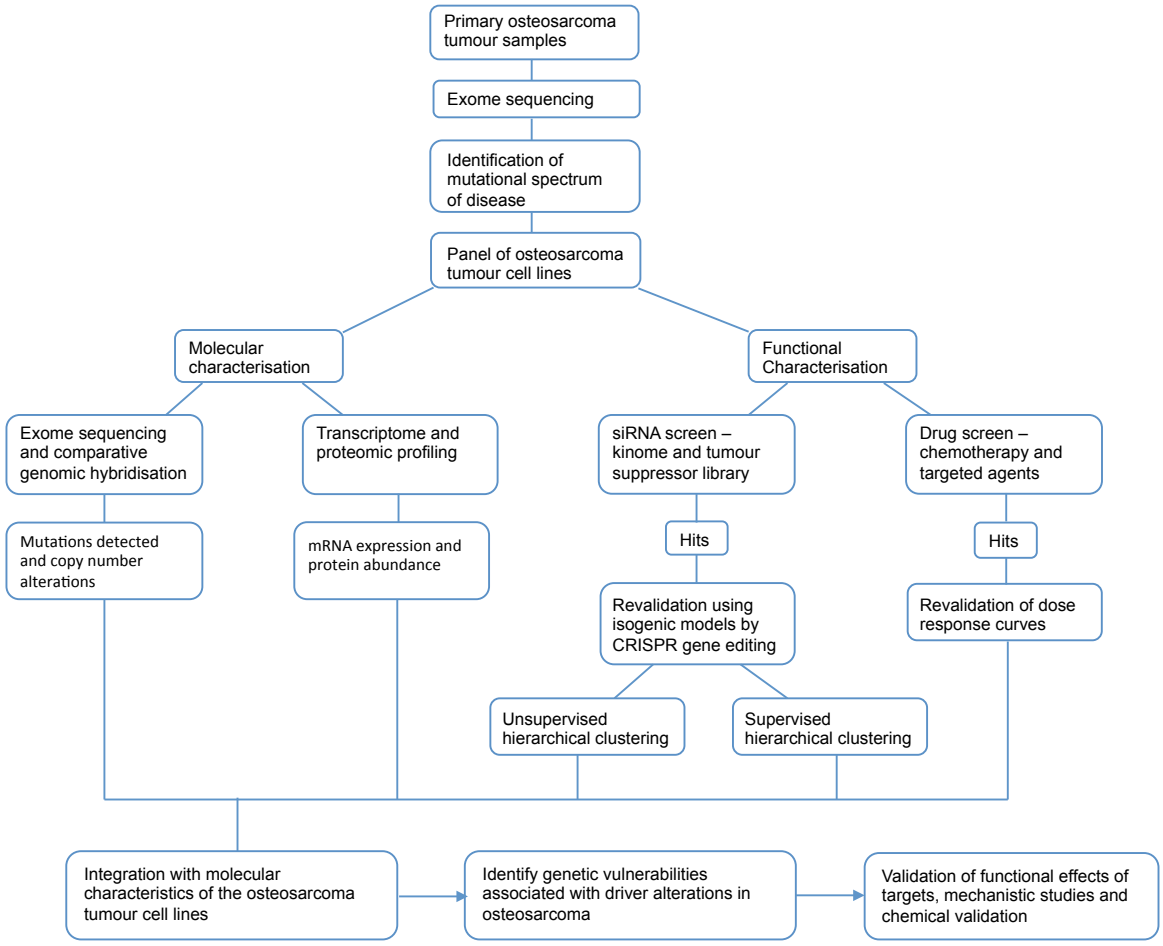

Figure 7 Project Overview – Framework for Identification of novel therapeutic dependencies in osteosarcoma.

Characterisation by parallel siRNA and drug screens was performed to identify candidate genetic dependencies ('hits'). The molecular characterisation of the tumour cells lines was integrated with the candidate genetic dependencies generated from the screens, and used to perform 'class analyses' to identify genetic vulnerabilities associated with driver alterations in osteosarcoma such as *RB1* status, prior to validation and mechanistic studies.

3.2 RESULTS

3.2.1 Characterisation of the panel of osteosarcoma tumour cell line models

A panel of 18 non-isogenic OS tumour cell lines, representing histological subtypes of OS was profiled (Table 8). Molecular profiling some of the lines (MG63, MHM, HOSMMNG, 143B, OSA/SJSA-1, U2OS, SAOS2, OHS, KPD, and HAL) was performed (DNA copy number, DNA methylation status of ~27,000 CpG sites, and global mRNA expression data) by the EuroBoNeT, a European Network of Excellence on bone tumours (http://www.eurobonet.eu) (Ottaviano, Schaefer, Gajewski, *et al.*, 2010). Further characterisation including exome sequencing and RNAseq on the remaining tumour cell lines (NY, HU03N1, HU09, HOS, G292 clone A141B1, NOS-1, CAL72, and LM7) was undertaken by Ultan McDermott, Wellcome Trust, Sanger Institute. Thirteen of these tumour cell lines are capable of tumour formation in mice (Lauvrak, Munthe, Kresse, *et al.*, 2013) (Table 8), and have been shown to have similar mRNA profiles to tumour samples (Kresse, Rydbeck, Skårn, *et al.*, 2012). The tumour cell lines were also profiled for the TP53 and CDKN2A status (Table 9).

3.2.2 Exome Sequencing

To assess whether the mutations found amongst the OS tumour cell line panel included candidate driver mutations found in clinical OS, these osteosarcoma models were compared to the known mutation profiles of OS tumours. Seventeen of the osteosarcoma tumour cell lines have been exome sequenced in collaboration with the Wellcome Trust Sanger Institute (information kindly provided by Dr Ultan McDermott). LM7 and SAOS2 underwent exome sequencing at the Tumour Profiling Unit at the Institute of Cancer Research, London.

Table 8: Origin and growth characteristics of osteosarcoma tumour cell lines

Subtype	**Cell Lines**	**Age (years) and sex of patient from whom the tumour originates**	**Tumorigenic potential in mouse model**	**Metastatic potential in mouse models**	**Note**	**Source**
Osteoblastic	CAL72	10 Male	Yes (Lauvrak, Munthe, Kresse, *et al.*, 2013)	N/A		COSMIC* German Collection of Microorganisms and Cell Cultures
	NOS-1	16 Male	N/A			COSMIC* Cell Bank, RIKEN BioResource Centre, Japan
	HAL	15 Male	Yes (Lauvrak, Munthe, Kresse, *et al.*, 2013) No (Mohseny, Machado, Cai, *et al.*, 2011)	N/A		(Kresse, Rydbeck, Skårn, *et al.*, 2012)
	HU09	unknown	N/A			COSMIC*
	OHS	14 Male	Yes (Lauvrak, Munthe, Kresse, *et al.*, 2013; Mohseny, Machado, Cai, *et al.*, 2011)	No (Mohseny, Machado, Cai, *et al.*, 2011)	Bilateral retinoblastoma and multiple lesions of OS at presentation	(Fodstad, Brøgger, Bruland, *et al.*, 1986)
Chondroblastic	KPD	7 Female	Yes (Lauvrak, Munthe, Kresse, *et al.*, 2013) No (Mohseny, Machado, Cai, *et al.*, 2011)	No (Mohseny, Machado, Cai, *et al.*, 2011)		(Bruland, Fodstad, Stenwig, *et al.*, 1988)
	MHM	41 Female	Yes (Lauvrak, Munthe, Kresse, *et al.*, 2013; Mohseny, Machado, Cai, *et al.*, 2011)	No (Mohseny, Machado, Cai, *et al.*, 2011)	Fibroblastic or metastaisis from parosteal OS lesion	(Kjønniksen, Winderen, Bruland, *et al.*, 1994)
Osteoblastic / Telangectatic	G292 clone A141B1	9 Female	Yes (Lauvrak, Munthe, Kresse, *et al.*, 2013)	N/A		ATCC CRL-1423

Fibroblastic	OSA/SJSA-1	19 Male	Yes (Lauvrak, Munthe, Kresse, *et al.*, 2013; Mohseny, Machado, Cai, *et al.*, 2011)	No (Mohseny, Machado, Cai, *et al.*, 2011)		ATCC CRL-2098
	MG63	14 Male	Yes (Lauvrak, Munthe, Kresse, *et al.*, 2013) No (Mohseny, Machado, Cai, *et al.*, 2011)	No (Mohseny, Machado, Cai, *et al.*, 2011)		ATCC CRL-1427
	LM7		N/A		Created from lung metastases of SAOS2 passaged through a mouse model (Jia, Worth & Kleinerman, 1999)	
	HOS	13 Female	Yes (Lauvrak, Munthe, Kresse, *et al.*, 2013) No (Mohseny, Machado, Cai, *et al.*, 2011)	No (Dass, Ek, Contreras, *et al.*, 2006)		ATCC CRL-1543
Epithelial	143B	13 Female	Yes (Lauvrak, Munthe, Kresse, *et al.*, 2013; Mohseny, Machado, Cai, *et al.*, 2011)	Yes (Dass, Ek, Contreras, *et al.*, 2006; Mohseny, Machado, Cai, *et al.*, 2011)	Dervied from HOS	ATCC CRL-8303
	HOSMNNG	13 Female	Yes (Lauvrak, Munthe, Kresse, *et al.*, 2013; Mohseny, Machado, Cai, *et al.*, 2011)	Yes (Lauvrak, Munthe, Kresse, *et al.*, 2013) No (Mohseny, Machado, Cai, *et al.*, 2011)	Derived from HOS	ATCC CRL-547
	SAOS2	11 Female	Yes (Lauvrak, Munthe, Kresse, *et al.*, 2013) No (Mohseny, Machado, Cai, *et al.*, 2011)	Yes (Dass, Ek, Contreras, *et al.*, 2006)		ATCC HTB-85

Mixed	U2OS	15 Female	Yes (Lauvrak, Munthe, Kresse, *et al.*, 2013; Mohseny, Machado, Cai, *et al.*, 2011)	No (Mohseny, Machado, Cai, *et al.*, 2011)		ATCC HTB-96
Unknown	HUO3N1	15 Female	N/A			COSMIC* Health Science Research Resources Bank, Japan
	NY	unknown	N/A			COSMIC* Health Science Research Resources Bank, Japan

*COSMIC: Catalogue of somatic mutations in cancer

http://cancer.sanger.ac.uk/cancergenome/projects/cosmic/

N/A: not all tumour cell lines have been studied for their tumourigenic potential

Table 9: Further characterisation of OS tumour cell lines in the EuroBoNet Consortium

Adapted from Ottaviano *et al*. (Ottaviano, Schaefer, Gajewski, et al., 2010)

Tumour Cell Line	***CDKN2A**** (Ottaviano, Schaefer, Gajewski, *et al.*, 2010)	**aCGH of *CDKN2A*** (Ottaviano, Schaefer, Gajewski, *et al.*, 2010)	**Mutation status of *TP53*** (Ottaviano, Schaefer, Gajewski, *et al.*, 2010)
HAL	Diploid	Diploid	Wildtype
HOS	Homozygous deletion	Homozygous loss	p.Arg156Pro
143b	Homozygous deletion	Homozygous loss	p.Arg156Pro
HOSMNNG	Homozygous deletion	Homozygous loss	p.Arg156Pro
KPD	Diploid	Hemizygous loss	Wildtype
MG63	Homozygous deletion	Homozygous loss	Wildtype
MHM	Hemizygous deletion	Diploid	Wildtype
OHS	Diploid	Gain	p.Glu286Lys
OSA / SJSA1	Hemizygous deletion	Hemizygous loss	Wildtype
SAOS2	Diploid	Diploid	del2>EX4-EX8
U2OS	Hemizygous deletion	Diploid	Wildtype

**CDKN2A* homozygous deletion by muliplex ligation-dependent probe amplification (MLPA)(Ottaviano, Schaefer, Gajewski, *et al.*, 2010)

Of the 17 OS tumour cell lines sequenced and analysed by the Sanger Institute, there were 11864 exonic mutations were identified, with 3606 classified as insertions, deletions or complex. The most recurrent mutations are shown in Table 10, and the details of mutations seen in two or more tumour cell lines shown in Table 11.

Five tumour cell lines had mutations in RB1 (HU09, HU03N1, NY, OHS and SAOS2), five had mutations in CDKN2A (CAL72, HOS, HOSMNNG, 143b and MG63) and seven had mutations in TP53 (HOS, 143b, HOSMNNG, HU03N1, NOS-1, OHS and SAOS2). LM7 (daughter of SAOS2) was confirmed to have 95 private mutations (8 stopgain, 4 splicesite, 3 frameshift, and 80 missense), not shared with SAOS2. Conversely, across the entire exome SAOS2 only had 27 private mutations (1 splicesite, 3 frameshift, and 23 missense) not seen in LM7. Genetic alterations, (homozygous deletions, genomic amplification, essential splice, and indels) for each tumour cell line were diverse with few recurrent alterations observed.

3.2.3 Categorisation of RB1 and p16 (CDKN2A) by molecular profiling, mRNA expression, western blotting and proteomic profiling for the panel of non-isogenic osteosarcoma tumour cell lines

Mutations in *RB1* and *CDKN2A* are amongst the most common known recurrent mutational events in sporadic osteosarcoma (Gorlick, Anderson, Andrulis, *et al.*, 2003). Loss of function of RB1 is reported in many cancer types (Knudsen & Wang, 2010). Furthermore, germ-line mutations of *RB1* have been associated with occurrence of osteosarcoma, while structural alterations and point mutations of the *RB1* gene have been reported in up to 40% of sporadic cases (Araki, Uchida, Kimura, *et al.*, 1991). Furthermore, in patients with OS, inhibition of the RB pathway has been associated with poorer prognosis, reduction in chemo-sensitivity and increased risk of metastasis (Ren & Gu, 2015). Thus genetic dependencies associated with loss of function of *RB1* and *CDKN2A* are worthy of further investigation. One objective was to identify synthetic lethal effects associated with *RB1* or *CDKN2A* dysfunction. This necessitated clustering of the tumour cell lines according to wildtype and ‘deficient’ status for both RB1 and p16. Therefore, to augment the genomic profiling I used mRNA expression data, and western blotting to assess protein expression, and proteomic abundance of RB1 and p16 (*CDKN2A*).

Table 10 Perturbation grid of recurrent alterations identified by the Sanger Institute in a panel of 17 OS tumour cell lines

[blue; missense variant/insertion/deletion; red: homozygous deletion; green: amplification]

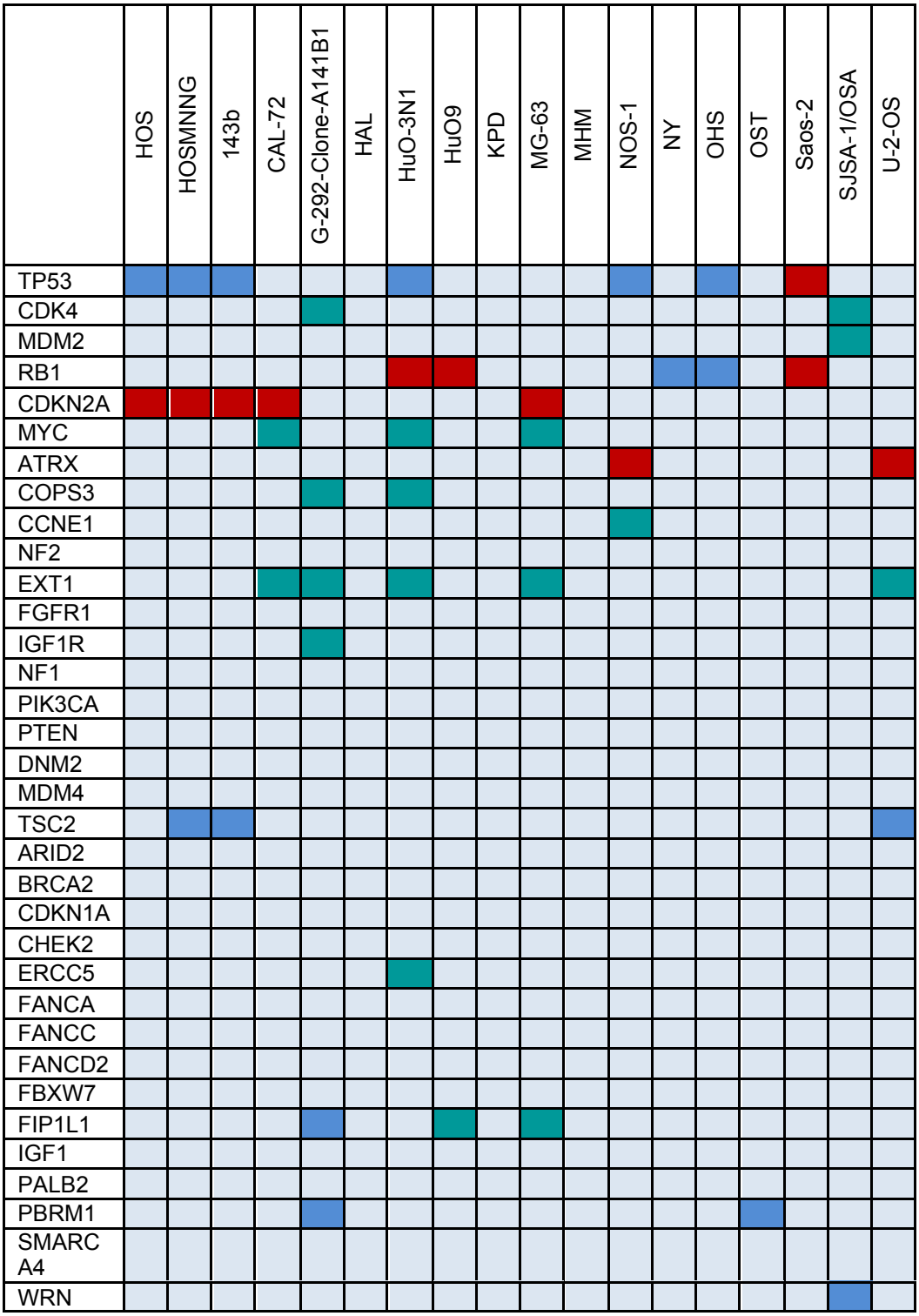

Table 11 Recurrent mutations identified in two or more of the OS tumour cell line panel by the Sanger Institute.

Homozygous mutations are highlighted in red. [TCL: tumour cell line panel]

OS TCL	*TP53*	*RB1*	*CDKN2A*	*ATRX*	*TSC2*	*PBRM1*
HOS	c.467G>C		Homozygous deletion			
HOSMNNG	c.467G>C		Homozygous deletion		c.5116C>T	
143B	c.467G>C		Homozygous deletion		c.5116C>T	
CAL72			Homozygous deletion			
G292 clone A141B1						c.4636+5_ 4636+6insGAG
HAL						
HU03N1	c.225_226insT	Homozygous deletion				
HU09		Homozygous deletion				
KPD						
MG63			Homozygous deletion			
MHM						
NOS-1	c.818G>A			Homozygous deletion		
NY		c.2107-4C>G				
OHS	c.856G>A	c.1183C>T				
OST						c.3204_3205 insCCTCTGTA
SAOS2	Homozygous deletion	Homozygous deletion				
SJSA1/OSA						
U2OS				Homozygous deletion	c.5051_5068 +16del34 c.3430G>A	

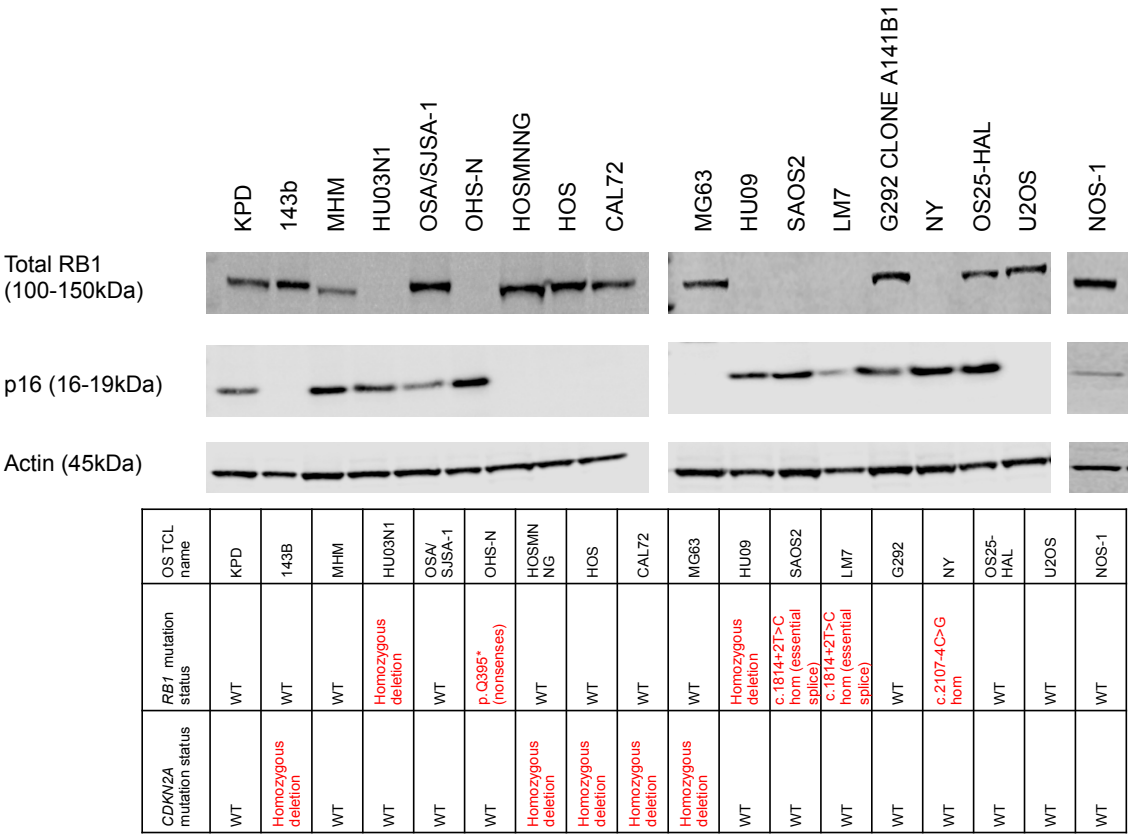

OS TCL name	KPD	143B	MHM	HU03N1	OSA/ SJSA-1	OHS-N	HOSMN NG	HOS	CAL72	MG63	HU09	SAOS2	LM7	G292	NY	OS25-HAL	U2OS	NOS-1
RB1 mutation status	WT	WT	WT	Homozygous deletion	WT	p.Q395* (nonsenses)	WT	WT	WT	WT	Homozygous deletion	c.1814+2T>C hom (essential splice)	c.1814+2T>C hom (essential splice)	WT	c.2107-4C>G hom	WT	WT	WT
CDKN2A mutation status	WT	Homozygous deletion	WT	WT	WT	WT	Homozygous deletion	Homozygous deletion	Homozygous deletion	Homozygous deletion	WT	WT	WT	WT	WT	WT	WT	WT

Figure 8 Comparison of exome sequencing and protein expression for RB1 and p16/CDKN2A of 18 osteosarcoma tumour cell lines.

Western blot and the mutation status for *RB1* and *CDKN2A* is shown for each tumour cell line. Exome sequencing was performed by the Wellcome Trust Sanger Institute for all OS tumour cell lines except LM7, which was undertaken by the Tumour Profiling Unit at the ICR. Total cell lysates from untreated cells were electrophoresed and immunoblotted as described in the Methods. Immunoblotting of actin was used as the loading control. The mutation status correlated with loss of protein expression for all tumour cell lines except U2OS and NY. NY harbours a homozygous substitution mutation of *RB1* (c.2107-4C>G) of unknown significance, but RB1 expression was not detected by western blotting. No mutations of *CDKN2A* have been reported for U2OS, but p16 expression was not detected by western blotting.

3.2.3.1 Determining expression of RB1 and p16 (CDKN2A) by western blotting

To confirm whether RB1 or CDKN2A mutations identified in OS tumour cell lines caused loss of wildtype protein the presence of RB1 and p16 (CDKN2A) were probed for by western blotting (Figure 8). The mutation status correlated with loss of protein expression for all tumour cell lines except U2OS and NY. NY harbours a homozygous substitution mutation of RB1 (c.2107-4C>G) of unknown significance, but RB1 expression was not detected by western blotting. No mutations of CDKN2A have been reported for U2OS, but p16 expression was not detected by western blotting.

3.2.3.2 Determining mRNA expression and copy number status for *RB1*

To categorise the tumour cell line panel according to RB1 expression, protein expression by western blotting was compared to known mutations of *RB1.* Absent protein expression of RB1 by western blotting in all tumour lines known to harbour non-functional mutations of *RB1* was seen, except for the tumour cell line NY. Wildtype protein expression on western blotting was compared to the known mutational status of the OS tumour panel. Of the tumour cell lines with absent expression of RB1 on western blot, HU031N1 and HU09 were known to have homozygous deletions of *RB1.* OHS-N had a nonsense mutation of *RB1*, while SAOS2 and LM7 had essential splice mutations. NY harboured a homozygous substitution mutation of *RB1* (c.2107-4C>G) of unknown significance, but RB1 expression was not detected by western blotting. Therefore, to identify if the mutation correlated with the loss of wildtype mRNA expression, as further confirmation of the RB1 status, both the copy number and mRNA expression of *RB1* obtained from the Catalogue Of Somatic Mutations In Cancer (COSMIC www.cancer.sanger.ac.uk) (Forbes, Beare, Gunasekaran, *et al.*, 2015) were compared to other tumour lines known to harbour homozygous deletions of *RB1* (HU03N1, HU09, and SAOS2). This demonstrated that NY had a level of expression and copy number of *RB1* comparable to those tumour cell lines and compatible with undetectable levels of protein expression on western blot (Figure 9). Therefore, NY was included in the RB1 deficient group. To confirm these observations, mRNA expression and copy number data from the Cancer Cell Line Encylopedia (CCLE www.broadinstitute.org/ccle) was obtained, but since data was only available for one OS tumour cell line with *RB1* deficiency, comparison was not possible (data not shown).

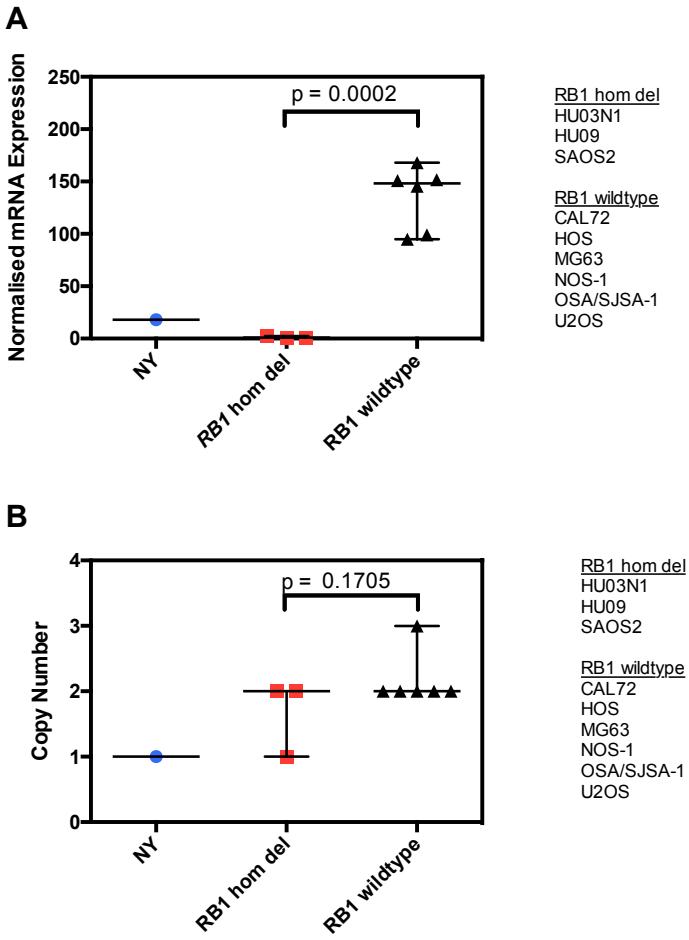

Figure 9 NY exhibited a level of expression and copy number of *RB1* comparable to those OS tumour cell lines with homozygous deletion of *RB1* and undetectable levels of protein on western blotting, and therefore included in the *RB1* deficient group.

NY was determined to have a homozygous substitution mutation of *RB1* (c.2107-4C>G) and absent expression of *RB1* on western blot.

(A) Scatter plot to illustrate expression of *RB1* using normalised mRNA expression data from COSMIC to compare the OS tumour cell lines with known homozygous deletion of *RB1* (HU03N1, HU09, and SAOS2), *RB1* wildtype OS tumour cell lines (CAL72, HOS, MG63, NOS1, OSA/SJSA1 and U2OS) with NY. Tumour cell lines with wildtype *RB1* exhibited significantly greater normalised mRNA *RB1* expression levels than tumour cell lines harbouring homozygous deletion of *RB1* (p = 0.0002).

(B) Scatter plot to illustrate copy number data for *RB1* from COSMIC was used to compare the OS tumour cell lines with known homozygous deletion of *RB1*, wildtype *RB1* and NY.

Median and range shown. P values calculated by Student's t test. [hom del: homozygous deletion; COSMIC: Catalogue of somatic mutations in cancer www.cancer.sanger.ac.uk (Forbes, Beare, Gunasekaran, *et al.*, 2015)]

3.2.3.3 Determining mRNA expression and copy number status for *CDKN2A*

To categorise the tumour cell panel according to expression of p16 (*CDKN2A*), protein expression determined by western blotting was compared to the known mutations of *CDKN2A* in the panel of tumour cell lines. Five cell lines had absent expression of p16 (*CDKN2A*) by western blot, and five of these were known to have homozygous deletions of *CDKN2A* (143b, HOSMNNG, HOS, CAL72 and MG63). Levels of p16 (*CDKN2A*) protein were undetectable for the tumour cell line U2OS by western blotting, despite an absence of reported mutations when profiled by exome sequencing. Therefore, to further characterise the tumour cell line, *CDKN2A* copy number data and mRNA expression data were used for further annotation. Copy number data obtained from COSMIC www.cancer.sanger.ac.uk (Forbes, Beare, Gunasekaran, *et al.*, 2015) confirmed that U2OS had two copies of *CDKN2A* in keeping with the wildtype sequencing (Figure 10). However, when mRNA expression of *CDKN2A* was plotted using data from COSMIC, it was apparent that the level of *CDKN2A* gene expression in U2OS was comparable with that seen in those tumour cell lines that were known to harbour a homozygous deletion (CAL72, HOS and MG63) (Figure 10). These observations were also confirmed using *CDKN2A* mRNA expression and copy number data from the CCLE (Figure 11). U2OS has been previously demonstrated to have undetectable levels of p16 (CDKN2A) on western blot and is used by anti-body manufactures as a negative control. On the basis of these results, U2OS was determined to be *CDKN2A* deficient.

3.2.3.4 Characterisation of RB1 and p16/CDKN2A status by proteomic profiling

In addition to the mRNA expression, protein expression by western blotting, and copy number described above, proteomic profiling undertaken by Colm Ryan, was used as another layer of annotation to further categorise the tumour cell lines into *RB1* and *CDKN2A* deficient or wildtype groups. Following lysis, protein purification, and tryptic digest, peptides were separated by liquid chromatography and measured by mass spectrometer. Label-free proteome quantification was performed using the MaxQuant software environment (Coscia, Watters, Curtis, *et al.*, 2016; Cox, Hein, Luber, *et al.*, 2014) to determine the quantitative abundance of 6696 proteins with a false discovery rate of less than one percent.

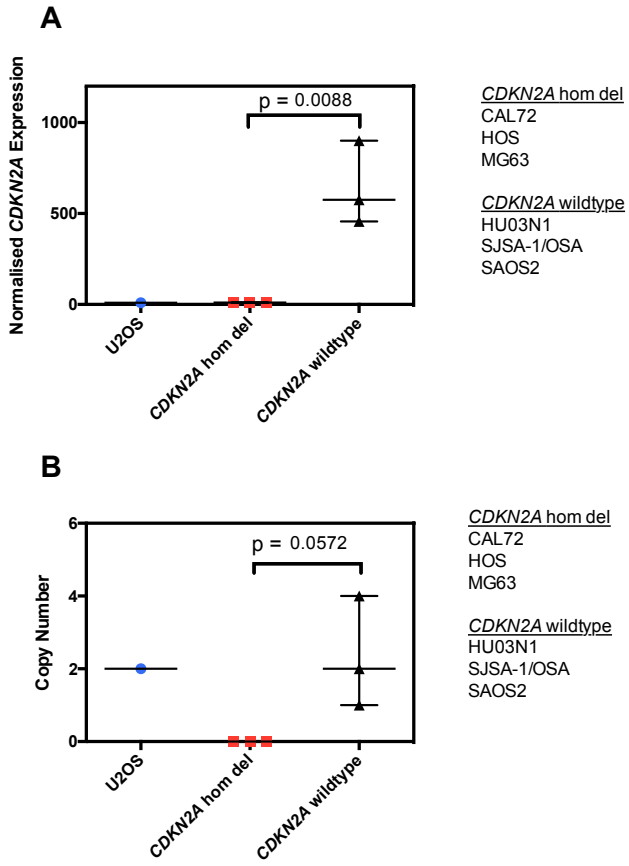

Figure 10 U2OS exhibited a copy number of *CDKN2A* comparable to those OS tumour cell lines with wildtype *CDKN2A,* but normalised mRNA expression levels of *CDKN2A were* undetectable comparable to those tumour cell lines with homozygous deletion of *CDKN2A* and absent expression by western blotting; therefore U2OS was categorised as *CDKN2A* deficient.

Levels of p16 (*CDKN2A*) protein were undetectable for the tumour cell line U2OS by western blotting, despite an absence of reported mutations when profiled by exome sequencing.

(A) Scatter plot to illustrate expression of *CDKN2A* using normalised mRNA expression data from COSMIC to compare the OS tumour cell lines with known homozygous deletion of *CDKN2A* (CAL72, HOS, and MG63), *CDKN2A* wildtype OS tumour cell lines (HU03N1, OSA/SJSA1 and SAOS2) with U2OS. Tumour cell lines with wildtype *CDKN2A* exhibited significantly greater normalised mRNA *CDKN2A* expression levels than tumour cell lines harbouring homozygous deletion of *CDKN2A* (p = 0.0088).

(B) Scatter plot of copy number data for *CDKN2A* from COSMIC to compare the OS tumour cell lines with known homozygous deletion of *CDKN2A*, wildtype *CDKN2A* and U2OS.

Median and range shown. P values calculated by Student's t test. [hom del: homozygous deletion; COSMIC: Catalogue of somatic mutations in cancer www.cancer.sanger.ac.uk (Forbes, Beare, Gunasekaran, *et al.*, 2015)]

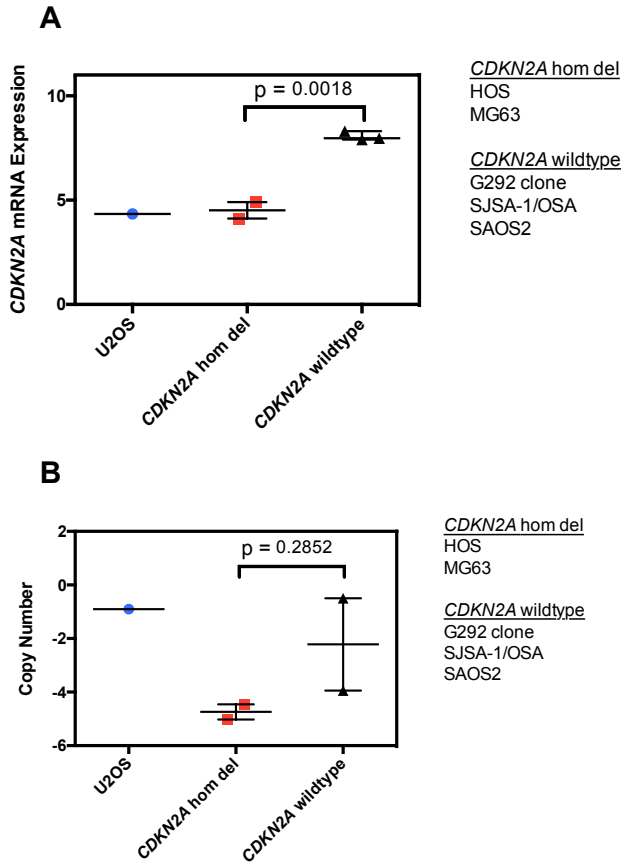

Figure 11 U2OS exhibited a copy number of *CDKN2A* comparable to those OS tumour cell lines with wildtype *CDKN2A,* but mRNA expression levels were comparable with tumour cell lines harbouring homozygous deletion using data from the CCLE, concordant with observations using data from COSMIC.

Levels of p16 (*CDKN2A*) protein were undetectable for the tumour cell line U2OS by western blotting, despite an absence of reported mutations when profiled by exome sequencing.

(A) Scatter plot illustrating expression of *CDKN2A* using normalised mRNA expression data from CCLE to compare the OS tumour cell lines with known homozygous deletion of *CDKN2A* (HOS, and MG63), *CDKN2A* wildtype OS tumour cell lines (G292 clone A141B1 OSA/SJSA1 and SAOS2) with U2OS. Tumour cell lines with wildtype *CDKN2A* exhibited significantly greater normalised mRNA *CDKN2A* expression levels than tumour cell lines harbouring homozygous deletion of *CDKN2A* (p = 0.0018).

(B) Scatter plot illustrating copy number data for *CDKN2A* from COSMIC to compare the OS tumour cell lines with known homozygous deletion of *CDKN2A*, wildtype *CDKN2A* and U2OS.

Median and range shown. P values calculated by Student's t test. [hom del: homozygous deletion; G292 clone: G292 clone A141B1; CCLE: Cancer cell line encylopedia www.broadinstitute.org/ccle]

Proteomic abundance of RB1 for all the OS tumour cell lines including the isogenic *RB1* deficient and wildtype U2OS models engineered by CRISPR-Cas9 mutagenesis, clustered into two groups, concordant with RB1 expression levels observed by western blotting (Figure 12). This provided further confirmation of the classification into *RB1* deficient and wildtype groups (Figure 12). NY had the lowest level of RB1 protein abundance in the panel of tumour cell lines, providing further confirmation that the known mutation in *RB1* leads to loss of expression at the protein level in this tumour cell line.

In addition, proteomic abundance of p16 (CDKN2A) for all the OS tumour cell lines, clustered into two groups, concordant with CDKN2A expression levels observed by western blotting. U2OS clustered with tumour cell lines with known loss of p16 (*CDKN2A*)(Figure 13).

3.2.4 Classification of Osteosarcoma Tumour Cell line panel into RB1 and CDKN2A deficient and wildtype groups

On the basis of the exome sequencing, protein expression as determined by western blotting, mRNA expression data, copy number and proteomic profiling the osteosarcoma tumour cell line panel was classified according to RB1 (Table 12) and CDKN2A (Table 13) status, for the purpose of identification of candidate genetic dependencies for these genetic markers.

3.2.5 TP53 mutation status and protein expression in the panel of non-isogenic osteosarcoma cell lines

A variety of stress signals can activate the p53 pathway, and loss of function of p53 is common feature in cancer (Muller & Vousden, 2014), with as many as 80% OS tumours harbouring a mutation (Chen, Bahrami, Pappo, *et al.*, 2014). It is not possible to determine the protein expression of p53 by *TP53* mutation status alone, since mutations can exert both a dominant-negative regulation over any remaining wildtype p53, or can acquire new oncogenic functions (Muller & Vousden, 2014).

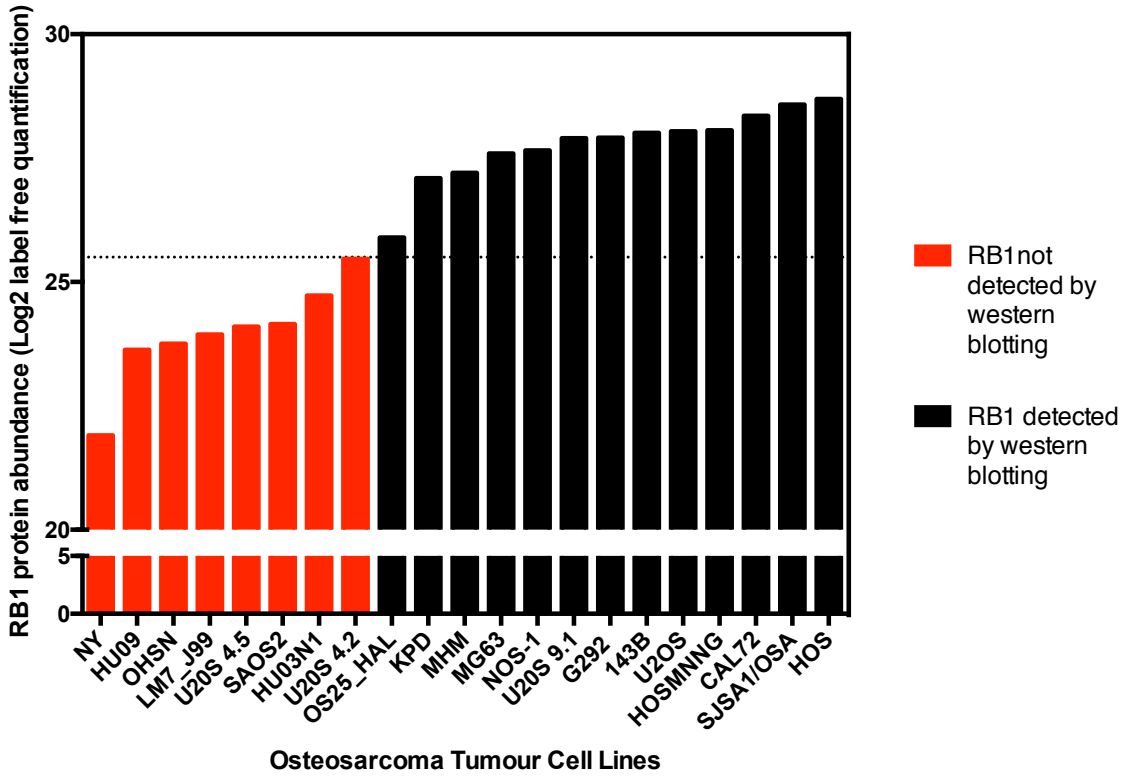

Figure 12 RB1 protein abundance in osteosarcoma tumour cell lines defined by mass spectroscopy proteomic profiling.

Bar chart illustrating protein abundance of RB1 for each OS tumour cell line; red columns indicate tumour cell lines classified as RB1 deficient by western blotting (Figure 8), copy number and mRNA expression levels (Figure 9). Isogenic *RB1* wildtype (U2OS 9.1) and mutant U2OS tumour cell lines (U2OS 4.2 and U2OS 4.5) generated by CRISPR-Cas9 mediated mutagenesis (described in next chapter) are shown as contrasts. Following lysis, protein purification, and tryptic digest, peptides were separated by liquid chromatography and measured by mass spectrometer. Label-free proteome quantification was performed using the MaxQuant software environment (Coscia, Watters, Curtis, *et al.*, 2016; Cox, Hein, Luber, *et al.*, 2014) to determine the quantitative abundance of 6696 peptides with a false discovery rate of less than one percent.

Therefore, in an attempt to determine the protein expression profile of p53 in the panel of OS tumour cell lines, all the OS tumour cell lines were exposed to 1μM doxorubicin for four hours to induce a DNA damage response and p53 expression. Lysates were collected at four and 24 hours post doxorubicin exposure. The protein expression of total p53, phosphorylated p53 (Serine 15) and p21 (downstream of p53) in the panel of OS tumour cell lines was determined by western blotting (Figure 14, Figure 15, Figure 16, Figure 17 and Figure 18).

Western blotting demonstrated that the expression of phosphorylated and total p53 in the presence of DNA damage was disrupted in the majority of OS tumour cell lines, in keeping with that observed in tumour samples (Chen, Bahrami, Pappo, *et al.*, 2014). Inspection of mutation alone was inadequate to determine the functional status of the pathway.

3.2.5.1 Characterisation of TP53 status of OS cells using proteomic expression

To further aid classification of the OS tumour cell line panel with regards p53 status, proteomic profiling was undertaken. Label-free proteome quantification was performed using the MaxQuant software environment (Coscia, Watters, Curtis, *et al.*, 2016; Cox, Hein, Luber, *et al.*, 2014) to determine the quantitative abundance of 6696 peptides with a false discovery rate of less than one percent. The majority of OS tumour cell lines with a mutation of *TP53* clustered together, with increased abundance of the protein (Figure 19).

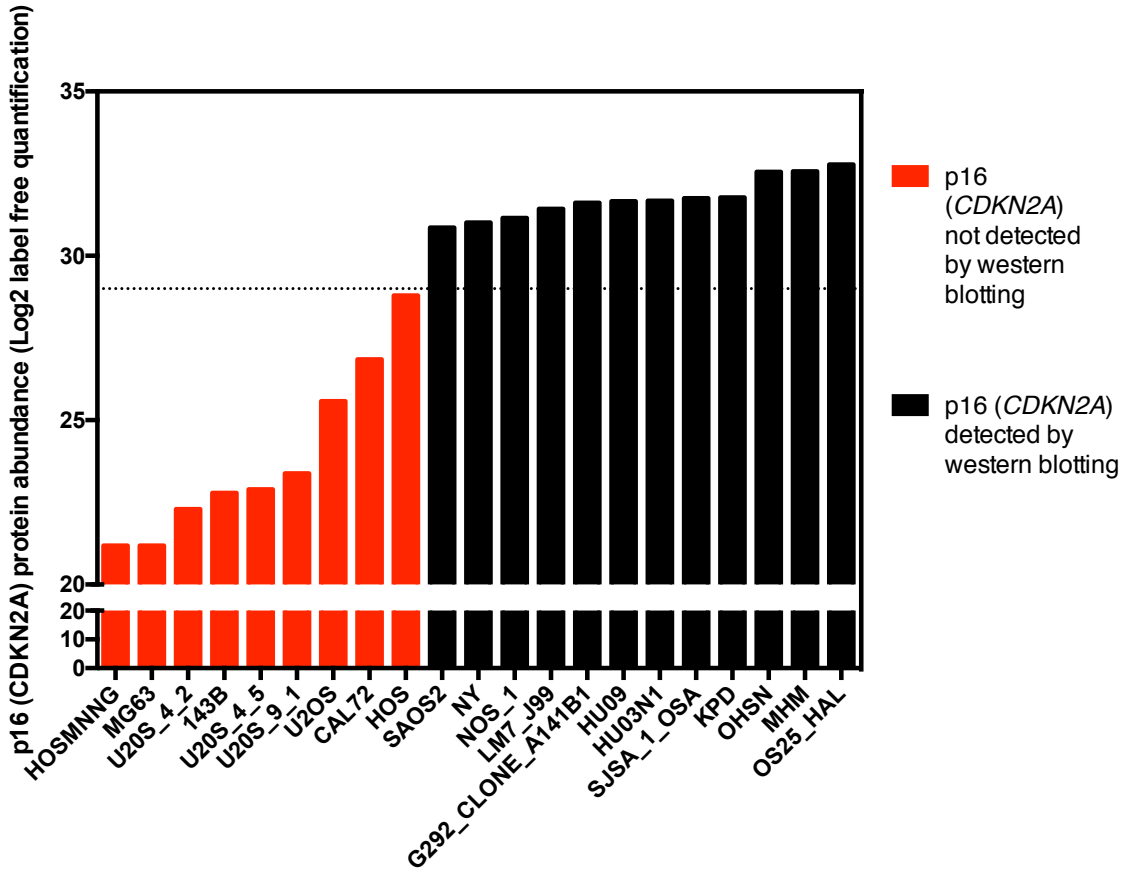

Figure 13 p16 (*CDKN2A*) protein abundance in osteosarcoma tumour cell lines defined by mass spectroscopy proteomic profiling.

Bar chart illustrating protein abundance of p16 (CDKN2A) for each OS tumour cell line; red columns indicate tumour cell lines classified as CDKN2A deficient by western blotting (Figure 8), copy number (Figure 10) and mRNA expression levels (Figure 11). Isogenic *RB1* wildtype (U2OS 9.1) and mutant U2OS tumour cell lines (U2OS 4.2 and U2OS 4.5) generated by CRISPR-Cas9 mediated mutagenesis (described in the next chapter) are shown as contrasts. Following lysis, protein purification, and tryptic digest, peptides were separated by liquid chromatography and measured by mass spectrometer. Label-free proteome quantification was performed using the MaxQuant software environment (Coscia, Watters, Curtis, *et al.*, 2016; Cox, Hein, Luber, *et al.*, 2014) to determine the quantitative abundance of 6696 peptides with a false discovery rate of less than one percent.

Table 12 Summary of classification of osteosarcoma tumour cell lines into *RB1* deficient and wildtype groups on the basis of exome sequencing, mRNA expression data, copy number and proteomic profiling.

RB1 defective	RB1 wildtype
HU09	OS25-HAL
HU03N1	MHM
NY	KPD
SAOS2	MG63
LM7	NOS-1
OHSN	U2OS
	143b
	HOSMNNG
	CAL72
	OSA/SJSA-1
	HOS
	G292 clone A141B1

Table 13 Summary of classification of osteosarcoma tumour cell lines into *CDKN2A* deficient and wildtype groups on the basis of exome sequencing, mRNA expression data, copy number and proteomic profiling.

p16 / CDKN2A defective	p16 / CDKN2A wildtype
HOSMNNG	OS25-HAL
MG63	MHM
U2OS	KPD
143b	OHS-N
CAL72	NOS-1
HOS	NY
	SAOS2
	LM7
	HU09
	OSA/SJSA-1
	HU03N1
	G292 clone A141B1

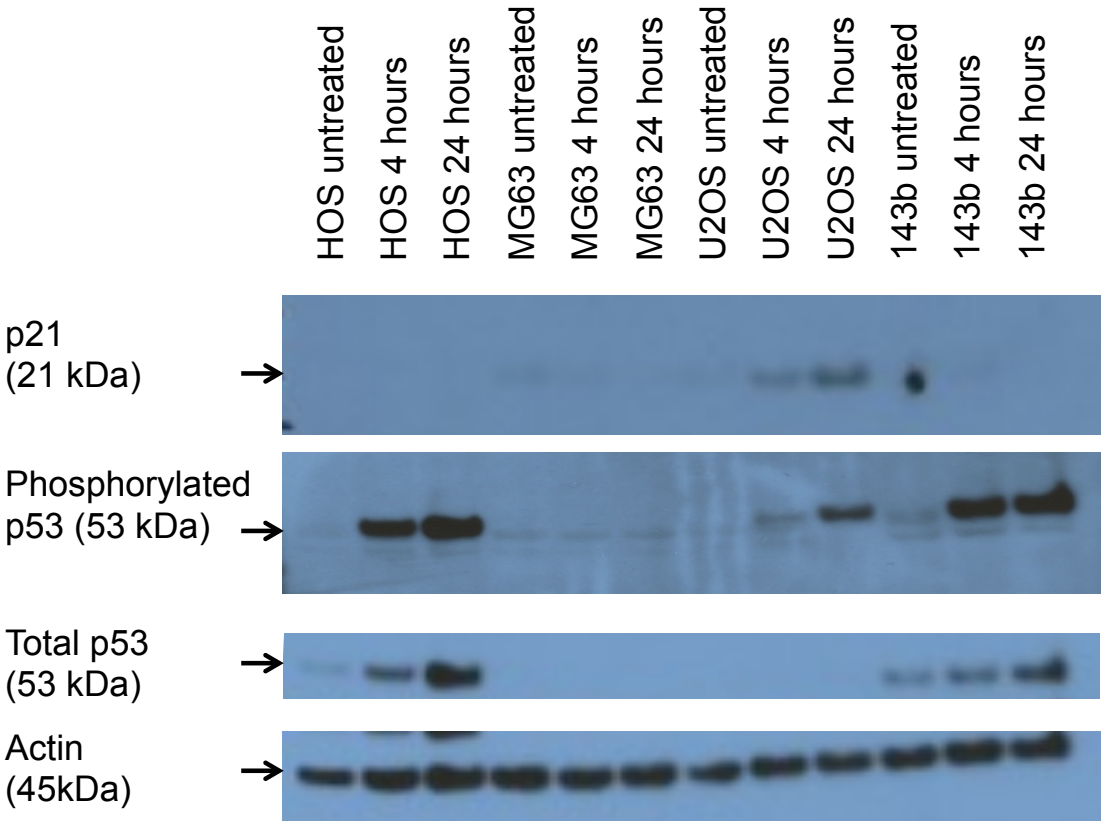

Figure 14 Heterogeneity of p21, p53 and phospho serine 15-p53 responses to doxorubicin in OS tumour cell lines (HOS, MG53, U2OS and 143b).

Western blot is shown. OS tumour cell lines were exposed to the DNA damaging agent doxorubicin (1μM) or drug vehicle, DMSO ("untreated") for four or 24 hours to induce DNA damage. Total cell lysates isolated after drug exposure were electrophoresed and immunoblotted as described in the Methods. Immunoblotting of actin was used as the loading control. All OS tumour cell lines with the exception of MG63, exhibited p53 and phospho-p53 induction in response to doxorubicin; only U2OS exhibited induction of p21 in response to doxorubicin.

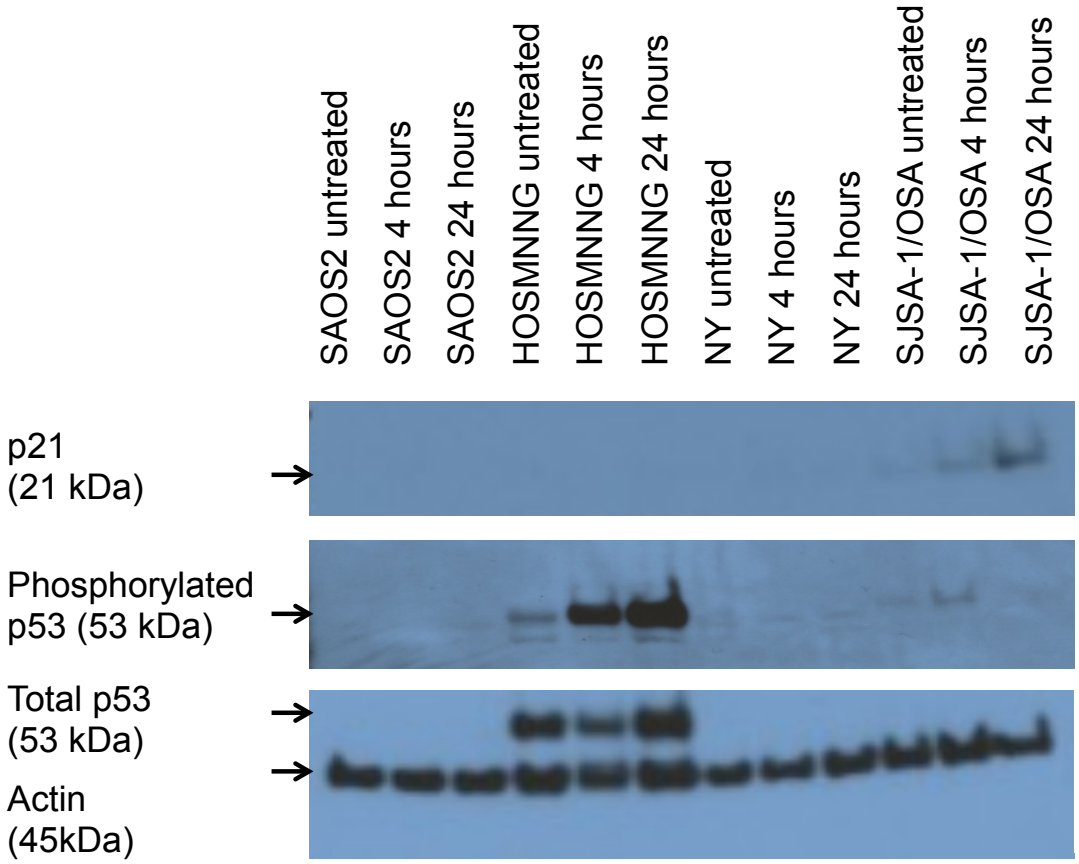

Figure 15 Heterogeneity of p21, p53 and phospho serine 15-p53 responses to doxorubicin in OS tumour cell lines (SAOS2, HOSMNNG, NY and SJSA-1/OSA).

Western blot is shown. OS tumour cell lines were exposed to the DNA damaging agent doxorubicin (1μM) or drug vehicle, DMSO ("untreated") for four or 24 hours to induce DNA damage. Total cell lysates isolated after drug exposure were electrophoresed and immunoblotted as described in the Methods. Immunoblotting of actin was used as the loading control. Only HOSMNNG exhibited p53 and phospho-p53 induction in response to doxorubicin; only SJSA-1/OSA exhibited induction of p21 in response to doxorubicin.

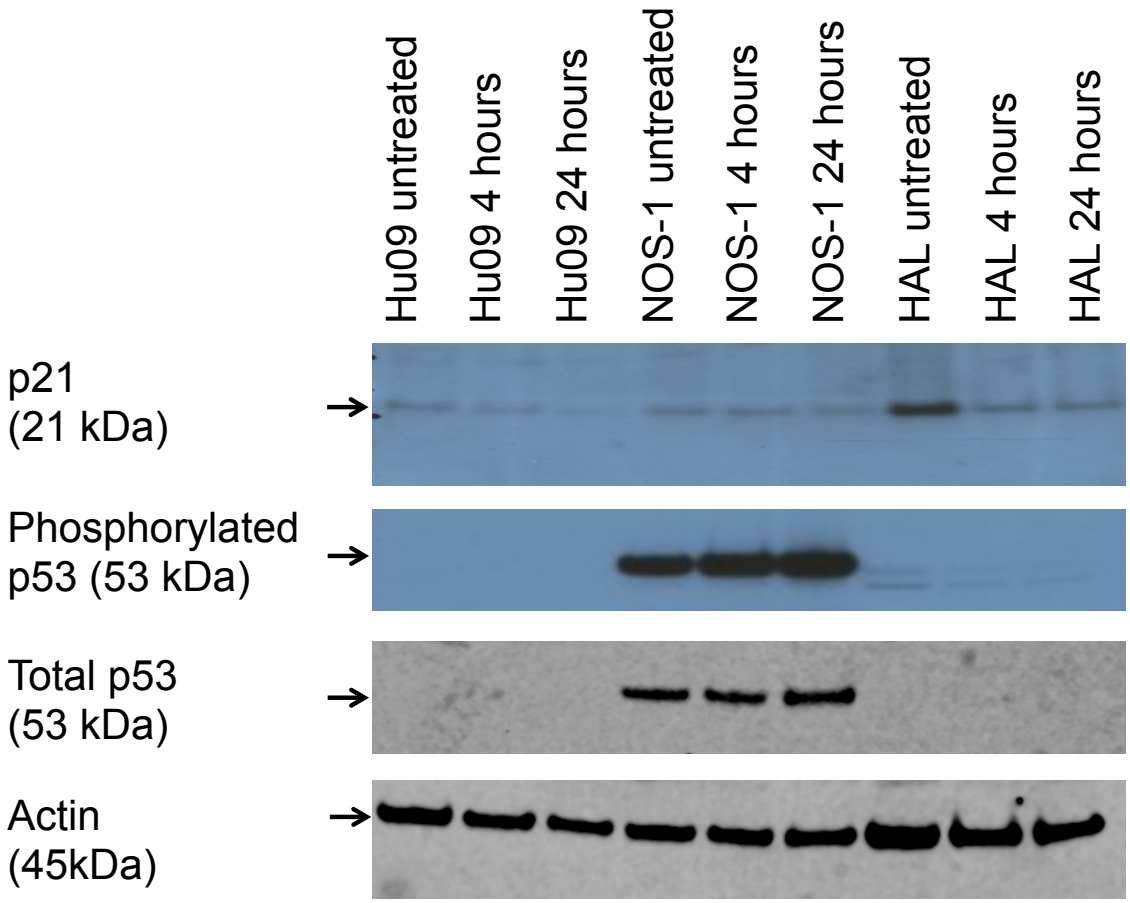

Figure 16 Heterogeneity of p21, p53 and phospho serine 15-p53 responses to doxorubicin in OS tumour cell lines (HU09, NOS1 and HAL).

Western blot is shown. OS tumour cell lines were exposed to the DNA damaging agent doxorubicin (1μM) or drug vehicle, DMSO ("untreated") for four or 24 hours to induce DNA damage. Total cell lysates isolated after drug exposure were electrophoresed and immunoblotted as described in the Methods. Blots for p21 and phosphorulated p53 were developed using film, while total p53 and actin were processed on the Liquor. Immunoblotting of actin was used as the loading control. Only NOS1 exhibited p53 and phospho-p53 induction in response to doxorubicin and was constitutively activated in DMSO; none of the tumour cell lines exhibited induction of p21 in response to doxorubicin.

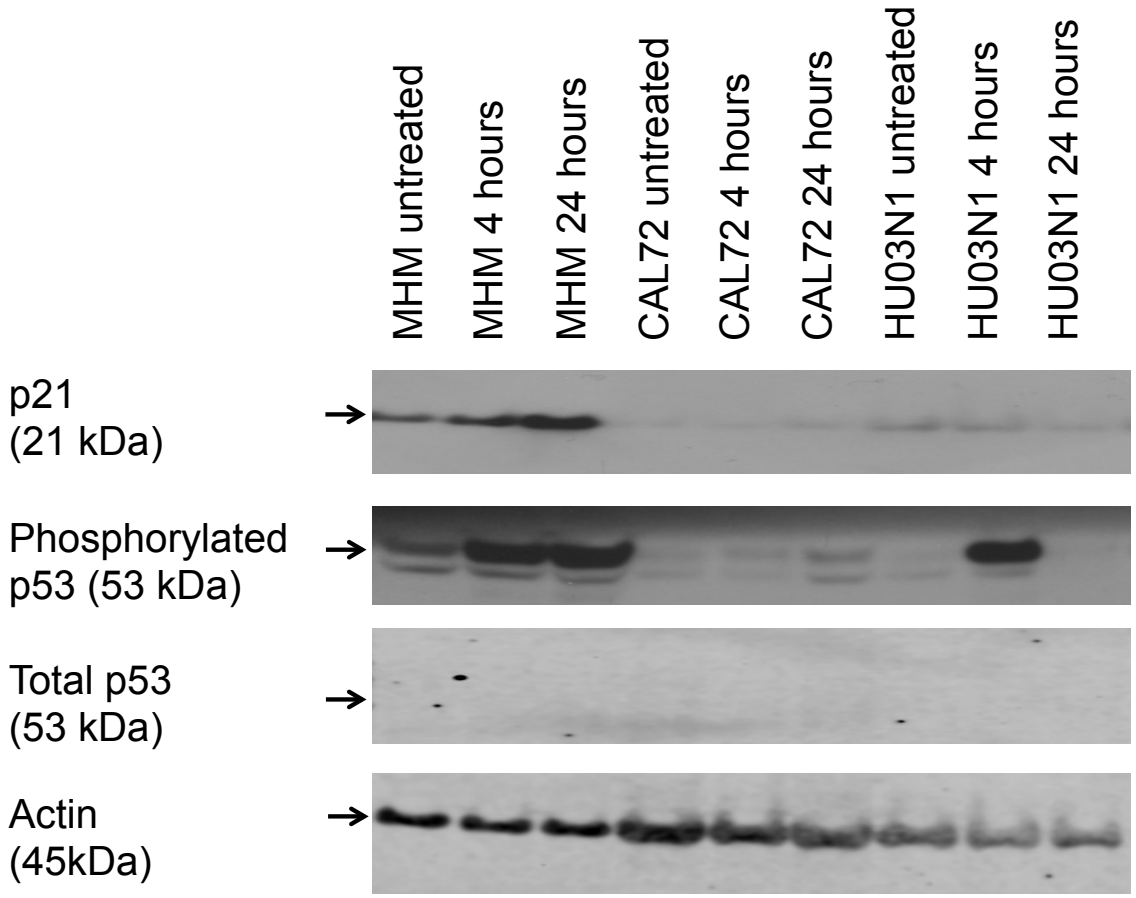

Figure 17 Heterogeneity of p21, p53 and phospho serine 15-p53 responses to doxorubicin in OS tumour cell lines (MHM, CAL72 and HU03N1).

Western blot is shown. OS tumour cell lines were exposed to the DNA damaging agent doxorubicin (1μM) or drug vehicle, DMSO ("untreated") for four or 24 hours to induce DNA damage. Total cell lysates isolated after drug exposure were electrophoresed and immunoblotted as described in the Methods. Immunoblotting of actin was used as the loading control. MHM exhibited phospho-p53 induction in response to doxorubicin, while an increase of phospho-p53 was seen only at four hours with HU03N1; only MHM exhibited induction of p21 in response to doxorubicin, and was constitutatively activated by DMSO.

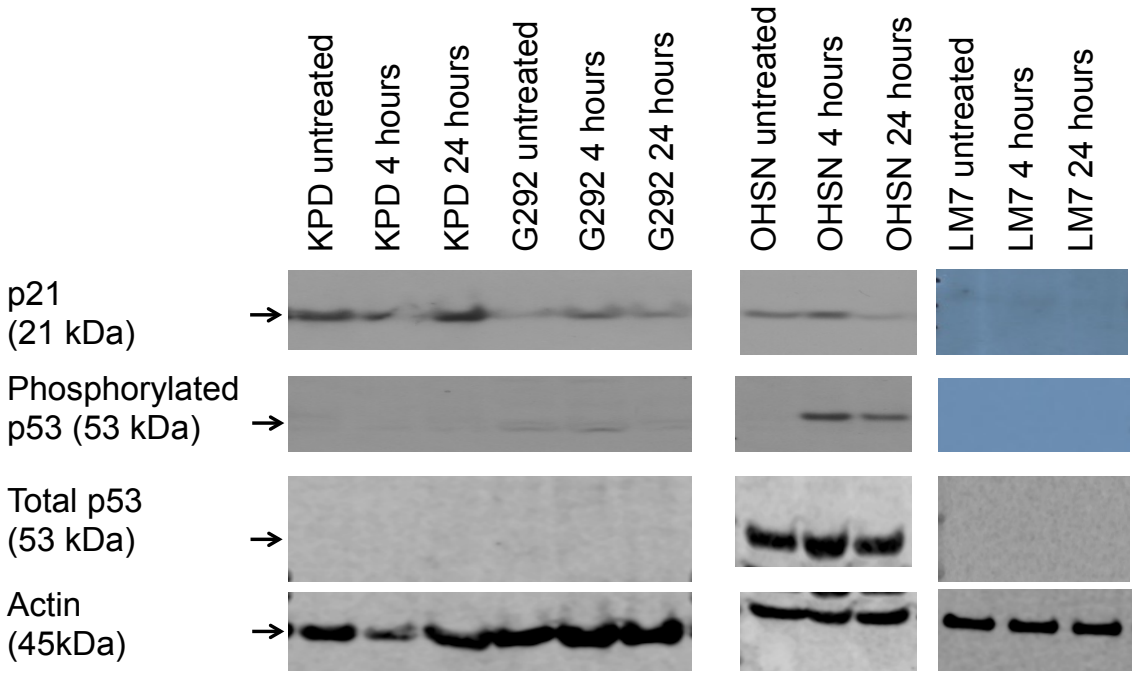

Figure 18 Heterogeneity of p21, p53 and phospho serine 15-p53 responses to doxorubicin in OS tumour cell lines (KPD, G292 clone A141B1, OHSN and LM7).

Western blot is shown. OS tumour cell lines were exposed to the DNA damaging agent doxorubicin (1μM) or drug vehicle, DMSO ("untreated") for four or 24 hours to induce DNA damage. Total cell lysates isolated after drug exposure were electrophoresed and immunoblotted as described in the Methods. Immunoblotting of actin was used as the loading control. Only OHSN exhibited p53 and phospho-p53 induction in response to doxorubicin; none of the tumour cell lines exhibited induction of p21 in response to doxorubicin, but p21 expression was constiuatively activated in KPD and OHS-N.

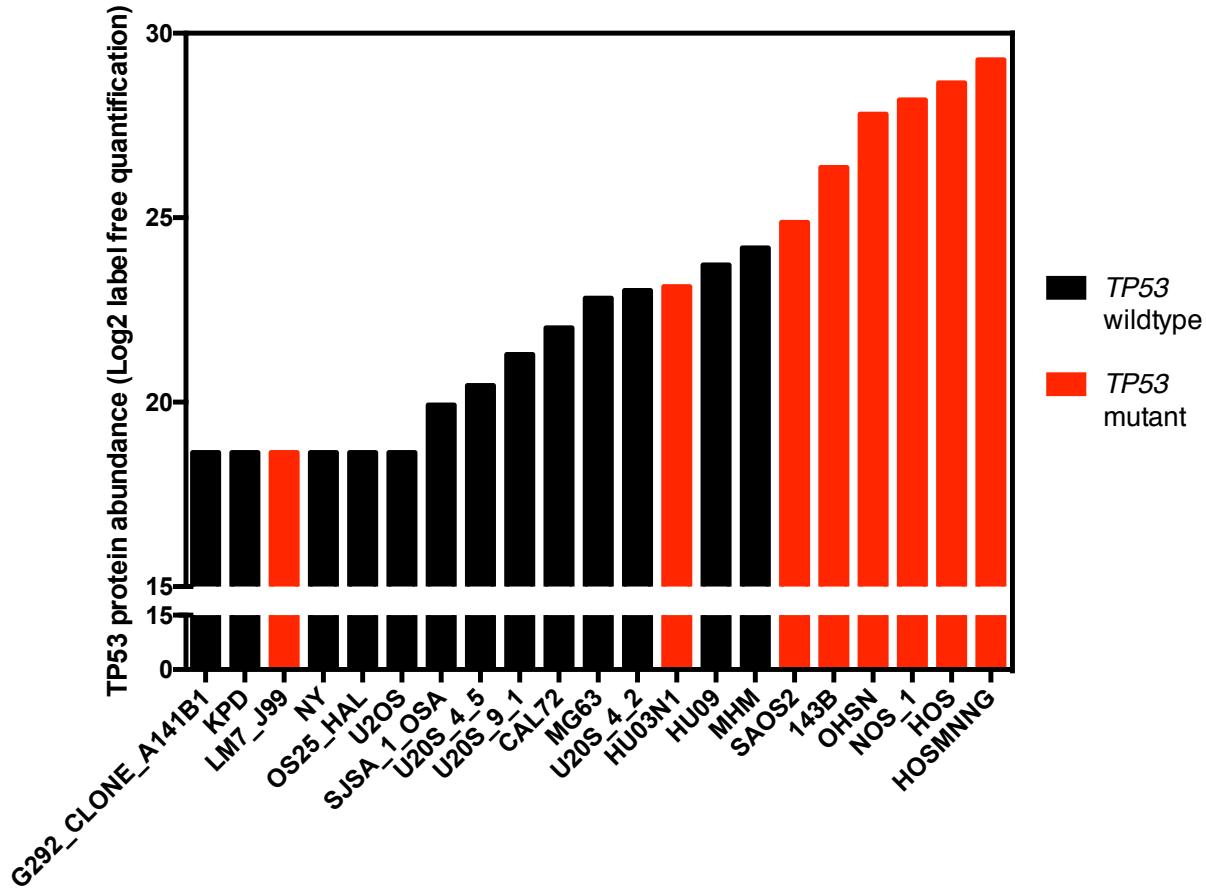

Figure 19 TP53 protein abundance in osteosarcoma tumour cell lines defined by mass spectroscopy bated proteomic profiling.

Bar chart illustrating protein abundance of TP53 for all the OS tumour cell lines; red columns indicated tumour cell lines classified as *TP53* mutant by exome sequencing, and black columns *TP53* wildtype. Tumour cell lines with known mutations in *TP53* (HOS, HOSMNNG, 143b, SAOS2, NOS-1, HU03N1 and OHS-N) clustered together with the exception of LM7. Isogenic *RB1* wildtype (U2OS 9.1) and mutant U2OS tumour cell lines (U2OS 4.2 and U2OS 4.5) generated by CRISPR-Cas9 mediated mutagenesis (described in the next chapter), were shown as contrasts. Following lysis, protein purification, and tryptic digest, peptides were separated by liquid chromatography and measured by mass spectrometer. Label-free proteome quantification was performed using the MaxQuant software environment (Coscia, Watters, Curtis, *et al.*, 2016; Cox, Hein, Luber, *et al.*, 2014) to determine the quantitative abundance of 6696 peptides with a false discovery rate of less than one percent.

3.2.6 Comparison of OS tumour cell line panel with OS tumour samples

Characterisation of the panel of OS tumour cell lines was performed with the primary aim of comparison with the reported molecular landscape of tumour samples to determine whether the panel of OS tumour cell lines represented a valid model to investigate recurrent driver mutations. For this comparison, the isogenic daughter tumour cell lines 143b and HOSMNNG (daughters of HOS), and LM7 (daughter of SAOS2), were excluded to prevent skewing of the data set. Whole exome sequencing data confirmed that the pattern of somatic mutations seen in the tumour cell line panel, was similar to that observed in clinical tumour samples (Kansara & Thomas, 2007; Chen, Bahrami, Pappo, *et al.*, 2014). The frequency of OS tumour samples that harbour mutations of *TP53* vary between cohorts from 20-80% (Gokgoz, Wunder, Mousses, *et al.*, 2001; Chen, Bahrami, Pappo, *et al.*, 2014). Mutations of *TP53* were seen in 26% (4/15) of the tumour cell line panel.

Mutations of *RB1* were seen in 33% (5/15) of the tumour cell lines, compared to up to 35% in sporadic cases of osteosarcoma (Araki, Uchida, Kimura, *et al.*, 1991). Mutations in *CDKN2A* and *ATRX* were present in 20% (3/15), and 13% (2/15) of the tumour cell lines respectively. Less than 25% of tumour samples have been reported to harbour mutations of *CDKN2A* (Nielsen, Burns, Rosenberg, *et al.*, 1998; Kansara & Thomas, 2007). Mutations of *ATRX* are seen at a frequency of 29% in the clinical disease, (Chen, Bahrami, Pappo, *et al.*, 2014), slightly higher than seen in the tumour cell line panel.

Of these candidate driver mutations it was only possible to study those with sufficient statistical power. Only two tumour cell lines had mutations of ATRX (NOS-1 and U2OS), lower than the frequency seen in the clinical disease (29%) (Chen, Bahrami, Pappo, *et al.*, 2014), which prevented further investigation. Cells harbouring mutations of *TP53* and expression of p53 post exposure to DNA damage were too ambiguous to cluster into two definite groups. Therefore, given the recurrent nature of the driver mutations *RB1* and *CDKN2A* and sufficient cohorts for deficient and wildtype groups, these two genes were chosen for investigation of synthetic lethality.

To further confirm the clinical relevance of the tumour cell line models used, comparison of the OS tumour cell line panel to a library of 112 tumour samples at the Wellcome Institute, Sanger Centre, was sought. (Behjati, Tarpey, Haase, *et al.*, 2017) Whole

genome sequencing of the tumour samples was performed and a schematic of the driver mutations is shown in Figure 20 (Behjati, Tarpey, Haase, *et al.*, 2017). The frequency and specificity of the driver mutations observed in these tumour samples closely resembles those seen in the panel of 18 OS tumour cell lines. However, it is likely that the frequency of driver mutations recorded probably represents an under estimate of the molecular changes seen in OS tumour samples, due to the lack of matched normal genomes for comparison (Behjati, Tarpey, Haase, *et al.*, 2017).

3.3 ISOGENIC MODELS

Isogenic models derive from a single progenitor cell line, with minimal genetic differences between the daughter and parental cell lines, so that any observed differences are more likely to be due to the gene of interest (Rehman, Lord & Ashworth, 2010). Therefore to identify candidate genetic dependencies associated with the driver mutations of *RB1* or a specific phenotype such as PARP sensitivity (LM7 and SAOS2), isogenic models were sought. In the absence of any available models of *RB1* deficiency and wildtype in osteosarcoma, breast models were used, while the generation of a model in osteosarcoma was undertaken by CRISPR-Cas9 mediated mutagenesis.

3.3.1 Osteosarcoma isogenic models

Two isogenic models were included amongst the OS tumour cell line panel. The OS tumour cell line HOS has been virally transformed using a *K-Ras* oncogene to 143B, and was previously chemically transformed by *N*-methyl-*N*-nitro-*N*-nitrosoguanidine to HOSMNNG (Rhim, Park, Arnstein, *et al.*, 1975). HOS and its derivatives 143B and HOSMMNG, have been shown to cluster together in terms of gene expression, DNA methylation, and DNA copy number but within this clustering, HOS and HOSMMNG were more similar in terms of gene expression and methylation, and 143B and HOS in terms of copy number (Kresse, Rydbeck, Skårn, *et al.*, 2012). The second LM7, was developed by multiple *in vivo* selection of SAOS2 cells in nude mice with pulmonary metastases (Jia, Worth & Kleinerman, 1999).

3.3.2 RB1 isogenic breast models

To provide a robust model to investigate specific genetic lethalities associated with loss of *RB1* function, an isogenic model of *RB1* loss was sought. Two *RB1* deficient and wildtype breast models were kind gifts from Eric Knudsen, Thomas Jefferson University, Philadelphia, USA; metastatic breast adenocarcinoma tumour cell line (MDAMB231) and a non-tumourigenic epithelial breast cell line (MCF10A) both created by shRNA mediated silencing of *RB1*. RB1 status was confirmed by western blotting (Figure 21).

3.4 DISCUSSION

At the commencement of this thesis, no human isogenic models of loss of *RB1*, or *CDKN2A* in osteosarcoma had been described. Therefore, a panel of tumour cell lines was used to describe the genetic dependencies in osteosarcoma with the aim of identification of candidate synthetic lethalities, while an isogenic model was created using CRISPR-Cas9 mutagenesis (described in the next chapter).

Some of these models were already partially characterised by the EuroBoNet Consortium (Ottaviano, Schaefer, Gajewski, *et al.*, 2010). The principle aim of completion of the exome sequencing of the remaining tumour cell lines was to ascertain their similarity with OS tumour samples, and confirm a clinically relevant model for investigation of the recurrent driver mutations *RB1* and *CDKN2A*. After exclusion of 143b and HOSMNNG (daughters of HOS), and LM7 (daughter of SAOS2), to prevent skewing of the data set, the whole exome sequencing confirmed a pattern of mutations representative of those seen in the tumour samples at similar frequencies (Gokgoz, Wunder, Mousses, *et al.*, 2001; Chen, Bahrami, Pappo, *et al.*, 2014; Araki, Uchida, Kimura, *et al.*, 1991; Nielsen, Burns, Rosenberg, *et al.*, 1998; Kansara & Thomas, 2007) with recurrent mutations in *TP53, RB1, CDKN2A,* with the exception of *ATRX* which was seen at a lower frequency than expected.

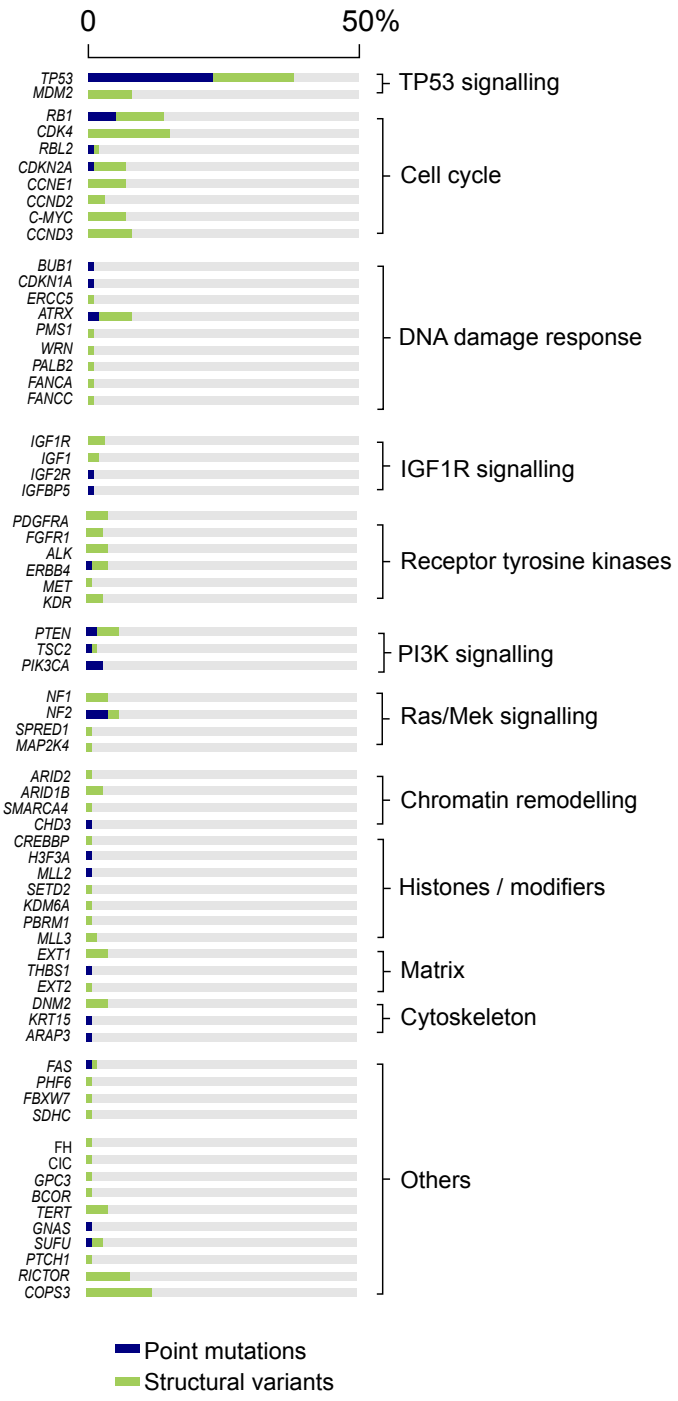

Figure 20 Summary of the driver events in osteosarcoma tumour samples.

Bar chart illustrating the percentage driver mutations in each mutated cancer gene observed in 112 OS tumours that under went exome (n = 75) or whole genome (n = 37) sequencing at the Wellcome Trust Sanger Institute. Mutations were subdivided by mutation type; blue: point mutation (substitutions; indels); and green: structural variant (amplification, homozygous deletion or disruptive breakpoint). Reproduced from Behjati *et al.* (Behjati, Tarpey, Haase, *et al.*, 2017).

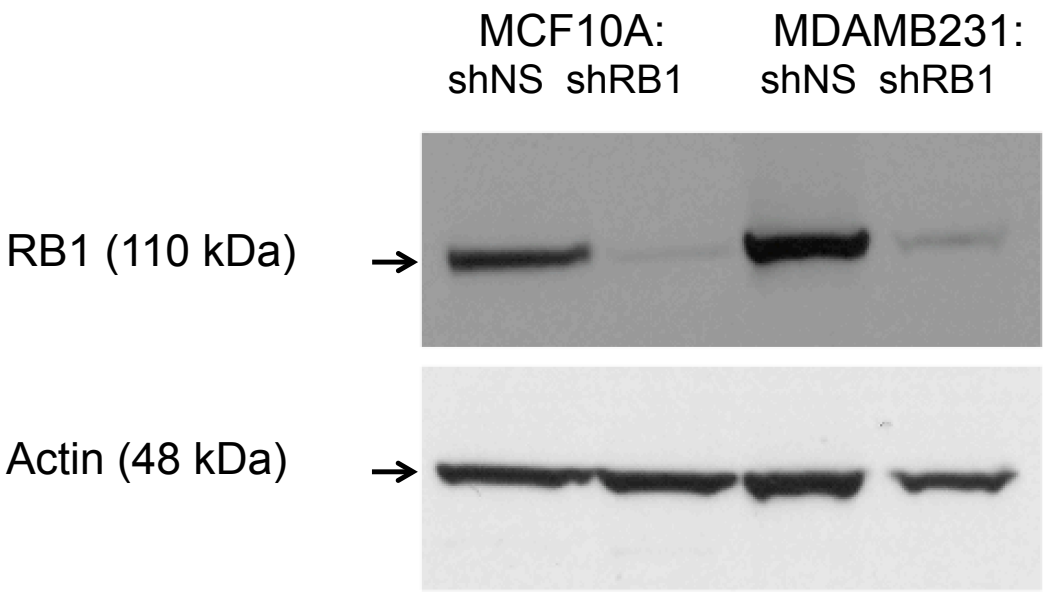

Figure 21 *RB1* deficient stable isogenic breast cancer cell line MDMAM231 and non-tumourigenic epithelial breast cell line MCF10A do not express RB1.

Western blot shown. The metastatic breast adencarcinoma tumour cell line (MDAMB231) and a non-tumourigenic epithelial breast cell line (MCF10A), both kind gifts from Eric Knudsen, were both created by shRNA mediated silencing of *RB1* and a non-targeting control (shNS). Cell lysates were collected from untreated cells, electrophoresed and immunoblotted as described in the Methods. Immunoblotting of actin was used as the loading control. [shRB1: shRNA RB1 specific RNA; shNS: non-silencing RNA.]

This panel of OS tumour cell lines was comprised of both non-isogenic and isogenic models that have inherent advantages and disadvantages as discussed in section 3.1. Therefore, both isogenic and non-isogenic OS tumour cell line models were used to investigate for candidate genetic vulnerabilities and drug dependencies.

The OS tumour cell line panel was classified according to *RB1* and *CDKN2A* deficiency by comparison of mutation status, mRNA expression, copy number, proteomic abundance and protein expression via western blotting to enable a 'class analysis' and identification of genetic vulnerabilities and drug dependencies associated with these recurrent alterations observed in both tumour samples and the TCL panel. This analysis forms the basis of Chapter six.

In order to investigate the transcriptional changes associated with *RB1* and *CDKN2A* deficiency, whole transcriptome analysis was performed in *RB1* isogenic U2OS tumour cell lines created by CRISPR-Cas9 mutagenesis. As another layer of annotation to further categorise the tumour cell lines into *RB1* and *CDKN2A* deficient or wildtype groups, proteomic profiling was undertaken. Only a preliminary analysis of this data-set has been performed as the data was only available towards the end of this PhD, therefore only initial descriptive results are reported here and form the basis of future work.

4 Characterisation of *RB1* deficient U2OS tumour cell lines engineered by CRISPR-Cas9 mutagenesis

4.1 INTRODUCTION

One of the limitations of using the combination of both breast and osteosarcoma tumour cell lines for loss of function of *RB1*, was the uncertainty of tissue specific genetic co-occurrences, which had the potential to make interpretation of candidate genetic dependencies more challenging. Therefore, to identify candidate genetic dependencies in OS specific to *RB1* deficiency, an isogenic model was developed. The advantages and limitations of isogenic and non-isogenic models have already been discussed previously section 3.1. In the absence of human isogenic models of *RB1* deficiency and wildtype in osteosarcoma, I engineered a stable isogenic model of *RB1* deficiency by genomic editing using clustered regularly interspaced short palindromic repeat and associated protein 9 (CRISPR-Cas9) mediated mutagenesis using the OS tumour cell line U2OS.

While RNAi is a well-established method for high-throughput screening, siRNA are only able to temporarily silence the target gene. However, gene editing by CRISPR-Cas9 mutagenesis is able to permanently inactivate the target gene and thus provides an alternative for validation. A schematic of the CRISPR-Cas9 methodology is shown in Figure 22.

Bacteria rely on CRISPR-Cas9 mediated systems for acquired immunity against invading foreign nucleic acids, including those of viruses and plasmids, by sequence specific detection and silencing via RNA-guided DNA cleavage (Wiedenheft, Sternberg & Doudna, 2012). This system has been adapted for use in human cells, by the co-delivery of plasmids expressing the CRISPR-associated protein 9 (Cas9) nuclease isolated from *Streptococcus pyogenes* and guide RNA (Gaj, Gersbach & Barbas, 2013). Cas9 is directed to a specific target DNA site by 20 nucleotides at the 5' end of the guide RNA (Sander & Joung, 2014). The correct protospacer adjacent motif (PAM) sequence must immediately follow the target sequence to allow successful binding of Cas9 (Sander & Joung, 2014). This means that the CRISPR-Cas9 system is highly maneuverable, simply by altering the guide RNA sequence, reviewed by (Sander & Joung, 2014). Double-strand breaks (DSBs) induced by Cas9, lead to both non-homologous end-joining (NHEJ) mediated indel mutations and homology-directed repair (HDR) (Sander & Joung, 2014).

The CRISPR-Cas9 methodology provides a rapid and efficient alternative to Zinc-Finger Nucleases (ZFNs) and Transcription-Activator Like Effector Nuclease (TALENs) for gene editing (Gaj, Gersbach & Barbas, 2013) because of reliance on RNA-guided nucleases which use simple, base-pairing rules between the target DNA site and the engineered RNA, as opposed to protein-DNA interactions (Sander & Joung, 2014). One of the disadvantages of CRISPR-Cas9 is the potential for off-target effects due to mis-match of the guide RNA and target DNA, although the true frequency of these effects is unknown (Sander & Joung, 2014). One method of combating this problem is the use of multiple separate CRISPR guides against the length of the target gene, and robust confirmation of inactivity.

4.2 GENERATION OF NEW ISOGENIC OSTEOSARCOMA MODELS OF RB1 DEFICIENCY

In the absence of previously described models of *RB1* deficiency in OS, generation of *RB1* deficient models by CRIPSR-Cas9 were undertaken using an OS tumour cell line U2OS (Figure 23). This generated two clones U2OS 4.2 and 4.5 with premature stop (nonsense) mutations.

4.2.1 Characterisation of two U2OS RB1 deficient isogenic models engineered by CRISPR-Cas9

To determine the *RB1* status of both U2OS clones 4.2 and 4.5, characterisation by Sanger sequencing, exome sequencing, mRNA expression, RB1 protein expression by western blotting, and proteomic abundance described below were undertaken.

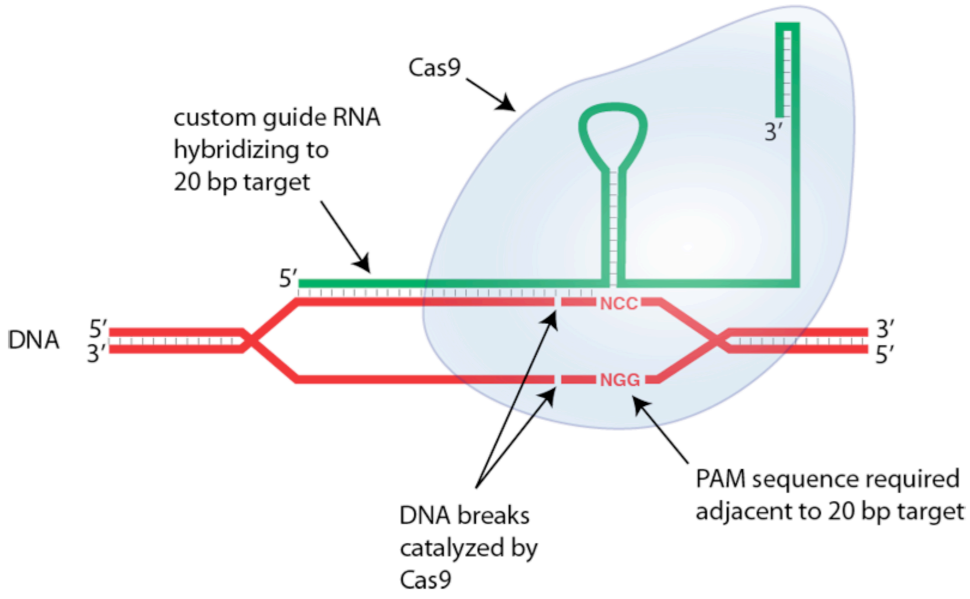

Figure 22: Schematic of targeted gene editing by CRISPR (clustered regularly interspaced short palindromic repeat) Cas9.

The Cas9 protein, shown in blue is directed to the target DNA sequence by 20 nucleotides at the 5' end of the guide RNA and the protospacer adjacent motif (PAM) sequence that follows the target sequence. Binding of the Cas9 causes double–strand breaks (DSBs) that can be repaired by non-homologous end-joining (NHEJ) which mediate indel mutations and homology-directed repair (HDR). Using this methodology, stable isogenic cell lines with the inactivation of a targeted gene can be produced (reproduced from http://ko.cwru.edu/services/directtargeting.shtml)

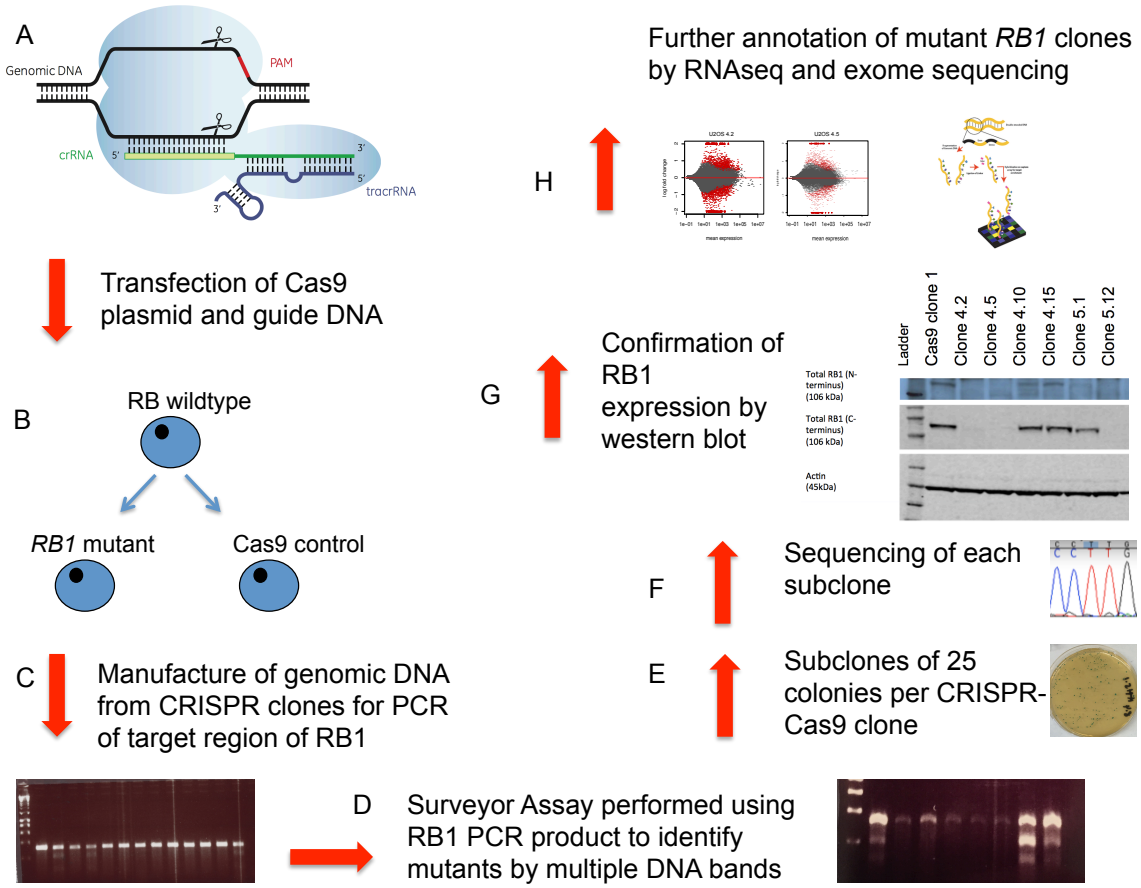

Figure 23 Schematic of generation of *RB1* isogenic osteosarcoma model by CRISPR (clustered regularly interspaced short palindromic repeat) Cas9 mutagenesis.

A: U2OS cells were reverse transfected with Cas9 and guide DNA, or Cas9 alone (control); B: Transfection efficiency was monitored using an EGFP control. Cells were selected by blastocydin, and seeded for colony formation. 100 colonies were picked and expanded; C: Manufacture of genomic DNA from single colony clones, and subsequent amplification of target region of *RB1* by PCR; D: Surveyor Assay performed using the *RB1* PCR product of all clones to further identify possible mutants by multiple DNA bands; E: Subclones of mutant clones identified, using 25 colonies per clone; F: Sanger sequencing of all subclones, for comparison with sequencing from Cas9 control (parental) clone; G: Confirmation of expression of RB1 protein level using western blot of both N-terminus and C-terminus of RB1; H: Further annotation of the *RB1* mutant clones by RNAseq and exome sequencing.

4.2.1.1 Sanger sequencing confirms nonsense mutations of RB1

Sanger sequencing of subclones of both U2OS clones 4.2 and 4.5 was performed to determine the mutation status of each clone, and the translational effect on the protein (Figure 26). Both clones were confirmed to have premature stop (nonsense) mutations (Table 14). Translation of mutant product for the U2OS CRISPR-Cas9 clone 4.2 demonstrated truncation of the protein at p.61 (TAA). Translation of mutant product for U2OS CRISPR-Cas9 clone 4.5 demonstrated truncation of the protein at p.30 (TGA) by insertion of a T insertion (c.87Tins), highlighted by the red box.

Only one AUG start codon with a single protein coding transcript has been reported for RB1. Other splice variants are subject to nonsense mediated decay.

4.2.1.2 Exome sequencing of the isogenic *RB1* deficient and wildtype U2OS tumour cell lines

The exome sequences of the U2OS *RB1* mutant clones were each compared to the *RB1* wild type (U2OS 9.1) clone separately. Contrastive analysis of the U2OS 4.2 and U2OS 9.1 exome sequences identified a total of 85 protein-altering mutations, 43 of which were specific to the *RB1* wild type U2OS 9.1 clone and 42 were specific to the *RB1* deficient U2OS 4.2 clone. Of 85 protein-altering mutations, 67 were missense, eight were frameshifts, four were splice site alterations and six were nonsense (stop-gained) mutations depicted in red in Figure 27. The 10 base pair deletion of *RB1* previously identified by Sanger sequencing was confirmed by exome sequencing in U2OS 4.2, not seen in the parental 9.1.

A contrastive analysis of the U2OS 4.5 and U2OS 9.1 exome sequences identified a total of 49 protein-altering mutations that were present in either U2OS 4.5 or U2OS 9.1 clones. Of these 49 mutations, 23 were specific to the RB1 wild type U2OS 9.1 clone and 26 were specific to the *RB1* deficient U2OS4.5 clone (Figure 27). Of these 49 mutations, 40 were missense mutations, five were frame shift mutations, two were splice site alterations and two were nonsense mutations. The frameshift mutation of *RB1* caused by T insertion in U2OS 4.5 identified by Sanger sequencing was also confirmed by exome sequencing.

A summary of the genetic alterations of the protein altering mutations at splice sites, or causing frameshifts or stop-gains is shown in Table 15. Apart from the engineered mutations in *RB1* in both daughter cell lines, none of the other alterations were in known key driver genes, and are therefore unlikely to significantly influence the therapeutic response of the models.

The number of genetic alterations in addition to the mutations identified in *RB1* are small, and most likely represent a combination of processes; the process of CRISPR-Cas9 mediated mutagenesis requires a number of passages during cell culture, and given that U2OS is a tumour cell line, genetic drift could occur between the cell lines during routine culture; some alterations could be the result of off-target effects of the CRISPR guide, although the majority of the alterations noted are in the parental 9.1 clone; although the parental clone was not transfected with a guide sequence, it was still transfected with Cas9, which is stably expressed. Theoretically there is the potential for some nonspecific activity of the Cas9 nuclease (Jinek, Chylinski, Fonfara, *et al.*, 2012). Without the formation of the Cas9 complex with CRISPR guide RNA, the Cas9 is not thought to mediate non-specific double strand breaks (Anders, Niewoehner, Duerst, *et al.*, 2014). Therefore, the presence of RNA sequences that can act as a guide RNA substrate, and the expression level of Cas9, will likely determine the extent of the off target effect. In addition the majority of reported mutations were single base pair alterations, which were potentially false discovery errors.

Table 14 Characteristics of the mutations generated in *RB1* in two isogenic *RB1* deficient U2OS CRISPR-Cas9 engineered clones

	U2OS CRISRP-Cas9 clone 4.2	U2OS CRIPSR-Cas9 clone 4.5
CRISPR guide used	AA4	AA4
Generated mutation	10bp deletion (c.90-99del)	T insertion (c.87Tins)
Effect of mutation	p.61 stop	p.30 stop

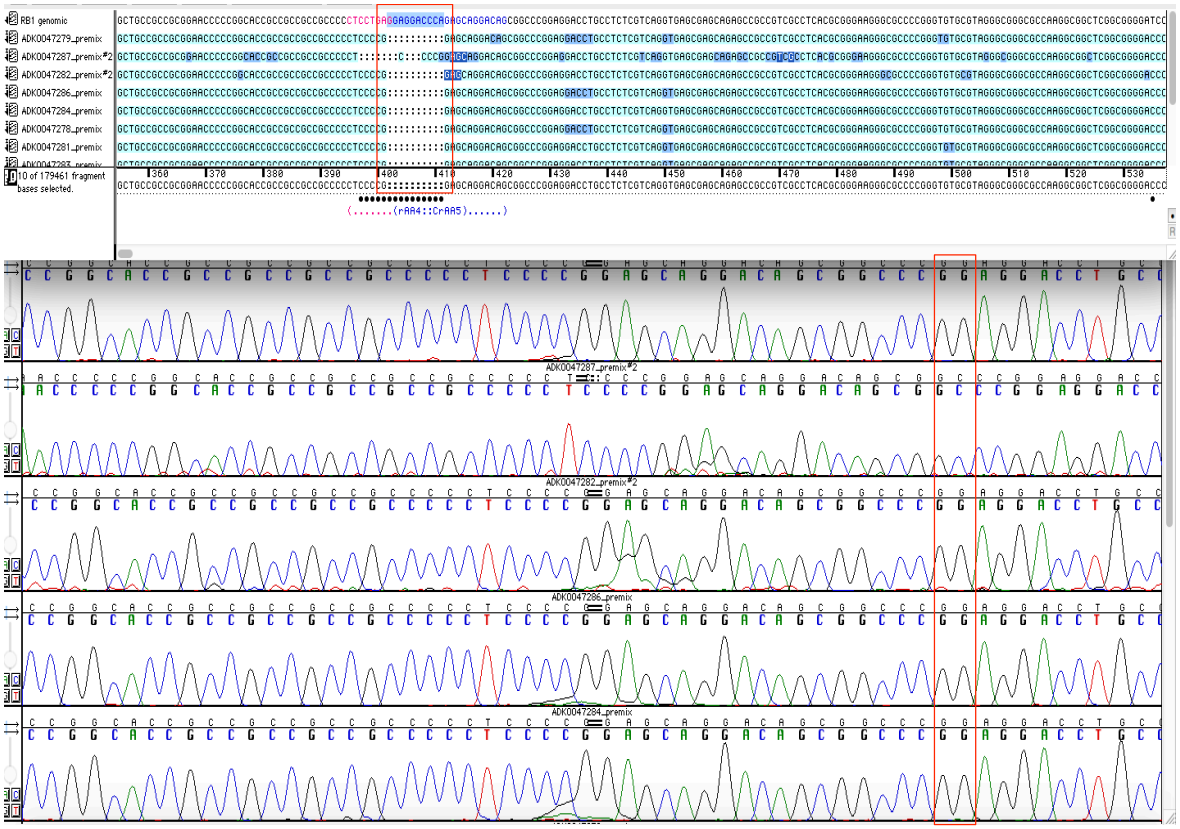

Figure 24 Sanger sequencing from five subcloned products for U2OS CRISPR-Cas9 clone 4.2 confirm a 10 base pair deletion (c.90-99del) in all alleles.

Sanger sequencing from five subclones for the *RB1* Exon 1 PCR product were aligned to the reference sequence of *RB1* cDNA to identify any alterations, and enable naming based on standard nomenclature. Highlighted by the red box is a 10 base pair deletion identified in this clone, replicated in five subcloned sequences, depicted alphabetically and also by electropherogram. The U2OS clone 4.2 was subcloned, DNA isolated and Exon one of *RB1* amplified by PCR. Sanger sequencing for five representative subclones are shown. Sequencher DNA Sequence Analysis Software was (www.genecodes.com) was used to visualise the sequencing.

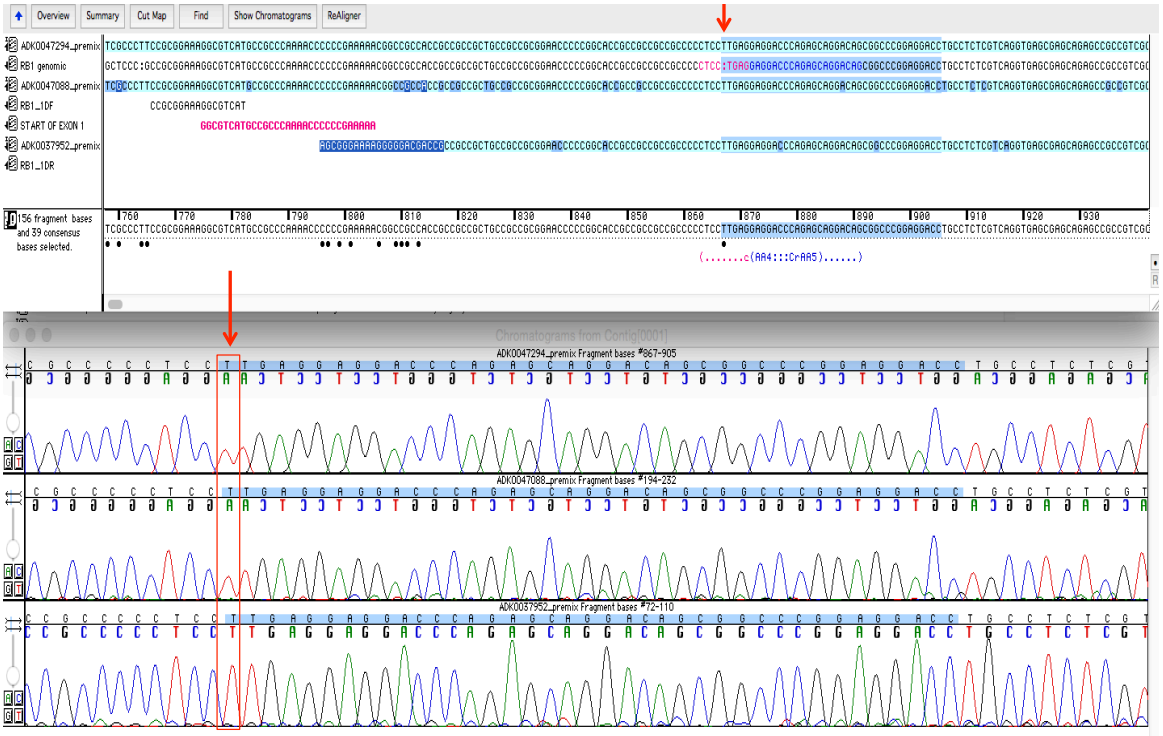

Figure 25 Sanger sequencing from three subcloned products for U2OS CRISPR-Cas9 clone 4.5 confirm an insertion of T (c.87Tins) in all alleles.

Sanger sequencing from three subclones for the *RB1* Exon 1 PCR product were aligned to the reference sequence of *RB1* cDNA to identify any alterations, and enable naming based on standard nomenclature. Highlighted by the red arrow and box is a single T insertion identified in this clone, replicated in three subcloned sequences, depicted alphabetically and also by electropherogram. The U2OS clone 4.5 was subcloned, DNA isolated and Exon one of *RB1* amplified by PCR. Sanger sequencing for three representative subclones are shown. Sequencher DNA Sequence Analysis Software was (www.genecodes.com) was used to visualise the sequencing.

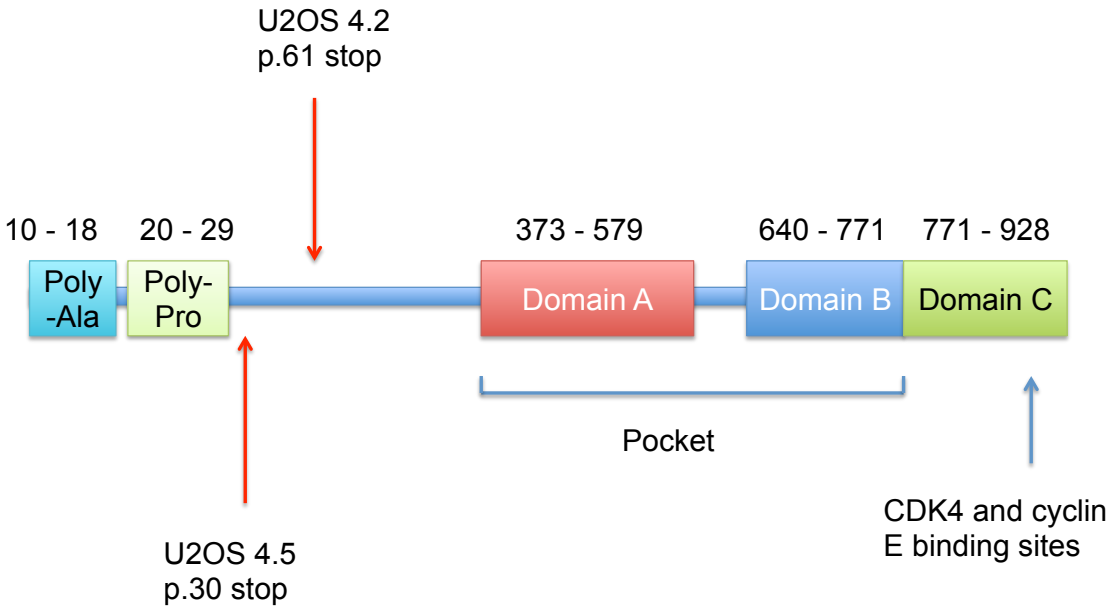

Figure 26 Schematic of the structure of the RB1 protein, and predicted effects of mutations seen in U2OS CRIPSR-Cas9 clones 4.2 and 4.5.

The RB1 protein comprises 3 domains (A, B and C). Together the region between Domains A and B comprise the Pocket, which binds to Domain C preventing interaction with heterodimeric E2F/DP transcription factor complexes (adapted from www.uniprot.org/uniprot/P06400#family_and_domains) (Dick, 2007). Only one AUG start codon with a single protein coding transcript has been reported for RB1. Other splice variants are subject to nonsense mediated decay.

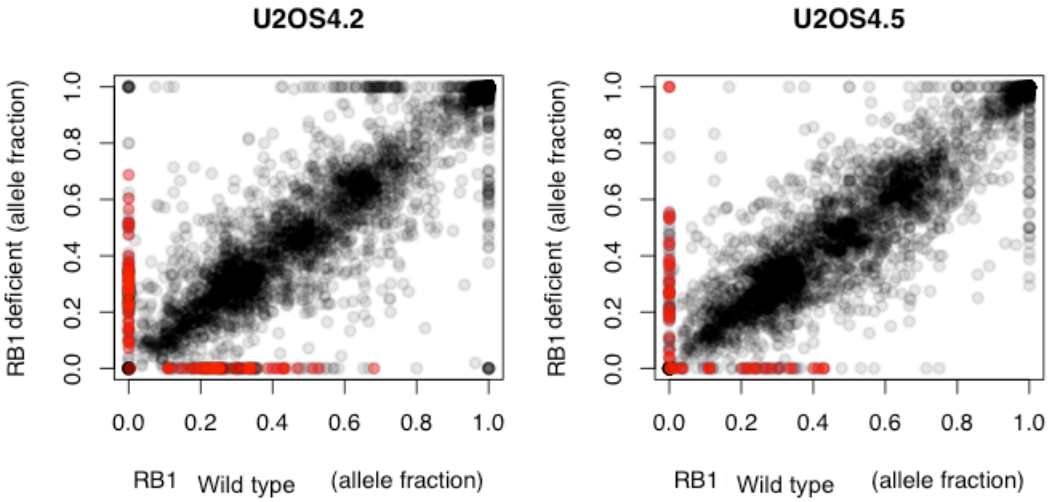

Figure 27 Contrast analysis of the exome sequencing of U2OS clones 4.2 and 4.5 compared to the parental line U2OS 9.1, determined mutations specific to each clone.

Scatter plots of the protein changing mutation profiles of *RB1* wildtype (U2OS 9.1) and *RB1* deficient cell line models (U2OS 4.2 and 4.5) determined by exome sequencing. The points highlighted in red along the x-axis represent the mutations unique to *RB1* wildtype model, while the points highlighted in red along the y-axis represent the mutations unique to *RB1* deficient models U2OS 4.2 and 4.5. Black dots represent mutations seen in both parental and daughter clones. The exome sequences of the U2OS *RB1* mutant clones were each compared to the *RB1* wild type (U2OS 9.1) clone separately. Contrastive analysis of the U2OS 4.2 and U2OS 9.1 exome sequences identified a total of 85 protein-altering mutations, 43 of which were specific to the *RB1* wild type U2OS 9.1 clone and 42 were specific to the *RB1* deficient U2OS 4.2 clone. A contrastive analysis of the U2OS 4.5 and U2OS 9.1 exome sequences identified a total of 49 protein-altering mutations, of these 23 were specific to the *RB1* wild type U2OS 9.1 clone and 26 were specific to the *RB1* deficient U2OS 4.5 clone. DNA was extracted from the OS tumour cell lines U2OS 4.2, 4.5 and 9.1 and members of the TPU (ICR) performed targeted exome capture. James Campbell (ICR) aligned the reads to the human reference genome, and performed somatic variant calling. Graphical depiction by James Campbell and Aditi Gulati (ICR) using R.

4.2.1.3 Whole Transcriptome Sequencing of *RB1* isogenic models

RNAseq was also performed on the *RB1* isogenic models MDAMB231 and MCF10A within the laboratory group. Comparison of all the RB1 deficient cell line models (U2OS 4.2, U2OS 4.5, MDAMB231 and MCF10A), to identify up-regulated and down-regulated genes that were in common between the models was performed. Nine genes (Centromere Protein E (*CENPE*), Ankyrin Repeat Domain 50 (*ANKRD50*), RP11-492E3.1, Glucosamine (UDP-N-Acetyl)-2-Epimerase/N-Acetylmannosamine Kinase (*GNE*), Tet Methylcytosine Dioxygenase 2 (*TET2*), Paralemmin 2 (*PALM2*), UDP-N-Acetylglucosamine Pyrophosphorylase 1 Like 1 (*UAP1L1*), Glia Maturation Factor Gamma (*GMFG*) and RP11-420A23.1) were up-regulated in all models, of which, CENPE, GNE and ANKRD50 are known to be involved in cell division. Four genes (Baculoviral IAP Repeat Containing 3 (*BIRC3*), ST6 Beta-Galactoside Alpha-2,6-Sialyltransferase 1 (*ST6GAL1*), Cytochrome B Reductase 1 (*CYBRD1*) and Mitochondrial Ribosomal Protein L45 (*MRPL45*)), other than RB1, were down regulated in all cell line models.

It was not possible to compare expression levels of *RB1* in the *RB1* deficient daughter models U2OS 4.2 and 4.5 with that of OS tumour cell lines from the panel with known homozygous deletion of *RB1,* due to lack of values for mRNA expression of *RB1* from publically available data sets (COSMIC and CCLE).

Further annotation of the list of genes with protein altering mutations that differed between *RB1* wildtype and deficient tumour cell line models was performed to determine if they were also differentially expressed. Seven genes (*RB1, ERG1C1,* WD Repeat Domain 60 (*WDR60*)*,* TBC1 Domain Family Member 9B (*TBC1D9B*)*,* Ubiquitin Specific Peptidase 53 (*USP53*)*,* Keratin 8 (*KRT8*)*,* and Caspase 10 (*CASP10*)), were differentially expressed in U2OS 4.2, and five genes (*RB1, KRT8,* Chromosome 17 Open Reading Frame 75 (*C17orf75*)*,* Coatomer Protein Complex Subunit Beta 2 (*COPB2*)*,* and *USP53*)*,* as differentially expressed in U2OS 4.5. Interestingly in addition to *RB1*, differential expression was seen in both daughter tumour cell lines in *KRT8,* and *USP53*, an ubiquitin specific peptidase.

Table 15 Alterations identified by exome sequencing of the *RB1* deficient clones U2OS 4.2 and 4.5 and parental 9.1

Gene	U2OS 9.1	U2OS 4.2	U2OS 4.5
RB1		CCTGAGGAGGA>C	C>CT
ERG1C1	G>GT		G>GT
TBC1D9B	G>GTA		G>GTA
TTC6		GGGCCCTGCAT>G	
NOS2	AG>A		
GLT6D1		CA>C	
EFCAB13	CAGTG>C		CAGTG>C
C8orf34			TCCGGCTCTCAGCGC>T
PHACTR1			CTCTTT>C
GLT6D1			CA>C
NUDT1	G>T		
KLK12	C>T		
ECSCR		C>T	
WIPF2	T>G		T>G
PYROXD1	C>A		C>A
DMGDH	G>T		G>T
FAM98A	C>A		
SSTR1	C>CGCTCTGAGCCCGGGCCACGCAGGG		C>CGCTCTGAGCCCGGGCCACGCAGGG
CCL25	G>A		G>A
FAM98A	C>A		
KRT8	G>A		

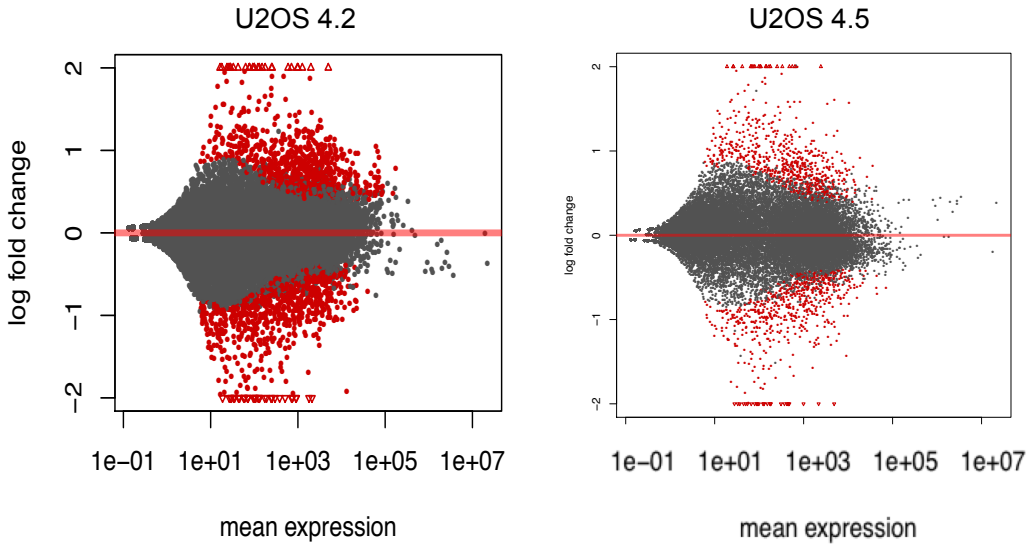

Figure 28 MA plots to visualise the relationship between log fold change in expression and mean expression of each gene for the RB1 isogenic pairs.

Scatter plots of differentially expressed genes between U2OS 4.2 and 4.5 compared to the parental clone U2OS 9.1 were defined using a False Discovery Rate (FDR) p-value of < 0.05 and are shown in red. RNA was extracted from the OS tumour cell lines U2OS 4.2, 4.5 and 9.1. Members of the TPU (ICR) performed mRNA sequencing and James Campbell and Aditi Gulati aligned the reads and performed a differential expression analysis in R using the Bioconductor package, DESeq2 (v1.14.1) which was used to generate the MA plots by Aditi Gulati. Triplicates measures of gene expression in each tumour cell line were performed.

4.2.1.4 Protein Expression of RB1 in the *RB1* isogenic models

Profiling of the clones by western blot confirmed that both 4.2 and 4.5 had lost expression of *RB1* at both the N and C-termini (Figure 29).

As another layer of annotation to further categorise the tumour cell lines into *RB1* and *CDKN2A* deficient or wildtype groups, proteomic profiling was undertaken. Proteomic abundance of RB1 demonstrated the U2OS mutants clustered with tumour cell lines harbouring known homozygous deletion of *RB1* (Figure 12).

4.3 DISCUSSION

At the commencement of this thesis, no human isogenic models of loss of *RB1* in osteosarcoma had been described. Therefore, a panel of tumour cell lines was used to describe the genetic dependencies in osteosarcoma with the aim of identification of candidate synthetic lethalities, while an isogenic model was created using CRISPR-Cas9 mediated mutagenesis.

The advantages and disadvantages of isogenic versus non-isogenic models have already been discussed. Employment of both types of models has the potential to increases the success of generating candidate genetic dependencies which are synthetically lethal with *RB1* loss, but which can also be extrapolated across a wider panel of tumour cell lines.

Two *RB1* deficient models of OS were engineered using CRISPR-Cas9, which were both confirmed to have homozygous loss of function mutations by both Sanger and whole exome sequencing, and loss of expression of both the N and C terminus of RB1 by western blotting. Proteomic profiling provided further annotation, which demonstrated that the level of abundance of RB1 was comparable with the OS tumour cell lines known to harbour homozygous deletions of *RB1*. In order to investigate the transcriptional changes associated with *RB1* deficiency, whole transcriptome analysis was performed in the *RB1* isogenic U2OS models. *RB1* mRNA levels were significantly reduced (false discovery rate ≤ 0.05) in both the *RB1* deficient models. Therefore, these models were robustly determined to suitable models to investigate the phenotype of *RB1* deficiency in OS.

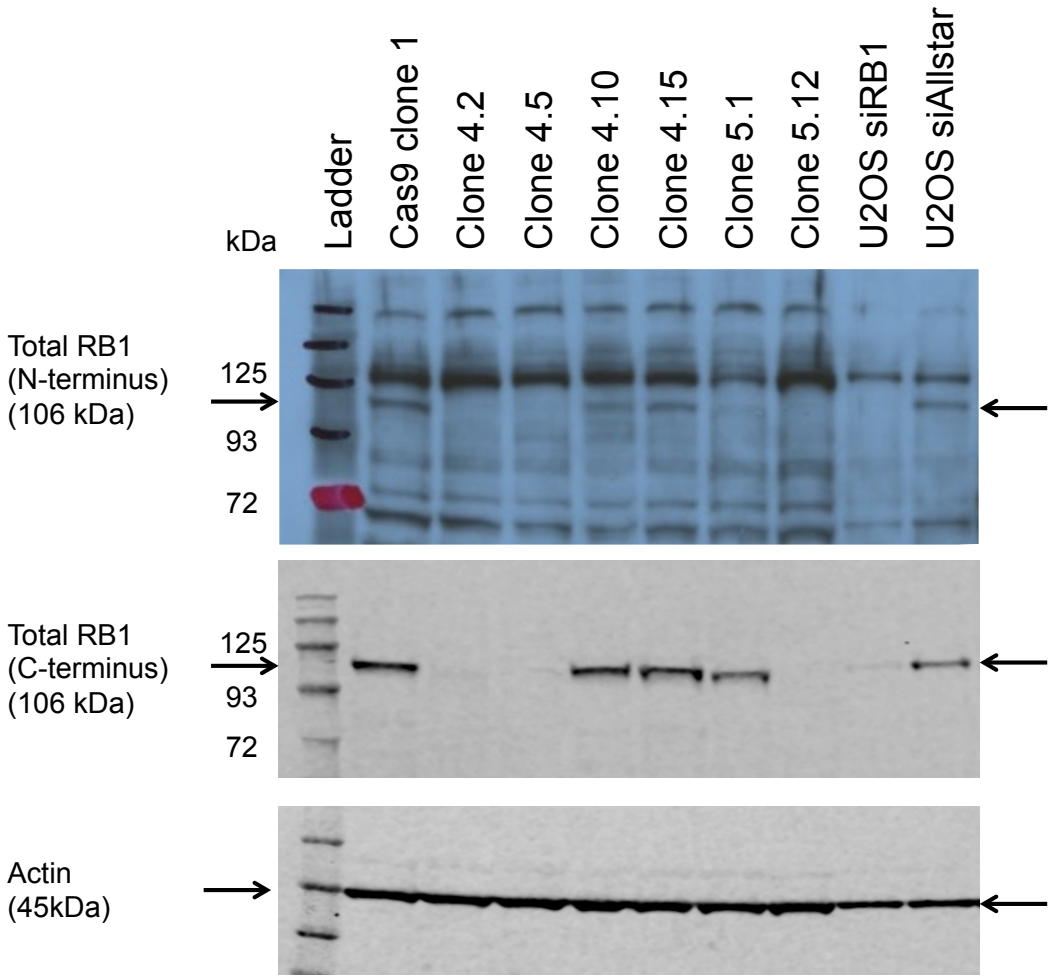

Figure 29 U2OS *RB1* mutant clones (4.2 and 4.5) generated by CRISPR-Cas9 do not express RB1 unlike *RB1* wildtype parental U2OS 9.1.

Western blotting of RB1 using antibodies to both the N and C termini for U2OS clones 4.2, 4.5, 4.10, 4.15, 5.1 and 5.12 and the Cas9 only control 9.1. Lysates of U2OS collected 48 hours post transfection with siRNA targeting *RB1* and the non-targeting siAllstar were used as positive and negative controls. Molecular weight of protein markers (ladder) shown in kilodaltons. Whole cell lysates were collected from untreated tumour cells, electrophoresed and immunoblotted as described in Methods. Immunoblotting of actin was used as the loading control.

5 Identifying genetic dependencies in osteosarcoma

5.1 INTRODUCTION

This chapter describes the use of a high-throughput cell-based screen using a custom library of short interfering RNA (siRNA) oligonucleotides to identify candidate genetic dependencies in osteosarcoma. This system offers a relatively unbiased and rapid approach to systematically assessing the genetic contribution to a particular cellular phenotype. Although whole genome RNAi screens are possible, a focused screening using a subset of the most tractable genes was chosen to generate genetic dependency profiles of multiple models of osteosarcoma.

RNA interference (RNAi) enables post-transcriptional gene silencing and has been performed using either small interfering RNA (siRNA) or small hairpin RNA (shRNA) (Willingham, Deveraux, Hampton, *et al.*, 2004; Lord, Martin & Ashworth, 2009; Brough, Frankum, Sims, *et al.*, 2011; Iorns, Lord, Turner, *et al.*, 2007) to identify novel genes involved in biological processes.

Non-protein coding miRNAs are transcribed from the genome and then processed in the nucleus into shorter RNA species bearing a hairpin structure (shRNAs) (Lord, Martin & Ashworth, 2009). shRNAs are exported from the nucleus and further processed into small RNA duplexes (siRNAs), which are loaded into the RNA-induced silencing complex (RISC) which facilitates binding between one of the siRNA strands and protein-coding mRNAs that have nucleotide sequence complementary to the siRNA (Lord, Martin & Ashworth, 2009). Once siRNA/mRNA binding has occurred, and the target mRNA transcript recognised, a nuclease in RISC degrades the mRNA, thereby ultimately reducing the amount of mRNA that is available for translation and protein production (Lord, Martin & Ashworth, 2009). These steps are summarised in Figure 30.

Small or short hairpin RNA (shRNA) comprise approximately 65 nucleotide sequences that are cloned into a viral vector backbone, enabling production of viral particles capable of transduction of the cell of choice. shRNA libraries can be classified by the type of vector used; such as non-viral (plasmid), retroviral, adenoviral or lentiviral (Iorns, Lord, Turner, *et al.*, 2007). Screens based on shRNA vectors can provide long-term gene silencing since the vectors used are able to integrate into genomic DNA and are thus copied along with cellular DNA (Iorns, Lord, Turner, *et al.*, 2007). One of the main

limitations of shRNA is the inherent instability of some of the viral systems used to express them, limiting their wider exploitation. In contrast, siRNA are approximately 20 base pairs in length and do not require a vector for transfer, but do require the target cells to be transfectable (Lord, Martin & Ashworth, 2009). Synthetic synthesis of siRNA results in consistent quality of reagents (Lord, Martin & Ashworth, 2009). siRNA only provide a relatively short period of silencing, as they are most likely degraded by the target cell, and not replicated with the genomic DNA (Lord, Martin & Ashworth, 2009).

Analysis of siRNA screen data demonstrates a wide range of effects across cell lines. It has been reasoned that siRNAs causing significant loss of cell viability in all cell lines assayed are likely to target genes that have an essential ubiquitous function in both normal and tumour cells (Brough, Frankum, Sims, *et al.*, 2011). Similarly, siRNAs with no major effect on viability in any of the cell lines either are not functional or target nonessential genes (Brough, Frankum, Sims, *et al.*, 2011). Therefore, Brough *et al.* postulated that siRNAs causing significant lethality in the majority, but not all, cell lines most likely identify genes that represent tumour-specific dependencies and candidate therapeutic targets (Figure 31) (Brough, Frankum, Sims, *et al.*, 2011). This approach generated a measure of viability for each of the siRNAs in the cell lines, expressed as Z scores, to allow comparison of data across the panel of cell lines, and to minimise the impact of variation caused by transfection efficiency between cell lines (Brough, Frankum, Sims, *et al.*, 2011).

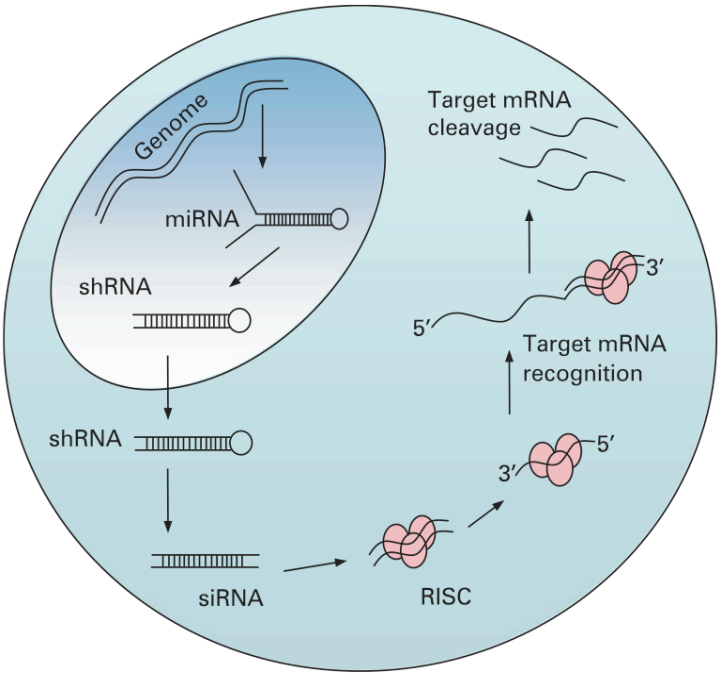

Figure 30: Schematic describing RNA interference.

Non-protein coding miRNAs are transcribed from the genome and then processed in the nucleus into shorter RNA species bearing a hairpin structure (shRNAs). shRNAs are exported from the nucleus and further processed into small RNA duplexes (siRNAs), which are loaded into the RNA-induced silencing complex (RISC) which facilitates binding between one of the siRNA strands and protein-coding mRNAs that have nucleotide sequence complementary to the siRNA. Once siRNA/mRNA binding has occurred, and the target mRNA transcript recognised, a nuclease in RISC degrades the mRNA, thereby ultimately reducing the amount of mRNA that is available for translation and protein production. (Reproduced from Lord *et al.* (Lord, Martin & Ashworth, 2009)).

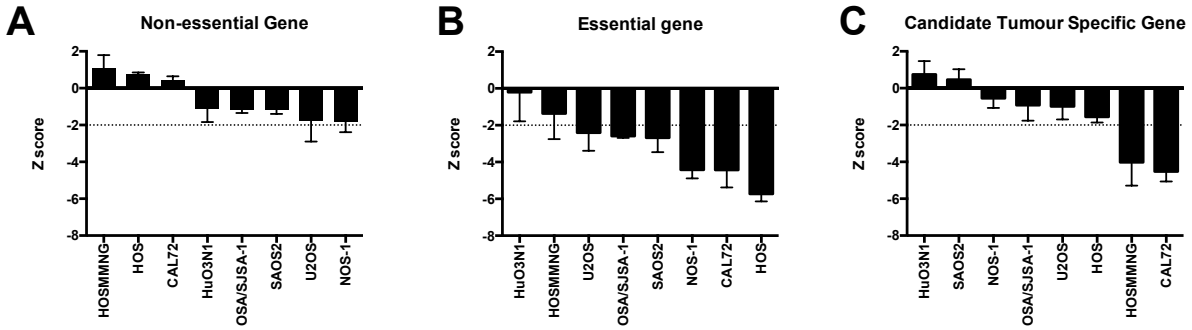

Figure 31 Example of discrimination of essential and non-essential genes via waterfall plot of Z-scores.

(A) siRNAs with no major effect on viability in any of the cell lines are either not functional or target nonessential genes.

(B) siRNAs causing significant loss of cell viability in all cell lines assayed are more likely to target genes that have an essential ubiquitous function.

(C) siRNAs causing significant lethality in the majority, but not all, cell lines are most likely to identify genes representing tumour-specific dependencies and candidate therapeutic targets (Brough, Frankum, Sims, *et al.*, 2011).

Adapted from Brough *et al.* (Brough, Frankum, Sims, *et al.*, 2011).

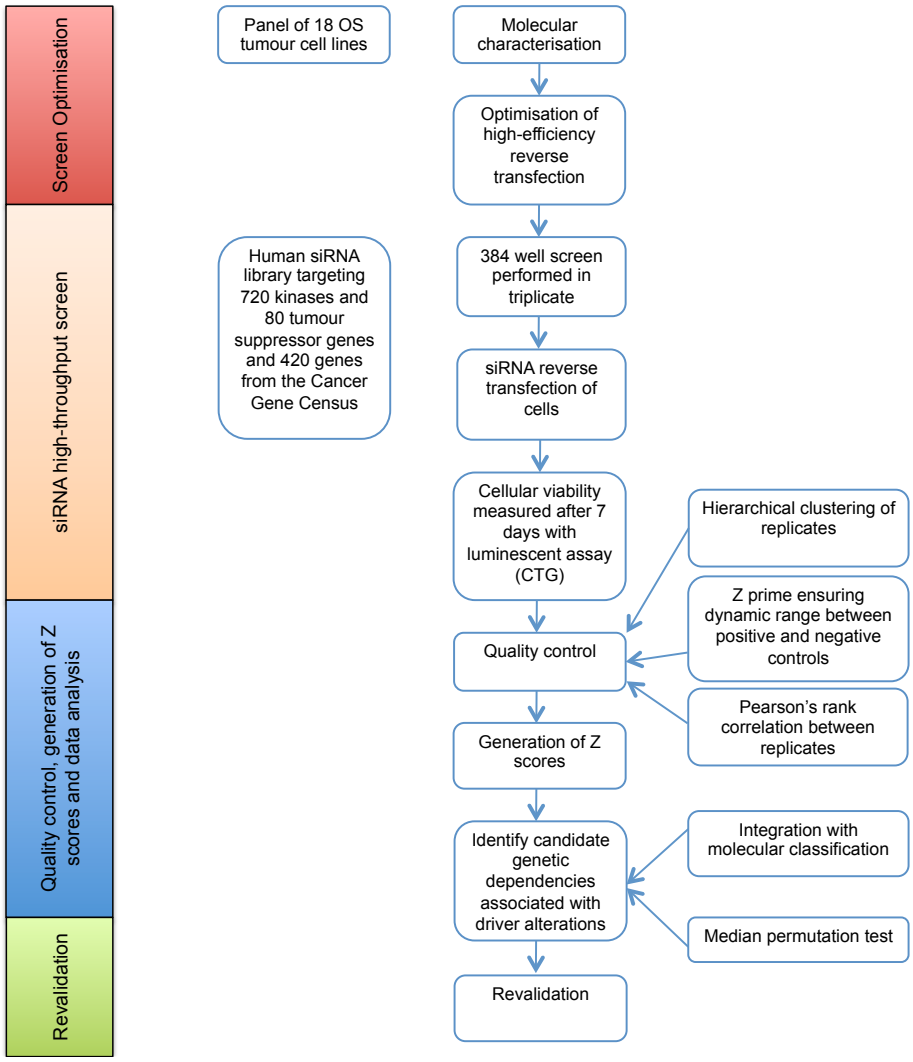

Figure 32 Schematic of overview of high-throughput siRNA screen.

First, transfection conditions for the panel of characterised OS tumour cell lines were optimised for each cell line. Cells were arrayed in triplicate and reverse transfected in 384-well plate format in variable densities and transfection reagents. After seven days, cell viability was measured using a luminescence assay that measures the metabolic activity of the cell using CellTiter-Glo (Promega). Optimal conditions were chosen which demonstrated the greatest dynamic range between negative and positive controls, with high reproducibility between the replicates. Secondly, the siRNA screens were performed in triplicate in 384 well plate format using an in-house library containing 720 kinases, 80 tumour suppressor genes and 480 genes from the Cancer Gene Census (Futreal, Coin, Marshall, *et al.*, 2004). Thirdly, each screen was subjected to rigorous quality control measures to ensure reproducibility, and a sufficient dynamic range. Only screens that passed these pre-define criteria were analysed further. Cell viability scores were plate centred and transformed to Z scores, for further analysis. The median permutation test was used to identify candidate genetic dependencies associated with gene alterations.

In order to maximise the potential for identification of candidate genetic dependencies specific to OS, a siRNA screen was performed in the panel of 18 OS tumour cell lines described in Chapter three. A schematic of the steps performed is shown in Figure 32. Optimisation of high-efficiency reverse transfection was performed for all of the tumour cell lines. Optimal conditions were chosen which demonstrated the greatest dynamic range between negative and positive controls, with high reproducibility between the replicates. Secondly, the siRNA screens were performed in triplicate in 384 well plate format using an in-house library containing 720 kinases, 80 tumour suppressor genes and 420 genes from the Cancer Gene Census (Futreal, Coin, Marshall, *et al.*, 2004). A complete list of the genes included in each RNA sub-library is provided in Appendix Tables 1-3. Thirdly, each screen was subjected to rigorous quality control measures to ensure reproducibility, and a sufficient dynamic range. Only screens that passed these pre-define criteria were analysed further. Cell viability scores were plate centred and transformed to Z scores, for further analysis. The median permutation test and T-tests were used to identify candidate genetic dependencies associated with gene alterations.

5.2 RESULTS

5.2.1 Screen optimisation

Eighteen osteosarcoma tumour cell lines (described previously in Chapter three), to be used for subsequent screening, were reversed transfected in 384-well plate format to determine the optimal cell density and transfection reagent. The ideal transfection reagent would permit efficient entry of the siRNA following membrane permeabilisation without any toxicity to the cell in the absence of siRNA since non-specific toxicity to the cell could reduce the screen specificity. To allow efficient transfection, the density of cells was titrated such that the cells did not reach confluence at the end point of the experiment (day seven). Cells were seeded at 250 and 500 cells per well, and three transfection reagents (Lipofectamine 2000, Dharmafect 4, and RNAMax) were tested to determine the optimal cell density and transfection reagent for each cell line. As a positive control to ensure successful transfection, an siRNA targeting Polo-like kinase (siPLK), which is essential for viability was used (Strebhardt & Ullrich, 2006). Three non-targeting controls (siControl1, siControl2, and siAllstar) were used as negative controls. Cell density and transfection reagent was decided on the basis of which produced the

maximum separation difference between survival fraction in the positive and negative controls. Within each plate 16 “mocks” at each cell density consisting of the same volume of media (35µL) with the addition of 10µL optimem to reach the same final volume (45µL) as the samples were plated. The survival fraction (SF) was calculated by the division of each sample by the median of the negative controls (non-targeting siRNA):

Survival fraction = sample / median of the ‘mocks’

Selected optimisation conditions for each of the OS tumour cell line panel, determined by comparison of the survival fractions for each siRNA condition (siCON1, siCON2, Allstar, and PLK) are demonstrated in Figure 33 and summarised in Table 16. Optimal conditions were considered to be: (i) viability of <30% in siPLK wells; and (ii) viability relative to the ‘mocks’ (wells without siRNA reagents) of >60% in two or more negative controls (Brough, Frankum, Sims, *et al.*, 2011). Two cell lines (G292 Clone A141B1 and KPD) initially failed this first optimisation stage because of survival fractions of less than 50% in the negative controls and so were repeated successfully at higher cell densities of 750 and 1000 cells per well. For 15 of the tumour cell lines the SF for the positive control (siPLK) was less than 30% and greater than 60% in at least two of the three negative controls (siCON1, siCON2 and allstar). Three (U2OS, KPD and OSA) had a SF of less than 50% in two of the three negative controls. However, all PLK values for these tumour cell lines were all less than 10%, thus deemed to have adequate separation of controls and resulting dynamic range for screening.

5.2.2 siRNA screen overview

A siRNA library targeting 720 known and putative human protein kinases, 80 tumour suppressor genes and 480 genes included in the Cancer Gene Census (Futreal, Coin, Marshall, *et al.*, 2004) was obtained in 384-well plates from Dharmacon (GE, 3135 Easton Turnpike, Fairfield, CT 06828, United States of America). A complete list of the genes included in each RNA sub-library provided in Appendix Tables 1-3. Each well contained 5µL (200nM) of a SMART pool of four distinct siRNA species targeting different sequences of the single target transcript. Additional positive (siRNA targeting PLK1) and negative (non-targeting siRNA: siControl1, siControl2 and siAllstar (Qiagen)) controls were added to the edges of each plate (8 wells of each control) (Figure 34), with an

internal well of siPLK within the first plate (each screen consists of three 384 well plates). Each siRNA screen was carried out in triplicate.

5.2.3 Osteosarcoma siRNA screen quality control

To determine that the screening process was robust and reproducible, specific parameters were used as measures of quality control. Calculation of the Spearman's rank correlation coefficient was used as a measure of the reproducibility between the replicates of each screen (Table 17). A Spearman's rank value of one represented strong correlation, and zero no correlation. All tumour cell lines passed the stringent quality control with a mean Spearman's Rank correlation of all three replicates approaching 1 (>0.7) (Turner, Lord, Iorns, *et al.*, 2008; Iorns, Turner, Elliott, *et al.*, 2008).

A measure of the quality of the screen, the Z prime, based on the dynamic range of negative and positive controls was calculated (Figure 35). The dynamic range of each screen was determined by calculating Z prime values (Zhang, Chung & Oldenburg, 1999), based on positive (siPLK) and negative (siCON1, siCON2 and allstar) control wells in each plate, which were used as a marker of quality (Figure 35). A minimum of two negative controls and one positive control was used for each analysis. Z prime values greater than >0.3 have been shown to be representative of reproducible data (Zhang, Chung & Oldenburg, 1999), and were considered acceptable, with a Z prime 0.5 – 1 demonstrating a robust and powerful screen (Brough, Frankum, Sims, *et al.*, 2011). Spearman Rank Correlation (as described above) determined the reproducibility between the replicates.

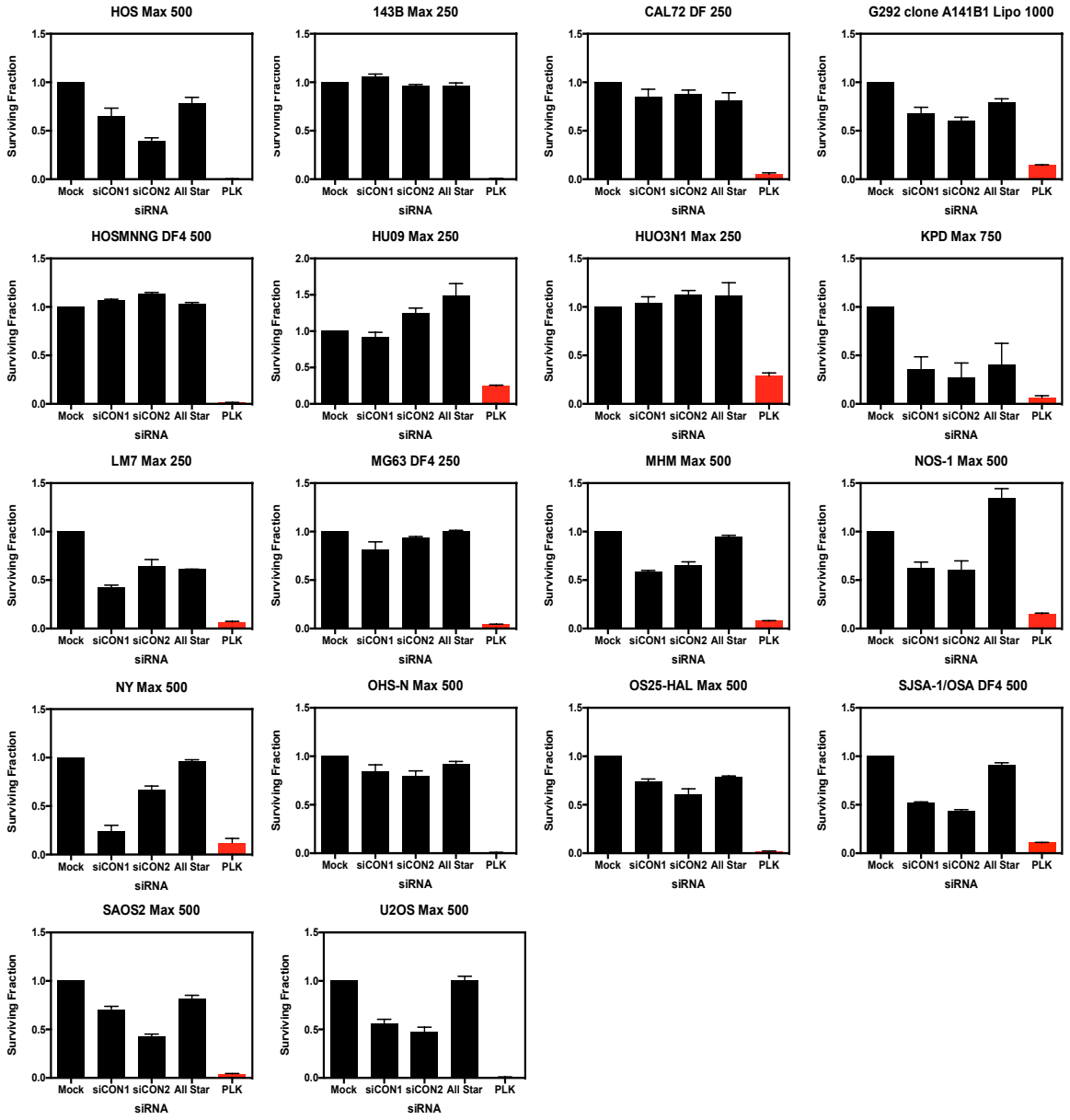

Figure 33 Selected optimisation conditions for high efficiency reverse transfection of the panel of osteosarcoma tumour cell lines.

Bar charts illustrate the effect of siRNA non-targeting negative (siControl1, siControl2, and siAllstar) and positive control (siPLK) on viability. Viability was calculated relative to mock transfection, where mock refers to treatment with lipid transfection mix only, with no addition of siRNA. Each graph represents the optimal transfection reagent and cell density for each cell line in 384-well plate format. For the majority (15/18) of the tumour cell lines, the siPLK reduced the surviving fraction to <30%, while the negative control siRNA (siCON1, siCON2, or siAllstar), resulted in a surviving fraction of >60% in two out of three controls. Error bars represent standard error of mean (SEM). [LF2000; Lipofectamine 2000; DF4: Dharmafect 4; Max: RNAmax]

Table 16 Summary of optimised reverse transfection conditions for each tumour cell line screened in the RNAi viability profiling

Cell Line	Lipid	Number of cells per well (384 well plate)
CAL72	Dharmafect 4	250
HU03N1	RNA max	250
HOSMNNG	Dharmafect 4	500
OSA/SJSA-1	Dharmafect 4	500
NOS-1	RNA max	500
MG63	Dharmafect 4	250
SAOS2	RNA max	500
U2OS	RNA max	500
HOS	RNA max	500
OHS-N	RNA max	500
MHM	RNA max	500
OS25-HAL	RNA max	500
LM7	RNA max	500
KPD	RNA max	750
HU09	RNA max	500
NY	RNA max	500
G292 clone A141B1	Lipofectamine 2000	1000
143B	RNA max	250

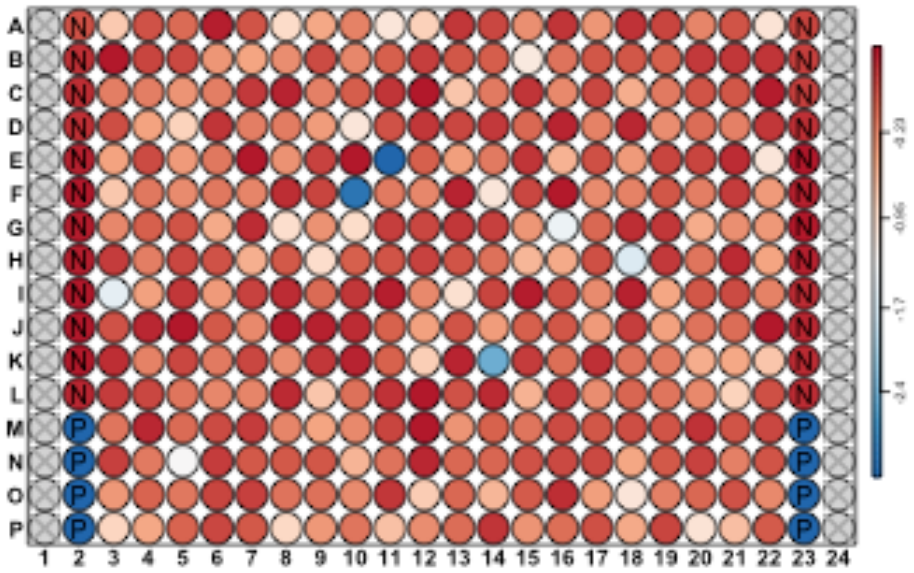

Figure 34: Illustrative example of luminosity read-out as a measure of viability for a 384 well siRNA screening plate.

Graphic illustrating cellular viability where blue represented loss of viability, orange represented some loss of viability, while red represented no loss of viability. Graphical representation of viability enables easy recognition of any edge effects or plating errors, and preliminary confirmation of successful controls. Cell lines were transfected with SMART pool siRNA using RNAiMax (Invitrogen), Lipofectamine 2000 (Invitrogen) or Dharmafect4 (Dharmacon) as per the results of prior optimisation described in section 5.2.1. After the addition of 35µL cell suspension to each well, the final concentration of siRNA was 20nM. Each cell line was screened in triplicate on the same day. After seven days cell viability was quantified via a highly sensitive luminescent assay measuring cellular ATP levels (CellTiter Glo; Promega). [Controls plated in Columns 2 and 23 (siCON1: rows A-D; siCON2: rows E-H; siALLSTAR: rows I-L; siPLK1: rows M-P). N= negative control, P = positive control.]

A Z prime of less than 0.3 was calculated in five tumour cell lines (KPD, HU09, NY, CAL72, and OSA/SJSA-1), because of reduced impact on viability by siPLK and/or more effect on viability by the negative controls. Using a subset of other cell lines that had undergone the same screening process by other members of the laboratory (n=99: 27 breast; 19 ovary; 19 lung; 14 oesophagus; 5 pancreas; 5 head and neck; 4 cervical; 4 central nervous system; 2 endometrium)(Campbell, Ryan, Brough, *et al.*, 2016), I was able to compare the magnitude of effects on viability of siRNA directed against *PLK* and other mitotic check points such as Aurora Kinase A (*AURKA*) and WEE1 G2 Checkpoint Kinase (*WEE1*) in a wider panel of tumour cell lines (Figure 36). From the non-osteosarcoma tumour cell line panel dataset four mitotic cell-cycle checkpoint kinases (*PLK1, AURKA, WEE1*, Chekpoint Kinase 1 (*CHEK1*)), Cyclin Dependent Kinase 11A (*CDK11A*), and Guanylate Cyclase 2D (GUCY2D) represented candidate genetic dependencies in more than 70% of the tumour cell lines screened (Campbell, Ryan, Brough, *et al.*, 2016). Therefore, comparison of loss of viability for these genes was deemed a robust alternative method of confirming dynamic range. Comparison of the viability by silencing these additional genes (*AURKA, WEE1* and *GUCY2D*) demonstrated that these OS screens were similar to those with a Z prime greater than 0.3 (Figure 36). This suggested that siPLK did not have a uniform effect on viability in all tumour cell lines but for tumour cell lines with a Z prime of greater than 0.3, siPLK was usually the most negative Z score. Whereas for the five tumour cell lines with a Z prime of less than 0.3, this was not the case, since hits from the screening library had a greater effect on viability. These five screens were therefore determined to be valid, and included in the panel, resulting in all 18 screens with robust viability profiles.

5.2.4 Analysis of Raw data

To account for the plate-to-plate variation common in high-throughput screens, raw luminescence readings from each well were $\log_2$ transformed and centred by the plate median. The data was normalised in this way, to also adjust for systemic errors of the screen for example variations in incubation time, differences in time when measuring luminescence values, or reagent evaporation, whilst preserving biologically relevant variation (Boutros, Brás & Huber, 2006). To allow data comparison between siRNA screens from individual tumour cell lines, the data was standardised by the use of a Z-score statistic; the plate-centred data was standardised to median effects of the library and the median absolute deviation (MAD). A Z score of zero represented no effect on

viability, while negative Z-scores represented loss of viability (Brough, Frankum, Sims, *et al.*, 2011). All three replicates for each cell line were combined in the final analysis; the median Z-score for each individual siRNA was calculated using the median normalised value of each siRNA and the MAD in order to account for the variance within each screen (Boutros, Brás & Huber, 2006). The Z score statistic assumes a normal distribution, with the assumption that the majority of siRNA tested would have little or no effect on viability. The distribution of each screen was assumed to approximate to normal, allowing comparison of the individual siRNA effects in multiple tumour cell lines. A schematic detailing data analysis from raw luminescence values to Z scores is shown in Figure 37.

5.2.5 Compilation of the dataset

There are a number of possible methods to align multiple distributions of data sets to aid comparison of the Z scores of screens with a large difference in magnitude. Normalised percentage inhibition (NPI), is one such method which has been used in a similar high-throughput RNAi screen (Mendes-Pereira, Lord & Ashworth, 2012). Calculation of NPI requires limits to be defined, usually as the maximal inhibitory effect as that caused by siRNAs targeting PLK, and the minimal effect as that caused by non-targeting control siRNAs. Since, siPLK did not have uniform effects on viability in the tumour cell lines, quantile normalisation (QN) (Bolstad, Irizarry, Astrand, *et al.*, 2003; Qiu, Wu & Hu, 2013) of the data set was chosen instead. QN enables alignment of multiple distributions with consideration of rank and magnitude.

Table 17 RNAi screen quality control: spearman's rank correlation coefficient for correlation of replicates and Z prime.

All OS tumour cell lines had Spearman's rank correlation coefficients approaching one (>0.7) and therefore, deemed to be reproducible (Turner, Lord, Iorns, *et al.*, 2008; Iorns, Turner, Elliott, *et al.*, 2008).

Cell Line	Spearman's Rank Correlation Coefficient			Z Prime		
	R1 v. R2	R2 v. R3	R1 v. R3	R1	R2	R3
CAL72	0.8977	0.9087	0.8917	0.06	0.18	0.06
HU03N1	0.7340	0.7888	0.7563	0.43	0.26	0.35
HOSMNNG	0.9216	0.9108	0.9119	0.81	0.81	0.80
OSA/SJSA-1	0.9512	0.9515	0.9478	-0.09	-0.29	-0.45
NOS-1	0.8650	0.8524	0.8239	0.55	0.50	0.59
MG63	0.8880	0.8830	0.8101	0.64	0.65	0.71
SAOS2	0.7914	0.6632	0.6623	0.35	0.56	0.52
U2OS	0.9203	0.9018	0.8644	0.36	0.34	0.39
HOS	0.7899	0.8079	0.9470	0.68	0.67	0.72
OHS-N	0.8776	0.8740	0.8900	0.37	0.45	0.39
MHM	0.8511	0.8557	0.8072	0.66	0.59	0.57
OS25-HAL	0.7983	0.8073	0.7316	0.61	0.59	0.61
LM7	0.8570	0.8319	0.7772	0.69	0.64	0.60
KPD	0.8784	0.9105	0.8916	0.24	0.16	0.25
HU09	0.8023	0.7806	0.7147	0.02	-0.16	-0.41
NY	0.8882	0.8774	0.8123	0.14	0.01	0.09
G292 clone A141B1	0.9243	0.9120	0.8898	0.45	0.48	0.49
143B	0.9052	0.9045	0.8911	0.76	0.75	0.79

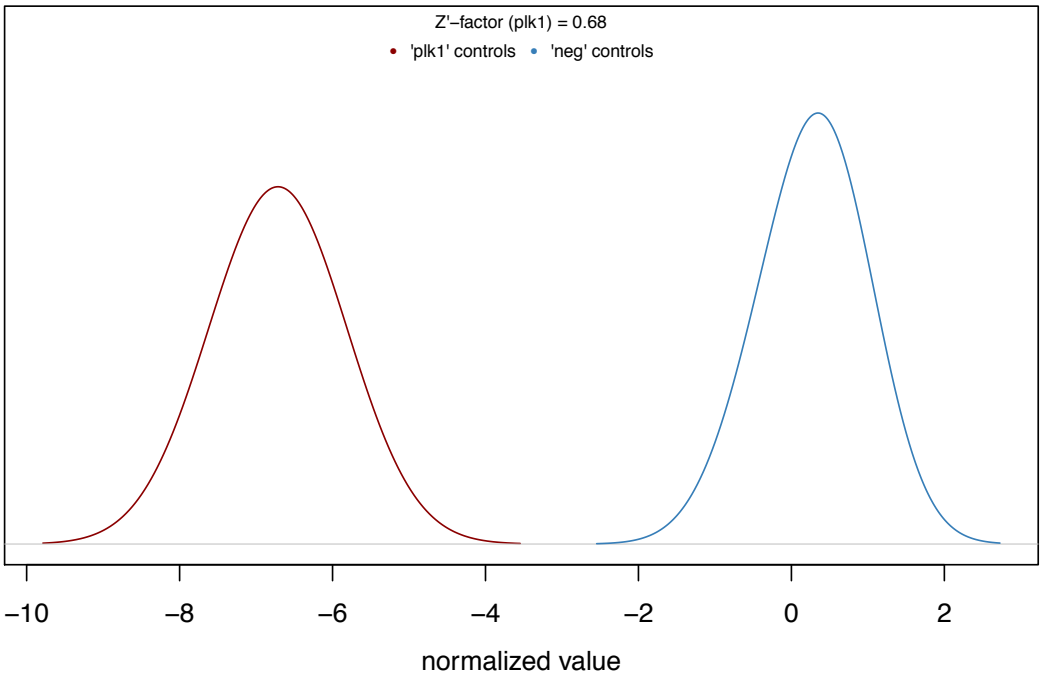

Figure 35 Clear separation of positive and negative controls confirmed by a Z prime of greater than 0.3.

Distribution plot illustrating Z score values for positive and negative controls, which show clear separation, for one replicate of the siRNA screen performed in the OS tumour cell line HOS. Negative controls (siCON1, siCON2, siALLSTAR) shown in blue, positive controls (siPLK1) shown in red. The dynamic window shown by calculation of the separation of negative and positive controls, was termed Z prime. Cells were reverse transfected, and after seven days viability estimated using CellTiter Glo as described in the Methods. Raw luminescence values were processed using the CellHTS package of the R software suit (BioConductor), used to generate this distribution plot and calculate the Z prime. [plk: siPLK positive control; neg: non-targeting siRNA species used as negative controls]

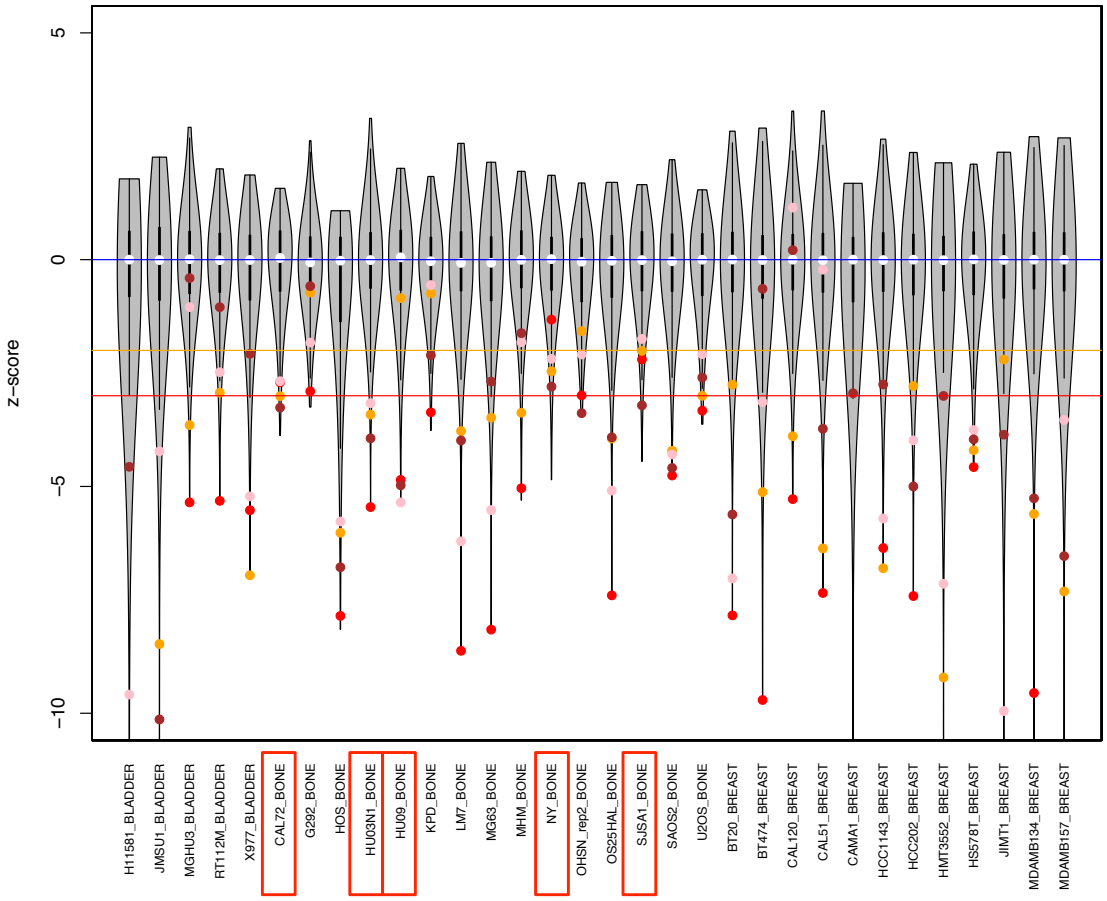

Figure 36 Comparison of Z scores from RNAi screens in osteosarcoma, bladder and breast tumour cell lines highlighted the variance of Z scores and effects on viability by the mitotic check-point kinases (siPLK, siAURKA, siWEE1) and siGUCY2D.

Violin plot of Z scores for each RNAi screen in OS, bladder and breast tumour cell lines to compare the magnitude of effects of viability of siRNA targeting *GUCY2D* (orange) and the mitotic check-point kinases *PLK* (red), *AURKA* (pink), and *WEE1* (brown). Tumour cell lines with Z prime of less than 0.3 were highlighted in red. Comparison of the viability by silencing (*AURKA, WEE1* and *GUCY2D*) demonstrated that these OS screens were similar to those with a Z prime greater than 0.3 and deemed to be valid. From the RNAi data set of 117 tumour cell lines (including OS), a set of six kinase-coding genes (*PLK1, AURKA, WEE1, CHEK1, CDK11A*, and *GUCY2D*) has been determined to represent candidate genetic dependencies in greater than 70% of the tumour cell lines screened (Campbell, Ryan, Brough, *et al.*, 2016). Cells were arrayed in triplicate 384 well plates, reverse transfected, and after seven days viability estimated using CellTiter Glo as described in the Methods. Raw luminescence values were converted to Z score statistics to enable comparison between screens. CAL72 had identical Z scores (-2.8) for PLK1 and AURKA. [Red: siPLK; orange: Guanylate Cyclase 2D (GUCY2D); pink: Aurora Kinase A (AURKA); brown: WEE1 G2 Checkpoint Kinase (WEE1)]

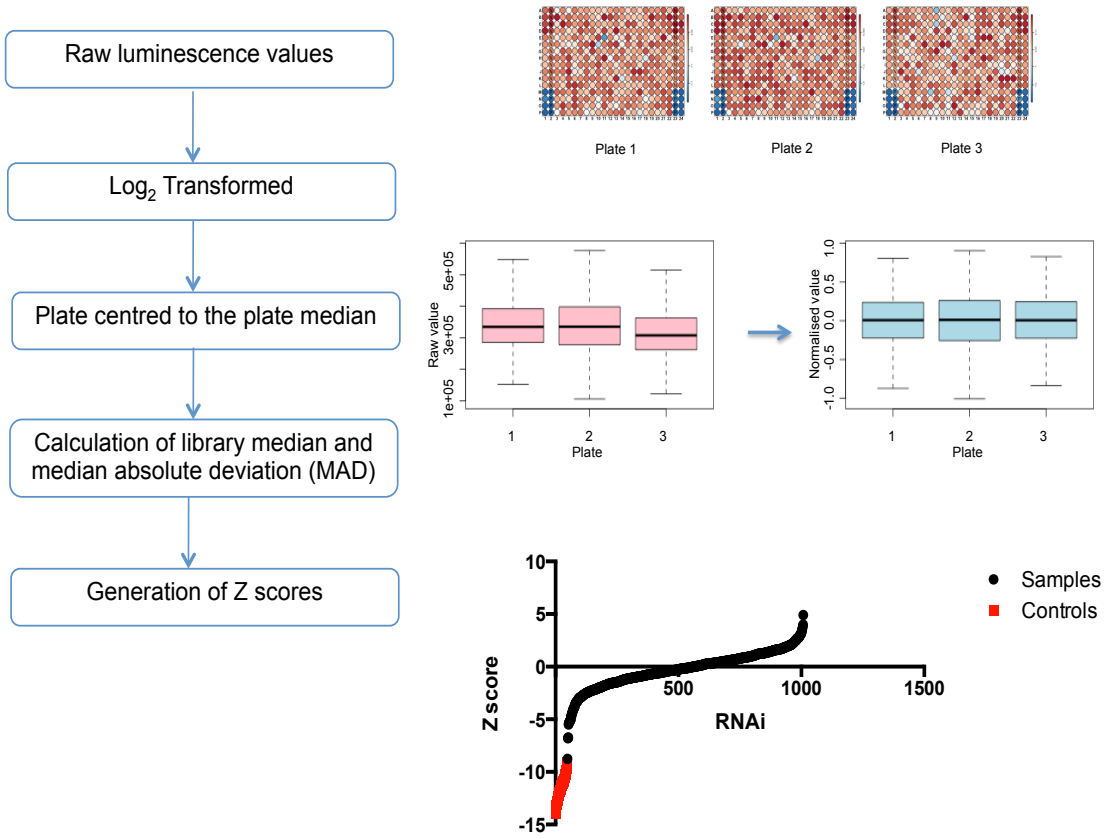

Figure 37 Schematic of data analysis from raw luminescence values to generation of Z scores.

Raw luminescence values from the siRNA screens performed in triplicate were first log_2 transformed and then plate centred by the plate median to account for plate-to-plate variation. To allow data comparison between siRNA screens from individual tumour cell lines, the data was standardised by the use of a Z-score statistic; the plate-centred data was standardised to median effects of the library and the median absolute deviation (MAD). A Z score of zero represented no effect on viability, while negative Z-scores represented loss of viability (Brough, Frankum, Sims, *et al.*, 2011). Each replicate of the screen for each tumour cell line was used in the analysis and the median Z-score for each individual siRNA was calculated using the median normalised valued of each siRNA and the MAD, to account for the variance within the screen. Illustrative examples of triplicate raw luminosity read-outs as a measure of viability for 384 well siRNA screening plates are shown. Box and whisker plots of median and range of Log2 transformed data for each replicate of the screen shown in pink, and in blue after plate centred by the plate median (normalised data). Scatter plot illustrating range of the median Z scores for an individual RNAi screen in an OS tumour cell, with the positive controls (siPLK) highlighted in red and genes of interest (samples) in black.

Quantile normalisation of the Z scores was kindly performed by James Campbell using the preProcessCore package (Bioconductor). This method (originally described by Bolstad et al. (Bolstad, Irizarry, Astrand, et al., 2003)) adjusts the distribution of z-scores for each cell line so as to make each of them identical whilst maintaining the approximate magnitude of the original z-scores. The principle of quantile normalisation is to first rank order (sort) z-scores for each cell line, average the values across each rank and then return the averaged values to the original order. The effect of QN on alignment of the distribution of the Z scores across the panel of 18 tumour cell lines can be seen in Figure 38 and Figure 39. A Z score threshold of <-1.5 representing 1.5 median absolute deviation (MAD) effects from the median effect was used to define significant loss of viability.

From this data set, it was possible to determine the genes whose depletion by siRNA caused loss of viability with a QN Z score less than minus 1.5 for each cell line (Figure 39). This analysis shows the predominant genetic dependencies for each cell line, and the QN Z scores were used as a basis for all further comparisons.

5.2.6 Identification of candidate genetic dependencies

The median permutation test and Student's t-tests were used to identify candidate genetic dependencies associated with gene alterations between groups of tumour cell lines. The Student's t test was calculated using Microsoft Excel or GraphPad Prism. James Campbell, at the ICR, performed the median permutation test (MPT) using a custom script on R. The MPT is a random sampling test to calculate the median difference between two groups. One million random samples for the two groups are performed. A false discovery rate (FDR) was set at 0.1. The median permutation test does not assume that both data sets have a normal distribution, unlike the T-test, and so is a more rigorous selection method for identification of candidate genetic dependencies.

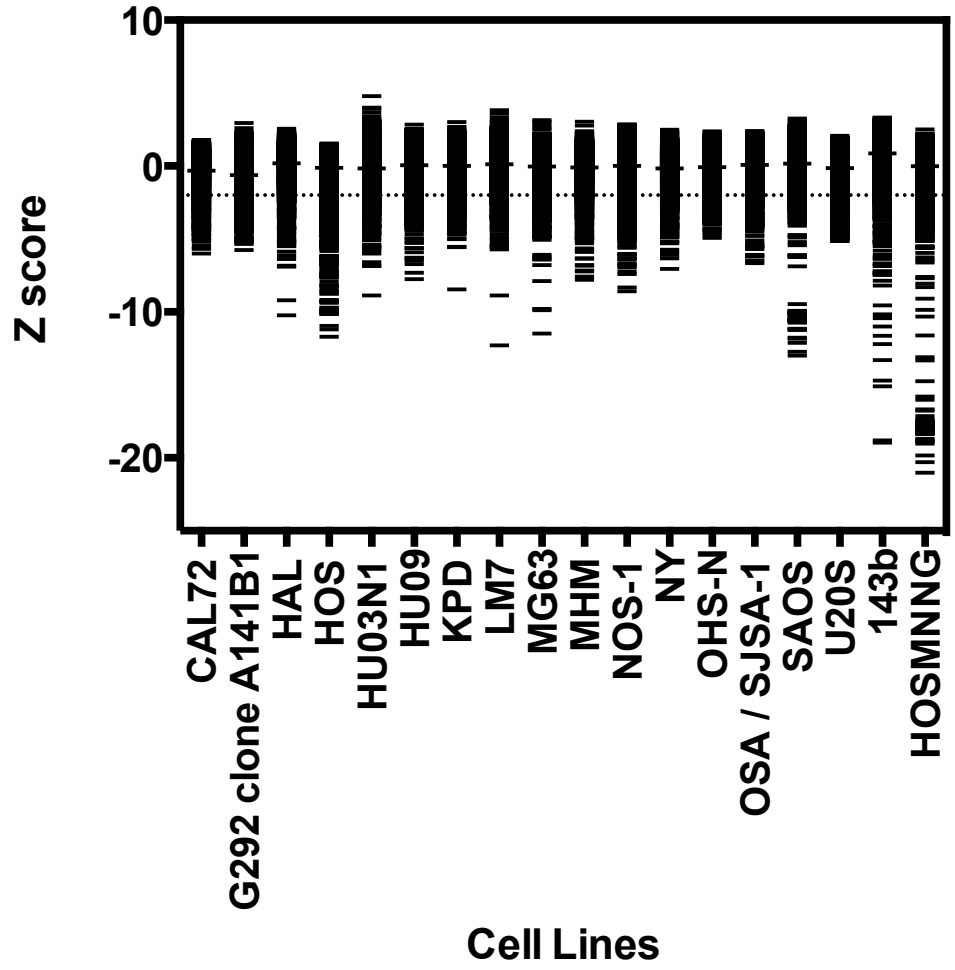

Figure 38 Range of Z scores for each RNAi screen for 18 OS tumour cell lines.

Dot plot of range of Z scores for each OS tumour cell line, where each line represented a median Z score for each individual siRNA within the RNAi library, and the median Z score for the entire screen shown by a wider line. It was apparent that the range of Z scores varied between OS tumour cell lines. Cells were arrayed in triplicate 384 well plates, reverse transfected and after seven days viability was estimated using CellTiter Glo as described previously. Raw luminescence values were log2 transformed, plate centred to the plate median, and standardised to median effects of the library and MAD into Z scores. Each replicate of the screen for each tumour cell line was used in the analysis, and the median Z score for each individual siRNA was calculated using the median normalised value of each siRNA and the MAD to account for variance within the screen.

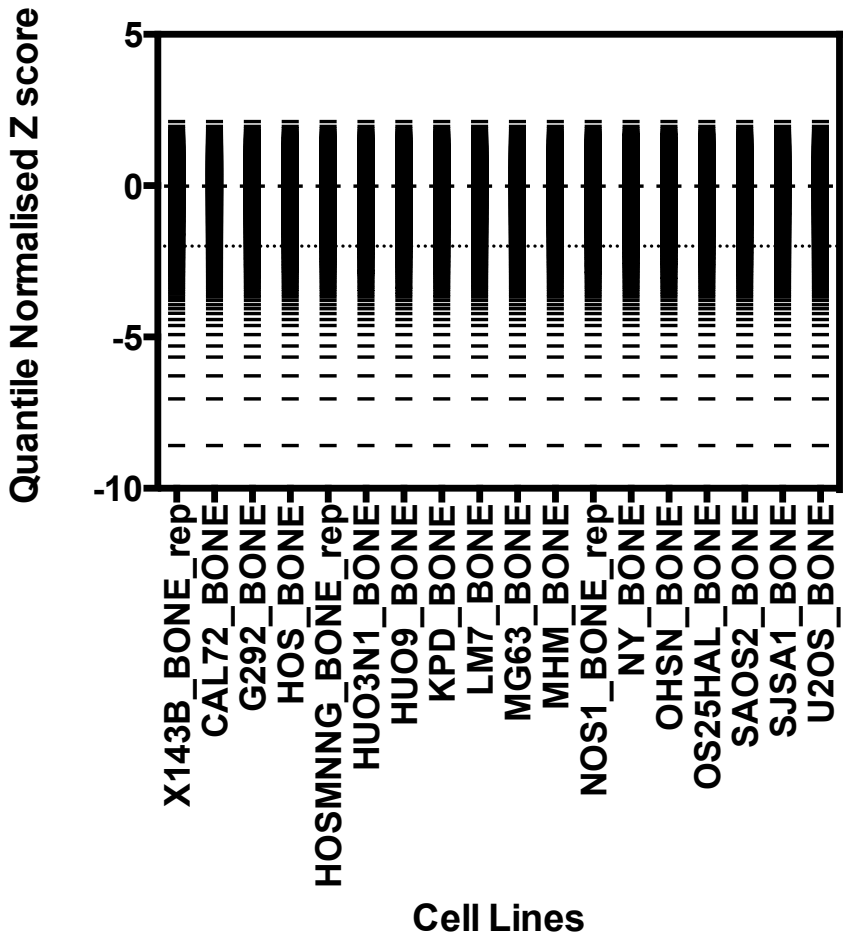

Figure 39 Effects of quantile normalisation on Z scores for each RNAi screen performed on the OS tumour cell line panel.

Dot plot of range of quantile normalised (QN) Z scores for each OS tumour cell line, where each line represented a QN median Z score for each individual siRNA within the RNAi library, and the median QN Z score for the entire screen shown by a wider line. Cells were arrayed in triplicate 384 well plates, reverse transfected and after seven days viability was estimated using CellTiter Glo as described in the Methods. Raw luminescence values were transformed into Z scores as previously described. Quantile normalisation of the Z scores for each screen was then used to align the multiple distributions of data and aid comparison of Z scores of screens with a large difference in magnitude, without loss of consideration of rank and magnitude of each screen. QN adjusts the distribution of z-scores for each cell line so as to make each of them identical whilst maintaining the approximate magnitude of the original z-scores (Bolstad, Irizarry, Astrand, *et al.*, 2003). The principle of quantile normalisation is to first rank order (sort) z-scores for each cell line, average the values across each rank and then return the averaged values to the original order. Quantile normalisation of the Z scores was kindly performed by James Campbell using the preProcessCore package (Bioconductor).

5.2.7 Unsupervised hierarchical clustering of osteosarcoma replicates

To confirm reproducibility of the data set, unsupervised hierarchal clustering of a subset of the viability data for 15 of the 18 osteosarcoma tumour cell lines that were available at the time, all screened using the same library, was undertaken using Gene-e (http://www.broadinstitute.org/cancer/software/GENE-E/) (Figure 40). These results demonstrated that the biological replicates for each cell line cluster together except SAOS2, which was likely due to an edge effect on one of the replicates and hence was excluded from the analysis and final data set. Edge effects cause a larger degree of loss of viability around the edge of the plate, which has the potential to skew that data-set leading to a greater risk of identifying false positive effects. Hence, to mediate against this risk, low profile lids were used on the 384 well plates to reduce evaporation, and the screens performed in triplicate so that outlying replicates can be identified and discarded. SAOS2 and LM7 (which was cycled through the lungs of mice to form a metastatic cell line) clustered together. Tumour cell lines did not cluster according to date of experiment.

5.2.8 Identification of skeletal system morphogenesis pathway as osteosarcoma-specific genetic dependencies

In order to identify genetic dependencies specific to osteosarcoma, supervised hierarchical cluster analysis of all 18 osteosarcoma tumour cell lines compared to the 99 non-osteosarcoma tumour cell lines (Campbell, Ryan, Brough, *et al.*, 2016) was performed and a heatmap generated as a visual measure of the differences of the two groups (Figure 41 and Figure 42). A significant difference in quantile normalised Z scores reflecting viability was seen in 163 genes between the two groups (OS and the non-osteosarcoma tumour cell line panel). In addition, a heatmap of the most profound genentic dependencies seen in the OS panel alone is shown in Figure 43. No genetic dependencies lead to ubiquitous cell death (QN Z<-2) across all 18 OS tumour cell lines.

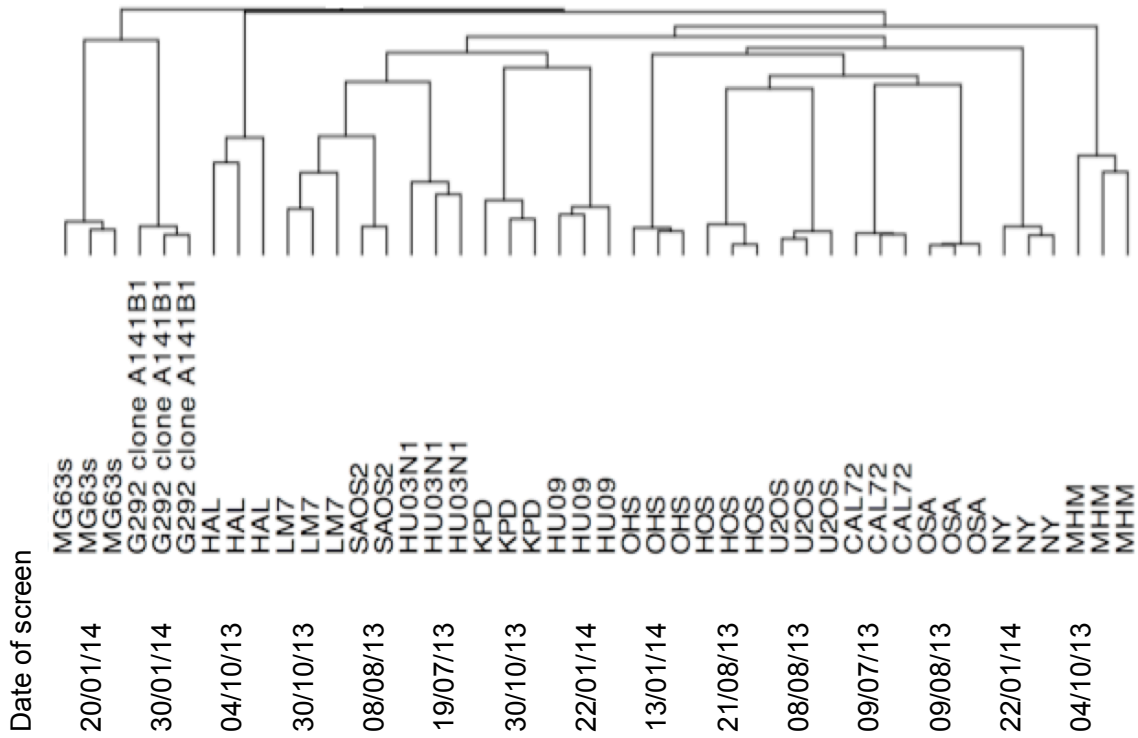

Figure 40 Unsupervised hierarchical clustering of the triplicate replicates for each siRNA screen in 15 OS tumour cell lines confirm reproducibility of the data set.

Unsupervised hierarchical clustering of a subset of the viability data for 15 of the 18 OS tumour cell lines that were available at the time, all screened using the same RNAi library was performed. All biological replicates for each tumour cell line clustered together except SAOS2, which was likely due to an edge effect on one replicate and so was excluded from this analysis and final data set. SAOS2 and LM7 (which was cycled through the lungs of mice to form a metastatic cell line) clustered together. Tumour cell lines did not cluster according to date of experiment. Gene-e software (http://www.broadinstitute.org/cancer/software/GENE-E/) was used to perform this analysis.

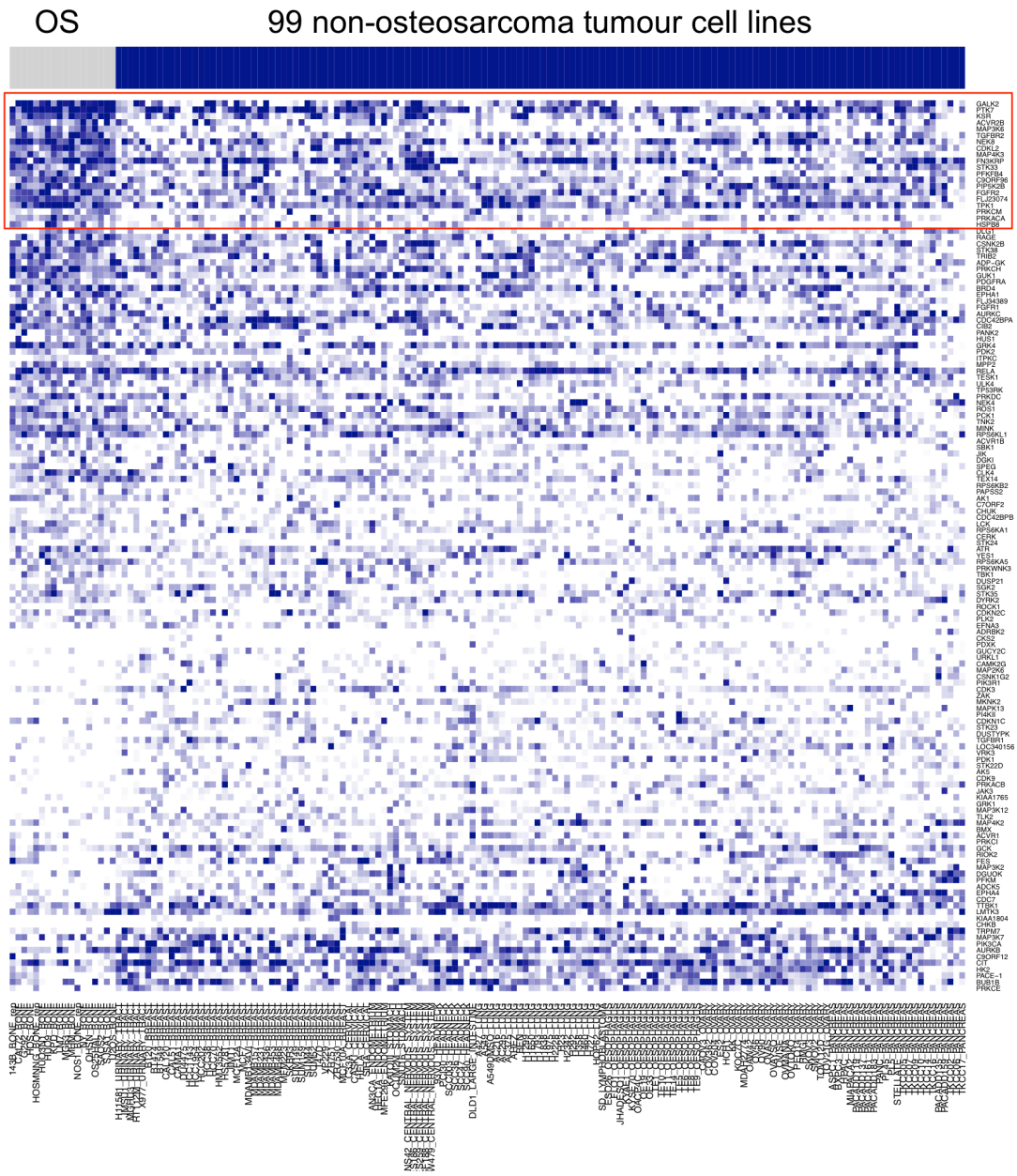

Figure 41 Heatmap of osteosarcoma tumour cell lines and 99 non-osteosarcoma tumour cell lines, by comparison of the QN Z scores in each group.

Only significant ($p<0.05$) genetic dependencies are shown. Each row represents viability effects of silencing of a target gene, while each column represents a tumour cell line. Dark blue represents loss of viability, whereas white represents no effect on viability. James Campbell (ICR) used a custom script in R to perform this analysis and generate the heatmap. The 20 most significant candidate genetic dependencies are highlighted by a red box and shown in Figure 42. P values calculated by median difference permutation test.

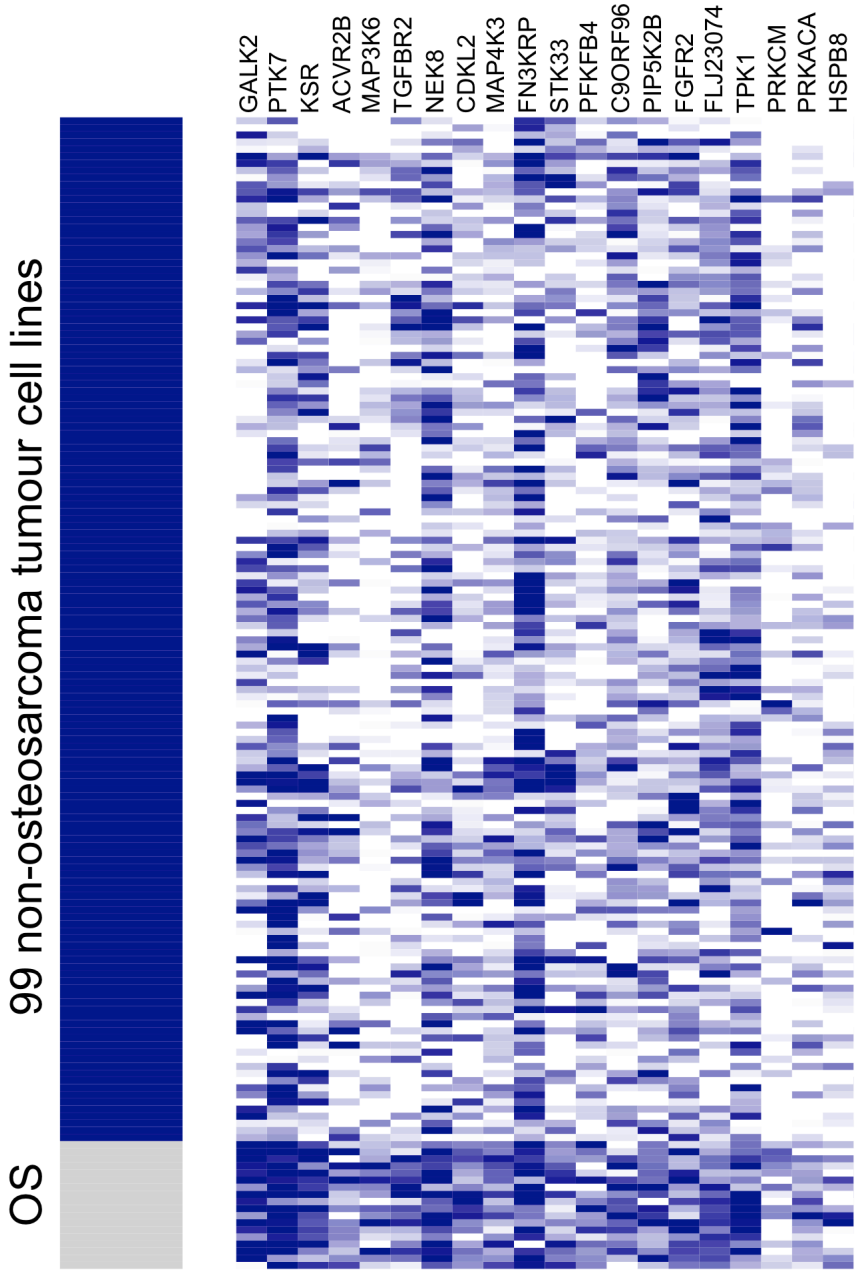

Figure 42 Heatmap of osteosarcoma tumour cell lines and 99 non-osteosarcoma tumour cell lines, by comparison of the QN Z scores in each.

Each row represents viability effects of silencing of a target gene, while each column represents a tumour cell line. Dark blue represents loss of viability, whereas white represents no effect on viability. James Campbell (ICR) used a custom script in R to perform this analysis and generate the heatmap. The twenty most significant candidate genetic dependencies are shown ($p<0.05$). p values calculated by the median difference permutation test.

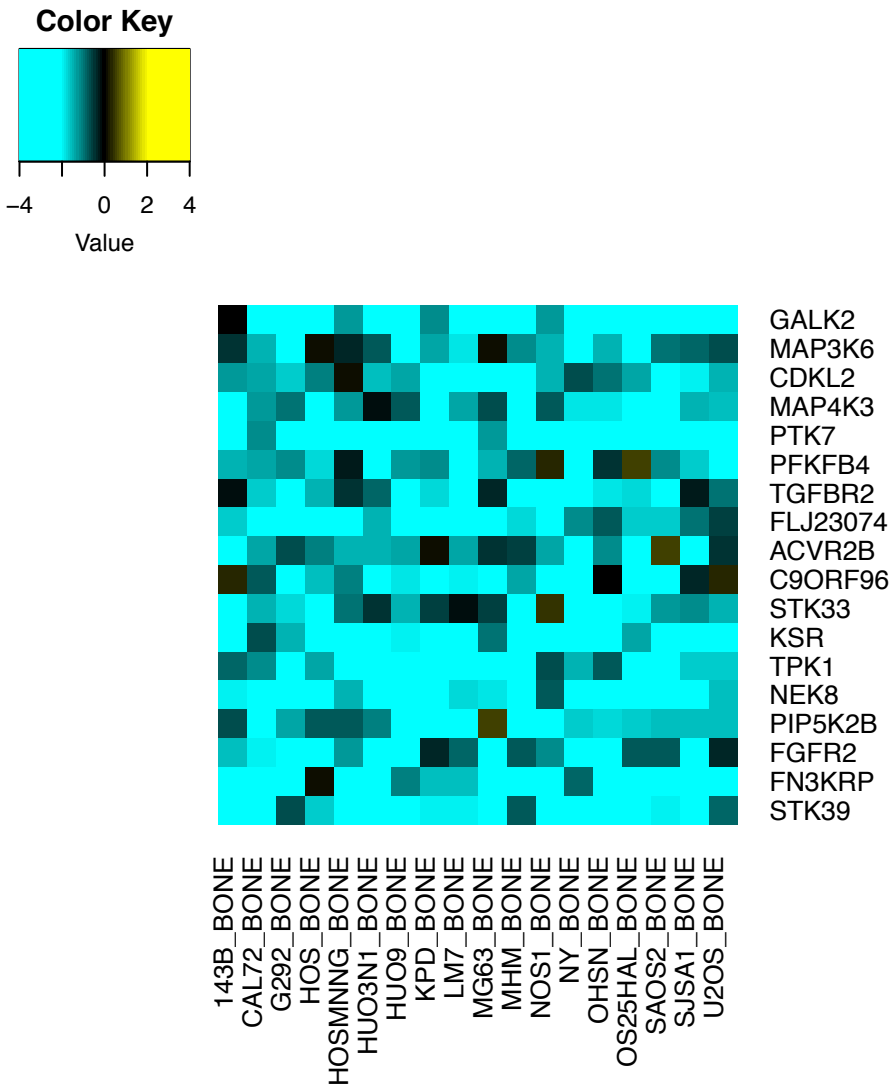

Figure 43 Heatmap of osteosarcoma tumour cell lines by comparison of the QN Z scores in each.

Each row represents viability effects of silencing of a target gene, while each column represents a tumour cell line. Turquoise represents loss of viability, whereas black represents no effect on viability, and yellow positive effects on viability. Aditi Agulati (ICR) used a custom script in R to perform this analysis and generate the heatmap. The eighteen significant candidate genetic dependencies are shown ($p<0.05$). p values calculated by the median difference permutation test.

The heatmap demonstrated a number of genes which caused significant lethality amongst the osteosarcoma models, but minimal effect on viability in the non-osteosarcoma tumour cell line panel models, which were considered most likely to represent tumour-specific dependencies and candidate therapeutic targets (Brough, Frankum, Sims, et al., 2011). Two of the most significant genes were mitogen-activated protein kinase kinase kinase 6 (MAP3K6) and mitogen-activated protein kinase kinase kinase 3 (MAP4K3) which are shown in Figure 44. Both of these genes code for proteins that are part of the mitogen-activated protein kinase (MAPK) family which link extracellular signals to the intracellular processes such as growth, proliferation, and differentiation (Dhillon, Hagan, Rath, et al., 2007). Additionally, a reliance on genes involved in 'skeletal system morphogenesis' including PDGFRA, ACVR2B, TGFBR2, DLG1, FGFR1 and FGFR2 was identified (Campbell, Ryan, Brough, *et al.*, 2016) (Figure 45 and Figure 46).

The *FGFR1* and *FGFR2* kinase genetic dependencies suggested that osteosarcoma models might be especially sensitive to small molecule FGFR inhibitors, and these associations are shown in the next chapter. Another of the genes identified in 'skeletal system morphogenesis' was Platelet derived growth factor receptor alpha (*PDGFRA*). Olaratumab is a new antibody targeting PDGFRA, currently undergoing Phase 1b clinical trial (NCT02659020) in patients with advanced soft tissue sarcoma.

5.3 DISCUSSION

This chapter described the steps to the generation of the first kinome-wide genetic dependency maps of multiple OS tumour cell line models on this scale. This data-set was made a publically available resource for the identification of OS genetic dependencies by the inclusion in Cancer GD www.cancergd.org which provides a searchable collection of genetic vulnerabilities associated with the alteration of driver genes in cancer cell lines as part of a collaboration between the Institute of Cancer Research, Systems Biology Ireland, University College Dublin and the Health Research Board.

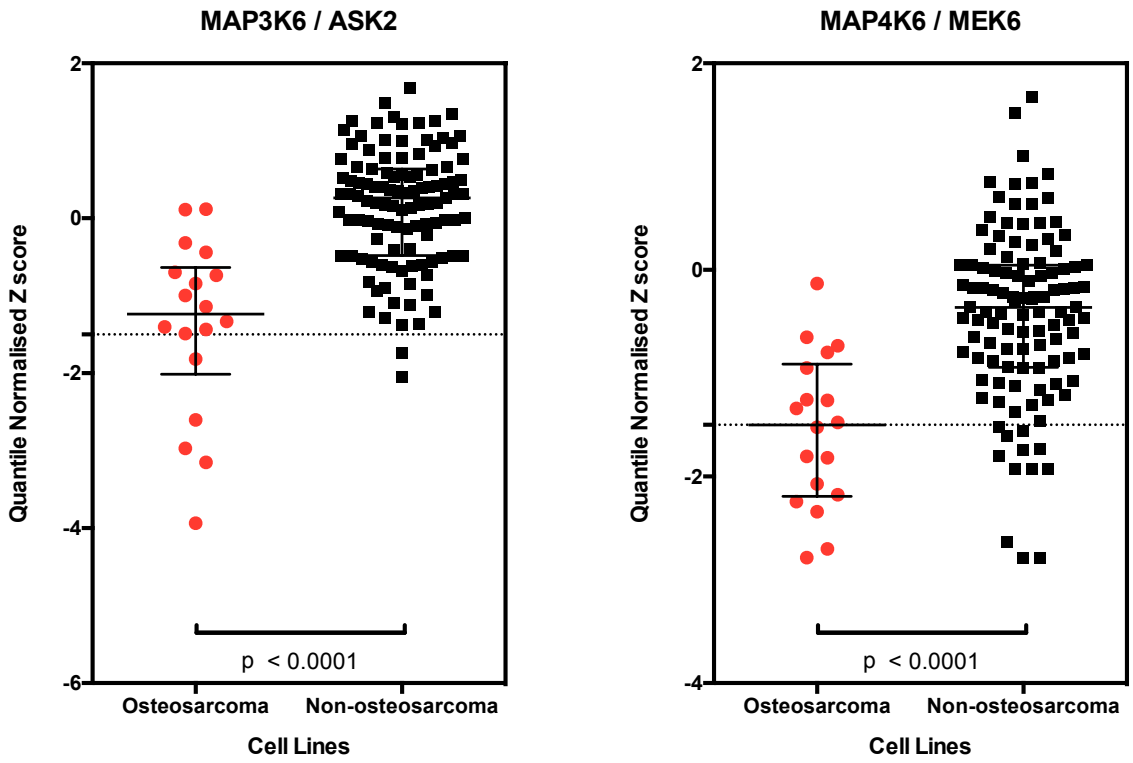

Figure 44 OS tumour cells demonstrated a candidate genetic dependency on *MAP3K6/ASK2* and *MAP4K6/MEK6* genes when compared to non-osteosarcoma tumour cell lines (n=99).

Dot plots of quantile normalised Z scores for *MAP3K6/ASHK2* and *MAP4K6/MEK6* in 18 osteosarcoma tumour cell lines and 99 non-osteosarcoma tumour cell lines (n=99: 27 breast; 19 ovary; 19 lung; 14 oesophagus; 5 pancreas; 5 head and neck; 4 cervical; 4 central nervous system; 2 endometrium). Tumour cell lines were arrayed in triplicate 384 well plates, and reverse transfected using the siRNA library described in Appendix Tables 1-3. After seven days, cell viability was estimated by CellTiter Glo reagent as described in the methods. A custom script on R was used to quantile normalise the Z scores across the non-osteosarcoma tumour cell line panel by James Campbell (ICR). Tumour cell lines were clustered into two groups, Osteosarcoma and non-osteosarcoma. Median and interquartile range highlighted. P values calculated by Median Permutation Test.

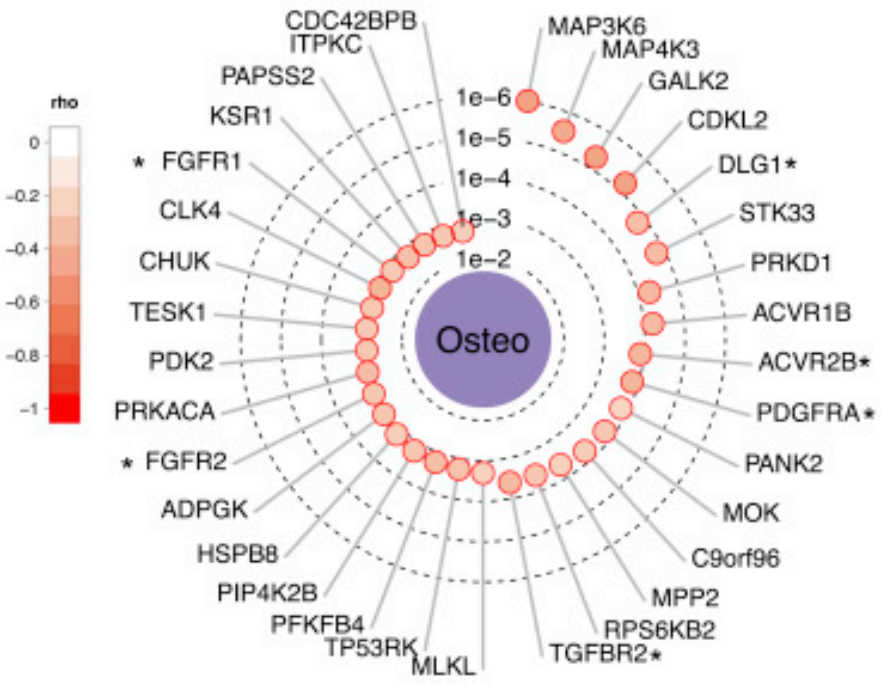

Figure 45 Radar plot (generated by James Campbell), summarizing the candidate genetic dependencies associated with the osteosarcoma histotype.

The concentric circles indicate the statistical significance and the depth of colour indicates the separation of Z scores between the osteosarcoma histotype (n = 18) and the non-osteosarcoma group of tumour cell lines (n=99: 27 breast; 19 ovary; 19 lung; 14 oesophagus; 5 pancreas; 5 head and neck; 4 cervical; 4 central nervous system; 2 endometrium). A set of six kinases annotated as involved in skeletal system morphogenesis in the Gene Ontology are annotated with asterisks (Campbell, Ryan, Brough, *et al.*, 2016). A custom R script was used by James Campbell to generate this radar plot.

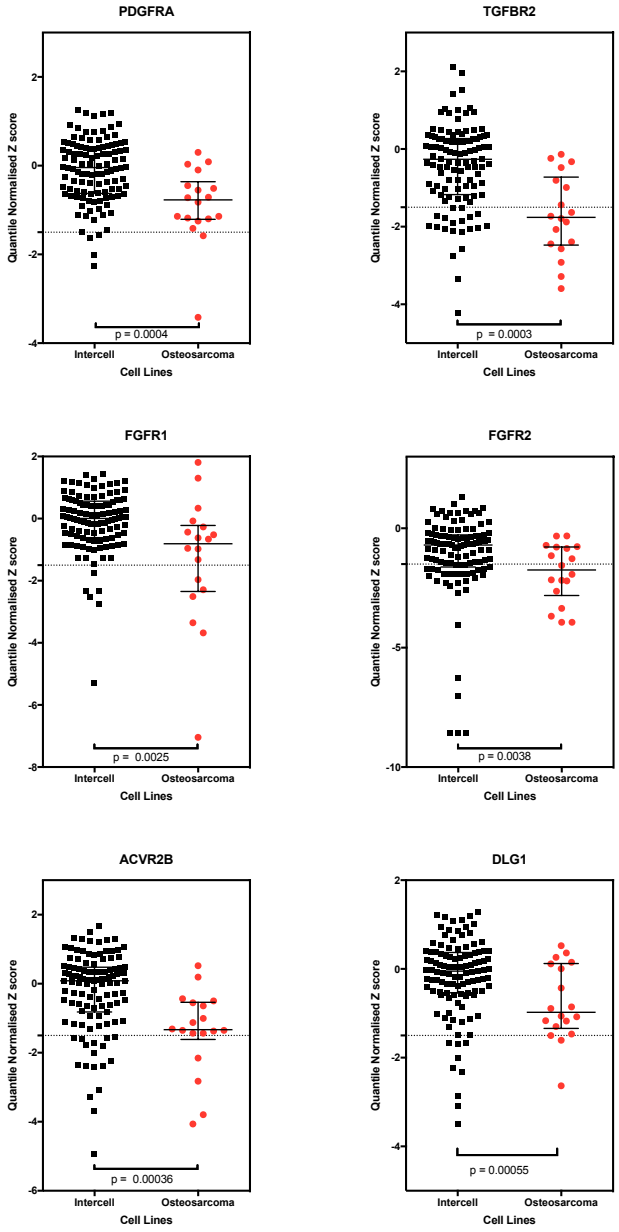

Figure 46 Six candidate genetic dependencies annotated as involved in skeletal system morphogenesis in the Gene Ontology, associated with the osteosarcoma histotype.

Dot plots of quantile normalised Z scores for six genes involved skeletal system morphogenesis, in 18 osteosarcoma tumour cell lines and 99 non-osteosarcoma tumour cell lines (n=99: 27 breast; 19 ovary; 19 lung; 14 oesophagus; 5 pancreas; 5 head and neck; 4 cervical; 4 central nervous system; 2 endometrium). Tumour cell lines were arrayed in triplicate 384 well plates, and reverse transfected using the siRNA library described in Appendix Tables 1-3. After seven days, cell viability was estimated using the CellTiter Glo reagent as described in the methods. A custom script on R was used to quantile normalise the Z scores across the non-osteosarcoma tumour cell line panel. Tumour cell lines were clustered into two groups, Osteosarcoma and non-osteosarcoma. Median and interquartile range highlighted. P values calculated by MPT.

This analysis was based on unbiased RNAi screening of a panel of tumour cell lines, and it is therefore particularly interesting that a reliance on this skeletal morphogenesis pathway was identified in osteosarcoma, given that osteosarcoma derives from primitive bone-forming mesenchymal stem cells (MSC) (Gorlick, 2009). MSC are pluripotent cells that via the complex process of osteogenic differentiation and the appropriate stimuli, can give rise to multiple lineages including osteocytes, myocytes, adipocytes, and chondrocytes (Tang, Song, Luo, *et al.*, 2008). Although the exact mechanisms of pathogenesis of OS is unknown, it is postulated that disruption of differentiation of these MCS (Tang, Song, Luo, *et al.*, 2008) leads to cellular arrest as undifferentiated precursors, supported by the many similarities seen between OS and primitive osteoblasts (Wagner, Luther, Zhu, *et al.*, 2011).

Genetic dependencies specific to osteosarcoma were identified, with a reliance of genes involved in 'skeletal system morphogenesis' including *FGFR1* (Campbell, Ryan, Brough, *et al.*, 2016). 'Skeletal system morphogenesis' is a Gene Ontology term (Ashburner, Ball, Blake, *et al.*, 2000) which encompasses four subcategories; cartilage condensation; embryonic skeletal system morphogenesis; bone trabecular formation; and bone morphogenesis. Platelet-derived growth factor receptor A (PDGFRA) is a cell surface tyrosine-protein kinase receptor that is required for normal skeletal development, and plays an important role in the differentiation of bone marrow-derived mesenchymal stem cells (Uezumi, Fukada, Yamamoto, *et al.*, 2014). It mediates activation of the MAP kinases (MAPK1/ERK2 and MAPK3/ERK1), and the Signal Transducer And Activator Of Transcription (STAT) family (STAT1, STAT3, and STAT5A/B). Actin A Receptor Type 2B (ACVR2B) is a member of the transforming growth factor-beta (TGF-beta) superfamily, and is a growth and differentiation factor involved in cell surface to cytoplasmic signalling (Olsen, Wader, Hella, *et al.*, 2015). Olaratumab a novel antibody targeting PDGFRA, has recently been seen to improve overall survival for patients with metastatic soft tissue sarcoma in combination with doxorubicin compared to doxorubicin alone (Tap, Jones, Van Tine, *et al.*, 2016). As a result olaratumab is now licenced for this indication. Olaratumab demonstrates anti-tumour activity in models of paediatric sarcoma including osteosarcoma (May, Loizos, Novosiadly, *et al.*, 2015). The observation of increased reliance on *PDGFRA* in osteosarcoma provides further rationale to support a clinical trial in this disease.

Transforming Growth Factor Beta Receptor 2 (TGFBR2), another member of the TGF-beta receptor superfamily, regulates transcription of a subset of genes related to cell proliferation and is involved in control of mesenchymal cell proliferation and differential, and extracellular matrix production (Wu, Chen & Li, 2016). A paralog of this gene is ACVR2A, which has very similar roles to ACVR2B (Olsen, Wader, Hella, *et al.*, 2015). Discs Large MAGUK Scaffold Protein 1 (DLG1) encodes a scaffolding protein required for normal development, with a possible role in cell proliferation, signal transduction, and adherens junction assembly. Fibroblast Growth Factor Receptor 1 (FGFR1) and 2 (FGFR2) are members of the fibroblast growth factor receptor (FGFR) family of trans-membrane catalytic receptors with intracellular tyrosine kinase activity. FGFR1 and FGFR2 play an essential role in the regulation of embryonic development, cell proliferation, differentiation and migration. Both are also required for normal skeletal genesis, and function upstream of the MAP kinase and phosphoinositide 3-kinase (AKT1) signalling pathways (Su, Jin & Chen, 2014). FGFR2 also plays a role in regulation of osteogenesis, osteoblast differentiation, and promotes apoptosis in differentiated osteoblasts (Su, Jin & Chen, 2014). Although there is a possibility of any given dependency being the result of off-target siRNA effects (Jackson & Linsley, 2010), the likelihood of an entire pathway being identified through off-target effects is likely to be much lower.

Genes identified as essential for viability in osteosarcoma but not in the non-osteosarcoma tumour cell line panel may represent key drivers of cellular survival in osteosarcoma. Two FGFR chemical inhibitors AZD4547 and PD173074 were both found to be more selective for osteosarcoma than a panel of 58 non-osteosarcoma tumour cell lines, described in the next chapter.

In the next chapter, I will demonstrate how the RNAi profiling of this OS tumour cell line panel enabled identification of candidate genetic dependencies specific to loss of *RB1* and *CDKN2A* deficiency.

6 Identification of genetic dependencies associated with driver mutations in osteosarcoma

6.1 INTRODUCTION

6.1.1 Identification of candidate genetic dependencies

In the previous chapter, the genetic dependencies of the panel of OS tumour cell lines were compared to that of 99 non-osteosarcoma cell lines, which identified a particular reliance on genes involved in skeletal system morphogenesis. To identify genetic dependencies associated with specific driver mutations, the data set viability scores described in Chapter 5, were integrated with the molecular profiling of the tumour cell lines, to enable identification of genetic vulnerabilities associated with driver alterations in osteosarcoma. As stated in Chapter 2, in addition to *TP53*, *RB1* and *CDKN2A* are the most common recurrent mutational events in sporadic osteosarcomas (Gorlick, Anderson, Andrulis, *et al.*, 2003). Loss of function of RB1 is reported in many cancer types (Knudsen & Wang, 2010). Furthermore, germ-line mutations of *RB1* have been associated with occurrence of osteosarcoma and structural alterations of the *RB1* gene have been reported in up to 30% of sporadic cases (Araki, Uchida, Kimura, *et al.*, 1991). Thus genetic dependencies associated with loss of function of *RB1* and *CDKN2A* were worthy of further investigation. Chapter three described the characterisation of the tumour cell line panel into 'deficient' and 'wildtype' groups for both of these genes (*CDKN2A* and *RB1*), which were used as the basis for class analysis in this Chapter. The most significant and reproducible differential effect identified between the *RB1* mutant and wildtype tumour cell lines in the high-throughput siRNA screen, was seen with siRNA targeting DYRK1A (dual-specificity tyrosine-regulate kinase 1A).

6.2 RESULTS

6.2.1 Identification of genetic dependencies associated with loss of function of CDKN2A in osteosarcoma

To identify candidate genetic dependencies associated with loss of function of *CDKN2A*, osteosarcoma tumour cell lines were clustered into 'deficient' and 'wildtype' groups, described in Chapter 3. A Z score threshold of < -1.5, representing 1.5 Median Absolute Deviation (MAD) effects from the median effect was used to define significant loss of

viability. To exclude any genes which had an effect on all tumour cell lines, and therefore more likely to represent an essential gene, a Z score of > -1.0 was used in the *CDKN2A* wildtype cohort. Therefore, the following criteria were used to select genes for revalidation: (i) median Z score in the *CDKN2A* deficient cells lines of < - 1.5; (ii) median Z score in the *CDKN2A* wildtype group of > -1.0; (iii) probability of the difference between the Z scores in both the *CDKN2A* deficient and wildtype groups seen by chance of $p<0.05$. Using these criteria, 99 genes demonstrated significant differential effects in the two groups (Figure 47 and Figure 48), and those with the most significant effects are shown in Figure 49.

Serine/Threonine-Protein Kinase 22C (*STK22C*) is a kinase involved in germ cell differentiation and mature sperm function. Fucokinase (*FUK*) mediates the fucose salvage pathway and FUK may have a role in metastasis, with a reduced expression in advanced murine melanomas observed (Lau, Feng, Claps, *et al.*, 2015). Two members of the Cyclin Dependent Kinase Family, *PCTK3* and *CDKN1C* were also identified. Cyclin Dependent Kinase 18 (*PCTK3*) controls actin cytoskeleton dynamics by negatively regulating the FAK/Rho signalling pathway, and silencing of *PCTK3* by siRNA has been associated with increased cell motility (Matsuda, Kawamoto, Miyamoto, *et al.*, 2017). Cyclin Dependent Kinase Inhibitor 1C, also known as $p57^{KIP2}$, inhibit G1 cyclin-dependent kinases thereby negatively regulating cell proliferation (Riccio & Cubellis, 2012). *CDKN1C* is part of a cluster of imprinted genes on Chromosome 11p15.5, reduced expression or activity is associated with the overgrowth syndrome Beckwith-Wiedermann Syndrome and a range of sporadic cancers (Riccio & Cubellis, 2012; Borriello, Caldarelli, Bencivenga, *et al.*, 2011). Branched Chain Ketoacid Dehydrogenase Kinase (*BCKDK*) is a rate-limiting enzyme in branched-chain amino acids catabolism and expression has been negatively correlated with survival in patients with colorectal cancer (Xue, Zeng, Duan, *et al.*, 2017). N-Acetylglucosamine Kinase (*NAGK*) is a salvage enzyme that is involved in mammalian amino-sugar metabolism and a member of the Heat Shock Protein 70 family (Islam, Sharif, Lee, *et al.*, 2015). Mitogen-Activated Protein Kinase Kinase Kinase 3 (*MAP3K3*), is a serine/threonine protein kinase within the MAP3K family (Fan, Ge, Wang, *et al.*, 2014). Amplification of MAP3K3 has been observed in 20% of breast cancers although the exact role of MAP3K3 is still unknown (Fan, Ge, Wang, *et al.*, 2014). Pyrroline-5-Carboxylate Synthetase (Glutamate Gamma-Semialdehyde Synthetase) (*PYCS*) is a member of the aldehyde dehydrogenase family. Further validation of these effects, and mechanistic understanding was not prioritised.

6.2.2 Identification of candidate genetic vulnerabilities associated *RB1* deficiency

To identify candidate genetic dependencies associated with loss of function of *RB1,* the siRNA data-set from osteosarcoma tumour cell lines was clustered according to the status of *RB1* (described in Chapter 3), demonstrating differences in gene dependency between *RB1* deficient and wildtype groups by comparison of the QN *Z* scores in each group (Figure 50). The same criteria, described in 6.2.1 were used to select genes for revalidation. Based on these criteria eight genes (*CDKL4, JAK2, DYRK1A, NEK7, PRKCN, MYLK, GALK1* and *LAK*) were identified (Figure 51).

6.2.3 Revalidation of siRNA high-throughput screen candidate genetic dependencies

Limitations of siRNA screening are well known, and of primary significance are the off-target effects which occur when using siRNA particularly in mammalian systems (Iorns, Lord, Turner, *et al.*, 2007; Echeverri & Perrimon, 2006). Silencing of genes through the siRNA pathway requires the species to be highly complementary to the target mRNA, while off-target effects may require less in a similar manner to microRNA machinery (Iorns, Lord, Turner, *et al.*, 2007). At the 5' end of the anti-sense strand, a seven to eight 'seed' nucleotide region is most critical in generating off-target effects, particularly when this 'seed' region occurs in the 3' un-translated region of a potential off-target gene (Birmingham, Anderson, Reynolds, *et al.*, 2006). It is therefore important to perform 'redundancy' or rescue experiments to confirm the observed phenotype is due to a specific on-target effect of silencing the gene of interest (Echeverri & Perrimon, 2006). Therefore, robust revalidation was performed using deconvolution with four distinct siRNA species targeting different regions of the target gene, as well as the SMARTpool used in the original screen.

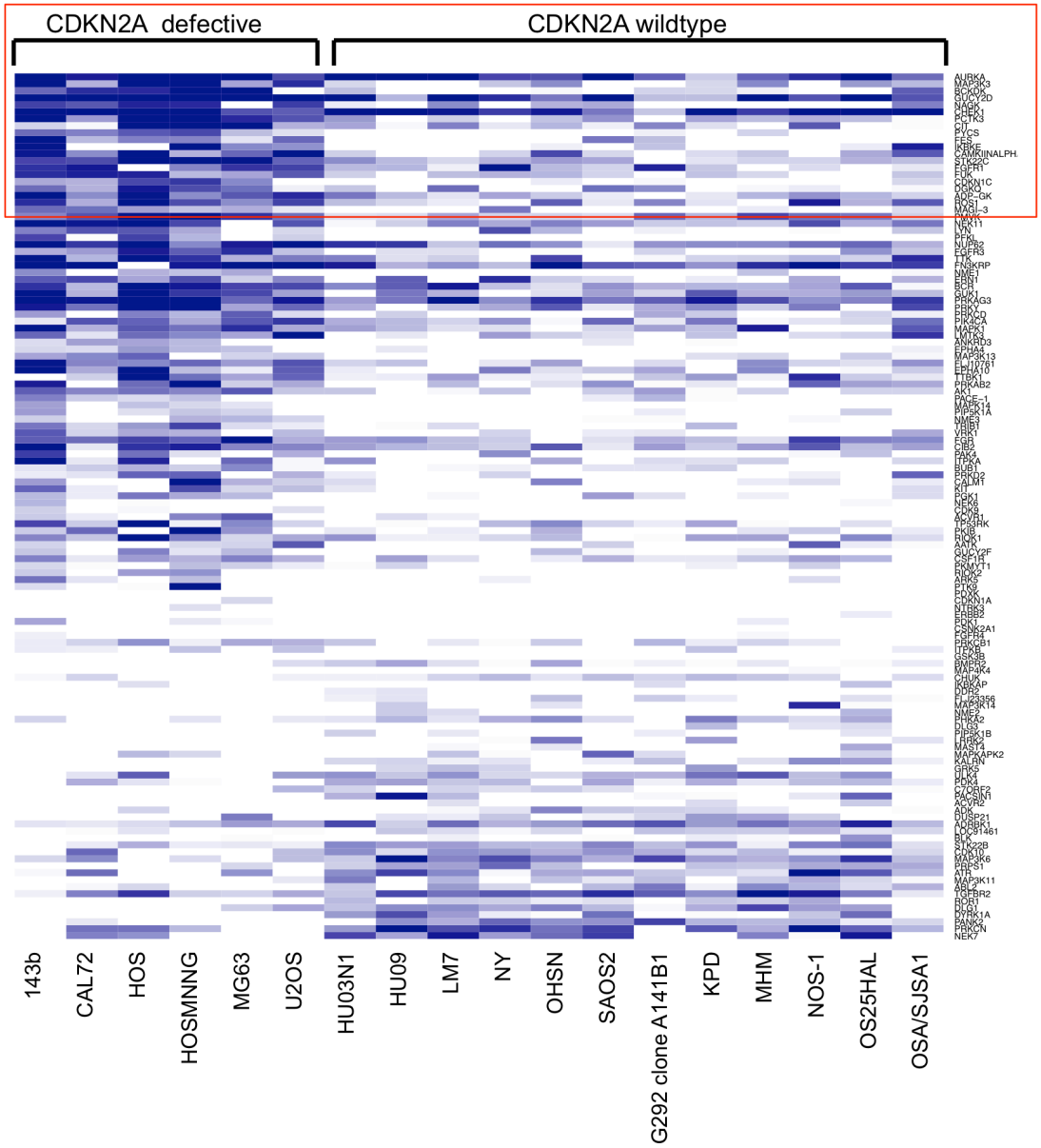

Figure 47 Heatmap of osteosarcoma tumour cell lines demonstrating the differences in gene dependency between *CDKN2A* deficient and wildtype groups by comparison of QN Z scores of each group.

Each row represents viability effects of silencing of a target gene, while each column represents a tumour cell line. Dark blue represents loss of viability, whereas white represents no effect on viability. Only significant (p<0.05) genetic dependencies are shown. The 20 most significant candidate genetic dependencies are highlighted by a red box and shown in Figure 48. P values calculated by median difference permutation test. James Campbell (ICR) used a custom script in R to perform this analysis and generate the heatmap.

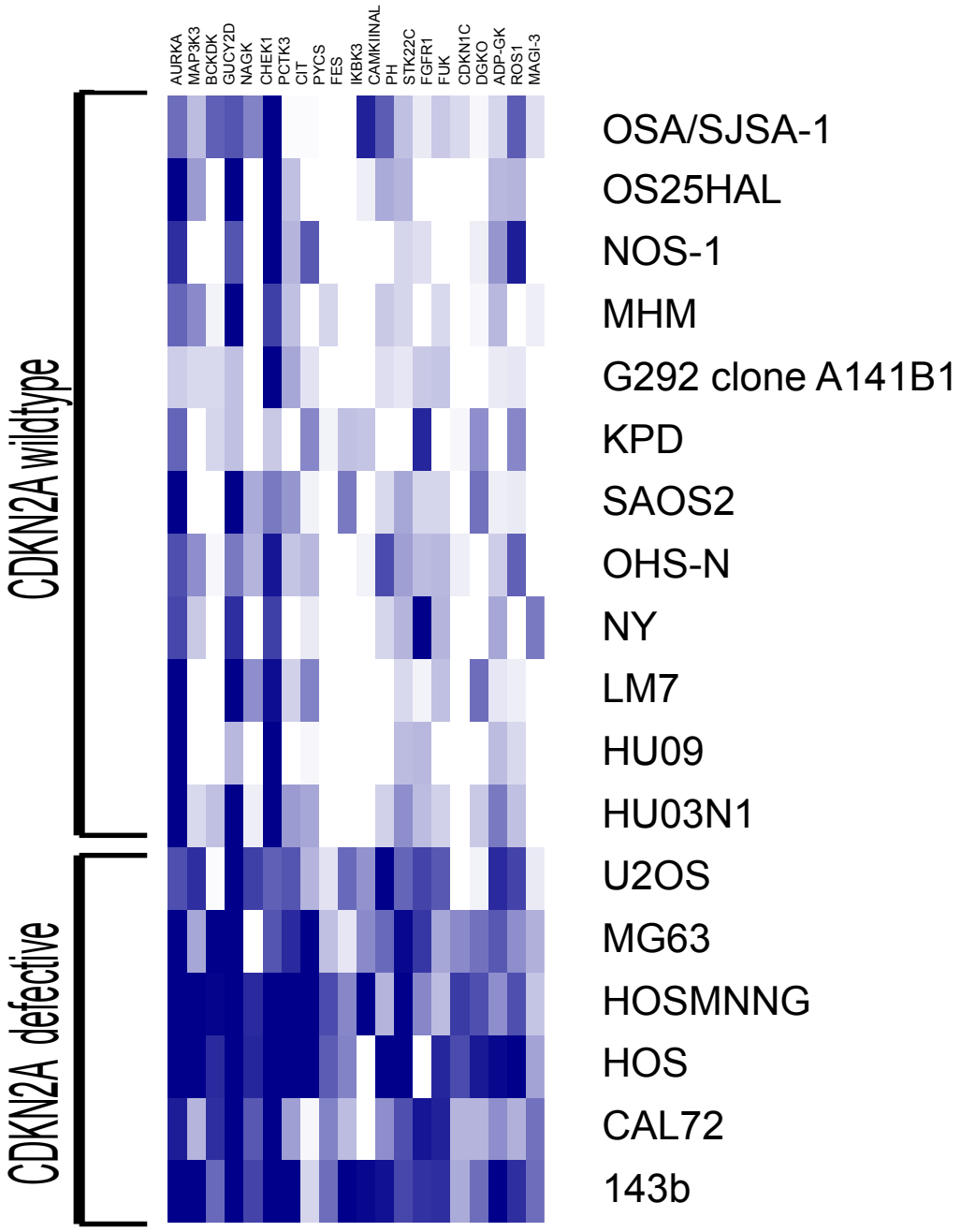

Figure 48 Heatmap of osteosarcoma tumour cell lines demonstrating the differences in gene dependency between *CDKN2A* deficient and wildtype groups by comparison of QN Z scores of each group.

Each row represents viability effects of silencing of a target gene, while each column represents a tumour cell line. Dark blue represents loss of viability, whereas white represents no effect on viability. James Campbell (ICR) used a custom script in R to perform this analysis and generate the heatmap. Only the 20 most significant candidate genetic dependencies are shown ($p<0.05$). P values calculated by median difference permutation test.

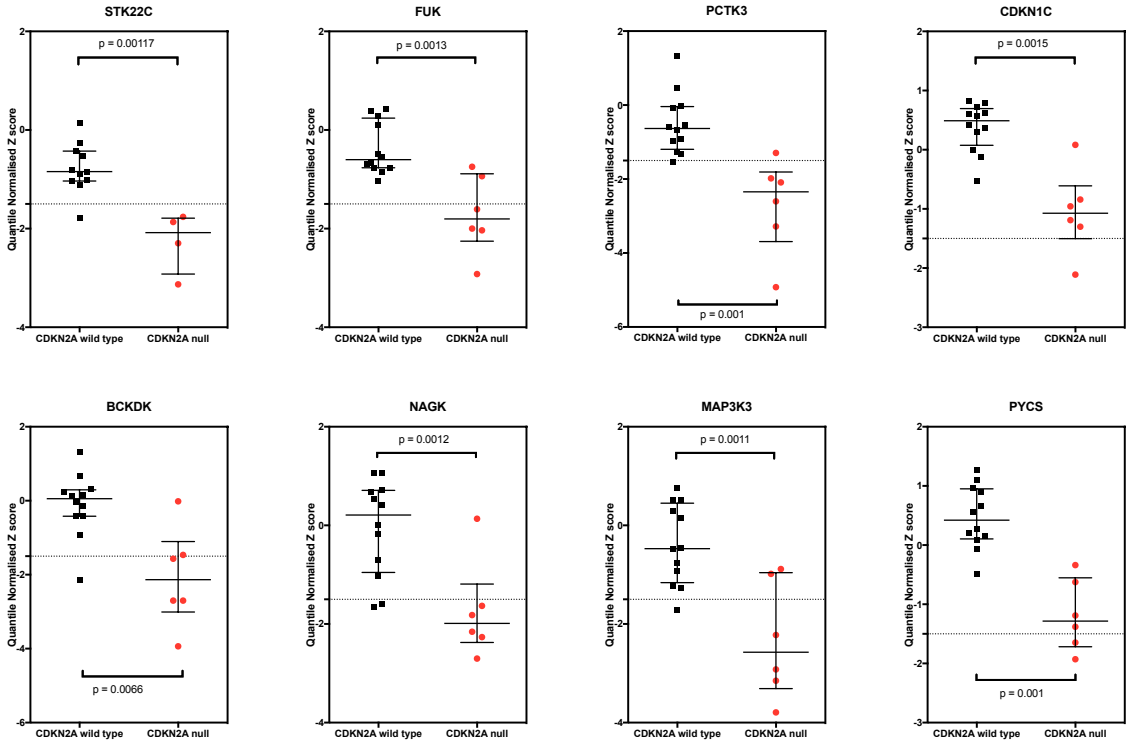

Figure 49 Candidate genetic dependencies associated with *CDKN2A* deficiency in osteosarcoma

Dot plots showing comparison of QN Z scores grouped by *CDKN2A* status. OS tumour cell lines were arrayed in triplicate 384 well plates and reverse transfected using the siRNA library described in Appendix Tables 1-3. After seven days, cell viability was estimated using the CellTiter Glo via a luminescence assay. A custom script on R was used to quantile normalise the Z scores across OS tumour cell line panel. Median and interquartile range represented by bars. *CDKN2A* wildtype shown in black, and *CDKN2A* deficient OS tumour cell lines shown in red. Median and interquartile range highlighted. P values calculated by MPT. [QN: quantile normalised]

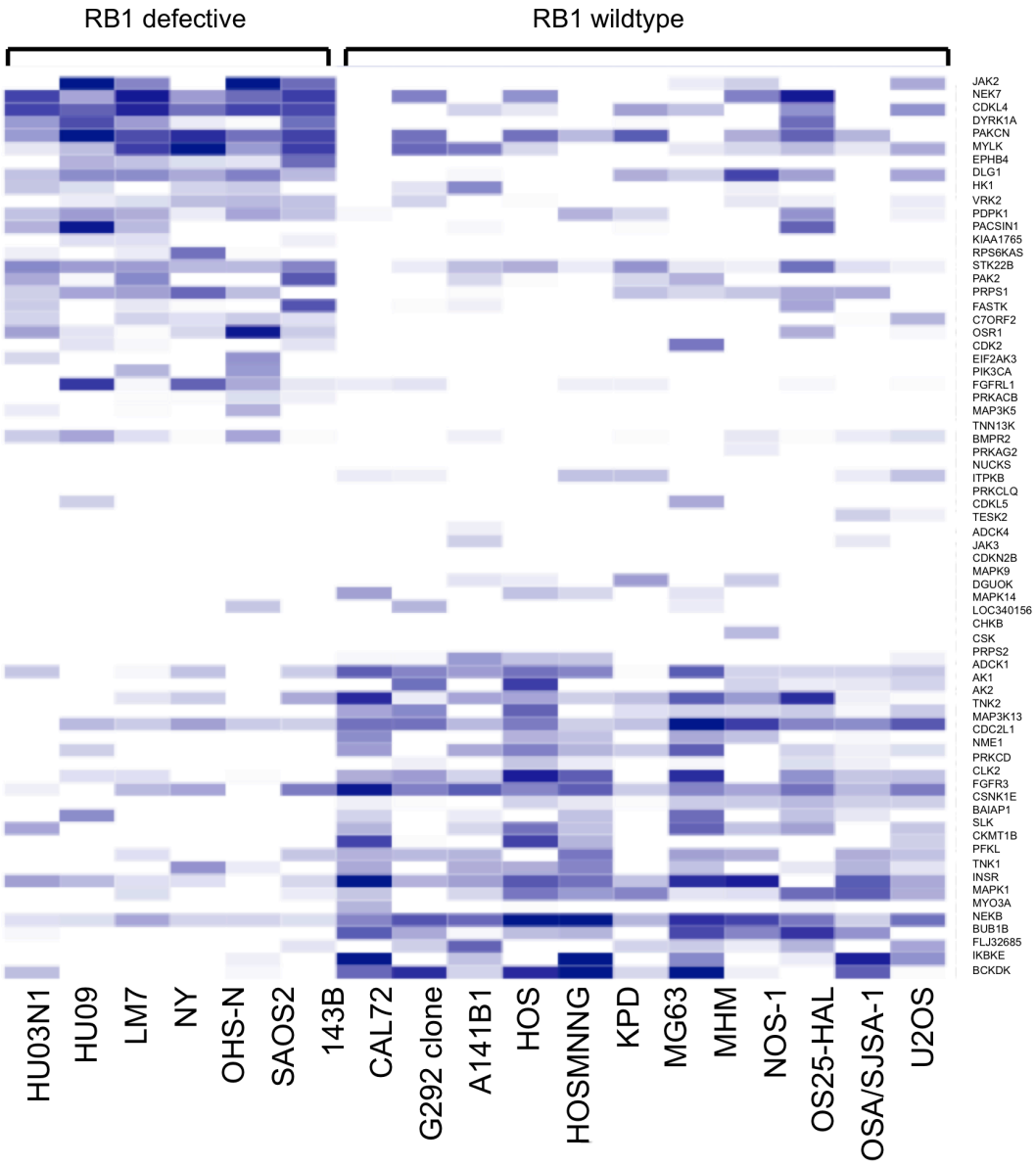

Figure 50 Heatmap of osteosarcoma tumour cell lines demonstrating differences in gene dependency between *RB1* deficient and wildtype groups by comparison of the QN Z scores in each group.

Only significant (p<0.05) genetic dependencies are shown. Each row represents viability effects of silencing of a target gene, while each column represents a tumour cell line. Dark blue represents loss of viability, whereas white represents no effect on viability. James Campbell (ICR) used a custom script in R to perform this analysis and generate the heatmap. P values calculated by median difference permutation test [QN: quantile normalised]

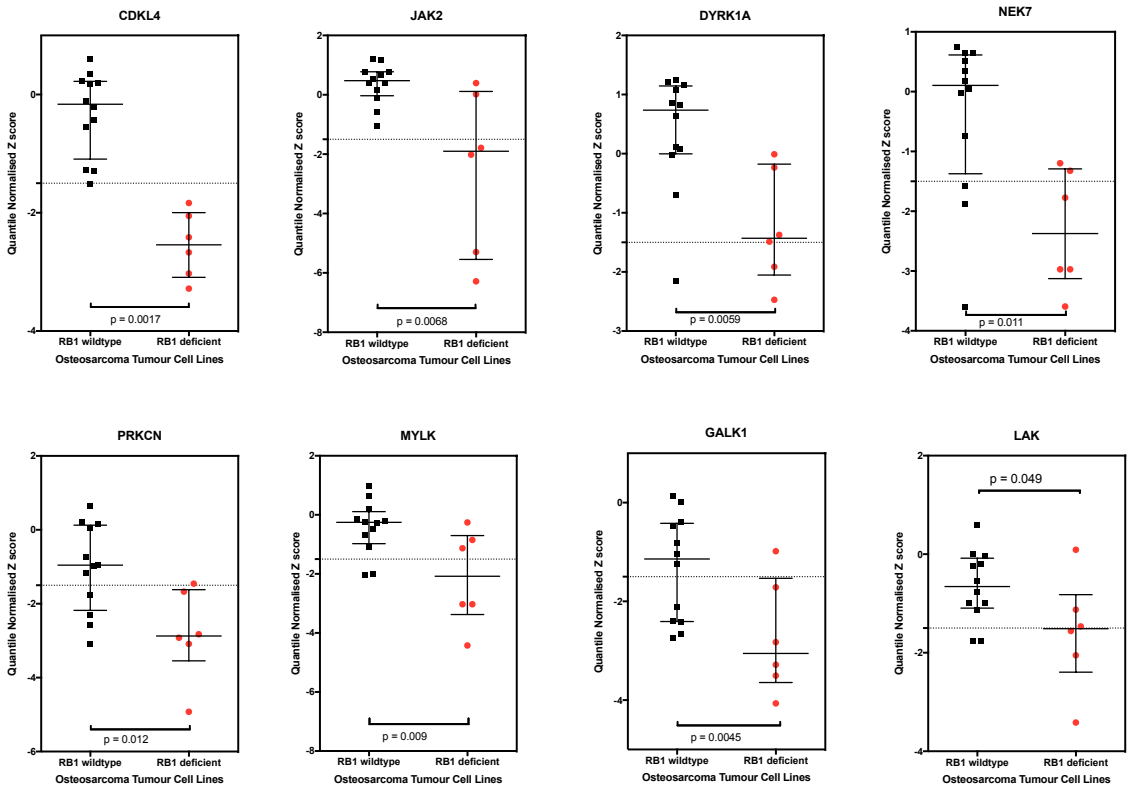

Figure 51 Candidate genetic dependencies chosen for revalidation according to *RB1* status in osteosarcoma tumour cell line models.

Dot plots showing comparison of QN Z scores grouped by *RB1* status with median and interquartile range. Tumour cell lines were arrayed in triplicate 384 well plates and reverse transfected using the siRNA library described in Appendix Tables 1-3. After seven days, cell viability was estimated using the CellTiter Glo via a luminescence assay. A custom script on R was used by James Campbell (ICR) to quantile normalise the Z scores across the non-osteosarcoma tumour cell line panel. Revalidation criteria were (i) median Z score in the *RB1* deficient cells lines of < - 1.5; (ii) median Z score in the *RB1* wildtype group of > -1.0; (iii) probability of the difference between the Z scores in both the *RB1* deficient and wildtype groups seen by chance of <0.05. p values calculated using the MPT. [QN: quantile normalised]

Based on these criteria 8 genes (*CDKL4, JAK2, DYRK1A, NEK7, PRKCN, MYLK, GALK1* and *LAK*) were selected for validation in the panel of non-isogenic osteosarcoma tumour cell lines. These genes were included in a custom 384-well plate of 231 other siRNA chosen for revalidation in other histologies (data not shown). It was assumed that the majority of these siRNA would not have an effect on viability in OS, and thus generation of Z scores were deemed valid. Observation of a phenotype caused by two different siRNA oligonucleotide species is considered unlikely that to be the result of an off-target effect (Echeverri & Perrimon, 2006). Therefore, validation of the effect was deemed successful if two out of the four individual oligonucleotides passed the above criteria. DYRK1A was the only candidate genetic dependency where these criteria were met (Figure 52 and Figure 53).

6.2.4 Investigation of the extent of the genetic dependency on DYRK1A in non-osteosarcoma tumour cell lines

To investigate the extent of the genetic dependency on DYRK1A, data from the non-osteosarcoma tumour cell line dataset (n=99 tumour cell lines derived from 10 cancer types) (Campbell, Ryan, Brough, *et al.*, 2016), and the 18 osteosarcoma tumour cell lines, was clustered according to *RB1* status. RNAi targeting DYRK1A resulted in a significant difference in viability between *RB1* wildtype and deficient osteosarcoma and breast tumour cell lines (Figure 54).

To further validate this observation in an independent data set, the publically available 'Achilles' data-set from the Broad Institute https://portals.broadinstitute.org/achilles which used lenti-virus to deliver 54,000 shRNA library in a panel of 216 cancer cell lines (Cowley, Weir, Vazquez, *et al.*, 2014) was used. Non-osteosarcoma tumour cell lines were annotated for *RB1* using a combination of protein expression by western blotting performed by Rachel Brough, publically available sequencing and mRNA expression data from COSMIC and CCLE using the same methodology to classify the OS tumour cell lines described in Chapter three. Only one osteosarcoma cell line, SJAS1/OSA was included in this data set. A similar significant difference of loss of viability in *RB1* deficient tumour cell lines compared to wildtype was seen with silencing of DYRK1A (Figure 55).

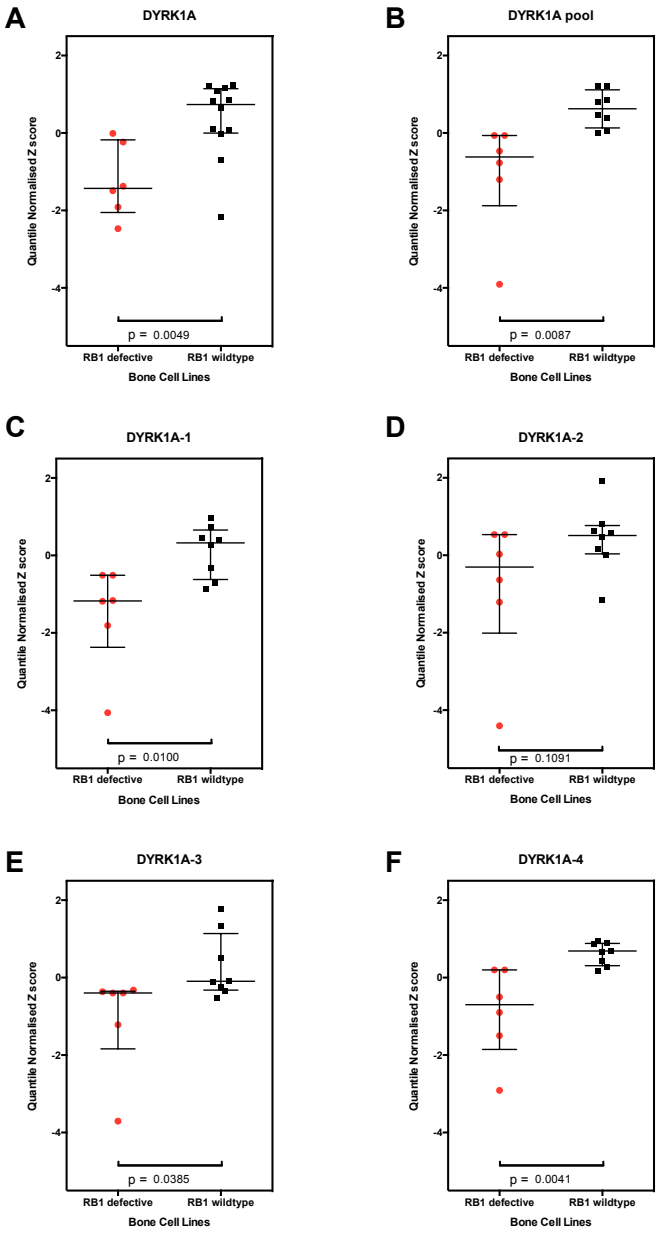

Figure 52 Revalidation of DYRK1A by deconvolution.

Dot plots of quantile normalised Z scores for DYRK1A clustered according to *RB1* in osteosarcoma tumour cell lines. (A) Data from the high-throughput screen of osteosarcoma tumour cell lines (*RB1* deficient: n = 6; *RB1* wildtype: n = 12), using a DYRK1A siRNA smartpool. (B) Validation using a DYRK1A smartpool and subset of OS tumour cell lines (*RB1* deficient: n = 6; *RB1* wildtype: n = 8). (C-F) Deconvolution using four different individual siRNAs targeting differing regions of DYRK1A. Tumour cell lines were reverse transfected using siRNA targeting DYKR1A. After seven days, cell viability was estimated using the CellTiter Glo via a luminescence assay. A custom script on R was used to quantile normalise the Z scores across the OS tumour cell line panel. Median and interquartile range highlighted. P values calculated by Student's t test.

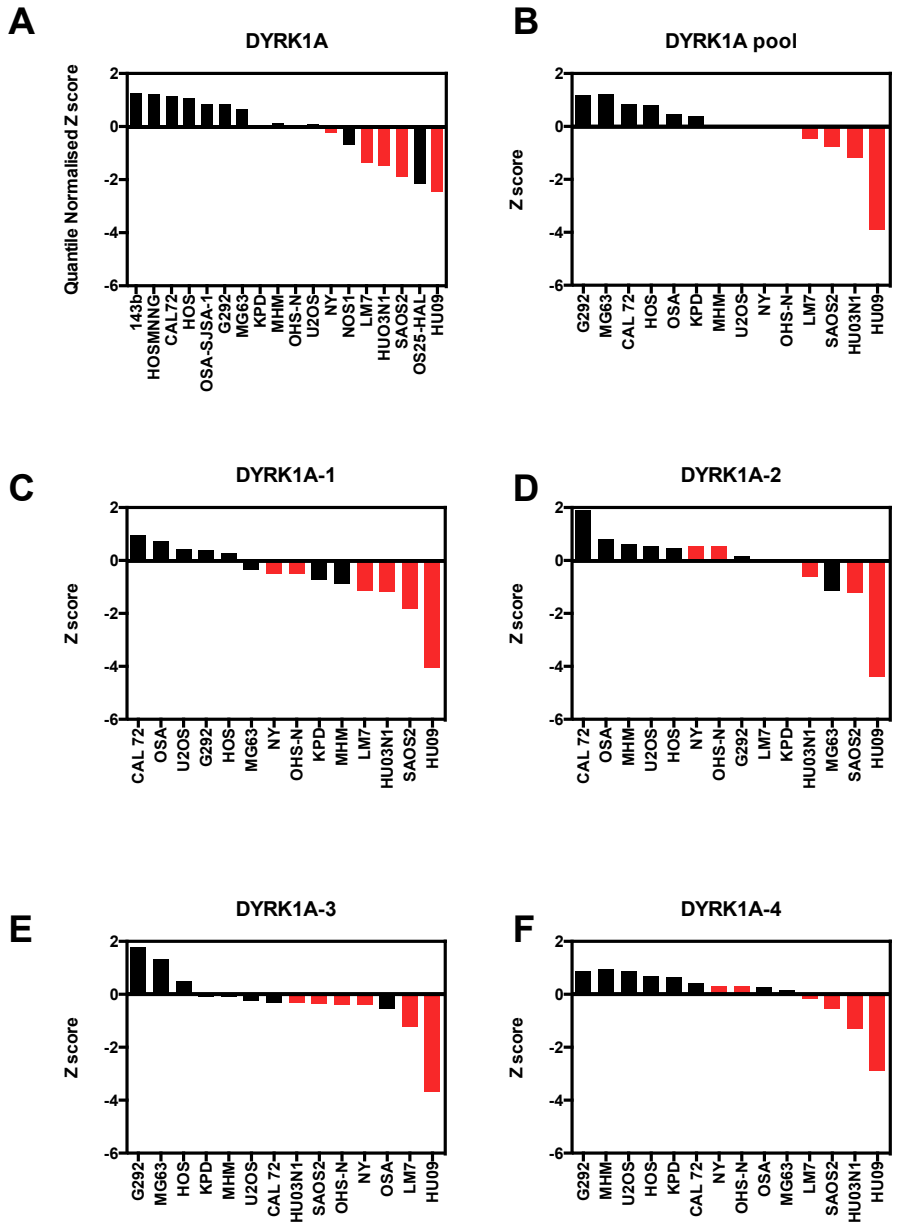

Figure 53 Waterfall plots of quantile normalised Z scores for DYRK1A revalidation using *RB1* deficient (red), and *RB1* wildtype (black) osteosarcoma tumour cell lines.

Each OS tumour cell line was ranked from least to most sensitive to DYRK1A silencing by siRNA, as measured by cell viability (Z score). (A) Data from the high-throughput screen of 18 osteosarcoma tumour cell lines using a DYRK1A siRNA smartpool. (B) Re-validation using a DYRK1A smartpool. (C-F) Deconvolution using four different individual siRNAs targeting differing regions of DYRK1A. A subset of the OS tumour cell lines (*RB1* deficient: n = 6; *RB1* wildtype: n = 8) was used for revalidation (B - F). Tumour cells were arrayed in triplicate 384 well plates, reverse transfected and viability was estimated after seven days using CellTiter Glo reagent as described in the methods.

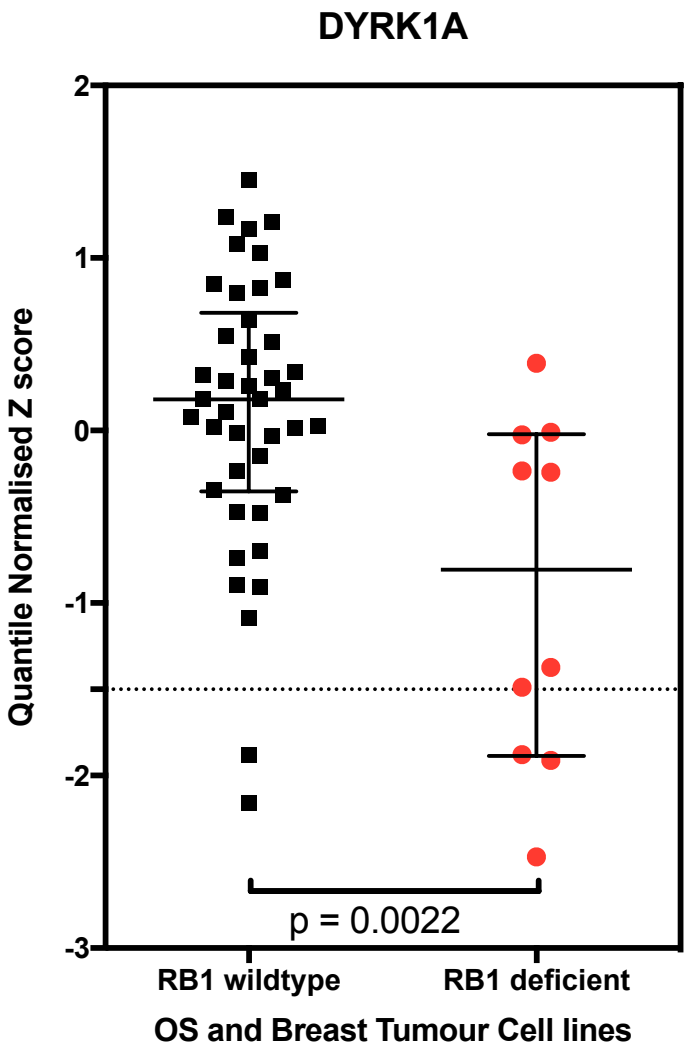

Figure 54 *RB1* deficient OS and breast tumour cell lines exhibit genetic vulnerability to silencing DYRK1A

Dot plot of quantile normalised Z scores for DYRK1A dependency with median and interquartile range clustered according to RB1 status. OS and breast tumour cell lines were arrayed in triplicate 348 well plates, and reverse transfected using the siRNA library described in Appendix Tables 1-3. After seven days, cell viability was estimated using the CellTiter Glo via a luminescence assay. A custom script on R was used to quantile normalise the Z scores across the panel of breast and OS tumour cell lines. Tumour cell lines were clustered into two groups, *RB1* deficient (OS: n = 6; breast: n = 4) and wildtype (OS: n = 12; breast n = 30). P values calculated by the MPT. [OS: osteosarcoma]

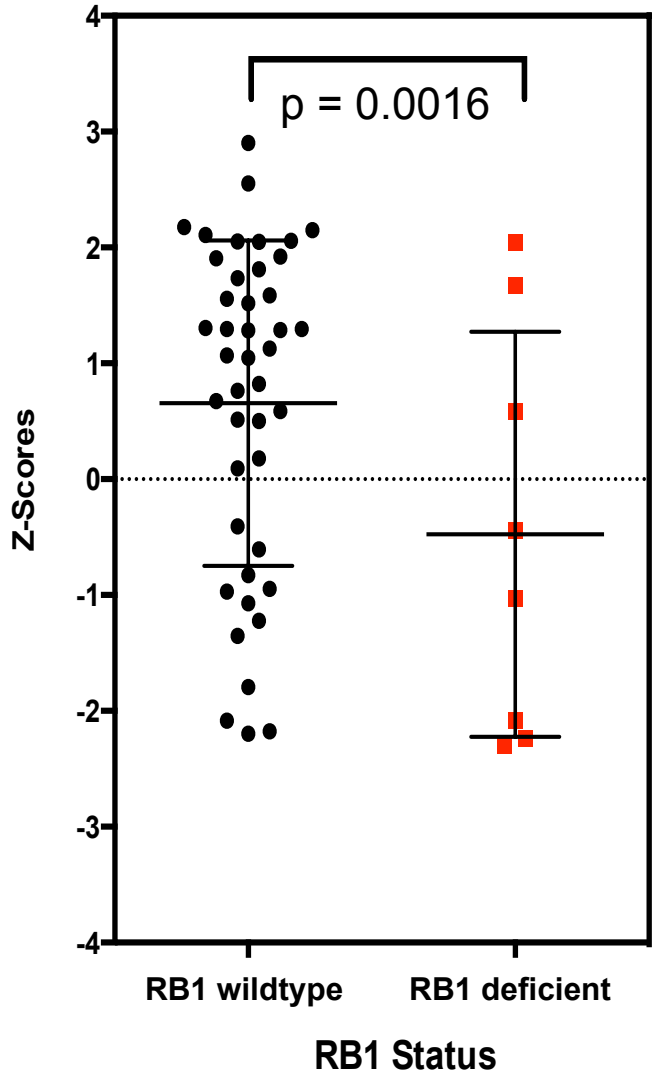

Figure 55 DYRK1A confirmed as a candidate genetic dependency in *RB1* deficient tumour cell lines using viability data from the independent publically available 'Achilles' data-set from the Broad Institute.

Dot plot of Z scores for DYRK1A using the 'Achilles' data set from the Broad Institute (https://portals.broadinstitute.org/achilles), which was comprised of a panel of 216 cancer cell lines with lenti-virally delivered genome-wide shRNA. Only one osteosarcoma cell line, SJAS1/OSA (*RB1* wildtype) was included in this data set. Silencing of DYRK1A resulted in a significantly decreased loss of viability in *RB1* deficient tumour cell lines compared to*RB1* wildtype. Non-osteosarcoma tumour cell lines were annotated for *RB1* using a combination of protein expression by western blotting performed by Rachel Brough, and publically available sequencing and mRNA expression data from COSMIC and CCLE using the same methodology to classify the OS tumour cell lines in Chapter 3. Median and interquartile range highlighted. P values calculated by the MPT.

In addition, Mittnacht *et al.* performed a siRNA screen of the kinome using a colon cancer derived cell line, which was irradiated to induce phosphorylation and activation of RB1 (Stockwell, Li, Aherne, *et al.*, 2012). *DYRK1A* was found to a be a candidate genetic dependency from this screen, with silencing in the absence of active RB1 associated with loss of viability (Stockwell, Li, Aherne, *et al.*, 2012).

6.3 INVESTIGATION OF THE *DYRK1A* AND *RB1* SYNTHETIC LETHALITY

6.3.1.1 Inhibitors of DYRK1A

There are a number of inhibitors of DYRK1A of varying efficacy, which can be broadly divided according to their action against Class I (DYRK1A and DYRK1B) and Class II (DYRK2, DYRK3, and DYRK4) targets (Ashford, Oxley, Kettle, *et al.*, 2014). Harmine, a plant alkaloid beta-carboline compound and the benzothiazole indy (INhibitor of DYRK1A), both exhibit selectivity to Class I over Class II, and have been co-crystallised with DYRK1A, bonding within the ATP binding-pocket (Ionescu, Dufrasne, Gelbcke, *et al.*, 2012). Harmine has an IC50 of 0.03-0.4μM for DYRK1A while 0.2-0.3μM for DYRK1B (Ionescu, Dufrasne, Gelbcke, *et al.*, 2012; Göckler, Jofre, Papadopoulos, *et al.*, 2009). Harmine also inhibits monoamine oxidase (MAO) A at a lower dose (IC50 5nM) than that required for inhibition of DYRK1A, which negatively impacts the side-effect profile (Ionescu, Dufrasne, Gelbcke, *et al.*, 2012; Ogawa, Nonaka, Goto, *et al.*, 2010). Indy has an IC50 of 0.01-0.9μM for DYRK1A while 0.24μM for DYRK1B (Ionescu, Dufrasne, Gelbcke, *et al.*, 2012; Ogawa, Nonaka, Goto, *et al.*, 2010). Indy has not been shown to have any action on MAO A (Ogawa, Nonaka, Goto, *et al.*, 2010). AZ191 also selectively targets Class I over Class II, and despite a lower IC50 for DYRK1B (0.017μM) than DYRK1A (IC50 0.08μM), it compairs to the IC50s for DYRK1A seen with harmine and indy (Ashford, Oxley, Kettle, *et al.*, 2014). There are no reports of use of AZ191 or indy *in vivo,* while harmine is reportedly well tolerated in mice with only side effects of tremble, twitching and jumping (Chen, Chao, Chen, *et al.*, 2005; Wang, Alvarez-Perez, Felsenfeld, *et al.*, 2015). A Phase I/II clinical trial (NCT02914769) of ayahuasca, an Amazonian botanical containing both harmine and a $5HT_{2A}$ agonist in 17 patients with recurrent depression, demonstrated that the drug was well tolerated, with the only adverse effect reported as vomiting in 47% (Sanches, de Lima Osório, Santos, *et al.*, 2016). These three drugs (harmine, indy, and AZ191) were chosen because they demonstrate inhibition of DYRK1A *in vitro* with the least recorded off-target effects.

6.3.2 Effects of silencing DYRK1A by siRNA

To further confirm the revalidation of DYRK1A, siRNA smart-pools targeting *RB1* and *DYRK1A* separately with non-targeting controls, and together, were used in the *RB1* wildtype OS tumour cell line U2OS (Figure 56). A significant difference in viability between silencing of either *RB1*, or *DYRK1A* in combination with negative controls, compared to silencing of both *RB1* and *DYRK1A* together was observed, confirming the genetic vulnerability. From this experiment silencing of *RB1* lead to an increase in cell viability compared to mock (tumour cells treated with lipid transfection mix alone), while silencing of *DYRK1A* had the opposite effect. Silencing of both *RB1* and *DYRK1A* demonstrated greater loss of viability than silencing *DYRK1A* alone.

6.3.3 Orthogonal validation of the DYRK1A and RB1 genetic vulnerability using inducible expression of DYRK1A

To further revalidate the *DYRK1A* and *RB1* genetic vulnerability, an orthogonal system was sought which enabled silencing of DYRK1A using an alternative to siRNA to confirm the observed phenotype was not an off-target effect of siDYRK1A. In the absence of an isogenic model of deficient and wildtype *DYRK1A*, exogenous kinase inactive *DYRK1A* known to have a dominant negative effect on endogenous *DYRK1A* (Yang, Ahn & Chung, 2001) (Litovchick, Florens, Swanson, *et al.*, 2011) was used. Three tumour cell lines (a generous gift from DeCaprio *et al.* (Litovchick, Florens, Swanson, *et al.*, 2011)) generated in OS tumour cell line U2OS with a tetracycline-on plasmid expression of empty vector (pRev), wildtype (WT), and kinase-inactive (KR) DYRK1A-K188R (created by site-directed mutagenesis using QuikChange: Aglient), were used. Kinase inactivation of *DYRK1A* by conversion of a critical Lys-188 residue in the catalytic domain to Arg-188 has been shown to have a dominant negative effect on wildtype *DYRK1A* (Yang, Ahn & Chung, 2001) (Litovchick, Florens, Swanson, *et al.*, 2011). Suppression of endogenous *DYRK1A* via the dominant negative effect of expression of exogenous kinase inactive *DYRK1A* was associated with a significant difference in fold change colony formation when *RB1* was silenced. No loss of viability with kinase inactive *DYRK1A* expression when *RB1* was not silenced was seen (Figure 57 and Figure 58).

Protein levels of *DYRK1A* were confirmed by western blot (Figure 59), and demonstrated endogenous expression of *DYRK1A* in pRev, increased expression of *DYRK1A* in both kinase inactive and wild-type exogenous *DYRK1A* expression. However, increased DYRK1A expression was observed in both the kinase inactive and wild-type conditions even when grown in tetracycline free media, suggesting expression of the target gene in the absence of the inducing agent, a frequent issue encountered in these systems (Pham, Moretti, Goodall, *et al.*, 2008). Despite this ambiguity, a difference in viability was still observed with this genetic vulnerability. This provided evidence that the genetic dependency observed is dependent on the kinase activity of DYRK1A.

6.3.4 Validation of the *DYRK1A* and *RB1* genetic vulnerability using a breast TCL with isogenic *RB1* deficiency

To provide a robust model to further investigate specific genetic lethalities associated with loss of *RB1* function, an isogenic model of *RB1* loss was developed. In the absence of an available *RB1* deficient isogenic model in osteosarcoma at the time, a breast cancer cell line model (MDAMB231) created by shRNA-mediated silencing of *RB1* was used. Reverse transfection in a 96-well plate format was used with 3000 cells per well. siRNA smart-pools targeting *DYRK1A*, with *PLK* as a positive control, and non-targeting negative controls (siCON1, siCON2, and siAllstar) were used. Cell viability was assessed using a CTG assay at seven days post reverse transfection. This experiment demonstrated that silencing of *DYRK1A* in a *RB1* deficient setting was associated with a significant increase in loss of viability, confirming the genetic vulnerability in an additional tissue type (Figure 60).

6.3.5 High-throughput siRNA screen in isogenic RB1 deficient and wildtype U2OS osteosarcoma models

After generation of a two isogenic *RB1* deficient and wildtype U2OS osteosarcoma tumour cell line models by CRISPR-Cas9, as detailed in Chapter four the models were screening using the same RNAi library as described previously (Appendix Tables 1-3). The screen was performed in triplicate using the same optimised transfection conditions already described for U2OS in Chapter 5. All three screens passed the same robust measures of quality control as previously set (5.2.3); U2OS 4.2: mean r^2 (Spearman's rank correlation coefficient) = 0.87, mean Z prime = 0.65; U2OS 4.5: mean r^2 = 0.93;

mean z prime = 0.66; U2OS 9.1: mean r^2 = 0.91; mean z prime = 0.68 (Figure 61 and Figure 62).

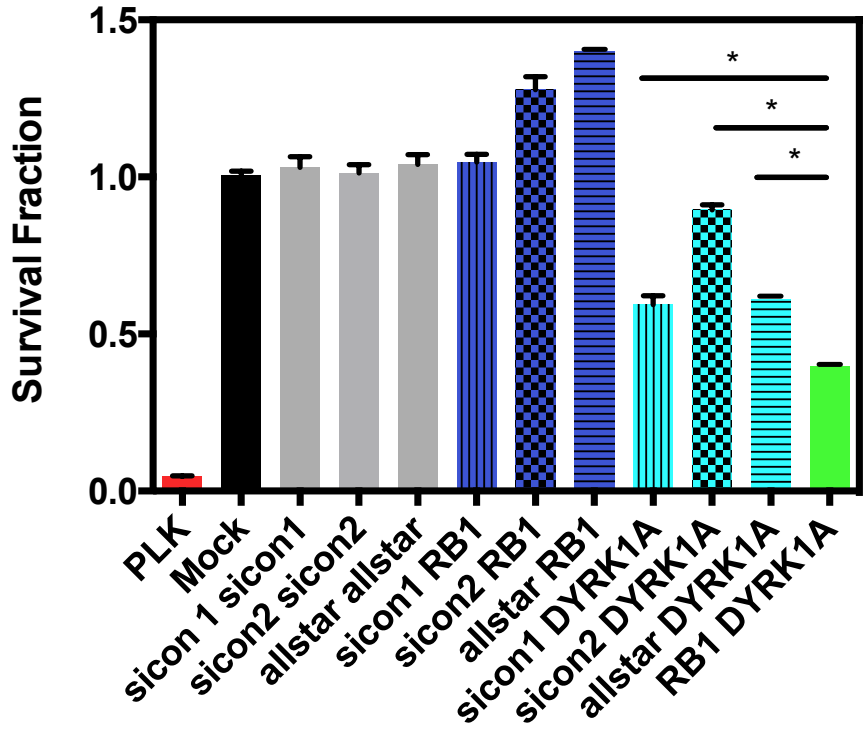

Figure 56 Silencing of both *RB1* and *DYRK1A* simultaneously by siRNA using the *RB1* wildtype OS tumour cell line U2OS confirmed the genetic vulnerability.

Bar chart illustrating survival fraction compared to 'mock'. Tumour cells were plated in 96 well format. Reverse transfection with siRNAs targeting the following combinations were undertaken: *RB1* and three different non-targeting controls (siAllstar, siCON1 and siCON2); *DYRK1A* and three different non-targeting controls (siAllstar, siCON1 and siCON2); *RB1* and *DYRK1A*; and *PLK*. Cells only treated with lipid transfection media without siRNA were termed 'mock'. After incubation for seven days, cell viability was assessed using CellTiter Glo reagent as described in the methods. A significant difference in viability (*$p<0.05$) between silencing of either *RB1*, or *DYRK1A* with negative controls, compared to silencing of both *RB1* and *DYRK1A* together was observed. P values calculated by Student's t test. Error bars represent SEM (standard error of the mean) from eight replicates.

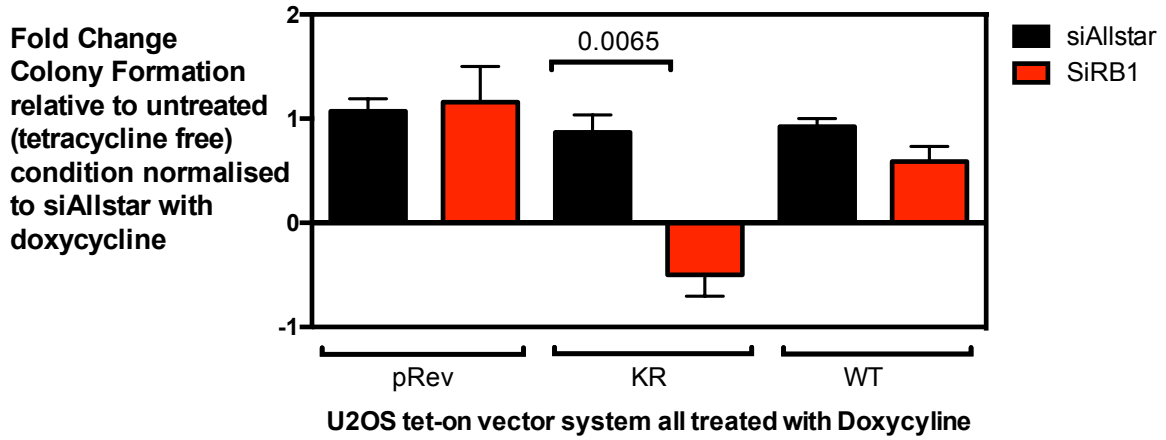

Figure 57 A significant difference between colony formation post silencing of *RB1* compared to non-targeting control (siAllstar) in the kinase inactive *DYRK1A-K188R* (KR) tumour cell line in the presence of doxycycline was observed.

Histogram of quantitation of colony formation post reverse transfection with siRNA targeting *RB1* using U2OS tumour cell lines with tetracycline inducible empty vector (pRev), kinase inactive *DYRK1A*-K188R (KR), and wildtype *DYRK1A* (WT). Fold change in colony formation from the tetracycline free condition normalised to the doxycycline treated non-targeting siRNA control (siAllstar) is shown. All three tumour cell lines were grown for one week in tetracycline free media, before division and the addition of doxycycline at 5µg/ml to half of the cells. After four days, cells were reverse transfected with a siRNA smart-pools targeting *RB1, PLK* and a non-targeting control (Allstar). At 24 hours, cells were then seeded in triplicate at low density (500 cells per well of six well plate), and after two weeks, the cells were fixed and stained. P values calculated using Student's t test. Error bars represent SEM (standard error of the mean) from three replicates. p = 0.0065 kinase inactive *DRYK1A*-K188R reverse transfected with siAllstar versus kinase inactive *DRYK1A*-K188R reverse transfected with siRB1.

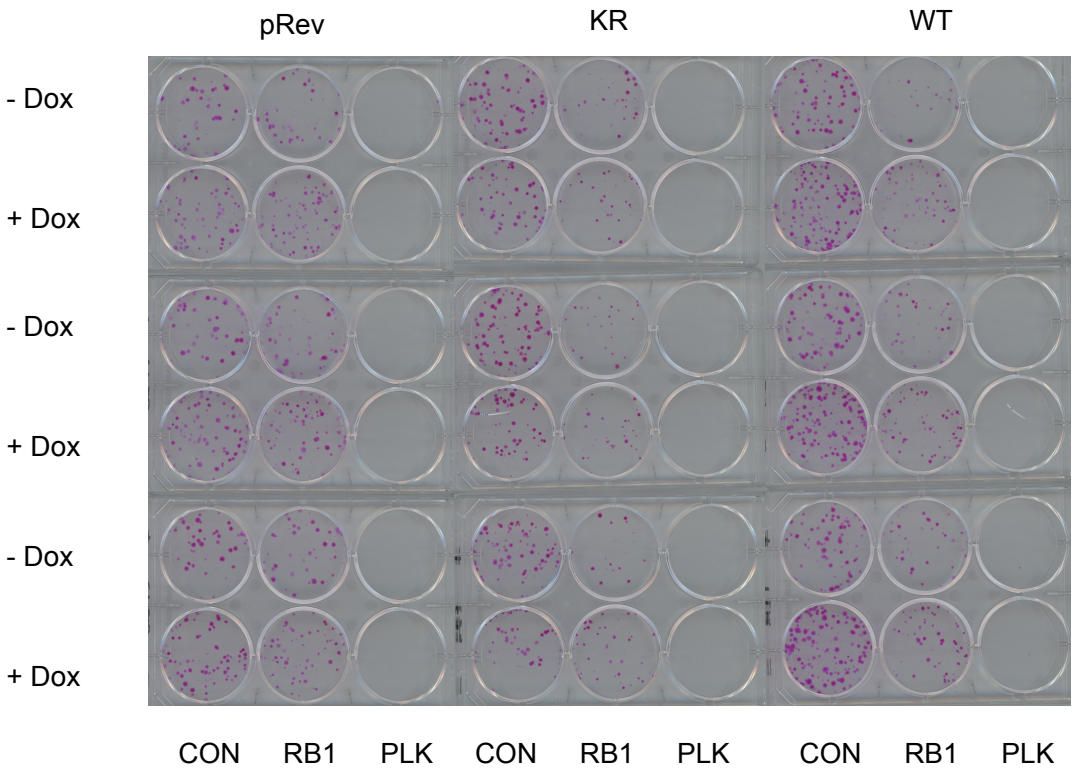

Figure 58 Colony formation post reverse transfection with siRNA targeting *RB1*

Three U2OS tumour cell lines were used with either a tetracycline inducible empty vector (pRev), kinase inactive *DYRK1A-K188R* (KR), or wildtype *DYRK1A* (WT). Each U2OS tumour cell line was expanded for a week in tetracycline free media, split and half were treated with doxycycline (5µg/ml) for five days. Cells were then reverse transfected with siRNA targeting *RB1*, Allstar (negative control), and *PLK* (positive control), and after 24 hours plated at low density (500 cells per well) for colony formation. After two weeks the colonies were fixed and stained. [- Dox: tetracycline free media; + Dox: doxycycline (5µg/ml); CON: siAllstar; RB1; siRB1; PLK; siPLK]

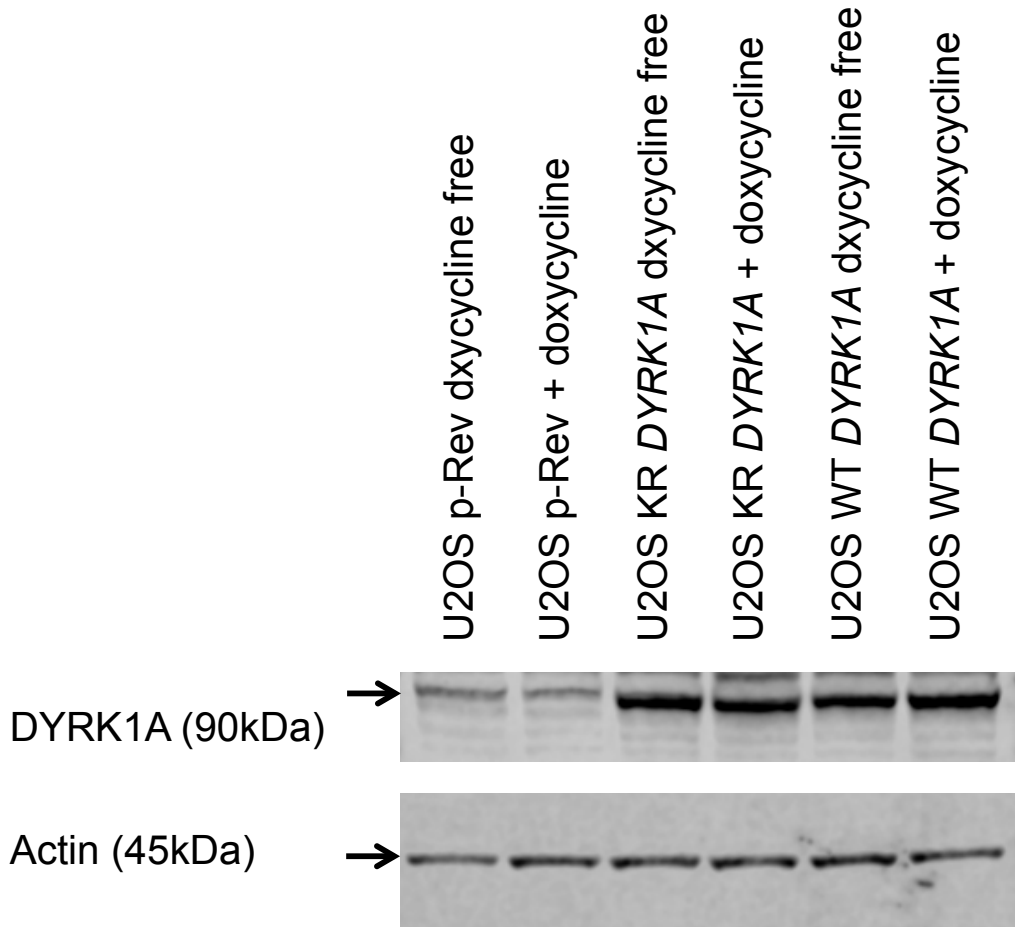

Figure 59 Increased exogenous levels of DYRK1A seen in both KR and WT DYRK1A vectors, both in the presence and absence of doxycycline, suggest some leakiness of the vector.

Western blot is shown. The OS tumour cell lines U2OS pRev, kinase inactive (KR) exogenous DYRK1A-K188R, and wild-type exogenous DYRK1A were exposed to tetracycline doxycycline (5µg/ml) for five days or grown in tetracycline free media. Total cell lysates isolated after drug exposure were electrophoresed and immunoblotted as described in the methods. Immuoblotting of actin was used as the loading control.

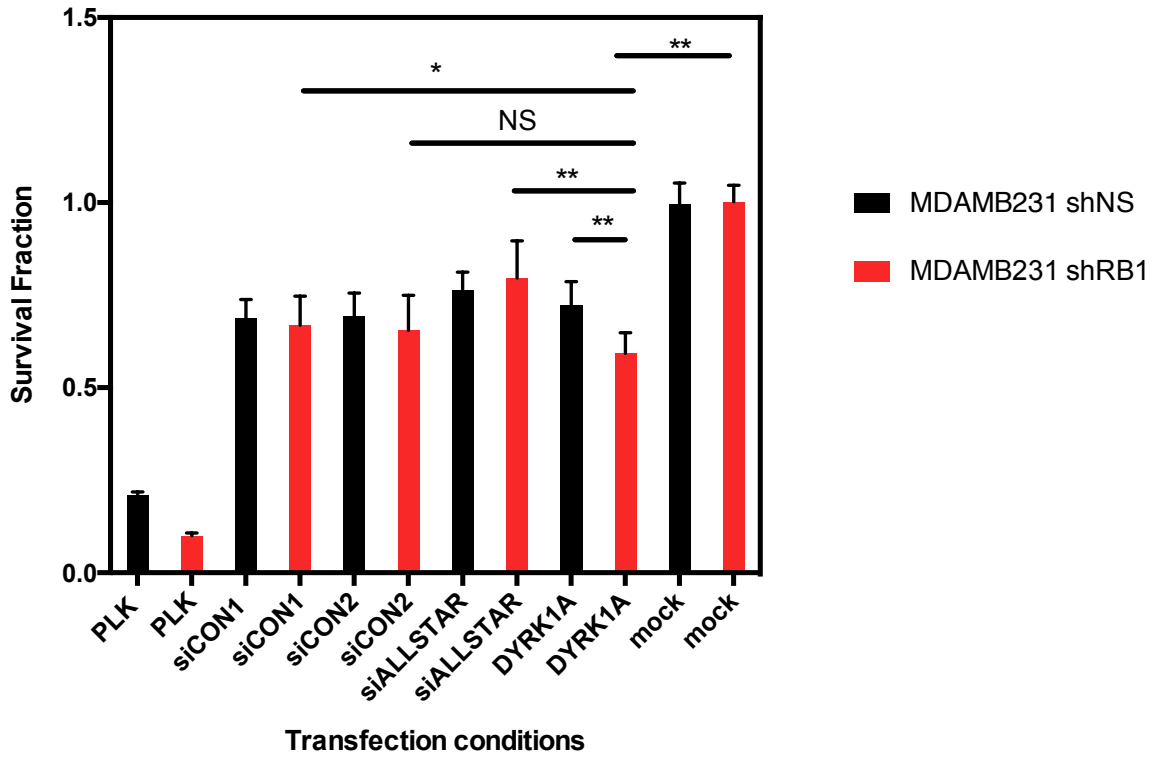

Figure 60 Genetic vulnerability to silencing of *DYRK1A* observed in the isogenic *RB1* deficient and wildtype breast cancer cell line MDMAMB231.

Bar chart illustrating survival fraction relative to 'mock'. Tumour cells that were only transfected with lipid transfection mix, but without siRNA were termed 'mock', and demonstrated no effect on viability of transfection mix alone. *RB1* deficient (shRB1) and wildtype (shNS) MDAMB231 tumour cell lines were arrayed in 96 well plates, and reverse transfected with non-targeting controls (siControl 1, siControl 2, and siAllstar), positive control siPLK, and siDYRK1A. After seven days, cell viability was assessed using CellTiter Glo reagent as described in the methods. Error bars represent SEM. P values calculated by Student's t test. Reverse transfection with the non-targeting controls had a minimal effect on viability, while siPLK demonstrated a profound loss of viability in both tumour cell lines. p = 0.0007 MDAMB231 shRB1 reverse transfected with siDYRK1A versus MDAMB213 shNS reverse transfected with siDYRK1A. [*: p<0.05; **: p<0.01; NS: non-significant; shNS: small non-targeting hairpins; shRB1: small hairpins targeting RB1]

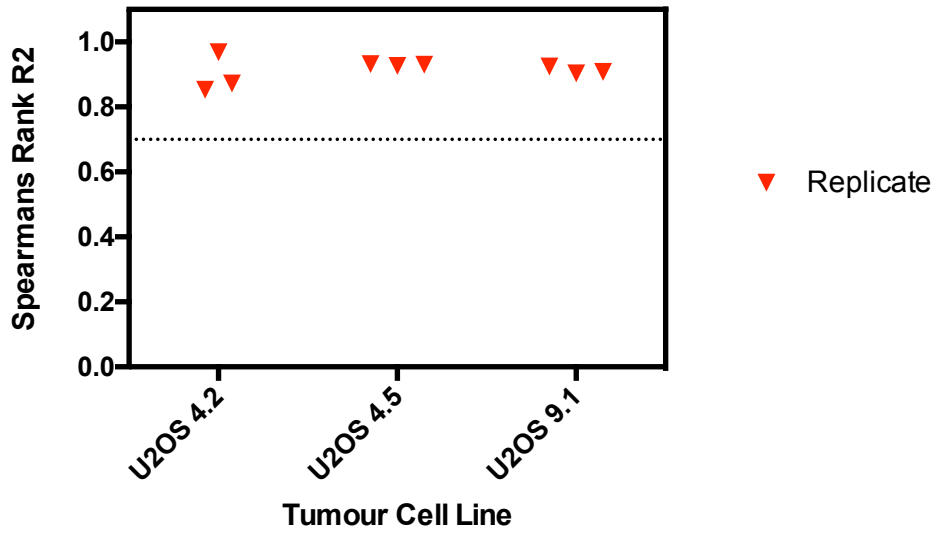

Figure 61 Spearman's rank correlation coefficient for each replicate of the siRNA screen performed using the isogenic *RB1* deficient U2OS 4.2 and 4.5 and *RB1* wildtype U2OS 9.1 tumour cell lines were >0.7.

Raw luminescence data from the RNAi screens was correlated using GraphPad Prism to determine the Spearman's rank correlation coefficient.

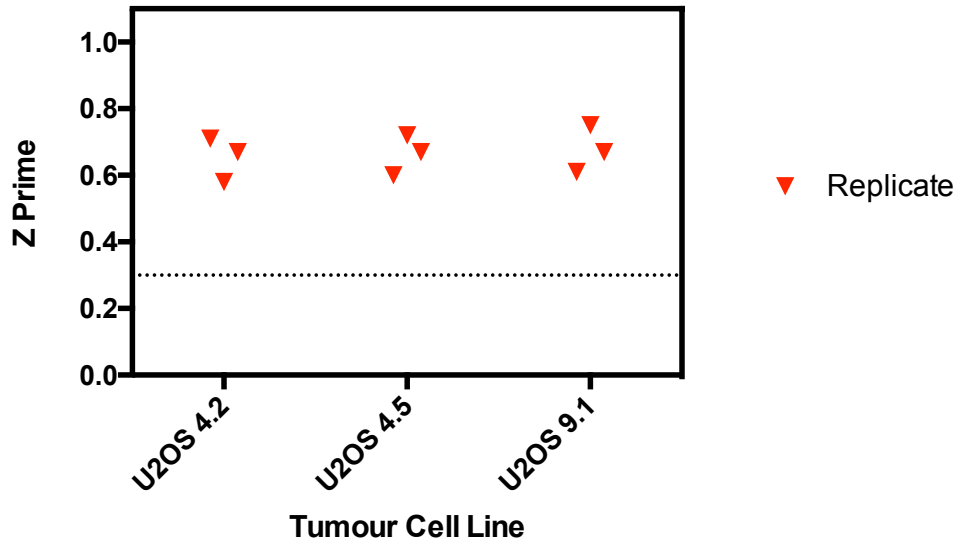

Figure 62 Z prime for each replicate of the siRNA screen performed using the isogenic *RB1* deficient U2OS 4.2 and 4.5 and *RB1* wildtype U2OS 9.1 tumour cell lines were >0.3.

Raw luminescence data from the RNAi screens was processed and Z prime values for each screen calculated using the CellHTS2 package of the R software suit (BioConductor).

The same criteria as previously described in section 6.2.1 were used to identify candidate genetic dependencies associated with *RB1* deficiency: (i) median Z score in both the *RB1* deficient tumour cells lines combined of < - 1.5; (ii) median Z score in the *RB1* wildtype parental line of > -1.0; (iii) probability of the difference between the Z scores in both the *RB1* deficient and wildtype groups seen by chance of <0.05. Twenty-seven genes met these criteria (Rho GTPase Activating Protein 26 (*ARHGAP26*), Heterogeneous Nuclear Ribonucleoprotein A2/B1 (*HNRNPA2B1*), Werner syndrome helicase (*WRN*), Calmodulin Binding Transcription Activator 1 (*CAMTA1*), Ras-Related C3 Botulinum Toxin Substrate 1 (*RAC1*), ERCC Excision Repair 3 TFIIH Core Complex Helicase Subunit (*ERCC3*), IKAROS Family Zinc Finger 1 (*IKZF1*), Motor Neuron And Pancreas Homeobox 1(*MNX1*), Programmed Cell Death 1 Ligand 2 (*PDCD1LG2*), Heat Shock Protein 90 Alpha Family Class A Member 1 (*HSP90AA1*), RecQ Like Helicase 5 (*RECQL5*), Cytochrome C Oxidase Subunit 6C (*COX6C*), Acyl-CoA Synthetase Long-Chain Family Member 3 (*ACSL3*), PALB2, Clathrin Heavy Chain (*CLTC*), Homeobox A13 (*HOXA13*), Ras Homolog Family Member H (*RHOH*), GATA Binding Protein 3 (*GATA3*), Epidermal Growth Factor Receptor Pathway Substrate 15 (*EPS15*), HRas Proto-Oncogene GTPase (*HRAS*), RAD50 Double Strand Break Repair Protein (*RAD50*), 8-Oxoguanine DNA Glycosylase (*OGG1*), Cyclin D3 (*CCND3*), WW Domain Containing Transcription Regulator 1 (*WWTR1*), Homeobox D13 (*HOXD13*), MYC Associated Factor X (*MAX*), and Solute Carrier Family 45 Member 3 (*SLC45A3*)), and the most profound are shown in Figure 63.

Network analysis demonstrated a number of connections between these candidate genetic dependencies (Figure 64). Of particular interest are the connections with DNA metabolism and damage repair (*WRN, RECQL5, RAD50, ERCC3, OGG1* and *PALB2*). In addition, mutations of *WRN* cause Werner Syndrome, also known as adult progeria, characterised by premature aging, short stature and distinctive skin changes, is also associated with an increased risk of OS and other malignancies (Calvert, Randall, Jones, *et al.*, 2012). Other DNA helicase disorders, Bloom Syndrome and Rothmund-Thomson Syndrome (RTS) are associated with germ-line mutations of *RECQL3* and *RECQL4* respectively (Vogelstein, Papadopoulos, Velculescu, *et al.*, 2013; Kansara & Thomas, 2007). Although mutations of *RECQL5* do not cause a monogenic disease, polymorphisms in this gene have been associated with an increased prevalence of OS in the Chinese Han population (Zhi, Ma, Zhang, *et al.*, 2014) and overexpression in the OS tumour cell line MG63 was associated with decreased viability (Wu, Zhi, Dai, *et al.*, 2015).

Analysis of the data generated by screening the *RB1* isogenic U2OS models separately identified one of the candidate genetic dependencies (*GALK1*) already selected for revalidation by the siRNA screen performed in the panel of OS tumour cell lines (Figure 65). Two other candidate genetic dependencies selected for revalidation including *DYRK1A* met one out of three of the criteria (Figure 66).

Further overlap of the genetic dependencies identified in this isogenic screen with those of the osteosarcoma tumour cell line panel, in particular *DYRK1A* were not observed. This could be due to other molecular characteristics of the tumour cell line U2OS that mitigate the genetic vulnerability of loss of *DYRK1A.*

6.3.6 DYRK1A expression in the panel of OS tumour cell lines

To determine if vulnerability to silencing of *DYRK1A* correlated with protein expression, expression of DYRK1A in the panel of OS tumour cell lines was determined by rtPCR, western blotting, and proteomic abundance. Levels of expression of *DYRK1A* by rtPCR (Figure 67), western blotting (Figure 68) and proteomic abundance of DYRK1A (Figure 69) varied across the tumour cell line panel with no discernable pattern with relation to *RB1* or *CDKN2A* deficiency.

A positive correlation was observed between *DYRK1A* mRNA expression delta delta cycle threshold levels by rtPCR and *DYRK1A* Z scores amongst the *RB1* deficient OS tumour cell lines (Figure 70). Delta delta cycle threshold levels are inversely correlated with mRNA, meaning increasing delta delta cycle threshold levels equates to decreased mRNA expression. Spearman's rank correlation coefficient (r^2) = 0.735 demonstrated that in the context of *RB1* deficiency, increased mRNA expression levels (decreased delta delta cycle threshold) of DYRK1A was associated with a greater loss of viability when *DYRK1A* was silenced by siRNA (more negative Z score).

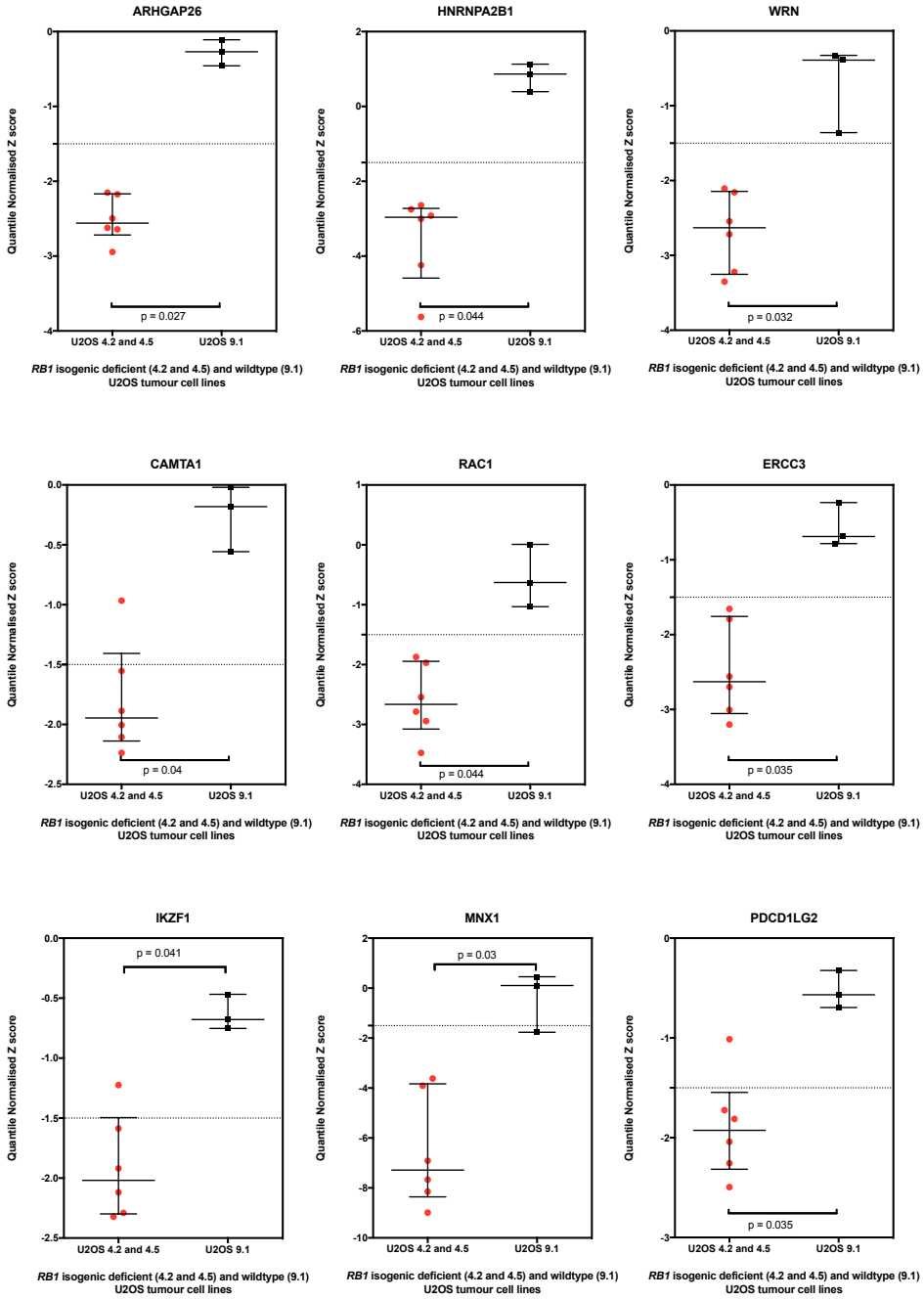

Figure 63 The most profound candidate genetic dependencies according to *RB1* status in isogenic *RB1* deficient and wildtype isogenic U2OS OS tumour cell lines.

Dot plots are shown illustrating the median effects on viability. U2OS 4.2 and 4.5 are *RB1* deficient mutant clones created by CRISPR-Cas9 mutagenesis, and U2OS 9.1 was the parental line (reverse transfected with Cas9 alone). Tumour cell lines were arrayed in triplicate 384 well plates, and reverse transfected using the siRNA library described in Appendix Tables 1-3. After seven days, cell viability was estimated using the CellTiter Glo reagent as described in the methods. A custom script on R was used to quantile normalise the Z scores across the tumour cell lines. P values calculated by the MPT. [QN: quantile normalised]

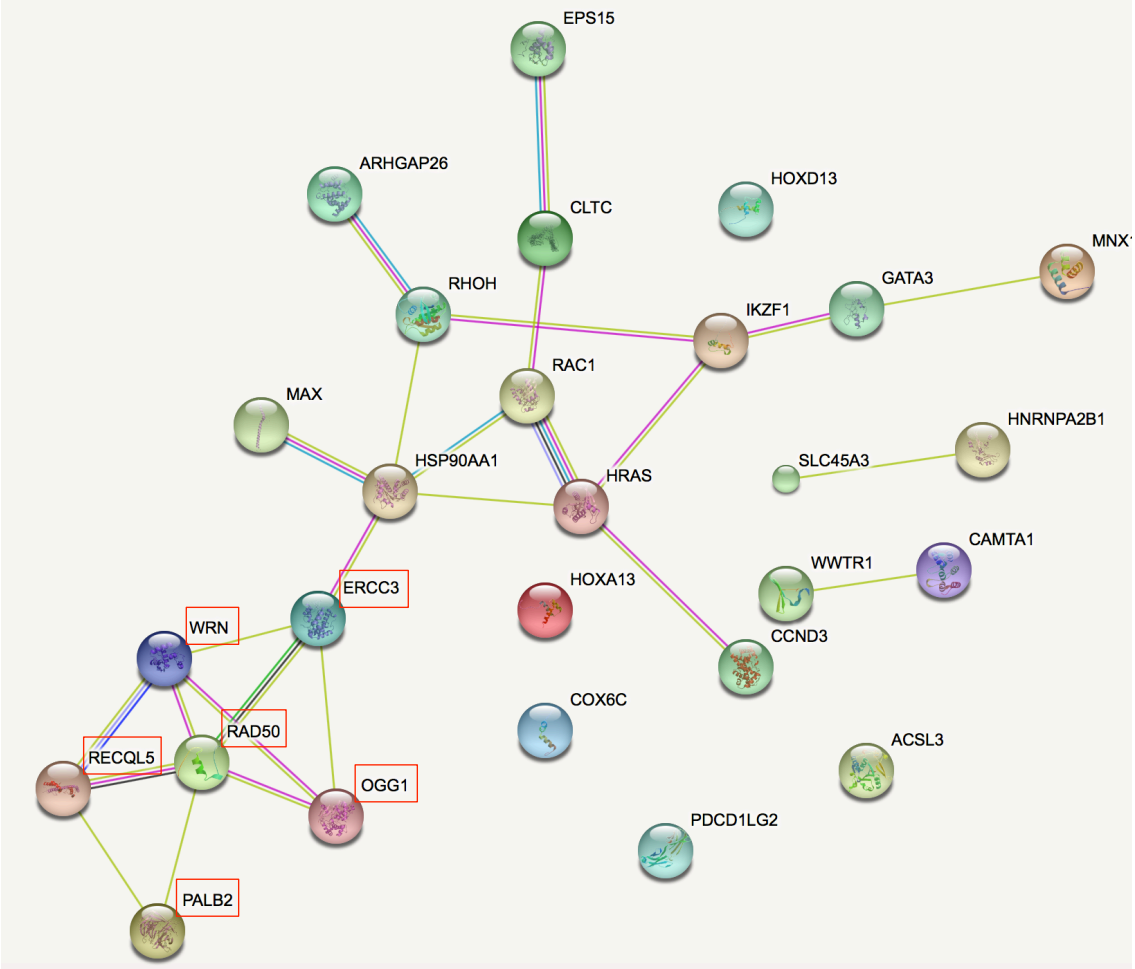

Figure 64 Protein-protein network analysis using String (string-db.org) highlights a reliance on genes involved in DNA metabolism and damage repair (*WRN, RECQL5, RAD50, ERCC3, OGG1* and *PALB2* highlighted by red boxes) associated with a *RB1* deficient phenotype.

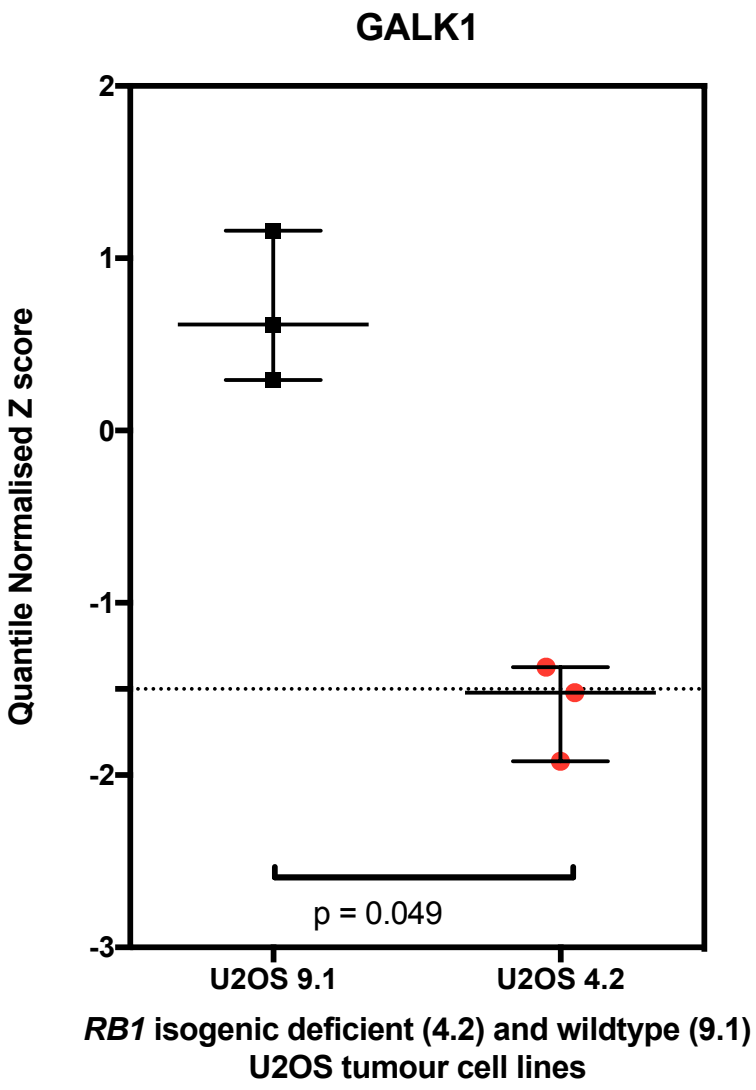

Figure 65 *RB1* deficient U2OS model demonstrates genetic dependency on *GALK1*.
Dot plot is shown illustrating viability. This candidate genetic dependency was previously selected from data generated by RNAi screen of the panel of 18 OS tumour cell lines for revalidation. In both screens, the median Z score in the *RB1* deficient cells lines was < - 1.5; median Z score in the *RB1* wildtype group was > -1.0; and the probability of the difference between the Z scores in both the *RB1* deficient and wildtype groups seen by chance of <0.05. Tumour cell lines (U2OS 4.2 and 9.1) were arrayed in triplicate in 384 well plates, and reverse transfected using the siRNA library described in Appendix Tables 1-3. After seven days, cell viability was estimated using CellTiter Glo reagent as described in the methods. A custom script on R was used to quantile normalise the Z scores across the non-osteosarcoma tumour cell line panel. Median and interquartile range highlighted. P values calculated by the MPT.

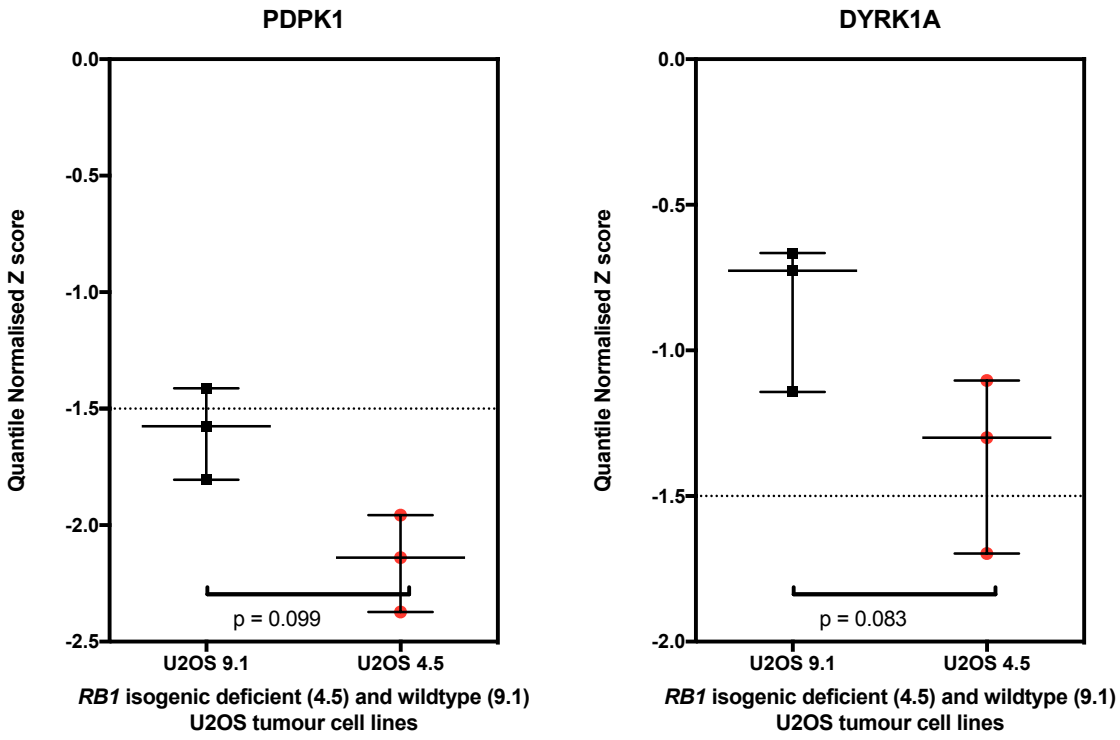

Figure 66 *RB1* deficient U2OS model demonstrates genetic dependency on *PDPK1* and *DYRK1A*.

Dot plot is shown illustrating viability. These candidate genetic dependencies were previously selected from data generated by RNAi screen of the panel of 18 OS tumour cell lines for revalidation. In this screen these genes met one of the three criteria set for selection for revalidation described previously. Tumour cell lines (U2OS 4.5 and 9.1) were arrayed in triplicate 384 well plates, and reverse transfected using the siRNA library described in Appendix Tables 1-3. After seven days, cell viability was estimated using CellTiter Glo reagent as descripted in the methods. A custom script on R was used to quantile normalise the Z scores across the non-osteosarcoma tumour cell line panel. Median and interquartile range highlighted P values calculated by MPT.

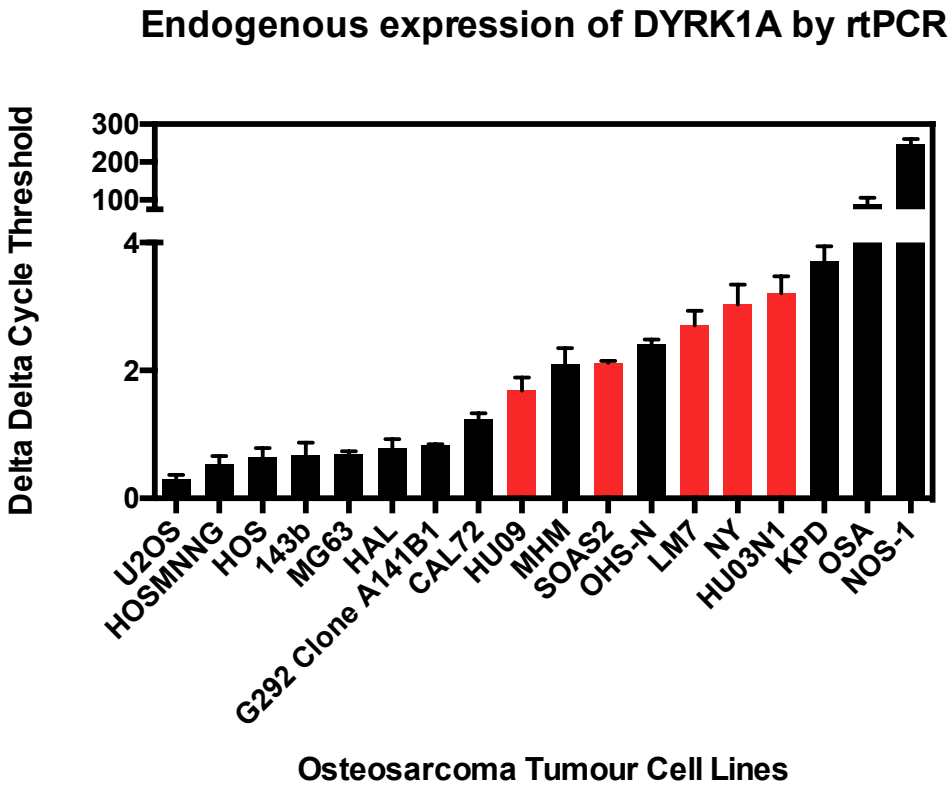

Figure 67 Endogenous mRNA expression levels of DYRK1A expression in the panel of OS tumour cell lines.

Bar chart illustrating delta delta cycle threshold levels for *DYRK1A* relative to endogenous expression of the control GAPDH. Delta delta cycle threshold levels are inversely correlated with mRNA, meaning increasing delta delta cycle threshold levels equates to decreased mRNA expression. *RB1* deficient tumour cell lines are shown in red, and *RB1* wildtype in black. cDNA was prepared from untreated tumour cells using the Supercript III First Strand Synthesis System for rt-PCR. Quantitive rtPCR was performed using Taqman Universal mastermix II with UNG using probes for DYRK1A and GAPDH. mRNA expression was detected using a 7900 HT Fast Real-Time PCR system RT-PCR. Target gene expression was calculated as expression relative to the expression of control cDNA after adjusting for expression of GAPDH as the endogenous control.

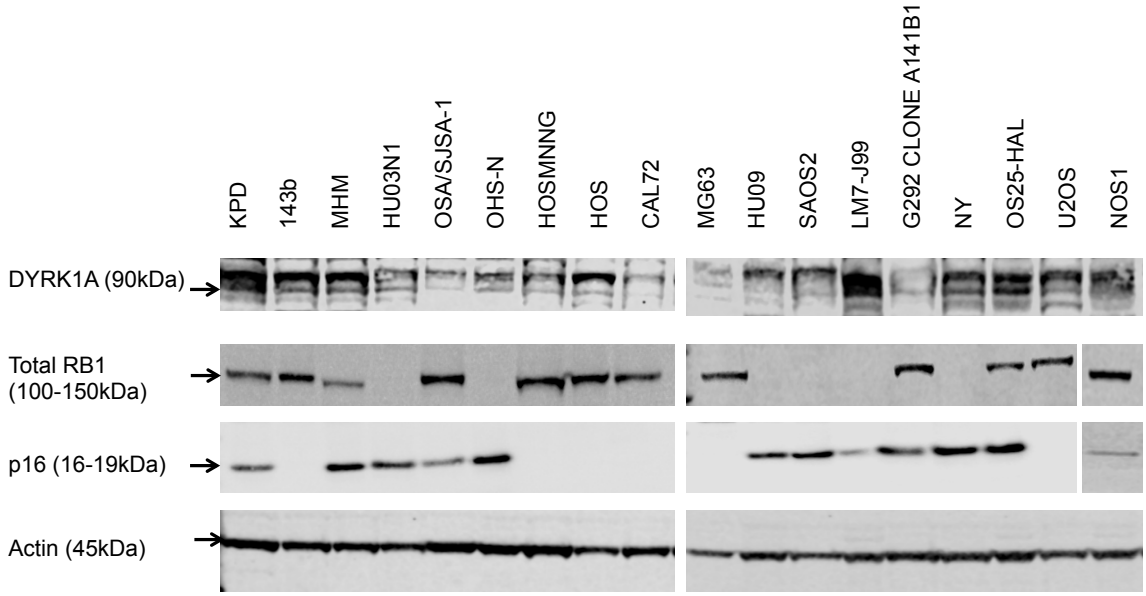

Figure 68 Heterogeneity of DYRK1A, RB1 and p16 (*CDKN2A*) protein expression in 18 osteosarcoma tumour cell lines.

Western blot is shown. Total cell lysates were collected from untreated cells, electrophoresed and immunoblotted as described in the methods. Immunoblotting of actin was used as the loading control. Levels of expression of DYRK1A varied across the tumour cell line panel with no discernable pattern with relation to *RB1* or *CDKN2A* deficiency. DYRK1A expression was seen in all *RB1* deficient tumour cell lines but did not correlate with genetic vulnerability.

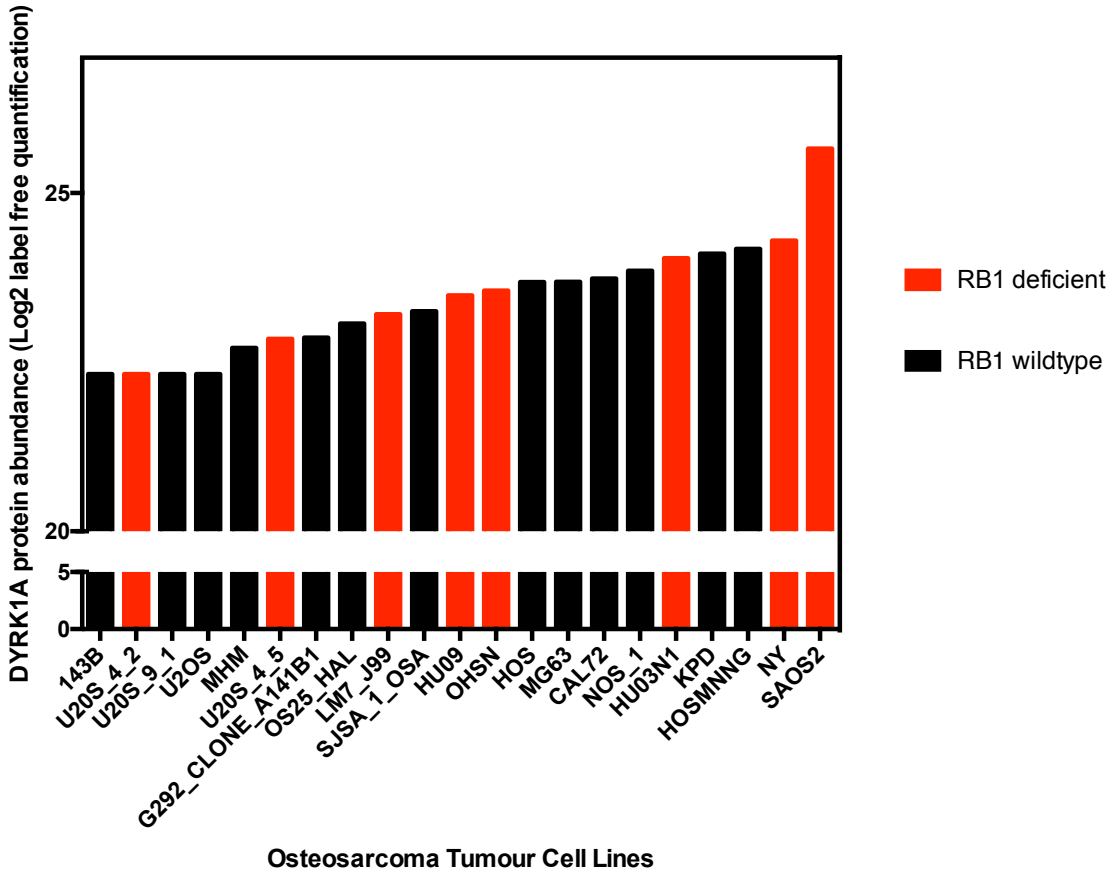

Figure 69 Proteomic abundance of DYRK1A in osteosarcoma tumour cell lines was not associated with *RB1* status.

Bar chart illustrating proteomic abundance of DRRK1A quantified by mass spectroscopy proteomic profiling performed by Colm Ryan (Systems Biology, Dublin, Ireland). Following lysis, protein purification, and tryptic digest, peptides were separated by liquid chromatography and measured by mass spectrometer. Label-free proteome quantification was performed using the MaxQuant software environment (Coscia, Watters, Curtis, *et al.*, 2016; Cox, Hein, Luber, *et al.*, 2014) to determine the quantitative abundance of 6696 peptides with a false discovery rate of less than one percent. Red columns indicate tumour cell lines classified as *RB1* deficient (Chapter 3). Isogenic *RB1* wildtype (U2OS 9.1) and *RB1* deficient U2OS tumour cell lines (U2OS 4.2 and U2OS 4.5) generated by CRISPR-Cas9 mediated mutagenesis (described in Chapter 4) are shown as contrasts. DYRK1A expression was seen in all *RB1* deficient tumour cell lines but did not correlate with genetic vulnerability to silencing of *DYRK1A.*

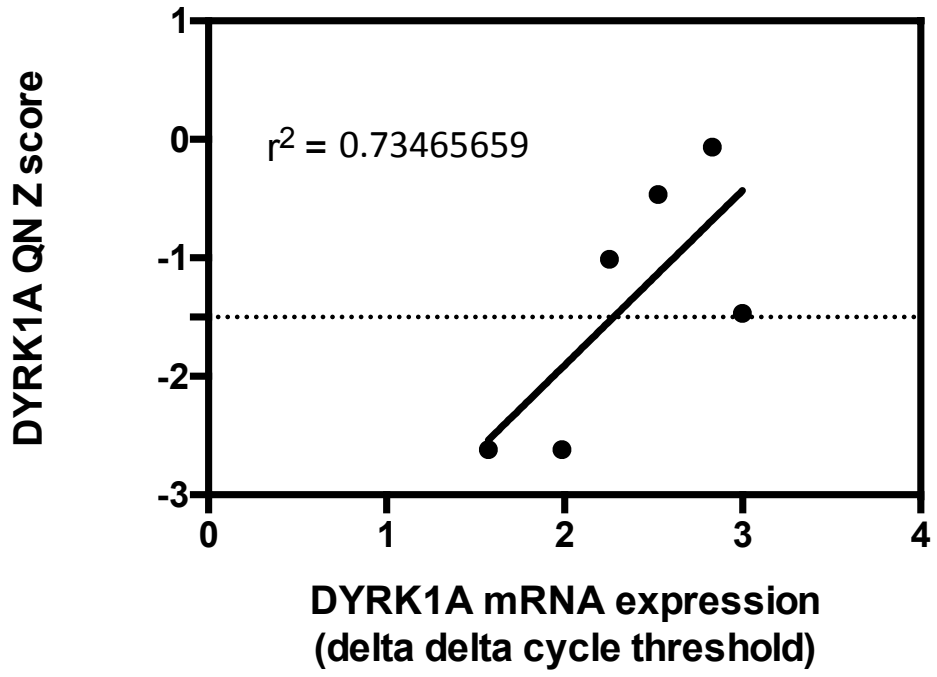

Figure 70 DYRK1A mRNA expression and siDYRK1A viability amongst the *RB1* deficient OS tumour cell lines are negatively correlated.

Scatter plot of DYRK1A quantile normalised Z scores and delta delta cycle threshold levels of *DYRK1A* using *RB1* deficient OS tumour cell lines only. cDNA was prepared from untreated tumour cells using the Supercript III First Strand Synthesis System for rt-PCR. Quantitive rtPCR was performed using Taqman Universal mastermix II with UNG using probes for DYRK1A and GAPDH. mRNA expression was detected using a 7900 HT Fast Real-Time PCR system RT-PCR. Target gene expression was calculated as expression relative to the expression of control cDNA after adjusting for expression of GAPDH as the endogenous control. Delta delta cycle threshold levels are inversely correlated with mRNA, meaning increasing delta delta cycle threshold levels equated to decreased mRNA expression. Spearman's rank correlation coefficient (r^2) = 0.735 demonstrated that in the context of *RB1* deficiency, increased mRNA expression levels (decreased delta delta cycle threshold) of DYRK1A were associated with a greater loss of viability when DYRK1A was silenced by siRNA (more negative Z score). [r^2: Spearman's rank correlation coefficient; QN: quantile normalised]

To determine if DYRK1A protein expression by western blotting correlated with genetic dependency, densitometry of DYRK1A relative to actin was performed prior to correlation; no significant correlation was observed (Figure 71). DYRK1A expression was seen in all *RB1* deficient tumour cell lines but did not correlate with genetic vulnerability. Proteomic abundance of DYRK1A defined by mass spectroscopy proteomic profiling did not correlate with genetic dependency to *DYRK1A* (Figure 72).

A positive correlation between a genetic dependency to *DYRK1A* and mRNA expression levels of DYRK1A but not protein levels was observed; this could be due to the linear relationship between binding of siDYRK1A via the RNA-induced silencing complex (RISC) which facilitates binding between one of the siRNA strands and protein-coding mRNAs that have nucleotide sequence complementary to the siRNA leading to mRNA degradation (Lord, Martin & Ashworth, 2009). Hence if a tumour cell has a high expression level of mRNA, silencing would require a high number of siDYRK1A. Given that there is the opportunity for considerable post-translational modification of protein expression level it is not unsurprising that no direct correlation was observed.

6.3.7 Small molecule inhibition of DYRK1A

To determine if small molecule inhibition of DYRK1A in an *RB1* deficient setting could recapitulate the genetic effects observed, a short-term five day assay was performed on a limited panel of osteosarcoma tumour cell lines (five *RB1* deficient and eight *RB1* wildtype), using two inhibitors of DYRK1A, harmine and indy (Ogawa, Nonaka, Goto, *et al.*, 2010; Ionescu, Dufrasne, Gelbcke, *et al.*, 2012). Of the two inhibitors, the greatest difference in loss of viability in the *RB1* deficient group was observed with Indy, although the effect was modest.

Median survival fractions were calculated for *RB1* wildtype and *RB1* deficient, with a significant difference between the two groups post exposure to indy (ANOVA plus Bonferroni post hoc test $p = 0.0028$) (Figure 73) but no significant difference in viability seen with harmine (ANOVA plus Bonferroni post hoc test $p = 0.83$) (Figure 74). After short-term exposure to indy, AUC for the range 0.05-50μM when grouped according to *RB1* status, demonstrated a statistically significant difference in median AUC shown in Figure 75. No significant difference in AUC was observed with harmine between the two groups (Figure 76).

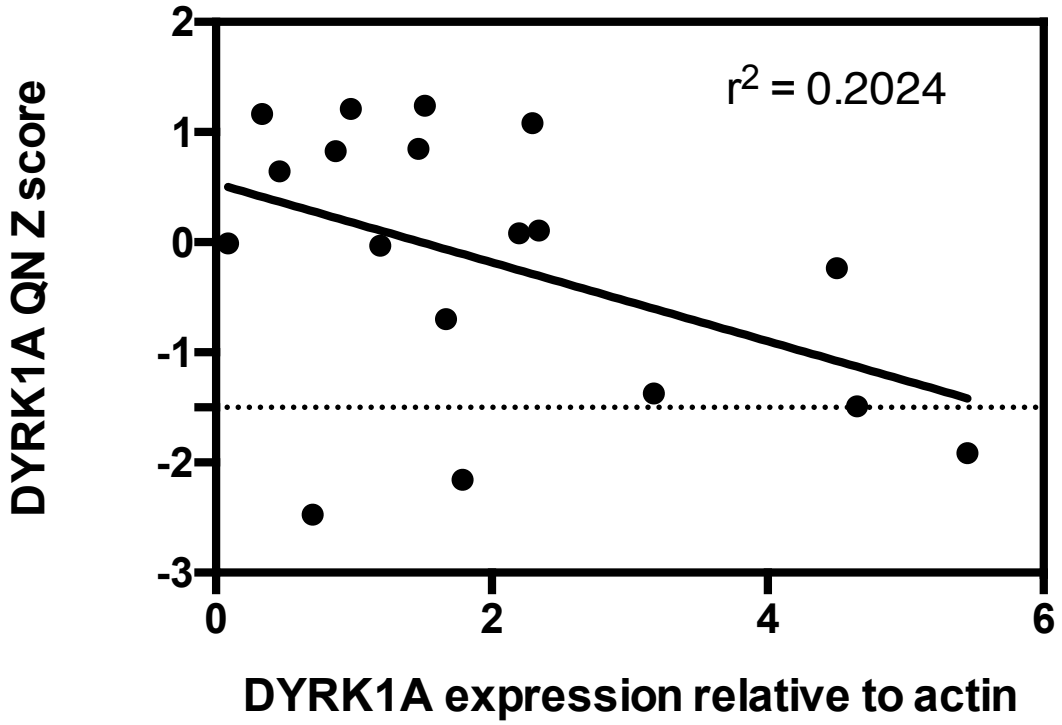

Figure 71 No significant correlation was observed between the density of DYRK1A expression and genetic dependency to *DYRK1A*

Scatter plot of DYRK1A expression by western blotting, relative to actin, and *DYRK1A* viability. Total cell lysates from untreated cells were electrophoresed and immunoblotted as described in the methods. Immunoblotting of actin was used as the loading control. Densitometry of DYRK1A expression relative to actin was calculated for each OS tumour cell line using ImageJ software. Spearman's rank correlation coefficient calculated using GraphPad Prism. No significant correlation between DYRK1A expression and quantile normalised Z score for DYRK1A was observed (Spearman's rank correlation coefficient 0.2024). [r^2: Spearman's rank correlation coefficient; QN: quantile normalised]

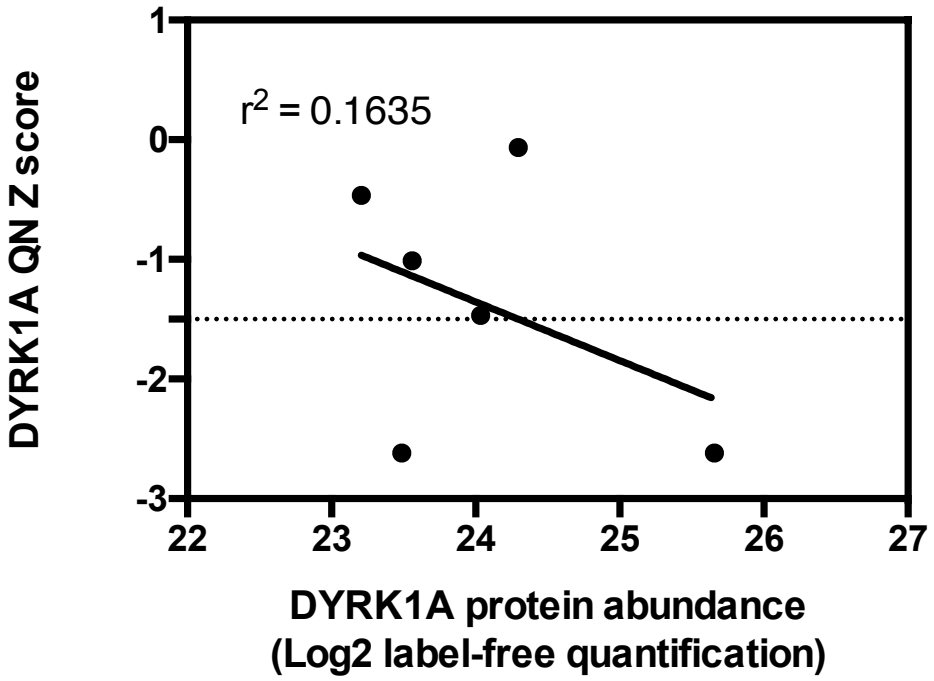

Figure 72 No significant correlation was observed between proteomic abundance of DYRK1A and genetic dependency to DYRK1A

Scatter plot of proteomic abundance of *DYRK1A* and viability in *RB1* deficient OS tumour cell lines only. Proteomic profiling of the OS tumour cell lines was performed by Colm Ryan (Systems Biology, Dublin, Ireland). Following lysis, protein purification, and tryptic digest, peptides were separated by liquid chromatography and measured by mass spectrometer. Label-free proteome quantification was performed using the MaxQuant software environment (Coscia, Watters, Curtis, *et al.*, 2016; Cox, Hein, Luber, *et al.*, 2014) to determine the quantitative abundance of 6696 peptides with a false discovery rate of less than one percent. Spearman's rank correlation coefficient (r^2) = 0.1635 did not demonstrate an association between *DYRK1A* quantile normalised Z score and proteomic abundance of DYRK1A in the setting of *RB1* deficient osteosarcoma tumour cell lines. Spearman's rank correlation coefficient calculated using GraphPad Prism. [r^2: Spearman's rank correlation coefficient; QN: quantile normalised]

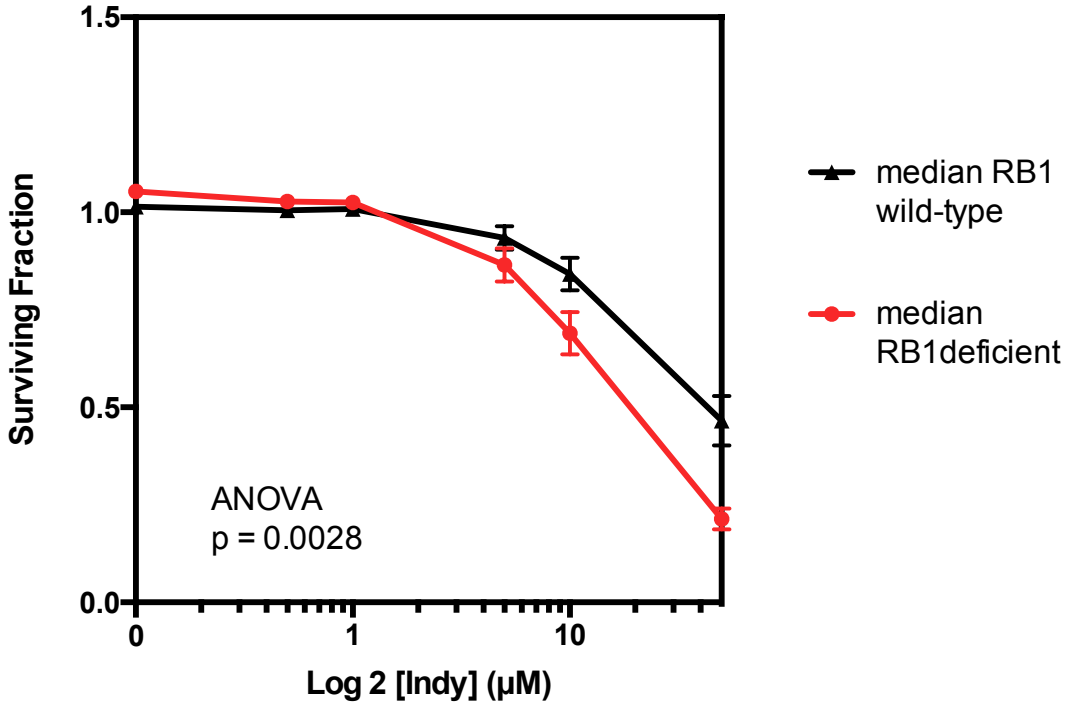

Figure 73 *RB1* deficient osteosarcoma tumour cell lines (TCLs) exhibit enhanced sensitivity to the DYRK1A small molecule inhibitor, indy.

Dose response curves are shown illustrating the median effects in a panel of five *RB1* deficient OS TCLs (LM7, HU03N1, HU09, OHSN, SAOS2) compared to the median effect in eight *RB1* wildtype OS TCLs (CAL72, KPD, U2OS, MHM, OSA/SJSA1, G292 clone A141B1, HOS, MG63). TCLs were arrayed in triplicate 384 well plates, and after twenty-four hours, were exposed to indy (0.05-50μM titration) for five continuous days as described in the methods, at which point cell viability was estimated by CellTiter Glo Reagent. Median survival fraction for *RB1* deficient tumour cell lines shown in red, and median survival fraction for *RB1* wildtype tumour cell lines shown in black. Error bars represent standard error of the mean (SEM). ANOVA plus Bonferroni post hoc test, p = 0.0028 *RB1* deficient versus *RB1* wildtype.

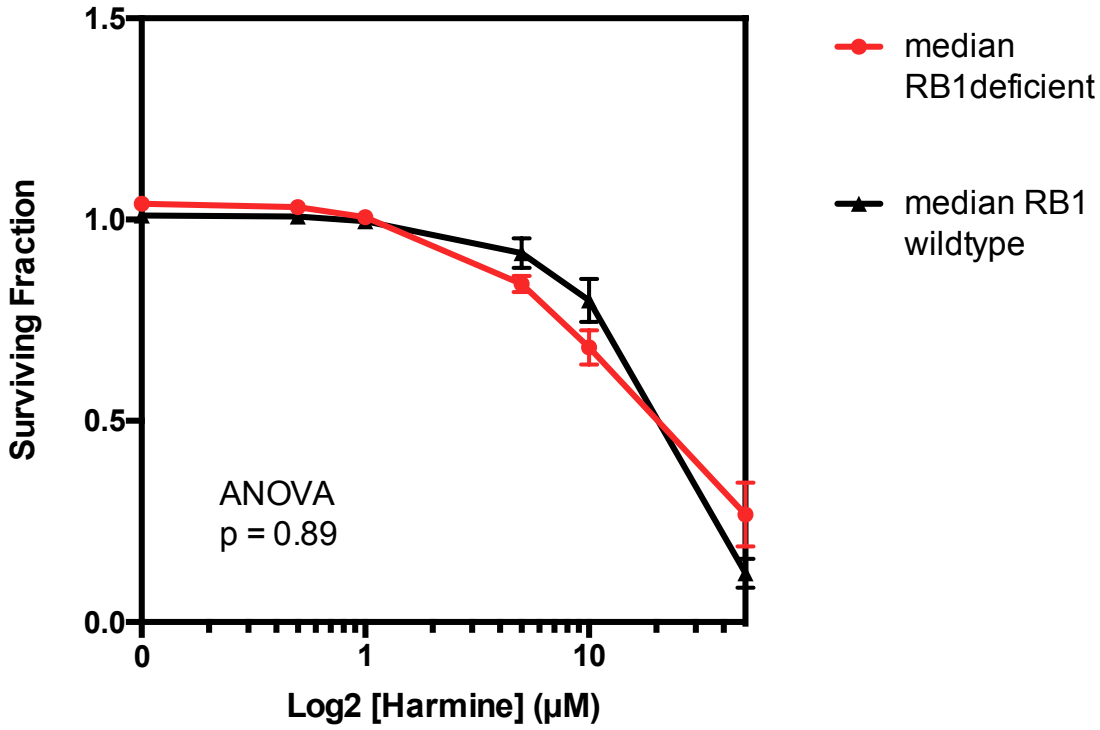

Figure 74 *RB1* deficient osteosarcoma tumour cell lines did not exhibit profound sensitivity to the DYRK1A small molecule inhibitor, harmine.

Dose response curves are shown illustrating the median effects in a panel of five *RB1* deficient OS TCLs (LM7, HU03N1, HU09, OHSN, SAOS2) compared to the median effect in eight *RB1* wildtype OS TCLs (CAL72, KPD, U2OS, MHM, OSA/SJSA1, G292 clone A141B1, HOS, MG63). TCLs were arrayed in triplicate 384 well plates, and after twenty-four hours, were exposed to harmine (0.05-50µM titration) for five continuous days as described in the methods, at which point cell viability was estimated by CellTiter Glo Reagent. Median survival fraction for *RB1* deficient tumour cell lines shown in red, and median survival fraction for *RB1* wildtype tumour cell lines shown in black. Error bars represent standard error of the mean (SEM). ANOVA plus Bonferroni post hoc test, p = 0.89 *RB1* deficient versus *RB1* wildtype.

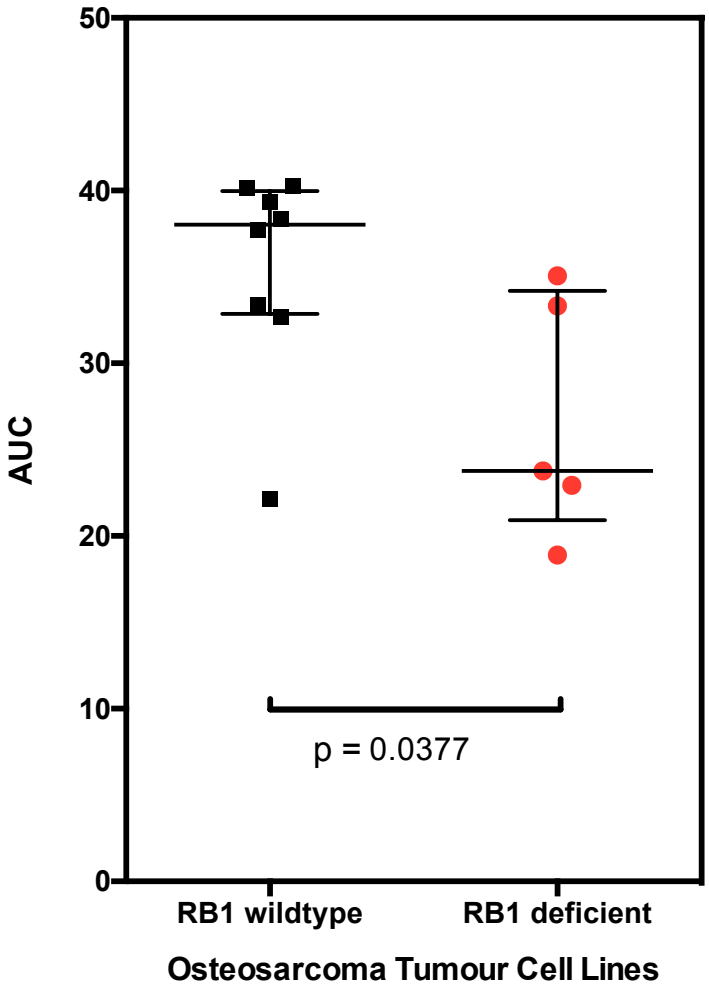

Figure 75 *RB1* deficient osteosarcoma tumour cell lines exhibit greater sensitivity to the DYRK1A small molecule inhibitor, indy.

Dot plot is shown illustrating AUC for indy, in a panel of five *RB1* deficient OS TCLs (LM7, HU03N1, HU09, OHSN, SAOS2) compared to the median effect in eight *RB1* wildtype OS TCLs (CAL72, KPD, U2OS, MHM, OSA/SJSA1, G292 clone A141B1, HOS, MG63). TCLs were arrayed in triplicate 384 well plates, and after twenty-four hours, were exposed to indy (0.05-50μM titration) for five continuous days as described in the methods, at which point cell viability was estimated by CellTiter Glo Reagent. AUC calculated from dose response curves using GraphPad Prism and p values calculated by Student's t test. Median and interquartile range shown. Median survival fraction for *RB1* deficient tumour cell lines shown in red, and median survival fraction for *RB1* wildtype tumour cell lines shown in black. Error bars represent standard error of the mean (SEM). P = 0.0377 *RB1* deficient versus *RB1* wildtype. [AUC: area under the curve]

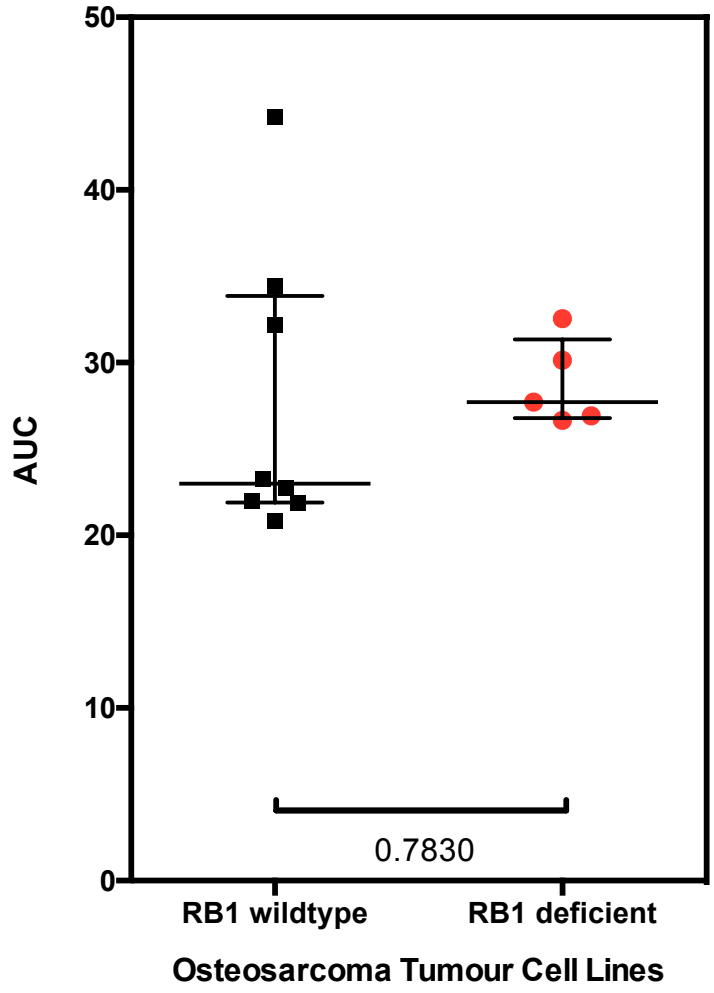

Figure 76 *RB1* deficient osteosarcoma tumour cell lines did not exhibit a profound sensitivity to the DYRK1A small molecule inhibitor harmine.

Dot plot is shown illustrating AUC for harmine, in a panel of five *RB1* deficient OS TCLs (LM7, HU03N1, HU09, OHSN, SAOS2) compared to the median effect in eight *RB1* wildtype OS TCLs (CAL72, KPD, U2OS, MHM, OSA/SJSA1, G292 clone A141B1, HOS, MG63). TCLs were arrayed in triplicate 384 well plates, and after twenty-four hours, were exposed to harmine (0.05-50μM titration) for five continuous days as described in the methods, at which point cell viability was estimated by CellTiter Glo Reagent. AUC calculated from dose response curves using GraphPad Prism and p values calculated by Student's t test. Median and interquartile range shown. Median survival fraction for *RB1* deficient tumour cell lines shown in red, and median survival fraction for *RB1* wildtype tumour cell lines shown in black. Error bars represent standard error of the mean (SEM). P = 0.7830 *RB1* deficient versus *RB1* wildtype. [AUC: area under the curve]

To establish if a greater difference in viability seen with inhibition of DYRK1A in the absence of *RB1* would be seen with multiple dosing, a longer-term assay over two weeks was performed. Although greater sensitivity to Indy was seen in the *RB1* deficient group, harmine was chosen for longer-term drug assay because it has previously been used in humans. No difference in sensitivity was seen with *RB1* deficiency (Figure 77). From these dose-response experiments it was possible to conclude that exposure to the DYRK1A inhibitors indy and harmine, were not able to clearly replicate the genetic effects already observed, potentially because of the inadequacy of the inhibitors. To determine if the synthetic lethality can be replicated using small molecule inhibition, other newer inhibitors of DYRK1A such as newer inhibitor GNF4877 (DYRK1A IC_{50} 6nM) (Shen, Taylor, Jin, *et al.*, 2015) should be investigated.

6.3.8 Exposure to DYRK1A inhibitor harmine increased apoptosis in RB1 deficient tumour cell line

To determine if the observed cellular inhibition phenotype seen post silencing of *DYRK1A* in *RB1* deficient OS tumour cell lines was due to cellular death via the role of DYRK1A as a negative regulator of apoptosis, or cell cycle exit into a quiescent G0 state, the role of apoptosis was investigated by measuring caspase 3/7 activation post exposure to small molecule inhibition of DYRK1A. In the absence of more potent chemical inhibitors of DYRK1A at the time, harmine was used. Two OS tumour cell lines both *CDKN2A* wildtype, one with wildtype *RB1* (G292 clone A141B1), and one with a homozygous deletion of *RB1* (HU09) were chosen as models. Exposure to 30μM of harmine caused a three-fold increase in apoptosis as measured by caspase 3/7 activity in the *RB1* deficient tumour cell line HU09 at both 24 and 48 hours, not observed in the *RB1* wildtype tumour cell line G292 clone A141B1 (Figure 78). In addition, a replicate experiment was used to assess viability at the same time points using CTG, which demonstrated a concomitant reduction in cell viability in the *RB1* deficient tumour cell line HU09, which was most notable at 48 hours (Figure 79). These experiments suggest that cellular inhibition observed in the *RB1* and *DYRK1A* synthetic lethality is due to the loss of DYRK1A as a negative regulator of apoptosis and thus more therapeutically attractive. Therefore, to determine if harmine had any synergistic effect in combination with cisplatin and doxorubicin, agents that already form part of the standard of care, combination experiments were performed.

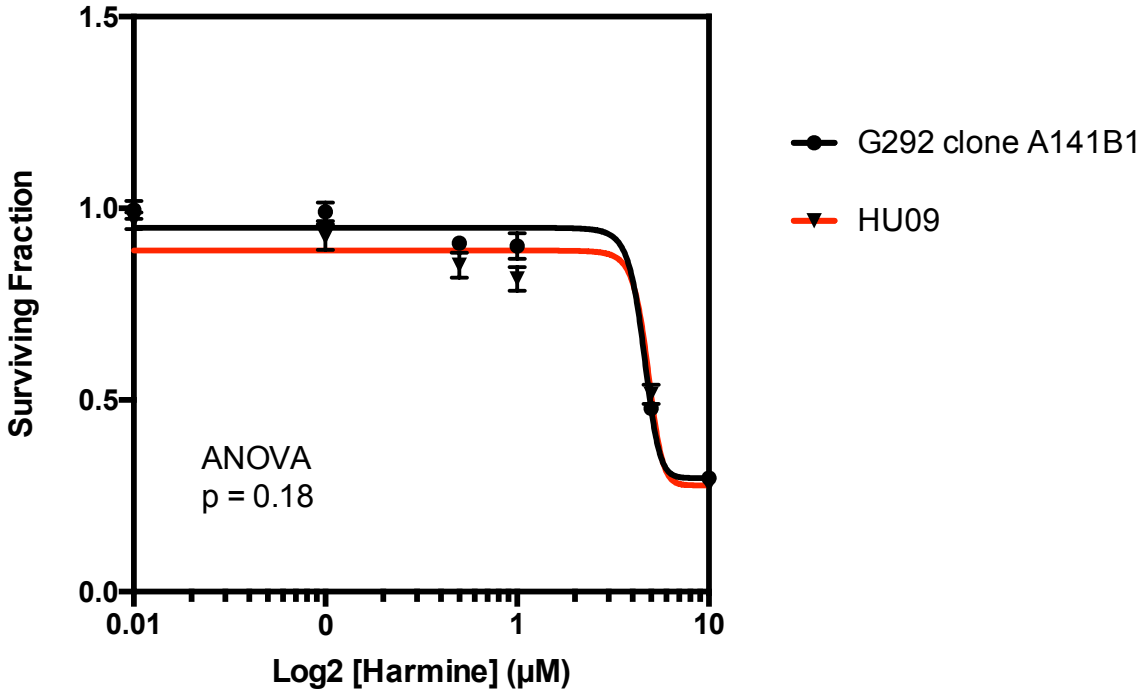

Figure 77 *RB1* deficient osteosarcoma tumour cell lines did not exhibit profound sensitivity to long term (two week) exposure to the DYRK1A small molecule inhibitor, harmine.

Dose response curves illustrating survival fractions for HU09 (*RB1* deficient) in red, and G292 clone A141B1 (*RB1* wildtype) in black. G292 clone A141B1 and HU09 cells were plated at a density of 500 cells/ml in 24 well plates and after 24 hours cells were drugged with five concentrations of harmine (0.1µM, 0.5µM, 1µM, 5µM and 10µM). Cells were drugged twice per week. After two weeks, cell viability was estimated using CellTiter Glo as described in the methods. Error bars represent standard error of the mean (SEM). ANOVA, p = 0.18 HU09 (*RB1* deficient) versus G292 clone A141B1 (*RB1* wildtype).

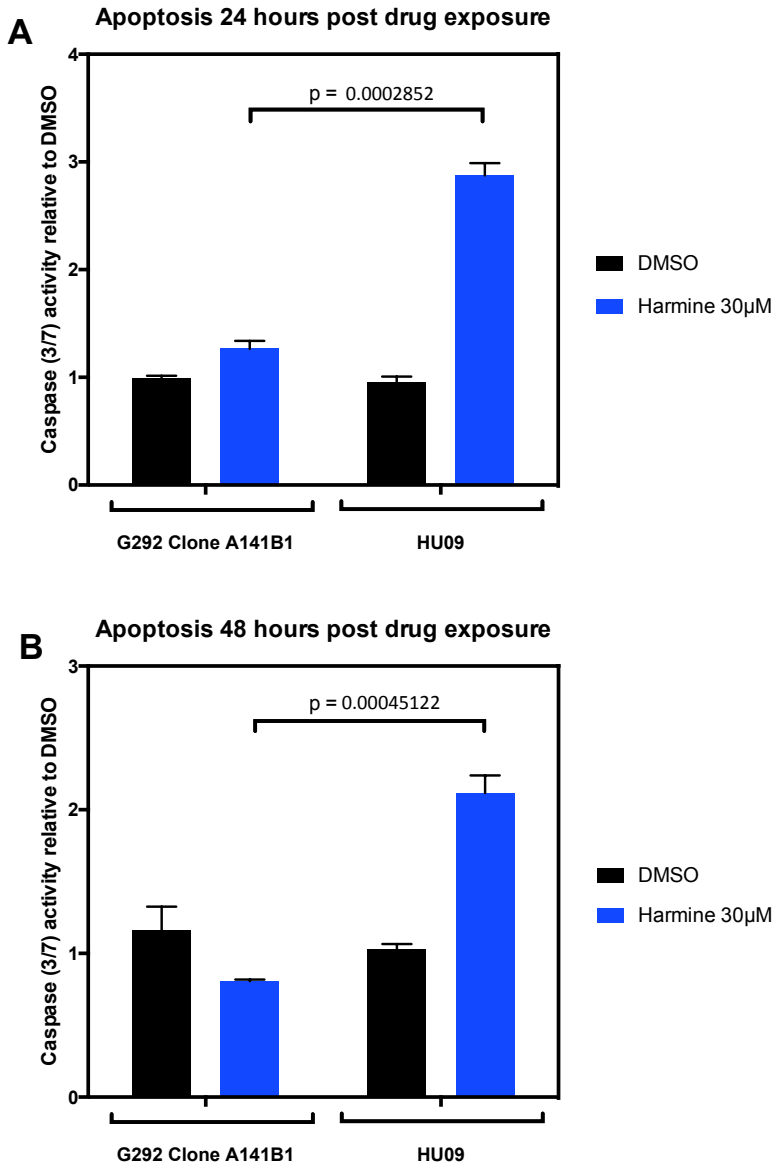

Figure 78 Harmine sensitivity in *RB1* deficient tumour cell line HU09 was characterised by an apoptotic response.

Bar charts illustrating caspase 3/7 activity relative to DMSO at (A) 24 and (B) 48 hours of exposure to harmine. Cells were plated at high density (10,000 cells per well) and exposed to harmine (10μM and 30μM) or drug vehicle, DMSO. At (A) 24 and (B) 48 hours post drug exposure, a luminogenic caspase 3/7 substrate was added, which resulted in cell lysis and caspase cleavage of the substrate with luminescence readout proportional to the caspase activity. P values calculated using Student's t test. Error bars represent SEM. Exposure to 30μM of harmine caused a two-fold increase in apoptosis as measured by caspase 3/7 activity in the *RB1* deficient tumour cell line HU09, not seen in the *RB1* wildtype tumour cell line G292 clone A141B1 (p = 0.0002852 at 24 hours and p = 0.00045122 at 48 hours).

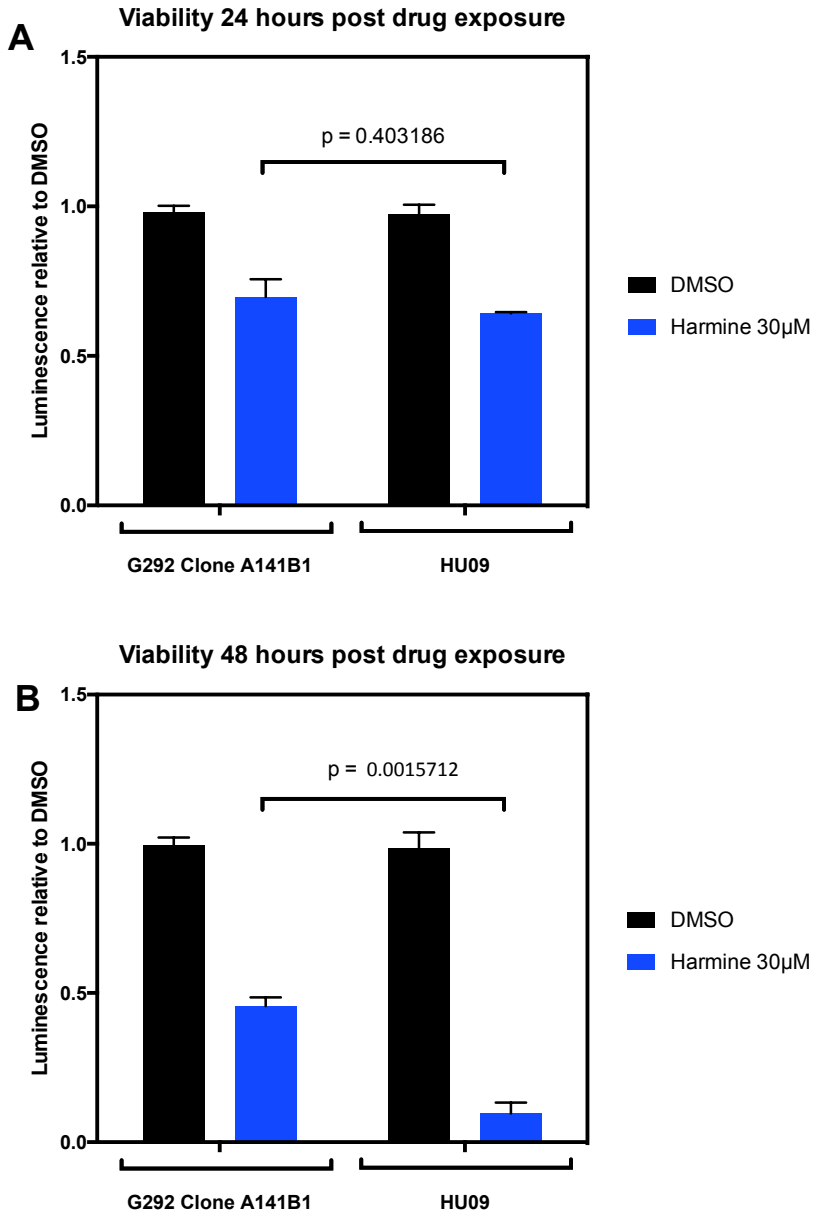

Figure 79 Harmine exposure in *RB1* deficient tumour cell line HU09 was characterised by decreased viability at 48 hours in the *RB1* deficient tumour cell line HU09.

Bar charts illustrating luminescence relative to DMSO as a measure of viability at (A) 24 hours and (B) 48 hours of exposure to harmine. Cells were plated at high density (10,000 cells per well) and exposed to DMSO, 10μM harmine or 30μM harmine. At (A) 24 and (B) 48 hours post drug exposure, a CTG was used to assess viability. Error bars represent SEM. P values calculated using Student's t test. Viability post exposure to harmine was significantly decreased in HU09 compared toG292 clone A141B1 at 48 hours (p = 0.0015712) but not 24 hours (p = 0.403186).

6.3.9 Combination of DYRK1A inhibitor and chemotherapeutic agents cisplatin and doxorubicin

MacDonald *et al.* suggested that targeting DYRK1A, and other members of the DREAM complex in ovarian tumour cell line spheroids causes cell death instead of increased proliferation, and is therefore a possible attractive therapeutic approach (MacDonald, Ramos-Valdes, Perampalam, *et al.*, 2016). They combined 30μM indy with 100-150μM carboplatin, an alkylating agent used in the treatment of ovarian malignancy, and demonstrated that after 48 hours, viability was decreased when these agents were combined (MacDonald, Ramos-Valdes, Perampalam, *et al.*, 2016). Furthermore in those tumour types where cells evade the effects of cytotoxic therapy by quiescence, inhibition of DREAM complex formation and resultant increase in cell cycling, may make them more susceptible to cytotoxic therapy.

Cisplatin and doxorubicin are two of the main chemotherapeutic modalities used to treat osteosarcoma. Cisplatin causes DNA cross-links which cause DNA damage and prohibit replication, subsequently inducing apoptosis (Dasari & Tchounwou, 2014). Doxorubicin also causes intercalation, DNA strand breakage and inhibition of topoisomerase II. ATR is activated during replication stress, by regions of single-stranded DNA and functions as part of the DNA damage response (Williamson, Miller, Pemberton, *et al.*, 2016).

To investigate if inhibition of DYRK1A by harmine or indy increased the sensitivity of the *RB1* deficient tumour cell line HU09 to exposure with cisplatin, doxorubicin or the ATR inhibitor VX970, short-term combination dose response experiments were performed. The ATR inhibitor VX970 was chosen as it has shown to be both a chemo-sensitiser to DNA damaging agents, and observed to increase the proportion of cells in non-replicating S phase (Figure 85 and Figure 86) and therefore might act synergistically with inhibition of DYRK1A. Two OS tumour cell lines both *CDKN2A* wildtype, one with wildtype *RB1* (G292 clone A141B1), and one with a homozygous deletion of *RB1* (HU09) were chosen as models. After incubation for five days, cell viability was assessed using a CTG luminescence assay. Dose response curves for harmine and cisplatin alone and in combination are shown in Figure 80. Moderate synergy was seen with both combinations of DYRK1A inhibitor and cisplatin and require further investigation using both longer-term exposure and use of one of the new agents with greater potency of inhibition to DYRK1A such as GNF4877 (DYRK1A IC_{50} 6nM) (Shen, Taylor, Jin, *et al.*, 2015) instead of harmine and indy.

The *RB1* deficient tumour cell line HU09 was more sensitive to doxorubicin, but this effect was not potentiated by the addition of harmine or indy. Dose response curves to harmine and indy alone, and in combination with doxorubicin are shown in Figure 81. Using these short-term assays, no synergistic effect was seen with the addition of either harmine or indy to the ATR inhibitor VX90 (Figure 82).

6.3.10 Silencing of DYRK1A and cell cycle profiling

DYRK1A has a number of roles within cell cycle control, which lead to G1 arrest via both direct and downstream interactions with Cyclin D1, $p27^{Kipl}$ and p21; cell cycle exit via DREAM complex formation, and repression of apoptosis via inhibition of Caspase 9 summarised in Figure 94. To determine if the loss of viability seen with the genetic vulnerability observed between *DRYK1A* and *RB1* was also mediated by the role of *DYRK1A* in the cell cycle, fluorescence activated cell sorting (FACS) was performed.

DYRK1A silencing has previously been associated with a shortened G1 duration (Chen, Lin, Tsai, *et al.*, 2013) and increased proportion of cells in S phase (Litovchick, Florens, Swanson, *et al.*, 2011). Therefore, I hypothesised that loss of *DYRK1A* could have multiple effects on the cell cycle; loss of DREAM complex formation could increase cell signalling and reduce senescence and quiescence; or degradation of Cyclin D1 or stabilisation of $p27^{Kip1}$ (and resultant decrease in Cyclin E), could decrease phosphorylation of RB1 and therefore stall cells in G1. However, in an *RB1* deficient setting, the role of cyclins D1 and E are unknown, since their main substrate is lost. Therefore, the effects of silencing DYRK1A in an *RB1* deficient setting could lead to increased cell cycling with loss of the DREAM complex and the RB dependent restriction point, leading to rapid unchecked-cycling and loss of viability (MacDonald, Ramos-Valdes, Perampalam, *et al.*, 2016).

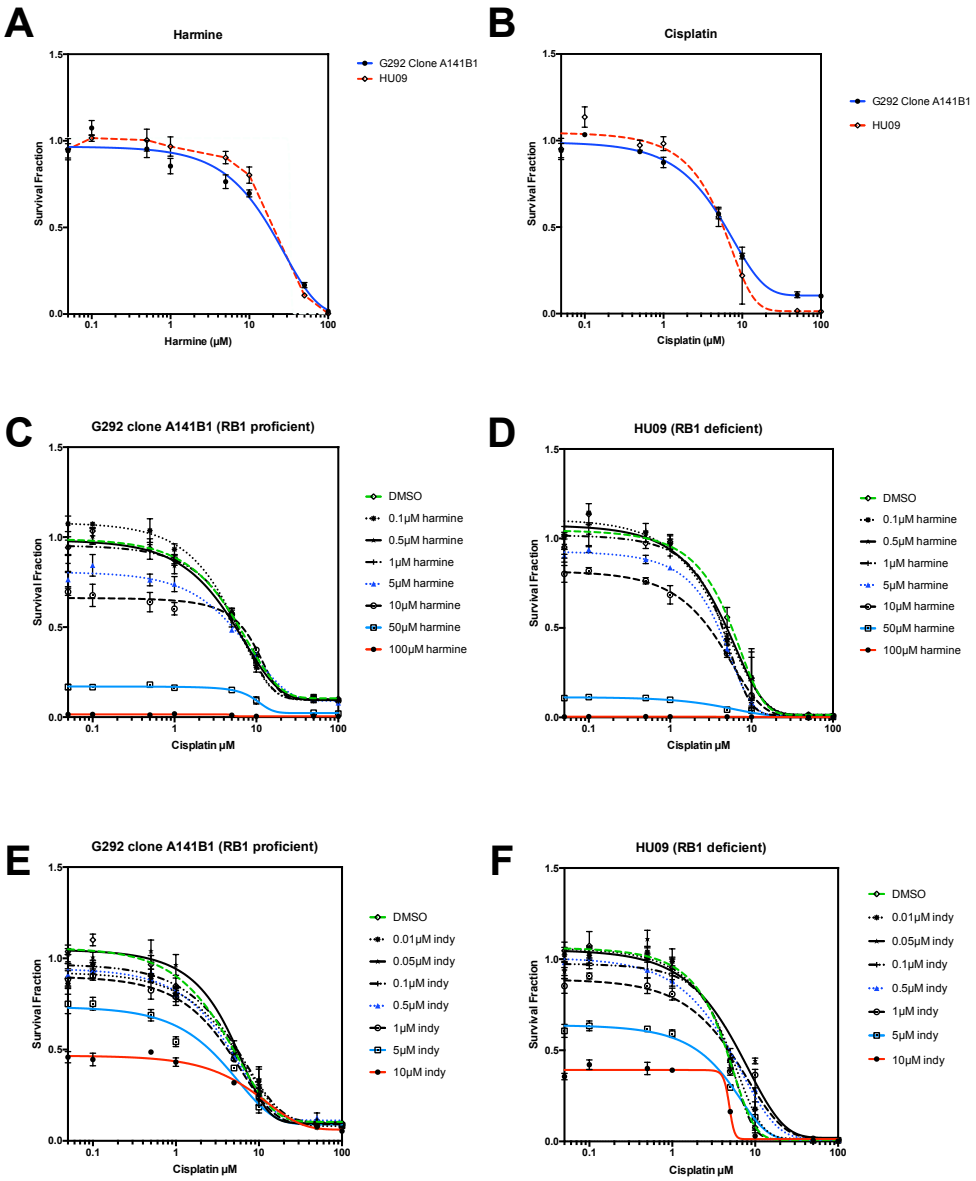

Figure 80 A modest synergistic effect was seen with the combination of harmine or indy with cisplatin in both tumour cell lines (G292 clone A141B1 and HU09).

Dose response curves illustrating survival fraction relative to DMSO. (A) Exposure to harmine alone. (B) Exposure to cisplatin alone. (C and E) Exposure to cisplatin and harmine in combination, (E and F) exposure to cisplatin and indy in combination using the *RB1* wildtype tumour cell line G292 clone A141B1 and *RB1* deficient tumour cell line HU09. HU09 and G292 clone A141B1 tumour cells were plated in triplicate 384 well plates, and after twenty four hours, were exposed to harmine (0.1-100μM titration) or indy (0.01-10μM titration) in combination with cisplatin (0.1-100μM titration) or drug vehicle, DMSO, for five continuous days, at which point cell viability was estimated using CellTiter Glo reagent as described in the methods. Error bars represent SEM.

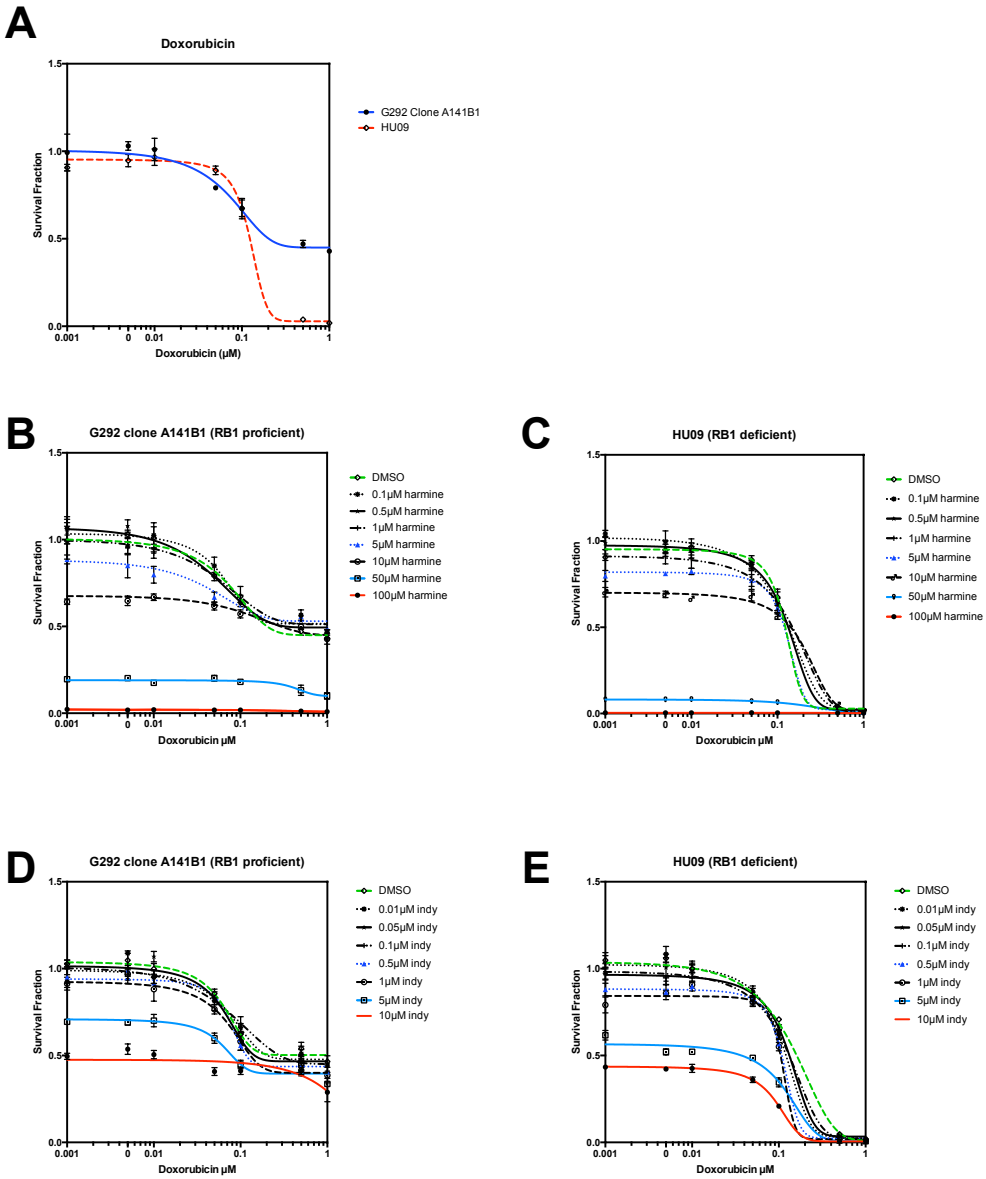

Figure 81 The *RB1* deficient tumour cell line HU09 was more sensitive to doxorubicin than the *RB1* wildtype tumour cell line G292 clone A141B1 but no synergistic effect with the addition of harmine or indy was seen.

Dose response curves illustrating survival fraction relative to DMSO. (A) Exposure to doxorubicin alone. (B and C) Exposure to doxorubicin and harmine in combination, (D and E) exposure to doxorubicin and indy in combination using the *RB1* wildtype tumour cell line G292 clone A141B1 and *RB1* deficient tumour cell line HU09. HU09 and G292 clone A141B1 tumour cells were plated in triplicate 384 well plates, and after twenty four hours, were exposed to harmine (0.1-100μM titration) or indy (0.01-10μM titration) in combination with doxorubicin (0.001-1μM titration) or drug vehicle, DMSO, for five continuous days, at which point cell viability was estimated using CellTiter Glo reagent as described in the methods. Error bars represent SEM.

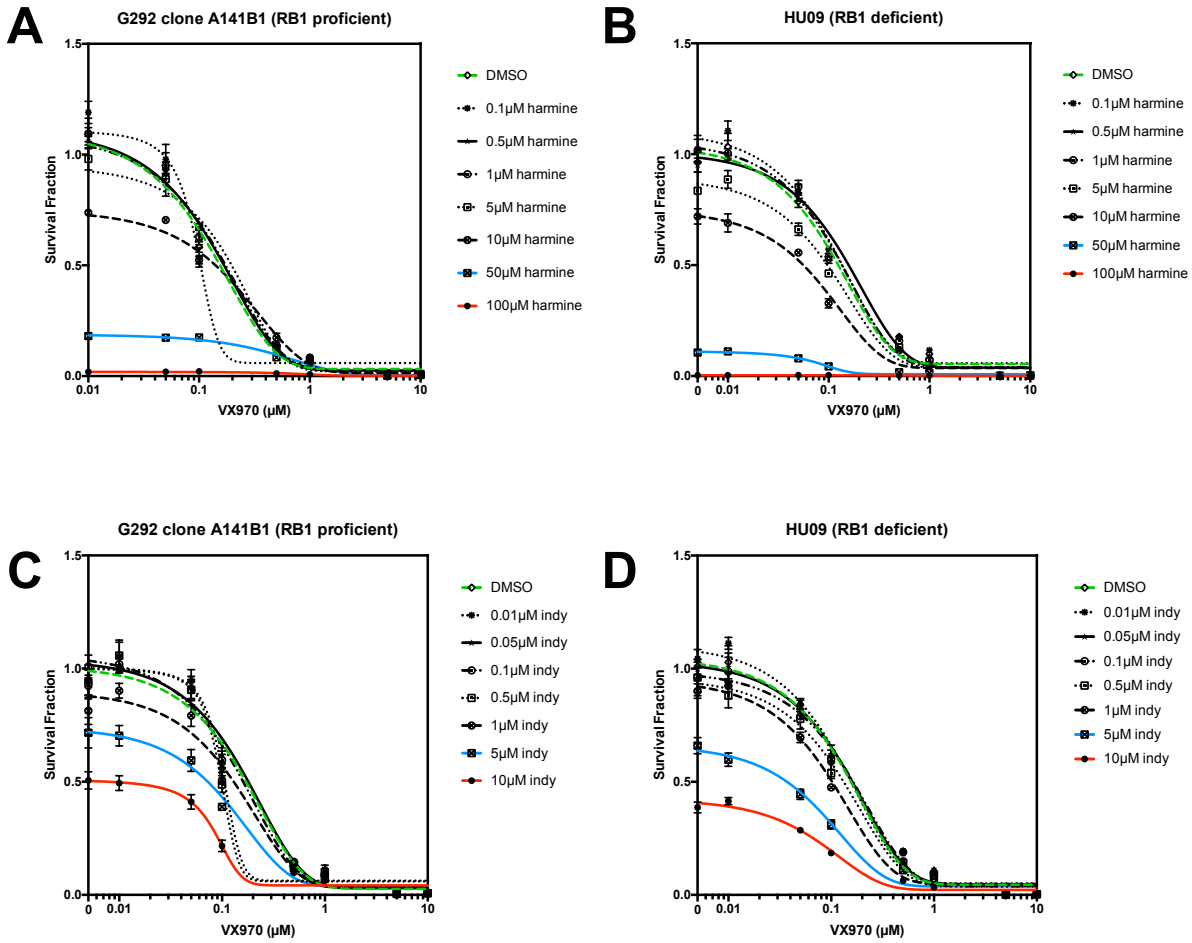

Figure 82 No synergistic effect was observed between the DYRK1A inhibitors harmine and indy in combination with VX970.

Dose response curves illustrating survival fraction relative to DMSO. (A and B) Exposure to VX970 and harmine in combination, (C and D) exposure to VX970 and indy in combination using the *RB1* wildtype tumour cell line G292 clone A141B1, and *RB1* deficient tumour cell line HU09. HU09 and G292 clone A141B1 tumour cells were plated in triplicate 384 well plates, and after twenty four hours, were exposed to harmine (0.1-100μM titration) or indy (0.01-10μM titration) in combination with VX970 (0.01-10μM titration) or drug vehicle, DMSO, for five continuous days, at which point cell viability was estimated using CellTiter Glo reagent as described in the methods. Error bars represent SEM.

Two osteosarcoma tumour cell lines both *CDKN2A* wildtype, one with wildtype *RB1* (G292 clone A141B1) and one with homozygous deletion of *RB1* (HU09) were chosen as models. Asynchronous cells were used for siRNA targeting and exposure to the DYRK1 inhibitor harmine at 10 and 30μM. Cells were collected 48 hours after reverse transfection with RNAi or exposure to inhibitor and fixed. Cells were stained with EDU and DAPI to identify replicating cells with the addition of an anti-phospho-histone H3 antibody identifying those in active mitosis. Silencing of S Phase Kinase-associated protein (SKP2) a genetic vulnerability associated with deficient *RB1* (Zhao, Wang, Bauzon, *et al.*, 2016) which leads to G0/G1 arrest (Lu, Gan, Cao, *et al.*, 2014), and ATR inhibitor VX970, known to target cells in S phase, were used as positive controls. FACS plots of siRNA transfection in both tumour cell lines are shown in Figure 83 and Figure 84. To further highlight these changes, percentage change from control (siControl1 or DMSO) for each phase of the cell cycle was calculated and shown in Figure 87 and Figure 88.

The cell cycle changes post reverse transfection were of low amplitude, particularly when compared to the positive control siSKP2. Cell cycling profiling of HU09 post reverse transfection with siDYRK1A resulted in increased S phase and G2, with a decrease in sub G1 and G1. This suggests that when DYRK1A is silenced, a decreased proportion enter the subG1 state, most likely via failure of formation of the DREAM complex, which is dependent on phosphorylation of LIN52 on serine 28 by DYRK1A (Litovchick, Florens, Swanson, *et al.*, 2011). In the absence of a functioning RB restriction point in G1, the *RB1* deficient tumour cells are able to proceed through G1, with increased cell numbers in S and G2 phases. These changes are concordant with an increase in S phase (Litovchick, Florens, Swanson, *et al.*, 2011) and decrease in G1 phase (MacDonald, Ramos-Valdes, Perampalam, *et al.*, 2016) observed previously although of lower amplitude. MacDonald *et al.* used transfected shDYRK1A in ovarian spheroids which potentially have a different phenotype compared to adherent cells, and they also observed a large increase in subG1 which was not seen here (MacDonald, Ramos-Valdes, Perampalam, *et al.*, 2016). Reverse transfection of siDYRK1A increased the percentage of *RB1* wildtype G292 clone A141B1 cells in G1 and S phase. In contrast to the effects seen with HU09, the proportion of *RB1* wildtype tumour cells in G1 increases, concordant with failure of formation of the DREAM complex, resulting in fewer cells exiting to subG1, and actions of the RB restriction point, stalling cells in G1. The changes observed here are not profound.

As expected, silencing of *SKP2* leads to G0/G1 arrest and decreased S phase (Lu, Gan, Cao, *et al.*, 2014), seen in both HU09 and G292 clone A141B1. In G292 clone A141B1, an additional increase in the proportion of cells in G2 was also observed.

Exposure to harmine at 10μM and 30μM concentrations resulted in a profound decrease in cells in G1 in both tumour cell lines, most noticeable in the *RB1* deficient tumour cell line HU09; a profound increase in cell in G2 was seen in both tumour cell lines, particularly HU09. A compensatory increase in active mitosis was only seen in the *RB1* wildtype tumour cell line G292 Clone A141B1. Some of the features seen are concordant with silencing of DYRK1A by siRNA, namely a decrease in G1 and increase in G2 was seen in HU09 for both conditions. In contrast, siDYRK1A caused an increase in G1 in G292 clone A141B1, whereas a decrease was seen post exposure to harmine, and instead the proportion of cells in G2/M increased. It is possible that these effects are due to off-target effects of harmine. Harmaline, another β-carboline alkaloid very similar harmine, has been shown to induce G2/M arrest via induction of p21, and activation of the Fas/FasL pathway (Wang, Wang, Jiang, *et al.*, 2015). Exposure to VX970 resulted in HU09 and G292 clone A141B1 tumour cells stalling in subG1 and non-replicating S phase, with compensatory decreases in other phases of the cell cycle, concordant with disruption of replication in S phase as predicted (Williamson, Miller, Pemberton, *et al.*, 2016).

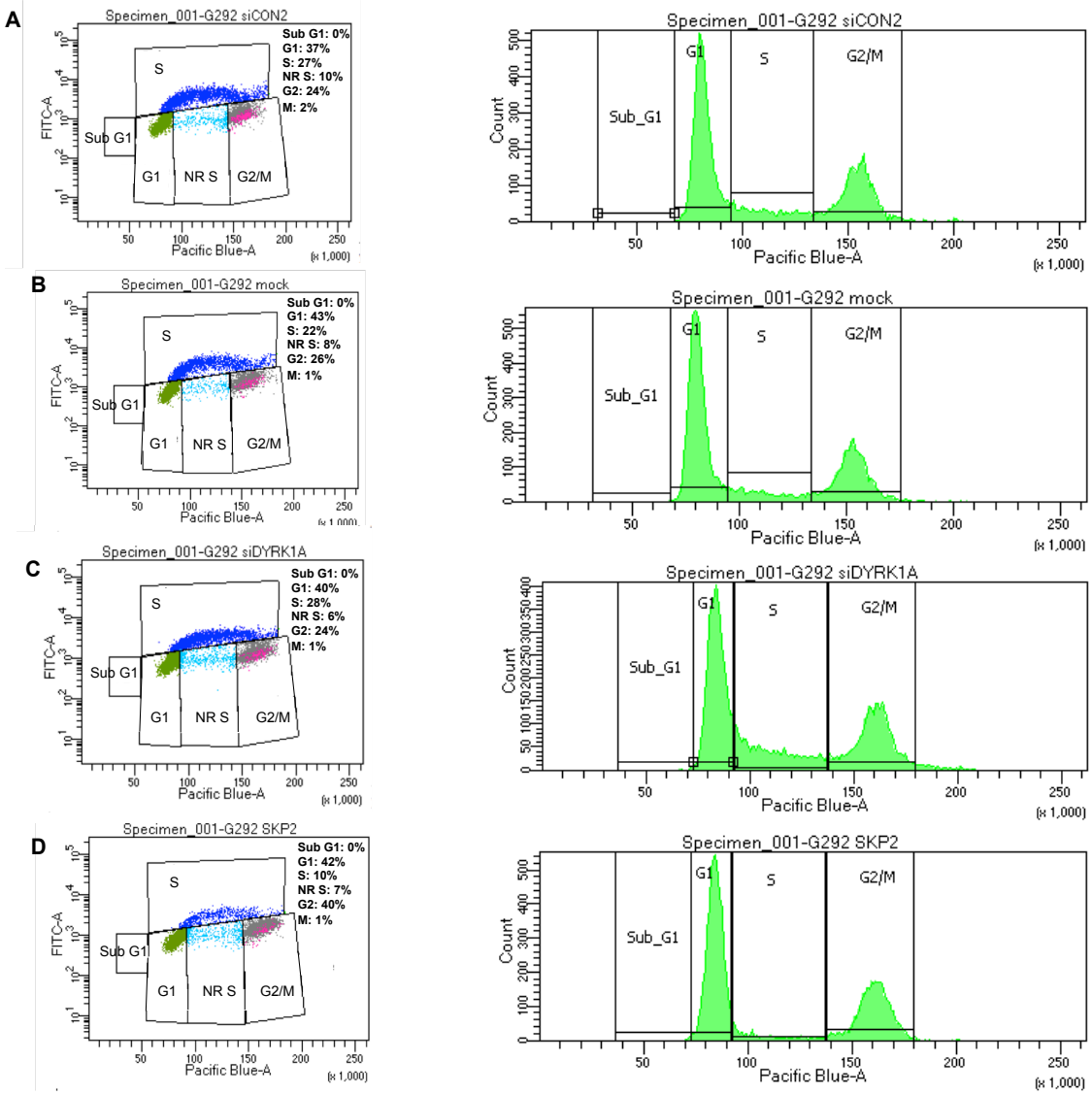

Figure 83 Increase in *RB1* wildtype OS tumour cells in G1 and S phase when DYRK1A is silenced.

FACS plots illustrating cell cycle fractions labelled with EDU, DAPI and anti-phospho-histone H3 antibody. G292 clone A141B1 tumour cells were fixed 48 hours post reverse transfection as described in the methods with (A) non-targeting control (siCON2), (B) 'mock', (C) siDYRK1A and (D) siSKP2. Reverse transfection of siDYRK1A in the *RB1* wildtype tumour cell line G292 clone A141B1 increased the percentage of cells in G1 and S phase, while decreased non-replicating S phase. Silencing of SKP2 demonstrated an increase of tumour cells in G1 and G2 phases, with a compensatory decrease in S phase. [NR S: non-replicating S phase]

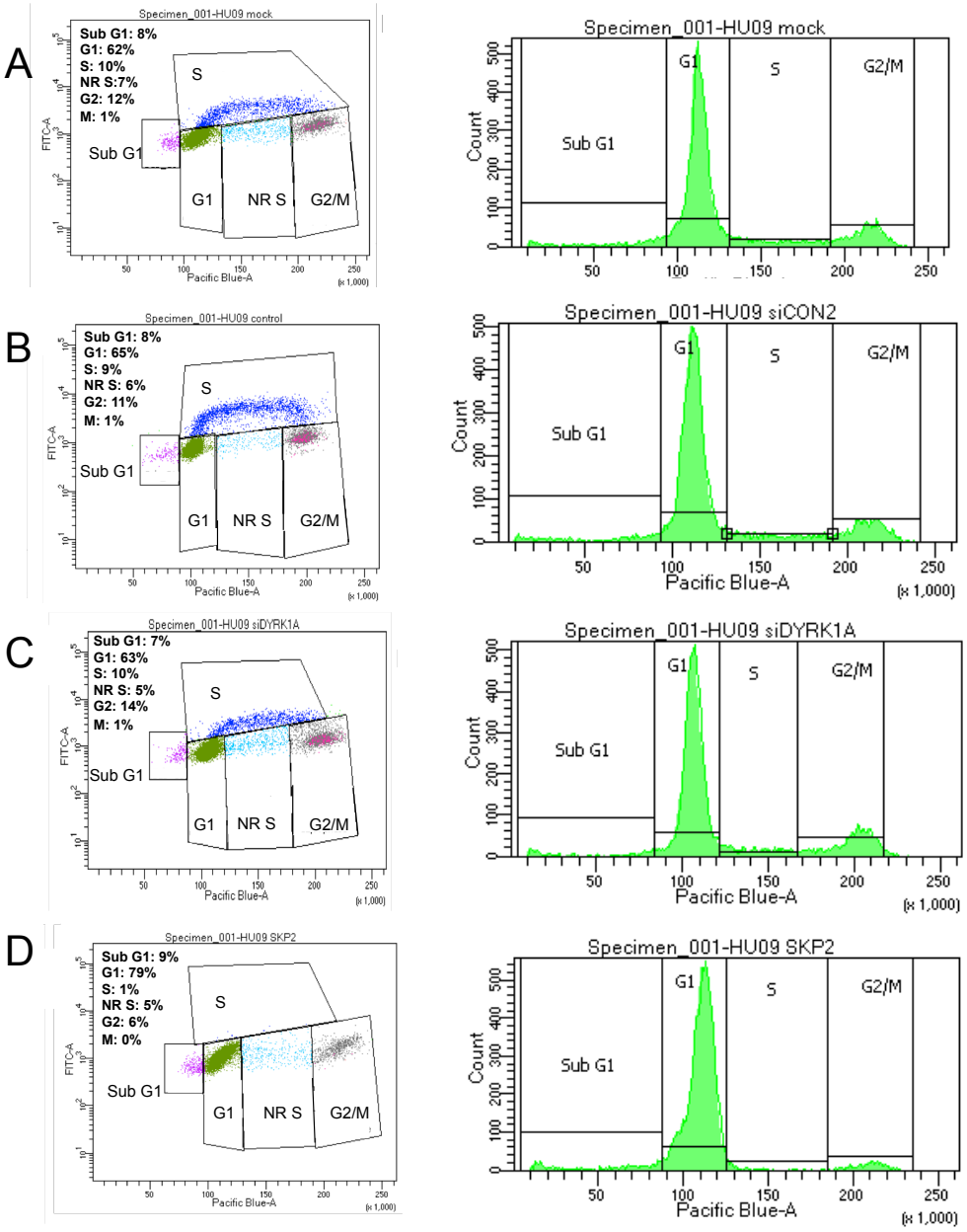

Figure 84 Increase in *RB1* deficient OS tumour cells in G2 and S phase when DYRK1A is silenced.

FACS plots illustrating cell cycle fractions labelled with EDU, DAPI and anti-phospho-histone H3 antibody. HU09 tumour cells were fixed 48 hours post reverse transfection as described in the methods with (A) non-targeting control (siCON2), (B) 'mock', (C) siDYRK1A and (D) siSKP2. Reverse transfection of siDYRK1A in the *RB1* deficient tumour cell line HU09 increased the percentage of cells in G2 and S phase, while decreased non-replicating S phase. Silencing of SKP2 stalled the tumour cells in G1, with a compensatory decrease in all other phases of the cell cycle. [NR S: non-replicating S phase]

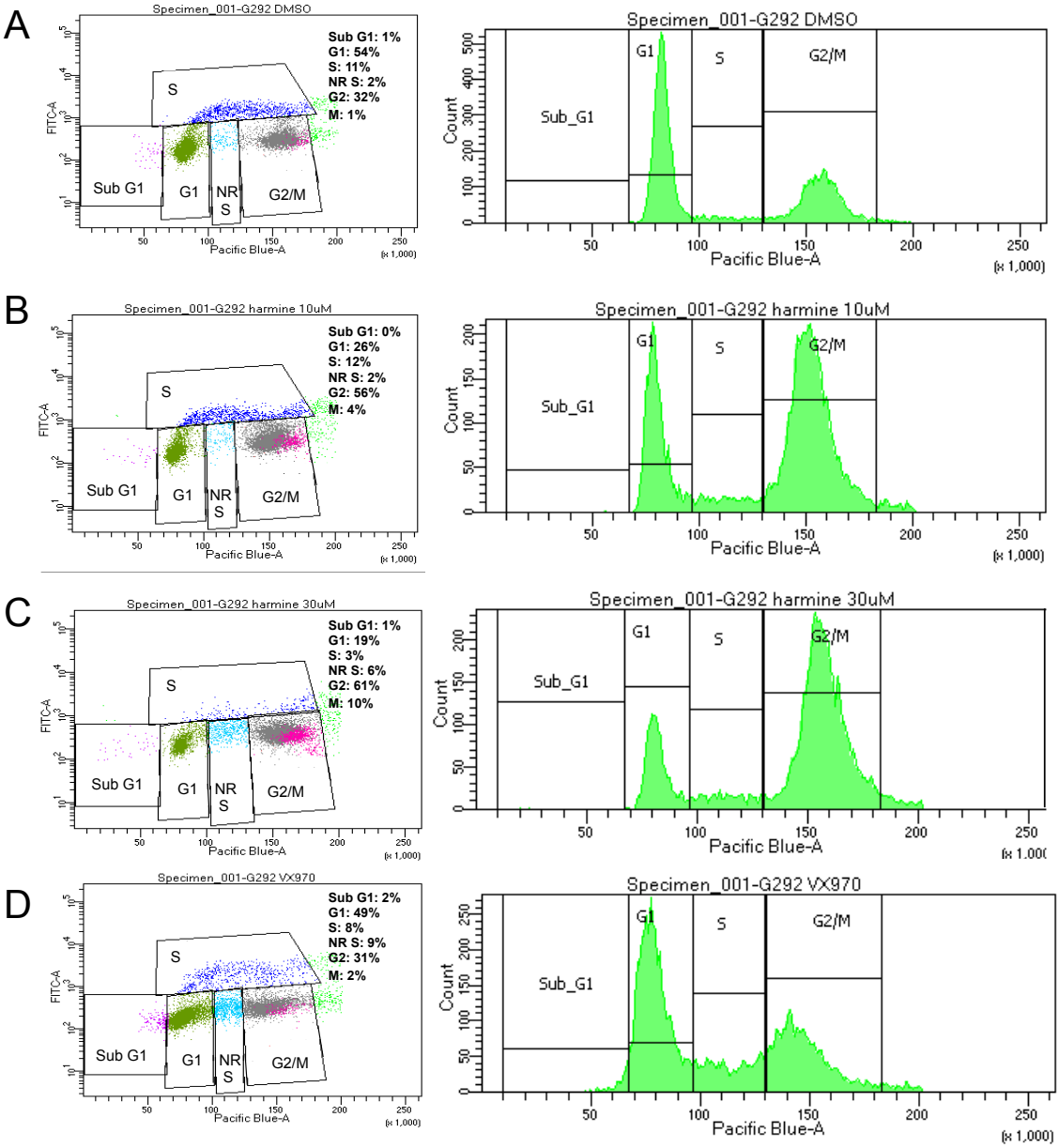

Figure 85 Profound increase in *RB1* wildtype OS tumour cells in G2 post exposure to the DYRK1A small molecule inhibitor, harmine.

FACS plots illustrating cell cycle fractions labelled with EDU, DAPI and anti-phospho-histone H3 antibody. G292 clone A141B1 tumour cells were fixed 48 hours post exposure to (A) DMSO, (B) harmine 10μM, (C) harmine 30μM and (D) 1μM VX970 as described in the methods. Exposure to harmine at both concentrations resulted in a profound decrease in cells in G1 and increase in G2, which was observed in both tumour cell lines. A compensatory increase in active mitosis was also seen. Exposure to VX970 resulted in stalling in subG1 and non-replicating S phase, with compensatory decreases in other phases of the cell cycle. [NR S: non-replicating S phase]

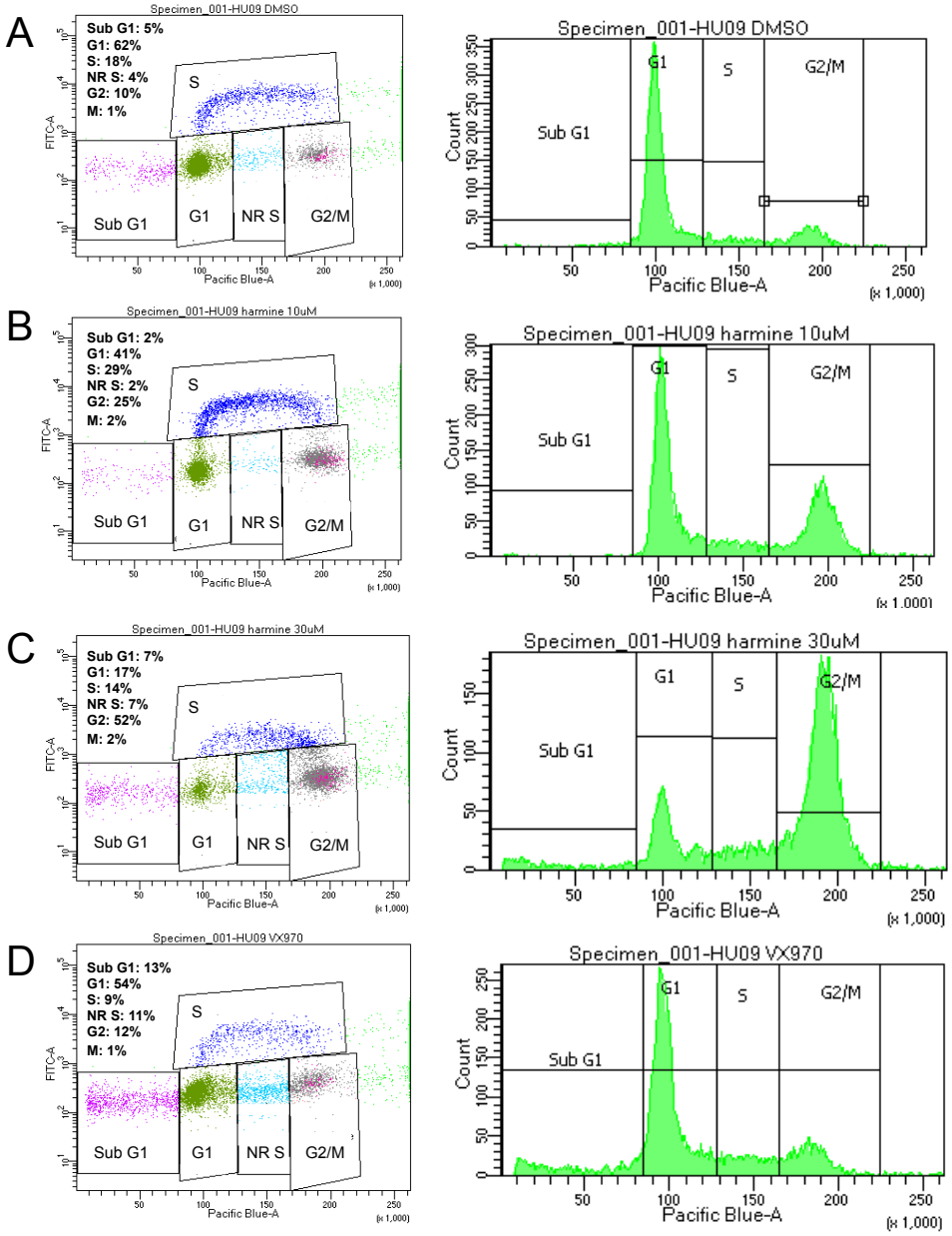

Figure 86 Profound increase in *RB1* deficient OS tumour cells in G2 post exposure to the DYRK1A small molecule inhibitor, harmine.

FACS plots illustrating cell cycle fractions labelled with EDU, DAPI and anti-phospho-histone H3 antibody. HU09 tumour cells were fixed 48 hours post exposure to (A) DMSO, (B) harmine 10μM, (C) harmine 30μM and (D) 1μM VX970 as described in the methods. Exposure to harmine at both concentrations resulted in a profound decrease in cells in G1, and increase in G2. A compensatory increase in active mitosis was not seen in HU09. Exposure to VX970 resulted in stalling in subG1 and non-replicating S phase, with compensatory decreases in other phases of the cell cycle. [NR S: non-replicating S phase]

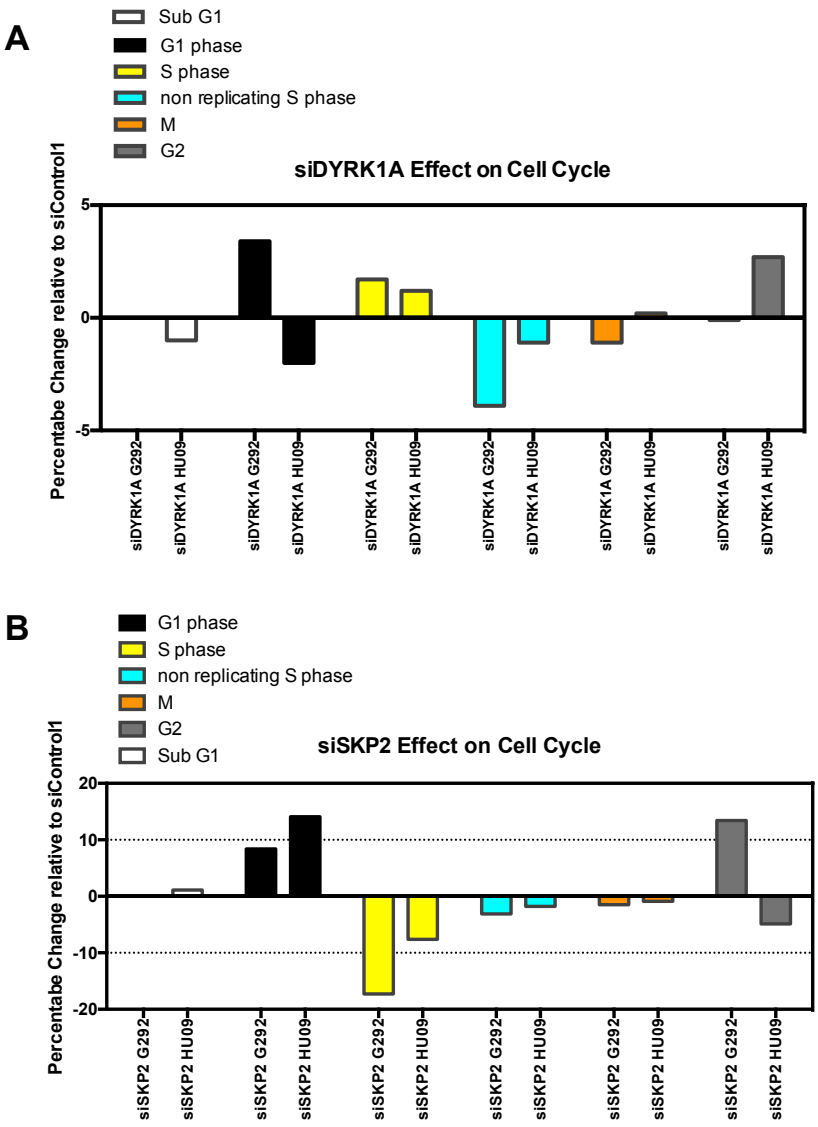

Figure 87 Percentage changes of the cell cycle post reverse transfection with siDYRK1A and siSKP2 are dependent on *RB1* status.

Bar charts illustrating percentage change of the cell cycle relative to control at 28 hours post reverse transfection. (A) Small changes in cell cycle were observed post reverse transfection with siDYRK1A; siDYRK1A increased the percentage of cells in S phase and decreased non-replicating S phase in both tumour cell lines. However, it also resulted in an increase in G2, with compensatory decrease in G1 in the *RB1* deficient tumour cell line HU09, while an increase in G1 in the *RB1* wildtype tumour cell line G292 Clone A141B1. (B) siSKP2 stalled *RB1* deficient HU09 tumour cells in G1, with a compensatory decrease in all other phases of the cell cycle. siSKP2 increased G292 clone A141B1 *RB1* wildtype tumour cells in G1 and G2 phases, with a compensatory decrease in S phase.

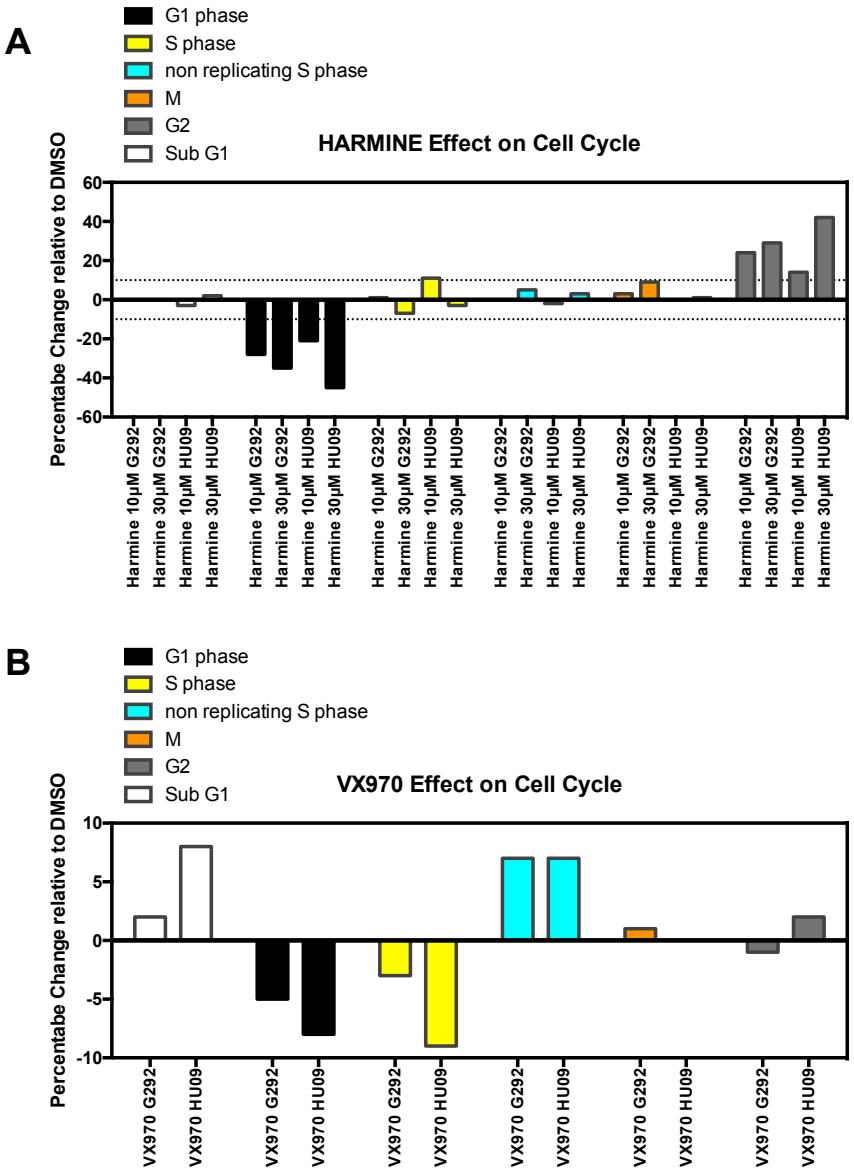

Figure 88 Exposure to the DYRK1A small molecule inhibitor, harmine, is associated with a profound increase in G2 independent of RB1 context, and compensatory rise in active mitosis only seen in the *RB1* wildtype tumour cell line.

Bar charts illustrating percentage change of the cell cycle relative to DMSO after 48 hours exposure to (A) harmine (10µM and 30µM) and (B) VX970 (1µM) using the RB1 deficient tumour cell line HU09, and RB1 wildtype tumour cell line G292 Clone A141B1. (A) Harmine resulted in a profound decrease in cells in G1 and increase in cells in G2 in both tumour cell lines. A compensatory increase in active mitosis was only seen in the *RB1* wildtype tumour cell line G292 Clone A141B1. (B) Exposure to VX970 resulted in HU09 and G292 clone A141B1 tumour cells stalling in subG1 and non-replicating S phase, with compensatory decreases in other phases of the cell cycle.

6.3.11 Protein expression changes by western blotting associated with silencing DYRK1A

To further investigate the nature of cell cycle profile changes post silencing by RNAi or inhibition of DYRK1A, protein expression of some of the Cyclins and known key substrates of DYRK1A were investigated. One of the key substrates of DYRK1A is $p27^{Kipl}$, known to play a role in cell cycle transition from G0 to S phase transition, by a decrease in translation of $p27^{Kipl}$ during G1 progression (Chu, Hengst & Slingerland, 2008). DYRK1A phosphorylates $p27^{Kipl}$ at Serine10, leading to enhanced stability, and supressed levels of Cyclin E, thereby maintaining RB1 in its active, unphosphorylated state causing cell cycle arrest (Ishida, Kitagawa, Hatakeyama, *et al.*, 2000). SKP2 negatively regulates expression of $p27^{Kipl}$, hence silencing of SKP2, leads to increase $p27^{Kipl}$ with stalling in G1/0 and decreased S phase (Lu, Gan, Cao, *et al.*, 2014). Active RB1 in an unphosphorylated form, negatively regulates SKP2 to maintain cells in G1/0 (Lu, Bauzon, Fu, *et al.*, 2014). To establish if $p27^{Kipl}$ levels decrease with silencing of *DYRK1A*, western blotting was undertaken using lysates collected 48 hours post reverse transfection (Figure 89). To highlight these changes densitometry of $p27^{Kipl}$ expression was performed, and corrected to actin, relative to siAllstar at each time point (Figure 90). Only the time points at 48 and 72 hours post reverse transfection are shown here, as they likely represent maximal effect of the siRNA prior to dilution with cell expansion.

In G292 clone A141B1, expression of $p27^{Kipl}$ was high at 48 hours, but decreased with time. Expression of $p27^{Kipl}$ did not rise in HU09, in keeping with diminished stability in the absence of phosphorylation by DYRK1A, and absence of active RB1. In both tumour cell lines $p27^{Kipl}$ increased with silencing of SKP2 as expected. The increased expression of $p27^{Kipl}$ at 48 hours in tumour cell line G292 clone A141B1 could relate to the presence of wildtype active un-phosphorylated *RB1*, and it's regulation of $p27^{Kipl}$ via SKP2. Since levels of $p27^{Kipl}$ are controlled by phosphorylation and stabilisation by DYRK1A, but also negative inhibition by SKP2, silencing of DYRK1A may lead to a change in balance of $p27^{Kipl}$ regulation in tumour cell lines with active *RB1.* Whereas, in the *RB1* deficient tumour cell line HU09, in the absence of inhibitory regulation of SKP2 by active un-phosphorylated RB1, baseline $p27^{Kipl}$ levels are low compared to the *RB1* wildtype tumour cell line. Increased p27 expression was not maintained at 72 hours in G292 clone A141B1 post reverse transfection with either siDYRK1A or siSKP2. This could reflect a faster growth characteristic than HU09, and therefore greater dilution of the siRNA, and therefore earlier return to baseline expression levels.

To further understand the cell cycle changes seen by FACS profiling when DYRK is silenced, western blots examining the cyclins A2, D1 and E1 were performed using lysates 48 hours post reverse transfection with siCON2 (non-targeting control), siSKP2, siDYRK1A and mock (untreated) (Figure 91). Silencing of *DYRK1A* by siRNA caused a decreased expression of DYRK1A in both tumour cell lines. Baseline Cyclin D1 levels were high in G292 clone A141B1 with a slight increase in cyclin D1 with silencing of *DYRK1A*. Baseline expression of Cyclin D1 was absent in HU09, but detectable post silencing of DYRK1A. This is accordant with loss of negative regulation of Cyclin D1 by DYRK1A, leading to increased levels of Cyclin D1.

Decreased expression of Cyclin E1 was seen in the RB1 wildtype tumour cell line G292 clone A141B1, in keeping with the increase in p27Kipl levels seen at 48 hours (Figure 89). Levels of p27Kipl were low in the RB1 deficient tumour cell line HU09, and hence no significant change of expression of Cyclin E1 was seen. Cyclin A1 expression levels were low for both tumour cell lines, without significant changes to expression levels. DYRK1A is known to phosphorylate and activate Sirtuin1 (SIRT1), which deacetylates p53, a negative regulator of p21 activation (Guo, Williams, Schug, et al., 2010). Silencing of DYRK1A, would therefore be expected to increase p21 activation, however, increased expression of p21 is seen in neither tumour cell line. This is perhaps because p21 expression is also negatively regulated by SKP2 expression, and therefore other homeostatic control measures prevent a significant increase.

Silencing of *SKP2,* used as a positive control, lead to loss of inhibitory control of $p27^{Kipl}$ with resultant increase in $p27^{Kipl}$ expression (Figure 90), and subsequent decrease in Cyclin E1, seen in both tumour cell lines. Furthermore, p21 expression was significantly increased in both tumour cell lines, in keeping with loss of inhibitory control by SKP2. Resultant increase in the proportion of cells in G1 and decreased S phase was seen in both cell lines by FACS as expected.

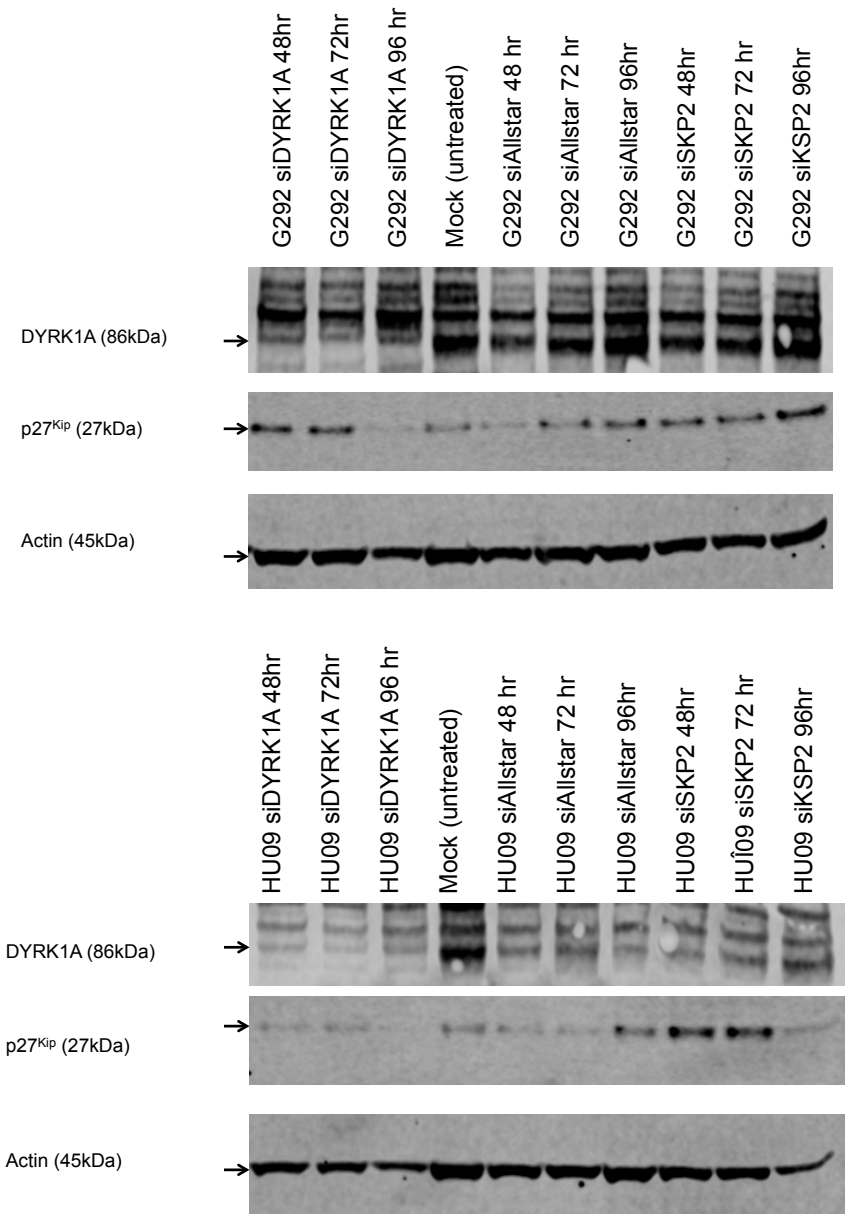

Figure 89 DYRK1A expression when targeted by siDYRK1A in both G292 clone A141B1 (*RB1* wildtype), and HU09 (*RB1* deficient) tumour cell lines decreased.

Western blotting of DYRK1A and p27 expression in G292 clone A141B1 and HU09. Both tumour cell lines were reverse transfected with siRNA targeting siDYRK1A, siAllstar (non-targeting control) and siSKP2, whole cell fractions collected after 48, 72 and 96 hours, electrophoresed and immunoblotted as described in the methods. Immunoblotting of actin was used a loading control. In G292 clone A141B1, expression of $p27^{Kipl}$ was high at 48 hours, and decreased with time. Expression of $p27^{Kipl}$ did not rise in HU09 and expression was absent at 96 hours, in keeping with diminished stability in the absence of phosphorylation by DYRK1A. In both tumour cell lines $p27^{Kipl}$ increased with silencing of SKP2 as expected.

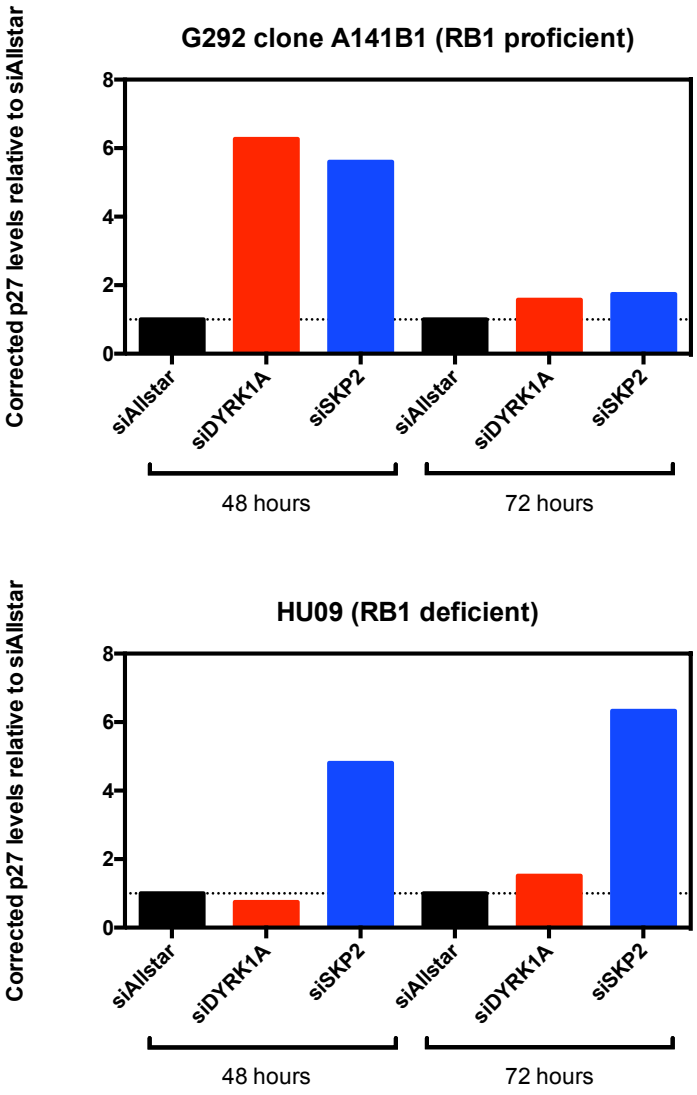

Figure 90 Densitometry of $p27^{Kipl}$ expression corrected to actin, relative to siAllstar at 48 and 72 hours post reverse transfection.

Bar chart of corrected p27 expression levels relative to siAllstar by western blotting. G292 clone A141B1 and HU09 were reverse transfected with siRNA targeting siDYRK1A, siAllstar (non-targeting control) and siSKP2, whole cell fractions collected after 48, 72 and 96 hours, electrophoresed and immunoblotted as described in the methods. Immunoblotting of actin was used a loading control. Densitometry of DYRK1A expression relative to actin was calculated for each OS tumour cell line using ImageJ software. In G292 clone A141B1, expression of $p27^{Kipl}$ was high at 48 hours, and decreased with time. Expression of $p27^{Kipl}$ did not rise in HU09. In both tumour cell lines $p27^{Kipl}$ increased with silencing of SKP2 as expected. Increased p27 expression was not maintained at 72 hours in G292 clone A141B1 post reverse transfection with either siDYRK1A or siSKP2. This could reflect a faster growth characteristic than HU09, and therefore greater dilution of the siRNA. [p27: $p27^{Kipl}$]

In conclusion, the most profound changes seen post silencing of DYRK1A in RB1 deficient tumour cells are decreased $p27^{Kipl}$ and an increase in Cyclin D1 at this time point. Expression of p21 and Cyclin E1 did not change. On inspection of the known targets of DYRK1A, at this time point, it is possible to exclude Cyclin E1 and p21 from the mechanism of synthetic lethality. It is most likely the following changes occur: firstly, reduction of phosphorylation of Cyclin D1 by DYRK1A leads to stabilisation, reflected in increased protein expression in both cell lines. In the RB1 wildtype context, loss of repression of Cyclin D1 leads to activation of RB1 (Soppa, Schumacher, Florencio Ortiz, et al., 2014; Ashford, Oxley, Kettle, et al., 2014). Secondly, reduction of phosphorylation of $p27^{Kipl}$ at Serine10 by DYRK1A, leads to decreased stability (Ishida, Kitagawa, Hatakeyama, et al., 2000), reflected in decreased $p27^{Kipl}$ expression in HU09. However, with decreased expression of $p27^{Kipl}$, no compensatory rise in Cyclin E1 was seen, but this could be because 48 hours was too early for this to be observed, or because of redundancy of regulation of Cyclin E1, for example by p21 acting via Cyclin D1. The cell cycle profile changes identified by FACS were not profound, and so it is possible that some of the expected increase of Cyclin A2 with the tumour cell line HU09, was too small to observe.

Lysates collected 48 hours post exposure to 3μM harmine and 3μM AZ191 were also used to investigate cyclin and DYRK1A substrate expression (Figure 92). AZ191 had become available from Astra Zenica on a material transfer agreement, and given its nanomolar IC50 inhibition of DYRK1A and DYRK1B, was used in addition to harmine. Decreased expression of DYRK1A was seen post inhibition of DYRK1A using both agents in both cell lines. After exposure to harmine and AZ191, no significant changes in Cyclin D1, Cyclin E1 or Cyclin A2 were seen. It is possible that the profound changes seen in cell cycling by FACS after exposure to 30μM harmine are off target effects given that no profound changes in Cyclin profiles were seen with a lower drug dose or silencing by siRNA.

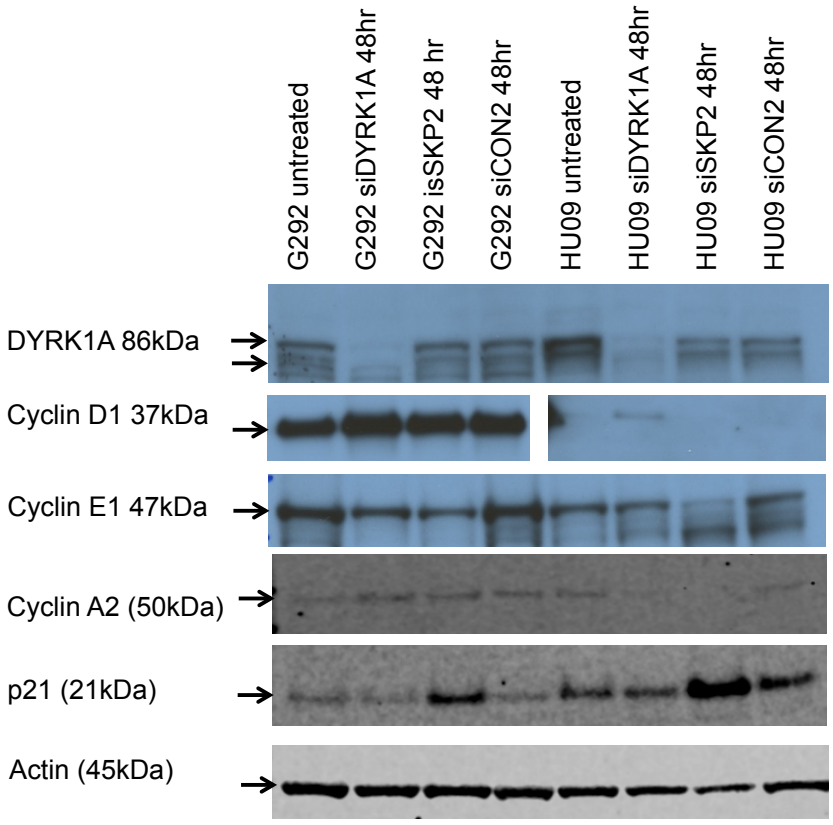

Figure 91 Expression of DYRK1A substrates and markers of the cell cycle at 48 hours post reverse transfection with siDYRK1A and siSKP2.

Western blotting is shown. Tumour cells were reverse transfected with siRNA (siAllstar, siDYRK1A, and siSKP2). After 48 hours, total cell lysates were collected, electrophoresed and immunoblotted Immunoblotting of actin was used as the loading control. Silencing of *DYRK1A* by siRNA caused a decreased expression of DYRK1A in both tumour cell lines. Baseline Cyclin D1 levels were high in G292 clone A141b1 with an increase in cyclin D1 with silencing of *DYRK1A*. Baseline expression of Cyclin D1 was absent in HU09, but detectable with silencing of DYRK1A. This is accordant with loss of negative regulation of Cyclin D1 by DYRK1A, leading to increased levels of Cyclin D1. Decreased expression of Cyclin E1 was seen in the *RB1* wildtype tumour cell line G292 clone A141B1, in keeping with the increase in $p27^{Kipl}$ levels seen at 48 hours. Silencing of *DYRK1A* leads to decreased phosphorylation of $p27^{Kipl}$ and therefore decreased stability. Levels of $p27^{Kipl}$ were low in the *RB1* deficient tumour cell line HU09, and hence no significant change of expression of Cyclin E1 was seen. Cyclin A1 expression levels were low for both tumour cell lines, without significant changes to expression levels. Levels of expression of p21 were unchanged in both tumour cell lines. Silencing of *SKP2,* used as a positive control, leads to loss of inhibitory control of $p27^{Kipl}$ (shown previously) and p21, with subsequent decrease in Cyclin E1, seen in both tumour cell lines.

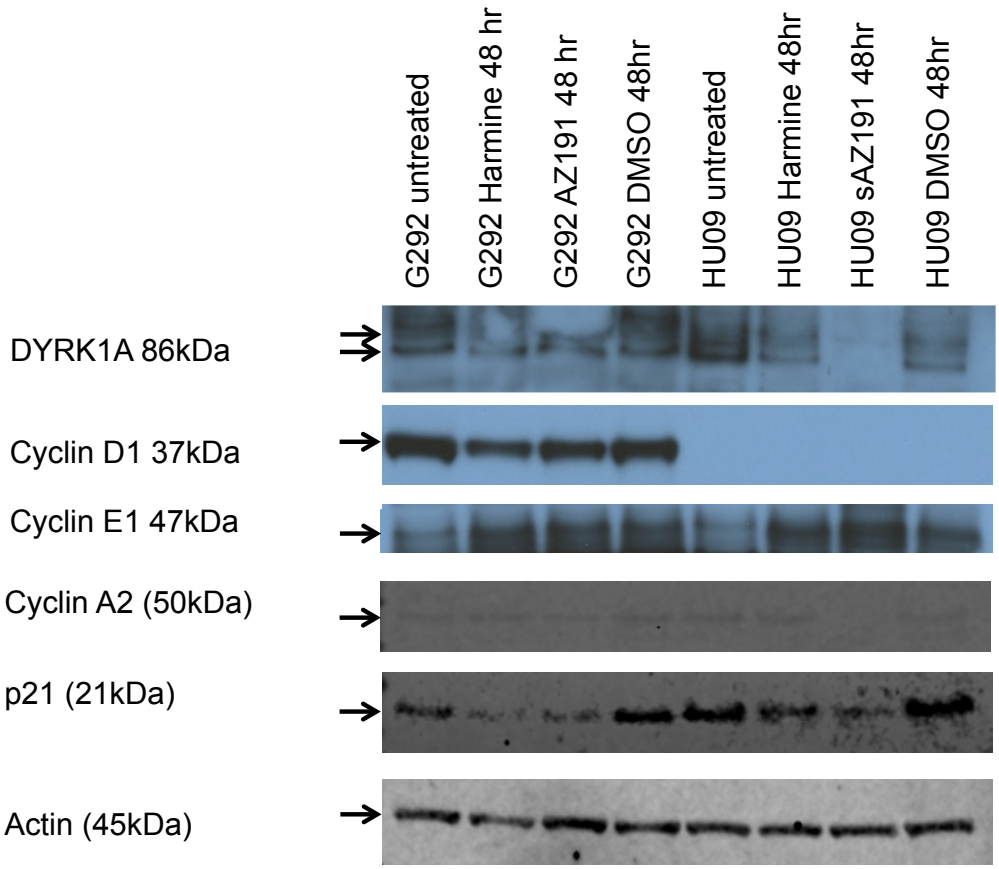

Figure 92 Expression of DYRK1A substrates and markers of the cell cycle responses to inhibition of DYRK1A by 3μM harmine and 3μM AZ191 in OS tumour cell lines.

Western blot is shown. G292 clone A141B1 and HU09 were exposed to 3μM harmine or 3μM AZ191 or drug vehicle, DMSO or untreated. After 48 hours, total cell lysates were isolated after drug exposure, electrophoresed and immunoblotted as described in the methods. Immunoblotting of actin was used as a loading control. Decreased expression of DYRK1A is seen post inhibition of DYRK1A using both agents in both tumour cell lines. After exposure to harmine and AZ191, no significant changes in Cyclin D1, Cyclin E1 or Cyclin A2 were seen. A decrease in expression of p21 was seen in both tumour cell lines, reflecting progression through G1 into S and beyond to G2.

6.4 DISCUSSION

This chapter descried the results of two parallel cell-based siRNA screens (OS panel of 18 tumour cell lines, and isogenic *RB1* deficient OS models) to identify genetic vulnerabilities associated with the recurrent driver mutations of *RB1* and *CDKN2A*.

Genetic vulnerabilities associated with *CDKN2A* deficiency were identified and revalidation of these genes could form the basis for future work. Genetic dependencies associated with *RB1* deficiency were also identified, and eight genes underwent revalidation by deconvolution. High-throughput cell-based screening has the advantage of allowing multiple individual genes to be targeted simultaneously, although type I and II errors may occur (Martis & Radhakrishnan, 2011). The incidence of false positive (Type I) errors can be reduced by performing multiple parallel screens with subsequent validation of generated hits. As discussed previously, both isogenic and non-isogenic models have inherent limitations, and thus in an attempt to overcome these limitations both models were screened to increase the likelihood of identifying a clinically relevant *RB1* synthetic lethal effect.

Twenty-seven genes were selected using the criteria set to identify candidate genetic dependencies associated with *RB1* deficiency using the isogenic *RB1* deficient U2OS models. Network analysis demonstrated a number of connections between these candidate genetic dependencies and reliance on DNA metabolism and damage repair (*WRN, RECQL5, RAD50, ERCC3, OGG1* and *PALB2*). Revalidation of these genes could provide the basis for future work. Of eight candidate genetic dependencies associated with *RB1* deficiency in the OS tumour cell line panel chosen for revalidation by deconvolution, only *DYRK1A* met the stringent criteria set for revalidation. To investigate the robustness of this synthetic lethal observation, combination of both the osteosarcoma and breast tumour cell line panels identified DYRK1A as a candidate genetic dependency associated with *RB1* deficiency. This observation was also seen in an independent publically available data set called ‘Achilles’ created by the Broad Institute using lenti-viral delivered genome-wide shRNA in a panel of 216 cancer cell lines (Cowley, Weir, Vazquez, *et al.*, 2014). A further independent data set derived from siRNA screening using a colon cancer cell line, which was irradiated to induce phosphorylation and inactivation of RB1 also demonstrated a genetic dependency on *DYRK1A* (Stockwell, Li, Aherne, *et al.*, 2012).

Further overlap of the genetic dependencies identified in isogenic *RB1* deficient U2OS cell line models with those of the osteosarcoma tumour cell line panel, in particular *DYRK1A* was not observed. This could be that other molecular characteristics of the tumour cell line U2OS mitigate the genetic vulnerability of loss of *DYRK1A.* Deficiency of *CDKN2A* (p16) was found in this panel of tumour cell lines to be mutually exclusive with deficiency of *RB1.* U2OS, although *CDKN2A* wildtype*,* p16 expression is not detectable by western blot, and mRNA expression and proteomic abundance levels are comparable with other tumour cell lines with homozygous deletion of *CDKN2A,* and so previously classified as *CDKN2A* deficient (described in Chapter three). It is possible that a deficiency of *CDKN2A* abrogates genetic vulnerabilities specific to acquired deficiencies associated with deficiency of *RB1.* Absence of p16 (*CDKN2A*) leads to loss of repression of Cyclin D1, and therefore phosphorylation and inactivation of RB1. CRISPR-Cas9 mediated mutagenesis of *RB1* was attempted in a number of osteosarcoma tumour cell lines (G292 clone A141B1, KPD, MHM and OS25-HAL) before success in U2OS. These tumour cell lines all had wildtype *CDKN2A*, and post reverse transfection, all CRISPR-Cas9 transfected clones demonstrated rapid loss of viability. It is possible that acquired deficiency of *RB1* is only possible in tumour cells with concomitant deficiency of *CDKN2A*, and have therefore adapted to a cellular state in which *RB1* is inactivated, which could impact on possible genetic vulnerabilities. Given that CRISPR-Cas9 mutagenesis was attempted in a number of other *CDKN2A* wildtype tumour cell lines without success, it is possible sudden acquired complete deficiency of *RB1* is lethal without prior deficiency of *CDKN2A,* and that a deficiency of *CDKN2A* abrogates genetic vulnerabilities specific to acquired deficiencies associated with deficiency of *RB1.*

All of these models have their limitations. Isogenic models that derive from a single progenitor cell line, with minimal genetic differences between the daughter and parental cell lines, so that any observed differences are more likely to be due to the gene of interest (Rehman, Lord & Ashworth, 2010), were sought. However, given the heterogeneity of osteosarcoma *in vivo*, a panel of representative tumour cell lines was attractive, but does make isolation of genetic vulnerabilities with a molecular deficiency such as *RB1* more difficult.

Kinase inactivation of *DYRK1A* by conversion of a critical Lys-188 residue in the catalytic domain to Arg-188 has been shown to have a dominant negative effect on wildtype *DYRK1A* (Yang, Ahn & Chung, 2001; Litovchick, Florens, Swanson, *et al.*, 2011). Using a

tetracycline inducible model of kinase inactivated and wildtype *DYRK1A*, colony formation assay post reverse transfection with siRNA targeting *RB1,* demonstrated suppression of colony formation. This confirmed that the genetic dependency observed was dependent on the kinase activity of DYRK1A.

Many different roles for DYRK1A have been recorded, with those in the DREAM complex and the cell cycle most annotated. DYRK1A is a critical component of the DREAM complex. Litovchick *et al.* established that the DREAM complex controls cell cycle exit into G0, and is composed of RB Transcriptional Co-repressor Like 2 (p130), E2F Transcription Factor 4 (E2F4), dimerization protein 1 (DP), and a stable core complex of five MuvB-like proteins which form the multi-vulval class B (MuvB) core: LIN9, LIN37, LIN52, LIN54 and RB Binding Protein 4, Chromatin Remodelling Factor (RBBP4); the MuvB core binds p130-E2F4 dimerisation partner (DP) to form the DP, RB like E2F and MuVB (DREAM) complex in G0 to repress all cell cycle-dependent gene expression (Litovchick, Florens, Swanson, *et al.*, 2011; Sadasivam & Decaprio, 2013), totalling more than 800 human promoters and is required for repression of E2F target genes (Litovchick, Sadasivam, Florens, *et al.*, 2007).

Formation of the MuvB core with p130 and E2F4 is dependent on phosphorylation of Serine28 on LIN52 by DYRK1A. Silencing or kinase inactivation (DYRK1A-K188R) of DYRK1A, or mutagenesis of Serine28 on LIN52, prevents DREAM complex formation, reducing the ability of the cell to enter quiescence or undergo Ras-induced senescence (Litovchick, Florens, Swanson, *et al.*, 2011). DRYK1B has also been shown to phosphorylate LIN52 *in vitro*, but no specific role for endogenous DYRK1B *in vivo* has been established, however, exogenous overexpression does rescue the effects of depletion of DYRK1A (Litovchick, Florens, Swanson, *et al.*, 2011).

If RB1 is active, cells are arrested at the restriction point. The activator E2Fs, (E2F1, E2F2, and E2F3) contribute to the control of early cell cycle gene expression and G1 to S phase transition. Cyclins D and E in complex with the cyclin-dependent kinases (CDKs) mitigate repression of E2F by phosphorylation of active RB1 to its inactive form. In the absence of DREAM complex formation, the MuvB core recruits BMYB during S phase and then forkhead box protein M1 (FOXM1) to the promoters of the G2/M phase-expressed genes (Sadasivam & Decaprio, 2013). The MuvB core is essential for targeting each of the three complexes (DREAM, BMYB and FOXM1) to specific sets of

cell cycle gene promoters (Sadasivam & Decaprio, 2013). A schematic of the DREAM complex and it's role in the cell cycle is shown in Figure 93.

The balance between the quiescent DREAM complex and the proliferative phase BMYB–MuvB–FOXM1 complex is frequently disrupted in cancer (Sadasivam & Decaprio, 2013). Disruption of the DREAM complex and RB1 by deregulated cyclin and cyclin dependent kinase (CDK) activity leads to decreased expression of the E2F-dependent cell cycle genes and instead activation of the late cell cycle genes (Sadasivam & Decaprio, 2013). Increased DREAM formation by over expression of DRYK1A or decreased levels of BMYB may result in cancer cells exiting the cell cycle and remaining dormant. It is unknown if the loss of RB1 and the perturbation of the DREAM complex can be distinguished in cancer, and thus whether there are separate roles during quiescence and senescence (Sadasivam & Decaprio, 2013).

Defective DREAM complex assembly, results in the loss of transcriptional repression of cell cycle genes (MacDonald, Ramos-Valdes, Perampalam, *et al.*, 2016). Loss of endogenous expression of DYRK1A appears to result in two fates, either proliferation or cell death; chemical silencing of DYRK1A in non cancerous pancreatic beta-cells increases proliferation (Shen, Taylor, Jin, *et al.*, 2015; Wang, Alvarez-Perez, Felsenfeld, *et al.*, 2015). Conversely, retention of the MuvB-BYMB complex, after loss of DYRK1A in epithelial ovarian cancer spheroids, leads to increased DNA synthesis that is concomitant with cell death (MacDonald, Ramos-Valdes, Perampalam, *et al.*, 2016). Ovarian tumour cell lines induced to produce spheroids enter G0, with DYRK1A acting as the primary kinase responsible for DREAM complex assembly (MacDonald, Ramos-Valdes, Perampalam, *et al.*, 2016). DYRK1A depleted ovarian tumour cell line spheroids, created by lentiviral shRNA infection, resulted in a significantly increased level of DNA synthesis at 6 hours post transfer to non-adherent conditions (MacDonald, Ramos-Valdes, Perampalam, *et al.*, 2016). Although this effect was abrogated by 24 hours, extensive subG1 death was observed and spheroid viability was reduced (MacDonald, Ramos-Valdes, Perampalam, *et al.*, 2016). Exposure of ovarian spheroids to a DYRK1A inhibitor, Indy in combination with carboplatin resulted in greater loss of viability than with either agent alone (MacDonald, Ramos-Valdes, Perampalam, *et al.*, 2016). Targeting DYRK1A, and other members of the DREAM complex, in such a setting instead of leading to proliferation, caused cell death, suggesting a possible attractive therapeutic approach

(MacDonald, Ramos-Valdes, Perampalam, *et al.*, 2016). Furthermore in those tumour types where cells evade the effects of cytotoxic therapy by quiescence, inhibition of DREAM complex formation and resultant increase in cell cycling, may make them more susceptible to cytotoxic therapy. One example is with Imatinib, the primary treatment of gastrointestinal stromal tumours (GIST), which has been shown to induce DREAM mediated quiescence *in vivo*. Inhibition of the DREAM complex formation by depletion of DYRK1A or LIN52 by siRNA or treatment with harmine, reduced quiescence and increased imatinib induced apoptosis (Boichuk, Parry, Makielski, *et al.*, 2013).

DYRK1A is also pro-survival with a role as a negative regulator of the intrinsic apoptotic pathway in the mouse retina (Laguna, Aranda, Barallobre, *et al.*, 2008). DYRK1A phosphorylates caspase-9 on threonine residue 125, which is crucial in protecting cells in the retina from apoptosis (Laguna, Aranda, Barallobre, *et al.*, 2008). DYRK1A also phosphorylates and activates Sirtuin1 (SIRT1), which deacetylates p53 leading to cell survival despite DNA damage (Guo, Williams, Schug, *et al.*, 2010). Deacetylation of p53 by SIRT1 leads to transcriptional inactivation and repression of the p53-mediated cell growth arrest and apoptosis in response to DNA damage and oxidative stress (Brooks & Gu, 2011). In addition, SIRT1 mediated deacetylation process has been associated with increased cellular senescence (Brooks & Gu, 2011). The p53-dependent transactivation of p21 is also prevented by this deacetylation (Brooks & Gu, 2011). p21 negatively regulates CDK1 activation, a promoter of cell cycle progression from G2 to mitosis (Ronco, Martin, Demange, *et al.*, 2017). Silencing of endogenous DYRK1A and DYRK3 leads to hypo-phosphorylation of SIRT1, and sensitisation of cells to DNA damage-induced cell death (Guo, Williams, Schug, *et al.*, 2010). DYRK1A also selectively binds and phosphorylates huntingtin-interacting protein 1 (Hip-1) during the neuronal differentiation of embryonic hippocampal neuro-progenitor cells, which results in the blockade of Hip-1 mediated neuronal cell death (Kang, Choi, Park, *et al.*, 2005).

The diverse roles of DYRK1A are summarised in Figure 94.

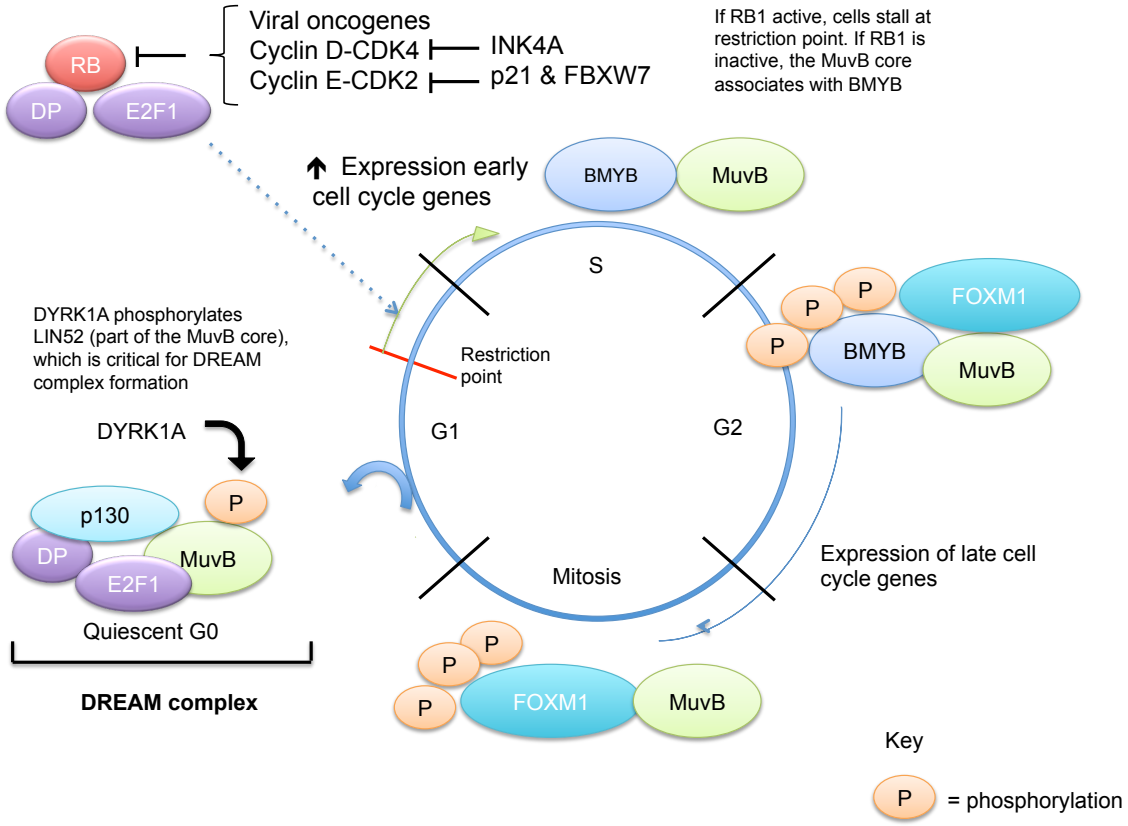

Figure 93 Schematic of the DREAM complex and role in the cell cycle adapted from Sadasivam *et al.* (Sadasivam & Decaprio, 2013).

The DREAM complex is composed of p130, E2F4, dimerization protein 1 (DP), and a stable core complex of five MuvB-like proteins which form the multi-vulval class B (MuvB) core: LIN9, LIN37, LIN52, LIN54 and RBBP4 (Litovchick, Florens, Swanson, *et al.*, 2011). Formation of the DREAM complex (multi-vulval class B (MuvB) core with p130 and E2F4) is dependent on phosphorylation of LIN52 by DYRK1A (Litovchick, Florens, Swanson, *et al.*, 2011). MuvB binds p130-E2F4 dimerisation partner (DP) to form the DP, RB-like E2F and MuVB (DREAM) complex in G0 to repress all cell cycle-dependent gene expression. If RB1 is active, cells are arrested at the restriction point. The activator E2Fs, (E2F1, E2F2, and E2F3) contribute to the control of early cell cycle gene expression and G1 to S phase transition (represented by the green arrow). Cyclins D and E in complex with the cyclin-dependent kinases (CDKs) mitigate repression of E2F by phosphorylation of active RB1 to its inactive form. In the absence of DREAM complex formation, the MuvB core recruits BMYB during S phase and then forkhead box protein M1 (FOXM1) to the promoters of the G2/M phase-expressed genes (Sadasivam & Decaprio, 2013). The MuvB core is essential for targeting each of the three complexes (DREAM, BMYB and FOXM1) to specific sets of cell cycle gene promoters (Sadasivam & Decaprio, 2013). Reproduced with alteration from Sadasivam *et al* (Sadasivam & Decaprio, 2013). [P: phosphorylation; DP: dimerization partner]

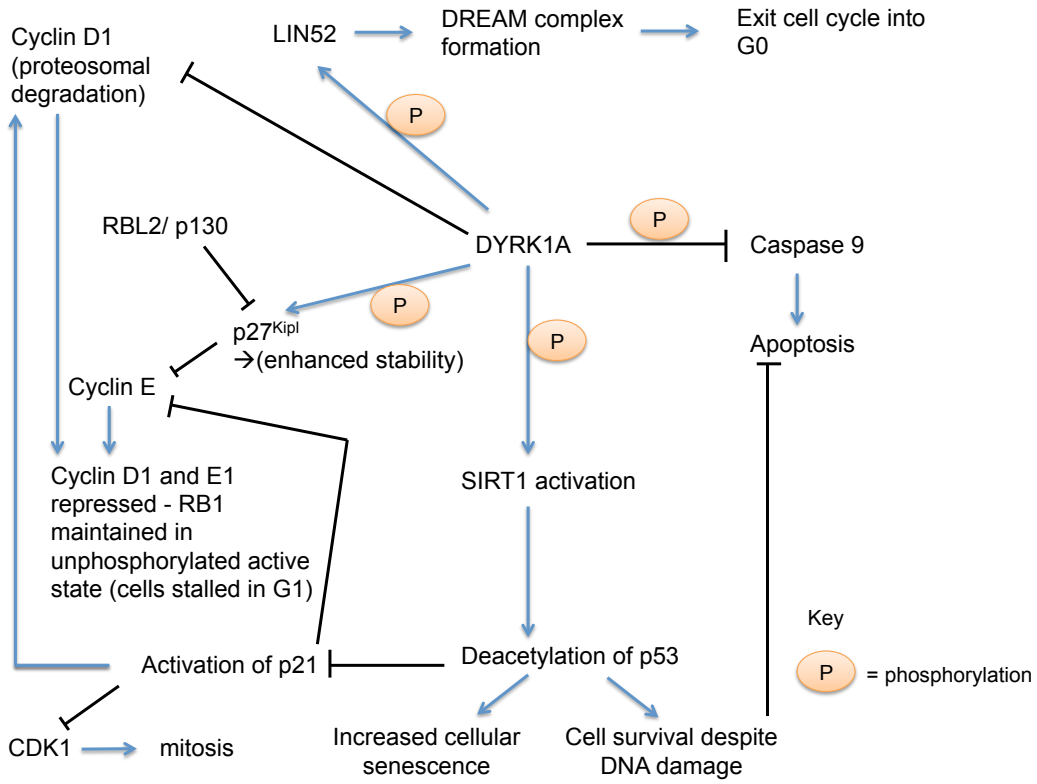

Figure 94 Schematic summarising the multiple reported roles of dual-specificity tyrosine-regulate kinase 1A (DYRK1A).

The formation of the DREAM complex is dependent on the phosphorylation of Serine28 on LIN52 by DYRK1A, which promotes cell cycle exit into G0 (Litovchick, Florens, Swanson, *et al.*, 2011; Sadasivam & Decaprio, 2013); DYRK1A phosphorylates Cyclin D1 leading to protosomal degradation, meaning RB1 remains in an un-phosphorylated active state (Soppa, Schumacher, Florencio Ortiz, *et al.*, 2014); DYRK1A phosphorylates $p27^{Kipl}$ at Serine10, leading to enhanced stability, and supressed levels of Cyclin E, thereby maintaining RB1 in its active, unphosphorylated state causing cell cycle arrest (Ishida, Kitagawa, Hatakeyama, *et al.*, 2000); DYRK1A phosphorylates caspase-9 on threonine residue 125, preventing apoptosis (Laguna, Aranda, Barallobre, *et al.*, 2008); DYRK1A phosphorylates and activates Sirtuin1 (SIRT1), which deacetylates p53 leading to cell survival despite DNA damage (Guo, Williams, Schug, *et al.*, 2010). Deacetylation of p53 by SIRT1 leads to transcriptional inactivation and repression of the p53-mediated cell growth arrest and apoptosis in response to DNA damage and oxidative stress (Brooks & Gu, 2011). In addition, this SIRT1 mediated deacetylation process has been associated with increased cellular senescence (Brooks & Gu, 2011). The p53-dependent transactivation of p21 is also prevented by this deacetylation (Brooks & Gu, 2011). p21 negatively regulates CDK1 activation, a promoter of cell cycle progression from G2 to mitosis (Ronco, Martin, Demange, *et al.*, 2017). pRb2/ p130 also induces $p27^{Kipl}$ levels by impeding cyclin E/CDK2 phosphorylation of $p27^{Kipl}$, which in turn generates the proteolytic degradation of $p27^{Kipl}$ (Neganova & Lako, 2008).

In addition to roles in both cell cycle exit to G0 via formation of the DREAM complex (Litovchick, Florens, Swanson, et al., 2011; Sadasivam & Decaprio, 2013), DYRK1A also represses Cyclin D1 and E1, both directly via proteosomal degradation of Cyclin D1 (Chen, Lin, Tsai, et al., 2013; Soppa, Schumacher, Florencio Ortiz, et al., 2014), and indirectly via enhanced stability of $p27^{Kipl}$ which negatively controls Cyclin E1 (Ishida, Kitagawa, Hatakeyama, et al., 2000). Repression of Cyclin D1 and E1 leads to maintenance of RB1 in an active unphosphorylated stated, and stalling of cells in G1 (Figure 95). It is logical therefore, that inhibition of DYRK1A would lead to decreased cell cycle exit into G0, and increased cell cycling through G1 and beyond depending on the function of the RB restriction point.

Litovchick *et al.* identified a link between DYRK1A and LIN52, one of the components of the DREAM complex which regulates quiescence and senescence (Litovchick, Florens, Swanson, *et al.*, 2011). They performed similar cell cycle experiments in both serum positive (10% FBS) and serum starved (0% FBS) conditions using T98G cells of glioblastoma origin, that have previously been shown to have cell cycle control that is dependent on functional pRB1 (Paggi, Felsani & Giordano, 2003). Forty-eight hours post reverse transfection with siDYRK1A and 20 hours post exposure to 10μM harmine, cell cycle profiling using FACS showed that S phase was increased in both treatment and serum conditions (Litovchick, Florens, Swanson, *et al.*, 2011). From this they concluded that DYRK1A must be essential to DREAM complex assembly and entry into G0/quiescence (Litovchick, Florens, Swanson, *et al.*, 2011). Notably Litovchick *et al.* only used EDU and DAPI stains, and so without the addition of a phospho-histone H2 antibody were unable to identify active mitosis. Concordant with these observations, in both tumour cell lines regardless of RB1 context, there was a modest increase in S phase post exposure to siDYRK1A. However, the observations of Litovchick *et al.* did not correspond with the dramatic decrease of S phase seen in the *RB1* wildtype tumour cell line G292 clone A14B1 post exposure to 30μM harmine from 3% as compared to 11% in the control (DMSO). It is possible that at higher doses of harmine off-target effects such as G2/M arrest via induction of p21, and activation of the Fas/FasL pathway (Wang, Wang, Jiang, *et al.*, 2015) mask the on-target effects of increased S-phase or temporal effects of a later time point used (48 hours not 20 hours as per Litovchick *et al*.).

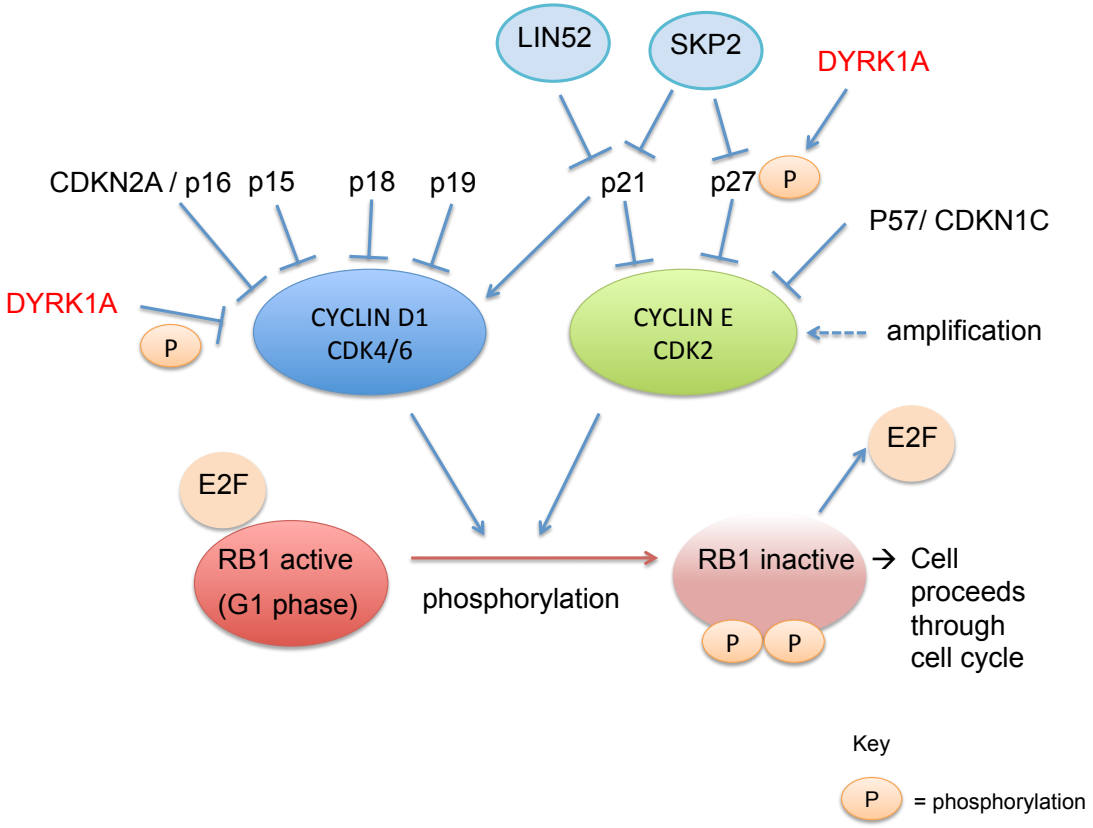

Figure 95 Schematic of RB pathway in a non-manipulated cell adapted from Mittnacht *et al.* (Mittnacht, 2005).

RB1 in its active state is hypo-phosphorylated and binds E2F. Cyclins D1 and E lead to hyper-phosphorylation and inactivation of RB1, and dissociation of the E2F transcription factors, enabling the cell to proceed through the cell cycle. DYRK1A phosphorylates Serine10 of $p27^{Kip1}$ leading to enhanced stability and suppression of levels of Cyclin E (Ishida, Kitagawa, Hatakeyama, *et al.*, 2000). Phosphorylation at Thr286 by DYRK1A and DYRK1B induces proteosomal degradation of Cyclin D1 during G1 phase (Soppa, Schumacher, Florencio Ortiz, *et al.*, 2014) meaning RB1 remains in an un-phosphorylated active state.

Chen *et al.* also demonstrated that silencing of DYRK1A by siRNA or by harmine, decreased the duration of G1 phase (Chen, Lin, Tsai, *et al.*, 2013). MacDonald *et al.* observed a decrease in G1, and an increase in subG1 population 20 hours post spheroid formation in ovarian tumour cell lines which stably expressed shDYRK1A (MacDonald, Ramos-Valdes, Perampalam, *et al.*, 2016). Although I do not see an increase in the subG1 population, this could be a function of the time point analysed. It is also important to note that these experiments (MacDonald, Ramos-Valdes, Perampalam, *et al.*, 2016) were performed in spheroid systems, not adherent cells which are likely to have different cell cycle profiles, and clinical implications for future extrapolation.

In accordance with the hypothesis that inhibition of DYRK1A decreases the proportion of cells exiting the cell cycle into G0, it appeared from the FACS experiments that inhibition of DYRK1A by harmine increased the proportion of cells in G2. In the *RB1* wildtype tumour cell line, cells continued to undergo mitosis, with a corresponding increase in mitosis (1% DMSO; 4% 10μM harmine; 10% 30μM harmine). However, in the *RB1* deficient tumour cell line, an increase in mitosis was not seen (1% DMSO; 2% 10μM harmine; 2% 30μM harmine), consistent with stalling in G2. It is possible that these effects are due to off-target effects of harmine. Harmaline, another β-carboline alkaloid very similar harmine, has been shown to induce G2/M arrest via induction of p21, and activation of the Fas Cell Surface Death Receptor (Fas/FasL) pathway (Wang, Wang, Jiang, *et al.*, 2015), since these profound changes were not seen with lower concentrations of harmine, or post silencing of DYRK1A by siRNA. In addition, the increase in apoptosis seen post exposure to harmine at 10μM and 30μM concentrations may partially be explained by off target-effects of activation of the Fas/FasL pathway, which have been shown to activate Caspase-8 and Caspase-3 (Wang, Wang, Jiang, *et al.*, 2015). However, this would not explain the statistically significant difference in levels of apoptosis seen between the two tumour cell lines. Tumour cells deficient in *RB1* have been shown to be resistant to apoptosis induced via the Fas/FasL pathway, because of a deficiency in caspase-8 expression secondary to epigenetic gene silencing by over methylation (Poulaki, Mitsiades, McMullan, *et al.*, 2005). It is therefore unlikely that potential off-target effects of harmine explain this observation.

Exposure to harmine was associated with a decreased viability and increased level of apoptosis at 48 hours in the *RB1* deficient tumour cell line HU09, compared to the *RB1* wildtype tumour cell line G292 clone A141B1. Although single agent DYRK1A inhibitors

have shown little selectivity towards tumour cells with *RB1* deficiency, a modest synergistic effect was observed with the combination of harmine and cisplatin in combination in the *RB1* deficient tumour cell line HU09. To further establish any possible synergistic relationship, a longer-term assay with multiple dosing could be performed. Furthermore, combination of harmine or one of the new agents with greater potency of inhibition to DYRK1A such as GNF4877 (DYRK1A IC_{50} 6nM) (Shen, Taylor, Jin, *et al.*, 2015) could be screened in combination with other cytotoxic agents, in particular anti-mitotic agents such as paclitaxel or vinblastine to look for synergy.

Interpretation of the protein expression data is complicated by the many roles of DYRK1A and unknown consequences of an *RB1* deficient context. As predicted, silencing of DYRK1A leads to reduction of phosphorylation of Cyclin D1 and subsequent stabilisation, reflected in increased protein expression in both tumour cell lines. In the *RB1* wildtype context, loss of repression of Cyclin D1 leads to activation of RB1 (Soppa, Schumacher, Florencio Ortiz, *et al.*, 2014; Ashford, Oxley, Kettle, *et al.*, 2014). In addition, $p27^{Kipl}$ levels were increased and Cyclin E1 decreased, which could explain the increase in proportion of *RB1* wildtype G292 clone A141B1 tumour cells in G1 post reverse transection with siDYRK1A, but why despite an increase in Cyclin D1, the *RB1* deficient HU09 tumour cells progress past the non-functional RB restriction point.

Therefore, it is likely that a combination of increase in Cyclin D1, together with loss of formation of the DREAM complex increases the number of cells actively cycling. Cell cycle progression past G1 is determined by the cellular context and presence of functioning RB restriction point. Cyclin profiles, $p27^{Kipl}$ and members of the Fas/FasL pathway expression after exposure to 30μM harmine could be performed to confirm the findings seen by flow cytometry and determine if these were more likely off-target effects. Further investigation of the effects of blockade of DYRK1A by other small molecule inhibitors could be undertaken using the newer inhibitor GNF4877 (DYRK1A IC_{50} 6nM) (Shen, Taylor, Jin, *et al.*, 2015). Unlike harmine and harmaline, which are beta-carboline compounds, GNF4877 is based on an aminopyrazine scaffold and structurally different. Therefore, cell cycle analysis after exposure to GNF4877 has the potential to confirm the effects of silencing DYRK1A without the potential for off-target effects seen with harmine.

Deficiency of active *RB1* has been associated with mis-regulation of E2F targets leading to RB1 pathway defects which have been associated with over expression of mitotic

checkpoint protein (*MAD2)*, and mitotic defects (Hernando, Nahlé, Juan, *et al.*, 2004), increasing the incidence of multipolar spindles, anaphase bridges, lagging chromosomes and micronuclei harbouring whole chromosomes (Amato, Schillaci, Lentini, *et al.*, 2009), preventing progression through mitosis (Manning & Dyson, 2012). It is therefore conceivable that *RB1* deficient tumour cells are stalled in G2, because *RB1* deficiency affects progression through mitosis (Dyson, 2016) forming the basis of the genetic vulnerability to loss of DYRK1A. Increased apoptosis observed in the *RB1* deficient cell line, could be mediated by decreased phosphorylation of caspase-9 on threonine residue 125 by DYRK1A, with resultant increase in apoptosis (Laguna, Aranda, Barallobre, *et al.*, 2008) or from mitotic catastrophe. To further confirm these changes the following experiments could be performed: firstly, silencing of LIN52 by siRNA or CRIPSR-Cas9 mutagenesis of the Serine28, critical for formation of the DREAM complex, should lead to the same phenotype observed, if failure of DREAM complex formation occurs. Secondly, expression of functional RB1 should reverse the phenotype and decrease apoptosis. Thirdly a DNA fibre assay could be performed to identify fork stalling, while γH2AX assay could investigate for increased DNA damage. A schematic summarising the proposed hypothesis for the DYRK1A and RB1 synthetic lethality is shown in Figure 96.

To further confirm this genetic vulnerability, a solution would be a rescue experiment, by silencing of endogenous expression of DRYK1A by CRISPR mutagenesis in an *RB1* deficient OS tumour cell line, and then controlled expression of exogenous wild type DYRK1A or kinase inactive (K188R) DYRK1A using a cre:lox system (Figure 97). This would enable further robust investigation of the mechanism without using siRNA.

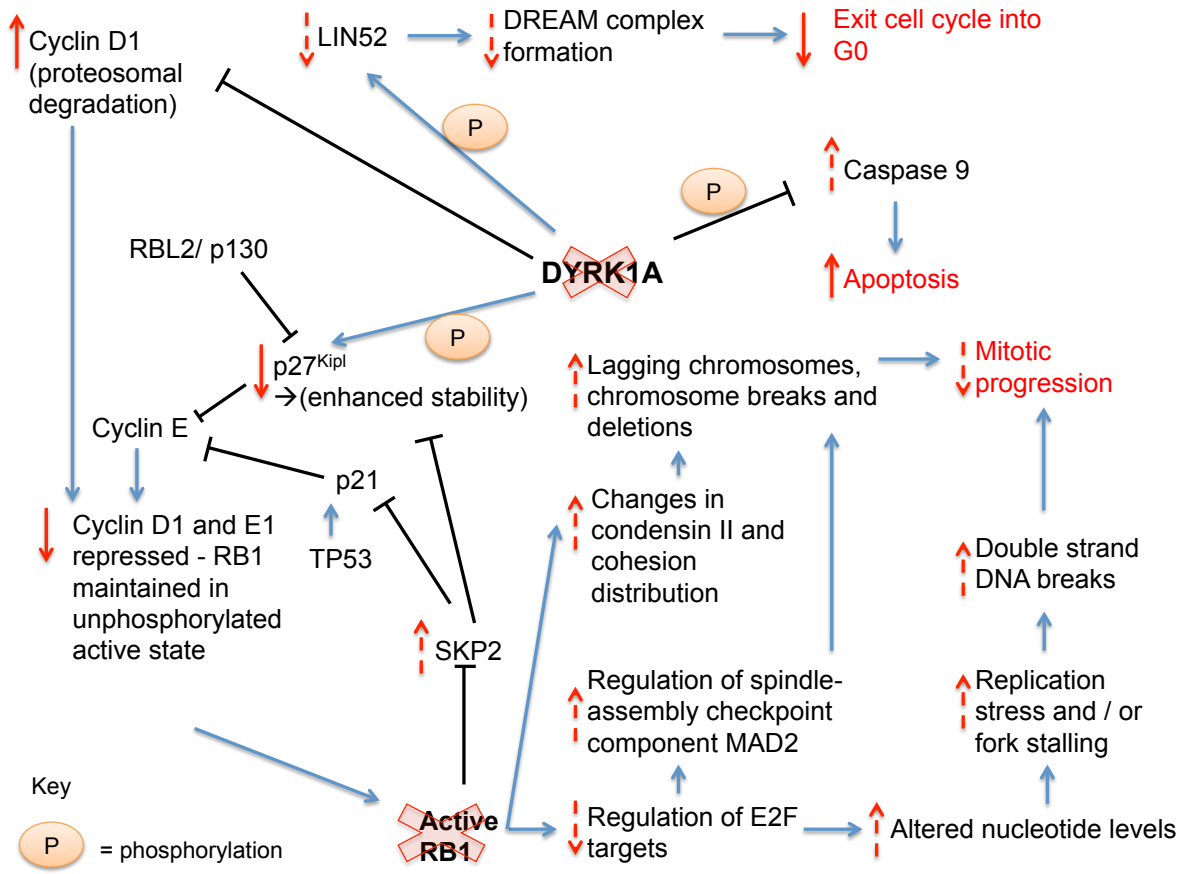

Figure 96 Schematic of the proposed hypothesis for the *DYRK1A* and *RB1* synthetic lethality

It is likely that a combination of increase in Cyclin D1, together with loss of formation of the DREAM complex increases the number of cells actively cycling. Deficiency of active RB1 has been associated with mis-regulation of E2F targets leading to firstly up-regulation of the spindle-assembly checkpoint component MAD2 and resultant hyper-activated checkpoint with impaired cleavage of cohesion, leading to lagging chromosomes, chromosome breaks, deletions (Hernando, Nahlé, Juan, *et al.*, 2004; Manning & Dyson, 2012),double strand DNA breaks, compromised centromere structure and function (Manning & Dyson, 2012). It is therefore conceivable that *RB1* deficient tumour cells are stalled in G2, because deficient *RB1* affects progression through mitosis (Dyson, 2016) forming the basis of the genetic vulnerability to loss of DYRK1A. Increased apoptosis observed in the *RB1* deficient cell line, could be mediated by decreased phosphorylation of caspase-9 on threonine residue 125 by DYRK1A, with resultant increase in apoptosis (Laguna, Aranda, Barallobre, *et al.*, 2008) or from mitotic catastrophe. [Red text: highlights outcomes; dashed red arrows: proposed effects; solid red arrows: observed effects]

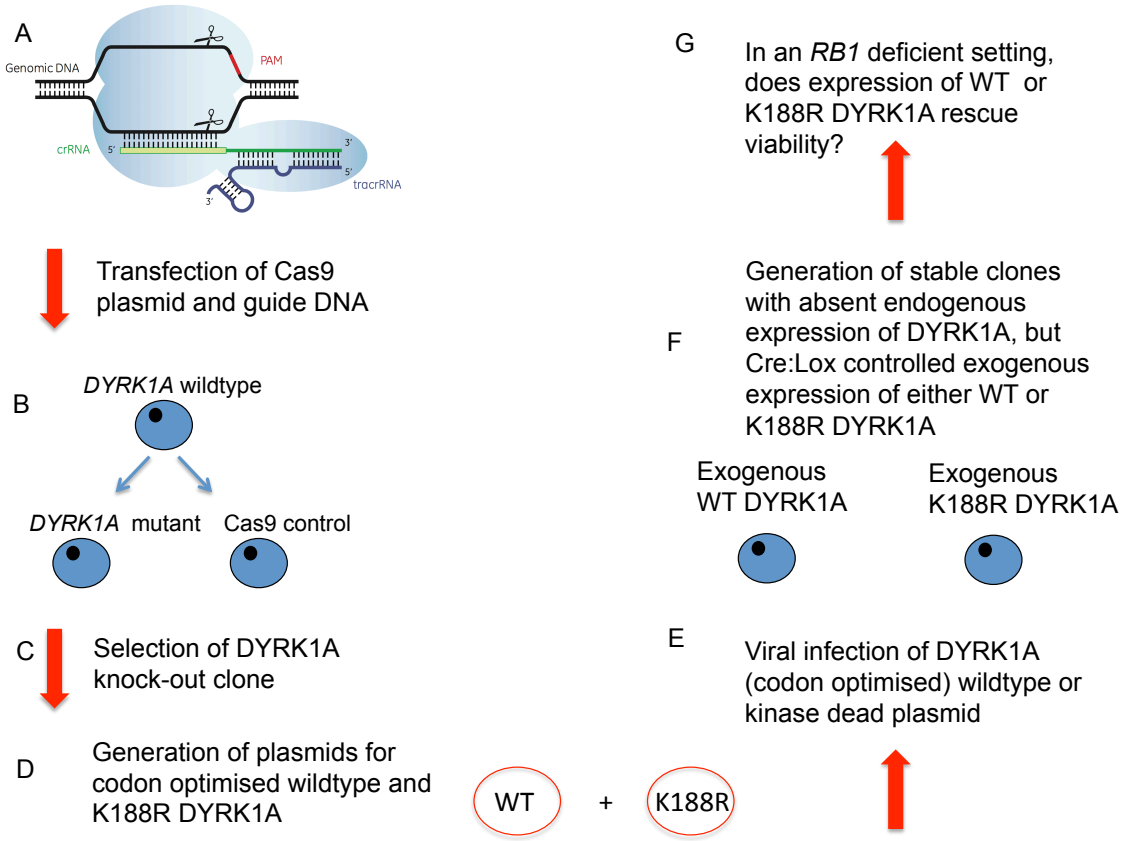

Figure 97 Schematic of future rescue experiment to further confirm the DYRK1A and RB1 synthetic lethality.

A: Transfection of Cas9 plasmid and guide DNA targeting Exon 1 of *DYRK1A* or Cas9 alone into a *RB1* deficient OS tumour cell line; B: Transfection efficiency monitored using a EGFP control. Cells selected by blastocydin, and seeded for colony formation. 100 colonies were picked and expanded. Generation of *DYKR1A* mutant and control (Cas9 alone) clones. C: Manufacture of genomic DNA from single colony clones, and subsequent amplification of target region of *DYRK1A* by PCR. Selection of mutant clones with the Surveyor Assay performed using the *DYRK1A* PCR product of all clones by identification of multiple DNA bands; sub-clone mutant clones, and sanger sequence for comparison with Cas9 control (parental) clone. Confirmation of expression of loss of DYRK1A expression by western blot of both N and C-termini of DYRK1A; D: Codon optimise genomic DYRK1A within the CRISPR guide target region only. Generation of plasmids for both wildtype and kinase inactive (K188R) *DYRK1A*; E: viral infection of DYRK1A plasmids into DYRK1A silenced CRISPR mutants; F: generation of stable tumour cell lines with cre:lox control of exogenous expression of wildtype and K188R DYRK1A. G: In the *RB1* deficient setting, does expression of wildtype DYRK1A rescue the synthetic lethality? Is rescue of the synthetic lethality by exogenous expression of DYRK1A dependent on the activity of the kinase domain or will kinase inactive K188R DYRK1A also rescue the synthetic lethality?

7 Identifying drug dependencies in osteosarcoma using a focused high-throughput cell based drug screen

7.1 INTRODUCTION

Unfortunately despite international collaboration, there has been little improvement in survival for patients with OS over the past two decades (Kempf-Bielack, Bielack, Jürgens, *et al.*, 2005; Janeway, Barkauskas, Krailo, *et al.*, 2012; Mirabello, Troisi & Savage, 2009; Luetke, Meyers, Lewis, *et al.*, 2014) with 5 year survival remaining in the order of 70% for young patients with localised disease. For those with metastatic disease at diagnosis, outcome is poor with only 20-30% surviving for 5 years (Koboldt, Fulton, McLellan, *et al.*, 2012), and remains even more dismal for those with recurrence (Luetke, Meyers, Lewis, *et al.*, 2014). There is a paucity of early phase clinical trials available for these patients and unfortunately results from these have generally been disappointing. Therefore, new or repositioned agents are needed for improvement of outcome. Currently no means of stratification of drugs for treatment of osteosarcoma or biomarkers of efficacy or sensitivity to treatment exist in the clinic. Targeting *RB1* deficiency in osteosarcoma represents a novel therapeutic approach and is attractive as up to 35% have structural rearrangements of *RB1* (Araki, Uchida, Kimura, *et al.*, 1991).

The aim of the parallel drug screen using a customised drug library was (i) to identify drugs with novel activity in osteosarcoma, (ii) further investigate drugs with known activity in osteosarcoma, (iii) more specifically to identify agents with sensitivity in *RB1* deficient models, (iv) validate potential therapeutic targets identified from the siRNA screens and (v) investigate the relative sensitivity of OS to PARP inhibition compared to HR deficient tumour cell lines. High-throughput approaches offer the benefit of rapidly examining the effects of multiple drugs or genes simultaneously (Boutros, Brás & Huber, 2006; Lord, Martin & Ashworth, 2009). Performing parallel screens with siRNA provided potential synergy whereby drugs and siRNA against the same target were identified to cause similar phenotypes and thus provide cross-validation. Chapter 3 described the rationale behind the models chosen for this thesis and the potential advantages and disadvantages of using isogenic and non-isogenic systems. In order to maximise the potential of identifying potential therapeutics for osteosarcoma, and *RB1* deficient tumours in particular, high-throughput drug screens were performed in the panel of OS tumour cell lines, and also isogenic *RB1* wildtype and deficient U2OS models.

The DNA damage response (DDR) is critical to genomic stability (Lord & Ashworth, 2012). DDR pathways encompass an analogous group of coordinated processes: detection of DNA damage; accumulation of DNA repair factors at the site of damage; and physical repair of the lesion (Lord & Ashworth, 2012). Ataxia-Telangiectasia Mutated (ATM), ATM-Rad3-related protein kinase (ATR) and the DNA-dependent protein kinase (DNA-PK) are kinases which transduce the DDR signals (Lord & Ashworth, 2012). Double strand breaks (DSB) in DNA are primarily repaired by homologous recombination (HR) and the more error prone non-homologous end joining (NHEJ) (Lord & Ashworth, 2012). HR involving resection of the sequence surrounding the DSB, and synthesis of replacement DNA using the homologous sister chromatid as a template, is primarily undertaken in the S and G2 phases of the cell cycle (Lord & Ashworth, 2012). Genes that encode proteins crucial to this process are *BRCA1, BRCA2, RAD51* and *PALB2* (Lord & Ashworth, 2012). In contrast to HR, NHEJ is active through-out the cell cycle and mediates repair by directly ligating the ends of a DSB together, which can lead to deletion or mutation of DNA sequences at or around the DSB site (Lord & Ashworth, 2012). The most well characterised role of DNA-PK is direct ligation of DNA double-strand breaks in NHEJ (Goodwin & Knudsen, 2014).

RB1, through its amino terminal (RB1N) domain, has been shown to bind to KU70, KU80 and DNA-PK, all components of the NHEJ machinery (Huang, Cook & Mittnacht, 2015). Furthermore, *RB1* deficient cells displayed an increased frequency of chromosomal aberrations after irradiation, a characteristic of defective NHEJ (Huang, Cook & Mittnacht, 2015). In addition, decreased NHEJ in *RB1* deficient cells and concomitant loss of the G1 checkpoint would lead to an increased reliance on the HR pathway. In tumour cells with a deficiency of *RB1* and loss of the G1 checkpoint, cells enter S phase with more unrepaired DNA damage. Therefore, *RB1* deficient cells would have a greater reliance on functional ATR to delay mitotic entry until all DNA damage repairs have been performed, and the DNA replicated (Nghiem, Park, Kim, *et al.*, 2001). Tumour suppressor genes, for example *RB1*, which when inactivated drive replication stress (Huang, Cook & Mittnacht, 2015) could potentially be therapeutically targeted with agents that disrupt the DNA damage repair, such as inhibitors of ATR.

DSBs activate primarily ATM and DNA-PK, while ATR responds to a wide spectrum of DNA damage, including DSBs, regions of single-stranded DNA and a variety of DNA lesions that interfere with replication (Goodwin & Knudsen, 2014; Maréchal & Zou, 2013;

Williamson, Miller, Pemberton, *et al.*, 2016). Replication stress leads to an increased proportion of single-stranded DNA, and a reliance upon an ATR checkpoint function (Williamson, Miller, Pemberton, *et al.*, 2016). Chemotherapeutic agents such as platinum salts (carboplatin and cisplatin) have a long history of clinical use by exploitation of DDR defects through DNA inter and intra-strand crosslinks repaired by nucleotide excision repair (NER) and HR (Lord & Ashworth, 2012). Recently new potent and specific inhibitors of ATR have been developed, VX970 (Vertex) and VE821 (Vertex) (Williamson, Miller, Pemberton, *et al.*, 2016); VE821 is a tool box compound while VX970 is currently in Phase I/II clinical trials in combination with topotecan (NCT02487095). In pre-clinical studies, in tumour cells with defects in the ATM/p53 pathway, VE821 has been shown to enhance the cytotoxic effects of DNA damaging agents suggesting a potential role for ATR inhibition as a chemo-sensitising agent (Williamson, Miller, Pemberton, *et al.*, 2016).

Inhibition of DNA-PK has been shown to sensitise tumour cells that depend on NHEJ for survival after induced DSB formation by chemotherapeutic agents such as doxorubicin and etoposide (Boucher, Hillier, Newsome, *et al.*, 2016; Tang, Yuan & Guo, 2014). VX984 (Vertex) a DNA-PK inhibitor has been shown to act synergistically with doxorubicin and etoposide in tumour cell lines and limited patient derived xenografts, leading to increased phosphorylated histone H2AX (gamma-H2AX), consistent with failed DSB repair (Boucher, Hillier, Newsome, *et al.*, 2016). An early phase Clinical Trial of VX984 in combination with pegylated liposomal doxorubicin is currently in progress (NCT02644278). In view of this evidence, an additional focused screen looking to determine if enhanced sensitivity to ATR and DNA-PK inhibition was observed in *RB1* deficient compared to *RB1* wildtype tumour cell lines was performed.

The concept of a BRCAness phenotype and potential applicability to osteosarcoma was discussed in 1.1.4.1 of Chapter 1. Given the great general interest amongst the OS community with regards the potential for clinical trial of PARP inhibitors in OS, this provided the rationale to investigate the representation of a ‘BRCAness’ phenotype in the OS tumour cell line panel and degree of sensitivity to PARP inhibition in relation to validated BRCA models.

7.2 RESULTS

7.2.1 Screen overview

To identify therapeutically activate agents in osteosarcoma, and also inhibitor dependencies specific for RB1 deficiency, all cell lines were profiled using a customised in-house drug library containing 80 drugs (Table 2, described in Chapter 2). These agents have either been licenced for clinical use in cancer or are in early phase clinical trials and were selected because of their potential for rapid clinical translation (17 under preclinical investigation, 24 in Phase I-III clinical trials, and 39 approved for use in cancer therapy). The library was chosen to cover a wide variety of proteins and biological processes relevant to cancer, including DNA repair, metabolism, cell cycle, DNA damaging chemotherapeutics, receptor and cytoplasmic tyrosine kinases, serine/threonine kinase and cytoskeleton assembly. Previous efforts within the Lord / Ashworth laboratory have screened a total of 99 tumour cell lines from a range of other ten other histologies (Campbell, Ryan, Brough, *et al.*, 2016), using the same screening format, making contextual comparison of relative drug sensitivity possible.

An additional library consisting of 395 drugs (Table 3, described in Chapter 2), which have either been licenced for clinical use in cancer or are in early phase clinical trials at 4 different concentrations (0.5, 5, 50, and 500nM) was also used to screen the isogenic *RB1* deficient U2OS models. This additional library was advantageous compared to the previous library, because it contained a wider selection of drugs, with redundancy of targets and pathways for example, three different Heat Shock Protein 90 (HSP90) inhibitors 17AAG, ganetesipib and geldanamycin providing additional internal validation. However, only 4 concentrations of each inhibitor were used compared to eight concentrations in the previous library. This additional library was a new addition to the laboratory and only available after the panel of OS tumour cell lines had been screened, and additional screening of the panel was not possible.

This methodology was described in Chapter 2 and summarised in Figure 98.

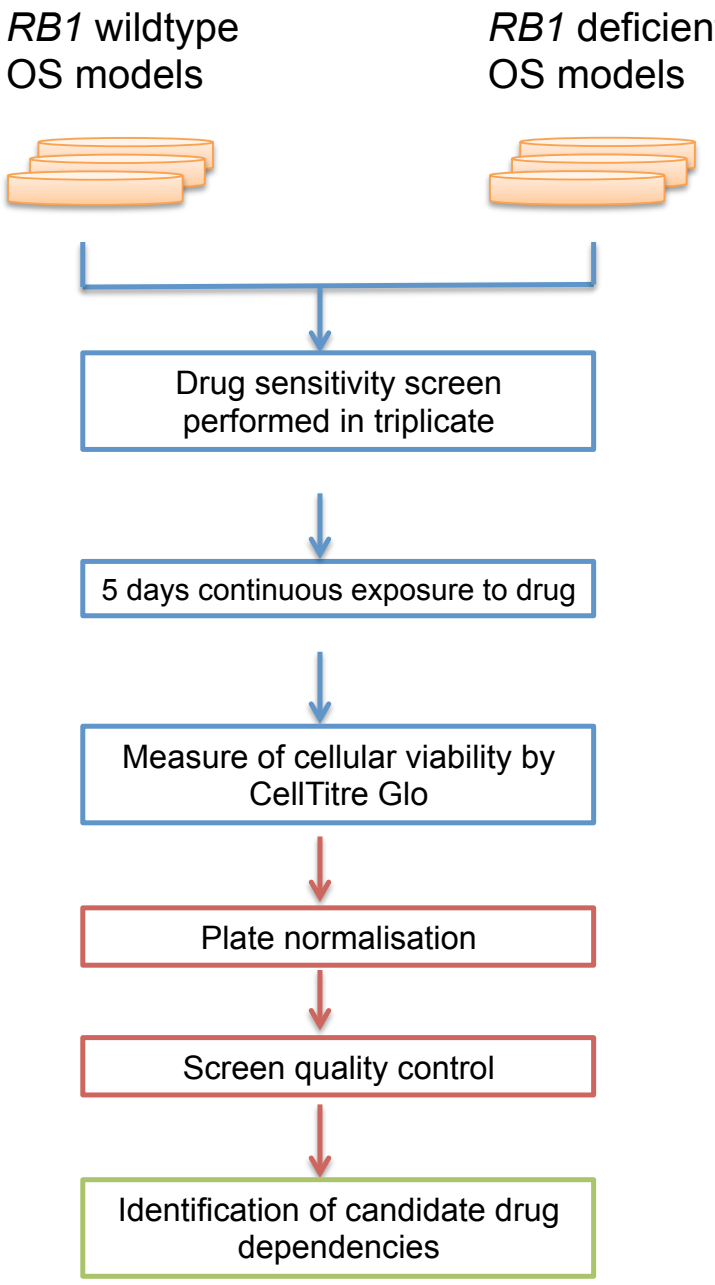

Figure 98 Schematic of high-throughput cell-based drug sensitivity screen overview.
The panel of 18 OS tumour cell lines and isogenic *RB1* deficient U2OS models were screened in triplicate. Cells were arrayed in 384-well plates, and after 24 hours the drug library was added. After five days of continuous drug exposure, cellular viability was estimated using CellTiter Glo reagent via a luminescence assay that measures cellular ATP, described in the methods. The raw data was processed using the CellHTS2 package of the R software suite (BioConductor), plate normalised, and subjected to robust quality control assessment by Spearman's Rank correlation and calculation of Z prime values to determine the dynamic range.

7.2.2 Screen quality control

The quality of the data was examined in a similar way to that of the data generated by siRNA screening already described in section 5.2.3 of Chapter 5. For the drug screen the Z prime (Zhang, Chung & Oldenburg, 1999), was based on positive (100% DMSO treated) and negative (0.2% (v/v) DMSO-treated) control wells in each plate to determine the dynamic range of the screen.

Spearman's Rank Correlation was performed to determine the reproducibility between the plates and was calculated on excel for the 3 combinations of pairs of replicates for each of the 2 drug plates for the main drug screen (Table 2), where a value of one represented strong correlation, and zero no correlation. All cell lines passed the stringent quality control with Spearman's Rank correlation approaching 1 (>0.7) and Z prime >0.3 (Turner, Lord, Iorns, *et al.*, 2008; Iorns, Turner, Elliott, *et al.*, 2008) (Figure 99, Table 18 and Table 19). The main drug library used to screen all 18 OS tumour cell lines and *RB1* deficient isogenic U2OS models, while an additional library (Table 3), was used as an additional screen for the *RB1* deficient isogenic U2OS models. It was possible to identify special abnormalities such as dispensing errors or edge effects using heatplots of CellTiter Glo values using CellHTS (Figure 100).

7.2.3 Raw data analysis

Raw luminescence values were first $\log_2$ transformed and normalised to eliminate the effects of plate-plate variation and adjust for unavoidable errors while maintain biologically relevant variation. Reagent evaporation, edge effects, time differences in the measurement of luminescence, and variation in incubation time could introduce systemic errors (Boutros, Brás & Huber, 2006; Makarenkov, Zentilli, Kevorkov, *et al.*, 2007). Three main approaches could have been employed for data analysis following normalisation: firstly calculation of a Z score statistic, which is a measure of the number of standard deviations from the mean. This was deemed inappropriate since calculation assumes a normal distribution and that the majority of drugs tested have little or no effect on viability. Secondly, normalised percent inhibition (NPI) allows for differential responses to the positive and negative controls between the models. Since 100% DMSO (positive control) lead to an almost complete loss of viability and 0.2% (v/v) DMSO (negative control) had no effect on viability in all models, this approach was not employed. Therefore calculation of the median survival fractions of the three replicates were chosen to identify both

osteosarcoma specific and *RB1* deficient selective effects. The Survival Fraction 50 (SF_{50}), the drug concentration required to elicit a 50 percent inhibition of the cell population, and the SF_{80} (concentration required to elicit an 80 percent inhibition of the cell population) were calculated from the dose response curves using GraphPad Prism. The Area Under the Curve (AUC) for each dose response curve was also calculated using GraphPad Prism. Comparison of SF_{50} and AUC was by a two-sided Student's t-test.

7.2.4 Identification of drug effects in a panel of osteosarcoma tumour cell lines

High-throughput drug screens in the panel of 18 osteosarcoma tumour cell line models demonstrated that the majority of the agents screened had a heterogeneous effect on the viability of osteosarcoma (at a dose of <1000nM thought to be most clinical relevant) with only a couple of OS tumour cell lines showing particular sensitivity or resistance, while the viability of the majority of tumour cell lines was not profoundly affected. Since there is no agreed definition of cellular sensitivity to a drug, an arbitrary cut-off of two or more tumour cell lines with an AUC <0.5 was used to identify drugs to which OS was most sensitive (Figure 101).

Out of these 11 drugs, six were cytotoxic (camptothecin, doxorubicin, gemcitabine, methotrexate, paclitaxel and vinorelbine). Methotrexate and doxorubicin are already incorporated within standard MAP chemotherapy in the treatment of OS. Cisplatin, one of the other standard therapeutic agents using in the treatment of OS, was not included in the drug screen. A number of chemotherapeutics are used for the treatment of advanced OS. Gemcitabine combined with docetaxel is commonly used as treatment for patients with relapsed disease as a study found that 13% of patients had a partial response to the combination, and 43% had stable disease (Palmerini, Jones, Marchesi, *et al.*, 2016). Although docetaxel was not included in this drug screen, the OS tumour cell lines did show sensitivity to another taxane, paclitaxel. Paclitaxel, a microtubule inhibitor, in the form of protein-bound nab paclitaxel is currently in Phase I/II study in children with advanced solid tumours including OS (NCT01962103). Nab-paclitaxel also in combination with gemcitabine is in currently in Phase II trial for patients with advanced sarcoma (NCT02945800).

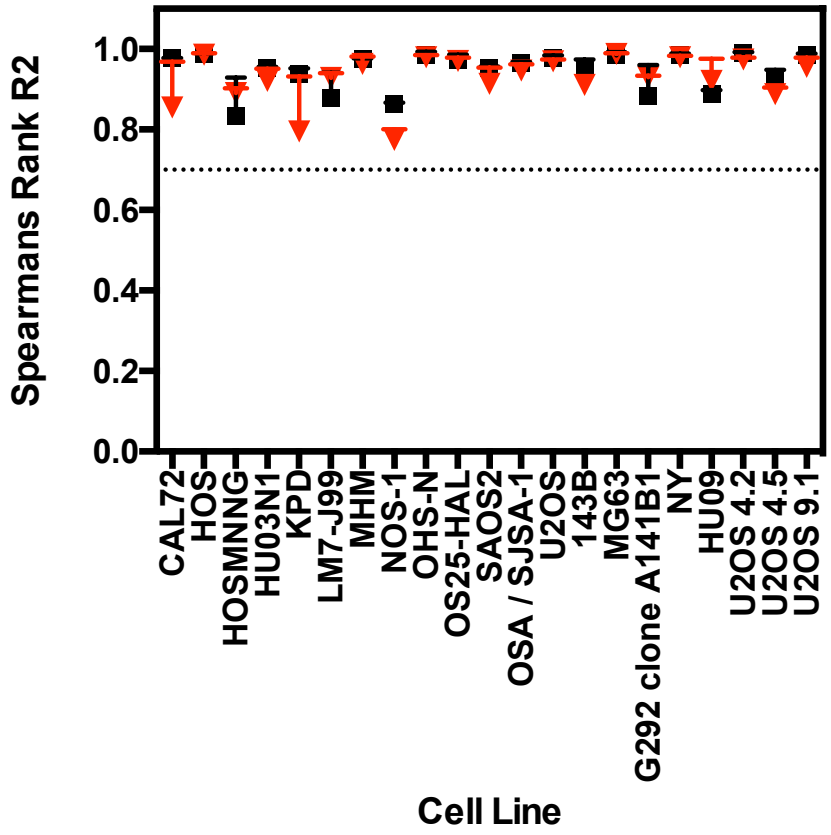

Figure 99 Drug screen quality control: Spearman's R^2 values for both plates of the drug library.

Dot plot illustrating Spearman's rank correlation coefficient values for both drug plates of the drug screen for all OS tumour cell lines including the isogenic *RB1* models engineered by CRISPR-Cas9 mutagenesis in U2OS (4.2, 4.5 and 9.1). All tumour cell lines passed the stringent quality control with Spearman's Rank correlation approaching 1 (>0.7). Mean and range for triplicate replicates are shown. Spearman's Rank Correlation coefficient calculated using GraphPad Prism. [Red: plate one; black: plate two]

Table 18 Drug screen quality control: Z prime scores for main drug screen.

All tumour cell lines passed the threshold of Z prime greater than 0.3.

Cell Line	Mean Z Prime
CAL72	0.69
HU03N1	0.76
HOSMNNG	0.60
OSA/SJSA-1	0.77
NOS-1	0.51
MG63	0.84
SAOS2	0.36
U2OS	0.66
HOS	0.84
OHS-N	0.78
MHM	0.89
OS25-HAL	0.82
LM7	0.58
KPD	0.65
HU09	0.63
NY	0.81
G292 clone A141B1	0.61
143B	0.75
U2OS 4.2	0.71
U2OS 4.5	0.71
U2OS 9.1	0.85

Table 19 Drug screen quality control: Z prime scores for additional drug screen for the isogenic *RB1* deficient U2OS tumour cell line models.

All tumour cell lines passed the threshold of Z prime greater than 0.3.

Cell Line	Mean Z Prime
U2OS 4.2	0.8266
U2OS 4.5	0.7340
U2OS 9.1	0.7206

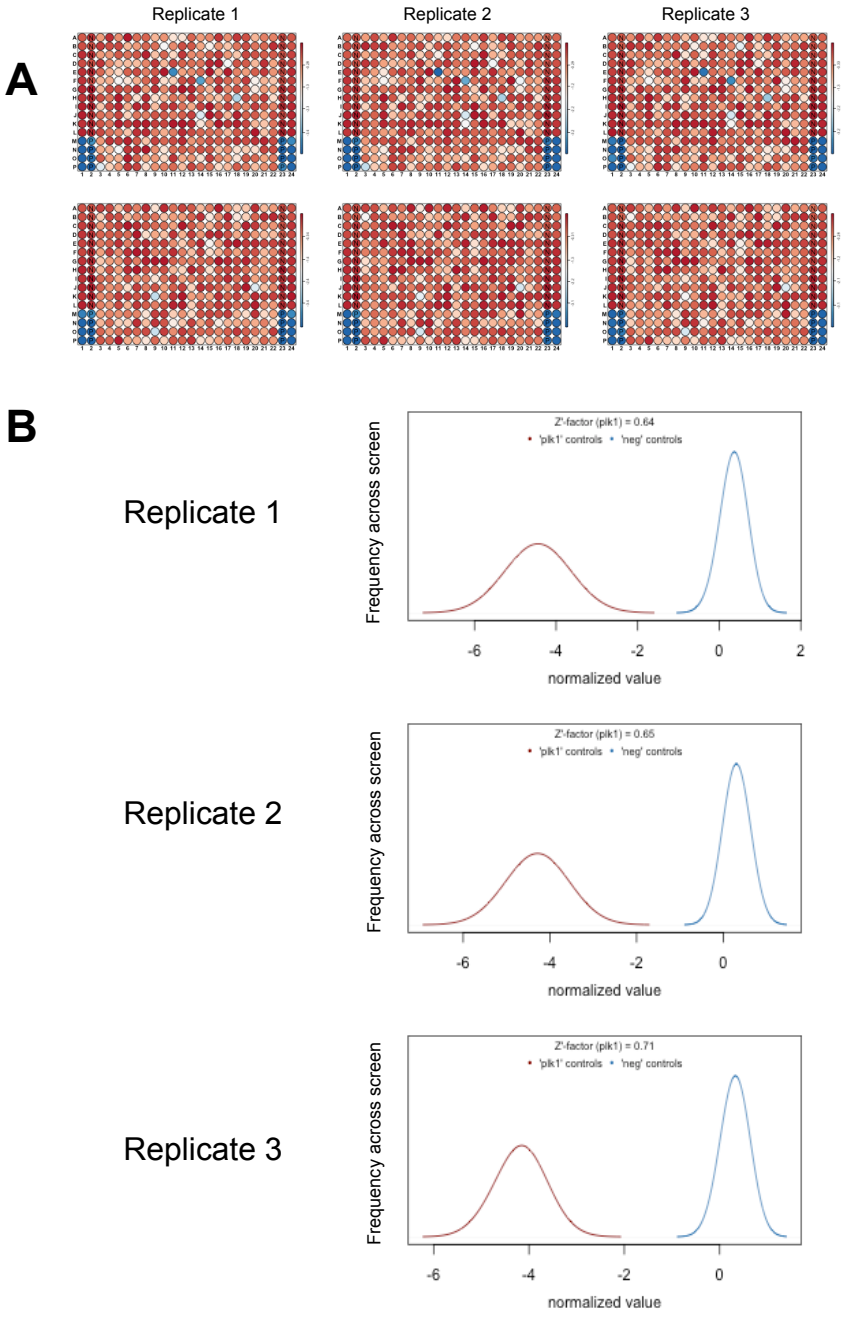

Figure 100 Quality control examples for OS tumour cell line MG63.

(A) Plate plots of raw luminescence intensities of CellTiter Glo values, generated by CellHTS for main drug screen performed in triplicate. These graphical representations provided easy identification of spatial abnormalities due to edge effect or dispensing errors. High cell viability was shown in red, while blue reflected loss of viability.

(B) Distribution blots for each replicate of the separation between negative (0.2% (v/v) DMSO) shown in blue and positive (100% DMSO) controls shown in red, demonstrating a good dynamic range and Z prime values of 0.64, 0.65 and 0.71 respectively.

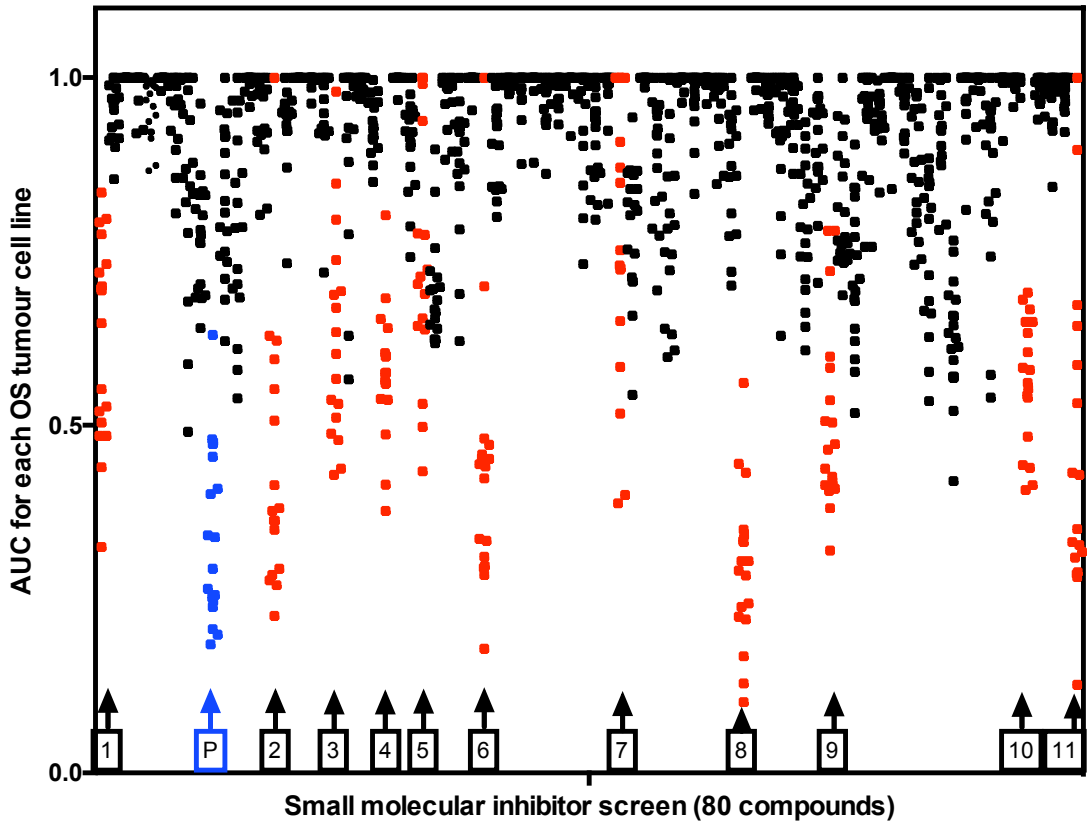

1: 17AAG (HSP90 inhibitor)
2: camptothecin (Topoisomerase inhibitor)
3: dasatinib (Bcr-Abl/Src inhibitor)
4: doxorubicin (Anthracyline)
5: everolimus (mTOR inhibitor)
6: gemcitabine (Anti-metabolite)
7: methotrexate (Anti-metabolite)
8: paclitaxel (microtubule poison)
9: PF-03758309 (PAK inhibitor)
10: vinorelbine (Anti-mitotic)
11: YM155 (Survivin- suppressant)

P: BI2536 (PLK inhibitor)

Figure 101 Drugs to which OS tumour cell lines demonstrated the greatest sensitivity.
Scatter plot of AUC (area under the curve) for each OS tumour cell line. Cells were arrayed in triplicate 384 well plates, and after 24 hours exposed to eighty drugs (0.5-1000nM titration). After five days of continuous exposure, cellular viability was estimated using CellTiter Glo reagent as described in the methods. Highlighted in red are the drugs to which OS tumour cell lines demonstrated the greatest sensitivity (two or more OS tumour cell lines with AUC < 0.5). The internal positive control, BI2536 (PLK inhibitor) was highlighted in blue. AUC were calculated using R. [P: internal positive control]

A number of the agents identified in the screen have already been investigated in OS. Dasatinib an inhibitor of the BCR-ABL fusion gene and SRC previously demonstrated sensitivity in three OS tumour cell lines (143b, HOS and SAOS2) (Hingorani, Zhang, Gorlick, *et al.*, 2009). These tumour cell lines were also represented in this panel and among the most sensitive in this screen. However, no effects on primary or metastatic tumour growth were observed in orthotopic mouse models using an oral dose of 50mg/kg/dose twice daily or intra-peritoneal administration of 25mg/kg/dose daily for four weeks (Hingorani, Zhang, Gorlick, *et al.*, 2009) and so potential clinical translation is unlikely.

Whole-exome sequencing of 59 OS tumour samples, whole genome sequencing of 13 tumour samples, and RNA-sequencing of 35 of the samples identified alterations in the Phosphoinositide-3-Kinase, Catalytic, Alpha Polypeptide / Mechanistic Target Of Rapamycin (PI3K/mTOR) pathway in 24% of patients with OS (Perry, Kiezun, Tonzi, *et al.*, 2014). Perry *et al*. therefore hypothesised that the PI3K/mTOR pathway was a unifying vulnerability required for OS tumour proliferation, which could be exploited therapeutically; they demonstrated sensitivity in four OS tumour cell lines to the dual PIK3CA/mTOR inhibitors GSK2126458 and BEZ235, comparable with the breast cancer cell line MCF7 known to harbour a PIK3CA p.E545K mutation previously established to undergo apoptosis in response to treatment with these inhibitors (Perry, Kiezun, Tonzi, *et al.*, 2014). BEZ235 was included in the drug screen, but a statistically significant difference between AUC for the OS panel compared to the non-osteosarcoma tumour cell line panel was not observed (Figure 102). MCF7 was used as a positive control for sensitivity to BEZ235.

OS tumour cell lines did demonstrate some sensitivity to everolimus, a first generation inhibitor of mTOR (Figure 101), but was not statistically significant compared to the non-osteosarcoma tumour cell line panel (Figure 103). Everolimus in combination with sorafenib, a multi-targeted kinase inhibitor, in Phase II study demonstrated an increased progression free survival time in 17 out of 35 (45%) patients with advanced OS (Grignani, Palmerini, Ferraresi, *et al.*, 2014). Another Phase II trial combined the mTOR inhibitor rapamycin with gemcitabine, and demonstrated a progression free survival rate of 28% in patients with advanced OS (Broto, Redondo, Valverde, *et al.*, 2015). Second generation mTOR inhibitors such as ridaforolimus have demonstrated efficacy in a Phase II study in 212 patients with advanced sarcomas (54 bone sarcomas), with a clinical benefit rate of

28.8%, four patients (two with OS) achieved partial remission (Chawla, Staddon, Baker, *et al.*, 2012). This lead to a Phase III study of maintenance therapy in 702 patients with metastatic sarcomas randomised to receive ridaforolimus or blinded placebo, which found a modest improvement in progression free survival rate (Hazard Ratio 0.72; p = 0.001) (Demetri, Chawla, Ray-Coquard, *et al.*, 2013).

OS tumour cell lines were sensitive to Heat shock protein 90 (HSP90), an evolutionarily conserved molecular chaperone, p-21 activated kinase 4 (PAK4) inhibitor PF-03758309, and the survivin inhibitor YM155. Assessment of these HSP90 inhibitors in OS tumour cell lines and limited mouse models have demonstrated limited efficacy (Hu, Bobb, He, *et al.*, 2015). A Phase I clinical trial of PAK4 inhibitor PF-03758309 in patients with advanced solid tumours was terminated due to pharmokinetic concerns (NCT00932126) and other inhibitors have yet to be studied. Limited *in vitro* studies using the OS tumour cell line MG63, demonstrated that doxorubicin resistant daughter clones had increased expression of survivin compared to the parental tumour cell line, and increased sensitivity to the combination of doxorubicin and YM-155 which was also replicated using a mouse model (Zhang, Zhang, Lv, *et al.*, 2015). Hence, survivin inhibition in pre-treated patients with advanced OS could be therapeutically attractive, but requires confirmation of efficacy in mouse models prior to clinical translation. Confirmation of increased survivin expression could be performed using immunohistochemistry of tumour samples from biobanks such as SARC Biospecimen Bank and at the Royal National Orthopaedic Hospital. BI2536 a PLK (Polo like Kinase 1) inhibitor was used as an internal positive control and demonstrates considerable loss of viability in this screen.

7.2.5 Identification of drugs that selectively target OS tumour cell lines

To investigate the relative sensitivity of the OS tumour panel to these drugs, comparison was made with identical drug screen data from non-osteosarcoma tumour cell lines (n=99 tumour cell lines derived from 10 cancer types) described previously (Figure 104). Although OS tumour cell lines may appear sensitive to an agent in isolation, comparison with the non-osteosarcoma tumour cell line panel highlights the utility of such a data set for contextual comparison, since agents that are universally toxic to all tumour cell lines are most likely to be toxic to non-malignant cells as well. OS tumour cell lines were demonstrated to be significantly more sensitive to the CHK1 inhibitor PF-004477736, and

FGFR1 inhibitors AZD4547 and PD173074 when compared to the non-osteosarcoma tumour cell line panel (Figure 104).

7.2.5.1 OS tumour cell line sensitivity to CHK1 inhibition

The cell cycle checkpoint kinase 1 (CHK1) is a serine/threonine-protein kinase that regulates S and G2/M phases of the cell cycle. It is highly expressed in OS tumours that demonstrate a poor response to neo-adjuvant chemotherapy (Man, Chintagumpala, Visvanathan, *et al.*, 2005) and has a role in the regulation of the DNA damage response and is essential for the repair of double-strand breaks by HR (Dai & Grant, 2010). The CHK1 inhibitor LY2606368 (Prexasertib) and siRNA targeting *CHK1* were observed to cause cell cycle arrest in G1/S and apoptosis (Strauss, Mistry, Mendoza, *et al.*, 2014) in OS tumour cell lines. In addition, sub-toxic concentrations *in vitro* potentiated the effect of methotrexate and doxorubicin and caused significantly more γH2AX than either agent alone concordant with increased DNA damage (Strauss, Mistry, Mendoza, *et al.*, 2014). While single agent LY2606368 significantly delayed tumour growth in a subcutaneous HOSMNNG mouse model (Strauss, Mistry, Mendoza, *et al.*, 2014) and a pulmonary adenocarcinoma xenograft tumour model using the tumour cell line Calu6 (King, Diaz, McNeely, *et al.*, 2015). Replication stress may increase sensitivity to CHK1 inhibition but the underlying mechanism is still unknown.

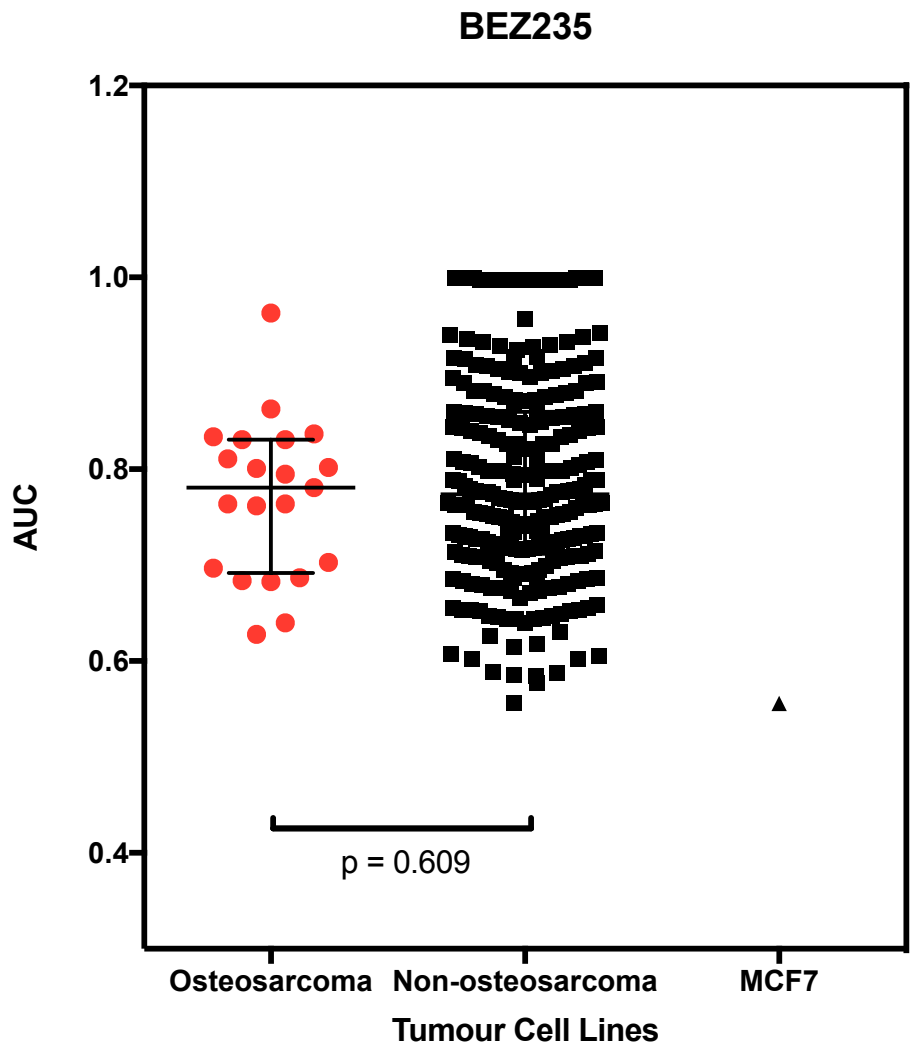

Figure 102 OS tumour cell lines did not exhibit profound sensitivity to BEZ235.

Dot plot illustrating AUC for BEZ235 for osteosarcoma (n = 18), non-osteosarcoma (n = 99) tumour cell lines and MCF7. Cells were arrayed in triplicate 384 well plates, and after 24 hours exposed to the drug library (0.5-1000nM titration). After five days of continuous exposure, cellular viability was estimated using CellTiter Glo reagent as described in the methods. AUC for BEZ235 were calculated using a custom script in R by Aditi Gulati and clustered into OS and non-OS groups. MCF7 used as a positive control with known sensitivity to this agent was shown for comparison. Median and interquartile ranges were shown. P values calculated by the MPT. Osteosarcoma tumour cell lines versus non-osteosarcoma tumour cell lines (p = 0.609).

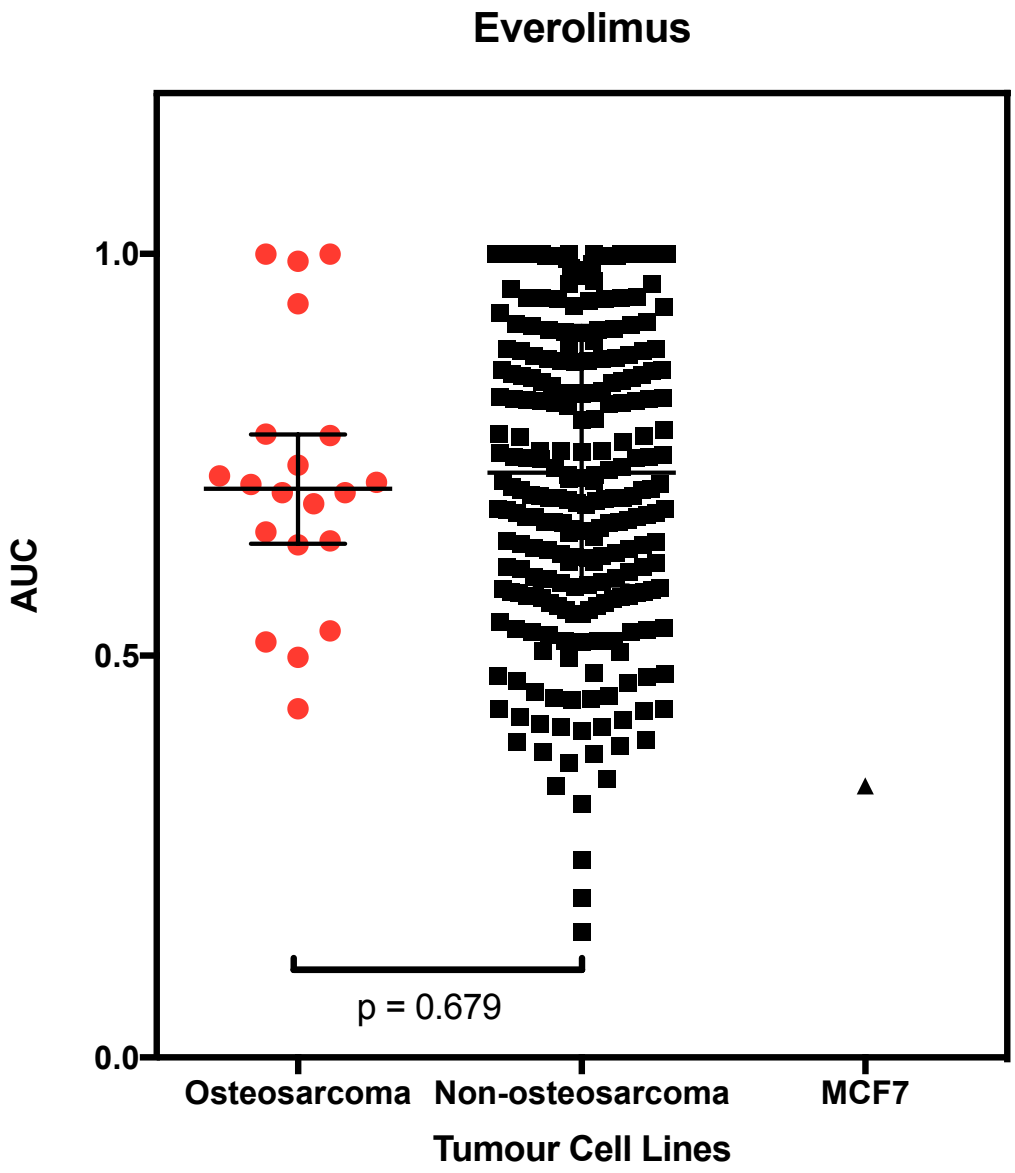

Figure 103 OS tumour cell lines did not exhibit profound sensitivity to everolimus.

Dot plot illustrating AUC for everolimus for osteosarcoma (n = 18), non-osteosarcoma (n = 99) tumour cell lines and MCF7. Cells were arrayed in triplicate 384 well plates, and after 24 hours exposed to the drug library (0.5-1000nM titration). After five days of continuous exposure, cellular viability was estimated using CellTiter Glo reagent as described in the methods. AUC for BEZ235 were calculated using a custom script in R by Aditi Gulati and clustered into OS and non-OS groups. MCF7 used as a positive control with known sensitivity to this agent was shown for comparison. Median and interquartile ranges were shown. P values calculated by the MPT. Osteosarcoma tumour cell lines versus non-osteosarcoma tumour cell lines (p = 0.679).

Figure 104 Comparison of sensitivity to the drug library between OS and non-osteosarcoma tumour cell lines.

Scatter plot of AUC for osteosarcoma tumour cell lines (n = 18: red circles), and non-osteosarcoma tumour cell lines (n = 99: black circles). Highlighted by red boxes are the drugs to which OS tumour cell lines demonstrated the greatest sensitivity, but were not shown to be significantly different from the non-OS panel. Green boxes highlight two FGFR1 inhibitors AZD4547 and PD173074, which were found to be more selective for OS models independent of amplification status, when compared to a subset of the non-OS panel. Also highlighted in green is the CHK1 inhibitor PF-004477736, which was found to be more selective for OS models. The internal positive control, BI2536 (PLK inhibitor) was highlighted in blue. Tumour cells were arrayed in triplicate 384-well plates, and after 24 hours eighty drugs (0.05-1000nM titration) were added. After five days of continuous exposure, cellular viability was estimated using CellTiter Glo reagent as described in the methods. A custom script in R was used by Aditi Gulati to calculate the AUC and generate this scatter plot.

Therefore, the AUC for the CHK1 inhibitor PF-004477736 for the OS and non-osteosarcoma tumour cell line panels were compared to the *BRCA1* deficient breast tumour cell line SUM149, and the *BRCA1* secondary mutant SUM149.B1*.S (c.2288delT, p.N723fsX13) known to restore *BRCA1* function and HR (Dréan, Williamson, Brough, *et al.*, 2017). SUM149 demonstrated considerable sensitivity to the agent, while SUM149.B1*.S was more resistant, suggesting a possible role for HR deficiency in CHK1 inhibitor sensitivity. One of the OS tumour cell lines, NY, was as sensitive as the *BRCA1* deficient SUM149. Two of the OS tumour cell lines LM7 and parental SAOS2 were assessed for an HR defect by assessment of nuclear RAD51 foci formation post IR, described in 7.2.9.1.1. LM7 cells exhibited significantly lower RAD51 foci formation than SAOS2, suggestive of an acquired HR defect. Therefore, to identify if the acquired HR defect of LM7 also predisposed to greater sensitivity to CHK1, tumour cell lines were ranked according to the AUC for the CHK1 inhibitor PF-004477736 (Figure 106). No significant difference in sensitivity was seen between LM7 and SAOS2 and suggests that HR deficiency may not be used as a robust biomarker for CHK1 inhibitor sensitivity.

To identify if the OS tumour cell lines also demonstrated a genetic dependency to *CHK1*, comparison of quantile normalised Z scores from RNAi was made with the non-osteosarcoma tumour cell line panel. A significant difference was not observed (Figure 107). This could reflect the possibility of a false negative within the siRNA screen, or possible off-target effects of PF-004477736 and could be confirmed using small-scale deconvolution with multiple individual siRNA targeting *CHK1,* and drug screen with a structurally different inhibitor of CHK1 such as LY2606368.

7.2.5.2 OS tumour cell line sensitivity to FGFR1 inhibition

The *FGFR1* and *FGFR2* kinase genetic dependencies described in the previous chapter, suggested that osteosarcoma models might be particularly sensitive to small molecule FGFR inhibitors. A sub-set of the non-osteosarcoma tumour cell line panel, consisting of 58 tumour cell lines, that included cell lines with *FGFR1/2* amplification were tested for FGFR inhibitor sensitivity, using two FGFR1 inhibitors AZD4547 (Gavine, Mooney, Kilgour, et al., 2012) and PD173074 (Gavine, Mooney, Kilgour, et al., 2012). These agents were found to be more selective for osteosarcoma models independent of amplification status (AZD4547, $p = 7.6x10-3$, PD173074 $p = 3.9x10-2$) (Figure 108).

The cBioPortal was used to access Comparative Genomic Hybridisation (CGH) data from the Broad Institute CCLE, scored via the GISTIC algorithm to define amplification (score +2) of *FGFR1* (Mermel, Schumacher, Hill, *et al.*, 2011). Amplification data for five OS tumour cell lines (143b, HOS, G292 clone A141B1, U2OS and MB63) was available using this method, and only G292 Clone A141B1 was found to harbour amplification of *FGFR1*. Additionally Fluorescent in situ hybridisation (FISH) was performed by Fernanda Amary on fixed pellets of five OS tumour cell lines, and G292 Clone A141B1, CAL72 and NOS-1 were identified as positive for amplification for *FGFR1* while HU09 and NY were scored as polysomy (Fernanda Amary, Ye, Berisha, *et al.*, 2014). Using data from both these sources, the OS tumour cell line panel was clustered into four groups: (i) positive for amplification; (ii) polysomy (three to five copies); (iii) not amplified; and (iv) unknown amplification status (Table 20). On this basis median dose response curves were plotted (Figure 109) which demonstrated that OS tumour cell lines positive for *FGFR1* amplification were significantly more sensitive to both FGFR1 inhibitors (AZ547 and PD173074) than unknown or non-amplified (ANOVA plus Bonferroni post hoc test $p<0.0001$).

While *FGFR1* amplification in OS tumour cell lines has previously been determined to be a marker of sensitivity to FGFR inhibition by the pan-FGFR inhibitor NVP-BGJ398 (Guagnano, Kauffmann, Wöhrle, *et al.*, 2012), the finding that OS tumour cell lines with *FGFR1* polysomy were also more sensitive to FGFR1 inhibition by two different FGFR1 inhibitors (ANOVA plus Bonferroni post hoc test $p < 0.0001$), suggests that an additional cohort of patients may benefit and adds further weight to the importance of the role of FGFR in OS.

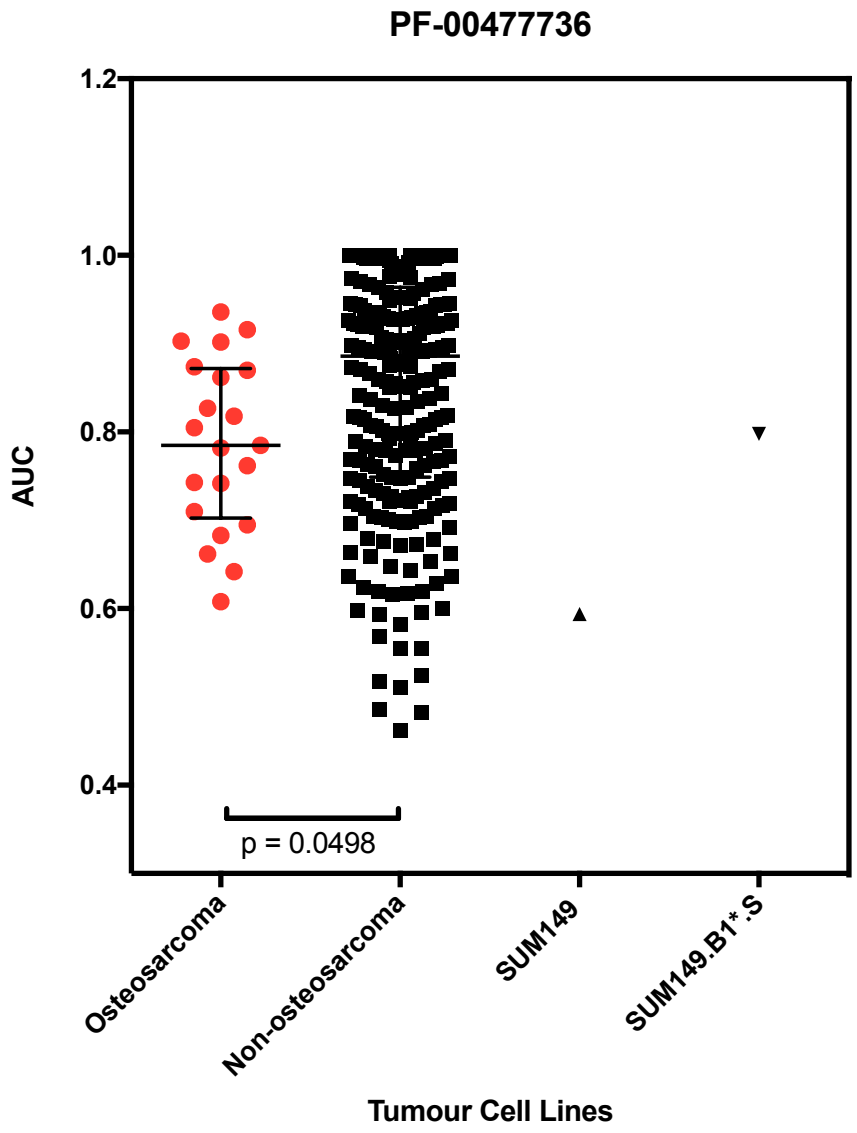

Figure 105 OS tumour cell lines exhibit enhanced sensitivity to CHK1 inhibition by PF004477736.

Dot plot of AUC for PF004477736 for OS (n = 18), non-OS (n = 99), SUM149 and SUM149.B1*.S tumour cell lines. Cells were arrayed in triplicate 384 well plates, and after 24 hours exposed to the drug library (0.5-1000nM titration). After five days of continuous drug exposure, cellular viability was estimated using CellTiter Glo reagent as described in the methods. Comparison was also made with the *BRCA1* deficient breast cancer cell line SUM19 and the *BRCA1* secondary mutant SUM149.B1*.S. The secondary *BRCA1* mutant SUM149.B1*.S (c.2288delT, p.N723fsX13) was engineered by CRISPR Cas9 mutagenesis, which restored the open reading frame of *BRCA1*, restoring *BRCA1* function and HR (Dréan, Williamson, Brough, *et al.*, 2017). Aditi Gulati used a custom script in R to calculate the AUC for PF-004477736. Median and interquartile ranges were shown. P values calculated by the MPT. OS tumour cell lines versus non-osteosarcoma cell lines (p = 0.0498).

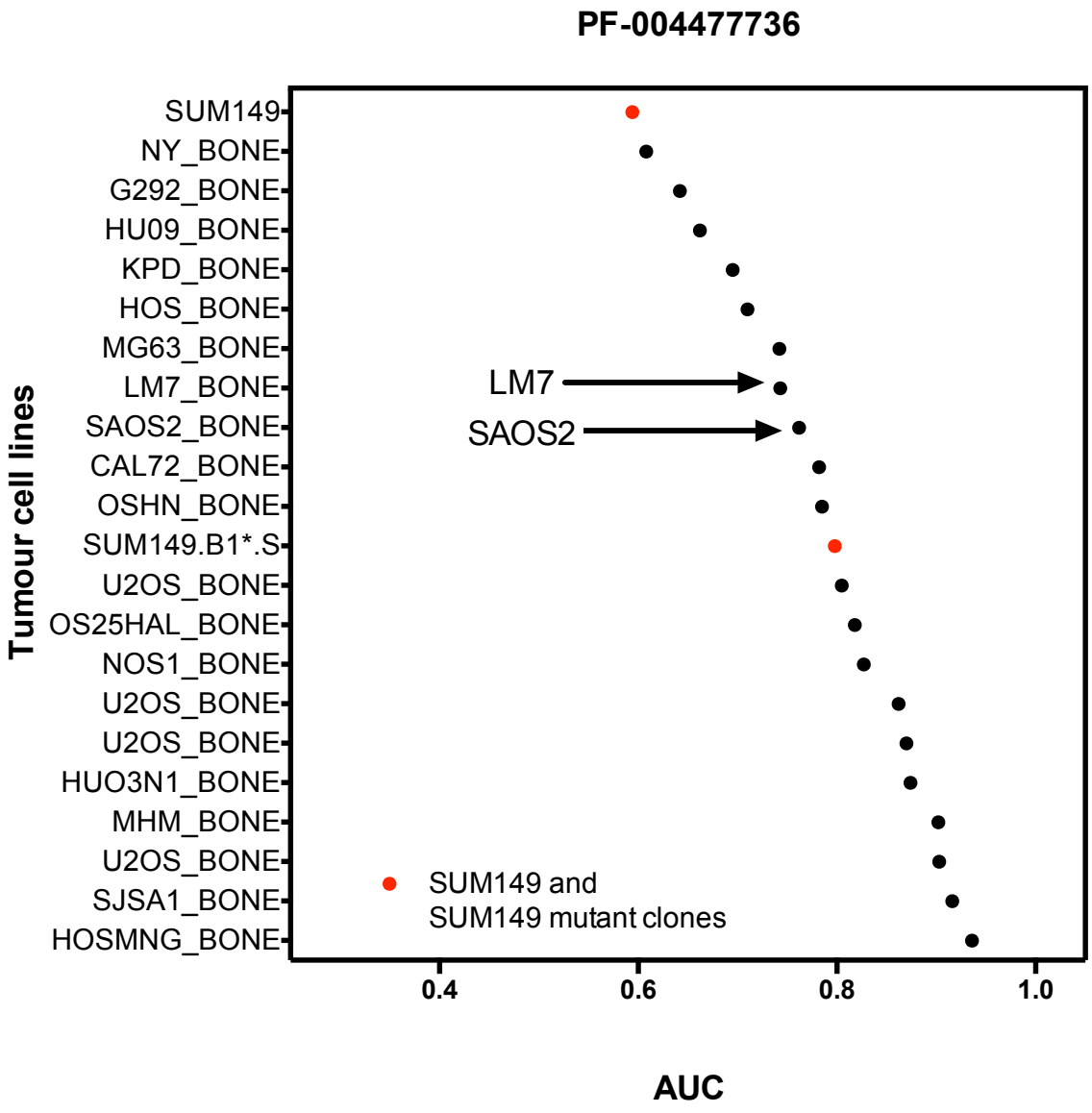

Figure 106 Comparison of CHK1 inhibition in OS tumour cell lines, *BRCA1* deficient SUM149 and secondary *BRCA1* mutant SUM149.B1*.S.

Waterfall plot of AUC for PF004477736 for OS (n = 18), non-OS (n = 99), SUM149 and SUM149.B1*.S tumour cell lines. Cells were plated in 384-well plate format in triplicate, and after 24 hours the drugs (0.5-1000nM titration) were added. After five days of continuous drug exposure, cellular viability was estimated using CellTiter Glo (Promega), as described previously. LM7 the daughter of SAOS2 did not demonstrate acquired sensitivity to PF-04477736 despite an acquired HR defect. The secondary *BRCA1* mutant SUM149.B1*.S (c.2288delT, p.N723fsX13) was engineered by CRISPR Cas9 mutagenesis, which restored the open reading frame of *BRCA1*, restoring *BRCA1* function and HR were highlighted in red (Dréan, Williamson, Brough, *et al.*, 2017). Aditi Gulati used a custom script in R to calculate the AUC for PF-004477736.

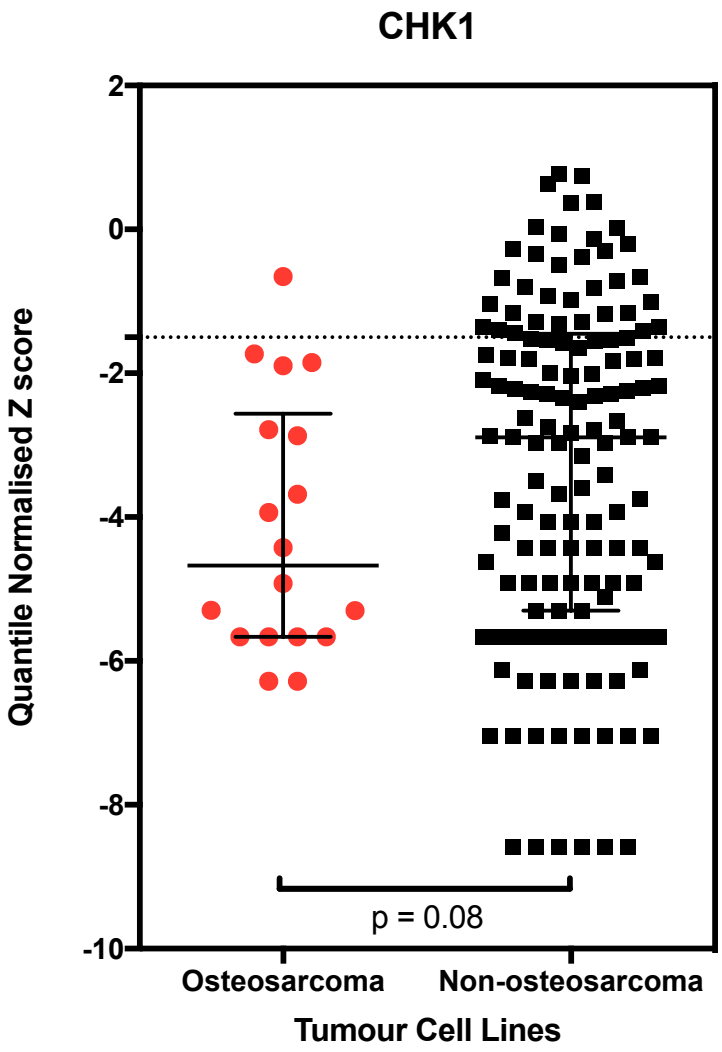

Figure 107 OS tumour cell lines do not exhibit enhanced genetic vulnerability to *CHK1.*
Dot plot of quantile normalised Z score for CHK1 silencing by siRNA in osteosarcoma (n = 18) and non-osteosarcoma tumour cell lines (n = 99). Tumour cell lines were reverse transfected using the siRNA library described in Appendix Tables 1-3. After seven days, cell viability was estimated using the CellTiter Glo reagent as described in the methods. A custom script on R was used to quantile normalise the Z scores across the entire tumour cell line panel by James Campbell (ICR). Tumour cell lines were clustered into two groups, Osteosarcoma and non-osteosarcoma. Median and interquartile ranges were shown. P values calculated by the MPT. OS tumour cell lines versus non-osteosarcoma tumour cell lines (p = 0.08).

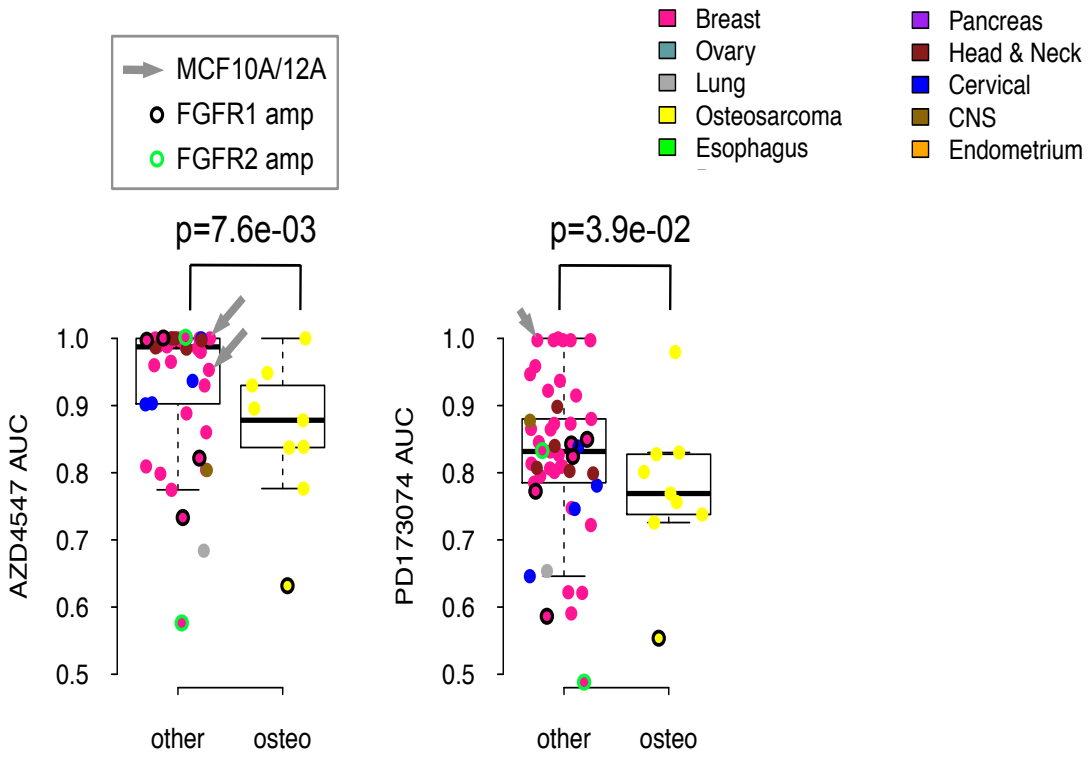

Figure 108 OS tumour cell lines exhibited enhanced sensitivity to FGFR1 inhibitors.

Box plots of AUC for the FGFR1 inhibitors AZD4547 and PD173074 for osteosarcoma (n = 18), and non-osteosarcoma (n = 58) tumour cell lines. Cells were arrayed in triplicate 384-well plates and after 24 hours the drug library (0.5-1000nM titration) was added. After five days of continuous drug exposure, cellular viability was estimated using CellTiter Glo reagent as described in the methods. FGFR1 and FGFR2-amplifed tumour cell lines are indicated with black and green circles, respectively. Grey arrows indicate the non-tumour epithelial cell lines MCF10A and MCF12A. FGFR1 amplification status was described using GISTIC comparative genomic hybridisation values from Broad Institute CCLE only. James Campbell (ICR) calculated AUC, and generated these box plots using a custom script in R. James Campbell (ICR) aslo used the cBioPortal to access the Comparative Genomic Hybridisation data, scored via the GISTIC algorithm to define *FGFR1* in a subset of the cell lines for which the data was available. The top and bottom of each box represents the median and interquartile range, while the whiskers extend to 1.5 times the interquartile distance from the box. P values calculated by use of a one-sided Mann Whitney U test on AUC values. AZD4547 and PD173074 were found to be selective for osteosarcoma models compared to other cancer cell line (AZD4547, $p = 7.6x10^{-3}$, PD173074 $p = 3.9x10^{-2}$). [osteo: osteosarcoma] reproduced from Campbell *et al.* (Campbell, Ryan, Brough, *et al.*, 2016).

Table 20 *FRF1* amplification status using GISTIC data from the Broad Institute CCLE and FISH hybridisation performed by Fernanda Amary (Royal National Orthopaedic Hospital).

Positive for amplification of *FGFR1*	Polysomy of *FGFR1* (3-5 copies)	*FGFR1* amplification not identified	Unknown *FGFR1* amplification status
G292 Clone A141B1	HU09	U2OS	LM7
NOS1	NY	MG63	SAOS2
CAL72		HOS	MHM
		143b	HU03N1
			KPD
			HOSMNNG
			OSA/SJSA-1
			OS25HAL
			OHSN

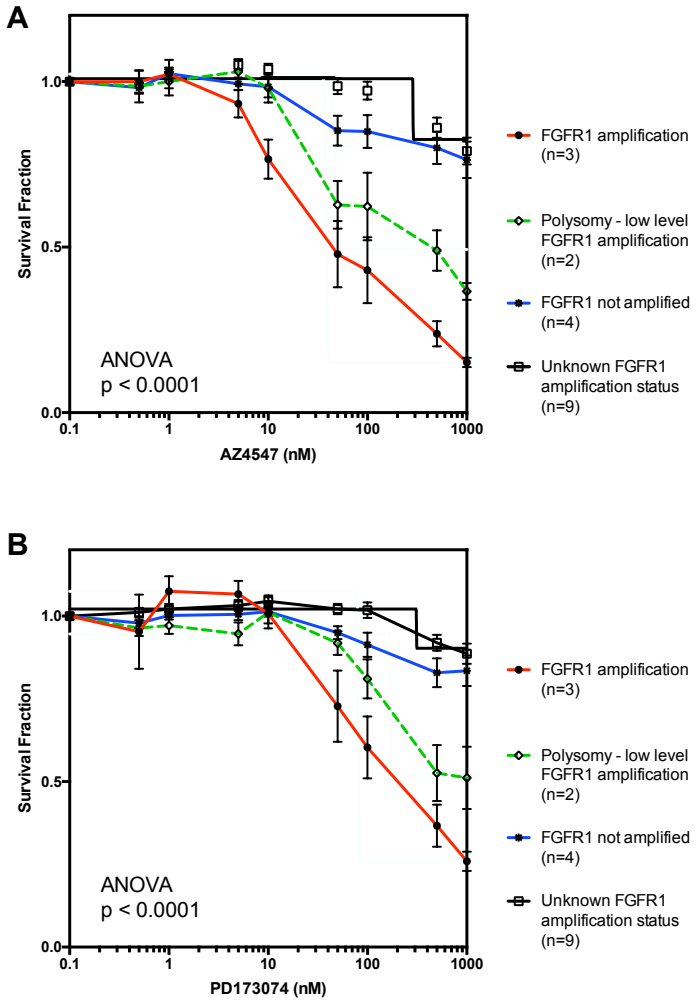

Figure 109 FGFR1 amplification and polysomy are associated with enhanced sensitivity to FGFR1 inhibition by AZ4547 and PD173074.

Dose response survival curves are shown illustrating the median effects for two FGFR1 inhibitors (A) AZ4547 and (B) PD173074 for OS tumour cell lines (n = 18). OS tumour cell lines (TCL) were clustered into groups according to *FGFR1* amplification status using GISTIC CGH data from the Broad Institute and FISH performed by Fernanda Amary. Cells were arrayed in triplicate 384 well plates, and after 24 hours the drug library (0.5-1000nM titration) was added. After five days of continuous drug exposure, cellular viability was estimated using CellTiter Glo reagent as described in the methods. Error bars represent SEM. OS tumour cell lines positive for amplification exhibited enhanced sensitivity to AZ4547 and PD173074 compared to those with an unknown (ANOVA plus Bonferroni post hoc test, $p<0.0001$), or negative amplification status (ANOVA plus Bonferroni post hoc test, $p<0.0001$). OS tumour cell lines positive for polysomy exhibited enhanced sensitivity to AZ4547 and PD173074 compared to those with an unknown (ANOVA plus Bonferroni post hoc test, $p<0.0001$), or negative amplification status (ANOVA plus Bonferroni post hoc test, $p<0.0001$).

Lenvatinib, a multi-targeted kinase inhibitor, is currently in Phase I/II clinical investigation alone and in combination with ifosfamide and etoposide in children and young adults with osteosarcoma (NCT02432274) and although marketed as a VEGFR inhibitor, also inhibits FGFR1 (IC50 = 46nmol/L) (Cabanillas & Habra, 2016). Therefore, the relative sensitivity of OS tumour cell lines to lenvatinib, compared to the non-osteosarcoma tumour cell line panel was investigated, but determined to be non-significant (p=0.06) (Figure 110). However, it was apparent that there was a spectrum of sensitivity to lenvatinib amongst the OS tumour cell line panel. To determine if sensitivity to lenvatinib was determined by *FGFR1* amplification, the OS tumour cell lines were clustered according to the same classification outlined in Table 20 and AUC for lenvatinib compared. Neither OS tumour cell lines with *FGFR1* amplification nor polysomy were significantly more sensitive to lenvatinib than tumour cell lines known to be not amplified (Figure 111). In the absence of a specific inhibitor for vascular endothelial growth factor receptor (VEGFR), a similar analysis was performed using the AUC for cabozantinib, another multi-tyrosine kinase inhibitor with preferential activity against VEGFR2 (IC_{50} 0.035nM), c-MET Proto-Oncogene (c-MET) (IC_{50} 1.3nM), Ret Proto-Oncogene (RET) (IC_{50} 4nM), KIT Proto-Oncogene Receptor Tyrosine Kinase (KIT) (IC_{50} 4.6nM), Fms Related Tyrosine Kinase 1/3/4 (FLT-11/3/4) (IC_{50} 12/11.3/6nM), TEK Receptor Tyrosine Kinase (TIE2) (IC_{50} 14.3nM) and AXL Receptor Tyrosine Kinase (AXL) (7nM), was used to further determine the role of VEGFR inhibition in OS. OS tumour cell lines were not preferentially sensitive to cabozantinib compared to the non-osteosarcoma tumour cell line panel (Figure 110), and *FGFR1* amplification or polysomy did not predict sensitivity (Figure 111). These results are potentially confounded by the multi-tyrosine kinase inhibition of this agent, and further clarification of the role of VEGFR inhibition in OS could be determined using a more specific inhibitor with fewer off target effects. Sorafenib, a multi-kinase inhibitor of Raf1 (IC50 6nM), B-Raf (IC50 22nM) and VEGFR-2 (ICF50 90nM) has already demonstrated some activity in OS in phase II trial (Grignani, Palmerini, Dileo, *et al.*, 2012), but activity may be confounded by Raf inhibition.

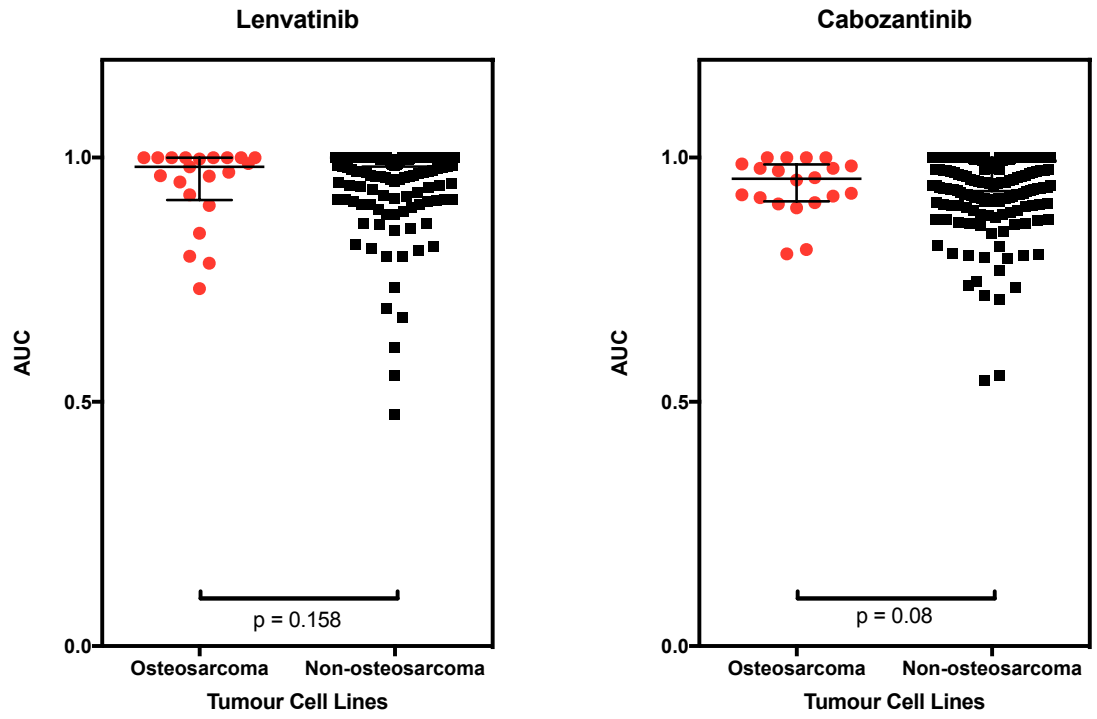

Figure 110 OS tumour cell lines did not exhibit enhanced sensitivity to mulit-targeted kinase inhibitors with preferential activity against VEGFR.

Dot plots are shown illustrating AUC for lenvatinib and cabozantinib clustered into osteosarcoma (n = 18) and non-osteosarcoma tumour cell lines (n = 99). Tumour cells were arrayed in triplicate 384 well plates, and after 24 hours the drug library (0.5-1000nM titration) was added. After five days of continuous drug exposure, cellular viability was estimated using CellTiter Glo reagent as described in the methods. AUC for lenvatinib and cabozantinib were calculated using a custom script in R by Aditi Gulati. Median and interquartile ranges were shown. OS tumour cell lines did not exhibit enhanced sensitivity to lenvatinib (p = 0.158) or carbozantinib (p = 0.08) compared to non-OS tumour cell lines. P values calculated by the MPT.

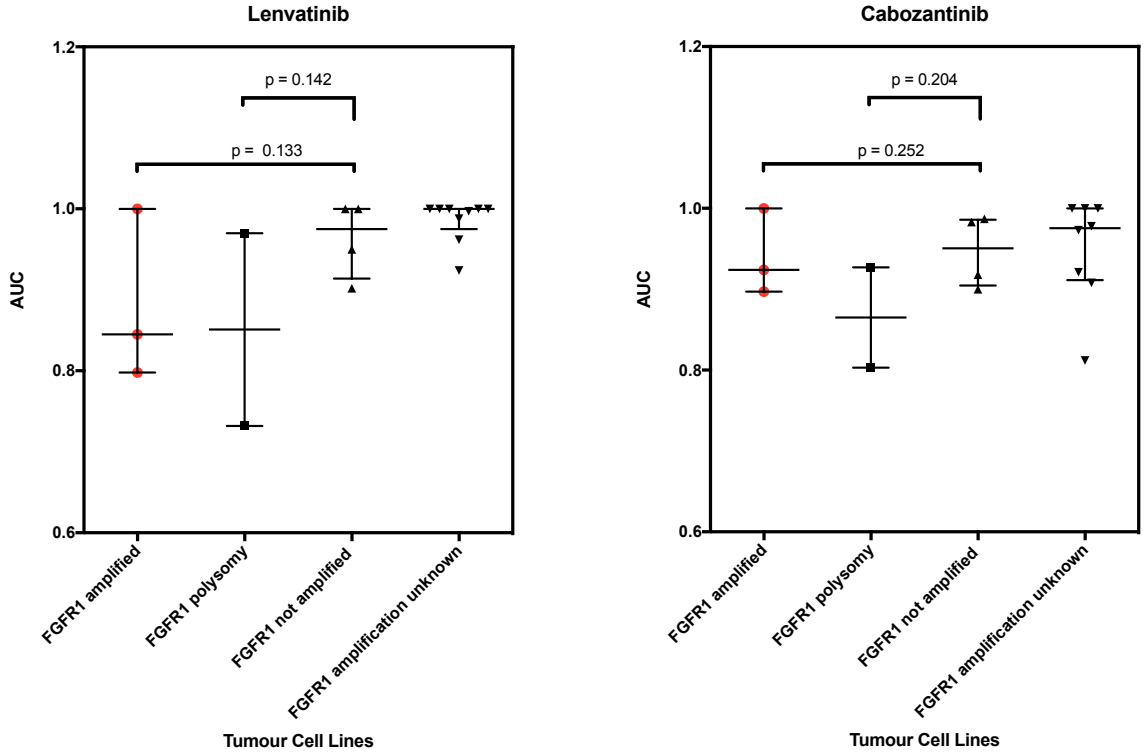

Figure 111 OS tumour cell lines harbouring amplification or polysomy of *FGFR1* did not exhibit enhanced sensitivity to lenvatinib or cabozantinib.

Dot plots are shown illustrating AUC for lenvatinib and cabozantinib. OS tumour cell lines were clustered into groups according to *FGFR1* amplification status using GISTIC CGH data from the Broad Institute and FISH performed by Fernanda Amary. OS tumour cells were arrayed in triplicate 384 well plates and after 24 hours the drug library (0.5-1000nM titration) was added. After five days of continuous drug exposure, cellular viability was estimated using CellTiter Glo reagent as described in the methods. AUC for lenvatinib and cabozantinib were calculated by Aditi Gulati using a custom script in R and clustered according to *FGFR1* amplification and polysomy. Median and interquartile ranges were shown. OS tumour cell lines with *FGFR1* amplification did not exhibit enhanced sensitivity to lenvatinib (p = 0.133) or carbozantinib (p = 0.252) compared to non-amplified OS tumour cell lines. OS tumour cell lines with *FGFR1* polysomy did not exhibit enhanced sensitivity to lenvatinib (p = 0.142) or carbozantinib (p = 0.204) compared to non-amplified OS tumour cell lines. P values calculated by MPT.

7.2.5.3 IGF-1R/IR inhibition in OS tumour cell lines

Dependency on insulin like growth factor 1 receptor (IGF-1R) signalling and activation of IGF-1R by IGF-1 leading to stimulation of the growth of OS tumour cells both *in vitro* (Kappel, Velez-Yanguas, Hirschfeld, *et al.*, 1994) and *in vivo* (Kolb, Gorlick, Houghton, *et al.*, 2008) has been described. Recent findings of insulin like growth factor (IGF) signalling pathway alterations (focal amplification of *IGF1R* (n=3) and *IGF1* (n=2); frameshift indels in *IGF2R* (n=2) and Insulin like growth factor binding protein 5 (*IGFBP5*) (n=1)) in eight out of 112 tumour OS samples which were either whole genome or exome sequenced (Behjati, Tarpey, Haase, *et al.*, 2017), has provided a rationale to further explore this pathway again as a therapeutic target. In targeted blockade of IGR-1R alone, the Insulin Receptor (IR) has been shown to activate the same downstream signalling pathways as IGF-1R (Kuijjer, Peterse, van den Akker, *et al.*, 2013), therefore, targeting both IGF-1R and IR might have greater effect. Given this interest, sensitivity to two dual inhibitors of IGR-1R and IR in the OS tumour cell line panel was investigated. OS tumour cell lines did not show significant sensitivity to the dual IGF-1R and IR inhibitors linsitinib (OSI-906) or GSK1904529A compared to the non-osteosarcoma tumour cell line data (Figure 112). However, a considerable range of sensitivity in the OS tumour cell line panel was observed with exposure to OSI-906 (range AUC 0.701-1).

Two OS tumour cell lines (LM7 and KPD) demonstrated particular sensitivity to linsitinib; LM7 did not harbour mutations or amplification of the IGF pathway members but KPD harbours a missense mutation of unknown significance of IGFBP4 (p.A161V). Therefore, mutation status of all the OS tumour cell lines was used to determine if mutation status of IGF pathway way members predicted sensitivity to linsitinib and GSK1904529A. In the OS tumour cell line panel, point substitution missense mutations of *IGF1R* (n=2: HU03N1, G292 clone A141B1), *IGFBP4* (n=1; KPD), *IGF2R* (n=1; SAOS2), *IGFBP6* (n=1: G292 clone A141B1) and Insulin Like Growth Factor Binding Protein Like 1 (*IGFBPL1*) (n=1; G292 clone A141B1) were identified and are of unknown significance but did predict sensitivity to linsitinib ($p = 0.0286$) but not GSK1904529A (Figure 113). No frameshift, or in/del mutations were identified. Only G292 clone A141B1 was found to have *IGF1R* amplification and was amongst the most sensitive to linsitinib (AUC 0.772) but this observation was not replicated with GSK1904529A.

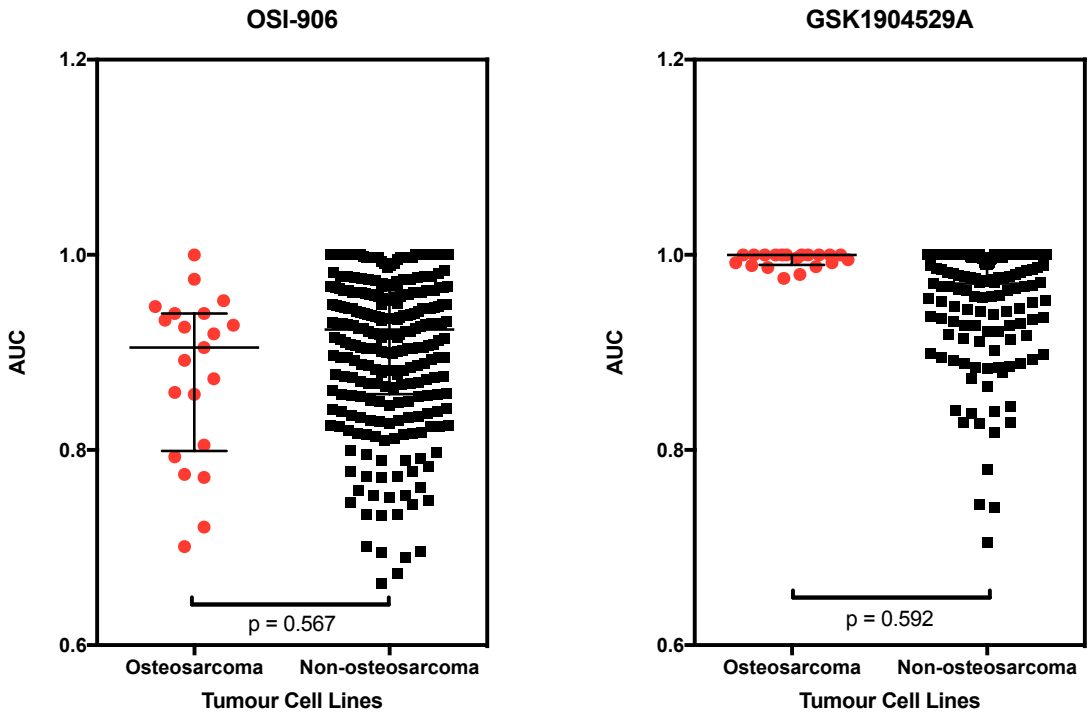

Figure 112 OS tumour cell lines did not exhibit enhanced sensitivity to dual IGF-1R / IR inhibitors.

Dot plots are shown illustrating AUC for OSI-906 and GSK1904592A for OS (n = 18) and non-osteosarcoma (n = 99) tumour cell lines. Tumour cells were arrayed in triplicate 384 well plates, and after 24 hours the drug library (0.5-1000nM titration) was added. After five days of continuous drug exposure, cellular viability was estimated using CellTiter Glo reagent as described previously. Two OS tumour cell lines (LM7 and KPD) demonstrated particular sensitivity to linsitinib; LM7 did not harbour mutations or amplification of the IGF pathway members but KPD harboured a missense mutation of unknown significance of *IGFBP4* (p.A161V). AUC for OSI-906 and GSK1904529A were calculated by Aditi Gulati using a custom script in R and clustered into OS and non-OS groups. Median and interquartile ranges were shown. OS tumour cell lines versus non-osteosarcoma tumour cell lines, OSI-906 (p = 0.567) and GSK1904592A (p = 0.592). P values calculated by the MPT.

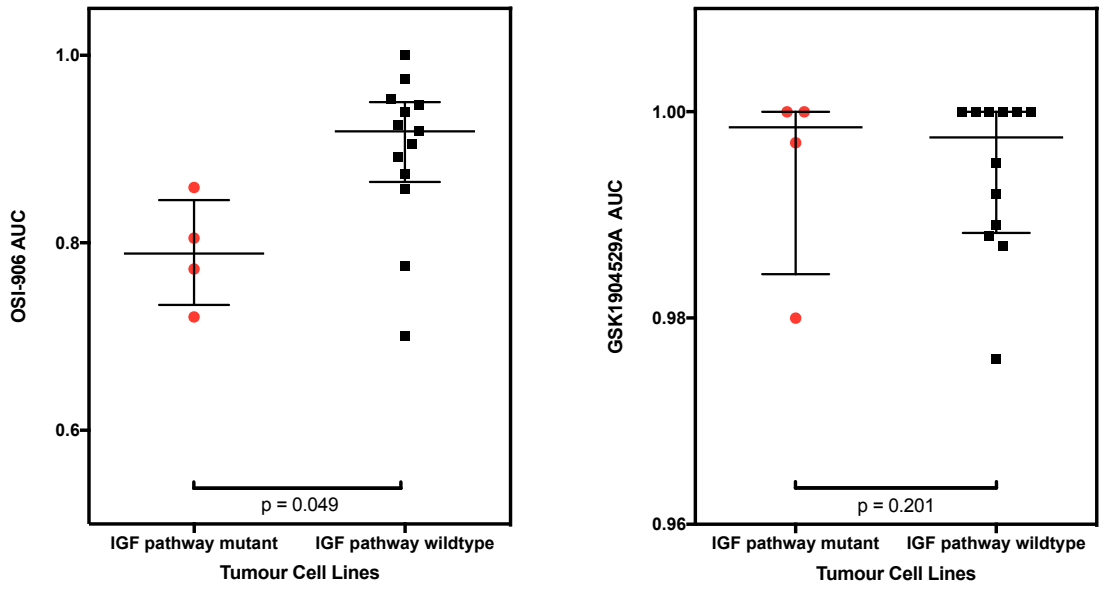

Figure 113 Mutations of the IGF pathway were associated with enhanced sensitivity to OSI-906 but not GSK1904529A.

Dot plots are shown illustrating the AUC for OSI-906 and GSK1904529A for 18 OS tumour cell lines that were clustered according to known mutation status of IGF pathway genes (substitution mutations of *IGF1R* (n=2: HU03N1, G292 clone A141B1), *IGF2R* (n=1; SAOS2), *IGFBP4* (n=1; KPD), *IGFBP6* (n=1: G292 clone A141B1) and Insulin Like Growth Factor Binding Protein Like 1 (*IGFBPL1*) (n=1; G292 clone A141B1). Tumour cells were arrayed in triplicate 384 well plates, and after 24 hours the drug library (0.5-1000nM titration) was added. After five days of continuous drug exposure, cellular viability was estimated using CellTiter Glo reagent as described in the methods. AUC for OSI-906 and GSK1904529A were calculated by Aditi Gulati using a custom R script. Median and interquartile ranges were shown. OS tumour cell lines with mutation of the IGF pathway versus OS tumour cells without known mutation of the IGF pathway, OSI-906 (p = 0.049) and GSK1904592A (p = 0.201). P values calculated by the MPT.

7.2.6 Identification of *CDKN2A* selective drug effects

In order to identify *CDKN2A* deficient selective effects, the median survival fraction (SF) of the *CDKN2A* deficient OS tumour cell lines (n=6) and *CDKN2A* wildtype OS tumour cell lines (n=12) were compared at each drug and concentration. Drugs were ranked according to the difference in median SF between the two cohorts, to identify drugs that had a selective effect on viability in the *CDKN2A* deficient cohort only. *CDKN2A* deficiency was associated with increase sensitivity to methotrexate (ANOVA plus Bonferroni post hoc test p = 0.0109) (Figure 114).

MTAP deficiency is a known sensitiser to methotrexate sensitivity, and is co-located on Chromosome 9 with *CDKN2A.* Cells deficient in Methylthioadenosine Phosphorylase (*MTAP)* by deletion or inactivation via methylation of the *MTAP* promoter are more sensitive to methotrexate (Bertino, Waud, Parker, *et al.*, 2011). Therefore, I hypothesised that *CDKN2A* deficiency in OS tumour cell lines could be used as a surrogate marker for methotrexate sensitivity. To categorise the tumour cell lines into *MTAP* deficient or wildtype groups, proteomic profiling was undertaken (Figure 115). It was possible to segregate the level of MTAP abundance by proteomic profiling into two groups. All cell lines with homozygous deletion of *CDKN2A* (HOS, CAL72, HOSMMNG, 143b, and MG63) had low levels of MTAP and clustered together, except for CAL72. This likely represents the partial loss of *MTAP,* and expression of shorter isoforms of MTAP. It must also be noted that HOSMNNG and 143b are isogenic derivates of the same cell line HOS, and so would be expected to cluster together. As described in section 3.2.4 of Chapter 3, although U2OS was not known to harbour mutations of *CDKN2A*, and had a normal copy number, protein expression of CDKN2A was absent by western blot, and proteomic expression clustered with the other tumour cell lines known to harbour homozygous deletions of *CDKN2A* and hence it was categorised previously as *CDKN2A* deficient. It is therefore, not unsurprising that given that U2OS has wildtype *MTAP*, that out of the *CDKN2A* group, U2OS had the largest AUC for methotrexate.

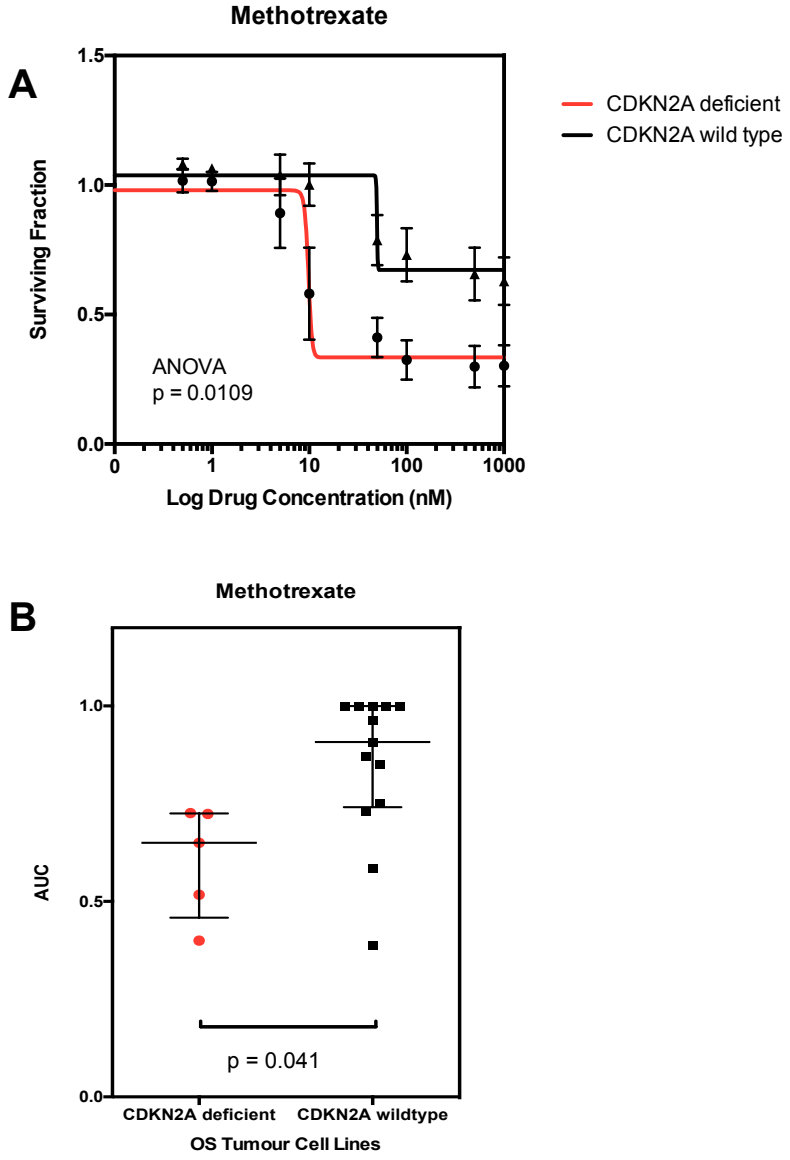

Figure 114 *CDKN2A* deficiency is associated with enhanced sensitivity to methotrexate

Tumour cells were arrayed in triplicate 384 well plates, and after 24 hours the drug library (0.5-1000nM titration) was added. After five days of continuous drug exposure, cellular viability was estimated using CellTiter Glo reagent as described in the methods.

(A) Dose response survival curves illustrating the median effects for *CDKN2A* deficient (n = 5) and *CDKN2A* wildtype (n = 13) OS tumour cell lines. Error bars represent SEM. ANOVA plus Bonferroni post hoc test p = 0.0109 *CDKN2A* deficient versus *CDKN2A* wildtype.

(B) Dot plot illustrating the AUC for methotrexate clustered according to *CDKN2A* deficiency for *CDKN2A* deficient (n = 5) and *CDKN2A* wildtype (n = 13) OS tumour cell lines. Median and interquartile ranges were shown. AUC for methotrexate was calculated using a custom script on R by Aditi Gulati. p=0.0193 *CDKN2A* deficient versus *CDKN2A* wildtype. P values calculated by the MPT.

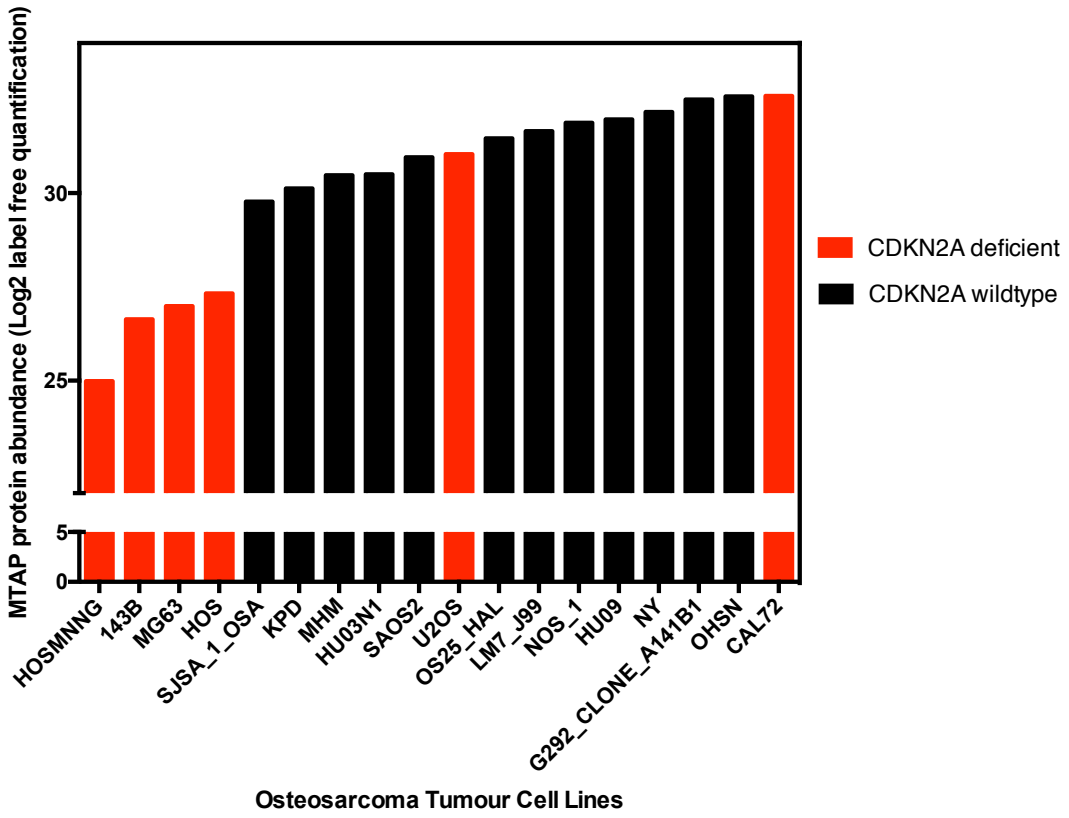

Figure 115 Proteomic abundance of MTAP in osteosarcoma tumour cell lines was significantly lower in *CDKN2A* deficient OS tumour cell lines.

Bar chart illustrating proteomic abundance of MTAP defined by mass spectroscopy performed by Colm Ryan, (Systems Biology, Dublin, Ireland) in the OS tumour cell line panel. Following lysis, protein purification, and tryptic digest, peptides were separated by liquid chromatography and measured by mass spectrometer. Label-free proteome quantification was performed using the MaxQuant software to determine the quantitative abundance of 6696 peptides with a false discovery rate of less than one percent. Red columns indicate tumour cell lines classified as *CDKN2A* deficient by a combination of western blotting, copy number and mRNA expression levels. It was possible to segregate the level of MTAP abundance by proteomic profiling into two groups. All cell lines with homozygous deletion of *CDKN2A* (HOS, CAL72 HOSMMNG, 143b, and MG63) had low levels of MTAP and clustered together, except for CAL72. This likely represented the partial loss of MTAP, and expression of shorter isoforms of MTAP. Although U2OS was not known to harbour mutations of *CDKN2A*, and had a normal copy number, protein expression of CDKN2A was absent, and hence it was categorised as *CDKN2A* deficient. No mutations of MTAP in the tumour cell line U2OS were recorded. p=0.0036 proteomic abundance of MTAP in osteosarcoma tumour cell lines was significantly lower in *CDKN2A* deficient and *CDKN2A* wildtype OS tumour cell lines. P values calculated by Student's t test.

7.2.7 Identification of *RB1* selective drug effects

7.2.7.1 OS tumour cell line panel

In order to identify *RB1* deficient selective effects, the median survival fraction (SF) of the *RB1* deficient OS tumour cell lines (n=6) and *RB1* wildtype OS tumour cell lines (n=12) were compared at each drug and concentration. Drugs were ranked according to the difference in median SF between the two cohorts, to identify drugs that had a selective effect on viability in the *RB1* deficient cohort only. Paclitaxel, vinorelbine and camptothecin were the only drugs with a significant difference ($p<0.05$) at 2 or more concentrations and are shown in Figure 15 and Figure 117. OS *RB1* deficient tumour cell lines were significantly more sensitive to paclitaxel, vinorelbine and camptothecin than those with wildtype *RB1* (ANOVA plus Bonferroni post hoc test $p<0.0001$). To ensure clinical relevance and ascertain relative sensitivity compared to other cancer types, comparison of the AUC for these drugs was made with the data from the non-osteosarcoma tumour cell line panel (Figure 116 and Figure 117). *RB1* deficient OS tumour cell lines all demonstrated relative sensitivity to paclitaxel, vinorelbine and camptothecin when compared to other cancer types. In addition, publically available data from COSMIC drug sensitivity in cancer, (http://www.cancerrxgene.org/translation/Gene/1330) confirmed that a diverse panel of tumour cell lines with a mutation in *RB1* were more sensitive to paclitaxel.

Perturbation of the RB1 pathway is well recognised in small-cell lung cancer (Knudsen & Knudsen, 2008), and increased paclitaxel sensitivity has been correlated with increased E2F3 expression, consistent with deregulation of E2F secondary to deficient *RB1* and absence of un-phosphorylated RB1 which bind the E2Fs (Kurtyka, Chen & Cress, 2014).

Sensitivity to camptothecin in the *RB1* deficient OS tumour cell line SAOS2, has previously been demonstrated due to increased apoptosis (Lauricella, Calvaruso, Carabillò, *et al.*, 2001); expression of exogenous wildtype *RB1* rescued sensitivity, via an anti-apoptotic influence through the control of c-Jun N-terminal kinase (JNK) activity (Lauricella, Calvaruso, Carabillò, *et al.*, 2001). Sensitivity to both paclitaxel and camptothecin demonstrate the mechanistic relevance of these findings in the drug screen.

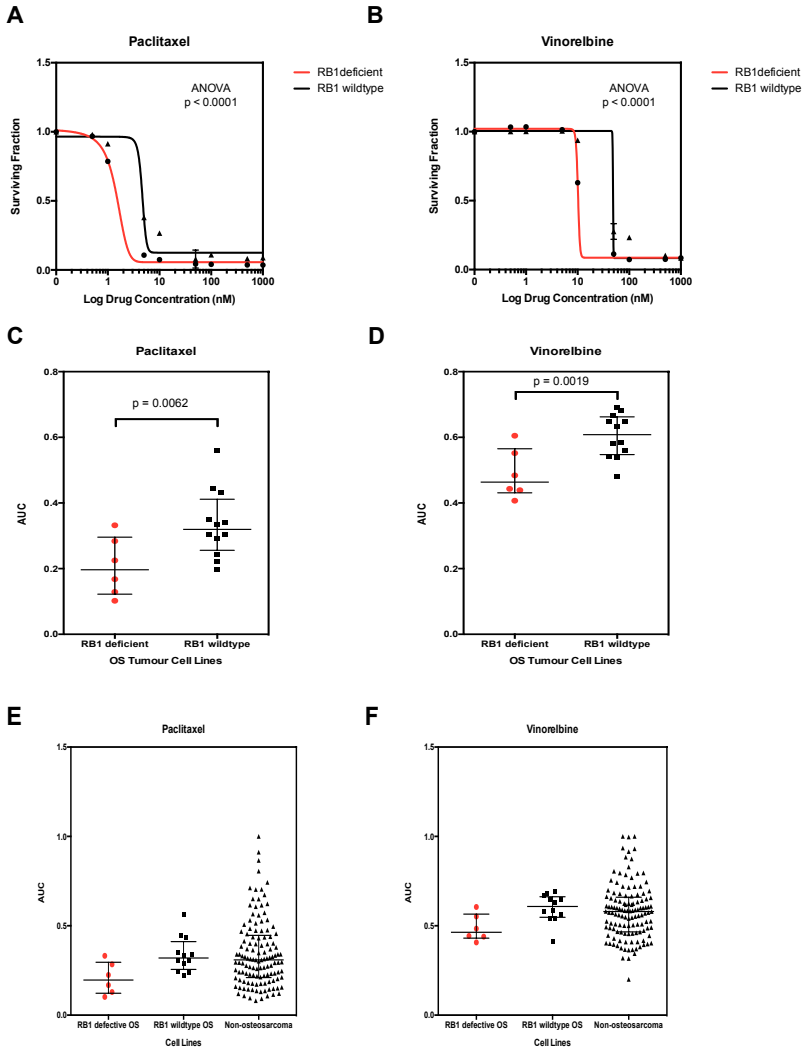

Figure 116 *RB1* deficiency was associated with increased sensitivity to paclitaxel and vinorelbine.

Tumour cells were arrayed in triplicate 384 well plates, and after 24 hours the drug library (0.5-1000nM titration) was were added. After five days of continuous drug exposure, cellular viability was estimated using CellTiter Glo reagent as described in the methods. (A and B) Dose response survival curves illustrating median effects for *RB1* deficient (n = 6) and *RB1* wildtype (n = 12) OS tumour cell lines. Error bars represent SEM. *RB1* deficient versus *RB1* wildtype, paclitaxel (ANOVA plus Bonferroni post hoc test p<0.0001) and vinorelbine (ANOVA plus Bonferroni post hoc test p<0.0001). (B and C) Dot plots illustrating AUC for paclitaxel and vinorelbine for the OS tumour cell line panel. Median and interquartile ranges are shown. *RB1* deficient versus *RB1* wildtype, paclitaxel (p = 0.0062) and vinorelbine (p = 0.0019). P values calculated by Student's t test. (E and F) Dot plots illustrating AUC for paclitaxel and vinorelbine for the OS tumour (n = 18) and non-osteosarcoma (n = 99) tumour cell line panels to demonstrate relative context of sensitivity. Median and interquartile ranges were shown. P values calculated by the MPT.

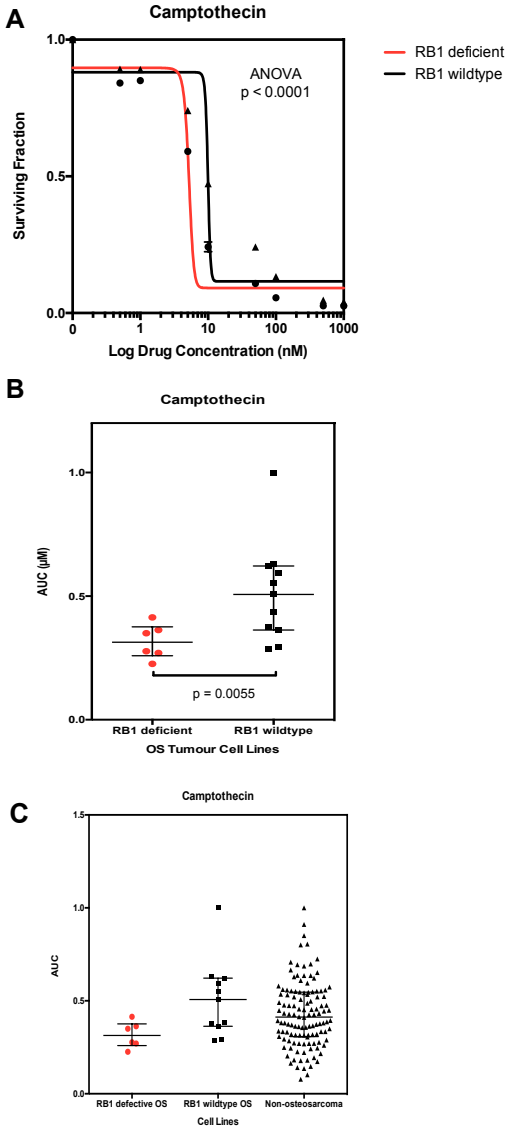

Figure 117 *RB1* deficiency was associated with enhanced sensitivity to camptothecin.

Tumour cells were arrayed in triplicate 384 well plates, and after 24 hours the drug library (0.5-1000nM titration) was added. After five days of continuous drug exposure, cellular viability was estimated using CellTiter Glo reagent as described in the methods. (A) Dose response survival curves illustrating median effects for *RB1* deficient (n = 6) and *RB1* wildtype (n = 12) OS tumour cell lines. Error bars represent SEM. ANOVA plus Bonferroni post hoc test, p<0.0001 *RB1* deficient versus *RB1* deficient. (B) Dot plots illustrating AUC for camptothecin for the OS tumour cell line panel clustered into *RB1* deficient and wildtype groups. Median and interquartile ranges were shown. p = 0.0055 *RB1* deficient versus *RB1* wildtype. (C) Dot plots illustrating AUC for camptothecin (0.5-1000nM range) for the OS tumour (n = 18) and non-osteosarcoma (n = 99) tumour cell line panels to demonstrate relative context of sensitivity. Median and interquartile ranges were shown. P values calculated by the MPT.

7.2.7.2 Isogenic models of RB1 deficiency in osteosarcoma

Given the molecular heterogeneity of the panel of OS tumour cell lines, to determine the drugs with greatest sensitivity in an *RB1* deficient setting, the isogenic *RB1* deficient U2OS models were used. Isogenic *RB1* deficient U2OS models generated by CRISPR-Cas9 mutagenesis and described in Chapter 4 were screened using both drug libraries described in section 2.1.2 of Chapter 2. Statistically significant increased sensitivity in the *RB1* deficient models compared to *RB1* wildtype model, to vinorelbine, camptothecin and paclitaxel were not seen in this screen (data not shown). Similar to limited overlap between the siRNA screens performed on the OS tumour cell line panel and isogenic *RB1* deficient U2OS models, drug sensitivity might be mediated by the other molecular characteristics of the tumour cell U2OS such as *CDKN2A* deficiency, not seen in the OS tumour cell lines with endogenous *RB1* deficiency.

Three groups of inhibitors in the additional drug screen, targeting Heat Shock Protein 90 (HSP90) (Figure 118), kinesin spindle protein (Figure 119), and Nicotinamide adenine dinucleotide (NAD) biosynthesis (Figure 120) showed the greatest difference in sensitivity according to *RB1* status. Unfortunately, because these agents were in the additional drug library, it was not possible to compare these results with the non-osteosarcoma tumour cell line panel data.

7.2.8 DNA damage repair

7.2.8.1 Investigation of sensitivity to small molecule inhibition of ATR and DNA-PK depending on *RB1* context

RB1 deficient tumour cells are known to have defective NHEJ, which combined with concomitant loss of the G1 checkpoint leads to an increase reliance on the HR pathway (Huang, Cook & Mittnacht, 2015). *RB1* deficient tumour cells therefore enter S phase with more unrepaired damage, and could have a greater reliance on functional ATR to delay mitotic entry until all DNA damage repairs have been performed, and the DNA replicated (Nghiem, Park, Kim, *et al.*, 2001). Therefore, *RB1* deficient models of OS were used to determine if *RB1* deficiency is associated with increased sensitivity to ATR and DNA-PK inhibition.

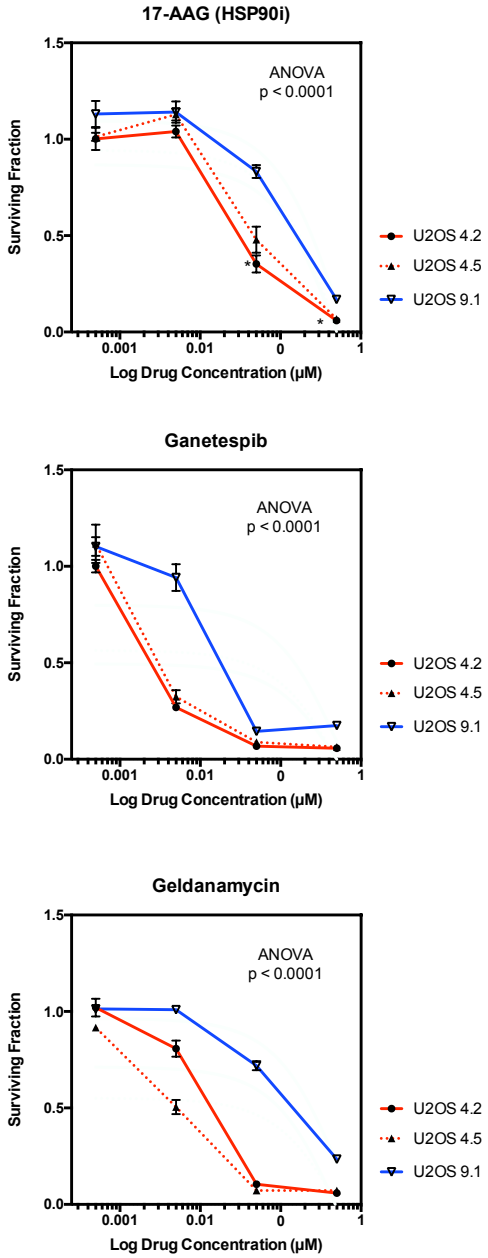

Figure 118 *RB1* deficiency was associated with enhanced sensitivity to HSP90 inhibitors.
Dose response survival curves illustrating the effects of the HSP90 inhibitors (17-AAG, ganetespib and geldanamycin) in the isogenic *RB1* deficient (4.2 and 4.5) and wildtype (9.1) U2OS models. Tumour cells were arrayed in triplicate 384 well plates, and after 24 hours the drug library (0.5-500nM titration) was added. After five days of continuous drug exposure, cellular viability was estimated using CellTiter Glo reagent as described in the methods. Error bars represent SEM. *RB1* deficient versus *RB1* wildtype, 17-AAG (ANOVA, p<0.0001), ganetespib (ANOVA, p<0.0001) and geldanamycin (ANOVA, p<0.0001). [U2OS 4.2 and 4.5 are *RB1* deficient created by CRISPR-Cas9 mediated mutagenesis. U2OS 9.1: *RB1* wildtype parental cell line]

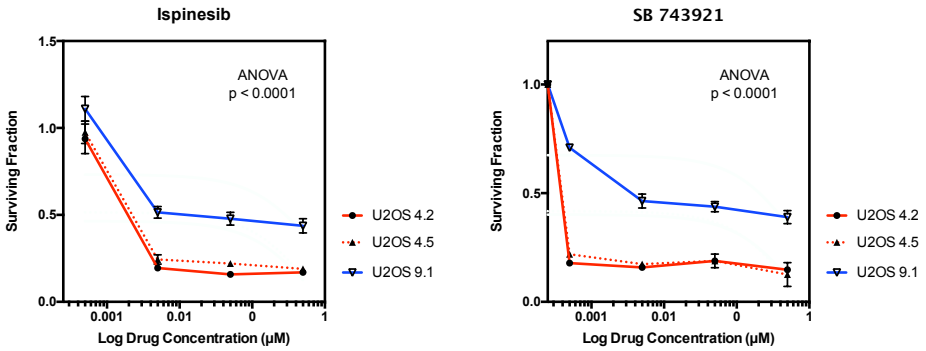

Figure 119 *RB1* deficiency was associated with enhanced sensitivity to kinesin spindle protein inhibitors.

Dose response survival curves illustrating the effects of the kinesin spindle protein inhibitors (ispinesib and SB743921), in the isogenic *RB1* deficient (4.2 and 4.5) and wildtype (9.1) U2OS models. Tumour cells were arrayed in triplicate 384 well plates, and after 24 hours the drug library (0.5-500nM titration) was added. After five days of continuous drug exposure, cellular viability was estimated using CellTiter Glo reagent as described in the methods. Error bars represent SEM. *RB1* deficient versus *RB1* wildtype, ispinesib (ANOVA, p<0.0001) and SB743921 (ANOVA, p<0.0001). [U2OS 4.2 and 4.5 are *RB1* deficient created by CRISPR-Cas9 mediated mutagenesis. U2OS 9.1: *RB1* wildtype parental cell line]

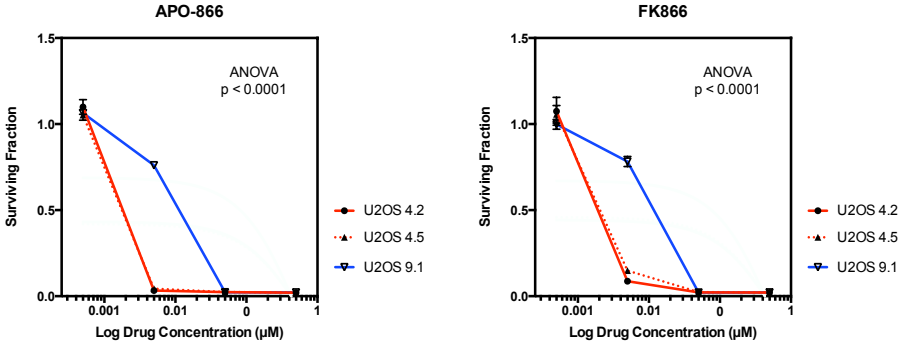

Figure 120 *RB1* deficiency was associated with enhanced sensitivity to NAD biosynthesis inhibitors.

Dose response survival curves illustrating the effects of the NAD biosynthesis inhibitors (APO-886 and FK866), in the isogenic *RB1* deficient (4.2 and 4.5) and wildtype (9.1) U2OS models. Tumour cells were arrayed in triplicate 384 well plates, and after 24 hours the drug library (0.5-500nM titration) was added. After five days of continuous drug exposure, cellular viability was estimated using CellTiter Glo reagent as described in the methods. Error bars represent SEM. *RB1* deficient versus *RB1* wildtype, APO-886 (ANOVA, p<0.0001) and FK866 (ANOVA, p<0.0001). [U2OS 4.2 and 4.5 are *RB1* deficient created by CRISPR-Cas9 mediated mutagenesis. U2OS 9.1: *RB1* wildtype parental cell line]

As described previously, inhibitors of ATR, have been shown in pre-clinical studies to enhance the cytotoxic effects of DNA damaging agents (Williamson, Miller, Pemberton, et al., 2016). Cisplatin, a well recognised chemotherapeutic agent which is part of established therapy for OS (Bacci, Longhi, Fagioli, et al., 2005) that causes DNA crosslinks, which activate several signal transduction pathways including ATR (Siddik, 2003) thus was chosen for combination experiments to investigate whether RB1 deficiency was associated with increased sensitivity to combination therapy with ATR inhibitors. Inhibitors of DNA-PK have already been shown to sensitise tumour cells that depend on NHEJ for survival after induced DSB formation by chemotherapeutic agents such as doxorubicin (Boucher, Hillier, Newsome, et al., 2016; Tang, Yuan & Guo, 2014). As doxorubicin is part of established therapy for OS, it was therefore chosen for combination experiments with DNA-PK inhibition. The clinical aim was to establish if OS tumour cells deficient in *RB1* could be sensitised to cisplatin and doxorubicin by ATR and DNA-PK inhibition respectively.

Generation of an isogenic *RB1* deficient and wildtype model in osteosarcoma by CRIPSR-Cas9 mutagenesis (described in Chapter 4), enabled investigation of the effects of ATR and DNA-PK inhibition in osteosarcoma in an isogenic system. The tumour cell lines were exposed to the ATR inhibitor VX970 and cisplatin, alone and in combination (Figure 121). Exposure to VX970 demonstrated that both *RB1* deficient clones were more sensitive than the *RB1* wildtype parental tumour cell line (ANOVA $p<0.001$). Although *RB1* context did not determine sensitivity to cisplatin, VX970 was found to potentiate the therapeutic effect of cisplatin in both *RB1* deficient clones compared to the parental *RB1* wildtype tumour cell line (ANOVA $p<0.001$).

The isogenic U2OS tumour cell lines were also exposed to the DNA-PK inhibitor VX984 alone and in combination with doxorubicin (Figure 122). No synergy was observed or increased sensitivity depending on *RB1* context.

Using the data generated from siRNA screen of the isogenic *RB1* deficient U2OS models to identify genetic dependencies associated with *RB1* deficiency, the same revalidation criteria as previously were used (median Z score in the group 1 of < -1.5; median Z score in group 2 of > -1.0; probability of the difference between the Z scores in both groups seen by chance of <0.05), *PRKDC,* also known as DNA-PK, was isolated (Figure 123).

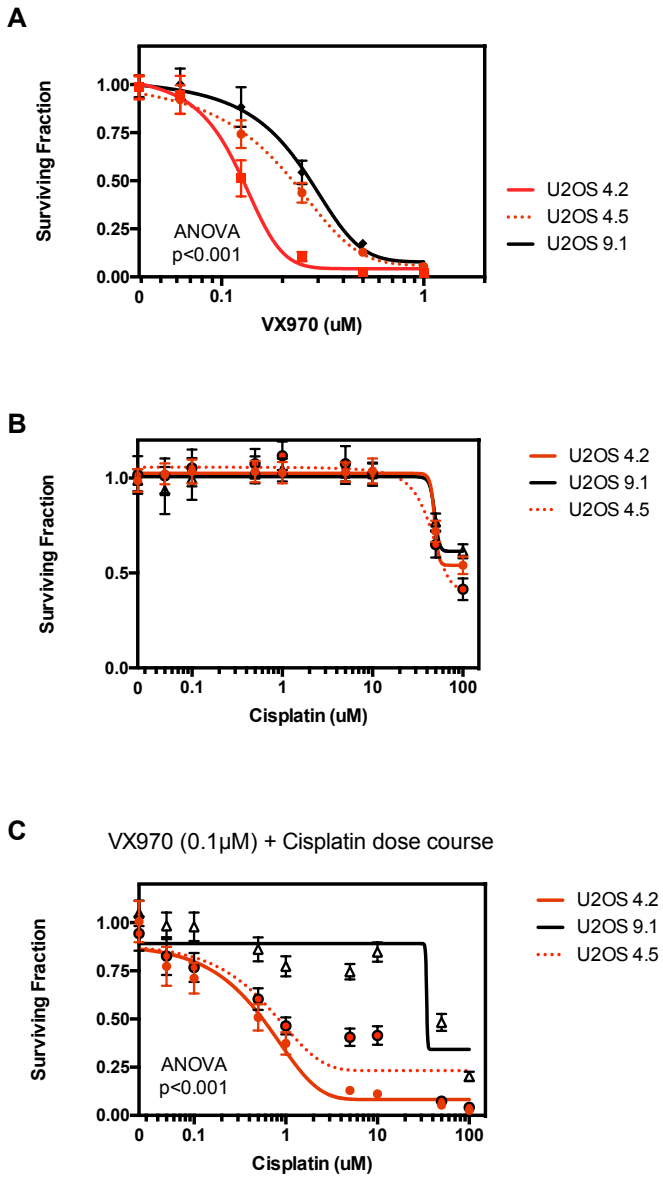

Figure 121 *RB1* deficiency was associated with enhanced sensitivity to VX970 alone and in combination with cisplatin.

Dose response survival curves for (A) VX970 (B) cisplatin (C) cisplatin in combination with 0.1μM VX970.

Cells were arrayed in 384 well plates and after 24 hours the drugs were added. Sixteen replicates for each drug dose were used. After five days of continuous drug exposure, cellular viability was estimated using CellTiter Glo (Promega), as described previously. Error bars represent SEM. *RB1* deficient versus *RB1* wildtype, VX970 (ANOVA p<0.001) and VX970 in combination with cisplatin (ANOVA p<0.001). *RB1* context did not determine sensitivity to cisplatin in these OS tumour cell lines. [U2OS 4.2 and 4.5 are *RB1* deficient created by CRISPR-Cas9 mediated mutagenesis. U2OS 9.1: *RB1* wildtype parental cell line]

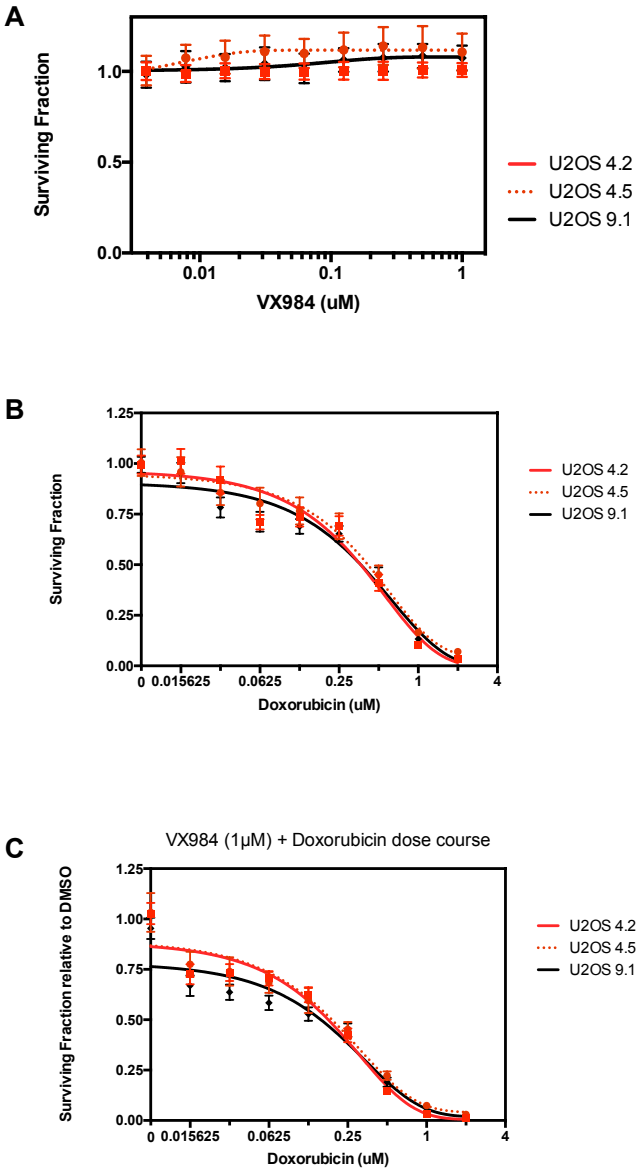

Figure 122 *RB1* deficiency did not determine sensitivity to the DNA-PK inhibitor VX984, doxorubicin, or in combination.

Dose response survival curves for (A) VX984 (B) doxorubicin (C) doxorubicin in combination with 1μM VX970. Cells were arrayed in 384-well plate format, and after 24 hours the drugs were added. Sixteen replicates for each drug dose were used. After five days of continuous drug exposure, cellular viability was estimated using CellTiter Glo reagent as described in the methods. Error bars represent SEM. *RB1* deficient tumour cell lines (U2OS 4.2 and 4.5) did not exhibit enhanced sensitivity to VX984, nor VX984 in combination with doxorubicin, nor doxorubicin alone compared to the *RB1* wildtype (U2OS 9.1) parental tumour cell line. [U2OS 4.2 and 4.5 are *RB1* deficient created by CRISPR-Cas9 mediated mutagenesis. U2OS 9.1: *RB1* wildtype parental cell line]

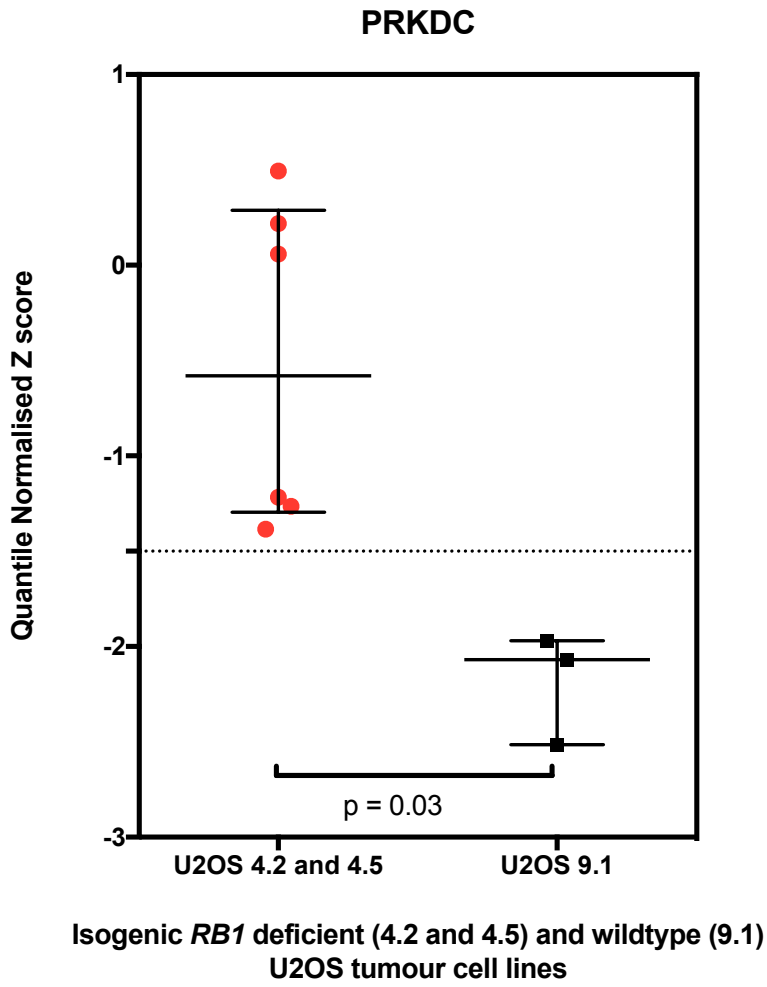

Figure 123 *RB1* deficiency is associated with decreased genetic dependency on *PRKDC* than *RB1* wildtype.

Dot plot illustrating quantile normalised Z scores for *PRKDC* for the isogenic *RB1* deficient (4.2 and 4.5) wildtype (9.1) U2OS tumour cell lines. Loss of *PRKDC* has little effect on viability in the absence of *RB1*. This could be because in the absence of active RB1, NHEJ is defective, so further silencing of *PRKDC* has little additional effect. p = 0.03 *RB1* deficient versus *RB1* wildtype Median and interquartile range shown. P values calculated by the MPT.

Although this effect has yet to be revalidated using deconvolution, it does suggest that silencing of *PRKDC* has little effect on viability in the absence of *RB1*. This could be because in the absence of active RB1, NHEJ is defective, so further silencing of *PRKDC* has little additional effect, concordant with no loss of viability seen with DNA-PK inhibition by VX984.

7.2.9 Investigation of 'BRCAness' in osteosarcoma in cellular models

7.2.9.1 Identification of an isogenic model of PARP sensitivity in osteosarcoma

As described previously in sections 1.1.4.1 and 7.1, given the recent interest in the potential 'BRCAness' phenotype in OS (Kovac, Blattmann, Ribi, *et al.*, 2015; Engert, Kovac, Baumhoer, *et al.*, 2016) the sensitivity of OS tumour cell lines to PARP inhibition was determined. From the drug screen described in 7.2.1 it was apparent that some of the OS tumour panel showed outlying sensitivity to inhibitors of PARP. Tumour cell lines with loss of functions of *BRCA1/2* are associated with an increased sensitivity to PARP inhibition (Bryant, Schultz, Thomas, *et al.*, 2005; Farmer, McCabe, Lord, *et al.*, 2005). To investigate the scale of sensitivity of the OS tumour cell line panel, and provide context for comparison, the OS tumour cell line panel was compared to tumour cell lines with loss of function of *BRCA1/2* as described in Table 18. The triple negative breast tumour cell line SUM149, which harbours a loss of function mutation of *BRCA1* (p.P724fs*12 homozygous), and mutant clones of SUM149 generated by CRISPR-Cas9 mutagenesis with loss of function mutations of *REV7*, *53BP1*, *PARP1* and gain of function of *BRCA2,* which have acquired resistance to PARP inhibition were used as a negative controls for comparison (Table 21). In addition, the pancreatic ductal adenocarcinoma cell line CAPAN1, known to be sensitive to PARP inhibition (Edwards, Brough, Lord, *et al.*, 2008), which harbours a *BRCA2* mutation and mutant daughter clone (CAPAN1.B2*.S), with a secondary mutation of *BRCA2,* which restored the native open reading frame and BRCA2 function were also used as controls. CAPAN1.B2.S* and SUM149.B1.S* have been shown to be profoundly less sensitive to PARP inhibition by olaparib than their isogenic parental cell lines (Figure 124), demonstrated BRCA expression by western blotting, and both demonstrate the ability to form RAD51 foci in response to ionising radiation (Dréan, Williamson, Brough, *et al.*, 2017). Using these tumour cell lines as controls, a good dynamic range was seen in all three PARP inhibitors demonstrating the utility of comparison with the isogenic SUM149 models (Figure 125).

Comparison of the OS tumour cell lines with tumour cell lines derived from 78 other tissue types comprised of breast (n = 42), head and neck (n = 11), synovial sarcoma (n = 5), prostate (n = 4), lung (n= 4), cervical (n = 4), soft tissue (n = 3), large intestine (n = 3), autonomic ganglion (n = 1), and haematological (n = 1), demonstrated a spectrum of sensitivities to PARP inhibition by rucaparib (Figure 126), talazoparib (Figure 127), and olaparib (Figure 128). LM7, daughter of SAOS2, created by repeated passage of SAOS2 through the lungs of nude mice (Jia, Worth & Kleinerman, 1999), demonstrated profound acquired sensitivity to short-term exposure to PARP inhibition, similar to that of triple negative breast tumour cell lines with known loss of function of *BRCA1* such as MDAMB436 and HCC1395. The other OS tumour cell lines demonstrated a spectrum of sensitivity to PARP inhibition (Figure 129).

To further investigate the sensitivity of LM7 and SAOS2, compared to *BRCA1* and *BRCA2* isogenic breast tumour models, longer term drug exposure was performed. The PARP inhibitors olaparib and talazoparib were refreshed twice per week. After two weeks of continuous drug exposure, cellular viability was estimated using CellTiter Glo (Promega), and the survival fractions calculated relative to DMSO (Figure 130). LM7 exhibited comparable olaparib sensitivity to CAPAN1 (ANOVA $p=0.587$) and SUM149 (ANOVA $p=0.183$) but significantly greater sensitivity than CAPAN1.B2*.S cells with a secondary gain of function *BRCA2* mutation (ANOVA $p<0.0001$) and SUM149.B1*.S (ANOVA $p<0.0001$) with secondary *BRCA1* mutation. In addition, LM7 exhibited comparable talazoparib sensitivity compared to SUM149 (ANOVA $p=0.326$), but significantly greater sensitivity than CAPAN1 (ANOVA $p=0.007$), SUM149.B1*.S cells with a secondary *BRCA2* mutation (ANOVA $p<0.0001$) and CAPAN1.B2*.S (ANOVA $p<0.0001$) with secondary *BRCA1* mutation.

Table 21 *BRCA1* or *BRCA2* mutant tumour cells used in PARP inhibitor sensitivity profiling studies.

To assess the scale and context of OS PARP inhibitor sensitivity, breast or pancreatic tumour cell lines with defects in either *BRCA1* or *BRCA2* as positive controls were used.

Tumour cell line	**Histology**	***BRCA gene* alteration**
MDAMB436	Triple negative breast cancer	*BRCA1* c.5277+1G>A splice site, homozygous mutation
SUM149	Triple negative breast cancer	*BRCA1* p.P724fs*12, homozygous mutation (Dréan, Williamson, Brough, *et al.*, 2017)
HCC1395	Triple negative breast cancer	*BRCA1* p.R1751*, homozygous mutation
HCC38	Triple negative breast cancer	*BRCA1* promoter hypermethylation
CAPAN1	Adenocarcinoma of the pancreas	*BRCA2*, p.S1982fs*22, homozygous mutation (Dréan, Williamson, Brough, *et al.*, 2017)

Table 22 Secondary mutant tumour cells used in PARP inhibitor sensitivity profiling studies.

To assess the scale and context of PARP inhibitor resistance in the OS tumour cell line panel, tumour cell lines generated from *BRCA1* or *BRCA2* mutant tumour cells, with secondary mutations engineered by CRISPR-Cas9 mutagenesis, that caused PARP inhibitor resistance were used as negative controls.

Tumour cell line	**Secondary mutation**
SUM149.B1*.S (BRCA1 revertant)	Intragenic mutation in *BRCA1* that restored the native open reading frame (Dréan, Williamson, Brough, *et al.*, 2017)
SUM149 REV7 mutant	Truncating mutation in REV7 (MAD2L2) that causes PARPi resistance (Inga Brandsma, ICR)
SUM149 PARP1 mutant	Missense mutation in PARP1 that causes PARPi resistance (Stephen Pettitt, ICR)
SUM149 53BP1 mutant	Truncating mutation in 53BP1 that causes PARPi resistance (Inga Brandsma, ICR)
CAPAN1.B2*.S (BRCA2 revertant)	Intragenic mutation in *BRCA1* that restored the native open reading frame (Dréan, Williamson, Brough, *et al.*, 2017)

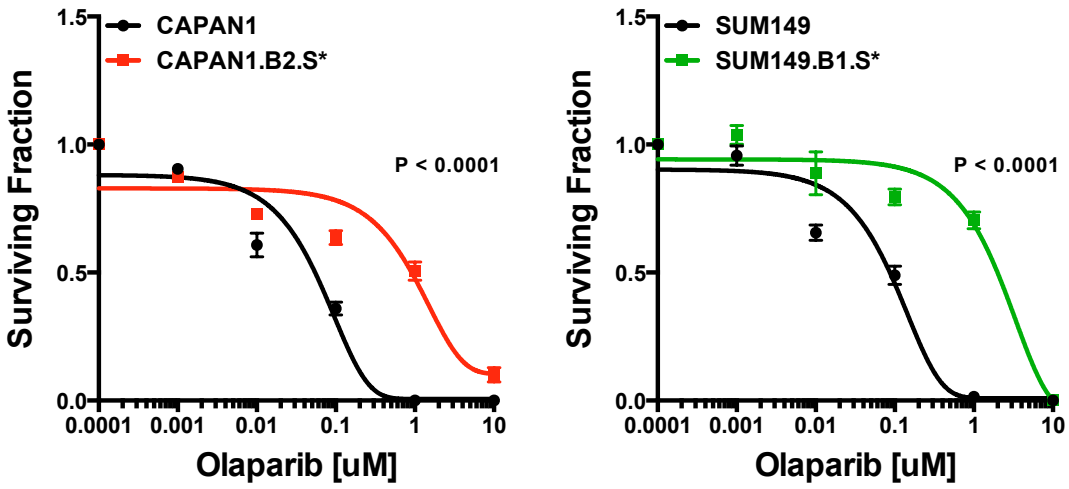

Figure 124 Secondary mutation of *BRCA2* or *BRCA1,* which lead to restoration of function were associated with a significant decrease in sensitivity to PARP inhibition.

Dose response survival curves for olaparib in the isogenic tumour cell lines CAPAN1 and SUM149 were generated by Amy Dréan (ICR). CRISPR-Cas9 mutagenesis by Amy Dréan of the pancreatic ductal adenocarcinoma cell line CAPAN1 (BRCA2 defective: c.6174delT, p.S1982fs*22) and *BRCA1* deficient breast tumour cell line SUM149 *BRCA1* mutant c.2288delT, p.N723fsX13) was used to restore BRCA2 and BRCA1 function respectively, profoundly decreasing sensitivity to olaparib (Dréan, Williamson, Brough, *et al.*, 2017). Cells were arrayed by Amy Dréan in triplicate 384 well plates, and after 24 hours olaparib (0.001-10μM titration) was added. After five days of continuous exposure, cellular viability was estimated using CellTiter Glo reagent as described in the methods. CAPAN1.B2.S* tumour cells exhibited enhanced resistance to olaparib compared to CAPAN1 (ANOVA $p<0.0001$). SUM149.B1.S* tumour cells exhibited enhanced resistance to olaparib compared to SUM149 (ANOVA $p<0.0001$). [Bx.S*: *BRCA* secondary mutation]

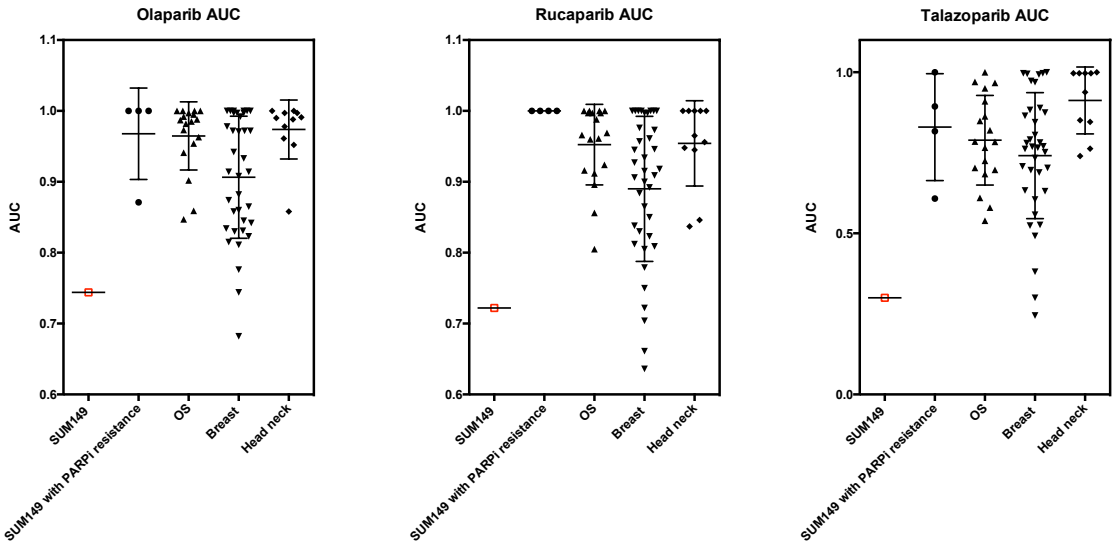

Figure 125 PARP inhibitor sensitivity in tumour cell lines derived from OS, breast cancer or head and neck cancers.

Dot plots illustrating AUC for three different inhibitors of PARP (rucaparib, talazoparib, and olaparib), for the OS tumour cell line panel (n = 18), breast tumour cells (n = 36), and head and neck (n = 11) tumour cell lines. Tumour cell lines were arrayed in triplicate 384 well plates, and after 24 hours exposed to the drug library (0.5-1000nM titration). After five days, cell viability was estimated using CellTiter Glo reagent as described in the methods. Raw luminescence values were plate normalised to account for plate to plate variation and then used to calculate AUC values for each drug in each cell line. Aditi Gulati used a custom script in R to calculate AUC. Median and interquartile range shown.

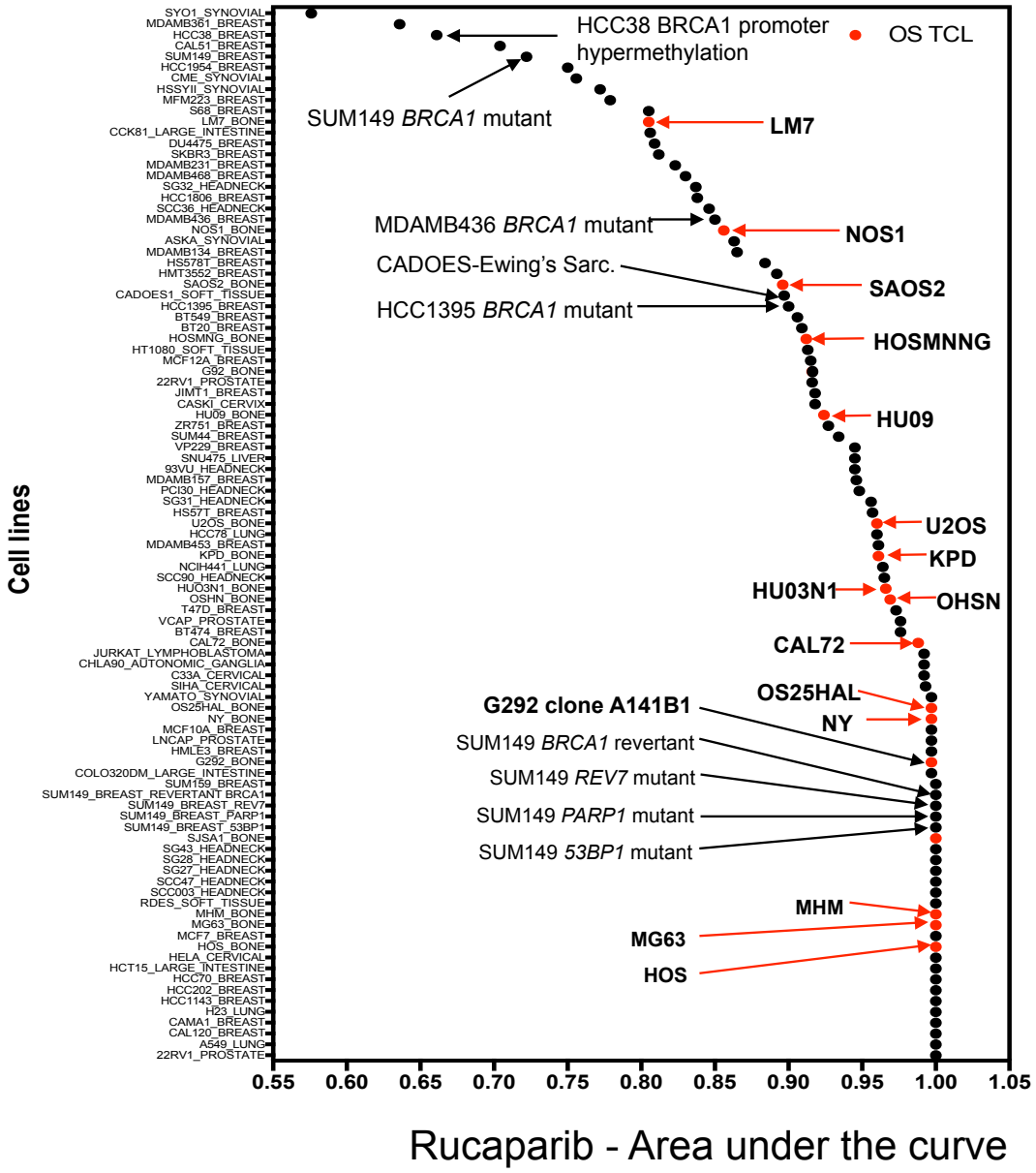

Figure 126 Rucaparib sensitivity in 96 tumour cell lines.

Waterfall plot illustrating rucaparib AUC is shown. Breast tumour cell lines with *BRCA1* alterations are shown, as are SUM149 daughter clones with mechanisms of PARP inhibitor resistance (SUM149 REV7 mutant, PARP1 mutant, 53BP1 mutant and SUM149.B1*.S). Ewing's sarcoma tumour cell lines are also annotated. Osteosarcoma tumour cell lines are highlighted (red dots and bold). Tumour cell lines were arrayed in triplicate 384 well plates, and after 24 hours exposed to the drug library (0.5-1000nM titration). After five days, cell viability was estimated using CellTiter Glo reagent as described in the methods. Raw luminescence values were plate normalised to account for plate to plate variation and then used to calculate AUC values for each drug in each cell line. Aditi Gulati (ICR) used a custom script in R to calculate AUC. Ilirjana Bajrami and Chris Lord (ICR) determined the *BRCA1/2* mutations in the non-osteosarcoma tumour cell line panel.

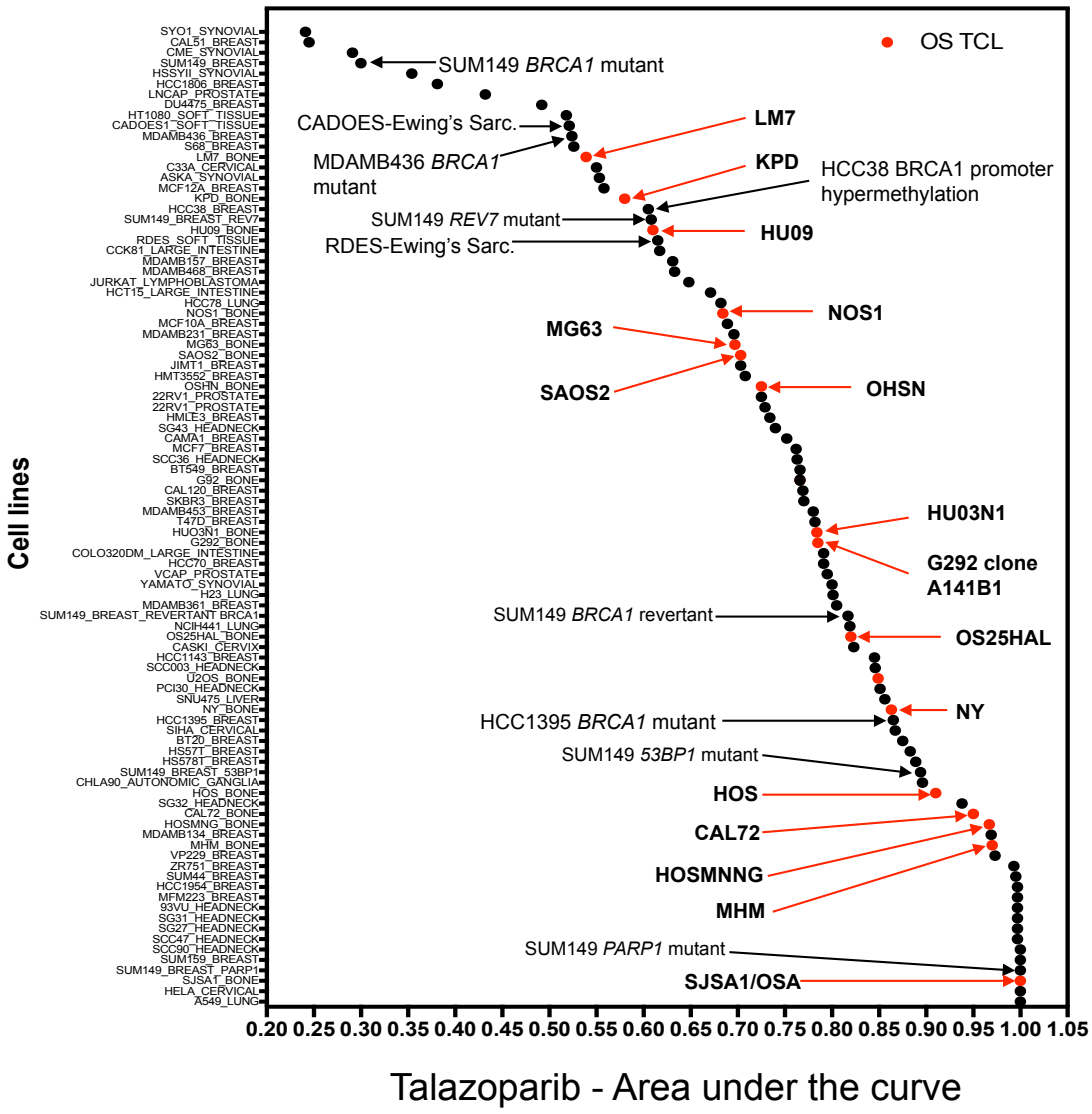

Figure 127 Talazoparib sensitivity in 96 tumour cell lines.

Waterfall plot illustrating talazoparib AUC is shown. Breast tumour cell lines with *BRCA1* alterations are shown, as are SUM149 daughter clones with mechanisms of PARP inhibitor resistance (SUM149 REV7 mutant, PARP1 mutant, 53BP1 mutant and SUM149.B1*.S). Ewing's sarcoma tumour cell lines are also annotated. Osteosarcoma tumour cell lines are highlighted (red dots and bold). Tumour cell lines were arrayed in triplicate 384 well plates, and after 24 hours exposed to the drug library (0.5-1000nM titration). After five days, cell viability was estimated using CellTiter Glo reagent as described in the methods. Raw luminescence values were plate normalised to account for plate to plate variation and then used to calculate AUC values for each drug in each cell line. Aditi Gulati (ICR) used a custom script in R to calculate AUC. Ilirjana Bajrami and Chris Lord (ICR) determined the *BRCA1/2* mutations in the non-osteosarcoma tumour cell line panel.

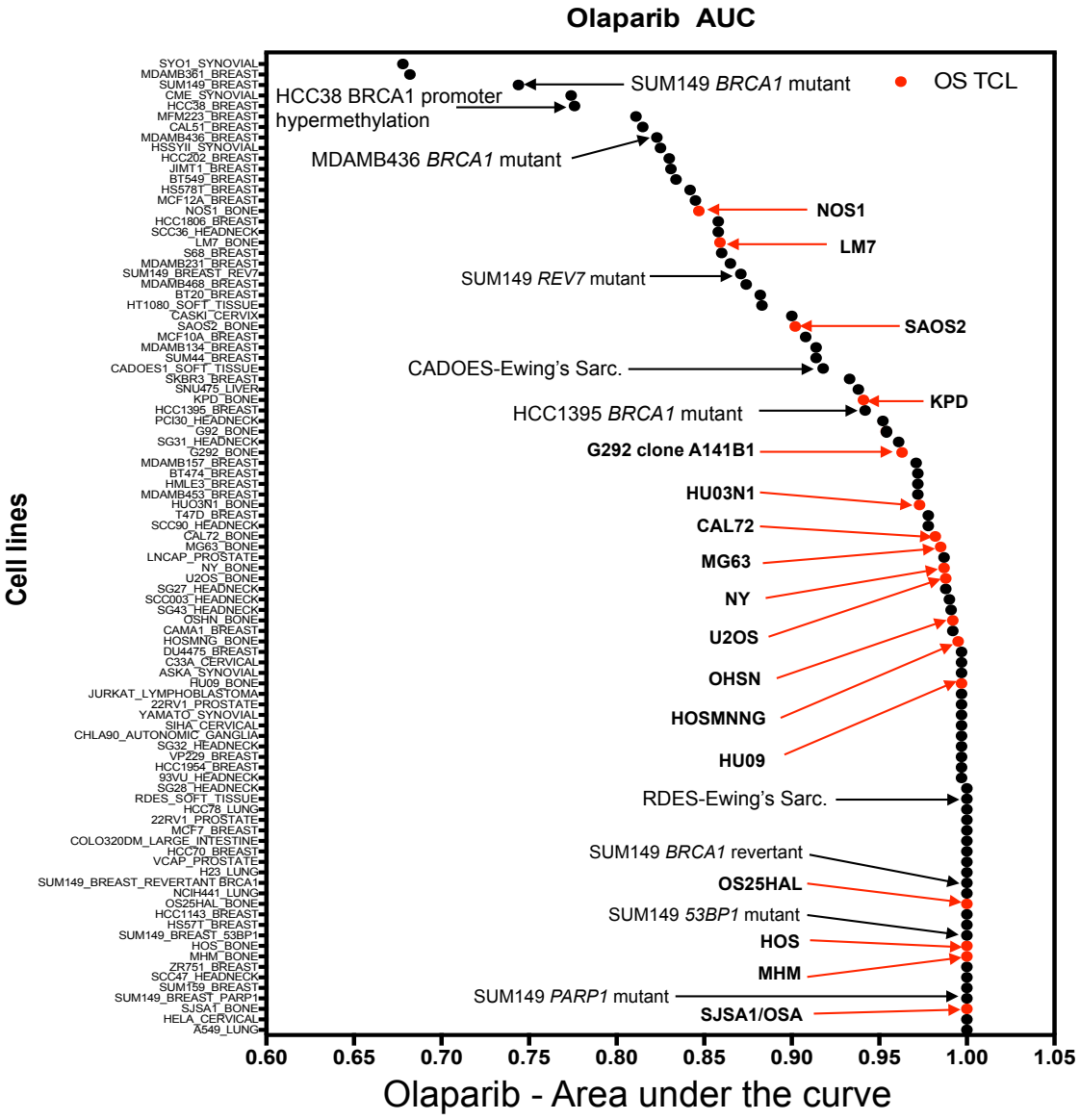

Figure 128 Olaparib sensitivity in 96 tumour cell lines.

Waterfall plot illustrating olaparib AUC is shown. Breast tumour cell lines with *BRCA1* alterations are shown, as are SUM149 daughter clones with mechanisms of PARP inhibitor resistance (SUM149 REV7 mutant, PARP1 mutant, 53BP1 mutant and SUM149.B1*.S). Ewing's sarcoma tumour cell lines are also annotated. Osteosarcoma tumour cell lines are highlighted (red dots and bold). Tumour cell lines were arrayed in triplicate 384 well plates, and after 24 hours exposed to the drug library (0.5-1000nM titration). After five days, cell viability was estimated using CellTiter Glo reagent as described in the methods. Raw luminescence values were plate normalised to account for plate to plate variation and then used to calculate AUC values for each drug in each cell line. Aditi Gulati (ICR) used a custom script in R to calculate AUC. Ilirjana Bajrami and Chris Lord (ICR) determined the *BRCA1/2* mutations in the non-osteosarcoma tumour cell line panel.

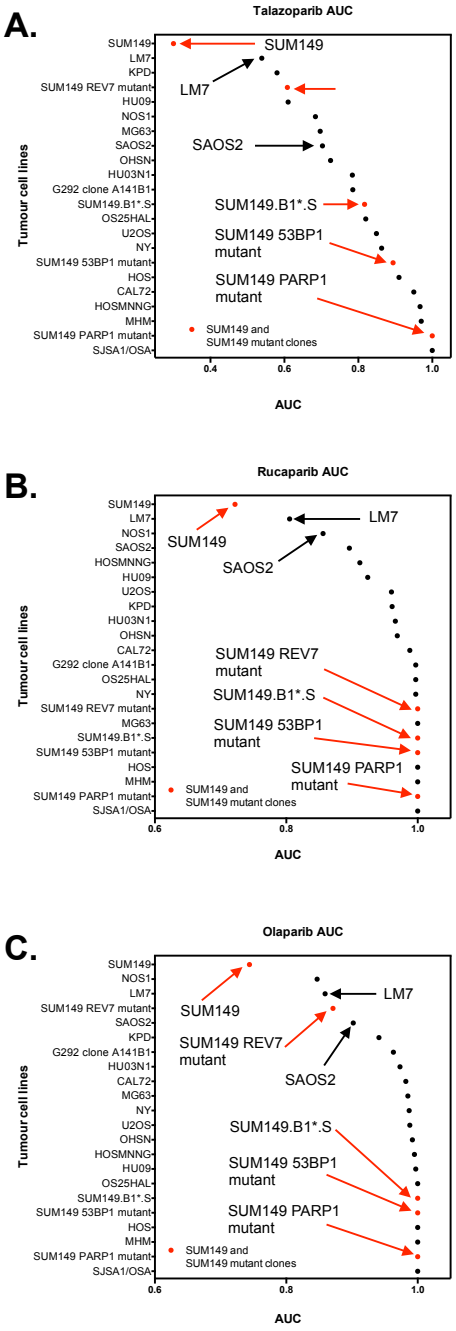

Figure 129 Comparison of PARP inhibitor sensitivity in OS tumour cell lines and SUM149-derived positive and negative controls.

Waterfall plot illustrating AUC for (A) talazoparib, (B) rucaparib, and (C) olaparib. Tumour cells were arrayed in triplicate 384 well plates, and after 24 hours the drug library (0.5-1000nM titration) was added. After five days of continuous drug exposure, cellular viability was estimated using CellTiter Glo reagent as described in the methods. Aditi Gulati used a custom script in R to calculate AUC. LM7 the daughter of SAOS2 demonstrated acquired sensitivity to PARP inhibition by talazoparib, rucaparib and olaparib.

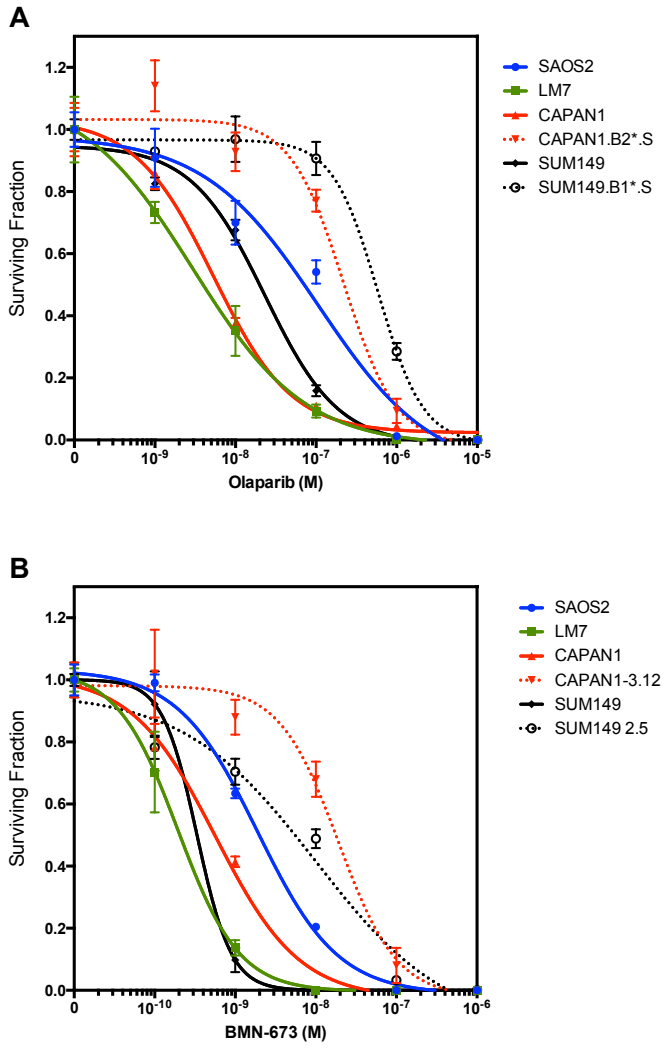

Figure 130 Fourteen day PARP inhibitor survival characteristics in SAOS2 and LM7 compared to *BRCA2* mutant CAPAN1 cells, *BRCA1* mutant SUM149 cells and PARP inhibitor resistant daughter clones.

Tumour cells were plated in a 6-well plate format and continuously exposed to PARP inhibitor for a two-week period at which point cell survival was estimated. Dose response curves from triplicate experiments are shown. Error bars represent SEM.

A. LM7 exhibited comparable olaparib sensitivity to CAPAN1 (ANOVA p=0.587) and SUM149 (ANOVA p=0.183) but significantly greater sensitivity than CAPAN1.B2*.S cells with a secondary *BRCA2* mutation (ANOVA p<0.0001) and SUM149.B1*.S (ANOVA p<0.0001) with secondary *BRCA1* mutation.

B. LM7 exhibited comparable talazoparib sensitivity to SUM149 (ANOVA p=0.326) but significantly greater sensitivity than CAPAN1 (ANOVA p=0.007), SUM149.B1*.S cells with a secondary *BRCA2* mutation (ANOVA p<0.0001) and CAPAN1.B2*.S (ANOVA p<0.0001) with secondary *BRCA1* mutation. [BMN673: talazoparib]

Neither LM7 nor SAOS2 harbour a *BRCA1* or *BRCA2* mutation. Given that SAOS2, the parent of LM7 did not demonstrate the same sensitivity to PARP inhibition, and in the absence of any OS tumour cell lines with loss of function of *BRCA*, this was conceived to have the potential to be an isogenic model for the investigation of PARP sensitivity in osteosarcoma. NOS-1 was reported to have a homozygous missense mutation of BRCA1 (c.154C>T) but this mutation was not postulated to cause loss of function.

Comparison of the relative sensitivity of the panel of OS by use of AUC for talazoparib with data from three OS tumour cells (MG63, SAOS2, and HOSMNNG) reported by (Engert, Kovac, Baumhoer, et al., 2016) did not demonstrate a particular sensitivity to this agent for these tumour cell lines (Figure 129). The AUC for HOSMNNG was very similar to that seen for the SUM149 *PARP1* and *53BP1* mutants, and greater than SUM149.B1*.S, which were used markers of resistance to PARP inhibition.

7.2.9.1.1 Marked decrease in RAD51 foci in LM7

To investigate if the LM7 had an acquired HR defect that could explain increased sensitivity to PARP, γH2AX and RAD51 foci formation were performed in both SAOS2 and LM7. Deficiency of formation of RAD51 foci is known to be a mechanistic determinant of PARP-inhibitor sensitivity (Lord & Ashworth, 2012). CAPAN1 (*BRCA2* deficient) and CAPAN1.B2*.S (*BRCA2* proficient) were used as positive and negative controls. 10Gray of irradiation was used to induce γH2AX foci. Four hours post irradiation the cells were fixed and stained. Confocal microscopy was used to visualise and score the γH2AX and RAD51 foci (Figure 131). After irradiation, γH2AX foci formation was increased in all cell lines, reflecting DSBs consistent with genotoxic stress. RAD51 foci, critical to HR (Tarsounas, Davies & West, 2004) were observed post irradiation only in SAOS2 and CAPAN1.B2*.S. *BRCA2* acts as a co-factor for RAD51, and is critical to HR, in accordance with the absence of RAD51 foci seen in the CAPAN1 tumour cells. LM7 also failed to form RAD51 foci in the presence of γH2AX foci post irradiation, suggestive of an HR defect.

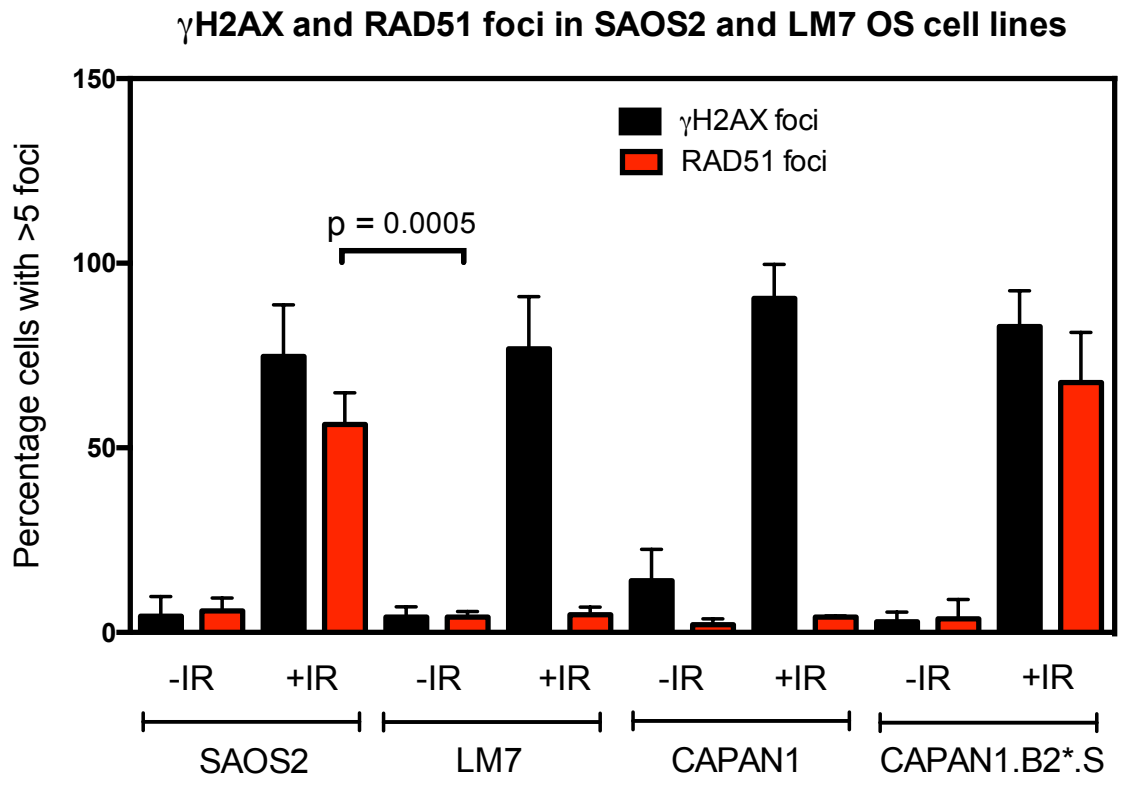

Figure 131 LM7 cells exhibit a defect in nuclear RAD51 foci formation.

Bar chart illustrating quantitation of nuclear RAD51 foci after exposure to ionising radiation. Cells were plated in triplicate in 6 well plates on coverslips. After 24 hours, tumour cells were irradiated (10 Gray) and cultured for a subsequent four hours, at which point cells were fixed and immunostained. Confocal microscopy was used to visualise and score the nuclear γH2AX and RAD51 foci. Cells containing more than 5 foci were considered positive. Mean ± SEM for three independent experiments are shown. LM7 cells exhibited significantly decreased nuclear RAD51 foci formation compared to SAOS2 (p = 0.0005). p values were calculated using Student's t test.

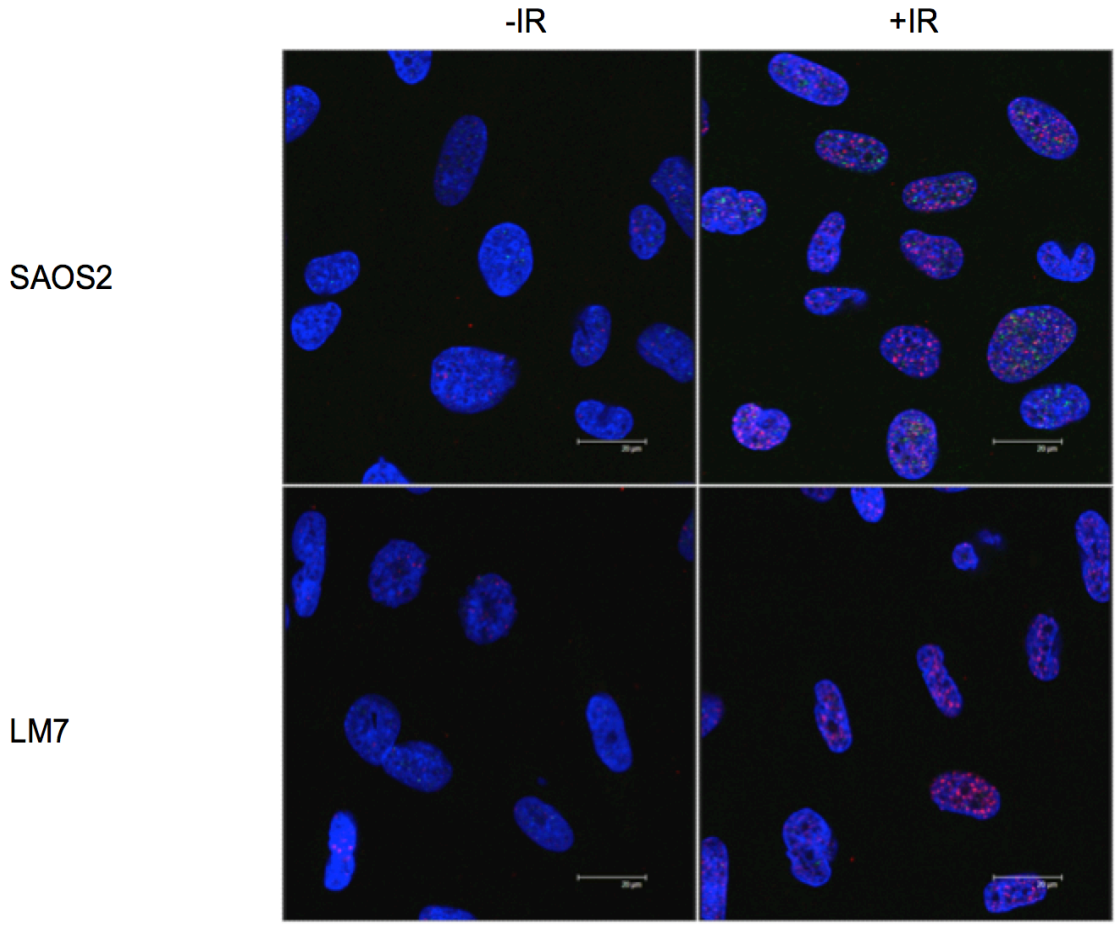

Figure 132 LM7 cells exhibited a defect in nuclear RAD51 foci formation, suggestive of an acquired HR defect.

Representative confocal images for nuclear RAD51 foci formation in LM7 and SAOS2 cells following IR exposure with staining to demonstrate γH2AX (pink) and RAD51 foci (green). Cells were plated in triplicate in 6 well plates on coverslips. After 24 hours, tumour cells were irradiated (10 Gy) and cultured for a subsequent four hours, at which point cells were fixed and immunostained. Confocal microscopy was used to visualise and score the nuclear gH2AX and RAD51 foci. Cells containing more than five foci were considered positive. Scale bar = 30 μm. [-IR: not exposed to irradiation; +IR: exposed to 10Gy radiation]

7.2.9.1.2 siRNA screen in combination with olaparib

To investigate the mechanism of sensitivity to PARP inhibition in osteosarcoma, the cell lines LM7 and SAOS2 were screened using the same siRNA library as described in Chapter 5 with the addition of continuous exposure to DMSO or 500nM of olaparib (SF50 for LM7) for five days. The Drug Effect (DE) on each gene was calculated (described in 2.3.1.4 section of Chapter 2), where scores of -2 < or > 2 were considered significant for sensitising and resistance causing effects. The Delta Drug Effect was calculated as the difference between the DE for each tumour cell line.

Selection criteria for candidate genetic dependencies that caused selective loss of viability in the presence of olaparib were set as follows: statistically significant ($p<0.05$) difference between viability in the presence of DMSO or olaparib; drug effect < - 2 in either cell line. Using these criteria, for LM7 the following 24 genes were identified: *BRCA1, BRCA2, FANCM, RAD51, SHFM1, PALB2,* Essential Meiotic Structure-Specific Endonuclease Subunit 2 (*EME2*), Tight Junction Protein 2 (*TJP2*), *Homeobox C13* (*HOXC13*), X-ray repair cross-complementing 3 (*XRCC3*), Glypican 3 (*GPC3*), Rho Associated Coiled-Coil Containing Protein Kinase 2 (*ROCK2*), *FGFR3,* Serine/Threonine Kinase 40 (STK40) (*MGC4796*), Calcium/Calmodulin Dependent Protein Kinase IV (*CAMK4*), Pyruvate Kinase Muscle (*PKM2*), *MUTYH,* Membrane Palmitoylated Protein 3 (*MPP3*), Advanced Glycosylation End-Product Specific Receptor (*RAGE*), Vaccinia Related Kinase 2 (*VRK2*), DNA Polymerase Gamma, Catalytic Subunit (*POLG*), *MAP4K2,* Protein Kinase N1 (*PRKCL1*), and Protein Kinase C Delta (*PRKCD*); and for SAOS2 the following ten genes were identified: *BRCA1, FANCM, SHFM1,* Cyclin E1 (*CCNE1*), *RAD51,* Eukaryotic Translation Initiation Factor 4A2 (*EIF4A2*), Replication Protein A3 (*RPA3*), Transcription Factor 7 Like 2 (*TCF7L2*), Nuclear Receptor Coactivator 4 (*NCOA4*), and X-Ray Repair Cross Complementing 1 (*XRCC1*). Protein-protein network analysis using String (string-db.org) highlighted a reliance on nine genes involved in DNA damage repair associated with a phenotype sensitive to PARP inhibition (Figure 133). Some genes for example *BRCA1* and *BRCA2* were in the siRNA library twice, and therefore provide further internal revalidation. To attempt to determine a mechanism of sensitivity to olaparib in LM7, candidate genetic dependencies that cause loss of viability of SAOS2 (Z score < -1.5) in the presence of olaparib, but without an effect on viability of LM7 (Z score > - 1.0), were sought. No candidate genetic dependencies were identified.

7.2.9.1.3 Exome sequencing and Transcriptome profiling of LM7 and SAOS2

Given the evidence of an acquired sensitivity to PARP and HR defect in LM7, exome sequencing and mRNA transcriptome profiling of LM7 and SAOS2 was performed by the Tumour Profiling Unit at the Institute of Cancer Research, London. Differences were sought between the two tumour cell lines to further understand the acquired sensitivity to PARP inhibition by LM7. The focus was set on genes known to be involved in DNA repair. Mutations, copy number changes and mRNA expression changes that were seen in both cell lines were excluded, since it is likely these effects do not cause a differential sensitivity to PARP. Therefore, only changes seen in either LM7 or SAOS2 are described.

122 protein-altering mutations present in either SAOS2 or LM7 were identified; 104 were missense; four (Autophagy Related 4A Cysteine Peptidase (*ATG4A*), Complement Factor H Related 2 (*CFHR2*), Ring Finger Protein 20 (*RNF20*), Tectonic Family Member 3 (*TCTN3*)) were found in splice sites; eight (Kelch Like Family Member 29 (*KLHL29*), Meiotic Double-Stranded Break Formation Protein 1 (*MEI1*), ATP Binding Cassette Subfamily A Member 12 (*ABCA12*), Churchill Domain Containing 1 (*CHURC1*), Complement C7 (*C7*), EH Domain Containing 1 (*EHD1*), Protocadherin Alpha 1 (*PCDHA1*), Protocadherin Beta 5 (*PCDHB5*)) were nonsense mutations (stop gained); and six (Contactin Associated Protein-Like 2 (*CNTNAP2*), Insulin Receptor Substrate 4 (*IRS4*), H2B Histone Family Member W Testis Specific (*H2BFWT*), *RP4-724E16.2,* Serpin Family B Member 10 (*SERPINB10*), Protein Tyrosine Phosphatase, Receptor Type C (*PTPRC*)) were frame shift mutations. Three missense mutations in LM7 in three genes (HUS1 Checkpoint Clamp Component (*HUS1*), INTS3 And NABP Interacting Protein (*INIP*), and EYA Transcriptional Coactivator And Phosphatase 4 (*EYA4*)) encoding proteins involved in DNA repair and HR were identified. *HUS1* has a critical role in the S-phase checkpoint in leading to cell cycle arrest in response to DNA damage (Weiss, Leder & Vaziri, 2003). *INIP* is a component of the sensor of single strand DNA (SOSS) complex, which functions to promote DNA repair and plays a critical role in the repair of DSB by HR (Huang, Gong, Ghosal, *et al.*, 2009). *EYA4* promotes DNA repair by the recruitment of DNA repair complexes and dephosphorylation of H2AX (Wilson, Vucic, Enfield, *et al.*, 2014). EYA4 was found to also have very low transcript expression in LM7.

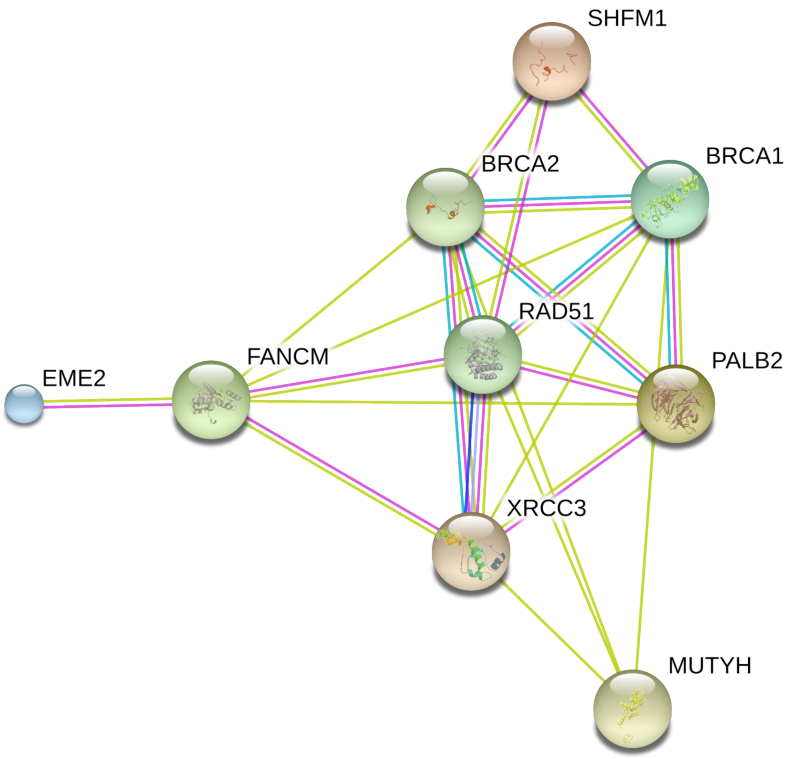

Figure 133 Protein-protein network analysis using String (string-db.org) highlighted a reliance on nine genes involved in DNA damage repair associated with a phenotype sensitive to PARP inhibition (LM7).

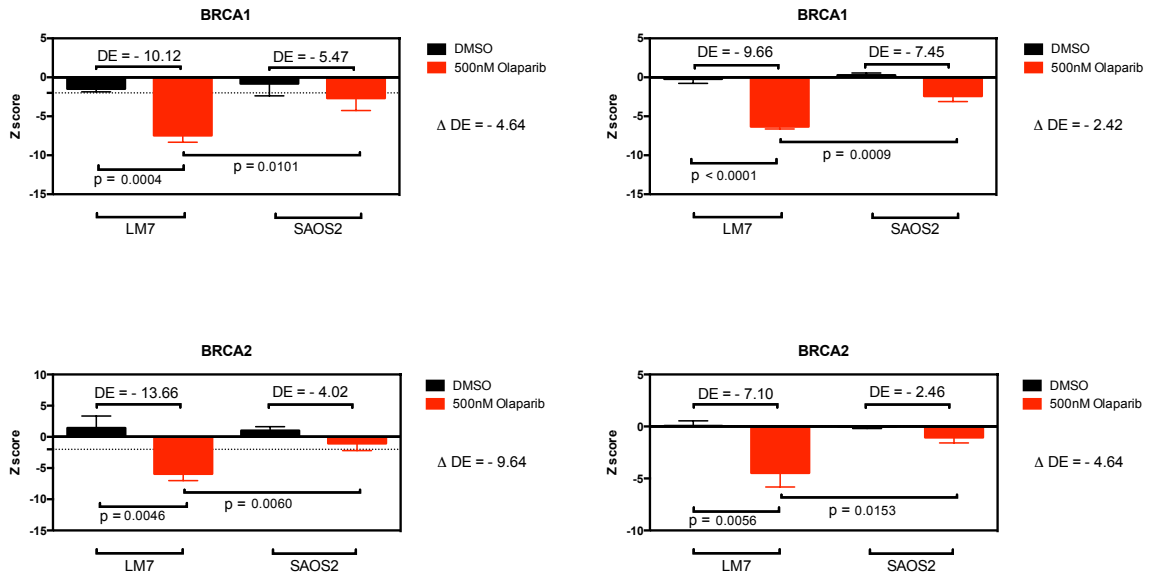

Figure 134 Silencing of *BRCA1* and *BRCA2* was associated with loss of viability in the presence of olaparib in both OS tumour cell line, but particularly LM7.

Bar charts illustrating viavility are shown for LM7 and SAOS2 in the presence of DMSO or olaparib. Tumour cell lines were reverse transfected using the siRNA library described in Appendix Tables 1-3. After 24 hours, cells were exposed to DMSO or 500nM olaparib. Post a further six days, cell viability was estimated using the CellTiter Glo reagent as described in the methods. The effect of each siRNA on olaparib (500nM) sensitivity was determined by calculation of a drug effect (DE) score for each siRNA. DE scores were calculated by the difference between the median of replicate wells with drug and median of replicate corresponding wells with no drug for each siRNA. The median absolute deviation (MAD) was used to account for variance of the DE data. Delta drug effect was calculated as the difference between the DE for each tumour cell line. Some genes such as *BRCA1* and *BRCA2* were in the siRNA library twice, and therefore provide further internal revalidation. Box and whisker plots showing mean and standard deviation. Bar represents mean value and error bars standard deviation. P values calculated by the Student's t test. [DE: drug effect; Δ DE: Delta drug effect]

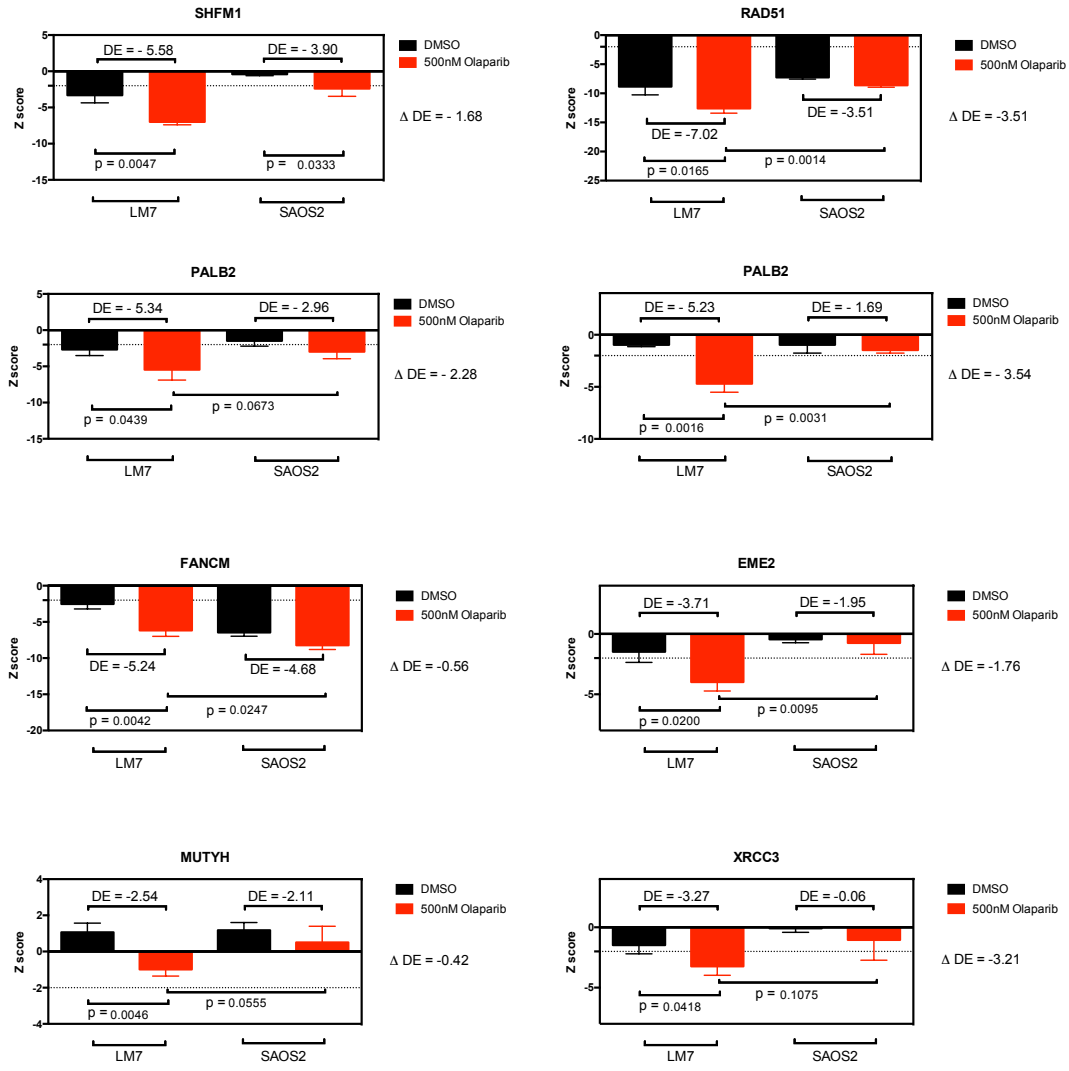

Figure 135 Candidate genetic dependencies associated with sensitivity to PARP inhibition by olaparib.

Bar charts illustrating viavility are shown for LM7 and SAOS2 in the presence of DMSO or olaparib. Tumour cell lines were reverse transfected using the siRNA library described in Appendix Tables 1-3. After 24 hours, cells were exposed to DMSO or 500nM olaparib. Post a further six days, cell viability was estimated using the CellTiter Glo reagent as described in the methods. The effect of each siRNA on olaparib sensitivity was determined by calculation of a drug effect (DE) score for each siRNA. DE scores were calculated by the difference between the median of replicate wells with drug and median of replicate corresponding wells with no drug for each siRNA. The median absolute deviation (MAD) was used to account for variance of the DE data. Delta drug effect was calculated as the difference between the DE for each tumour cell line. Some genes such as *PALB2* were in the siRNA library twice, and therefore provide further internal revalidation. Bars represent mean and error bars standard deviation. P values calculated by the Student's t test. [DE: drug effect; Δ DE: Delta drug effect]

There were 14 genes with copy number changes only seen in LM7 (SLX1 Homolog A, Structure-Specific Endonuclease Subunit (*SLX1A*), PARP1 Binding Protein (*PARPBP*), *CHEK2, EYA2,* Ubiquitin C (*UBC*), Mortality Factor 4 Like 2 (*MORF4L2*), Ubiquitin Conjugating Enzyme E2 A (*UBE2A*), Acyl-CoA Synthetase Long-Chain Family Member 4 (*ACSL4*), Cullin 4B (*CUL4B*), Iduronate 2-Sulfatase (*IDS*), Nuclear Receptor Coactivator 6 (*NCOA6*), *RUNX1,* 1-Acylglycerol-3-Phosphate O-Acyltransferase 3 (*AGPAT3*), Solute Carrier Family 19 Member 1 (*SLC19A1*)) involved in DNA repair. Of these, three genes (*SLX1A*, *PARPBP* and *CHEK2*) were known to be involved in HR-mediated DNA repair. There was no evidence of differential mRNA expression of these 14 DNA repair genes. Loss of homozygosity regions were identified in six genes (*FANCM,* Ring Finger Protein 168 (*RNF168*), 3-Hydroxybutyrate Dehydrogenase 1 (*BDH1*), NIMA Related Kinase 1 (*NEK1*), *WBSCR22* and *WBSCR27*) in LM7, with known involvement in DNA repair pathways. Two out of these six genes (*FANCM* and *RNF168*) have known involvement in HR dependent DNA repair.

7.2.9.1.4 Investigation of differences in expression of proteins known to be involved in DNA damage repair pathways

To investigate if proteins known to be sensitisers to PARP inhibition were expressed at differential levels between LM7 and SAOS2 and therefore potential biomarkers of sensitivity to PARP inhibition, western blotting of selected proteins was undertaken. To identify changes in phosphorylated CHK1, tumour cells were exposed to DMSO or 10μM olaparib for 24 hours. No difference in levels of expression was seen between the two tumour cell lines for BRCA1, BRCA2, CHK1, phosphorylated CHK1 (Serine 345), phosphorylated CHK2 (Threonine 68), ATM or ATR (Figure 136, Figure 137 and Figure 138). Total CHK2 expression was slightly decreased in SAOS2. However, no obvious differential expression of known sensitisers to PARP inhibition that could explain the acquired sensitivity to PARP inhibition by LM7 was observed.

7.2.9.1.5 Investigation of differences in abundance of proteins known to be involved in DNA damage repair pathways

To further identify differences in protein expression between the two tumour cell lines that could explain the acquired sensitivity to PARP inhibition by LM7, proteomic profiling was kindly undertaken by Colm Ryan using the methodology described in section 2.2.3.2 of

Chapter 2. Proteins with the greatest differential abundance between LM7 and SAOS2, with lowest abundance in LM7, were selected. SWI/SNF Related Matrix Associated Actin Dependent Regulator Of Chromatin Subfamily A Member 1 (SMARCA1), Fanconi Anaemia Complementation Group D2 (FANCD2) and Histone Cluster 2 H2B Family Member A (HIST2H2AB) exhibited the greatest difference (Figure 139). Protein abundance values for BRCA1, BRCA2, SHFM1, XRCC3, and PALB2 were not available and therefore likely represent low abundance.

SMARCA1 is a member of the SWI/SNF family of proteins that contribute to the chromatin remodelling of transcription. These complexes also function in HR, NHEJ and DNA damage associated signalling (Lans, Marteijn & Vermeulen, 2012). Inhibition of *SMARCA1*, has been shown to selectively activate the DNA damage response, leading to inhibition of growth and apoptosis of tumour cells (Aydin, Vermeulen & Lans, 2014). Potentially decreased expression of SMARCA1 leading to constitutive activation of the DNA damage response could increase sensitivity to PARP inhibition. HIST2H2AB is a pseudo-gene of the histone family of proteins primarily responsible for nucleosome structure of the chromosomal fibre. As a pseudo-gene its relevance is unknown. FANCD2 co-localises with BRCA1 and is directly involved in HR and cell cycle checkpoint response to DNA damage (Bogliolo & Surrallés, 2013).

Although, there are no supportive genomic correlates of *SMARCA1, FANCD2* or *HIST2H2AB*, seen in the whole exome sequencing, or mRNA transcriptome profiling, loss of heterozygosity (LOH) for *FANCM* was identified in LM7 but not SAOS2. FANCD2 controls FANCM, and the combination of LOH of FANCM and decreased abundance of FANCD2, both key proteins in DDR may explain the acquired sensitivity to PARP by LM7.

Unfortunately, siRNA targeting *SMARCA1* and *HIST2H2AB* were not part of the RNAi library used in 7.2.9.1.2, and could not be used to cross-reference and validate these findings. Small-scale revalidation to test the hypothesis that silencing of *SMARCA1* or *HIST2H2AB* in SAOS2 could increase sensitivity to PARP inhibition could be investigated, or if over expression using a plasmid could rescue the sensitivity to PARP inhibition, and increase the resistance in LM7. Silencing of *FANCD2* in this screen did not cause a loss of viability (median Z score < -1.5) in LM7 or SAOS2. This could be because of redundancy of the protein or a false negative in the screen.

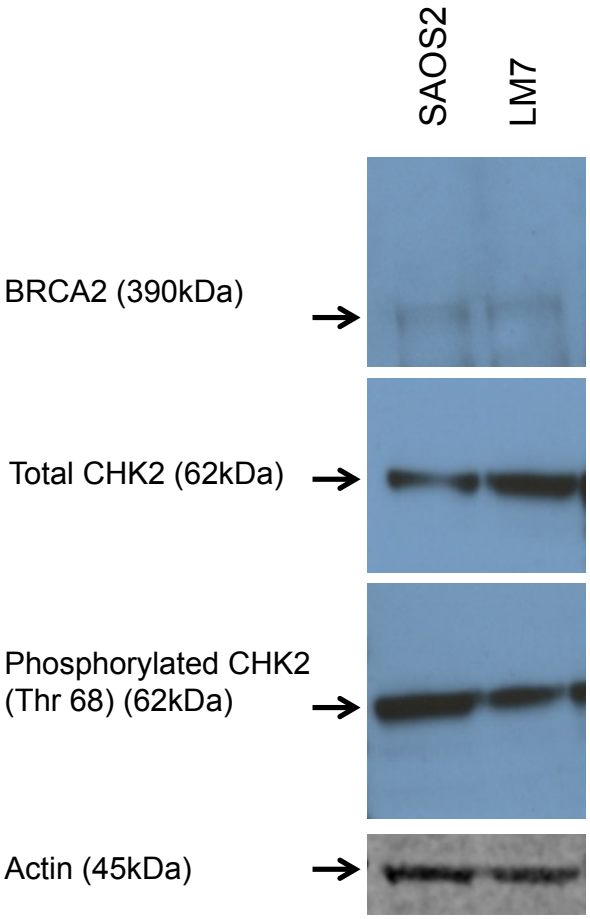

Figure 136 LM7 and SAOS2 exhibit similar expression levels of BRCA2, total CHK2 and phospho threonine 65-CHK2.

Western blot is shown. Total cell lysates were collected from untreated cells, electrophoresed, and immunoblotted as described in the methods. Immunoblotting of actin was used as the loading control. No difference in expression levels of BRCA2 or phosphorylated CHK2 (Threonine 68) was observed between the two tumour cell lines. Expression of total CHK2 was slightly decreased in SAOS2.

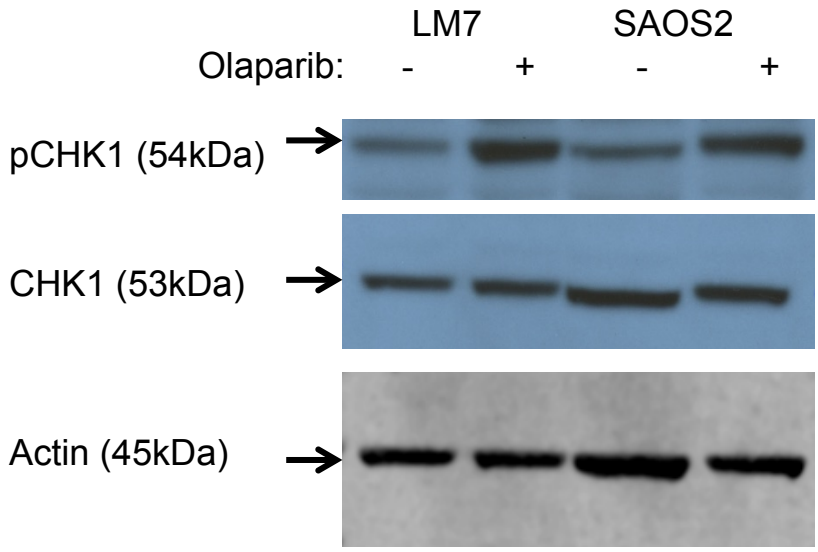

Figure 137 LM7 and SAOS2 exhibit similar protein expression levels of phosphor serine 345-CHK1 and total CHK1.

Western blot is shown. Tumour cells were exposed 10μM olaparib or DMSO for 24 hours. Total cell lysates isolated after drug exposure were electrophoresed, and immunoblotted as described in the methods. Immunoblotting of actin was used as the loading control. [-: 24 hour exposure to DMSO; +: 24 hour exposure to 10μM olaparib; pCHK1: phosphorylated CHK1 (Serine 345)].

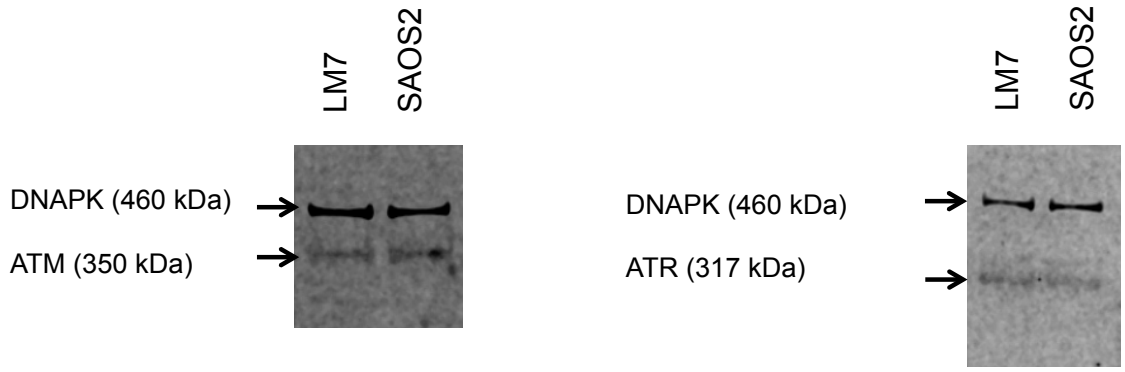

Figure 138 LM7 and SAOS2 exhibit similar protein expression of ATM and ATR by western blotting.

Western blot is shown. Total cell lysates were collected from untreated cells, electrophoresed, and immunoblotted as described in the methods. Immunoblotting of DNA-PK was used as the loading control.

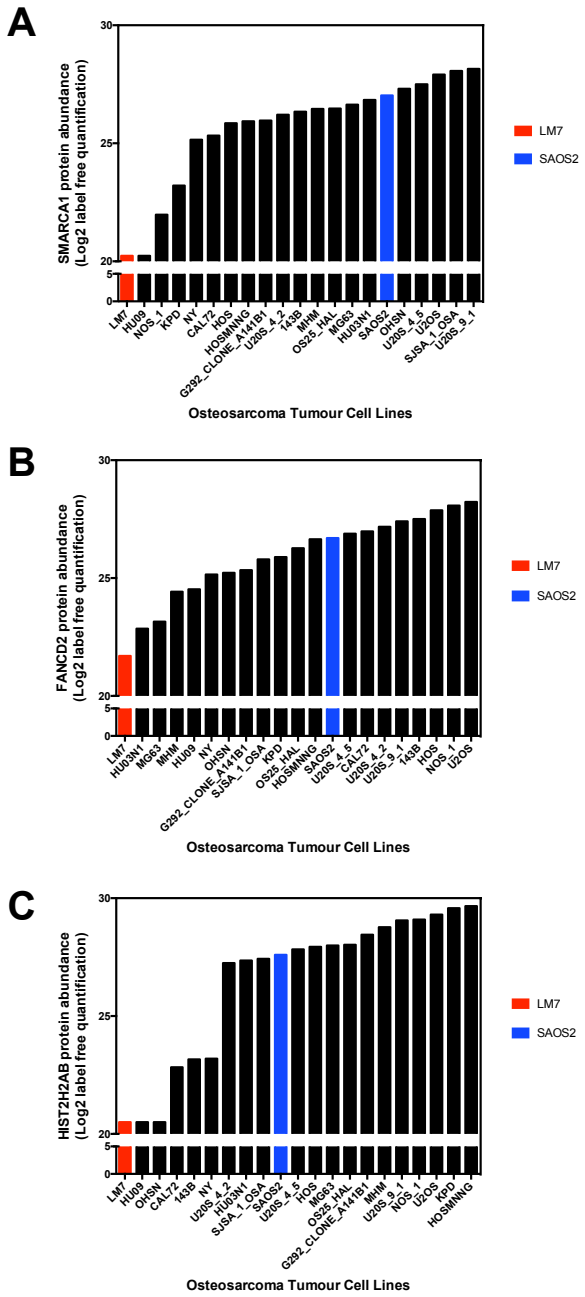

Figure 139 Proteomic abundance of (A) SMARCA1, (B) FANCD2, and (C) HIST2H2AB in LM7 and SAOS2, exhibited large differential in abundance.

Bar charts of protein abundance of (A) SMARCA1, (B) FANCD2, and (C) HIST2H2AB in LM7 and SAOS2 defined by mass spectrometry that was performed Colm Ryan (Systems Biology, Dublin, Ireland). Following lysis, protein purification, and tryptic digest, peptides were separated by liquid chromatography and measured by mass spectrometer. Label-free proteome quantification was performed using the MaxQuant software environment to determine the quantitative abundance of 6696 peptides with a false discovery rate of less than one percent.

7.3 DISCUSSION

This chapter describes high-throughput screening of the panel of 18 OS tumour cell lines and isogenic *RB1* deficient and wildtype U2OS tumour cell line generated by CRISPR-Cas9 mutagenesis, with the aim of identification of drugs with novel activity in OS that may facilitate development of clinical trials and or stratification of patients for clinical trials. The heterogeneity of the molecular landscape of OS makes finding new molecular targets challenging, and the overall resistance of OS to the majority of small molecule inhibitors and chemotherapeutics compared to other cancer types makes identification of novel agents also difficult. It is therefore imperative to have a range of useful models for studying this disease further, and context for comparison of sensitivity. The small molecule screens described in this chapter demonstrate that sensitivity to most inhibitors was seen only in a minority of models, thus diminishing the statistical power and possible clinical relevance. Due to the heterogeneity of the disease, appropriate patient selection using biomarkers of sensitivity will be critical. For a disease that is not common, further division of the patient population into a number of minority subsets, could present challenges with trial recruitment nationally, and necessitate international collaboration.

The drug screen demonstrated that OS tumour cell lines exhibit sensitivity to chemotherapeutics that already form the standard of care (methotrexate and doxorubicin) (Marina, Smeland, Bielack, *et al.*, 2016), and are frequently used in the advanced setting (gemcitabine) (Palmerini, Jones, Marchesi, *et al.*, 2016). Others such as mTOR inhibitors have demonstrated clinical activity in OS but not sufficient to be incorporated into treatment protocols (Chawla, Staddon, Baker, *et al.*, 2012; Demetri, Chawla, Ray-Coquard, *et al.*, 2013). Whole-exome sequencing, whole genome sequencing, and RNA-sequencing of OS tumour samples, identified alterations in the PI3K/mTOR pathway in 24% of patients with OS (Perry, Kiezun, Tonzi, *et al.*, 2014). Mutations of *PTEN* and *PIK3CA* were found in by multivariable analysis of clinical trial data to be predictive of response to rapamycin in advanced cancer (Janku, Hong, Fu, *et al.*, 2014). However, no mutations of PI3K/mTOR pathway members (*PI3K, PTEN, PDPK1, AKT1* and *EIF4B*) were observed in the panel of OS tumour cell lines, and so make these models less attractive for further study in this area.

Recent findings of IGF signalling pathway mutations or amplification in eight out of 112 tumour OS samples which were either whole genome or exome sequenced (Behjati, Tarpey, Haase, *et al.*, 2017), has provided a novel insight into the pathway as a potential

avenue worthy of investigation once again. Response to robatumumab, a fully human antibody that binds and inhibits IGF-1R, was found in Phase II trial to be related to disease burden, imparting a complete or partial response in three of 31 patients with resectable osteosarcoma metastases, but not in patients with un-resectable metastases (Anderson, Bielack, Gorlick, *et al.*, 2016), while a monoclonal antibody targeting IGF-1R, R1507, showed limited activity in OS with only two of 38 patients with advanced OS, achieving partial remission, as part of a larger study (Pappo, Vassal, Crowley, *et al.*, 2014). However, all clinical trials in sarcoma have been closed or halted due to perceived lack of activity and no biomarker to stratify patients for therapy. In blockade of IGR-1R alone, the IR has been shown to activate the same downstream signalling pathways as IGF-1R (Kuijjer, Peterse, van den Akker, *et al.*, 2013). Therefore, targeting both IGF-1R and IR might have greater effect. A phase II study of linsitinib (NCT02546544) in patients with relapsed or refractory advanced Ewing's sarcoma has closed and the results are awaited. The OS tumour cell lines did not show significant sensitivity to the dual IGF-1R and IR inhibitors linsitinib (OSI-906) or GSK1904529A compared to the non-osteosarcoma tumour cell line data. However, a considerable range of sensitivity in the OS tumour cell line panel was observed with exposure to linsitinib (OSI-906), and mutation of the IGF pathway genes (*IGF1R, IGF2R, IGFBP4*, *IGFBP6* and *IGFBPL1*) were found to correlate with sensitivity. One of the tumour cell lines harboured *IGF1R* amplification and was amongst the most sensitive to linsitinib, however, these results were not replicated with GSK1904529A. Further validation of these observations using tumour samples is needed to determine applicability of any IGF pathway mutation as a potential biomarker for linsitinib, and IGF pathway inhibitors in general, since these observations were not replicated with GKS1904529A. A robust biomarker for sensitivity to IGF1R/IR inhibition could be therapeutically attractive but as yet has proven illusive.

An OS specific dependency to the CHK1 inhibitor PF-004477736 was identified, although an OS specific genetic dependency on *CHK1* was not observed. This could be a false negative from the siRNA screen described in Chapter 5, or an off-target effect of the drug leading to a false positive. To further establish the role of *CHK1* in this panel of OS tumour cell lines, a small-scale deconvolution reverse transfection using multiple siRNA species each targeting a different region of *CHK1* could be performed. In addition, a drug screen using other structurally different inhibitors of CHK1, and also confirmation of cell cycle arrest in G2/M. Interestingly, the *BRCA1* deficient breast cancer cell line SUM149 was particularly sensitive to PF-004477736, while the secondary *BRCA1* mutant

SUM149.B1*.S demonstrated acquired resistance. However, acquired sensitivity to this agent was not observed in LM7 compared toSAOS2, despite an acquired HR defect.

A number of CHK1 inhibitors are currently in development and early clinical trials. A Phase I trial of PF-004477736 was commenced in combination with gemcitabine in patients with advanced solid tumours, but was terminated for financial reasons (NCT00437203). A phase I trial of LY2606368 to determine the safety and toxicity profile in patients with advanced solid tumours has been performed (no patients with OS were enrolled) (Hong, Infante, Janku, *et al.*, 2016). Grade 4 neutropenia occurred in 73% of patients but was transient, and otherwise well tolerated; two of 45 patients had a partial response, while 15 had stable disease (Hong, Infante, Janku, *et al.*, 2016). A number of clinical trials of LY2606368 in patients with advanced solid tumours are currently recruiting. The potential for CHK1 inhibitor use is likely to be limited by absence of a sufficient biomarker of sensitivity. It will be interesting to observe if a relationship between HR deficiency and CHK1 sensitivity is established in a clinical trial setting (NCT02873975).

The previous chapter described a reliance on genes involved in 'skeletal system morphogenesis' including *FGFR1* (Campbell, Ryan, Brough, *et al.*, 2016). Two FGFR inhibitors AZD4547 and PD173074, were found to be selective for osteosarcoma models independent of amplification status. In addition, amplification and polysomy of *FGFR1* in this panel of OS tumour cell lines was shown to be associated with significantly greater sensitivity to the *FGFR1* inhibitors than OS tumour cell lines for which *FGFR1* amplification was unknown or negative. Using 145 tumour cell lines of lineages which for which Guagnano *et al.* reported *FGFR1* amplification, in breast, lung and OS, they demonstrated that *FGFR1* amplification was significantly associated with sensitivity to the FGFR inhibitor NVP-BGJ398 (Guagnano, Kauffmann, Wöhrle, *et al.*, 2012). Validation of these findings in OS tumour samples, identified one of 17 samples with *FGFR1* amplification (defined as log2 ratio ≥1: equal to ≥4 normalized DNA copies) (Guagnano, Kauffmann, Wöhrle, *et al.*, 2012). A c-Fos oncogene-induced orthotopic mouse model of OS was used to demonstrate that treatment with the FGFR inhibitor AZD4547 lead to a reduction of the number and size of pulmonary nodules (Weekes, Kashima, Zandueta, *et al.*, 2016). In addition, silencing of *FGFR1* by use of shRNA targeting FGFR prior to injection, decreased the number of spontaneous pulmonary metastases (Weekes, Kashima, Zandueta, *et al.*, 2016).

Recently a study analysed *FGFR1* amplification using interphase fluorescence in situ hybridisation (FISH) in 352 OS tumour samples from 288 patients. *FGFR1* amplification was defined as positive if ≥10% of the cells showed (a) *FGFR1*/Centromere 8 (*CEN8*) ratio >2, (b) clusters of *FGFR1* signals, or (c) >15 copies of *FGFR1* per cell. Amplification of *FGFR1* was observed in 18.5% of patients in whose tumours revealed a poor response to chemotherapy (<90% necrosis) (Fernanda Amary, Ye, Berisha, *et al.*, 2014) and present disproportionally higher in the rarer histological variants of OS such as fibroblastic and pleomorphic subgroups (Fernanda Amary, Ye, Berisha, *et al.*, 2014). Patients with a good response to chemotherapy did not harbour *FGFR1* amplification (Fernanda Amary, Ye, Berisha, *et al.*, 2014). Nearly 10% of OS tumour samples from 288 patients exhibited *FGFR1* amplification, while approximately 50% of tumour samples were observed to have polysomy (Fernanda Amary, Ye, Berisha, *et al.*, 2014). It was not possible to establish if *FGFR1* amplification increased the risk of metastatic disease because of relatively small data set (Fernanda Amary, Ye, Berisha, *et al.*, 2014). Thus, from the results of the drug screen, there are indications of possible treatment opportunities of a significant proportion of OS patients with *FGFR1* amplification and/or polysomy. Given that *FGFR1* amplification was seen in patients who had a poorer response to chemotherapy, and associated with rarer histological variants (Fernanda Amary, Ye, Berisha, et al., 2014), finding an association that *FGFR1* amplification in this panel of OS tumour cell lines was associated with significantly greater sensitivity to the *FGFR1* inhibitors provides further rationale for finding inhibitors.

There are a number of monoclonal antibodies and specific tyrosine kinase inhibitors that target the FGFR receptor family that are currently in Phase I/II clinical trials. One such study, of the inhibitor AZD4547, added a basket cohort to explore efficacy of the agent in FGFR amplified osteosarcoma (NCT01795768). Unfortunately the study is currently “on hold” due to unexpected side effects identified. Lenvatinib, a multi-targeted kinase inhibitor was investigated in osteosarcoma in a phase I study initially developed by the Innovative Therapies for Children with Cancer (ITCC), and identified 14mg/m^2/day as the recommended dose (Gaspar, Melcon, Venkatramani, *et al.*, 2017). The efficacy of this agent is currently being explored in a phase II expansion of the single agent in osteosarcoma and Phase Ib study in combination with ifosfamide and etoposide in osteosarcoma (NCT02432274). Although marketed as a VEGFR inhibitor, it is also an FGFR1 inhibitor with an IC50 of 46nmol/L (Cabanillas & Habra, 2016). However, data from the drug screen in this thesis cautions the clinical translation of lenvatinib, since no

significant sensitivity was seen in OS compared to non-OS tumour cell lines, and sensitivity did not correlate with *FGFR1* amplification status. A more specific FGFR1 inhibitor might be more effective.

While *FGFR1* amplification in OS tumour cell lines has previously been determined to be a marker of sensitivity to FGFR inhibition by the pan-FGFR inhibitor NVP-BGJ398 (Guagnano, Kauffmann, Wöhrle, *et al.*, 2012), the finding that OS tumour cell lines with *FGFR1* polysomy are also sensitive to FGFR1 inhibition by two different FGFR1 inhibitors, in addition to a panel wide reliance on genes involved in 'skeletal system morphogenesis' including *FGFR1* (Campbell, Ryan, Brough, *et al.*, 2016), suggests that an additional cohort of patients may benefit from FGFR1 inhibition. These findings add further weight to the importance of the role of FGFR in OS and rationale for a clinical trial of *FGFR1* inhibitors in an enriched patient population with *FGFR1* amplification or polysomy. In addition, it would be valuable to measure *FGFR* status in patients on current clinical trials to determine whether there is any correlation with response to the therapy.

Sensitivity to drugs depending on deficiency of *CDKN2A* and *RB1* were identified. *CDKN2A* deficiency was demonstrated to be predictive of methotrexate sensitivity, as *MTAP*, a known sensitiser to methotrexate is collocated on Chromosome 9 with *CDKN2A.* Cells deficient in *MTAP* by deletion or inactivation via methylation of the *MTAP* promoter are more sensitive to methotrexate (Bertino, Waud, Parker, *et al.*, 2011). Cells deficient in MTAP, have a defective salvage pathway for adenine and methionine, increasing sensitivity to inhibitors of de novo purine synthesis such as methotrexate, and methionine deprivation (Bertino, Waud, Parker, *et al.*, 2011). Interestingly, four out of the five of the OS tumour cell line panel (HOS, HOSMMNG, 143b and MG63) with homozygous deletions of *CDKN2A* also had homozygous deletions of *MTAP.* CAL72 has a region of loss from 21894035 – 22183163 base pairs on chromosome 9. This included *CDKN2A* (21967751 – 21995300 base pairs), but only part of *MTAP* (21802543 – 21937651 base pairs), meaning that some isoforms of MTAP are still possible. Methotrexate is one of the three principal chemotherapeutics used for the treatment of OS. At present there is no biomarker for determining potential response to therapy, however, deficiency of *CDKN2A* or *MTAP* could have the potential for use as a biomarker. It would be valuable to measure *CDKN2A* or *MTAP* status by immunohistochemistry in patients on current clinical trials to determine whether there is any correlation with response to the therapy. However, this is confounded by likely co-

treatment with doxorubicin and cisplatin in addition to methotrexate. Determining if patients whose tumours harbour *CDKN2A* or *MTAP* deficiency would have a similar outcome post dose-reduction of methotrexate as compared to standard therapy would be limited by the need for a large phase III trial. Given the toxicity of high-dose methotrexate at the standard doses, combined with that of doxorubicin and cisplatin, it would be difficult to envisage increasing the dose of methotrexate in those patients who were *CDKN2A* or *MTAP* wildtype. Therefore, possible benefit would be most likely if an additional agent could be used in combination with or instead of methotrexate in this potential cohort.

Given the heterogeneity of OS *in vivo,* a panel of representative tumour cell lines is attractive, but does make isolation of drug dependencies associated with a molecular deficiency such as *RB1* more challenging. Isogenic models that derive from a single progenitor cell line, with minimal differences between the daughter and parental cell lines, so that any observed differences are more likely to be due to the gene of interest (Rehman, Lord & Ashworth, 2010) have the potential to make isolation of drug dependencies more accessible. However, these isogenic models also have their limitations, since the observed dependency may be specific to the molecular landscape of the model, with limited wider applicability and require further validation in a panel of representative tumour cell lines. Hence, both methodologies were employed, with drug screens in both the panel of OS tumour cell lines, and the isogenic *RB1* deficient U2OS models. Similar to the observed genetic dependencies described in the previous chapter, different drug dependencies were found using the different models. As discussed in the previous chapter, *RB1* and *CDKN2A* deficiency were found to be mutually exclusive in the OS tumour cell line panel. The OS tumour cell line U2OS was classified in Chapter three as *CDKN2A* deficient. Given that CRISPR-Cas9 mutagenesis was attempted in a number of other *CDKN2A* wildtype OS tumour cell lines without success, it is possible sudden acquired complete deficiency of *RB1* is lethal without prior deficiency of *CDKN2A,* and that a deficiency of *CDKN2A* abrogates vulnerabilities specific to acquired deficiencies associated with deficiency of *RB1.* This presents future challenges for the isolation of both genetic and drug dependencies associated with *RB1* deficiency, given the heterogeneity of the panel and difficulty of creation of an isogenic model representative of the disease.

Paclitaxel, vinorelbine and camptothecin were the only drugs that demonstrated increased sensitivity with *RB1* deficiency in the panel of OS tumour cell lines and could

be avenues for future investigation using mouse models prior to clinical translation. Although paclitaxel and camptothecin appear mechanistically relevant to tumour cells harbouring *RB1* deficiency (Kurtyka, Chen & Cress, 2014; Lauricella, Calvaruso, Carabillò, *et al.*, 2001), and statistically significant, the scale of effect observed was modest, and is unlikely to be a priority.

The isogenic *RB1* deficient U2OS models generated by CRISPR-Cas9 mutagenesis demonstrated sensitivity to HSP90, kinesin spindle protein and NAD biosynthesis inhibitors. HSP90 is recognised as a crucial facilitator of oncogene addiction and cancer cell survival, via its protection of an array of mutated and overexpressed oncoproteins from mis-folding and degradation (Trepel, Mollapour, Giaccone, *et al.*, 2010). Despite over twenty clinical trials, only moderate single agent activity has been observed in diseases such as *HER-2* amplified breast cancer and *ALK* rearranged and *EGFR* mutant lung cancer where the tumour cells are addicted to a HSP90 client protein (Neckers & Workman, 2012). Assessment of efficacy of HSP90 in osteosarcoma has been on *in vivo* tumour cell lines (Hu, Bobb, He, *et al.*, 2015) and limited mouse models (Hu, Bobb, He, *et al.*, 2015) that have shown limited efficacy.

Kinesin spindle protein (KSP) inhibitors are a family of molecular motors that travel uni-directionally along tracks to support cell division (Rath & Kozielski, 2012). In *RB1* deficient tumour cell lines, decreased ϒ-tubulin, an important regulator of microtubule formation, has been demonstrated to induce cell death (Lindström, Villoutreix, Lehn, *et al.*, 2015). Mechanistically an increased reliance on KSP might also be explained in *RB1* deficient tumour cells by an increase in cell cycling, due to the loss of inhibitory control of RB1. Unfortunately, they have also shown limited efficacy in the clinic, with frequent mutation of the binding pocket (Jiang & You, 2013). Relatively recent discovery of an ATP competitive KSP inhibitor which has the potential to overcome mutation-mediated resistance to the allosteric inhibitors, or combination with chemotherapeutic agents, could provide increased efficacy for these agents (Jiang & You, 2013; El-Nassan, 2013).

These *RB1* deficient models also demonstrated increased sensitivity to a NAD biosynthesis inhibitor and the potential for combination treatment with PARP inhibition could be explored by combination experiments in the OS tumour cell line panel. The PARP family of enzymes add ADP-ribose moieties onto proteins, using b-NAD^+ as substrate termed PARylation (De Vos, Schreiber & Dantzer, 2012). Nicotinamide

phosphoribosyltransferase (NAMPT) is a rate-limiting enzyme involved in the generation of the PARP substrate b-NAD^+ from the natural precursor nicotinamide essential for cellular survival (Bajrami, Kigozi, Van Weverwijk, *et al.*, 2012; Nahimana, Attinger, Aubry, *et al.*, 2009). Inhibition of NAMPT has a negative impact on the catalytic activity of PARP enzymes (Bajrami, Kigozi, Van Weverwijk, *et al.*, 2012). PARP inhibitors are selective for tumour cells with homologous recombination (HR) gene defects (Bajrami, Kigozi, Van Weverwijk, *et al.*, 2012). Two inhibitors of PARP, rucaparib and olaparib also part of the same screen were not found to be selective for *RB1* deficiency in these models, nor in the wider OS tumour cell line panel. However, inhibition of NAMPT has been shown to increase the tumour cell inhibitor effect of the clinical PARP inhibitor olaparib both *in vitro* and an *in vivo* model of triple-negative breast cancer (Bajrami, Kigozi, Van Weverwijk, *et al.*, 2012). It is therefore possible, that inhibition of NAMPT might sensitise osteosarcoma tumour cells to PARP inhibition. These effects were not prioritised for smaller scale revalidation and confirmation of effects, but are potential avenues for further investigation. *RB1* has been reported to have a role DNA damage repair, predominantly by NHEJ (Huang, Cook & Mittnacht, 2015; Cook, Zoumpoulidou, Luczynski, *et al.*, 2015), but also regulation of HR (Yang, Tian, Brown, *et al.*, 2013) with *RB1* deficiency associated with chromosomal instability (CIN) (Huang, Cook & Mittnacht, 2015; Manning, Longworth & Dyson, 2010). It is therefore possible to postulate that *RB1* deficient tumour cells might have a dependency on NAMP and PARP inhibitors because of increased reliance on HR, but this dependency would be conditional on the level of deregulation of HR, and unless significant, unlikely to translate to the clinic.

A targeted drug screen of the ATR inhibitor VX970 in combination with cisplatin, using the isogenic *RB1* deficient U2OS model generated by CRISPR-Cas9 mutagenesis demonstrated a synergistic effect in both *RB1* deficient clones compared to the parental *RB1* wildtype tumour cell line. VX970 has already been demonstrated to increase sensitivity to DNA damaging agents such as cisplatin in lung xenograft models (Hall, Newsome, Wang, *et al.*, 2014). In a trial to identify biomarkers of response to neo-adjuvant cisplatin in patients with bladder cancer, genomic alterations of *ATM, RB1* and *FANCC* predicted response and clinical benefit (Plimack, Dunbrack, Brennan, *et al.*, 2015). As discussed in section 7.1, *RB1* deficient cells have defective NHEJ (Huang, Cook & Mittnacht, 2015), an increased reliance on the HR pathway, a greater reliance on the DNA damage G2 checkpoint, and functional ATR to delay mitotic entry (Nghiem, Park, Kim, *et al.*, 2001; Eguchi, Takaki, Itadani, *et al.*, 2007). Cell cycling could be

investigated by FACS, presence of pan-nuclear γH2AX in response to replication fork stress, and presence of DSB by nuclear γH2AX foci (Ward & Chen, 2001), and both speed of replication forks, and also replication fork collapse, which is associated with ATR inhibition in combination with cisplatin (Reaper, Griffiths, Long, *et al.*, 2011). Further investigation into the mechanism of ATR and cisplatin inhibition in *RB1* deficient tumour cell lines, using some of the models described in this thesis is planned and supports the potential relevance of *RB1* in OS (personal correspondence Sybille Mittnacht, UCL). Further investigation of the combined activity of VX970 and cisplatin could be performed using colony formation assays to establish the presence of a longer-term effect, and effect on cellular inhibition. In addition, exposure to the combination of VX970 and cisplatin in the panel of 18 osteosarcoma cell lines would provide a measure of efficacy given the heterogeneity of the panel. Prior to clinical translation, confirmation of efficacy using *RB1* deficient and wildtype mouse models with treatment arms comprised of vehicle, VX970, cisplatin, and VX970 in combination with cisplatin, would need to be performed. If successful a clinical trial to compare the efficacy of standard MAP chemotherapy compared to addition of VX970. Given that cisplatin is one of the established therapeutic agents in OS, and VX970 is already in Phase I/II development in other tumour types, VX970 has the potential to be used as a biomarker driven chemo-sensitiser in a molecularly defined population. Although VX970 has reportedly been well tolerated, most frequently reported toxicities are of myelo-suppression, and given that cisplatin and doxorubicin in combination are already significantly myelo-suppressive, the practicalities of addition to the current schedule could be challenging, and possibly require a longer duration between cycles for count recovery or dose reduction of cisplatin. Any benefit would need to be balanced with possible deleterious effect on outcome due to reduction of dose-intensity and explored in a trial setting.

In view of recent interest in exploring the role of PARP inhibitors in OS, a comprehensive analysis of OS tumour cell line sensitivity was undertaken. A minority of OS tumour cell lines were determined to be sensitive to PARP inhibition by talazoparib, rucaparib and olaparib. Comparison with tumour cell lines with *BRCA1/2* deficiency such as SUM149 and CAPAN1 demonstrated that LM7, the daughter of SAOS2 had acquired increased sensitivity to PARP inhibition, in both short and longer-term exposure. The panel of OS tumour cell lines demonstrated a spectrum of sensitivity to PARP inhibition. Determinants of sensitivity to PARP inhibition are known to primarily be genes encoding proteins which modulate HR (Lord & Ashworth, 2012). It was not surprising that the top candidate

genetic dependencies seen from the siRNA screen with the addition of olaparib using LM7 and SAOS2 were involved in DNA damage repair. The most profound candidate genetic dependencies with greatest drug effect were *BRCA1* and *BRCA2.* Silencing of *BRAC1* and *BRCA2* in both LM7 and SAOS2 caused loss of viability in the presence of olaparib but not DMSO. Other genetic dependencies involved in DNA damage repair were isolated in LM7. PALB2 (partner and localizer of BRCA2) is involved in stability and nuclear localization, and required for some functions of BRCA2 in double-strand break repair and homologous recombination (Rahman, Seal, Thompson, *et al.*, 2007). MUTYH (MutY DNA Glycosylase) is a DNA glycosylase involved in oxidative DNA damage repair, and functions to remove inappropriately paired adenine bases from the DNA backbone (Torrezan, da Silva, Santos, *et al.*, 2013). XRCC3 is RAD51 paralog that functions as part of a PALB2-scaffolded HR complex containing BRCA2 and RAD51, involved in HR repair of DNA DSBs (Brenneman, Weiss, Nickoloff, *et al.*, 2000). Split Hand/Foot Malformation (Ectrodactyly) Type 1 (SHFM1) is a component of the Three Prime Repair Exonuclease 2 (TREX-2) complex which binds and stabilizes BRCA2 (Huen & Chen, 2008). Tumour cells depleted of SHFM1 do not form RAD51 foci in response to DNA damage (Huen & Chen, 2008). Fanconi Anaemia Complementation Group M (FANCM) is one the 19 proteins which comprise the Fanconi anaemia (FA) pathway which repair DNA inter-strand cross-links (ICLs) (Ceccaldi, Sarangi & D'Andrea, 2016). Essential Meiotic Structure-Specific Endonuclease Subunit 2 (EME2) functions as a DNA structure-specific endonuclease in DNA repair (Ciccia, Ling, Coulthard, *et al.*, 2007). Although, it might be expected that any tumour cell line in the presence of PARP inhibition would exhibit genetic dependencies to these genes involved in DNA damage repair, different genetic dependencies were observed between LM7 and SAOS2, which suggests some residual reliance on HR by LM7. Although the RAD51 assay demonstrated the presence of an HR defect in LM7, this screen in the presence of olaparib suggested that HR has not been completely abrogated, since silencing of *BRCA1* and *BRCA2* still leads to a decrease in viability in the presence of PARP inhibition. In addition, silencing of *SHFM1* (*DDS)*, required for DNA damage induced RAD51 foci formation and *PALB2*, the partner and localiser of *BRCA2,* both had the same effect. Small-scale revalidation of these candidate genetic dependencies by deconvolution could be performed. Silencing of proteins involved in the HR response such as *XRCC3* and *RAD52*, by targeted siRNA in U2OS tumour cells induced a HR defect, PARP hyper-activation and increased sensitivity to PARP inhibitors (Michels, Vitale, Saparbaev, *et al.*, 2014). Therefore, further experiments to determine if exogenous expression of the genetic dependencies observed in LM7

rescue sensitivity to PARP inhibition, might help both with further understanding of the biology and could also be used as a biomarker for sensitivity to PARP inhibition. Tractable genetic dependencies of both LM7 and SAOS2, for example RAD51 and FANC proteins, in the presence of olaparib could also be used to explore possible combination therapies with PARP inhibition, although these drugs are still in pre-clinical investigation.

Deficiency of formation of RAD51 foci is known to be a mechanistic determinant of PARP-inhibitor sensitivity (Lord & Ashworth, 2012). At present, determination of RAD51 foci formation is an *ex vivo* assay that requires either treatment of *in* vitro cells with ionising radiation, or the patient to have had radiotherapy prior to tumour biopsy. Therefore, using RAD51 foci formation to determine potential sensitivity to PARP inhibition in a clinical trial setting is problematic. However, new techniques that do not have these requirements are in development and could provide a useful biomarker for patient selection and inclusion in clinical trials of PARP inhibitors.

Comparison of exome sequencing and mRNA transcriptome data of LM7 and SAOS2 was performed to identify any molecular differences between the two cells that could explain the sensitivity of LM7 to PARP inhibition. A number of molecular differences were observed, focussed on DNA damage repair such as missense mutations in LM7 of *HUS1, INIP,* and *EYA4*, and copy number changes in *SLX1A*, *PARPBP* and *CHEK2*; these could be investigated further to identify if these changes can explain the increased sensitivity to PARP by LM7 and therefore, if silencing could impart PARP sensitivity on SAOS2. Further confirmation could be investigated by a rescue experiment to determine if over expression of these genes impart PARP resistance on LM7. At a protein level, no significant changes in a subset (*BRCA2, CHK1, pCHK1, ATR* and *ATM)* of the known sensitisers to PARP inhibition were seen, but further work to clarify all sensitisers such as RAD51, ATRX, SHFM1, RPA1, NBN, miR-182, CDK1, SWI5–SFR1, USP1/ UAF1 and the Fanconi anaemia proteins could be performed. Proteomic profiling of LM7 and SAOS2 was performed and identified 11 proteins with the greatest differential abundance between the two tumour lines. Of these proteins, SMARCA1 involved in the DNA damage response and HIST2H2AB, a pseudo-gene of the histone family of proteins primarily responsible for nucleosome structure of the chromosomal fibre, and FANCD2 that co-localises with BRCA1 and directly involved in HR, were identified as having lower abundance in LM7 than SAOS2. These findings merit further investigation, to identify if silencing the genes encoding these proteins confers an increased sensitivity to PARP

inhibition on SAOS2, and if over expression using cDNA in a plasmid, rescues the PARP sensitivity seen with LM7. Potential differences of molecular or gene expression or proteomic abundance could lead to a biomarker for PARP sensitivity ensuring an enriched population for subsequent trials. At present, only mutations of *BRCA1/2* have been established as robust markers of PARP sensitivity (Brown, Kaye & Yap, 2016), or the use of a surrogate marker such as deficiency of RAD51 foci, which using the current methodology has considerable limitations. Increased expression of *PARPBP*, observed in LM7, and reported in pancreatic cancers, leads to PARP hyper-activation which may reflect DNA damage repair, and has already been postulated as a potential biomarker of PARP sensitivity (Michels, Vitale, Saparbaev, *et al.*, 2014). Further understanding of this relationship is required by investigation of *PARPBP* expression status and PARP sensitivity in tumour cell lines, or primary tumour models, with potential utility as an attractive biomarker. The LM7 and SAOS2 models could be used to determine the comparative status of other postulated biomarkers of PARP inhibitor sensitivity such increased *53BP1, PAR, EMSY. HER2, NF-kB* and *AURKA*, or decreased expression of *POLB, MRE11, XRCC1, CDK5, PLK3* and *MAPK12* (Michels, Vitale, Saparbaev, *et al.*, 2014).

Clarification of the protein expression status of phosphorylated CHK2 post exposure to olaparib, and also BRCA1 could be sought by western blotting. Expression of other molecular features characteristic of BRCAness such as *BAP1, BARD1,* and *FANCD2* could be investigated (Engert, Kovac, Baumhoer, *et al.*, 2016) along with other known determinants of sensitivity to PARP inhibition for example *RAD51, ATRX, SHFM1, RPA1, NBN*, miR-182, *CDK1, SWI5–SFR1, USP1/ UAF1* and the Fanconi anaemia proteins (Lord & Ashworth, 2012). Homozygous deletion of *ATRX* was observed in the OS tumour cell lines NOS-1 and U2OS that both exhibited moderate sensitivy to PARP inhibition. Whole genome sequencing of 34 OS tumour samples identified structural variants and point mutations of *ATRX* in 10 tumours (29%) (Chen, Bahrami, Pappo, *et al.*, 2014). *ATRX* mutations were observed in 11/31 (35%) OS tumour samples which were exome sequenced (Kovac, Blattmann, Ribi, *et al.*, 2015). Point mutations and structural variants of *ATRX* were also identified by whole genome and exome sequencing in another sequencing study of 112 OS tumour samples (Behjati, Tarpey, Haase, *et al.*, 2017). Determination of the potential utility of *ATRX* as a biomarker would require further correlation of precise mutation status with PARP sensitivity in a wider tumour panel.

The molecular phenotype of 'BRCAness' (Turner, Tutt & Ashworth, 2004) was described in section 1.1.4.1 of Chapter 1. As discussed above, a recent publication revealed a significant proportion of OS to potentially have a 'BRCAness' phenotype (Kovac, Blattmann, Ribi, *et al.*, 2015). There has been much recent debate as to the applicability of this phenotype in OS. On the basis of Kovac *et al.'s* findings investigation of the potential therapeutic opportunity in OS was undertaken using four OS tumour cell lines (MG63, ZK58, SAOS2, and HOSMMNG) which they reported to have disruptive gains in *PTEN* and *FANCD2* and / or losses of *ATM, BAP1, BARD1, FANCA* or *CHK2* and therefore functionally analogous to *BRCA* mutations, were observed to be susceptible to PARP inhibition by talazoparib (BMN-673) (Engert, Kovac, Baumhoer, *et al.*, 2016). However, very large doses of talazoparib (0.01-100μM), were needed to demonstrate sensitivity to the OS cell lines (Engert, Kovac, Baumhoer, *et al.*, 2016), which are unlikely to be clinically relevant, with no comparison of context by use of *BRCA 1/2* deficient cell lines for scale of sensitivity. Inspection of the screen data after short-term exposure to talazoparib (range 0.5-1000nM) did not demonstrate a profound sensitivity to PARP inhibition in the OS tumour cell line panel. In addition, data from the Wellcome Trust Sanger Institute demonstrated that of the whole-genome sequencing performed on 37 osteosarcoma tumour samples, only one, a radiation-induced OS, harboured evidence of HR deficiency using HRdetect methodology (mutation signature three) (Behjati, Tarpey, Haase, *et al.*, 2017; Davies, Glodzik, Morganella, *et al.*, 2017). From this series, nine different mutational signatures were represented, the most prevalent were signatures five (age-related mutational process), and eight (unknown origin) (Behjati, Tarpey, Haase, *et al.*, 2017). It was determined from that analysis that detection of the BRCAness molecular phenotype should only be performed on whole genome sequencing, not the whole-exome sequencing performed by Kovac *et al.* (Kovac, Blattmann, Ribi, *et al.*, 2015).

It is therefore likely that the degree of BRCAness of OS has been overstated by Kovac *et al.* due to differences in methodology (Kovac, Blattmann, Ribi, *et al.*, 2015). Nevertheless, exploiting the BRCAness phenotype in a subset of OS tumours could be therapeutically attractive. LM7 demonstrated differential sensitivity to PARP inhibition in both short and longer-term multi-dosing experiments. In addition, a marked deficiency in RAD51 foci formation after ionising radiation compared to SAOS2 was observed, suggestive of an HR defect that could explain the increased sensitivity seen with this tumour cell line. To further investigate a BRCAness phenotype in OS, LM7 the "daughter" of SAOS2, has the

potential to be an attractive model for investigation of mechanisms and potential biomarkers for patient selection for OS and more widely.

A number of PARP inhibitors are licenced for the treatment of cancer (Brown, Kaye & Yap, 2016), for example rucaparib and niraparib have been granted approval by the American Food and Drug Administration (FDA) for patients with BRCA mutant ovarian cancer, there are a number of Phase II Clinical trials of talazoparib, and olaparib has been licenced for use in *BRCA* mutant ovarian cancer by the National Institute of Clinical Excellence (NICE). These agents could be easily repositioned for use in OS, and their oral bioavailability with relatively fewer toxicity effects than traditional chemotherapy agents makes them attractive. Finding the appropriate subset of patients with OS that could benefit from these agents, by use of a biomarker, is therefore paramount for the translation of these pre-clinical findings into the clinic. Confirmation of an *in vivo* differential sensitivity to PARP inhibition using orthotopic mouse models of LM7 and SAOS2 that are already available (Jia, Worth & Kleinerman, 1999) is required. Considering the role of PARP inhibition is OS is challenging, not least due to the need for a biomarker for appropriate selection, but also determining the best combination therapy, and timing of PARP inhibitor treatment. Standard MAP chemotherapy is particularly toxic, and it is unlikely that addition of PARP therapy alongside MAP would be acceptable to the patient population, and delays to the current treatment schedule caused by any increase in toxicity profile could worsen outcomes. Consideration of PARP inhibition as a maintenance therapy after MAP chemotherapy therefore appears most plausible, similar to the approval of olaparib maintenance for ovarian carcinoma (Ledermann, Harter, Gourley, *et al.*, 2016), but PARP inhibitor monotherapy is unlikely to be effective in OS. For the addition of PARP inhibitor combination maintenance therapy to be successful, a balance must be struck between providing a sufficient survival extension with acceptable drug-related toxicity profile, to warrant use in an already heavily treated patient who would otherwise have an asymptomatic, treatment-free interval before progression (Graybill, Pothuri, Chase, *et al.*, 2017). One option would therefore be to perform a double-blinded clinical trial with randomisation at the end of MAP to PARP inhibitor combination therapy or placebo. In the absence of an appropriate biomarker to enrich the study population, parallel molecular characterisation of tumour samples could be undertaken in an attempt to determine a clinical biomarker.

An important consideration is the noticeable challenge of translating a drug from promising pre-clinical studies into the clinic. One example is the discovery that Ewing sarcoma cell lines that harboured the EWS-FLI1 rearrangement were particularly sensitive to single agent PARP inhibition by olaparib and rucaparib (Garnett, Edelman, Heidorn, *et al.*, 2012). Given strong pre-clinical data with a mechanistically plausible explanation, there was great enthusiasm in the community, which resulted in a Phase II clinical trial of olaparib in patients with refractory Ewing sarcoma following failure of chemotherapy (Choy, Butrynski, Harmon, *et al.*, 2014). However, it was closed at the interim analysis for lack of activity (Choy, Butrynski, Harmon, *et al.*, 2014). Unfortunately the profound responses seen both *in vitro* and *in vivo* were not replicated by this study. There are a number of possible explanations for this; (i) confirmation of *EWS-FLI1* rearrangement was not confirmed in patients enrolled in the study; (ii) the preclinical tumour cell line models might not be representative of the disease, for example might be chemotherapy naïve compared to patients with chemo-refractory disease; (iii) unknown secondary genomic or epigenomic alterations or tumour environment interactions leading to PARP inhibitor resistance (Choy, Butrynski, Harmon, *et al.*, 2014). There is however, also strong preclinical evidence of synergy of PARP inhibition given in combination with alkylating agents and topoisomerase inhibitors such as temozolomide or irinotecan which might prove more successful, and a phase I clinical trial to determine the safety of the PARP inhibitor niraparib in combination with temozolomide or irinotecan in patients with advanced Ewing sarcoma is currently in progress (NCT02044120). This example highlights the many challenges of drug translation into the clinic, confirming the need for reproducible models that are representative of the disease, and provides greater understanding of why so few agents are successful in the journey from bench to bedside.

This chapter has described a number of potential drugs for further validation for which are selective for *RB1* deficient OS tumour cells using the OS isogenic models. The drug screens presented are limited by both their potential applicability depending on the models used, and also by potential false positives and negatives via off-target effects and practicalities such as human error, reinforcing the need for robust revalidation. Further experiments to understand if these observations are confirmed firstly in the wider panel of OS tumour cell lines, and then *in vivo,* needs to be established prior to any further clinical translation. The challenges of identification of therapeutically relevant targets given the heterogeneity of the tumour, and difficulty of establishing a representative isogenic model of *RB1* deficiency in OS have been discussed; the synergy observed between VX970 and

cisplatin may be confined to the molecular background of U2OS, and will need further investigation in the tumour cell line to determine potential wider applicability.

The complexity of drug screens and challenge of validation in OS was confirmed in this chapter, however possible targets were identified which have therapeutic potential. However, what appears statistically significant in a drug screen may not necessarily be clinically relevant. Comparison of activity with appropriate models to determine context is very important, and thus highlights the investigation of PARP sensitivity in OS, where comparison was possible with models that are known to be reflective of sensitive disease in clinic. The most promising targets from this Chapter are FGFR1 inhibition in OS patients with *FGFR1* polysomy in addition to amplification, the use of *CDKN2A* or *MTAP* as a potential biomarker for methotrexate sensitivity, VX9070 in combination with cisplatin in *RB1* deficient tumours and PARP combination maintenance therapy in OS. The recent establishment of patient derived xenograph (PDX) models in osteosarcoma which more closely resemble the human disease on a morphological, histological and genomic level (Blattmann, Thiemann, Stenzinger, *et al.*, 2015) than previously used orthotopic models are well placed to investigate further the potential of PARP combinations. These agents are well positioned for clinical translation, methotrexate is already included in standard therapy, PARP inhibitors are licenced for use in other malignancies, and VX970 is in early Phase I/II trials. Specific inhibition of FGFR1 might prove more challenging, after one of the more promising agents (AZD4547) was withdrawn due to unwanted side effects. The data presented here supports the hypothesis that the multi-kinase inhibitor lenvatinib might be less effective in this population than a specific inhibitor of FGFR1. A more specific FGFR1 inhibitor has the potential for a better side effect profile, without hypertension and proteinuria associated with VEGFR blockade (Lewin & Siu, 2015). JNJ-42756493 an oral, selective pan-FGFR inhibitor that is reported to exhibit minimal activity against other kinases has completed Phase I trial in advanced solid tumours (Tabernero, Bahleda, Dienstmann, *et al.*, 2015), and due to start Phase II trial in paediatric patients with advanced solid malignancies (NCT03210714) and could be repositioned in OS.

8 General Discussion

8.1 RATIONALE FOR PROJECT

Since the introduction of MAP (methotrexate, doxorubicin and cisplatin) therapy, despite international collaboration, there has been little improvement in survival over the past two decades (Kempf-Bielack, Bielack, Jürgens, *et al.*, 2005; Janeway, Barkauskas, Krailo, *et al.*, 2012; Mirabello, Troisi & Savage, 2009) with five year survival remaining in the order of 70% for young patients with localised disease. For those with metastatic disease at diagnosis, outcome is poor with only 20-30% surviving for five years (Koboldt, Fulton, McLellan, *et al.*, 2012), and remains even more dismal for those with recurrence (Luetke, Meyers, Lewis, *et al.*, 2014). Therefore, identification of new therapeutic targets is critical.

8.2 SUMMARY OF WORK PRESENTED WITHIN THIS THESIS

8.2.1 Characterisation of osteosarcoma tumour cell line panel

Firstly, described in this thesis are a panel of OS tumour cell lines. Although a number of these OS tumour cell lines had already been genetically characterised by EuroBoNeT, a European Network of Excellence on bone tumours (http://www.eurobonet.eu) (Ottaviano, Schaefer, Gajewski, *et al.*, 2010) (Mohseny, Machado, Cai, *et al.*, 2011) further genetic characterisation of the remainder of the panel was undertaken at the Wellcome Trust Sanger Institute and Tumour Profiling Unit of the Institute of Cancer Research (ICR). Using the whole exome sequencing for the panel of 18 OS tumour cell lines, I was able to confirm that although a considerable degree of heterogeneity was observed, the spectrum of recurrent somatic mutations identified was reflective of those seen in recent sequencing of the clinical samples, and the panel was therefore a suitable model for further investigation of genetic dependency profiling of OS.

8.2.2 Generation of isogenic *RB1* deficient osteosarcoma tumour cell line models

To date, no stable isogenic model of *RB1* deficiency in OS had been described. Using CRISPR-Cas9 mutagenesis I was able to generate two stable models of *RB1* deficiency using the OS tumour cell line U2OS. These models were extensively characterised by transcriptome profiling, whole exome sequencing and proteomics and were robustly determined to suitable models to investigate the phenotype of *RB1* deficiency in OS.

They have the potential to be used to create an isogenic orthotopic mouse model of *RB1* deficiency that could be used for revalidation. The advantages and limitations of isogenic and non-isogenic models have been discussed, and provided the rationale for use of both systems in this thesis as a complementary approach.

8.2.3 Identification of candidate genetic dependencies in osteosarcoma

This thesis described the production of the first kinome-wide genetic dependency maps of multiple OS tumour cell line models on this scale. This data-set was made a publicly available resource for the identification of OS genetic dependencies by the inclusion in Cancer GD www.cancergd.org which provides a searchable collection of genetic vulnerabilities associated with the alteration of driver genes in cancer cell lines as part of a collaboration between the Institute of Cancer Research, Systems Biology Ireland, University College Dublin and the Health Research Board. Comparison of this data set with the non-osteosarcoma tumour cell line panel, demonstrated a reliance on the skeletal morphogenesis pathway in osteosarcoma (Campbell, Ryan, Brough, *et al.*, 2016). This was a particularly interesting finding given, the unbiased nature of the screening, and that OS derives from primitive bone-forming mesenchymal stem cells (MSC) (Gorlick, 2009). Further interrogation of this data set and integration with additional molecular characterisation such as transcriptome profiling for the entire OS tumour cell line panel could provide a powerful basis for future pre-clinical and clinical investigation.

8.2.4 *DYRK1A* and *RB1* synthetic lethality

In Chapter 5 I described the genetic vulnerabilities associated with the recurrent driver mutations of *RB1* and *CDKN2A.* Results from this thesis have established *DYRK1A* as a specific vulnerability for *RB1* deficient OS tumour cell lines, an observation also seen in two independent data sets comprised of multiple histologies (Cowley, Weir, Vazquez, *et al.*, 2014; Stockwell, Li, Aherne, *et al.*, 2012). Interpretation of the mechanism of synthetic lethality between *DYRK1A* and *RB1*, was complicated by the many roles of DYRK1A and unknown consequences of an deficient *RB1* context. Of greatest clinical relevance was the synergistic effect seen between harmine and cisplatin, however, further work is required to understand the mechanism. The lack of potency of the available DYRK1A inhibitors such as harmine was also challenging. A new small molecule inhibitor, GNF4877, with lower IC50 than harmine and potential for fewer/different off-target effects

(Shen, Taylor, Jin, *et al.*, 2015) has the potential to overcome some of these challenges. The work presented in this thesis established that the selectivity of silencing DYRK1A in *RB1* deficient OS tumour cells is due to an increase in apoptosis, but clarification is needed to confirm that this observation is independent of activation of the Fas/FasL pathway by off-target effects of harmine.

8.2.5 Identification of tractable targets in osteosarcoma

In Chapter 6 I described the results from a high-throughput cell-based drug screen performed in a panel of OS tumour cell lines. These agents have either been licenced for clinical use in cancer or are in early phase clinical trials and were selected because of their potential for rapid clinical translation. The heterogeneity of molecular landscape of OS makes finding new molecular targets challenging, this was highlighted by only a minority of tumour cell lines demonstrating sensitivity to the majority of drugs. Given that osteosarcoma is not a common tumour, further subdivision of the patient population into a number of minority subsets, makes biomarker patient selection a priority and necessitates international collaboration for trial recruitment.

Further to demonstrating a reliance on genes involved in 'skeletal system morphogenesis' including *FGFR1,* two FGFR inhibitors AZD4547 and PD173074, were found to be selective for osteosarcoma models independent of amplification status (Campbell, Ryan, Brough, *et al.*, 2016). In addition, both *FGFR1* amplification and polysomy in this panel of OS tumour cell lines were shown to be associated with significantly greater sensitivity to the *FGFR1* inhibitors than cell lines unknown or negative for amplification. Since nearly 10% of OS tumour samples from 288 patients exhibited *FGFR1* amplification, while approximately 50% of tumour samples were observed to have polysomy (Fernanda Amary, Ye, Berisha, *et al.*, 2014), these findings provide further rationale for investigation of FGFR inhibition as a therapy in OS and the use of *FGFR1* amplification and/or polysomy as molecular biomarkers to target specific patient groups, which are predicated to include a significant proportion of patients.

Another of the genes identified in 'skeletal system morphogenesis' was Platelet derived growth factor receptor alpha (*PDGFRA*). Olaratumab a novel antibody targeting PDGFRA, has recently been seen to improve overall survival for patients with metastatic soft tissue sarcoma in combination with doxorubicin compared to doxorubicin alone (Tap,

Jones, Van Tine, *et al.*, 2016) and olaratumab is now licenced for this indication. Olaratumab demonstrates anti-tumour activity in models of paediatric sarcoma including osteosarcoma (May, Loizos, Novosiadly, *et al.*, 2015). However, in a phase II study, the multi-kinase inhibitor imatinib, which has an IC50 of 100nM against PDGFR, did not exhibit sufficient activity in soft tissue sarcoma to warrant further investigation (Chugh, Wathen, Maki, *et al.*, 2009) and at present no suitable biomarkers for patient selection have been identified. Therefore, caution as to the clinical applicability of PDGFR inhibition in OS in the absence of a biomarker for patient selection must be noted.

Additionally, using the isogenic *RB1* deficient U2OS model, the ATR inhibitor VX970 was observed to potentiate the therapeutic effect of cisplatin in both *RB1* deficient clones compared to the parental *RB1* wildtype tumour cell line. Further validation of this effect is required in both longer-term assays in a wider tumour cell line panel, as well as studies to understand the mechanism, but given that cisplatin is one of the established therapeutic agents in OS, VX970 has the potential to be used as a biomarker driven chemo-sensitising agent. This will form part of a recently awarded Children with Cancer Grant, exploring *RB1* deficiency as an actionable target in paediatric bone and soft tissue sarcoma, led by Sybille Mittnacht at the UCL Cancer Institute.

MTAP and CDKN2A were identified as potential biomarkers for sensitivity to methotrexate. Further validation using tumour samples is now required and there are now a growing number of biobanks containing OS tumour samples such as the SARC Biospecimen Bank and at the Royal National Orthopaedic Hospital, where clinical information on chemotherapeutics and outcome is also available. Using these samples *CDKN2A* and *MTAP* status by immunohistochemistry could be retrospectively assessed, and correlated with response to therapy. However, this is confounded by likely co-treatment with doxorubicin and cisplatin in addition to methotrexate. This evidence could provide rationale for a clinical biomarker driven trial to establish if patients with defective *MTAP* or *CDKN2A* could achieve the same outcome with dose-reduction of methotrexate or preferentially identify patients for whom methotrexate is not useful. However, both of these options are limited by either the need for a costly phase III trial to identify if dose reduction of methotrexate, or a different agent in *CDKN2A*/MTAP wildtype patients could achieve the same or better outcome than current standard therapy. It would be difficult to envisage dose reduction of methotrexate, since even in patients with localised, resectable disease and a ‘good’ histological response (>90% necrosis) to neo-adjuvant

chemotherapy, event free survival is only 70% whilst those with a 'poor' response this lies below 50% (Bielack, 2002). Given the toxicity of high-dose methotrexate at the standard doses, combined with that of doxorubicin and cisplatin, it would be difficult to envisage increasing the dose of methotrexate in those patients who were *CDKN2A* or *MTAP* wildtype. Possible benefit would be most likely if an additional agent could be used in combination with or instead of methotrexate in this potential cohort.

8.2.6 'BRCAness' in osteosarcoma

After the drug screen was performed in the panel of OS tumour cell lines, two manuscripts were published which suggested that the majority of OS tumours harbour a BRCAness molecular phenotype due to HR deficiency, with sensitivity to PARP inhibition identified in a subset of OS tumour cell lines (Kovac, Blattmann, Ribi, *et al.*, 2015; Engert, Kovac, Baumhoer, *et al.*, 2016). On the basis of this evidence, a PARP inhibitor trial is currently being considered in patients with OS. However, using the HRdetect methodology (Davies, Glodzik, Morganella, *et al.*, 2017) to assess the mutational signatures of whole genome sequencing data from 37 OS tumour samples at the WTSI, only one, which was radiation induced, has shown evidence of HR deficiency (Behjati, Tarpey, Haase, *et al.*, 2017). From this series, nine different mutational signatures were represented, the most prevalent were signatures five (age-related mutational process), and eight (unknown origin) (Behjati, Tarpey, Haase, *et al.*, 2017). Kovac *et al.* classified the molecular phenotype using whole-exome sequencing not whole-genome, and thus potentially over stated any effect observed. In addition, very large doses of talazoparib (0.01-100μM), which are unlikely to be clinically relevant, were needed to demonstrate sensitivity to the OS cell lines (Engert, Kovac, Baumhoer, *et al.*, 2016), with no comparison of context by use of *BRCA 1/2* deficient cell lines for scale of sensitivity. In Chapter 6, short-term exposure to talazoparib did not demonstrate a profound sensitivity to PARP inhibition in the OS tumour cell line panel. Instead, the OS tumour cell lines demonstrated a spectrum of sensitivity to the PARP inhibitors talazoparib, rucaparib, and olaparib, with only a minority harbouring sensitivity comparable to other tumour cell lines with a 'BRCAness' phenotype.

Exploiting the BRCAness phenotype in a subset of OS tumours could be therapeutically attractive since inhibitors such as olaparib are already approved for the treatment of BRCA mutant ovarian cancer by NICE, rucaparib is FDA approved for BRCA mutant

ovarian cancer, and talazoparib is in Phase II clinical trial. These agents could be easily repositioned for use in OS, and their oral bioavailability with relatively fewer toxicity effects than traditional chemotherapy agents makes them attractive. However, from the data presented in this thesis, demonstrating that only a minority of OS tumour cell lines harbour sensitivity to PARP inhibition at clinically relevant doses, and data from the WTSI described above (Behjati, Tarpey, Haase, *et al.*, 2017), it is likely that the degree of BRCAness of OS has been overstated by Kovac *et al.* and Engert *et al.* (Kovac, Blattmann, Ribi, *et al.*, 2015; Engert, Kovac, Baumhoer, *et al.*, 2016). Therefore, single agent PARP inhibition is unlikely to have a significant impact in the therapy of OS, but there could be potential for biomarker driven PARP inhibitor combination studies in a subset of patients with OS. Although the majority of OS tumour cell lines do not exhibit the profound PARP inhibitor sensitivity associated with BRCAness, one OS tumour cell line, LM7, clearly demonstrates this phenotype. The absence of RAD51 foci in LM7 identifies this as a suitable, mechanistically relevant, tool for studying BRCAness in this cancer histology. SMARCA1, HIST2H2AB, or FANCD2, were found to have the greatest differential proteomic abundance between LM7 and parental SAOS2 tumour cell lines. Further comparison of molecular features in LM7 versus the parental SAOS2 cell line might inform the identification of molecular drivers of PARP inhibitor sensitivity in LM7. Therefore, there are many unanswered questions regarding the degree of BRCAness seen in OS. Further investigation of the cell lines using a RAD51 assay to determine if any OS tumour cell lines in addition to LM7 harbour an HR defect would be interesting and informative. Given the sensitivity to PARP inhibition seen in the small molecule screen performed in Chapter 6, it is likely that only a small minority possess such a defect. Determining the BRCAness phenotype of a tumour sample requires either the application of HRdetect (Davies, Glodzik, Morganella, *et al.*, 2017) on whole-genome sequencing or the use of an *ex vivo* RAD51 assay on sample material that has been exposed to DNA damage *in vivo*. New technology that could circumvent these challenges and make rapid assessment of an HR defect and thus potential sensitivity to PARP inhibition would improve real-time patient selection for clinical trials of PARP inhibitors in tumours such as OS, where no simple genetic marker of sensitivity as been isolated, unlike *BRCA1/2* deficiency in breast and ovarian malignancies.

8.3 OVERALL CONTEXT OF THIS STUDY

8.3.1 Clinical advances in immunotherapy in osteosarcoma

Recent advances in molecular profiling over the last decade have lead to increasing availability of large-scale genetic profiling, driving towards truly personalised medicine. Clinical trials are increasingly looking at the molecular as well as clinical phenotypes of disease, and patient selection is increasingly biomarker driven. A large number of molecularly targeted cancer drugs have now gained regulatory approval. However, despite considerable unmet need in OS, and increased understanding of the molecular landscape of OS, this is only just beginning to translate into specific therapies. During this thesis, immunotherapies emerged as the latest trend in cancer therapies, and appear therapeutically attractive with fewer side effects than conventional cytotoxic agents. These agents stimulate the innate and adaptive immune system to inhibit the tumour tolerance usually seen. A number of agents are currently in early Phase trials including aerosolised proleukin (Interleukin 2) (NCT01590069), avelumab (anti-Programmed cell death ligand 1 (PD-L1) antibody) (NCT03006848), pembrolizumab (anti-PD-L1 antibody) (NCT03013127) and anti-ganglioside GD2 antibody (NCT00743496). Aerosol IL-2 has been observed to stimulate local Natural Killer (NK) cell proliferation and increase NK numbers in the lungs of mice, inducing metastatic regression and increased overall survival (Guma, Lee, Ling, *et al.*, 2014). Cytotoxic T lymphocytes (CTLs) express PD1, a member of the Tumour Necrosis Factor (TNF) receptor family. Inhibition of PD1 by tumours leads to decreased CTL proliferation, cytokine production and cytotoxicity, and associated tumour progression in mice (Zitvogel & Kroemer, 2012). Both the CTLs which infiltrate OS and the OS tumour cells themselves express PD-L1, while inhibition of PD1-PD-L1 interactions improves outcome, and suppression of PD1 by mono-clonal antibody suppresses OS growth in mice models (Kansara, Teng, Smyth, *et al.*, 2014). The anti-PD-L1 antibody pembrolizumab has already been approved by NICE in patients with advanced non-small cell lung cancer. The addition of PEG-interferon 2beta to standard MAP chemotherapy has not shown any additional benefit (Bielack, Smeland, Whelan, *et al.*, 2015). Many of the signalling pathways with key roles in the immune system such as TNF Receptor Superfamily Member 11a (RANK-RANKL) signalling and the cytokines Interleukin 1 (IL1), IL6, IL17 and transforming growth factor-β (TGFβ), also have an overlapping role in osteoclastogeneis (Kansara, Teng, Smyth, *et al.*, 2014) the equilibrium between bone resorption by osteoclasts and bone formation by osteoblasts (Yavropoulou & Yovos, 2008). This overlap has been termed osteo-immunology (Kansara, Teng,

Smyth, *et al.*, 2014). Altered bone phenotypes have been seen in mice which are deficient for some of these genes such as interferon (α and β) receptor 1 (Ifnar1), nuclear factor-κB (Nfkb) and interferon-γ (Ifng) (Kansara, Teng, Smyth, *et al.*, 2014). Interestingly significantly increased survival rates have been observed in those patients with OS who develop postoperative infections (84.5% compared to 62.3%) (Jeys, Grimer, Carter, *et al.*, 2007). At present MTP-PE is the only immunotherapy in OS that is approved by the National Institute of Clinical Excellence (NICE) in the treatment of OS, although the true value remains unevaluated. Understanding the potential for targeting osteoimmunity is in its infancy and the true value remains to be evaluated.

8.3.2 Clinical advances in FGFR inhibition in osteosarcoma

During this thesis a number of monoclonal antibodies and specific tyrosine kinase inhibitors that target the FGFR receptor family have translated into Phase I/II clinical trials. Unfortunately, one trial of the inhibitor AZD4547 that aimed to explore efficacy in FGFR amplified osteosarcoma (NCT01795768) was suspended due to side effects. The FGFR1-4 inhibitor PRN1371 is currently in Phase I trial of patients with advanced solid tumours, and an expansion cohort of 20 patients, enriched for solid tumours with fibroblast *FGFR1-4* genetic alterations (NCT02608125). In addition, other multi-targeted kinase inhibitors such as lenvatinib are now in phase II investigation as single agent treatment in OS, and in Phase Ib study in combination with ifosfamide and etoposide in osteosarcoma (NCT02432274). Although marketed as a VEGF inhibitor, lenvatinib also targets FGFR1 with an IC50 of 46nmol/L (Cabanillas & Habra, 2016). The FGFR1-3 inhibitor INCB054828 is currently in Phase I trial in patients with advanced solid tumours, with preliminary data confirming a tolerable safety profile, and signs of efficacy in bladder tumours with *FGFR* genetic alterations (NCT02872714) (personal correspondence with Mark Linch). These inhibitors have the potential to be the first targeted kinase inhibitor in osteosarcoma, but further research is needed to identify markers of greatest efficacy and if there is potential for a durable response. These findings from this thesis provide further rationale for investigation of FGFR inhibition as a therapy in OS and the use of both *FGFR1* amplification and polysomy as molecular biomarkers to target specific patient groups. It would be valuable to measure *FGFR* status in patients on current clinical trials to determine whether there is any correlation with response to the therapy. A study of OS tumour samples from 288 patients, identified *FGFR1* amplification in nearly 10%, and

polysomy in 50% of tumour samples which suggest that a significant cohort of patients might benefit from FGFR1 inhibition (Fernanda Amary, Ye, Berisha, *et al.*, 2014).

8.4 LIMITATIONS OF STUDY AND ALTERNATIVE APPROACHES

8.4.1 Tumour cell line panel

While use of tumour cell lines grown in two-dimensional culture can provide a pragmatic and utilitarian approach, all tumour cell line models have limitations, given that they are grown in monolayer cultures on plastic and lack interaction with the surrounding tumour microenvironments seen *in vivo.* Growth of osteosarcoma spheroids in three-dimensional culture using murine tumour cell lines (Akeda, Nishimura, Satonaka, *et al.*, 2009) may address some of these caveats. However, a recent study investigating genetic dependencies and drug sensitivity in breast cancer tumour cell line cultures demonstrated a difference between two and three-dimensional culture, although these differences have the potential for therapeutical exploitation (Maguire, Peck, Wai, *et al.*, 2016; Imamura, Mukohara, Shimono, *et al.*, 2015). An alternative approach could have been to perform RNAi and drug screens using both two and three-dimensional culture of osteosarcoma tumour cell lines to provide a more complete representation of dependencies. However, molecular differences have been observed between tumour cell lines and the tumour sample they were derived from (Goodspeed, Heiser, Gray, *et al.*, 2016). Patient derived xenograft (PDX) models may help to conserve more of the molecular characteristics of the tumour sample, but still lack the interactions with tumour microenvironment (Goodspeed, Heiser, Gray, *et al.*, 2016). Mouse models have traditionally not been used for unbiased high-throughput screening, but recently 1000 PDX models were used to screen 62 drugs (Gao, Korn, Ferretti, *et al.*, 2015). This methodology could improve clinical translation, but is costly to run, and as yet is nascent in OS requiring robust validation of the relevance of the models.

Additionally, OS tumour samples that are sufficient both in quality and quantity for molecular characterisation, are more likely to be from patients with tumours that have residual disease post chemotherapy, and thus may skew interpretation of cell line data. In particular, interpretation of sensitivity to PARP and platinum chemotherapeutics needs to be carefully considered when selecting informative cell lines to evaluate mechanistic

interactions, and potential clinical applicability to the wider OS population. Generation of PDX or tumour cell line models from chemotherapy naïve OS tumour samples at diagnosis and subsequent comparison with regular biopsies during treatment would provide a more complete understanding of both the molecular evolution of the disease, response to selection pressures from chemotherapeutics, and the potential for success of drugs such as PARP inhibitors. Tumour evolution has already been reported in other malignancies (Gerlinger, Horswell, Larkin, *et al.*, 2014), but the recent evolution of single cell based molecular characterisation by DNA and RNA sequencing has enabled even greater insights into tumour evolution, and the intra- and inter-heterogeneity of the tumour population (Ellsworth, Blackburn, Shriver, *et al.*, 2017; Abbosh, Birkbak, Wilson, *et al.*, 2017; Jamal-Hanjani, Wilson, McGranahan, *et al.*, 2017). Future fluidic systems to simultaneously isolate and analyse the molecular alterations of millions of cells in parallel, and comparison of these at different time points, from both the primary site and metastatic lesions, could provide further insight into the driver variants of the disease, tumour development due to chromosomal instability and response to therapeutics (Ellsworth, Blackburn, Shriver, *et al.*, 2017). Single cell profiling in non-small cell lung cancer has already provided further understanding of driver events in both clonal and subclonal populations (Jamal-Hanjani, Wilson, McGranahan, *et al.*, 2017), but as yet detailed DNA and RNA sequencing of single cells in OS remains uncharacterised.

The first genome-wide study of proteomic abundance in osteosarcoma in a tumour cell line panel on this scale was also performed, although only a preliminary analysis of this data-set has been performed by Colm Ryan, Systems Biology Ireland; as the data was only available towards the end of this PhD, only initial descriptive results were reported here and form the basis of future work to integrate this with the RNAi and drug dependency data set.

8.4.2 High-throughput cell-based screening

High-throughput screening can provide a rapid way of providing unbiased data, and combining parallel drug and siRNA screening has the potential to be complementary and provide some cross-validation. However, siRNA and drug screening can present technical challenges including off-target effects and identification of false positives and negatives (Williamson, Miller, Pemberton, *et al.*, 2016). In-built redundancy in the screens, by use of multiple different siRNA species and inhibitors of the same target or

pathway, and robust quality control measures can help to reduce these challenges (Lord & Ashworth, 2012). In addition, since gene silencing with siRNA is only temporary, as siRNA are not replicated, the effects become more diluted with each cell division, therefore only phenotypes which require short-term silencing can be observed (Williamson, Miller, Pemberton, *et al.*, 2016). Also, given that gene silencing by siRNA can be transient and incomplete, the negative predictive value of any siRNA screen is limited. High-complementarity to the target mRNA is required for silencing of target genes by endo-nucleolytic cleavage and degradation, while off-target effects require only partial complementarity (Birmingham, Anderson, Reynolds, *et al.*, 2006). A seven to eight nucleotide seed region at the 5' end of the anti-sense strand which binds to the 3' un-translated region of a potential off-target gene is most important in generation of off-target effects (Birmingham, Anderson, Reynolds, *et al.*, 2006). Hence, validation to confirm an observed phenotype is due to an on-target effect is important. Despite these limitations I have identified a number of potential candidate genetic dependencies associated with *RB1* deficiency, and *DYRK1A* was confirmed in two independent data sets, with subsequent revalidation experiments.

Given the recent advances in CRISPR-Cas9 gene editing technology, which have enabled genome-wide gene silencing studies to be performed in both *in vitro* (Wang, Wei, Sabatini, *et al.*, 2014) and mouse models (Chen, Sanjana, Zheng, *et al.*, 2015; Burgess, 2015), such a screen could now be performed in osteosarcoma. CRIPSR-Cas9 technology is advantageous compared to siRNA technology, providing a stable gene silencing instead of a transient reduction in gene expression (Wang, Wei, Sabatini, *et al.*, 2014) but was not available at the beginning of this thesis. Creation of an isogenic *DYRK1A* deficient model in osteosarcoma with cre:lox controlled expression of exogenous DYRK1A may have provided additional benefit during revalidation of the synthetic lethality observed with *RB1.* A CRISPR-Cas9 gene-silencing screen in combination with small molecule inhibition of PARP might have been a more powerful approach to investigate acquired sensitivity to PARP inhibition in LM7.

8.5 FINAL CONCLUSIONS AND FUTURE DIRECTIONS

This thesis has provided a framework and basis for identification of novel therapeutic dependencies in OS, and has provided a number of interesting observations. Future work

to understand these further will involve a parallel approach: (i) further understanding of the mechanism of the *RB1 DYRK1A* synthetic lethality, and potential therapeutic applicability; (ii) validation and investigation into both the additional *RB1* synthetic lethalities identified in the isogenic *RB1* deficient U2OS models, and *CDKN2A* synthetic lethalities identified in the OS tumour cell line panel; (iii) investigation of the association of *FGFR1* amplification and polysomy with increased sensitivity to *FGFR1* small molecule inhibition; (iv) further investigation of the synergistic effect of VX970 in combination with cisplatin seen in the isogenic *RB1* deficient U2OS tumour cell lines models; (v) investigation of the association of *MTAP* / *CDKN2A* deficiency and sensitivity to methotrexate using clinical tumour samples; (vi) further investigation of the mechanism of acquired HR deficiency and sensitivity to PARP inhibition in the OS tumour cell line LM7; and (vii) investigation if a subset of OS tumour cell lines are sensitive to PARP inhibition in combination with other chemotherapeutics and identification of a biomarker of sensitivity.

Whilst I've established a synthetic lethality between silencing of *RB1* and *DYRK1A*, dependent on the kinase activity of DYRK1A, mediated by increased apoptosis, the exact mechanism has not been fully determined, in part due to multiple functions of DYRK1A and the low potency of the inhibitors available. Although the increase in apoptosis seen post exposure to harmine may possibly be explained by off target-effects of activation of the Fas/FasL pathway, which have been shown to activate Caspase-8 and Caspase-3 (Wang, Wang, Jiang, *et al.*, 2015), this would not explain the statistically significant difference in levels of apoptosis seen dependent on RB1 context. In addition, tumour cells deficient in *RB1* haven been shown to harbour a deficiency in caspase-8 expression secondary to epigenetic gene silencing by over methylation which prevents apoptosis triggered via the Fas/FasL pathway (Poulaki, Mitsiades, McMullan, *et al.*, 2005). It is therefore unlikely that potential off-target effects of harmine explain this observation. To determine if the Fas/FasL pathway has a role in both G2/M arrest and increased apoptosis post exposure to harmine, replication of the apoptosis assay and cell cycle profile in the presence on Fas/FasL blockade, or use of a structurally different DYRK1A inhibitor such as GNF4877 could be performed with coincident western blotting to determine if the Fas/FasL pathway is activated. If the G2/M arrest and resultant apoptosis, seen in *RB1* deficient tumour cells is due to the deleterious effects of deficient *RB1* on progression through mitosis (Dyson, 2016), expression of functional RB1 should reverse the phenotype. A DNA fibre assay could be performed to identify fork stalling,

while gamma H2AX assay could investigate for increased DNA damage in *RB1* deficient cells. In addition to these mechanistic experiments, long-term multiple-dosing experiments using the DYRK1A inhibitor GNF4877, alone and in combination with other cytotoxic agents, in particular anti-mitotic agents such as cisplatin, paclitaxel or vinblastine to look for potential synergy. Future work is under way to establish if these findings are replicated in OS primary tumour cell lines, which are thought more likely to closely reflect the clinical disease. Further confirmation of any effects would be necessary in an orthotopic mouse model or PDX prior to clinical translation. If this effect was also replicated with GNF4877 firstly in OS tumour cell lines, and then using either an orthotopic mouse model, or PDX, this could provide the rationale for a Phase I clinical trial in patients of osteosarcoma tumours that harbour *RB1* deficiency.

A number of additional candidate genetic dependencies were identified in the isogenic *RB1* deficient U2OS models, and *CDKN2A* synthetic lethalities identified in the OS tumour cell line panel could be validated firstly by deconvolution using multiple individual siRNA species targeting different regions of the gene, followed by additional orthogonal validation such as use of a drug with the same target if available.

Amplification of *FGFR1* was found to be significantly associated with increased sensitivity to FGFR1 inhibition, concordant with the observation in a mixed panel of tumour cell lines which included OS (Guagnano, Kauffmann, Wöhrle, *et al.*, 2012). A novel finding was the polysomy was also associated with an increase in sensitivity to both FGFR1 inhibitors. Lenvatinib, a multi-targeted kinase inhibitor, marketed as a VEGF inhibitor, but with nanomolar inhibition of FGFR1, (IC50 of 46nmol/L (Cabanillas & Habra, 2016)) is already in Phase 1b/II investigation both alone and in combination with ifosfamide and etoposide, in children and young people with osteosarcoma (NCT02432274). Potential candidates are the FGFR1-4 inhibitor PRN1371 currently in Phase I trial of patients with advanced solid tumours, and an expansion cohort of 20 patients, enriched for solid tumours with fibroblast FGFR1-4 genetic alterations (NCT02608125). Given that the OS tumour cell lines demonstrated greater sensitivity to FGFR1 inhibition that the non-osteosarcoma tumour cell lines, independent of amplification status, ideally a clinical trial of an FGFR1 inhibitor in all patients with advanced OS would be performed, parallel to confirmation of molecular alterations of *FGFR1*. However, to increase the power of the study, it is likely that enrichment of the patient population by selection of those with alterations of *FGFR1* or *FGFR1* amplification and/or polysomy would be necessary.

The ATR inhibitor VX970 was demonstrated to have a synergistic effect in combination with cisplatin in the isogenic *RB1* deficient U2OS tumour cell line models. Further investigation of this effect in a longer-term multiple dosing experiment, in a panel of OS tumour cell lines characterised for *RB1* deficiency should be performed. Replication of the effect in *RB1* deficient and wildtype orthotopic mouse models or PDX models with treatment arms comprised of vehicle, VX970, cisplatin, and VX970 in combination with cisplatin would be needed prior to clinical translation. To investigate if this relationship is due to defective NHEJ, increased reliance on the HR pathway in *RB1* deficient tumour cells (Huang, Cook & Mittnacht, 2015), and resultant increased importance of the DNA damage G2 checkpoint and functional ATR (Nghiem, Park, Kim, *et al.*, 2001; Eguchi, Takaki, Itadani, *et al.*, 2007), a number of experiments could be performed to further understand the mechanism. FACS could be used to determine if cell cycling is unaffected by DNA damage imparted by cisplatin and ATR inhibition. Also the γH2AX assay could be used to identify an increase of pan-nuclear γH2AX in response to replication fork stress, and DSB by presence of nuclear γH2AX foci (Ward & Chen, 2001) if *RB1* deficient tumour cells are more sensitive due to an impairment in DNA damage repair. In addition, both speed of replication forks, and also replication fork collapse, associated with ATR inhibition in combination with cisplatin (Reaper, Griffiths, Long, *et al.*, 2011) could be investigated. Further investigation into the mechanism of ATR and cisplatin inhibition in *RB1* deficient tumour cell lines, using some of the models used in this thesis is planned and supports the potential relevance of *RB1* as an actionable target in OS (personal correspondence Sybille Mittnacht, UCL).

VX970 is already in early phase clinical trials, one in combination with PARP inhibition and cisplatin in patients with advanced solid tumours (NCT02723864) and could be easily repositioned. Given that cisplatin is one of the established therapeutic agents in OS, VX970 has the potential to be used as a biomarker (*RB1* deficiency) driven chemo-sensitiser. However, even though VX970 has reportedly been well tolerated, the most frequently reported toxicities are of myelo-suppression. Considering cisplatin and doxorubicin in combination are already significantly myelo-suppressive, the practicalities of addition to the current schedule could be challenging, and possibly require a longer duration between cycles for count recovery or dose reduction of cisplatin; this would need to be balanced with possible deleterious effect on outcome due to reduction of dose-intensity and explored in a trial setting.

MTAP and CDKN2A were identified as possible biomarkers for sensitivity to methotrexate. Further validation could be performed by immunohistochemistry to identify MTAP or CDKN2A deficiency on tumour samples from the Royal National Orthopaedic Hospital, Stanmore Musculoskeletal Biobank, a satellite of the UCL/UCLH Biobank for Studying Health and Disease, and correlated with response to MAP chemotherapy at resection. Although confounded by doxorubicin and cisplatin therapy in combination with high-dose methotrexate, it could provide the rationale for a clinical biomarker driven trial to establish if patients with wildtype *MTAP* or *CDKN2A* could achieve the same or better outcome with a different agent instead of methotrexate.

The isogenic model such as SAOS2 and LM7 which has acquired HR deficiency and sensitivity to PARP inhibition provides an attractive model to identify markers of a 'BRCAness' phenotype and PARP inhibitor sensitivity in OS and a wider context. Mouse models of these tumour cell lines are already available (Jia, Worth & Kleinerman, 1999). Further work is needed to establish if silencing the genes encoding the proteins SMARCA1, HIST2H2AB, or FANCD2, confer an increased sensitivity to PARP inhibition on SAOS2, and if over expression of these genes using cDNA in a plasmid, rescues the PARP sensitivity seen with LM7. Investigation if any of the other OS tumour cell lines harbour an HR defect, by use of the RAD51 assay, could provide further evidence of the proportion of BRCAness seen in OS tumour cell lines and inform clinical trials. Finding the right subset of patients with OS that could benefit from these agents, by use of a biomarker, is critical for the successful translation of these pre-clinical findings into the clinic. It is more likely that a PARP inhibitor in combination with other chemotherapeutics would be most attractive, although finding a biomarker for sensitivity to PARP combinations and choice of additional agents are not without challenges (Dréan, Lord & Ashworth, 2016). A high-throughput drug screen with the addition of a PARP inhibitor using LM7 and SAOS2 could be performed to isolate the most synergistic combination. Confirmation experiments in a mouse model would be needed prior to clinical translation.

In conclusion, the use of integrated screens in this thesis has provided a framework for pre-clinical identification and validation of a number of tractable therapeutic targets to facilitate translation into development of clinical trials.

9 Appendix

Appendix Table 1 Kinome siRNA library

Gene ID	Entrez gene ID	Gene ID	Entrez gene ID	Gene ID	Entrez gene ID
213H19.1	51765	FYN	2534	PFKM	5213
AAK1	22848	GAK	2580	PFKP	5214
AATK	9625	GALK1	2584	PFTK1	5218
ABL1	25	GALK2	2585	PGK1	5230
ABL2	27	GCK	2645	PGK2	5232
ACVR1	90	GK	2710	PHKA1	5255
ACVR1B	91	GK2	2712	PHKA2	5256
ACVR1C	130399	GNE	10020	PHKB	5257
ACVR2	92	GOLGA5	9950	PHKG1	5260
ACVR2B	93	GRK1	6011	PHKG2	5261
ACVRL1	94	GRK4	2868	PI4K2B	55300
ADCK1	57143	GRK5	2869	PI4KII	55361
ADCK2	90956	GRK6	2870	PIK3C2A	5286
ADCK4	79934	GRK7	131890	PIK3C2G	5288
ADCK5	203054	GSG2	83903	PIK3C2G	5288
ADK	132	GSK3A	2931	PIK3C3	5289
ADP-GK	83440	GSK3B	2932	PIK3CA	5290
ADRBK1	156	GTF2H1	2965	PIK3CB	5291
ADRBK2	157	GUCY2C	2984	PIK3CD	5293
AIP1	9863	GUCY2D	3000	PIK3CG	5294
AK1	203	GUCY2F	2986	PIK3R1	5295
AK2	204	GUK1	2987	PIK3R2	5296
AK3	205	HAK	115701	PIK3R3	8503
AK3L1	50808	HCK	3055	PIK3R4	30849
AK5	26289	HIPK1	204851	PIK4CA	5297
AK7	122481	HIPK2	28996	PIK4CB	5298
AKT1	207	HIPK3	10114	PIM1	5292
AKT2	208	HIPK4	147746	PIM2	11040
AKT3	10000	HK1	3098	PIM3	415116

ALK	238	HUNK	30811	PINK1	65018
ALS2CR2	55437	HUS1	3364	PIP5K1A	8394
ALS2CR7	65061	ICK	22858	PIP5K1B	8395
AMHR2	269	IGF1R	3480	PIP5K1C	23396
ANKK1	255239	IGF2R	3482	PIP5K2A	5305
ANKRD3	54101	IHPK1	9807	PIP5K2B	8396
ARAF1	369	IHPK2	51447	PIP5K2C	79837
ARK5	9891	IHPK3	117283	PIP5K3	200576
ASK	10926	IKBKAP	8518	PIP5KL1	138429
ATM	472	IKBKB	3551	PKIA	5569
ATR	545	IKBKE	9641	PKIB	5570
AURKA	6790	IKBKG	8517	PKLR	5313
AURKB	9212	ILK	3611	PKM2	5315
AURKC	6795	ILK-2	55522	PKMYT1	9088
AXL	558	INSR	3643	PKN3	29941
BAIAP1	9223	INSRR	3645	PLK1	5347
BCKDK	10295	IPMK	253430	PLK2	10769
BCR	613	IRAK1	3654	PLK3	1263
BLK	640	IRAK2	3656	PLK4	10733
BMP2K	55589	IRAK3	11213	PMVK	10654
BMPR1A	657	IRAK4	51135	PNCK	139728
BMPR1B	658	ITK	3702	PNKP	11284
BMPR2	659	ITPK1	3705	PRKAA1	5562
BMX	660	ITPKA	3706	PRKAA2	5563
BRAF	673	ITPKB	3707	PRKAB1	5564
BRD2	6046	ITPKC	80271	PRKAB2	5565
BRD3	8019	JAK1	3716	PRKACA	5566
BRD4	23476	JAK2	3717	PRKACB	5567
BRDT	676	JAK3	3718	PRKAR1B	5575
BTK	695	JIK	51347	PRKAR2A	5576
BUB1	699	KALRN	8997	PRKAR2B	5577
BUB1B	701	KCNH2	3757	PRKCA	5578
C10ORF89	118672	KCNH8	131096	PRKCB1	5579
C14ORF20	283629	KDR	3791	PRKCD	5580

C7ORF2	64327	KHK	3795	PRKCE	5581
C9ORF12	64768	KIAA0999	23387	PRKCG	5582
C9ORF96	169436	KIAA1361	57551	PRKCH	5583
CALM1	801	KIAA1639	57729	PRKCI	5584
CALM2	805	KIAA1765	85443	PRKCL1	5585
CALM3	808	KIAA1804	84451	PRKCL2	5586
CAMK1	8536	KIAA1811	84446	PRKCM	5587
CAMK1D	57118	KIAA1811	84446	PRKCN	23683
CAMK1G	57172	KIAA2002	79834	PRKCQ	5588
CAMK2A	815	KIT	3815	PRKCSH	5589
CAMK2B	816	KSR	8844	PRKCZ	5590
CAMK2D	817	KSR2	283455	PRKD2	25865
CAMK2G	818	KUB3	91419	PRKDC	5591
CAMK4	814	LAK	80216	PRKG1	5592
CAMKK1	84254	LATS1	9113	PRKG2	5593
CAMKK1	84254	LATS2	26524	PRKR	5610
CAMKK2	10645	LCK	3932	PRKWNK1	65125
CARKL	23729	LIMK1	3984	PRKWNK2	65268
CASK	8573	LIMK2	3985	PRKWNK3	65267
CCRK	23552	LMTK2	22853	PRKX	5613
CDADC1	81602	LMTK3	114783	PRKY	5616
CDC2	983	LOC340156	340156	PRPF4B	8899
CDC2L1	984	LOC390226	390226	PRPS1	5631
CDC2L2	728642	LOC91461	91461	PRPS1L1	221823
CDC42BPA	8476	LRRK1	79705	PRPS2	5634
CDC42BPA	8476	LRRK2	120892	PSKH1	5681
CDC42BPB	9578	LTK	4058	PSKH2	85481
CDC7	8317	LYK5	92335	PTK2	5747
CDK10	8558	LYN	4067	PTK2B	2185
CDK11	23097	MAGI-3	260425	PTK6	5753
CDK2	1017	MAK	4117	PTK7	5754
CDK3	1018	MAP2K1	5604	PTK9	5756
CDK4	1019	MAP2K2	5605	PTK9L	11344
CDK5	1020	MAP2K3	5606	PXK	54899

CDK5R1	8851	MAP2K4	6416	PYCS	5832
CDK5R2	8941	MAP2K5	5607	RAF1	5894
CDK6	1021	MAP2K6	5608	RAGE	5891
CDK7	1022	MAP2K7	5609	RBKS	64080
CDK8	1024	MAP3K1	4214	RELA	5970
CDK9	1025	MAP3K10	4294	RET	5979
CDKL1	8814	MAP3K11	4296	RFK	55312
CDKL2	8999	MAP3K12	7786	RFP	5987
CDKL3	51265	MAP3K13	9175	RIOK1	83732
CDKL4	344387	MAP3K14	9020	RIOK2	55781
CDKL5	6792	MAP3K15	389840	RIOK3	8780
CDKN1A	1026	MAP3K2	10746	RIPK1	8737
CDKN1B	1027	MAP3K3	4215	RIPK2	8767
CDKN1C	1028	MAP3K4	4216	RIPK3	11035
CDKN2B	1030	MAP3K5	4217	RNASEL	6041
CDKN2C	1031	MAP3K6	9064	ROCK1	6093
CDKN2D	1032	MAP3K7	6885	ROCK2	9475
CERK	64781	MAP3K7IP1	10454	ROR1	4919
CHEK1	1111	MAP3K8	1326	ROR2	4920
CHEK2	11200	MAP4K1	11184	ROS1	6098
CHKA	1119	MAP4K1	11184	RP6-	
CHKB	1120	MAP4K2	5871	RPS6KA1	6195
CHUK	1147	MAP4K3	8491	RPS6KA2	6196
CIB2	10518	MAP4K4	9448	RPS6KA3	6197
CIT	11113	MAP4K5	11183	RPS6KA4	8986
CK2A	55450	MAPK1	5594	RPS6KA5	9252
CKB	1152	MAPK10	5602	RPS6KA6	27330
CKM	1158	MAPK11	5600	RPS6KB1	6198
CKMT1B	1159	MAPK12	6300	RPS6KB2	6199
CKMT2	1160	MAPK13	5603	RPS6KC1	26750
CKS1B	1163	MAPK14	1432	RPS6KL1	83694
CKS2	1164	MAPK3	5595	RYK	6259
CLK1	1195	MAPK4	5596	SAST	22983
CLK2	1196	MAPK6	5597	SBK1	388228

CLK3	1198	MAPK7	5598	SCAP1	8631
CLK4	57396	MAPK8	5599	SCYL1	57410
COASY	80347	MAPK9	5601	SGK	6446
CRIM1	51232	MAPKAPK2	9261	SGK2	10110
CRK7	51755	MAPKAPK3	7867	SGK223	157285
CRKL	1399	MAPKAPK5	8550	SGKL	23678
CSF1R	1436	MARK1	4139	SIK2	23235
CSK	1445	MARK2	2011	SLK	9748
CSNK1A1	1452	MARK3	4140	SMG1	23049
CSNK1A1L	122011	MARK4	57787	SNARK	81788
CSNK1D	1453	MAST2	23139	SNF1LK	150094
CSNK1E	1454	MAST3	23031	SNRK	54861
CSNK1G1	53944	MAST4	375449	SPEG	10290
CSNK1G2	1455	MASTL	84930	SPHK1	8877
CSNK1G3	1456	MATK	4145	SPHK2	56848
CSNK2A1	1457	MELK	9833	SRC	6714
CSNK2A2	1459	MERTK	10461	SRMS	6725
CSNK2B	1460	MET	4233	SRP72	6731
DAPK1	1612	MGC16169	93627	SRPK1	6732
DAPK2	23604	MGC42105	167359	SRPK2	6733
DAPK3	1613	MGC45428	166614	SSTK	83983
DCAMKL1	9201	MGC4796	83931	SSTK	83983
DCK	1633	MGC4796	83931	STK10	6793
DDR1	780	MGC8407	79012	STK11	6794
DDR2	4921	MIDORI	57538	STK16	8576
DGKA	1606	MINK	50488	STK17A	9263
DGKB	1607	MKNK1	8569	STK17B	9262
DGKD	8527	MKNK2	2872	STK19	8859
DGKG	1608	MLCK	91807	STK22B	23617
DGKH	160851	MULK	55750	STK22C	81629
DGKI	9162	MUSK	4593	STK22D	83942
DGKK	139189	MVK	4598	STK22D	83942
DGKQ	1609	MYLK	4638	STK23	26576
DGUOK	1716	MYLK2	85366	STK24	8428

DLG1	1739	MYO3A	53904	STK25	10494
DLG2	1740	MYO3B	140469	STK29	9024
DLG3	1741	N4BP2	55728	STK3	6788
DLG4	1742	NAGK	55577	STK31	56164
DMPK	1760	NEK1	4750	STK32A	202374
DTYMK	1841	NEK11	79858	STK32B	55351
DUSP21	63904	NEK2	4751	STK32C	282974
DUSTYPK	25778	NEK3	4752	STK33	65975
DYRK1A	1859	NEK4	6787	STK35	140901
DYRK1B	9149	NEK5	341676	STK36	27148
DYRK2	8445	NEK6	10783	STK38	11329
DYRK3	8444	NEK7	140609	STK38L	23012
DYRK4	8798	NEK8	284086	STK39	27347
EEF2K	29904	NEK9	91754	STK4	6789
EFNA3	1944	NLK	51701	STYK1	55359
EFNA4	1945	NME1	4830	SYK	6850
EFNA5	1946	NME2	4831	TAF1	6872
EFNB3	1949	NME3	4832	TAF1L	138474
EGFR	1956	NME4	4833	TAO1	9344
EIF2AK3	9451	NME5	8382	TBK1	29110
EIF2AK4	440275	NME6	10201	TEC	7006
EPHA1	2041	NME7	29922	TEK	7010
EPHA10	284656	NPR2	4882	TESK1	7016
EPHA2	1969	NRBP	29959	TESK2	10420
EPHA3	2042	NRBP2	340371	TEX14	56155
EPHA4	2043	NRK	203447	TGFBR1	7046
EPHA5	2044	NTRK1	4914	TGFBR2	7048
EPHA6	285220	NTRK2	4915	TGFBR3	7049
EPHA7	2045	NTRK3	4916	THNSL1	79896
EPHA8	2046	NUCKS	64710	TJP2	9414
EPHB1	2047	NUP62	23636	TK2	7084
EPHB2	2048	NYD-SP25	89882	TLK1	9874
EPHB3	2049	OSR1	9943	TLK2	11011
EPHB4	2050	P101-PI3K	23533	TNIK	23043

EPHB6	2051	PACE-1	57147	TNK1	8711
ERBB2	2064	PACSIN1	29993	TNK2	10188
ERBB3	2065	PAK1	5058	TNNI3K	51086
ERBB4	2066	PAK2	5062	TOPK	55872
ERK8	225689	PAK3	5063	TP53RK	112858
ERN1	2081	PAK4	10298	TPK1	27010
ERN2	10595	PAK6	56924	TRIB1	10221
ETNK1	55500	PAK7	57144	TRIB2	28951
EXOSC10	5394	PANK1	53354	TRIB3	57761
FASTK	10922	PANK2	80025	TRIO	7204
FER	2241	PANK3	79646	TRPM6	140803
FES	2242	PANK4	55229	TRPM7	54822
FGFR1	2260	PAPSS1	9061	TSKS	60385
FGFR2	2263	PAPSS2	9060	TTBK1	84630
FGFR3	2261	PASK	23178	TTBK2	146057
FGFR4	2264	PCK1	5105	TTK	7272
FGFRL1	53834	PCK2	5106	TYK2	7297
FGR	2268	PCTK1	5127	TYRO3	7301
FLJ10761	55224	PCTK2	5128	UCK1	83549
FLJ13052	65220	PCTK3	5129	UHMK1	127933
FLJ23356	84197	PDGFRA	5156	UKL3	25989
FLJ23356	84197	PDGFRB	5159	ULK1	8408
FLJ23356	84197	PDGFRL	5157	ULK2	9706
FLJ25006	124923	PDIK1L	149420	ULK4	54986
FLJ32685	152110	PDK1	5163	UMP-CMPK	51727
FLJ34389	197259	PDK2	5164	UMPK	7371
FLT1	2321	PDK3	5165	URKL1	54963
FLT3	2322	PDK4	5166	VRK1	7443
FLT4	2324	PDPK1	5170	VRK2	7444
FN3K	64122	PDXK	8566	VRK3	51231
FN3KRP	79672	PFKFB1	5207	WEE1	7465
FRAP1	2475	PFKFB2	5208	WNK4	65266
FRDA	2395	PFKFB3	5209	XYLB	9942

FRK	2444	PFKFB4	5210	YES1	7525
FUK	197258	PFKL	5211	ZAK	51776

Appendix Table 2 Tumour suppressor gene siRNA library

Gene ID	Entrez gene ID	Gene ID	Entrez gene ID	Gene ID	Entrez gene ID
APC	324	FANCD2	2177	PRKAR1A	5573
ATM	472	FANCE	2178	PTCH	5727
BHD	201163	FANCF	2188	PTEN	5728
BLM	641	FANCG	2189	RB1	5925
BMPR1A	657	FAS	355	RECQL4	9401
BRCA1	672	FBXW7	55294	SBDS	51119
BRCA2	675	FH	2271	SDHB	6390
BRIP1	83990	FLJ21816	79728	SDHC	6391
BUB1B	701	FLJ39827	139285	SDHD	6392
CDH1	999	GPC3	2719	SMAD4	4089
CDKN2A	1029	HRPT2	79577	SMARCB1	6598
CHEK2	11200	MAP2K4	6416	SOCS1	8651
COPEB	1316	MEN1	4221	STK11	6794
CYLD	1540	MLH1	4292	SUFU	51684
DDB2	1643	MSH2	4436	TCF1	6927
EP300	2033	MSH6	2956	TP53	7157
ERCC2	2068	MUTYH	4595	TSC1	7248
ERCC3	2071	NBS1	4683	TSC2	7249
ERCC4	2072	NF1	4763	VHL	7428
ERCC5	2073	NF2	4771	WAS	7454
EXT1	2131	PHOX2B	8929	WRN	7486
EXT2	2132	PIK3R1	5295	WT1	7490
FANCA	2175	PMS1	5378	XPA	7507
FANCC	2176	PMS2	5395	XPC	7508
				ZNFN1A1	10320

Appendix Table 3 Cancer Gene Census siRNA library

Gene ID	Entrez gene ID	Gene ID	Entrez gene ID	Gene ID	Entrez gene ID
ABI1	10006	GAS7	8522	PMS2	5395
ACKR3	57007	GATA1	2623	PNKP	11284
ACSL3	2181	GATA3	2625	POLB	5423
ACSL6	23305	GEN1	348654	POLD1	5424
AFF3	3899	GMPS	8833	POLE	5426
AKAP9	10142	GNA11	2767	POLG	5428
ALDH2	217	GNAQ	2776	POLH	5429
ALKBH2	121642	GNAS	2778	POLI	11201
ALKBH3	221120	GOPC	57120	POLK	51426
AMER1	139285	GTF2H1	2965	POLL	27343
APEX1	328	GTF2H2	2966	POLM	27434
APEX2	27301	GTF2H3	2967	POLN	353497
APTX	54840	GTF2H4	2968	POLQ	10721
ARHGAP26	23092	GTF2H5	404672	POT1	25913
ARHGEF12	23365	H2AFX	3014	POU2AF1	5450
ARID1A	8289	H3F3A	3020	POU5F1	5460
ARID2	196528	H3F3A	3020	PPARG	5468
ARNT	405	HELQ	113510	PPP2R1A	5518
ASPSCR1	79058	HERPUD1	9709	PRCC	5546
ASXL1	171023	HEY1	23462	PRDM1	639
ATF1	466	HIP1	3092	SSX4	6759
ATM	472	HIST1H4I	8294	STAT3	6774
ATR	545	HMGA1	3159	STAT5B	6777
ATRX	546	HMGA2	8091	SUZ12	23512
AXIN1	8312	HMGN2P46	283651	TAF15	8148
BAP1	8314	HNRNPA2B1	3181	TAL1	6886
BCL10	8915	HOOK3	84376	TBL1XR1	79718
BCL11A	53335	HOXA11	3207	TCEA1	6917
BCL2	596	HOXA13	3209	TCF12	6938
BCL3	602	HOXA9	3205	TCF3	6929
BCL6	604	HOXC11	3227	TCF7L2	6934

BCL7A	605	HOXC13	3229	TDG	6996
BCL9	607	HOXD11	3237	TDP1	55775
BCOR	54880	HOXD13	3239	TDP2	51567
BIRC3	330	HRAS	3265	TERT	7015
BLM	641	HSP90AA1	3320	TET2	54790
BRCA1	672	HSP90AB1	3326	TFE3	7030
BRCA2	675	HUS1	3364	TFEB	7942
BRIP1	83990	IDH1	3417	TFG	10342
C15orf65	145788	IDH2	3418	TFRC	7037
C19orf40	91442	NFKB2	4791	THRAP3	9967
C2orf44	80304	NHEJ1	79840	TMPRSS2	7113
CAMTA1	23261	NIN	51199	TNFAIP3	7128
CANT1	124583	NKX2-1	7080	TNFRSF14	8764
CARD11	84433	NONO	4841	TNFRSF17	608
CBL	867	NOTCH1	4851	TNKS_TNKS2	8658_80351
CBLB	868	NOTCH2	4853	TOP1	7150
CBLC	23624	NPM1	4869	TP53	7157
CCDC6	8030	NR4A3	8013	TP53BP1	7158
CCNB1IP1	57820	NRAS	4893	TPM3	7170
CCND1	595	NSD1	64324	TPR	7175
CCND2	894	NT5C2	22978	TRAF7	84231
CCND3	896	NTHL1	4913	TREX1	11277
CCNE1	898	NUDT1	4521	TREX2	11219
CCNH	902	NUMA1	4926	TRIM24	8805
CCNL1	57018	NUTM1	256646	TRIM27	5987
CD74	972	NUTM2A	728118	TRIM33	51592
CDH11	1009	NUTM2B	729262	TRIP11	9321
CDK12	51755	OGG1	4968	TSHR	7253
CDK7	1022	OMD	4958	TTL	150465
FANCG	2189	P2RY8	286530	U2AF1	7307
FANCI	55215	PAFAH1B2	5049	UBE2A	7319
FANCL	55120	PALB2	79728	UBE2B	7320
FANCM	57697	PARP1	142	UBE2N	7334
FAS	355	PARP2	10038	UBE2V2	7336

FASN	2194	PATZ1	23598	UBR5	51366
FBXO11	80204	PAX3	5077	UNG	7374
FEN1	2237	PAX7	5081	USP6	9098
FEV	54738	PAX8	7849	VTI1A	143187
FGFR1OP	11116	PBRM1	55193	WHSC1	7468
FHIT	2272	PCM1	5108	WHSC1L1	54904
FIP1L1	81608	PCNA	5111	WIF1	11197
FLI1	2313	PCSK7	9159	WRN	7486
FNBP1	23048	PDCD1LG2	80380	WWTR1	25937
FOXL2	668	PDGFB	5155	XAB2	56949
FOXO1	2308	PHF6	84295	XPA	7507
FOXO3	2309	PICALM	8301	XPC	7508
FOXP1	27086	PLAG1	5324	XRCC1	7515
FUBP1	8880	PML	5371	XRCC2	7516
FUS	2521	PMS1	5378	XRCC3	7517

10 References

Abbosh, C., Birkbak, N.J., Wilson, G.A., Jamal-Hanjani, M., et al. (2017) Phylogenetic ctDNA analysis depicts early-stage lung cancer evolution. *Nature*. 545 (7655), 446–451.

Akeda, K., Nishimura, A., Satonaka, H., Shintani, K., et al. (2009) Three-dimensional alginate spheroid culture system of murine osteosarcoma. *Oncology reports*. 22 (5), 997–1003.

Alexandrov, L.B., Nik-Zainal, S., Wedge, D.C., Aparicio, S.A.J.R., et al. (2013) Signatures of mutational processes in human cancer. *Nature*.

Amato, A., Schillaci, T., Lentini, L. & Di Leonardo, A. (2009) CENPA overexpression promotes genome instability in pRb-depleted human cells. *Molecular cancer*. 8 (1), 119.

Anders, C., Niewoehner, O., Duerst, A. & Jinek, M. (2014) Structural basis of PAM-dependent target DNA recognition by the Cas9 endonuclease. *Nature*. 513 (7519), 569–573.

Anders, S., Pyl, P.T. & Huber, W. (2015) HTSeq--a Python framework to work with high-throughput sequencing data. *Bioinformatics*. 31 (2), 166–169.

Anderson, P.M., Bielack, S.S., Gorlick, R.G., Skubitz, K., et al. (2016) A phase II study of clinical activity of SCH 717454 (robatumumab) in patients with relapsed osteosarcoma and Ewing sarcoma. *Pediatric blood & cancer*. 63 (10), 1761–1770.

Angelini, A., Mavrogenis, A.F., Trovarelli, G., Ferrari, S., et al. (2016) Telangiectatic osteosarcoma: a review of 87 cases. *Journal of cancer research and clinical oncology*. 142 (10), 2197–2207.

Angstadt, A.Y., Motsinger-Reif, A., Thomas, R., Kisseberth, W.C., et al. (2011) Characterization of canine osteosarcoma by array comparative genomic hybridization and RT-qPCR: signatures of genomic imbalance in canine osteosarcoma parallel the human counterpart. *Genes, chromosomes & cancer*. 50 (11), 859–874.

Araki, N., Uchida, A., Kimura, T., Yoshikawa, H., et al. (1991) Involvement of the retinoblastoma gene in primary osteosarcomas and other bone and soft-tissue tumors. *Clinical orthopaedics and related research*. (270), 271–277.

Aranda, S., Laguna, A. & la Luna, de, S. (2011) DYRK family of protein kinases: evolutionary relationships, biochemical properties, and functional roles. *The FASEB Journal*. 25 (2), 449–462.

Arora, S., Gonzales, I.M., Hagelstrom, R.T., Beaudry, C., et al. (2010) RNAi phenotype profiling of kinases identifies potential therapeutic targets in Ewing's sarcoma. *Molecular cancer*. 9218.

Ashburner, M., Ball, C.A., Blake, J.A., Botstein, D., et al. (2000) Gene ontology: tool for the unification of biology. The Gene Ontology Consortium. *Nature genetics*. 25 (1), 25–29.

Ashford, A.L., Oxley, D., Kettle, J., Hudson, K., et al. (2014) A novel DYRK1B inhibitor AZ191 demonstrates that DYRK1B acts independently of GSK3β to phosphorylate cyclin D1 at Thr(286), not Thr(288). *The Biochemical journal*. 457 (1), 43–56.

Ashworth, A., Lord, C.J. & Reis-Filho, J.S. (2011) Genetic interactions in cancer progression and treatment. *Cell*. 145 (1), 30–38.

Aydin, Ö.Z., Vermeulen, W. & Lans, H. (2014) ISWI chromatin remodeling complexes in the DNA damage response. *Cell cycle*. 13 (19), 3016–3025.

Bacci, G., Briccoli, A., Longhi, A., Ferrari, S., et al. (2005) Treatment and outcome of recurrent osteosarcoma: experience at Rizzoli in 235 patients initially treated with neoadjuvant chemotherapy. *Acta oncologica*. 44 (7), 748–755.

Bacci, G., Longhi, A., Fagioli, F., Briccoli, A., et al. (2005) Adjuvant and neoadjuvant chemotherapy for osteosarcoma of the extremities: 27 year experience at Rizzoli Institute, Italy. *European journal of cancer*. 41 (18), 2836–2845.

Bacci, G., Mercuri, M., Longhi, A., Ferrari, S., et al. (2005) Grade of chemotherapy-induced necrosis as a predictor of local and systemic control in 881 patients with non-metastatic osteosarcoma of the extremities treated with neoadjuvant chemotherapy in a single institution. *European journal of cancer*. 41 (14), 2079–2085.

Bacci, G., Picci, P., Ruggieri, P., Mercuri, M., et al. (1990) Primary chemotherapy and delayed surgery (neoadjuvant chemotherapy) for osteosarcoma of the extremities. The Istituto Rizzoli Experience in 127 patients treated preoperatively with intravenous methotrexate (high versus moderate doses) and intraarterial cisplatin. *Cancer*. 65 (11), 2539–2553.

Bajrami, I., Kigozi, A., Van Weverwijk, A., Brough, R., et al. (2012) Synthetic lethality of PARP and NAMPT inhibition in triple-negative breast cancer cells. *EMBO molecular medicine*. 4 (10), 1087–1096.

Barbie, D.A., Tamayo, P., Boehm, J.S., Kim, S.Y., et al. (2009) Systematic RNA interference reveals that oncogenic KRAS-driven cancers require TBK1. *Nature*. 462 (7269), 108–112.

Becker, W. (2012) Emerging role of DYRK family protein kinases as regulators of protein stability in cell cycle control. *Cell cycle*. 11 (18), 3389–3394.

Behjati, S., Tarpey, P.S., Haase, K., Ye, H., et al. (2017) Recurrent mutation of IGF signalling genes and distinct patterns of genomic rearrangement in osteosarcoma. *Nature Communications*. 815936.

Berger, M.F., Lawrence, M.S., Demichelis, F., Drier, Y., et al. (2011) The genomic complexity of primary human prostate cancer. *Nature*. 470 (7333), 214–220.

Berman, S.D., Calo, E., Landman, A.S., Danielian, P.S., et al. (2008) Metastatic osteosarcoma induced by inactivation of Rb and p53 in the osteoblast lineage. *Proceedings of the National Academy of Sciences of the United States of America*. 105 (33), 11851–11856.

Bertino, J.R., Waud, W.R., Parker, W.B. & Lubin, M. (2011) Targeting tumors that lack

methylthioadenosine phosphorylase (MTAP) activity: current strategies. *Cancer biology & therapy*. 11 (7), 627–632.

Bielack, S.S. (2002) Prognostic Factors in High-Grade Osteosarcoma of the Extremities or Trunk: An Analysis of 1,702 Patients Treated on Neoadjuvant Cooperative Osteosarcoma Study Group Protocols. *Journal of Clinical Oncology*. 20 (3), 776–790.

Bielack, S.S., Kempf-Bielack, B., Delling, G., Exner, G.U., et al. (2002) Prognostic factors in high-grade osteosarcoma of the extremities or trunk: an analysis of 1,702 patients treated on neoadjuvant cooperative osteosarcoma study group protocols. *Journal of clinical oncology*. 20 (3), 776–790.

Bielack, S.S., Smeland, S., Whelan, J.S., Marina, N., et al. (2015) Methotrexate, Doxorubicin, and Cisplatin (MAP) Plus Maintenance Pegylated Interferon Alfa-2b Versus MAP Alone in Patients With Resectable High-Grade Osteosarcoma and Good Histologic Response to Preoperative MAP: First Results of the EURAMOS-1 Good Response Randomized Controlled Trial. *Journal of clinical oncology*. 33 (20), 2279–2287.

Bignell, G.R., Greenman, C.D., Davies, H., Butler, A.P., et al. (2010) Signatures of mutation and selection in the cancer genome. *Nature*. 463 (7283), 893–898.

Birch, J.M., Blair, V., Kelsey, A.M., Evans, D.G., et al. (1998) *Cancer phenotype correlates with constitutional TP53 genotype in families with the Li-Fraumeni syndrome.* 17 (9), 1061–1068.

Birmingham, A., Anderson, E.M., Reynolds, A., Ilsley-Tyree, D., et al. (2006) 3' UTR seed matches, but not overall identity, are associated with RNAi off-targets. *Nature methods*. 3 (3), 199–204.

Blattmann, C., Thiemann, M., Stenzinger, A., Roth, E.K., et al. (2015) Establishment of a patient-derived orthotopic osteosarcoma mouse model. *Journal of Translational Medicine*. 13 (1), 136.

Bogliolo, M. & Surrallés, J. (2013) *The Fanconi Anemia/BRCA Pathway: FANCD2 at the Crossroad between Repair and Checkpoint Responses to DNA Damage*.

Boichuk, S., Parry, J.A., Makielski, K.R., Litovchick, L., et al. (2013) The DREAM complex mediates GIST cell quiescence and is a novel therapeutic target to enhance imatinib-induced apoptosis. *Cancer research*. 73 (16), 5120–5129.

Bolstad, B.M., Irizarry, R.A., Astrand, M. & Speed, T.P. (2003) A comparison of normalization methods for high density oligonucleotide array data based on variance and bias. *Bioinformatics*. 19 (2), 185–193.

Borriello, A., Caldarelli, I., Bencivenga, D., Criscuolo, M., et al. (2011) p57(Kip2) and cancer: time for a critical appraisal. *Molecular cancer research : MCR*. 9 (10), 1269–1284.

Boucher, D., Hillier, S., Newsome, D., Wang, Y., et al. (2016) Preclinical characterization of the selective DNA-dependent protein kinase (DNA-PK) inhibitor VX-984 in combination with chemotherapy. *Annals of oncology*. 27 (suppl_6).

Boutros, M., Brás, L.P. & Huber, W. (2006) Analysis of cell-based RNAi screens. *Genome biology*. 7 (7), R66.

Brenneman, M.A., Weiss, A.E., Nickoloff, J.A. & Chen, D.J. (2000) XRCC3 is required for efficient repair of chromosome breaks by homologous recombination. *Mutation research*. 459 (2), 89–97.

Brooks, C.L. & Gu, W. (2011) The impact of acetylation and deacetylation on the p53 pathway. *Protein & Cell*. 2 (6), 456–462.

Broto, J.M., Redondo, A., Valverde, C.M., Salgado, M.A.V., et al. (2015) *Phase II trial of gemcitabine plus rapamycin as second line in advanced osteosarcoma: A Spanish Group for Sarcoma Research (GEIS) Study.*

Brough, R., Frankum, J.R., Sims, D., Mackay, A., et al. (2011) Functional viability profiles of breast cancer. *Cancer Discovery*. 1 (3), 260–273.

Brown, J.S., Kaye, S.B. & Yap, T.A. (2016) PARP inhibitors: the race is on. *British Journal of Cancer*. 114 (7), 713–715.

Bryant, H.E., Schultz, N., Thomas, H.D., Parker, K.M., et al. (2005) Specific killing of BRCA2-deficient tumours with inhibitors of poly(ADP-ribose) polymerase. *Nature*. 434 (7035), 913–917.

Burgess, D.J. (2015) Cancer genetics: CRISPR screens go in vivo. *Nature Reviews Genetics*. 16 (4), 194–195.

Burrell, R.A., McGranahan, N., Bartek, J. & Swanton, C. (2013) The causes and consequences of genetic heterogeneity in cancer evolution. *Nature*. 501 (7467), 338–345.

Cabanillas, M.E. & Habra, M.A. (2016) Lenvatinib: Role in thyroid cancer and other solid tumors. *Cancer treatment reviews*. 4247–55.

Cahill, D.P., Lengauer, C., Yu, J., Riggins, G.J., et al. (1998) Mutations of mitotic checkpoint genes in human cancers. *Nature*. 392 (6673), 300–303.

Calvert, G.T., Randall, R.L., Jones, K.B., Cannon-Albright, L., et al. (2012) At-risk populations for osteosarcoma: the syndromes and beyond. *Sarcoma*. 2012 (4), 152382–152389.

Campbell, J., Ryan, C.J., Brough, R., Bajrami, I., et al. (2016) Large-Scale Profiling of Kinase Dependencies in Cancer Cell Lines. *Cell Reports*. 14 (10), 2490–2501.

Ceccaldi, R., Sarangi, P. & D'Andrea, A.D. (2016) The Fanconi anaemia pathway: new players and new functions. *Nature Reviews Molecular Cell Biology*. 17 (6), 337–349.

Chawla, S.P., Staddon, A.P., Baker, L.H., Schuetze, S.M., et al. (2012) Phase II study of the mammalian target of rapamycin inhibitor ridaforolimus in patients with advanced bone and soft tissue sarcomas. *Journal of Clinical Oncology*. 30 (1), 78–84.

Chen, J.-Y., Lin, J.-R., Tsai, F.-C. & Meyer, T. (2013) Dosage of Dyrk1a shifts cells within a p21-cyclin D1 signaling map to control the decision to enter the cell cycle.

Molecular cell. 52 (1), 87–100.

Chen, Q., Chao, R., Chen, H., Hou, X., et al. (2005) Antitumor and neurotoxic effects of novel harmine derivatives and structure-activity relationship analysis. *International Journal of Cancer*. 114 (5), 675–682.

Chen, S., Sanjana, N.E., Zheng, K., Shalem, O., et al. (2015) Genome-wide CRISPR screen in a mouse model of tumor growth and metastasis. *Cell*. 160 (6), 1246–1260.

Chen, X., Bahrami, A., Pappo, A., Easton, J., et al. (2014) Recurrent Somatic Structural Variations Contribute to Tumorigenesis in Pediatric Osteosarcoma. *Cell Reports*. 7 (1), 104–112.

Chou, A.J., Kleinerman, E.S., Krailo, M.D., Chen, Z., et al. (2009) Addition of muramyl tripeptide to chemotherapy for patients with newly diagnosed metastatic osteosarcoma: a report from the Children's Oncology Group. *Cancer*. 115 (22), 5339–5348.

Choy, E., Butrynski, J.E., Harmon, D.C., Morgan, J.A., et al. (2014) Phase II study of olaparib in patients with refractory Ewing sarcoma following failure of standard chemotherapy. *BMC cancer*. 14 (1), 813.

Chu, I.M., Hengst, L. & Slingerland, J.M. (2008) The Cdk inhibitor p27 in human cancer: prognostic potential and relevance to anticancer therapy. *Nature reviews. Cancer*. 8 (4), 253–267.

Chugh, R., Wathen, J.K., Maki, R.G., Benjamin, R.S., et al. (2009) Phase II multicenter trial of imatinib in 10 histologic subtypes of sarcoma using a bayesian hierarchical statistical model. *Journal of Clinical Oncology*. 27 (19), 3148–3153.

Ciccia, A., Ling, C., Coulthard, R., Yan, Z., et al. (2007) Identification of FAAP24, a Fanconi anemia core complex protein that interacts with FANCM. *Molecular cell*. 25 (3), 331–343.

Cingolani, P., Platts, A., Wang, L.L., Coon, M., et al. (2012) A program for annotating and predicting the effects of single nucleotide polymorphisms, SnpEff: SNPs in the genome of Drosophila melanogaster strain w1118; iso-2; iso-3. *Fly*. 6 (2), 80–92.

Clarke, A.R., Maandag, E.R., van Roon, M., van der Lugt, N.M., et al. (1992) Requirement for a functional Rb-1 gene in murine development. *Nature*. 359 (6393), 328–330.

Cleton-Jansen, A.-M., Anninga, J.K., Briaire-de Bruijn, I.H., Romeo, S., et al. (2009) Profiling of high-grade central osteosarcoma and its putative progenitor cells identifies tumourigenic pathways. *British Journal of Cancer*. 101 (11), 1909–1918.

Cook, R., Zoumpoulidou, G., Luczynski, M.T., Rieger, S., et al. (2015) Direct involvement of retinoblastoma family proteins in DNA repair by non-homologous end-joining. *Cell Reports*. 10 (12), 2006–2018.

Coscia, F., Watters, K.M., Curtis, M., Eckert, M.A., et al. (2016) Integrative proteomic profiling of ovarian cancer cell lines reveals precursor cell associated proteins and functional status. *Nature Communications*. 712645.

Cowley, G.S., Weir, B.A., Vazquez, F., Tamayo, P., et al. (2014) Parallel genome-scale loss of function screens in 216 cancer cell lines for the identification of context-specific genetic dependencies. *Scientific data*. 1140035.

Cox, J., Hein, M.Y., Luber, C.A., Paron, I., et al. (2014) Accurate Proteome-wide Label-free Quantification by Delayed Normalization and Maximal Peptide Ratio Extraction, Termed MaxLFQ. *Molecular & Cellular Proteomics*. 13 (9), 2513–2526.

Dai, Y. & Grant, S. (2010) New insights into checkpoint kinase 1 in the DNA damage response signaling network. *Clinical cancer research: an official journal of the American Association for Cancer Research*. 16 (2), 376–383.

Dalla-Torre, C.A., Yoshimoto, M., Lee, C.-H., Joshua, A.M., et al. (2006) Effects of THBS3, SPARC and SPP1 expression on biological behavior and survival in patients with osteosarcoma. *BMC cancer*. 6237.

Dasari, S. & Tchounwou, P.B. (2014) Cisplatin in cancer therapy: molecular mechanisms of action. *European journal of pharmacology*. 740364–378.

Davies, H., Glodzik, D., Morganella, S., Yates, L.R., et al. (2017) HRDetect is a predictor of BRCA1 and BRCA2 deficiency based on mutational signatures. *Nature medicine*. 23 (4), 517–525.

De Vos, M., Schreiber, V. & Dantzer, F. (2012) The diverse roles and clinical relevance of PARPs in DNA damage repair: current state of the art. *Biochemical pharmacology*. 84 (2), 137–146.

DeLaney, T.F., Park, L., Goldberg, S.I., Hug, E.B., et al. (2005) Radiotherapy for local control of osteosarcoma. *International journal of radiation oncology, biology, physics*. 61 (2), 492–498.

Demetri, G.D., Chawla, S.P., Ray-Coquard, I., Le Cesne, A., et al. (2013) Results of an international randomized phase III trial of the mammalian target of rapamycin inhibitor ridaforolimus versus placebo to control metastatic sarcomas in patients after benefit from prior chemotherapy. *Journal of Clinical Oncology*. 31 (19), 2485–2492.

Dick, F.A. (2007) Structure-function analysis of the retinoblastoma tumor suppressor protein - is the whole a sum of its parts? *Cell division*. 2 (1), 26.

Doench, J.G., Petersen, C.P. & Sharp, P.A. (2003) siRNAs can function as miRNAs. *Genes & development*. 17 (4), 438–442.

Dowjat, W.K., Adayev, T., Kuchna, I., Nowicki, K., et al. (2007) Trisomy-driven overexpression of DYRK1A kinase in the brain of subjects with Down syndrome. *Neuroscience letters*. 413 (1), 77–81.

Dréan, A., Lord, C.J. & Ashworth, A. (2016) PARP inhibitor combination therapy. *Critical reviews in oncology/hematology*. 10873–85.

Dréan, A., Williamson, C.T., Brough, R., Brandsma, I., et al. (2017) Modelling therapy resistance in BRCA1/2 mutant cancers. *Molecular cancer therapeutics*.

Druker, B.J., Talpaz, M., Resta, D.J., Peng, B., et al. (2001) Efficacy and safety of a

specific inhibitor of the BCR-ABL tyrosine kinase in chronic myeloid leukemia. *New England Journal of Medicine*. 344 (14), 1031–1037.

Duan, X., Jia, S.-F., Koshkina, N. & Kleinerman, E.S. (2006) Intranasal interleukin-12 gene therapy enhanced the activity of ifosfamide against osteosarcoma lung metastases. *Cancer*. 106 (6), 1382–1388.

Duan, Z., Ji, D., Weinstein, E.J., Liu, X., et al. (2010) Lentiviral shRNA screen of human kinases identifies PLK1 as a potential therapeutic target for osteosarcoma. *Cancer letters*. 293 (2), 220–229.

Duan, Z., Zhang, J., Choy, E., Harmon, D., et al. (2012) Systematic kinome shRNA screening identifies CDK11 (PITSLRE) kinase expression is critical for osteosarcoma cell growth and proliferation. *Clinical Cancer Research*. 18 (17), 4580–4588.

Dyson, N.J. (2016) RB1: a prototype tumor suppressor and an enigma. *Genes & development*. 30 (13), 1492–1502.

Echeverri, C.J. & Perrimon, N. (2006) High-throughput RNAi screening in cultured cells: a user's guide. *Nature Reviews Genetics*. 7 (5), 373–384.

Edwards, S.L., Brough, R., Lord, C.J., Natrajan, R., et al. (2008) Resistance to therapy caused by intragenic deletion in BRCA2. *Nature*. 451 (7182), 1111–1115.

Eguchi, T., Takaki, T., Itadani, H. & Kotani, H. (2007) RB silencing compromises the DNA damage-induced G2/M checkpoint and causes deregulated expression of the ECT2 oncogene. *Oncogene*. 26 (4), 509–520.

Eilber, F., Giuliano, A., Eckardt, J., Patterson, K., et al. (1987) Adjuvant chemotherapy for osteosarcoma: a randomized prospective trial. *Journal of clinical oncology*. 5 (1), 21–26.

Eisenhauer, E.A., Therasse, P., Bogaerts, J., Schwartz, L.H., et al. (2009) New response evaluation criteria in solid tumours: revised RECIST guideline (version 1.1). *European journal of cancer.* 45 (2) pp.228–247.

El-Nassan, H.B. (2013) Advances in the discovery of kinesin spindle protein (Eg5) inhibitors as antitumor agents. *European journal of medicinal chemistry*. 62614–631.

Ellsworth, D.L., Blackburn, H.L., Shriver, C.D., Rabizadeh, S., et al. (2017) Single-cell sequencing and tumorigenesis: improved understanding of tumor evolution and metastasis. *Clinical and translational medicine*. 6 (1), 15.

Elstrodt, F., Hollestelle, A., Nagel, J.H.A., Gorin, M., et al. (2006) BRCA1 mutation analysis of 41 human breast cancer cell lines reveals three new deleterious mutants. *Cancer research*. 66 (1), 41–45.

Engert, F., Kovac, M., Baumhoer, D., Nathrath, M., et al. (2016) Osteosarcoma cells with genetic signatures of BRCAness are susceptible to the PARP inhibitor talazoparib alone or in combination with chemotherapeutics. *Oncotarget*. 5 (0).

Fan, Y., Ge, N., Wang, X., Sun, W., et al. (2014) Amplification and over-expression of MAP3K3 gene in human breast cancer promotes formation and survival of breast

cancer cells. *The Journal of pathology*. 232 (1), 75–86.

Farmer, H., McCabe, N., Lord, C.J., Tutt, A.N.J., et al. (2005) Targeting the DNA repair defect in BRCA mutant cells as a therapeutic strategy. *Nature*. 434 (7035), 917–921.

Fernanda Amary, M., Ye, H., Berisha, F., Khatri, B., et al. (2014) Fibroblastic growth factor receptor 1 amplification in osteosarcoma is associated with poor response to neo-adjuvant chemotherapy. *Cancer medicine*. 3 (4), 980–987.

Fernández-Martínez, P., Zahonero, C. & Sánchez-Gómez, P. (2015) DYRK1A: the double-edged kinase as a protagonist in cell growth and tumorigenesis. *Molecular & cellular oncology*. 2 (1), e970048.

Ferrari, S., Briccoli, A., Mercuri, M., Bertoni, F., et al. (2003) Postrelapse survival in osteosarcoma of the extremities: prognostic factors for long-term survival. *Journal of clinical oncology*. 21 (4), 710–715.

Fleuren, E.D.G., Versleijen-Jonkers, Y.M.H., Boerman, O.C. & van der Graaf, W.T.A. (2014) Targeting receptor tyrosine kinases in osteosarcoma and Ewing sarcoma: Current hurdles and future perspectives. *Biochimica et biophysica acta*. 1845 (2), 266–276.

Fong, P.C., Boss, D.S., Yap, T.A., Tutt, A., et al. (2009) Inhibition of poly(ADP-ribose) polymerase in tumors from BRCA mutation carriers. *New England Journal of Medicine*. 361 (2), 123–134.

Forbes, S.A., Beare, D., Gunasekaran, P., Leung, K., et al. (2015) COSMIC: exploring the world's knowledge of somatic mutations in human cancer. *Nucleic acids research*. 43 D805–D811.

Fujiwara-Okada, Y., Matsumoto, Y., Fukushi, J., Setsu, N., et al. (2013) Y-box binding protein-1 regulates cell proliferation and is associated with clinical outcomes of osteosarcoma. *British Journal of Cancer*. 108 (4), 836–847.

Futreal, P.A., Coin, L., Marshall, M., Down, T., et al. (2004) A census of human cancer genes. *Nature reviews. Cancer*. 4 (3), 177–183.

Gaj, T., Gersbach, C.A. & Barbas, C.F. (2013) ZFN, TALEN, and CRISPR/Cas-based methods for genome engineering. *Trends in biotechnology*. 31 (7), 397–405.

Gao, H., Korn, J.M., Ferretti, S., Monahan, J.E., et al. (2015) High-throughput screening using patient-derived tumor xenografts to predict clinical trial drug response. *Nature medicine*. 21 (11), 1318–1325.

Garnett, M.J., Edelman, E.J., Heidorn, S.J., Greenman, C.D., et al. (2012) Systematic identification of genomic markers of drug sensitivity in cancer cells. *Nature*. 483 (7391), 570–575.

Gaspar, N., Melcon, M.S.G., Venkatramani, R., Bielack, S.S., et al. (2017) Single-agent dose-finding cohort of a phase 1/2 study of lenvatinib (LEN) in children and adolescents with refractory or relapsed solid tumors. *Journal of Clinical Oncology*.

Gavine, P.R., Mooney, L., Kilgour, E., Thomas, A.P., et al. (2012) AZD4547: an orally

bioavailable, potent, and selective inhibitor of the fibroblast growth factor receptor tyrosine kinase family. *Cancer research*. 72 (8), 2045–2056.

Gerlinger, M., Horswell, S., Larkin, J., Rowan, A.J., et al. (2014) Genomic architecture and evolution of clear cell renal cell carcinomas defined by multiregion sequencing. *Nature genetics*. 46 (3), 225–233.

Gokgoz, N., Wunder, J.S., Mousses, S., Eskandarian, S., et al. (2001) Comparison of p53 mutations in patients with localized osteosarcoma and metastatic osteosarcoma. *Cancer*. 92 (8), 2181–2189.

Gonzalez-Vasconcellos, I., Anastasov, N., Sanli-Bonazzi, B., Klymenko, O., et al. (2013) Rb1 haploinsufficiency promotes telomere attrition and radiation-induced genomic instability. *Cancer research*. 73 (14), 4247–4255.

Goodspeed, A., Heiser, L.M., Gray, J.W. & Costello, J.C. (2016) Tumor-Derived Cell Lines as Molecular Models of Cancer Pharmacogenomics. *Molecular cancer research : MCR*. 14 (1), 3–13.

Goodwin, J.F. & Knudsen, K.E. (2014) Beyond DNA repair: DNA-PK function in cancer. *Cancer Discovery*. 4 (10), 1126–1139.

Gorlick, R. (2009) Current concepts on the molecular biology of osteosarcoma. *Cancer treatment and research*. 152467–478.

Gorlick, R., Anderson, P., Andrulis, I., Arndt, C., et al. (2003) Biology of childhood osteogenic sarcoma and potential targets for therapeutic development: meeting summary. *Clinical cancer research.* 9 (15), 5442–5453.

Göckler, N., Jofre, G., Papadopoulos, C., Soppa, U., et al. (2009) Harmine specifically inhibits protein kinase DYRK1A and interferes with neurite formation. *The FEBS journal*. 276 (21), 6324–6337.

Graybill, W.S., Pothuri, B., Chase, D.M. & Monk, B.J. (2017) Poly(ADP-ribose) polymerase (PARP) inhibitors as treatment versus maintenance in ovarian carcinoma. *Gynecologic oncology*. 146 (1), 11–15.

Grignani, G., Palmerini, E., Dileo, P., Asaftei, S.D., et al. (2012) A phase II trial of sorafenib in relapsed and unresectable high-grade osteosarcoma after failure of standard multimodal therapy: an Italian Sarcoma Group study. *Annals of oncology*. 23 (2), 508–516.

Grignani, G., Palmerini, E., Ferraresi, V., D'Ambrosio, L., et al. (2014) Sorafenib and everolimus for patients with unresectable high-grade osteosarcoma progressing after standard treatment: a non-randomised phase 2 clinical trial. *The lancet oncology*. (14)71136-2.

Grimer, R.J. (2005) Surgical options for children with osteosarcoma. *The lancet oncology*. 6 (2), 85–92.

Guagnano, V., Kauffmann, A., Wöhrle, S., Stamm, C., et al. (2012) FGFR genetic alterations predict for sensitivity to NVP-BGJ398, a selective pan-FGFR inhibitor. *Cancer Discovery*. 2 (12), 1118–1133.

Guimera, J., Casas, C., Estivill, X. & Pritchard, M. (1999) HumanMinibrainHomologue (MNBH/DYRK1): Characterization, Alternative Splicing, Differential Tissue Expression, and Overexpression in Down Syndrome. *Genomics*. 57 (3), 407–418.

Guma, S.R., Lee, D.A., Ling, Y., Gordon, N., et al. (2014) Aerosol interleukin-2 induces natural killer cell proliferation in the lung and combination therapy improves the survival of mice with osteosarcoma lung metastasis. *Pediatric blood & cancer*. 61 (8), 1362–1368.

Guo, X., Williams, J.G., Schug, T.T. & Li, X. (2010) DYRK1A and DYRK3 promote cell survival through phosphorylation and activation of SIRT1. *Journal of Biological Chemistry*. 285 (17), 13223–13232.

Hall, A.B., Newsome, D., Wang, Y., Boucher, D.M., et al. (2014) Potentiation of tumor responses to DNA damaging therapy by the selective ATR inhibitor VX-970. *Oncotarget*. 5 (14), 5674–5685.

Hawkins, M.M., Wilson, L.M., Burton, H.S., Potok, M.H., et al. (1996) Radiotherapy, alkylating agents, and risk of bone cancer after childhood cancer. *Journal of the National Cancer Institute*. 88 (5), 270–278.

Hernando, E., Nahlé, Z., Juan, G., Diaz-Rodriguez, E., et al. (2004) Rb inactivation promotes genomic instability by uncoupling cell cycle progression from mitotic control. *Nature*. 430 (7001), 797–802.

Himpel, S., Panzer, P., Eirmbter, K., Czajkowska, H., et al. (2001) Identification of the autophosphorylation sites and characterization of their effects in the protein kinase DYRK1A. *The Biochemical journal*. 359 (Pt 3), 497–505.

Hingorani, P., Zhang, W., Gorlick, R. & Kolb, E.A. (2009) Inhibition of Src Phosphorylation Alters Metastatic Potential of Osteosarcoma In vitro but not In vivo. *Clinical Cancer Research*. 15 (10), 3416–3422.

Hong, D., Infante, J., Janku, F., Jones, S., et al. (2016) Phase I Study of LY2606368, a Checkpoint Kinase 1 Inhibitor, in Patients With Advanced Cancer. *Journal of Clinical Oncology*. 34 (15), 1764–1771.

Hu, Y., Bobb, D., He, J., Hill, D.A., et al. (2015) The HSP90 inhibitor alvespimycin enhances the potency of telomerase inhibition by imetelstat in human osteosarcoma. *Cancer biology & therapy*. 16 (6), 949–957.

Huang, J., Gong, Z., Ghosal, G. & Chen, J. (2009) SOSS Complexes Participate in the Maintenance of Genomic Stability. *Molecular cell*. 35 (3), 384–393.

Huang, P.H., Cook, R. & Mittnacht, S. (2015) RB in DNA repair. *Oncotarget*. [Online] 6 (25), 20746–20747.

Huen, M.S.Y. & Chen, J. (2008) The DNA damage response pathways: at the crossroad of protein modifications. *Cell research*. 18 (1), 8–16.

Imamura, Y., Mukohara, T., Shimono, Y., Funakoshi, Y., et al. (2015) Comparison of 2D- and 3D-culture models as drug-testing platforms in breast cancer. *Oncology reports*. 33 (4), 1837–1843.

Ionescu, A., Dufrasne, F., Gelbcke, M., Jabin, I., et al. (2012) DYRK1A kinase inhibitors with emphasis on cancer. *Mini reviews in medicinal chemistry*. 12 (13), 1315–1329.

Iorns, E., Lord, C.J., Grigoriadis, A., McDonald, S., et al. (2009) Integrated functional, gene expression and genomic analysis for the identification of cancer targets. *PloS one*. 4 (4), e5120.

Iorns, E., Lord, C.J., Turner, N. & Ashworth, A. (2007) Utilizing RNA interference to enhance cancer drug discovery. *Nature reviews. Drug discovery*. 6 (7), 556–568.

Iorns, E., Turner, N.C., Elliott, R., Syed, N., et al. (2008) Identification of CDK10 as an important determinant of resistance to endocrine therapy for breast cancer. *Cancer Cell*. 13 (2), 91–104.

Ishida, N., Kitagawa, M., Hatakeyama, S. & Nakayama, K. (2000) Phosphorylation at serine 10, a major phosphorylation site of p27(Kip1), increases its protein stability. *The Journal of biological chemistry*. 275 (33), 25146–25154.

Islam, M.A., Sharif, S.R., Lee, H., Seog, D.-H., et al. (2015) N-acetyl-D-glucosamine kinase interacts with dynein light-chain roadblock type 1 at Golgi outposts in neuronal dendritic branch points. *Experimental & molecular medicine*. 47 (8), e177.

Jackson, A.L. & Linsley, P.S. (2010) Recognizing and avoiding siRNA off-target effects for target identification and therapeutic application. *Nature reviews. Drug discovery*. 9 (1), 57–67.

Jaffe, N., Frei, E., Traggis, D. & Bishop, Y. (1974) Adjuvant methotrexate and citrovorum-factor treatment of osteogenic sarcoma. *New England Journal of Medicine*. 291 (19), 994–997.

Jamal-Hanjani, M., Wilson, G.A., McGranahan, N., Birkbak, N.J., et al. (2017) Tracking the Evolution of Non-Small-Cell Lung Cancer. *New England Journal of Medicine*. 376 (22), 2109–2121.

Janeway, K.A. & Gorlick, R. (2016) The case for informative phase 2 trials in osteosarcoma. *The lancet oncology*. 17 (8), 1022–1023.

Janeway, K.A., Barkauskas, D.A., Krailo, M.D., Meyers, P.A., et al. (2012) *Outcome for adolescent and young adult patients with osteosarcoma: a report from the Children's Oncology Group.* 118 (18), 4597–4605.

Janku, F., Hong, D.S., Fu, S., Piha-Paul, S.A., et al. (2014) Assessing PIK3CA and PTEN in early-phase trials with PI3K/AKT/mTOR inhibitors. *Cell Reports*. 6 (2), 377–387.

Jeys, L.M., Grimer, R.J., Carter, S.R., Tillman, R.M., et al. (2007) Post operative infection and increased survival in osteosarcoma patients: are they associated? *Annals of surgical oncology*. 14 (10), 2887–2895.

Jia, S.F., Worth, L.L. & Kleinerman, E.S. (1999) A nude mouse model of human osteosarcoma lung metastases for evaluating new therapeutic strategies. *Clinical & experimental metastasis*. 17 (6), 501–506.

Jiang, C. & You, Q. (2013) Kinesin spindle protein inhibitors in cancer: a patent review

(2008 - present). *Expert opinion on therapeutic patents*. 23 (12), 1547–1560.

Jinek, M., Chylinski, K., Fonfara, I., Hauer, M., et al. (2012) A Programmable Dual-RNA–Guided DNA Endonuclease in Adaptive Bacterial Immunity. *Science (New York, N.Y.)*. 337 (6096), 816–821.

Jones, K.B. (2011) Osteosarcomagenesis: Modeling Cancer Initiation in the Mouse. *Sarcoma*. 2011 (3), 1–10.

Jullien, N., Dieudonné, F.-X., Habel, N., Marty, C., et al. (2013) ErbB3 silencing reduces osteosarcoma cell proliferation and tumor growth in vivo. *Gene*. 521 (1), 55–61.

Kang, J.E., Choi, S.A., Park, J.B. & Chung, K.C. (2005) Regulation of the proapoptotic activity of huntingtin interacting protein 1 by Dyrk1 and caspase-3 in hippocampal neuroprogenitor cells. *Journal of Neuroscience Research*. 81 (1), 62–72.

Kansara, M. & Thomas, D.M. (2007) Molecular pathogenesis of osteosarcoma. *Dna and Cell Biology*. 26 (1), 1–18.

Kansara, M., Teng, M.W., Smyth, M.J. & Thomas, D.M. (2014) Translational biology of osteosarcoma. *Nature reviews. Cancer*. 14 (11), 722–735.

Kappel, C.C., Velez-Yanguas, M.C., Hirschfeld, S. & Helman, L.J. (1994) Human osteosarcoma cell lines are dependent on insulin-like growth factor I for in vitro growth. *Cancer research*. 54 (10), 2803–2807.

Kempf-Bielack, B., Bielack, S.S., Jürgens, H., Branscheid, D., et al. (2005) Osteosarcoma relapse after combined modality therapy: an analysis of unselected patients in the Cooperative Osteosarcoma Study Group (COSS). *Journal of clinical oncology*. 23 (3), 559–568.

King, C., Diaz, H.B., McNeely, S., Barnard, D., et al. (2015) LY2606368 Causes Replication Catastrophe and Antitumor Effects through CHK1-Dependent Mechanisms. *Molecular cancer therapeutics*. 14 (9), 2004–2013.

Kleinerman, R.A., Schonfeld, S.J. & Tucker, M.A. (2012) Sarcomas in hereditary retinoblastoma. *Clinical Sarcoma Research*. 2 (1), 15.

Knudsen, E.S. & Knudsen, K.E. (2008) Tailoring to RB: tumour suppressor status and therapeutic response. *Nature reviews. Cancer*. 8 (9), 714–724.

Knudsen, E.S. & Wang, J.Y.J. (2010) Targeting the RB-pathway in cancer therapy. *Clinical cancer research : an official journal of the American Association for Cancer Research*. 16 (4), 1094–1099.

Koboldt, D.C., Fulton, R.S., McLellan, M.D., Schmidt, H., et al. (2012) Comprehensive molecular portraits of human breast tumours. *Nature*. 490 (7418), 61–70.

Kolb, E.A., Gorlick, R., Houghton, P.J., Morton, C.L., et al. (2008) Initial testing (stage 1) of a monoclonal antibody (SCH 717454) against the IGF-1 receptor by the pediatric preclinical testing program. *Pediatric blood & cancer*. 50 (6), 1190–1197.

Konopka, J.B., Watanabe, S.M. & Witte, O.N. (1984) An alteration of the human c-abl

protein in K562 leukemia cells unmasks associated tyrosine kinase activity. *Cell*. 37(3),1035-1042.

Kovac, M., Blattmann, C., Ribi, S., Smida, J., et al. (2015) Exome sequencing of osteosarcoma reveals mutation signatures reminiscent of BRCA deficiency. *Nature Communications*. 68940.

Kresse, S.H., Rydbeck, H., Skårn, M., Namløs, H.M., et al. (2012) Integrative Analysis Reveals Relationships of Genetic and Epigenetic Alterations in Osteosarcoma. *PloS one*. 7 (11).

Kuijjer, M.L., Hogendoorn, P.C.W. & Cleton-Jansen, A.-M. (2013) Genome-wide analyses on high-grade osteosarcoma: Making sense of a genomically most unstable tumor. *International Journal of Cancer*.

Kuijjer, M.L., Peterse, E.F.P., van den Akker, B.E.W.M., Briaire-de Bruijn, I.H., et al. (2013) IR/IGF1R signaling as potential target for treatment of high-grade osteosarcoma. *BMC cancer*. 13 (1), 245.

Kuijjer, M.L., Rydbeck, H., Kresse, S.H., Buddingh, E.P., et al. (2012) Identification of osteosarcoma driver genes by integrative analysis of copy number and gene expression data. *Genes, chromosomes & cancer.* 51 (7), 696–706.

Kurtyka, C.A., Chen, L. & Cress, W.D. (2014) E2F inhibition synergizes with paclitaxel in lung cancer cell lines. *PloS one*. 9 (5).

Lagmay, J.P., Krailo, M.D., Dang, H., Kim, A., et al. (2016) Outcome of Patients With Recurrent Osteosarcoma Enrolled in Seven Phase II Trials Through Children‘s Cancer Group, Pediatric Oncology Group, and Children’s Oncology Group: Learning From the Past to Move Forward. *Journal of Clinical Oncology*. 34 (25), 3031–3038.

Laguna, A., Aranda, S., Barallobre, M.J., Barhoum, R., et al. (2008) The Protein Kinase DYRK1A Regulates Caspase-9-Mediated Apoptosis during Retina Development. *Developmental cell*. 15 (6), 841–853.

Lans, H., Marteijn, J.A. & Vermeulen, W. (2012) ATP-dependent chromatin remodeling in the DNA-damage response. *Epigenetics & chromatin*. 5 (1), 4.

Lau, E., Feng, Y., Claps, G., Fukuda, M.N., et al. (2015) The transcription factor ATF2 promotes melanoma metastasis by suppressing protein fucosylation. *Science signaling*. 8 (406), ra124–ra124.

Lauricella, M., Calvaruso, G., Carabillò, M., D'Anneo, A., et al. (2001) pRb suppresses camptothecin-induced apoptosis in human osteosarcoma Saos-2 cells by inhibiting c-Jun N-terminal kinase. *FEBS letters*. 499 (1-2), 191–197.

Lauvrak, S.U., Munthe, E., Kresse, S.H., Stratford, E.W., et al. (2013) Functional characterisation of osteosarcoma cell lines and identification of mRNAs and miRNAs associated with aggressive cancer phenotypes. *British Journal of Cancer*. 109 (8), 2228–2236.

Ledermann, J.A., Harter, P., Gourley, C., Friedlander, M., et al. (2016) Overall survival in patients with platinum-sensitive recurrent serous ovarian cancer receiving olaparib

maintenance monotherapy: an updated analysis from a randomised, placebo-controlled, double-blind, phase 2 trial. *The lancet oncology*. 17 (11), 1579–1589.

Lewin, J. & Siu, L.L. (2015) Development of Fibroblast Growth Factor Receptor Inhibitors: Kissing Frogs to Find a Prince? *Journal of Clinical Oncology*. 33 (30), 3372–3374.

Li, F.P. & Fraumeni, J.F. (1969) *Soft-tissue sarcomas, breast cancer, and other neoplasms. A familial syndrome?* [71 (4), 747–752.

Lindström, L., Villoutreix, B.O., Lehn, S., Hellsten, R., et al. (2015) Therapeutic Targeting of Nuclear γ-Tubulin in RB1-Negative Tumors. *Molecular cancer research : MCR*. 13 (7), 1073–1082.

Litovchick, L., Florens, L.A., Swanson, S.K., Washburn, M.P., et al. (2011) DYRK1A protein kinase promotes quiescence and senescence through DREAM complex assembly. *Genes & development*. 25 (8), 801–813.

Litovchick, L., Sadasivam, S., Florens, L., Zhu, X., et al. (2007) Evolutionarily Conserved Multisubunit RBL2/p130 and E2F4 Protein Complex Represses Human Cell Cycle-Dependent Genes in Quiescence. *Molecular cell*. 26 (4), 539–551.

Liu, X., Choy, E., Hornicek, F.J., Yang, S., et al. (2011) ROCK1 as a potential therapeutic target in osteosarcoma. *Journal of orthopaedic research.* 29 (8), 1259–1266.

Lord, C.J. & Ashworth, A. (2016) BRCAness revisited. *Nature reviews. Cancer*. 16 (2), 110–120.

Lord, C.J. & Ashworth, A. (2013) Mechanisms of resistance to therapies targeting BRCA-mutant cancers. *Nature medicine*. 19 (11), 1381–1388.

Lord, C.J. & Ashworth, A. (2012) The DNA damage response and cancer therapy. *Nature*. 481 (7381), 287–294.

Lord, C.J., Martin, S.A. & Ashworth, A. (2009) RNA interference screening demystified. *Journal of clinical pathology*. 62 (3), 195–200.

Lord, C.J., Tutt, A.N.J. & Ashworth, A. (2015) Synthetic lethality and cancer therapy: lessons learned from the development of PARP inhibitors. *Annual review of medicine*. 66455–470.

Love, M.I., Huber, W. & Anders, S. (2014) Moderated estimation of fold change and dispersion for RNA-seq data with DESeq2. *Genome biology*. 15 (12), 550.

Lovejoy, C.A., Li, W., Reisenweber, S., Thongthip, S., et al. (2012) Loss of ATRX, genome instability, and an altered DNA damage response are hallmarks of the alternative lengthening of telomeres pathway. Hamish S Scott (ed.). *PLoS genetics*. 8 (7), e1002772.

Lu, H., Gan, M., Cao, X., Chen, L., et al. (2014) RNAi-mediated silencing of the Skp-2 gene causes inhibition of growth and induction of apoptosis in human renal carcinoma cells. *International journal of clinical and experimental pathology*. 7 (7), 3845–3852.

Lu, Z., Bauzon, F., Fu, H., Cui, J., et al. (2014) Skp2 suppresses apoptosis in Rb1-deficient tumours by limiting E2F1 activity. *Nature Communications*. 53463.

Luetke, A., Meyers, P.A., Lewis, I. & Juergens, H. (2014) Osteosarcoma treatment - Where do we stand? A state of the art review. *Cancer treatment reviews*. 40 (4), 523–532.

Luu, H.H., Kang, Q., Park, J.K., Si, W., et al. (2005) An orthotopic model of human osteosarcoma growth and spontaneous pulmonary metastasis. *Clinical & experimental metastasis*. 22 (4), 319–329.

MacDonald, J., Ramos-Valdes, Y., Perampalam, P., Litovchick, L., et al. (2016) A systematic analysis of negative growth control implicates the DREAM complex in cancer cell dormancy. *Molecular cancer research.*

Maguire, S.L., Peck, B., Wai, P.T., Campbell, J., et al. (2016) Three-dimensional modelling identifies novel genetic dependencies associated with breast cancer progression in the isogenic MCF10 model. *The Journal of pathology*. 240 (3), 315–328.

Makarenkov, V., Zentilli, P., Kevorkov, D., Gagarin, A., et al. (2007) An efficient method for the detection and elimination of systematic error in high-throughput screening. *Bioinformatics.* 23 (13), 1648–1657.

Mali, P., Yang, L., Esvelt, K.M., Aach, J., et al. (2013) RNA-guided human genome engineering via Cas9. *Science (New York, N.Y.)*. 339 (6121), 823–826.

Man, T.-K., Chintagumpala, M., Visvanathan, J., Shen, J., et al. (2005) Expression profiles of osteosarcoma that can predict response to chemotherapy. *Cancer research*. 65 (18), 8142–8150.

Man, T.-K., Lu, X.-Y., Jaeweon, K., Perlaky, L., et al. (2004) Genome-wide array comparative genomic hybridization analysis reveals distinct amplifications in osteosarcoma. *BMC cancer*. 445.

Manning, A.L. & Dyson, N.J. (2012) RB: mitotic implications of a tumour suppressor. *Nature reviews. Cancer*. 12 (3), 220–226.

Manning, A.L., Longworth, M.S. & Dyson, N.J. (2010) Loss of pRB causes centromere dysfunction and chromosomal instability. *Genes & development*. 24 (13), 1364–1376.

Maréchal, A. & Zou, L. (2013) DNA damage sensing by the ATM and ATR kinases. *Cold Spring Harbor perspectives in biology*. 5 (9), a012716–a012716.

Marina, N., Bielack, S., Whelan, J., Smeland, S., et al. (2009) International collaboration is feasible in trials for rare conditions: the EURAMOS experience. *Cancer treatment and research*. 152339–353.

Marina, N., Gebhardt, M., Teot, L. & Gorlick, R. (2004) Biology and therapeutic advances for pediatric osteosarcoma. *The oncologist*. 9 (4), 422–441.

Marina, N.M., Smeland, S., Bielack, S.S., Bernstein, M., et al. (2016) Comparison of MAPIE versus MAP in patients with a poor response to preoperative chemotherapy

for newly diagnosed high-grade osteosarcoma (EURAMOS-1): an open-label, international, randomised controlled trial. *The lancet oncology*. 17 (10), 1396–1408.

Martis, E.A. & Radhakrishnan, R. (2011) High-throughput screening: the hits and leads of drug discovery-an overview. *Journal of Applied Pharmaceutical Science 01 (01); 2011: 02-10*

Matsuda, S., Kawamoto, K., Miyamoto, K., Tsuji, A., et al. (2017) PCTK3/CDK18 regulates cell migration and adhesion by negatively modulating FAK activity. *Scientific reports*. 745545.

May, C., Loizos, N., Novosiadly, R., Blosser, W., et al. (2015) The Anti-platelet-derived Growth Factor Receptor A antibody Olaratumab (LY3012297/IMC-3G3) demonstrates anti-tumour activity in models of pediatric bone and soft tissue sarcoma. *CTOS*.

Mejia-Guerrero, S., Quejada, M., Gokgoz, N., Gill, M., et al. (2010) Characterization of the 12q15 MDM2and 12q13-14 CDK4amplicons and clinical correlations in osteosarcoma. *Genes, chromosomes & cancer*.

Mendes-Pereira, A.M., Lord, C.J. & Ashworth, A. (2012) NLK is a novel therapeutic target for PTEN deficient tumour cells. *PloS one*. 7 (10), e47249.

Mermel, C.H., Schumacher, S.E., Hill, B., Meyerson, M.L., et al. (2011) GISTIC2.0 facilitates sensitive and confident localization of the targets of focal somatic copy-number alteration in human cancers. *Genome biology*. 12 (4), R41.

Meyers, P.A., Schwartz, C.L., Krailo, M., Kleinerman, E.S., et al. (2016a) Osteosarcoma: A Randomized, Prospective Trial of the Addition of Ifosfamide and/or Muramyl Tripeptide to Cisplatin, Doxorubicin, and High-Dose Methotrexate. *Journal of Clinical Oncology*. 23 (9), 2004–2011.

Meyers, P.A., Schwartz, C.L., Krailo, M.D., Healey, J.H., et al. (2016b) Osteosarcoma: The Addition of Muramyl Tripeptide to Chemotherapy Improves Overall Survival—A Report From the Children's Oncology Group. *Journal of Clinical Oncology*. 26 (4), 633–638.

Michels, J., Vitale, I., Saparbaev, M., Castedo, M., et al. (2014) Predictive biomarkers for cancer therapy with PARP inhibitors. *Oncogene*. 33 (30), 3894–3907.

Miller, C.W., Aslo, A., Tsay, C., Slamon, D., et al. (1990) *Frequency and structure of p53 rearrangements in human osteosarcoma.* 50 (24), 7950–7954.

Mills, J., Matos, T., Charytonowicz, E., Hricik, T., et al. (2009) Characterization and comparison of the properties of sarcoma cell lines in vitro and in vivo. *Human cell*. 22 (4), 85–93.

Mirabello, L., Troisi, R.J. & Savage, S.A. (2009) *Osteosarcoma incidence and survival rates from 1973 to 2004: data from the Surveillance, Epidemiology, and End Results Program.* 115 (7), 1531–1543.

Mittnacht, S. (2005) The retinoblastoma protein--from bench to bedside. *European journal of cell biology*. 84 (2-3), 97–107.

Mohseny, A.B., Hogendoorn, P.C.W. & Cleton-Jansen, A.-M. (2012) Osteosarcoma Models: From Cell Lines to Zebrafish. *Sarcoma*. 2012 (397), 1–11.

Mohseny, A.B., Machado, I., Cai, Y., Schaefer, K.-L., et al. (2011) Functional characterization of osteosarcoma cell lines provides representative models to study the human disease. *Laboratory investigation; a journal of technical methods and pathology*. 91 (8), 1195–1205.

Muller, P.A.J. & Vousden, K.H. (2014) Mutant p53 in Cancer: New Functions and Therapeutic Opportunities. *Cancer Cell*. 25 (3), 304–317.

Mutsaers, A.J., Ng, A.J.M., Baker, E.K., Russell, M.R., et al. (2013) Modeling distinct osteosarcoma subtypes in vivo using Cre:lox and lineage-restricted transgenic shRNA. *Bone*. 55 (1), 166–178.

Møller, R.S., Kübart, S., Hoeltzenbein, M., Heye, B., et al. (2008) Truncation of the Down syndrome candidate gene DYRK1A in two unrelated patients with microcephaly. *American journal of human genetics*. 82 (5), 1165–1170.

Nahimana, A., Attinger, A., Aubry, D., Greaney, P., et al. (2009) The NAD biosynthesis inhibitor APO866 has potent antitumor activity against hematologic malignancies. *Blood*. 113 (14), 3276–3286.

Neckers, L. & Workman, P. (2012) Hsp90 molecular chaperone inhibitors: are we there yet? *Clinical cancer research : an official journal of the American Association for Cancer Research*. 18 (1), 64–76.

Neganova, I. & Lako, M. (2008) G1 to S phase cell cycle transition in somatic and embryonic stem cells. *Journal of anatomy*. 213 (1), 30–44.

Nghiem, P., Park, P.K., Kim, Y., Vaziri, C., et al. (2001) ATR inhibition selectively sensitizes G1 checkpoint-deficient cells to lethal premature chromatin condensation. *Proceedings of the National Academy of Sciences of the United States of America*. 98 (16), 9092–9097.

Nielsen, G.P., Burns, K.L., Rosenberg, A.E. & Louis, D.N. (1998) CDKN2A gene deletions and loss of p16 expression occur in osteosarcomas that lack RB alterations. *The American Journal of Pathology*. 153 (1), 159–163.

Nik-Zainal, S., Alexandrov, L.B., Wedge, D.C., Van Loo, P., et al. (2012) Mutational processes molding the genomes of 21 breast cancers. *Cell*. 149 (5), 979–993.

Ogawa, Y., Nonaka, Y., Goto, T., Ohnishi, E., et al. (2010) Development of a novel selective inhibitor of the Down syndrome-related kinase Dyrk1A. *Nature Communications*. 186.

Olive, K.P., Tuveson, D.A., Ruhe, Z.C., Yin, B., et al. (2004) Mutant p53 Gain of Function in Two Mouse Models of Li-Fraumeni Syndrome. *Cell*. 119 (6), 847–860.

Olsen, O.E., Wader, K.F., Hella, H., Mylin, A.K., et al. (2015) Activin A inhibits BMP-signaling by binding ACVR2A and ACVR2B. *Cell communication and signaling*. 13 (1), 27.

Ottaviano, L., Schaefer, K.-L., Gajewski, M., Huckenbeck, W., et al. (2010) Molecular characterization of commonly used cell lines for bone tumor research: A trans-European EuroBoNet effort. *Genes, chromosomes & cancer*. 49 (1), 40–51.

Paggi, M.G., Felsani, A. & Giordano, A. (2003) Growth Control by the Retinoblastoma Gene Family. In: *Tumor Suppressor Genes*. New Jersey, Humana Press. pp. 003–019.

Pakos, E.E., Nearchou, A.D., Grimer, R.J., Koumoullis, H.D., et al. (2009) Prognostic factors and outcomes for osteosarcoma: an international collaboration. *European journal of cancer.* 45 (13), 2367–2375.

Palmerini, E., Jones, R.L., Marchesi, E., Paioli, A., et al. (2016) Gemcitabine and docetaxel in relapsed and unresectable high-grade osteosarcoma and spindle cell sarcoma of bone. *BMC cancer*. 16 (1), 280.

Pappo, A.S., Vassal, G., Crowley, J.J., Bolejack, V., et al. (2014) A phase 2 trial of R1507, a monoclonal antibody to the insulin-like growth factor-1 receptor (IGF-1R), in patients with recurrent or refractory rhabdomyosarcoma, osteosarcoma, synovial sarcoma, and other soft tissue sarcomas: results of a Sarcoma Alliance for Research Through Collaboration study. *Cancer*. 120 (16), 2448–2456.

Perry, J.A., Kiezun, A., Tonzi, P., Van Allen, E.M., et al. (2014) Complementary genomic approaches highlight the PI3K/mTOR pathway as a common vulnerability in osteosarcoma. *Proceedings of the National Academy of Sciences of the United States of America*. 111 (51), E5564–E5573.

Pham, D., Moretti, P., Goodall, G. & Pitson, S. (2008) Attenuation of leakiness in doxycycline-inducible expression via incorporation of 3′ AU-rich mRNA destabilizing elements. *BioTechniques*. 45 (2), 155–162.

Plimack, E.R., Dunbrack, R.L., Brennan, T.A., Andrake, M.D., et al. (2015) Defects in DNA Repair Genes Predict Response to Neoadjuvant Cisplatin-based Chemotherapy in Muscle-invasive Bladder Cancer. *European urology*. 68 (6), 959–967.

PosthumaDeBoer, J., Witlox, M.A., Kaspers, G.J.L. & van Royen, B.J. (2011) Molecular alterations as target for therapy in metastatic osteosarcoma: a review of literature. *Clinical & experimental metastasis*. 28 (5), 493–503.

Poulaki, V., Mitsiades, C.S., McMullan, C., Fanourakis, G., et al. (2005) Human retinoblastoma cells are resistant to apoptosis induced by death receptors: role of caspase-8 gene silencing. *Investigative ophthalmology & visual science*. 46 (1), 358–366.

Qiu, X., Wu, H. & Hu, R. (2013) The impact of quantile and rank normalization procedures on the testing power of gene differential expression analysis. *BMC bioinformatics*. 14124.

Rahman, N., Seal, S., Thompson, D., Kelly, P., et al. (2007) PALB2, which encodes a BRCA2-interacting protein, is a breast cancer susceptibility gene. *Nature genetics*. 39 (2), 165–167.

Rath, O. & Kozielski, F. (2012) Kinesins and cancer. *Nature reviews. Cancer*. 12 (8),

527–539.

Raymond, A.K., Ayala, A.G. & Knuutila, S. *Who Classification of Tumours of Soft Tissue and Bone*.

Reaper, P.M., Griffiths, M.R., Long, J.M., Charrier, J.-D., et al. (2011) Selective killing of ATM- or p53-deficient cancer cells through inhibition of ATR. *Nature Chemical Biology*. 7 (7), 428–430.

Rehman, F.L., Lord, C.J. & Ashworth, A. (2010) Synthetic lethal approaches to breast cancer therapy. *Nature reviews. Clinical oncology*. 7 (12), 718–724.

Ren, W. & Gu, G. (2015) Prognostic implications of RB1 tumour suppressor gene alterations in the clinical outcome of human osteosarcoma: a meta-analysis. *European journal of cancer care*.

Rhim, J.S., Park, D.K., Arnstein, P., Huebner, R.J., et al. (1975) *Transformation of human cells in culture by N-methyl-N'-nitro-N-nitrosoguanidine.* 256 (5520), 751–753.

Riccio, A. & Cubellis, M.V. (2012) Gain of function in CDKN1C. *Nature genetics*. 44 (7), 737–738.

Ronco, C., Martin, A.R., Demange, L. & Benhida, R. (2017) ATM, ATR, CHK1, CHK2 and WEE1 inhibitors in cancer and cancer stem cells. *MedChemComm*. 8 (2), 295–319.

Ryan, C.J., Kennedy, S., Bajrami, I., Matallanas, D., et al. (2017) A Compendium of Co-regulated Protein Complexes in Breast Cancer Reveals Collateral Loss Events. *Cell systems*. 5 (4), 399–409.

Sadasivam, S. & Decaprio, J.A. (2013) The DREAM complex: master coordinator of cell cycle-dependent gene expression. *Nature reviews. Cancer*. 13 (8), 585–595.

Sadikovic, B., Park, P.C., Selvarajah, S. & Zielenska, M. (2013) Array comparative genomic hybridization in osteosarcoma. *Methods in molecular biology.*

Sanches, R.F., de Lima Osório, F., Santos, Dos, R.G., Macedo, L.R.H., et al. (2016) Antidepressant Effects of a Single Dose of Ayahuasca in Patients With Recurrent Depression: A SPECT Study. *Journal of clinical psychopharmacology*. 36 (1), 77–81.

Sander, J.D. & Joung, J.K. (2014) CRISPR-Cas systems for editing, regulating and targeting genomes. *Nature biotechnology*. 32 (4), 347–355.

Savage, S.A., Mirabello, L., Wang, Z., Gastier-Foster, J.M., et al. (2013) Genome-wide association study identifies two susceptibility loci for osteosarcoma. *Nature genetics*. 45 (7), 799–803.

Schlabach, M.R., Luo, J., Solimini, N.L., Hu, G., et al. (2008) *Cancer proliferation gene discovery through functional genomics.* 319 (5863), 620–624.

Schmitt, C.A., Fridman, J.S., Yang, M., Baranov, E., et al. (2002) Dissecting p53 tumor suppressor functions in vivo. *Cancer Cell*. 1 (3), 289–298.

Schwarz, R., Bruland, O., Cassoni, A., Schomberg, P., et al. (2009) The role of

radiotherapy in oseosarcoma. *Cancer treatment and research*. 152147–164.

Shen, W., Taylor, B., Jin, Q., Nguyen-Tran, V., et al. (2015) Inhibition of DYRK1A and GSK3B induces human β-cell proliferation. *Nature Communications*.

Siddik, Z.H. (2003) Cisplatin: mode of cytotoxic action and molecular basis of resistance. *Oncogene*. 22 (47), 7265–7279.

Siddiqui, R., Onel, K., Facio, F., Nafa, K., et al. (2005) *The TP53 mutational spectrum and frequency of CHEK2*1100delC in Li-Fraumeni-like kindreds.* 4 (2), 177–181.

Soppa, U., Schumacher, J., Florencio Ortiz, V., Pasqualon, T., et al. (2014) The Down syndrome-related protein kinase DYRK1A phosphorylates p27(Kip1) and Cyclin D1 and induces cell cycle exit and neuronal differentiation. *Cell cycle*. 13 (13), 2084–2100.

Stephens, P.J., Greenman, C.D., Fu, B., Yang, F., et al. (2011) *Massive genomic rearrangement acquired in a single catastrophic event during cancer development.* 144 (1), 27–40.

Stockwell, S.R., Li, H., Aherne, W., Cuomo, M.E., et al. (2012) PLOS ONE: Mechanism-Based Screen Establishes Signalling Framework for DNA Damage-Associated G1 Checkpoint Response. *PloS one*.

Strauss, S.J., Mistry, P., Mendoza, A., Robson, M., et al. (2014) 245 Chk1 is a potential novel therapeutic target that regulates cell survival and potentiates chemotherapy in osteosarcoma (OS) models. *European journal of cancer*. (14)70371-5.

Strebhardt, K. & Ullrich, A. (2006) Targeting polo-like kinase 1 for cancer therapy. *Nature reviews. Cancer*. 6 (4), 321–330.

Su, N., Jin, M. & Chen, L. (2014) Role of FGF/FGFR signaling in skeletal development and homeostasis: learning from mouse models. *Bone research*. 214003.

Sutow, W.W., Sullivan, M.P., Fernbach, D.J., Cangir, A., et al. (1975) Adjuvant chemotherapy in primary treatment of osteogenic sarcoma. A Southwest Oncology Group study. *Cancer*. 36 (5), 1598–1602.

Sutow, W.W., Sullivan, M.P., Wilbur, J.R. & Cangir, A. (1975) Study of adjuvant chemotherapy in osteogenic sarcoma. *Journal of clinical pharmacology*. 15 (7), 530–533.

Tabernero, J., Bahleda, R., Dienstmann, R., Infante, J.R., et al. (2015) Phase I Dose-Escalation Study of JNJ-42756493, an Oral Pan-Fibroblast Growth Factor Receptor Inhibitor, in Patients With Advanced Solid Tumors. *Journal of Clinical Oncology*. 33 (30), 3401–3408.

Talevich, E., Shain, A.H., Botton, T. & Bastian, B.C. (2016) CNVkit: Genome-Wide Copy Number Detection and Visualization from Targeted DNA Sequencing. *PLoS computational biology*. 12 (4), e1004873.

Tang, N., Song, W.-X., Luo, J., Haydon, R.C., et al. (2008) Osteosarcoma development and stem cell differentiation. *Clinical orthopaedics and related research*. 466 (9),

2114–2130.

Tang, X., Yuan, F. & Guo, K. (2014) Repair of radiation damage of U2OS osteosarcoma cells is related to DNA-dependent protein kinase catalytic subunit (DNA-PKcs) activity. *Molecular and cellular biochemistry*. 390 (1-2), 51–59.

Tap, W.D., Jones, R.L., Van Tine, B.A., Chmielowski, B., et al. (2016) Olaratumab and doxorubicin versus doxorubicin alone for treatment of soft-tissue sarcoma: an open-label phase 1b and randomised phase 2 trial. *Lancet.* 388 (10043), 488–497.

Tarkkanen, M., Karhu, R., Kallioniemi, A., Elomaa, I., et al. (1995) *Gains and losses of DNA sequences in osteosarcomas by comparative genomic hybridization.* 55 (6), 1334–1338.

Tarsounas, M., Davies, A.A. & West, S.C. (2004) RAD51 localization and activation following DNA damage. *Philosophical transactions of the Royal Society of London. Series B, Biological sciences*. 359 (1441), 87–93.

Tejedor, F.J. & Hämmerle, B. (2011) MNB/DYRK1A as a multiple regulator of neuronal development. *The FEBS journal*. 278 (2), 223–235.

Toguchida, J., Yamaguchi, T., Ritchie, B., Beauchamp, R.L., et al. (1992) Mutation spectrum of the p53 gene in bone and soft tissue sarcomas. *Cancer research*. 52 (22), 6194–6199.

Toomey, E.C., Schiffman, J.D. & Lessnick, S.L. (2010) *Recent advances in the molecular pathogenesis of Ewing's sarcoma.* 29 (32), 4504–4516.

Torrezan, G.T., da Silva, F.C.C., Santos, E.M.M., Krepischi, A.C.V., et al. (2013) Mutational spectrum of the APC and MUTYH genes and genotype-phenotype correlations in Brazilian FAP, AFAP, and MAP patients. *Orphanet journal of rare diseases*. 8 (1), 54.

Trepel, J., Mollapour, M., Giaccone, G. & Neckers, L. (2010) Targeting the dynamic HSP90 complex in cancer. *Nature reviews. Cancer*. 10 (8), 537–549.

Turner, N., Tutt, A. & Ashworth, A. (2004) Hallmarks of 'BRCAness' in sporadic cancers. *Nature reviews. Cancer*. [Online] 4 (10), 814–819. Available from: doi:10.1038/nrc1457.

Turner, N.C., Lord, C.J., Iorns, E., Brough, R., et al. (2008) A synthetic lethal siRNA screen identifying genes mediating sensitivity to a PARP inhibitor. *The EMBO Journal*. 27 (9), 1368–1377.

Tutt, A., Robson, M., Garber, J.E., Domchek, S.M., et al. (2010) Oral poly(ADP-ribose) polymerase inhibitor olaparib in patients with BRCA1 or BRCA2 mutations and advanced breast cancer: a proof-of-concept trial. *The Lancet*. 376 (9737), 235–244.

Uezumi, A., Fukada, S., Yamamoto, N., Ikemoto-Uezumi, M., et al. (2014) Identification and characterization of PDGFRα+ mesenchymal progenitors in human skeletal muscle. *Cell death & disease*. 5 (4), e1186.

van Maldegem, A.M., Bhosale, A., Gelderblom, H.J., Hogendoorn, P.C., et al. (2012a)

Comprehensive analysis of published phase I/II clinical trials between 1990-2010 in osteosarcoma and Ewing sarcoma confirms limited outcomes and need for translational investment. *Clinical Sarcoma Research*. 2 (1), 5.

Vogelstein, B., Papadopoulos, N., Velculescu, V.E., Zhou, S., et al. (2013) *Cancer genome landscapes.* 339 (6127), 1546–1558.

Wagner, E.R., Luther, G., Zhu, G., Luo, Q., et al. (2011) Defective osteogenic differentiation in the development of osteosarcoma. *Sarcoma*. 2011 (8), 325238–12.

Walkley, C.R., Qudsi, R., Sankaran, V.G., Perry, J.A., et al. (2008) Conditional mouse osteosarcoma, dependent on p53 loss and potentiated by loss of Rb, mimics the human disease. *Genes & development*. 22 (12), 1662–1676.

Wang, D., Luo, M. & Kelley, M.R. (2004) *Human apurinic endonuclease 1 (APE1) expression and prognostic significance in osteosarcoma: enhanced sensitivity of osteosarcoma to DNA damaging agents using silencing RNA APE1 expression inhibition.* 3 (6), 679–686.

Wang, L.L., Levy, M.L., Lewis, R.A., Chintagumpala, M.M., et al. (2001) *Clinical manifestations in a cohort of 41 Rothmund-Thomson syndrome patients.* 102 (1), 11–17.

Wang, P., Alvarez-Perez, J.-C., Felsenfeld, D.P., Liu, H., et al. (2015) A high-throughput chemical screen reveals that harmine-mediated inhibition of DYRK1A increases human pancreatic beta cell replication. *Nature medicine*. 21 (4), 383–388.

Wang, T., Wei, J.J., Sabatini, D.M. & Lander, E.S. (2014) Genetic screens in human cells using the CRISPR-Cas9 system. *Science (New York, N.Y.)*. 343 (6166), 80–84.

Wang, Y., Wang, C., Jiang, C., Zeng, H., et al. (2015) Novel mechanism of harmaline on inducing G2/M cell cycle arrest and apoptosis by up-regulating Fas/FasL in SGC-7901 cells. *Scientific reports*.

Ward, I.M. & Chen, J. (2001) Histone H2AX is phosphorylated in an ATR-dependent manner in response to replicational stress. *The Journal of biological chemistry*. 276 (51), 47759–47762.

Weekes, D., Kashima, T.G., Zandueta, C., Perurena, N., et al. (2016) Regulation of osteosarcoma cell lung metastasis by the c-Fos/AP-1 target FGFR1. *Oncogene*. 35 (22), 2852–2861.

Weinstein, I.B. & Joe, A. (2008) Oncogene addiction. *Cancer research*. [Online] 68 (9), 3077–3080.

Weiss, R.S., Leder, P. & Vaziri, C. (2003) Critical role for mouse Hus1 in an S-phase DNA damage cell cycle checkpoint. *Molecular and cellular biology*. 23 (3), 791–803.

Whelan, J., McTiernan, A., Cooper, N., Wong, Y.K., et al. (2012) Incidence and survival of malignant bone sarcomas in England 1979-2007. *International Journal of Cancer*. 131 (4), E508–E517.

Whelan, J.S., Bielack, S.S., Marina, N., Smeland, S., et al. (2015) EURAMOS-1, an

international randomised study for osteosarcoma: results from pre-randomisation treatment. *Annals of oncology*. 26 (2), 407–414.

Wiedenheft, B., Sternberg, S.H. & Doudna, J.A. (2012) RNA-guided genetic silencing systems in bacteria and archaea. *Nature*. 482 (7385), 331–338.

Williamson, C.T., Miller, R., Pemberton, H.N., Jones, S.E., et al. (2016) ATR inhibitors as a synthetic lethal therapy for tumours deficient in ARID1A. *Nature Communications*. 713837.

Willingham, A.T., Deveraux, Q.L., Hampton, G.M. & Aza-Blanc, P. (2004) RNAi and HTS: exploring cancer by systematic loss-of-function. *Oncogene*. 23 (51), 8392–8400.

Wilson, I.M., Vucic, E.A., Enfield, K.S.S., Thu, K.L., et al. (2014) EYA4 is inactivated biallelically at a high frequency in sporadic lung cancer and is associated with familial lung cancer risk. *Oncogene*. 33 (36), 4464–4473.

Wong, K.C., Lee, V., Shing, M.M.K. & Kumta, S. (2013) Surgical resection of relapse may improve postrelapse survival of patients with localized osteosarcoma. *Clinical orthopaedics and related research*. 471 (3), 814–819.

Wu, J., Zhi, L., Dai, X., Cai, Q., et al. (2015) Decreased RECQL5 correlated with disease progression of osteosarcoma. *Biochemical and biophysical research communications*. 467 (4), 617–622.

Wu, M., Chen, G. & Li, Y.-P. (2016) TGF-β and BMP signaling in osteoblast, skeletal development, and bone formation, homeostasis and disease. *Bone research*. 416009.

Wunder, J.S., Gokgoz, N., Parkes, R., Bull, S.B., et al. (2005) TP53 mutations and outcome in osteosarcoma: a prospective, multicenter study. *Journal of clinical oncology*. 23 (7), 1483–1490.

Xue, P., Zeng, F., Duan, Q., Xiao, J., et al. (2017) BCKDK of BCAA Catabolism Cross-talking With the MAPK Pathway Promotes Tumorigenesis of Colorectal Cancer. *EBioMedicine*.

Yamaguchi, U., Honda, K., Satow, R., Kobayashi, E., et al. (2009) Functional genome screen for therapeutic targets of osteosarcoma. *Cancer science*. 100 (12), 2268–2274.

Yang, E.J., Ahn, Y.S. & Chung, K.C. (2001) Protein kinase Dyrk1 activates cAMP response element-binding protein during neuronal differentiation in hippocampal progenitor cells. *The Journal of biological chemistry*. 276 (43), 39819–39824.

Yang, Y., Tian, S., Brown, B., Chen, P., et al. (2013) The Rb1 gene inhibits the viability of retinoblastoma cells by regulating homologous recombination. *International journal of molecular medicine*. 32 (1), 137–143.

Yavropoulou, M.P. & Yovos, J.G. (2008) Osteoclastogenesis--current knowledge and future perspectives. *Journal of musculoskeletal & neuronal interactions*. 8 (3), 204–216.

Zhang, J., Chung, T. & Oldenburg, K. (1999) A Simple Statistical Parameter for Use in Evaluation and Validation of High Throughput Screening Assays. *Journal of biomolecular screening*. 4 (2), 67–73.

Zhang, J., Walsh, M.F., Wu, G., Edmonson, M.N., et al. (2015) Germline Mutations in Predisposition Genes in Pediatric Cancer. *New England Journal of Medicine*. 373 (24), 2336–2346.

Zhang, J., Yang, P.L. & Gray, N.S. (2009) Targeting cancer with small molecule kinase inhibitors. *Nature reviews. Cancer*. 9 (1), 28–39.

Zhang, Z., Zhang, Y., Lv, J. & Wang, J. (2015) The survivin suppressant YM155 reverses doxorubicin resistance in osteosarcoma. *International journal of clinical and experimental medicine*. 8 (10), 18032–18040.

Zhao, H., Wang, H., Bauzon, F., Lu, Z., et al. (2016) Deletions of Retinoblastoma 1 (Rb1) and Its Repressing Target S Phase Kinase-associated protein 2 (Skp2) Are Synthetic Lethal in Mouse Embryogenesis. *Journal of Biological Chemistry*. 291 (19), 10201–10209.

Zhi, L.-Q., Ma, W., Zhang, H., Zeng, S.-X., et al. (2014) Association of RECQL5 gene polymorphisms and osteosarcoma in a Chinese Han population. *Tumour biology*. 35 (4), 3255–3259.

Zitvogel, L. & Kroemer, G. (2012) Targeting PD-1/PD-L1 interactions for cancer immunotherapy. *Oncoimmunology*. 1 (8), 1223–1225.